Advanced and Complete Functional Series Time-Dependent ARMA (FS-TARMA) Methods for the Identification and Fault Diagnosis of Non-Stationary Stochastic Structural Systems

ΠΑΝΕΠΙΣΤΗΜΙΟ ΠΑΤΡΩΝ
UNIVERSITY OF PATRAS

Minas Spiridonakos
Department of Mechanical Engineering and Aeronautics
University of Patras

A thesis submitted for the degree of
Doctor of Philosophy

April 2, 2012

Examination Committee

- **Spilios Fassois, Professor (supervisor)**
  Department of Mechanical Engineering & Aeronautics
  University of Patras, Greece

- **Anthony Tzes, Professor (advising committee member)**
  Department of Electrical & Computer Engineering
  University of Patras, Greece

- **Kostas Berberidis, Professor (advising committee member)**
  Department of Computer Engineering & Informatics
  University of Patras, Greece

- **Tassos Bountis, Professor**
  Department of Mathematics
  University of Patras, Greece

- **Ioannis Antoniadis, Associate Professor**
  School of Mechanical Engineering
  National Technical University of Athens, Greece

- **Manolis Manatakis, Assistant Professor**
  Department of Mechanical Engineering & Aeronautics
  University of Patras, Greece

- **Ioannis Sakellariou, Lecturer**
  Department of Mechanical Engineering & Aeronautics
  University of Patras, Greece

I would like to dedicate this thesis to my wife Angeliki and my family. Without their support I would not have been able to complete this work.

Acknowledgements

This thesis arose out of years of research that has been done since I came to SMSA group. By that time, I have worked with a great number of people whose contribution to the research and the making of the thesis deserves special mention. It is a pleasure to convey my gratitude to them all in my humble acknowledgement.

Firstly, I 'm grateful to my supervisor, Prof. Fassois, whose expertise, vast knowledge and skills in many areas added considerably to my graduate experience and guidance during the writing process. A very special thanks goes also to my advisory committee members, Prof. Anthony Tzes (Department of Electrical & Computer Engineering) and Prof. Kostas Berberidis (Department of Computer Engineering & Informatics), whose recommendations have been critical to my work.

I would like also to thank my beloved family and wife for the support they provide me through my life, in particular, without their love, encouragement and assistance, I would not have finished this thesis. I also feel obliged and I deeply appreciate my colleagues and friends Fotis, Aggelos, Vangelis, Dimos, Giannis, Paulos, Thodoris, Thanasis, Nikos and Zisis for the excellent cooperation and support during all these years. Although any expression of acknowledgment will fail to fully capture the importance of their role, I would still like to thank each of them, and also to say how much I appreciated their contributions and enjoyed our interactions.

Finally, I would like to thank everybody who was important to the successful realization of the thesis, as well as expressing my apology that I could not mention personally one by one.

Abstract

Non-stationary signals, that is signals with statistical properties that depend upon time, are commonly encountered in engineering practice. The vibration responses of structures, such as traffic-excited bridges, robotic devices, rotating machinery, deployable structures and so on, constitute typical examples of non-stationary signals. Such structures characterized by properties, either physical or geometrical, that vary with time are referred as Time-Varying (TV) structures and their vibration-based identification under normal operating conditions is a significant and yet challenging problem.

An important class of parametric methods for the effective solution of the above problem is based on Functional Series Time-dependent AutoRegressive Moving Average (FS-TARMA) models. These models have parameters that explicitly depend on time, with the dependence described by deterministic functions belonging to specific functional subspaces. The advantages of FS-TARMA models over alternative non-stationary models have been demonstrated in a number of studies and involve improved accuracy, improved tracking of the time-varying dynamics, increased predictive ability, and representation parsimony. The potential of FS-TARMA models for accurate vibration-based non-stationary modelling constitutes the primary motivation for this thesis.

The specific goal of the present work is the development of advanced and complete methods that offer important improvements in overcoming the drawbacks of existent FS-TARMA methods mainly regarding the functional subspace estimation problem. Additionally, a number of practical issues are presently considered. These include the extension of FS-TARMA modelling for non-stationary identification based on multivariate response measurements that are usually available in modern structures and the problem of fault detection and identification for time-varying structures.

More specifically, in Chapter 2 and after the introduction of this thesis, an experimental assessment and comparison of vibration based non-stationary parametric identification methods is presented. The methods considered are classified according to the mathematical structure imposed on the TV parameter evolution as unstructured, stochastic, and deterministic parameter evolution. A representative identification method from each class is outlined, while their performance characteristics are examined through their application to the problem of identification and model-based dynamic analysis of a "bridge-like" laboratory structure consisting of a beam with a mass moving on it. The results of this study demonstrate the parametric methods' applicability, effectiveness, and high potential for parsimonious and accurate identification and dynamic analysis of TV structures under unobservable excitation, with FS-TARMA method achieving the best performance in terms of TV dynamics tracking accuracy.

The problem of parametric output-only identification of a time-varying structure based on measured vector vibration response signals is considered in Chapter 3 of this thesis. More specifically, a Functional Series Vector Time-dependent AutoRegressive Moving Average (FS-VTARMA) method is introduced and employed for the identification of the aforementioned "bridge-like" laboratory structure. In this case, the identification is based on three simultaneously measured vibration response signals. The method is judged against baseline modelling based on multiple "frozen-configuration" stationary experiments, and is shown to be effective and capable of accurately tracking the structure's dynamics. Additional comparisons with

recursive and short-time subspace methods are made and demonstrate the FS-VTARMA method's superior achievable accuracy and model representation economy.

In Chapter 4 a new class of Adaptable FS-TARMA (AFS-TARMA) models is introduced. The novel models utilize adaptable functional subspaces with a-priori unknown characteristics for the expansion of their time-dependent parameters.In this way, the basis may be automatically adapted on the data in order to track the evolution of the system parameters with the highest possible accuracy. This is accomplished via proper basis function parametrizations and a Separable Nonlinear Least Squares (SNLS) type procedure which leads to a constrained nonlinear optimization problem of reduced dimensionality that is tackled via a hybrid optimization scheme. The latter consists of a global search procedure based on the gradient-free evolutionary Particle Swarm Optimization (PSO) algorithm and a gradient-type refinement based on an interior point algorithm. The method's effectiveness is shown in both numerical and experimental case studies. The numerical case studies concern Monte Carlo experiments based on the identification of simulated models characterized by abrupt parameter evolution, while the introduced method is also applied for the output-only identification of the time-varying dynamics of a pick-and-place mechanism. Comparisons with the classical FS-TARMA and alternative non-stationary methods are also presented. The results confirm the excellent performance and superior accuracy achieved by the introduced AFS-TARMA method with adaptable basis functions.

A critical survey with exhaustive literature review of FS-TARMA type methods for the identification and analysis of non-stationary signals and structures is presented in Chapter 5. The aim of this chapter is to provide a critical overview of the various FS-TARMA estimation methods and model structure selection schemes that have been proposed in the literature. The estimation methods considered include regression type methods based on the minimization of Prediction Error (PE) criteria, recursive estimation methods, multistage methods and the Maximum Likelihood (ML) method. For the model structure selection problem integer optimization schemes, and schemes based on the concept of backward and forward regression are reviewed. The study covers both theoretical and practical aspects on the subject while special emphasis is placed on promising new methods that aim at overcoming problems of previous approaches. The detailed comparison and assessment of the reviewed methods based on Monte Carlo experiments is also performed. More specifically, the most significant methods for FS-TARMA parameter estimation are employed for the identification of simulated systems. Several functional bases and various model structure selection methods are contrasted, while comparisons with alternative non-stationary methods are also carried out. The results of the study demonstrate the effectiveness and improvements offered by new FS-TARMA methods over previous counterparts, as well as the FS-TARMA approach overall accuracy and effectiveness.

Finally, in the last chapter of this thesis the problem of vibration-based fault detection and identification in inherently non-stationary structures is considered via a statistical time series method based on FS-TAR models combined with an appropriate statistical decision framework. Its performance is experimentally assessed via its application on the fault detection and identification in a time-varying pick-and-place mechanism. The mechanism consists of two electromagnetic linear motors that follow prescribed motion profiles while the whole mechanism is subject to broadband random force excitation. The faults considered are of various types and occurrence locations, while their detection is based solely on a single non-stationary vibration response signal acquired during operation. The method is shown to achieve effective fault detection and identification for all the fault scenarios.

Εξελιγμένες και Πλήρεις Μέθοδοι Συναρτησιακών Χρονικά Μεταβαλλόμενων Μοντέλων Αυτοπαλινδρόμησης και Κινητού Μέσου Όρου (FS-TARMA) για την Δυναμική Αναγνώριση και Διάγνωση Βλαβών σε Μη-Στάσιμα Στοχαστικά Συστήματα Κατασκευών

Περίληψη

Μη-στάσιμα σήματα, δηλαδή σήματα με στατιστικές ιδιότητες οι οποίες μεταβάλλονται με τον χρόνο, απαντώνται συχνά στην επιστήμη του μηχανικού. Τυπικά παραδείγματα αποτελούν οι ταλαντωτικές αποκρίσεις κατασκευών, όπως γέφυρες διεγειρόμενες από την κίνηση των οχημάτων, ρομποτικές διατάξεις, περιστρεφόμενες μηχανές, αναδιπλούμενες και επεκτεινόμενες κατασκευές, και άλλες. Τέτοιες κατασκευές οι οποίες χαρακτηρίζονται από ιδιότητες, είτε φυσικές είτε γεωμετρικές, οι οποίες μεταβάλλονται με τον χρόνο αναφέρονται ως μη-στάσιμες ή αλλιώς χρονικά μεταβαλλόμενες κατασκευές και η δυναμική αναγνώριση και ανάλυση τους επί τη βάση ταλαντωτικών σημάτων απόκρισης αποτελεί σημαντικό και ταυτόχρονα δύσκολο πρόβλημα.

Ο τελικός στόχος της διαδικασίας της δυναμικής αναγνώρισης μιας κατασκευή είναι η ανάπτυξη ενός μαθηματικού μοντέλου για την ακριβή περιγραφή της. Συνήθως, θεωρείται πως το μετρούμενο σήμα ταλαντωτικής απόκρισης μιας κατασκευής υπακούει σε μια παρόμοια αλλά άγνωστη σε εμάς μαθηματική έκφραση, η οποία θα αναπαριστά τα υποκείμενα δυναμικά χαρακτηριστικά της και αναφέρεται ως πραγματικό μοντέλο της κατασκευής. Εν συνεχεία, το εκτιμημένο μοντέλο μπορεί να χρησιμοποιηθεί για μη-στάσιμη δυναμική ανάλυση μέσω της εξαγωγής χρήσιμων φυσικών πληροφοριών όπως οι στατιστικές ροπές ή συνηθέστερα κάποια μορφή της χρονικά μεταβαλλόμενης συνάρτησης πυκνότητας φάσματος ισχύος και των χρονικά μεταβαλλόμενων ιδιομορφών. Επιπρόσθετα της δυναμικής ανάλυσης, ένα εκτιμημένο μοντέλο μπορεί να χρησιμοποιηθεί για σκοπούς πρόβλεψης, προσομοίωσης, διάγνωσης βλαβών και αυτομάτου ελέγχου.

Η μοντελοποίηση μη-στάσιμων ταλαντώσεων έχει λάβει ιδιαίτερη προσοχή τα τελευταία χρόνια. Οι διαθέσιμες μέθοδοι μη-στάσιμης μοντελοποίησης μπορούν κατ' αρχήν να ταξινομηθούν σε *μη-παραμετρικές* ή *παραμετρικές*. Έως σήμερα, οι μη-παραμετρικές μέθοδοι λαμβάνουν περισσότερης προσοχής, κυρίως λόγω της απλότητας τους. Βασίζονται σε μη-παραμετρικές αναπαραστάσεις του ταλαντωτικού σήματος ως συνάρτηση του χρόνου και της συχνότητας ταυτόχρονα (κατανομές χρόνου-συχνότητας). Οι μέθοδοι αυτές περιλαμβάνουν το ευρέως χρησιμοποιούμενο φασματογράφημα (spectrogram) το οποίο βασίζεται στον μετασχηματισμό Fourier βραχέως χρόνου (Short-Time Fourier Transform, STFT) και τις παραλλαγές του [Hammond and White, 1996], το εξελικτικό φάσμα του Priestley [Priestley, 1988], κατανομές όπως η Wigner-Ville και η Choi-Williams οι οποίες ανήκουν στην τάξη των κατανομών Cohen [Cohen, 1995], μέθοδοι οι οποίοι βασίζονται σε κυματίδια [Spanos and Failla, 2005] και άλλες.

Εν γένει, συγκρινόμενες με τις μη-παραμετρικές μεθόδους, οι μη-στάσιμες μέθοδοι που βασίζονται σε παραμετροποιημένες αναπαραστάσεις έχει δειχθεί πως δυνητικά προσφέρουν ένα πλήθος πλεονεκτημάτων, όπως (για παράδειγμα βλ. [Poulimenos and Fassois, 2006, Petsounis and Fassois, 2000, Conforto and D'Alessio, 1999b, Ben Mrad et al., 1998b, Fouskitakis and Fassois, 2002, Poulimenos and Fassois, 2009a, Zhan and Jardine, 2005a]): (i)

οικονομία παραμετροποίησης, καθώς τα εκτιμημένα μοντέλα συνήθως ορίζονται από περιορισμένο αριθμό παραμέτρων, (ii) αυξημένη ακρίβεια, (iii) βελτιωμένη ανάλυση στις αναπαραστάσεις των συναρτήσεων χρόνου-συχνότητας, (iv) καλύτερη ανίχνευση των χρονικά μεταβαλλόμενων δυναμικών χαρακτηριστικών, (v) ευελιξία κατά την ανάλυση, καθώς οι παραμετρικές μέθοδοι είναι ικανές για την άμεση αναπαράσταση των δυναμικών χαρακτηριστικών της κατασκευής τα οποία ευθύνονται για την μη-στάσιμη συμπεριφορά, και (vi) ευελιξία στην χρήση τους για σκοπούς προσομοίωσης και πρόβλεψης, διάγνωσης βλαβών και αυτομάτου ελέγχου.

Η παρούσα διατριβή εστιάζει στην μοντελοποίηση και ανάλυση μη-στάσιμων στοχαστικών σημάτων ταλάντωσης μέσω μιας συγκεκριμένης οικογένειας παραμετρικών χρονικά μεταβαλλόμενων μοντέλων. Τα μοντέλα αυτά ονομάζονται συναρτησιακά χρονικά μεταβαλλόμενα μοντέλα αυτοπαλινδρόμησης κινητού μέσου όρου (FS-TARMA, Functional Series Time-Dependent AutoRegressive Moving Average) και βασίζονται στην παραδοχή ότι οι παράμετροι τους ακολουθούν ένα καθοριστικό πρότυπο και κατά συνέπεια μπορούν να προβληθούν σε κατάλληλα επιλεγμένους συναρτησιακούς υποχώρους. Βάσει της *κλασσικής* προσέγγισης αυτοί οι συναρτησιακοί υποχώροι επιλέγονται απο ένα σύνολο γραμμικά ανεξάρτητων συναρτήσεων βάσης μιας συγκεκριμένης οικογένειας (όπως πολυωνυμικές, τριγωνομετρικές, κυματιδίων, ή άλλες). Υιοθετώντας αυτή την προσέγγιση, ένα *κλασσικό παραμετρικό μοντέλο FS-TARMA*$(n_a, n_c)_{[p_a,p_c,p_s]}$, με n_a, n_c να υποδηλώνουν τις τάξεις του AR και MA μέρους, αντίστοιχα, και p_a, p_c, p_s τις διαστάσεις των συναρτησιακών υποχώρων του AR, MA μέρους και της διασποράς της καινοτόμου ακολουθίας, ορίζεται ως ακολούθως [Poulimenos and Fassois, 2006]:

$$\boxed{\begin{gathered}
x[t] + \underbrace{\sum_{i=1}^{n_a} a_i[t] \cdot x[t-i]}_{\text{AR μέρος}} = e[t] + \underbrace{\sum_{i=1}^{n_c} c_i[t] \cdot e[t-i]}_{\text{MA μέρος}}, \qquad e[t] \sim \text{NID}(0, \sigma_e^2[t]) \\[2ex]
\mathcal{F}_{\text{AR}} = \left\{ G_{d_a(1)}[t], \ldots, G_{d_a(p_a)}[t] \right\}, \qquad \mathcal{F}_{\text{MA}} = \left\{ G_{d_c(1)}[t], \ldots, G_{d_c(p_c)}[t] \right\}, \\
\mathcal{F}_{\sigma_e^2[t]} = \left\{ G_{d_s(1)}[t], \ldots, G_{d_s(p_s)}[t] \right\} \\[2ex]
a_i[t] = \sum_{j=1}^{p_a} a_{i,j} \cdot G_{d_a(j)}[t], \quad c_i[t] = \sum_{j=1}^{p_c} c_{i,j} \cdot G_{d_c(j)}[t], \quad \sigma_e^2[t] = \sum_{j=1}^{p_s} s_j \cdot G_{d_s(j)}[t]
\end{gathered}}$$

όπου $x[t]$ υποδηλώνει την χρονοσειρά της ταλαντωτικής απόκρισης του συστήματος, $e[t]$ την καινοτόμο ακολουθία (ή αλλιώς τα υπόλοιπα) του μοντέλου, «$\mathcal{F}$» τον συναρτησιακό υποχώρο της υποδεικνυόμενης ποσότητας, $d_a(i)$ $(i = 1, \ldots, p_a)$, $d_c(i)$ $(i = 1, \ldots, p_c)$ και $d_s(i)$ $(i = 1, \ldots, p_s)$ τους δείκτες των συγκεκριμένων συναρτήσεων βάσης που περιλαμβάνονται σε κάθε υποχώρο, ενώ $a_{i,j}$, $c_{i,j}$, και s_j αντιπροσωπεύουν τους *συντελεστές προβολής* του AR, MA μέρους και της διασποράς της καινοτόμου ακολουθίας, αντίστοιχα. Έτσι, το πλήρες διάνυσμα των παραμέτρων $\boldsymbol{\theta}$ του μοντέλου αποτελείται από αυτούς τους συντελεστές προβολής, ενώ θεωρώντας μια συγκεκριμένη οικογένεια συναρτήσεων βάσης η διαδικασία επιλογής της δομής ενός μοντέλου FS-TARMA αφορά τον καθορισμό των AR και MA τάξεων n_a, n_c, και τα διανύσματα των δεικτών των συναρτήσεων βάσεων $\boldsymbol{d}_a = [d_{a(1)}, \ldots, d_{a(p_a)}]^T$, $\boldsymbol{d}_c = [d_{c(1)}, \ldots, d_{c(p_c)}]^T$, και $\boldsymbol{d}_s = [d_{s(1)}, \ldots, d_{s(p_s)}]^T$ του AR, MA μέρους και της διασποράς της καινοτόμου ακολουθίας, αντίστοιχα, δηλαδή:

$$\boxed{\begin{gathered}
\boldsymbol{\theta} = [\boldsymbol{\vartheta}_a^T \; \boldsymbol{\vartheta}_c^T \; \boldsymbol{\vartheta}_s^T]^T = [a_{1,1}, \ldots, a_{n_a,p_a} \; c_{1,1}, \ldots, c_{n_c,p_c} \; s_1, \ldots, s_{p_s}]^T \\
\mathcal{M} = \{n_a, n_c, \boldsymbol{d}_a, \boldsymbol{d}_c, \boldsymbol{d}_s\}
\end{gathered}}$$

Βάσει των παραπάνω, τα κύρια χαρακτηριστικά των μοντέλων FS-TARMA μπορούν να συνοψισθούν ως εξής:

- Είναι στοχαστικά παραμετρικά μοντέλα συγκεντρωμένων παραμέτρων. Στοχαστικά καθώς περιλαμβάνουν τυχαίες μεταβλητές, οι οποίες αντικατοπτρίζουν τους συντελεστές αβεβαιότητας που υπάρχουν στα σήματα ταλάντωσης και καθιστούν αδύνατη την ακριβή πρόβλεψη της απόκρισης των υπό μοντελοποίηση συστημάτων, και συγκεντρωμένων παραμέτρων καθώς περιγράφονται από πεπερασμένο αριθμό εξισώσεων διαφορών.
- Είναι μοντέλα διακριτού χρόνου καθώς αναπαριστούν το ταλαντωτικό σήμα σε διακριτές χρονικές στιγμές (για παράδειγμα $t = 1, 2, \ldots, N$), μέσω ενός σχετικά μικρού αριθμού παραμέτρων.
- Είναι γραμμικά μοντέλα απόκρισης, καθώς αναπαριστούν τα ταλαντωτικά σήματα μέσω γραμμικών σχέσεων που συμπεριλαμβάνουν παρελθοντικές τιμές μόνο των σημάτων απόκρισης και τυχαίων μεταβλητών.

Το *πλήρες πρόβλημα αναγνώρισης* ενός μοντέλου FS-TARMA μπορεί να διατυπωθεί ως εξής: *«Δοθέντων N παρατηρήσεων της ταλαντωτικής απόκρισης, έστω $x^N = \{x[1] \ldots x[N]\}$ και το σύνολο των μοντέλων FS-TARMA:*

$$\mathbb{M} \triangleq \Bigg\{ \mathcal{M}(\boldsymbol{\theta}): \; x[t] + \sum_{i=1}^{n_a} a_i[t,\boldsymbol{\theta}] \cdot x[t-i] = e[t,\boldsymbol{\theta}] + \sum_{i=1}^{n_c} c_i[t,\boldsymbol{\theta}] \cdot e[t-i,\boldsymbol{\theta}]; \\ \sigma_e^2[t] = \mathrm{E}\left\{ e^2[t,\boldsymbol{\theta}] \right\}, \qquad t = 1, \ldots N, \qquad \boldsymbol{\theta} \in \Re^{\dim(\boldsymbol{\theta})} \Bigg\},$$

επιλέξτε το στοιχείο του συνόλου $\mathbb{M}$ το οποίο περιγράφει κατά τον βέλτιστο τρόπο τις παρατηρήσεις».

Στην παραπάνω μαθηματική έκφραση, $e[t, \boldsymbol{\theta}]$ αναπαριστά την ακολουθία του σφάλματος πρόβλεψης ενός βήματος του μοντέλου (ακολουθία των υπολοίπων), η οποία, όπως και στην στάσιμη περίπτωση, συμπίπτει με την καινοτόμο ακολουθία του μοντέλου $e[t]$ [Poulimenos and Fassois, 2006]. Έτσι, η αναγνώριση μπορεί να θεωρηθεί ως το πρόβλημα προσδιορισμού του μοντέλου το οποίο περιγράφει κατά τον βέλτιστο τρόπο τις παρατηρήσεις της ταλαντωτικής απόκρισης x^N. Η καταλληλότητα του μοντέλου μπορεί να κριθεί επί τη βάση διαφόρων κριτηρίων, όπως η συνάρτηση πιθανοφάνειας ή κριτήρια σχετικά με το σφάλμα πρόβλεψης [Fassois, 2001a]. Τόσο η δομή $\mathcal{M}$ όσο και το διάνυσμα των παραμέτρων του μοντέλου $\boldsymbol{\theta}$ το οποίο αποτελείται από τους συντελεστές προβολής $a_{i,j}, c_{i,j}, s_j$ πρέπει να εκτιμηθούν από το δοθέν σήμα της ταλαντωτικής απόκρισης.

Τα μοντέλα FS-TARMA ανήκουν στην τάξη των μεθόδων Καθοριστικής Εξέλιξης των Παραμέτρων (Deterministic Parameter Evolution (DPE)) καθώς επιβάλλουν καθοριστική «δομή» στην εξέλιξη των χρονικά μεταβαλλόμενων παραμέτρων τους. Κατ' αυτόν τον τρόπο, μπορούν να θεωρηθούν ως ιδιαίτερα αποτελεσματικά για την αναγνώριση χρονικά μεταβαλλόμενων μηχανολογικών κατασκευών, οι οποίες συνήθως χαρακτηρίζονται από έναν καθοριστικό φυσικό μηχανισμό ο οποίος ευθύνεται για την μεταβλητότητα τους. Επιπλέον, συγκρινόμενα με εναλλακτικές παραμετρικές μεθόδους που ανήκουν στις τάξεις των μεθόδων αδόμητης εξέλιξης των παραμέτρων (Unstructured Parameter Evolution, UPE) ή στοχαστικής εξέλιξης των παραμέτρων (Stochastic Parameter Evolution, SPE), οι μέθοδοι που βασίζονται σε FS-TARMA μοντέλα παρουσιάζουν ένα πλήθος επιθυμητών ιδιοτήτων όπως [Poulimenos and Fassois, 2006, Conforto and D'Alessio, 1999b, Ben Mrad et al., 1998b, Petsounis and Fassois, 2000, Fouskitakis and Fassois, 2001, Niedźwiecki, 2000]: (i) Επιβάλλουν την μέγιστη «δομή» στην εξέλιξη των παραμέτρων επιτυγχάνοντας υψηλό βαθμό οικονομίας παραμετροποίησης, (ii) είναι ικανές να ανιχνεύουν τόσο ομαλές/αργές όσο και απότομες/γρήγορες μεταβολές των παραμέτρων μέσω της κατάλληλης επιλογής των συναρτήσεων βάσης, και (iii) επιτυγχάνουν υψηλή ακρίβεια μοντελοποίησης και ανάλυσης των αναπαραστάσεων των δυναμικών χαρακτηριστικών της κατασκευής.

Πράγματι, οι μέθοδοι της αδόμητης εξέλιξης αποτυγχάνουν να μοντελοποιήσουν τα μεταβατικά φαινόμενα των μη-στάσιμων ταλαντώσεων και είναι κατάλληλες για την περιγραφή κυρίως «αργών» μεταβολών των χαρακτηριστικών του σήματος, απαιτούν συμβιβασμό μεταξύ της δυνατότητας ανίχνευσης και της επιτυγχανόμενης ακρίβειας, και δεν οδηγούν σε οικονομικές αναπαραστάσεις. Οι μέθοδοι της στοχαστικής εξέλιξης, από την άλλη μεριά, προσφέρουν αυξημένη οικονομία, αλλά είναι κατάλληλες κυρίως για την περιγραφή στοχαστικών μεταβολών των χαρακτηριστικών του συστήματος. Τα πλεονεκτήματα των μοντέλων FS-TARMA έναντι εναλλακτικών μη-στάσιμων μοντέλων έχουν μάλιστα δειχθεί μέσω συγκριτικής μελέτης επί την βάση Monte Carlo πειραμάτων [Poulimenos and Fassois, 2006] αν και έως σήμερα τα αποτελέσματα αυτά δεν έχουν επιβεβαιωθεί από πειραματική μελέτη.

Τα μοντέλα FS-TARMA έχουν διαδραματίσει σημαντικό ρόλο στην ανάπτυξη και την εξέλιξη της μη-στάσιμης στοχαστικής μοντελοποίησης σημάτων τα τελευταία σαράντα χρόνια. Τα συναρτησιακά μοντέλα, στην απλούστερη μορφή των μοντέλων αυτοπαλινδρόμησης TAR εισήχθησαν το 1970 από τον Rao [Rao, 1970]. FS-TAR μοντέλα με παραμέτρους που ανήκουν σε υποχώρους πολυωνυμικών συναρτήσεων Legendre χρησιμοποιήθηκαν για πρώτη φορά εντός του πλαισίου της μοντελοποίησης και προσομοίωσης στοχαστικών σημάτων ταλάντωσης, και πιο συγκεκριμένα σεισμογραφημάτων, σε άρθρο του Kozin το 1977 [Kozin, 1977]. Ωστόσο, τα συναρτησιακά μοντέλα δεν βρήκαν μεγάλη απήχηση στην διεθνή επιστημονική κοινότητα πριν τις αρχές της δεκαετίας του 1980, οπότε και πλήθος ερευνητών ξεκίνησε να μελετά τις ιδιότητες τους και να εξετάζει την ικανότητα τους για ακριβή μοντελοποίηση μη-στασίμων σημάτων [Grenier, 1983b, Hall et al., 1983, Clergeot, 1984, Charbonnier et al., 1987, Niedźwiecki, 1988].

Έκτοτε, τα μοντέλα FS-TAR/TARMA έχουν χρησιμοποιηθεί σε διάφορες εφαρμογές γύρω από την δυναμική ανάλυση κατασκευών μέσω σημάτων ταλάντωσης, όπως για την ταλαντωτική ανάλυση περιστρεφόμενων μηχανών [Bardou and Sidahmed, 1994, Conforto and D'Alessio, 1999b, Zhang et al., 2010a], την μοντελοποίηση και την πρόβλεψη της κατανάλωσης ενέργειας σε σύστημα ενεργητικής ανάρτησης αυτοκινήτου [Ben Mrad et al., 1998b], την μοντελοποίηση και την ανάλυση προσομοιωμένης ταλάντωσης ρομποτικού μηχανισμού [Petsounis and Fassois, 2000], και την μοντελοποίηση και δυναμική ανάλυση πρότυπης εργαστηριακής κατασκευής η οποία αναπαριστά σύστημα γέφυρας με βαρύ κινούμενο όχημα επ' αυτής [Poulimenos and Fassois, 2009b].

Παρ' όλα αυτά, η πλειοψηφία των εργασιών που εξετάζουν ή εφαρμόζουν FS-TARMA μοντέλα περιορίζονται στην απλή βαθμωτή περίπτωση και την μοντελοποίηση μέσω ενός μόνο σήματος ταλάντωσης. Αν και η περίπτωση μοντελοποίησης πολλαπλών σημάτων ταλαντωτικής απόκρισης (διανυσματική ή πολυμεταβλητή) περίπτωση είναι πολύ πιο σημαντική από πρακτικής σκοπιάς, έως σήμερα έχει τύχει περιορισμένης προσοχής. Εν γένει, η διανυσματική αναγνώριση μπορεί να οδηγήσει σε πιο πλήρεις αναπαραστάσεις, μικρότερους χρόνους λήψης δεδομένων και χρόνων επεξεργασίας και επίσης αυξημένη ακρίβεια των μορφικών παραμέτρων [Fassois, 2001b]. Αν και η υποκατηγορία των διανυσματικών μοντέλων FS-TAR έχει χρησιμοποιηθεί σε ένα γενικότερο πλαίσιο από τους Gersch ανδ Kitagawa [Gersch and Kitagawa, 1982] και τον Sato και τους συνεργάτες του [Sato et al., 2007] για την μοντελοποίηση και ανάλυση οικονομετρικών και βιοϊατρικών χρονοσειρών αντίστοιχα, η περίπτωση των πληρέστερων διανυσματικών μοντέλων FS-TARMA δεν έχει θεωρηθεί έως σήμερα.

Σχετικά με το πρόβλημα της επιλογής της δομής των μοντέλων FS-TARMA, και παρότι η σημαντικότητα του προβλήματος της επιλογής των κατάλληλων συναρτησιακών υποχώρων είχε υπογραμμιστεί σε πάρα πολλές δημοσιεύσεις από τα πρώτα χρόνια της ιστορίας των μοντέλων FS-TARMA, μόλις το 1993 οι Tsatsanis και Giannakis παρουσίασαν ένα πλήρες σχήμα για την επιλογή της δομής των μοντέλων βασισμένο στην έννοια της οπισθοδρομικής παλινδρόμησης [Tsatsanis and Giannakis, 1993]. Πιο συστηματική διερεύνηση του ζητήματος έχει λάβει χώρα την τελευταία δεκαετία. Για παράδειγμα, ένα απλοποιημένο σχήμα βασιζόμενο στην οπισθοδρομική παλινδρόμηση έχει προταθεί από τους Poulimenos και Fassois [Poulimenos and Fassois, 2003b] ενώ μια διαδικασία βασισμένη στην πρόσω παλινδρόμηση (forward regression) και την ορθογωνοποίηση κατά Gram-Schmidt έχει επίσης προταθεί από τους Wei και Billings [Wei and Billings, 2002]. Τέλος, πρόσφατα έχει προταθεί μια πιο αυτοματοποιημένη διαδικασία η οποία βασίζεται σε σχήμα βελτιστοποίησης ακεραίων και γενετικούς αλγορίθμους [Poulimenos and Fassois, 2003a].

Προφανώς, πέρα από την μέθοδο επιλογής της δομής του μοντέλου, η επιλογή της οικογένειας των συναρτήσεων βάσης για την προβολή των χρονικά μεταβαλλόμενων παραμέτρων ενός συναρτησιακού μοντέλου είναι επίσης κρίσιμης σημασίας. Οι βάσεις που έχουν προταθεί στην βιβλιογραφία περιλαμβάνουν πολυωνυμικές συναρτήσεις βάσης όπως Chebyshev [Fouskitakis and Fassois, 2002] και Legendre [Kozin, 1977, Grenier, 1983b], τριγωνομετρικές συναρτήσεις βάσης [Petsounis and Fassois, 2000, Poulimenos and Fassois, 2009a], διάφορες οικογένειες κυματιδίων [Tsatsanis and Giannakis, 1993, Li et al., 2011] και άλλες. Πρόσφατα, έχουν επίσης προταθεί μέθοδοι για την ταυτόχρονη χρήση δύο ή περισσότερων οικογενειών συναρτήσεων βάσης οι οποίες στοχεύουν στον συνδυασμό των ετερόκλητων χαρακτηριστικών τους σε περιπτώσεις με μεταβολές των χρονικά μεταβαλλόμενων παραμέτρων που περιλαμβάνουν συνδυασμό ομαλών και απότομων μεταβολών κατά την διάρκεια του πειράματος [Chon et al., 2005, Li et al., 2011]. Ωστόσο, το κοινό χαρακτηριστικό όλων των προαναφερθέντων μελετών είναι ότι οι συναρτησιακοί υποχώροι τους οποίους θεωρούν, όπως κι αν αυτοί επιλέγονται, αποτελούνται πάντα από συναρτήσεις βάσης *προκαθορισμένης μορφής*, επιλεγμένων από ένα επίσης προκαθορισμένο σύνολο συναρτήσεων. Συνεπώς, η ακρίβεια της περιγραφής των δεδομένων είναι συνάρτηση της επιλεγμένης οικογένειας συναρτήσεων βάσης.

Τέλος, όπως ήδη αναφέρθηκε ένας από τους σημαντικότερους τομείς στους οποίους βρίσκουν πρακτική εφαρμογή τα παραμετρικά μοντέλα κατασκευών είναι η διάγνωση βλαβών, η οποία είναι κρίσιμης σημασίας για λόγους που σχετίζονται τόσο με την ασφάλεια λειτουργίας όσο και το κόστος συντήρησης των κατασκευών. Τα τελευταία χρόνια μάλιστα ιδιαίτερη έμφαση έχει δοθεί στην ανάπτυξη μεθόδων που βασίζονται σε μοντέλα τα οποία έχουν αναγνωρισθεί επί τη βάση σημάτων ταλάντωσης. Ωστόσο, η ραγδαία εξέλιξη τέτοιων μεθόδων για την διάγνωση βλαβών σε στάσιμες κατασκευές δεν έχει ακολουθηθεί από αντίστοιχη εξέλιξη στην περίπτωση των εγγενώς μη-στάσιμων κατασκευών. Έως σήμερα μόνο ένας μικρός αριθμός εργασιών έχει παρουσιασθεί στην διεθνή βιβλιογραφία επί του θέματος. Για παράδειγμα ένα στατιστικό πλαίσιο λήψης αποφάσεων το οποίο χρησιμοποιεί την ακολουθία των υπολοίπων ενός χρονικά μεταβαλλόμενου συναρτησιακού μοντέλου αυτοπαλινδρόμησης με εξωγενή διέγερση FS-TARX έχει εφαρμοσθεί για την διάγνωση βλάβης στην εργαστηριακή προαναφερθείσα κατασκευή που προσομοιάζει την αλληλεπίδραση γέφυρας με βαρύ κινούμενο όχημα επ' αυτής [Poulimenos and Fassois, 2004b]. Επίσης, για την αποτίμηση της επίδρασης βλάβης στα μορφικά χαρακτηριστικά ενός ενισχυμένου πλαισίου σκυροδέματος έχει εφαρμοστεί μοντελοποίηση FS-TARX σε δεδομένα ταλάντωσης από τον Huang και τους συνεργάτες του [Huang et al., 2009]. Εντούτοις, το κύριο μειονέκτημα των εργασιών που έχουν παρουσιασθεί έως σήμερα είναι ότι χρησιμοποιούν μοντέλα εισόδου-εξόδου, και έτσι απαιτούν πρόσβαση στην διέγερση της κατασκευής για την εφαρμογή τους. Τέτοια πληροφορία όμως, συνήθως δεν είναι διαθέσιμη σε πρακτικές εφαρμογές.

Λαμβάνοντας υπόψη τα παραπάνω, ως βασικός στόχος της παρούσας διατριβής ορίζεται η ανάπτυξη εξελιγμένων μεθόδων μοντελοποίησης FS-TARMA οι οποίες θα προσφέρουν σημαντικές βελτιώσεις στις υπάρχουσες προσεγγίσεις και θα βοηθήσουν στην αντιμετώπιση πρακτικών προβλημάτων που σχετίζονται τόσο με την αναγνώριση των δυναμικών χαρακτηριστικών όσο και την διάγνωση βλαβών σε μη-στάσιμες κατασκευές. Πιο συγκεκριμένα, η διατριβή αυτή επικεντρώνεται στο πρόβλημα της βέλτιστης εκτίμησης των συναρτησιακών υποχώρων FS-TARMA μοντέλων, την μη-στάσιμη αναγνώριση κατασκευών επί τη βάση πολυμεταβλητών μετρήσεων ταλαντωτικής απόκρισης καθώς και την ανάπτυξη μια στατιστικής μεθόδου για την αποτελεσματική λύση του προβλήματος της διάγνωσης βλαβών σε εγγενώς μη-στάσιμες κατασκευές.

Συνοψίζοντας, οι συγκεκριμένοι στόχοι της παρούσας διατριβής μπορούν να περιγραφούν ως ακολούθως:

- *(i).* Πειραματική αποτίμηση και σύγκριση των κυριοτέρων μεθόδων στοχαστικής μοντελοποίησης μη-στάσιμων σημάτων ταλάντωσης μέσω της εφαρμογής τους για την αναγνώριση μιας προτύπου εργαστηριακής κατασκευής. Περιγραφή των κυριοτέρων χαρακτηριστικών των μεθόδων και της εφαρμοσιμότητας τους, καθώς και διερεύνηση των πλεονεκτημάτων και μειονεκτημάτων τους.
- *(ii).* Η ανάπτυξη μιας διανυσματικής (πολυμεταβλητής) μεθόδου εκτίμησης μοντέλων FS-TARMA για την αναγνώριση των δυναμικών χαρακτηριστικών κατασκευών μέσα από διανυσματικά σήματα ταλαντωτικής απόκρισης. Ανάπτυξη αποδοτικών εργαλείων τόσο για το πρόβλημα εκτίμησης των παραμέτρων όσο και της επιλογής της δομής του μοντέλου. Αποτίμηση της μεθόδου μέσω εφαρμογής της για την αναγνώριση χρονικά μεταβαλλόμενης εργαστηριακής κατασκευής που προσομοιάζει κατασκευή γέφυρας με κινούμενο όχημα επ' αυτής.
- *(iii).* Η εισαγωγή μιας καινοτόμου τάξης προσαρμόσιμων AFS-TARMA μοντέλων και η ανάπτυξη κατάλληλης μεθόδου για την αποτελεσματική εκτίμηση τους. Τα μοντέλα AFS-TARMA είναι προσαρμόσιμα υπό την έννοια ότι δεν βασίζονται συναρτήσεις βάσης προκαθορισμένης μορφής, αλλά αντιθέτως, χρησιμοποιούν συναρτήσεις βάσης με εκ των προτέρων άγνωστες ιδιότητες και οι οποίες μπορούν να προσαρμοστούν στα χαρακτηριστικά συγκεκριμένου στοχαστικού σήματος. Διερεύνηση της αποτελεσματικότητας της μεθόδου μέσω της εφαρμογής της σε αριθμητικές και πειραματικές μελέτες και συγκρίσεις με υπάρχουσες μη-στάσιμες μεθόδους αναγνώρισης σημάτων.
- *(iv).* Η παρουσίαση – για πρώτη φορά – μιας διεξοδικής επισκόπησης των μοντέλων FS-TARMA η οποία καλύπτει τόσο θεωρητικά όσο και πρακτικά ζητήματα των προβλημάτων της εκτίμησης των παραμέτρων και της επιλογής της δομής των μοντέλων FS-TARMA. Προβολή υποσχόμενων νέων μεθόδων οι οποίες ευελπιστούν να ξεπεράσουν προβλήματα προηγούμενων προσεγγίσεων. Διεξοδική σύγκριση και αποτίμηση των θεωρημένων μεθόδων επί τη βάση Monte Carlo πειραμάτων και σύγκριση με εναλλακτικές μη-στάσιμες μεθόδους.
- *(v).* Η εισαγωγή μιας στατιστικής μεθόδου για την διάγνωση βλαβών σε εγγενώς μη-στάσιμες κατασκευές η οποία χρησιμοποιεί, για πρώτη φορά σε πρακτική εφαρμογή, τις ασυμπτωτικές ιδιότητες μιας πρόσφατα εισηγμένης εκτιμήτριας FS-TAR πολλαπλών σταδίων [Poulimenos and Fassois, 2007]. Εφαρμογή, της μεθόδου για την διάγνωση βλαβών σε έναν χρονικά μεταβαλλόμενο μηχανισμό δύο βαθμών ελευθερίας ο οποίος αποτελείται από ισάριθμους ηλεκτρομαγνητικούς γραμμικούς κινητήρες. Αποτίμηση της αποτελεσματικότητας της μεθόδου σε όρους ικανότητας επιτυχούς διάγνωσης για τα διάφορα σενάρια βλάβης που θεωρούνται.

Πιο συγκεκριμένα, στο Κεφάλαιο 2 και μετά την εισαγωγή αυτής της διατριβής, παρουσιάζεται μια πειραματική μελέτη για την αποτίμηση και σύγκριση των κυριοτέρων μη-στάσιμων παραμετρικών μεθόδων για την αναγνώριση κατασκευών μέσω σημάτων ταλάντωσης. Οι μέθοδοι που εξετάζονται ταξινομούνται σύμφωνα με την δομή την οποία επιβάλλουν στην εξέλιξη των χρονικά μεταβαλλόμενων παραμέτρων ως μέθοδοι αδόμητης, στοχαστικής και καθοριστικής εξέλιξης των παραμέτρων. Μια αντιπροσωπευτική μέθοδος από κάθε τάξη μεθόδων παρουσιάζεται συνοπτικά, ενώ τα κύρια χαρακτηριστικά τους εξετάζονται μέσω της εφαρμογής τους στο πρόβλημα της δυναμικής αναγνώρισης και ανάλυσης προτύπου εργαστηριακής κατασκευής η οποία προσομοιάζει κατασκευή γέφυρας με βαρύ κινούμενο όχημα επ' αυτής. Τα αποτελέσματα της μελέτης επιδεικνύουν την ικανότητα των παραμετρικών μοντέλων να παρέχουν ακριβείς και «οικονομικές» αναπαραστάσεις χρονικά μεταβαλλόμενων κατασκευών, ενώ σε όρους ακρίβειας ανίχνευσης των χρονικά μεταβαλλόμενων δυναμικών χαρακτηριστικών της κατασκευής, η μέθοδος μοντελοποίησης FS-TARMA επιτυγχάνει την συνολικά καλύτερη επίδοση μεταξύ των μεθόδων που χρησιμοποιούνται.

Το πρόβλημα της παραμετρικής αναγνώρισης χρονικά μεταβαλλόμενων κατασκευών επί τη βάση πολυμεταβλητών σημάτων ταλαντωτικής απόκρισης αντιμετωπίζεται στο Κεφάλαιο 3 της παρούσας διατριβής. Για το σκοπό αυτό, εισάγεται μια διανυσματική μέθοδος συναρτησιακών μοντέλων FS-TARMA η οποία χρησιμοποιείται για την αναγνώριση της προαναφερθείσας προτύπου εργαστηριακής κατασκευής που προσομοιάζει γέφυρα με βαρύ κινούμενο όχημα. Η αναγνώριση βασίζεται σε τρία ταυτόχρονα μετρούμενα ταλαντωτικά σήματα απόκρισης τα οποία λαμβάνονται κατά την διάρκεια ενός μη-στάσιμου πειράματος. Η αποτελεσματικότητα της μεθόδου κρίνεται σε σύγκριση με ένα μοντέλο το οποίο εκτιμάται επί τη βάση πολλαπλών στάσιμων πειραμάτων με την κατασκευή να βρίσκεται σε «παγωμένη διάταξη» και αποδεικνύεται πως είναι κατάλληλη για την επακριβή ανίχνευση των δυναμικών χαρακτηριστικών της κατασκευής. Συγκρίσεις με επαναληπτικές μεθόδους και μεθόδους που βασίζονται σε μοντέλα χώρου κατάστασης επιδεικνύουν την υπεροχή των διανυσματικών μοντέλων FS-TARMA τόσο ως προς την επιτυγχανόμενη ακρίβεια όσο και ως προς την οικονομία της παραμετροποίησης.

Στο τέταρτο κεφάλαιο, προτείνεται μια νέα τάξη προσαρμόσιμων μοντέλων AFS-TARMA τα οποία χρησιμοποιούν προσαρμόσιμους συναρτησιακούς υποχώρους με αρχικά άγνωστα χαρακτηριστικά για την προβολή των χρονικά μεταβαλλόμενων παραμέτρων τους. Αυτό επιτυγχάνεται μέσω κατάλληλων παραμετροποιήσεων των συναρτήσεων βάσης και τον ορισμό ενός προβλήματος διαχωριζόμενων μη-γραμμικών ελαχίστων τετραγώνων (Separable Nonlinear Least Squares (SNLS)), το οποίο αντιμετωπίζεται μέσω υβριδικού σχήματος βελτιστοποίησης. Η αποτελεσματικότητα των μοντέλων αποτιμάται μέσω προσομοιώσεων και πειραματικής μελέτης. Πιο συγκεκριμένα, οι αριθμητικές μελέτες αφορούν Monte Carlo πειράματα για την αναγνώριση προσομοιωμένων μοντέλων που χαρακτηρίζονται από απότομη εξέλιξη των χρονικά μεταβαλλόμενων παραμέτρων τους, ενώ η εισηγμένη μέθοδος εφαρμόζεται επίσης για το πρόβλημα της αναγνώρισης των χρονικά μεταβαλλόμενων δυναμικών χαρακτηριστικών ενός μηχανισμού δυο βαθμών ελευθερίας. Τέλος, παρουσιάζονται συγκρίσεις με την κλασσική μέθοδο FS-TARMA η οποία βασίζεται σε προκαθορισμένες συναρτησιακές βάσεις καθώς και με εναλλακτικές μη-στάσιμες μεθόδους. Τα αποτελέσματα φανερώνουν την εξαιρετική απόδοση και ακρίβεια που επιτυγχάνεται μέσω των νέων μοντέλων AFS-TARMA με προσαρμόσιμες συναρτήσεις βάσης.

Μια εκτενής παρουσίαση της βιβλιογραφίας και ενδελεχής επισκόπηση των μεθόδων για την αναγνώριση και ανάλυση μη-στάσιμων σημάτων μέσω μοντέλων FS-TARMA παρουσιάζεται στο Κεφάλαιο 5. Στόχος αυτού του κεφαλαίου είναι να παρέχει μια κριτική θεώρηση των διαφόρων μεθόδων που έχουν προταθεί έως σήμερα για την επίλυση των προβλημάτων της εκτίμησης των παραμέτρων και της επιλογής της δομής των μοντέλων FS-TARMA. Οι μέθοδοι εκτίμησης που εξετάζονται συμπεριλαμβάνουν μεθόδους παλινδρόμησης που βασίζονται στην ελαχιστοποίηση κριτηρίων πρόβλεψης, επαναληπτικές μεθόδους, μεθόδους πολλαπλών σταδίων και την μέθοδο μέγιστης πιθανοφάνειας. Αντίστοιχα για το πρόβλημα της επιλογής της δομής των μοντέλων, εξετάζονται διάφορα σχήματα που βασίζονται στις έννοιες της πρόσω και οπισθοδρομικής παλινδρόμησης άλλα και σε σχήματα βελτιστοποίησης ακεραίων. Στην εργασία αυτή εξετάζονται τόσο θεωρητικά όσο και πρακτικά ζητήματα ενώ ιδιαίτερη έμφαση δίνεται σε υποσχόμενες νέες μεθόδους που προσπαθούν να ξεπεράσουν προβλήματα προηγούμενων προσεγγίσεων. Η αποτελεσματικότητα των κυριότερων μεθόδων αποτιμάται μέσω πειραμάτων Monte Carlo για την αναγνώριση προσομοιωμένων μοντέλων και συγκρίσεις με εναλλακτικές μη-στάσιμες μεθόδους αναγνώρισης. Τα αποτελέσματα του κεφαλαίου επιβεβαιώνουν την γενικότερη αποτελεσματικότητα των μοντέλων FS-TARMA αλλά και τα πλεονεκτήματα που προσφέρουν πρόσφατα ανεπτυγμένες μέθοδοι.

Τέλος, στο Κεφάλαιο 6 εξετάζεται το πρόβλημα της διάγνωσης βλαβών επί τη βάση σημάτων ταλάντωσης σε μη-στάσιμες κατασκευές. Η μέθοδος που προτείνεται βασίζεται σε μοντέλα FS-TAR τα οποία συνδυάζονται με κατάλληλο στατιστικό πλαίσιο λήψης αποφάσεων. Η απόδοση της μεθόδου εξετάζεται πειραματικά μέσω της εφαρμογής της στο πρόβλημα της διάγνωση βλαβών σε χρονικά μεταβαλλόμενο μηχανισμό δυο βαθμών ελευθερίας. Ο μηχανισμός αποτελείται από δυο ηλεκτρομαγνητικούς γραμμικούς κινητήρες οι οποίοι ακολουθούν προκαθορισμένα προφίλ κίνησης ενώ ο μηχανισμός υπόκειται σε τυχαία ακολουθία διέγερσης. Τέτοιοι μηχανισμοί απαντώνται σε πλήθος βιομηχανικών εφαρμογών και η θεώρηση τους κατά την διάρκεια της λειτουργίας τους μέσω αυτοματοποιημένου πλαισίου λήψης αποφάσεως είναι κρίσιμης σημασίας. Οι βλάβες που εξετάζονται είναι διαφόρων τύπων και λαμβάνουν χώρα σε διάφορα σημεία του μηχανισμού, ενώ η διάγνωση τους βασίζεται αποκλειστικά σε σήμα της ταλαντωτικής απόκρισης του μηχανισμού το οποίο καταγράφεται κατά την διάρκεια ενός κύκλου λειτουργίας του. Η μέθοδος επιτυγχάνει εξαιρετικά αποτελέσματα όσο αφορά την διάγνωση των βλαβών για όλα τα σενάρια βλάβης που εξετάζονται.

Contents

Important Conventions and Symbols

- Bold-face upper/lower case symbols designate matrix/column-vector quantities, respectively.
- Matrix transposition is indicated by the superscript T.
- A functional argument in parentheses designates function of a real variable; for instance $x(t)$ is a function of analog time $t \in \Re$.
- A functional argument in brackets designates function of an integer variable; for instance $x[t]$ is a function of normalized discrete time ($t = 1, 2, \ldots$). The conversion from discrete normalized time to analog time is based on $(t-1)T_s$, with T_s standing for the sampling period. A time instant used as superscript to a function indicates the set of values of the function up to that time instant; for instance $x^t \triangleq \{x[i], i = 1, 2, \ldots, t\}$.
- A hat designates estimator/estimate of the indicated quantity; for instance $\hat{\boldsymbol{\theta}}$ is an estimator/estimate of $\boldsymbol{\theta}$.
- $\mathcal{B}$ stands for the backshift operator defined such that $\mathcal{B}^i \cdot \boldsymbol{x}[t] \triangleq \boldsymbol{x}[t-i]$.
- For simplicity of notation, no distinction is made between a random variable and its value(s).

Acronyms

2SLS	: Two Stage Least Squares (method)
2SSNLS	: Two Stage Separable Nonlinear Least Squares (method)
AFS-TAR	: Adaptable FS-TAR (model)
AFS-TARMA	: Adaptable FS-TARMA (model)
AIC	: Akaike Information Criterion
AR	: AutoRegressive
BIC	: Bayesian Information Criterion
CVA	: Canonical Variate Analysis (algorithm)
DPE	: Deterministic Parameter Evolution (method)
FS-TAR	: Functional Series TAR (model)
FS-TARMA	: Functional Series TARMA (model)
FS-VTAR	: Functional Series VTAR (model)
FS-VTARMA	: Functional Series VTARMA (model)
GA	: Genetic Algorithm
ISD	: Instantaneous Standard Deviation (method)
IV	: Instantaneous Variance (method)
MA	: Moving Average
ML	: Maximum Likelihood (method)
MS	: Multi-Stage (method)
MW	: Moving Window (method)
NID	: Normally Independently Distributed
OLS	: Ordinary Least Squares (method)
PE	: Prediction Error
PLR	: Pseudo-Linear Regression (method)
PLR-VTARMA	: PLR-estimated VTARMA (model)
PSO	: Particle Swarm Optimization
RELS	: Recursive Extended Least Squares (method)
RLS	: Recursive Least Squares (method)

RMS	:	Relaxed Multi Stage (method)
RSS	:	Residual Sum of Squares
SNLS	:	Separable Nonlinear Least Squares (method)
SP-TARMA	:	Smoothness Priors TARMA (model)
SPWV	:	Smoothed Pseudo Wigner Ville (method)
STFT	:	Short-Time Fourier Transform (method)
SPE	:	Stochastic Parameter Evolution (method)
SSI	:	Stochastic Subspace Identification
ST-SSI	:	Short Time SSI (method)
TAR	:	Time-dependent AR (model)
TARMA	:	Time-dependent ARMA (model)
TV	:	Time-Varying
UPE	:	Unstructured Parameter Evolution (method)
VP	:	Variable Projection (algorithm)
VTAR	:	Vector Time-dependent AR (model)
VTARMA	:	Vector Time-dependent ARMA (model)
WLS	:	Weighted Least Squares

Chapter 1

Introduction

1.1 The General Problem

The general problem that the present thesis deals with is the non-stationary vibration *modelling* (identification) and *analysis* based upon *equispaced* in time *digital* sampled vibration signal measurements of finite length obtained from a single realization. The problem of modelling based upon signal measurements is in general referred to as an *identification problem* (for instance see [Ljung, 1999, Soderstrom and Stoica, 1989]) and – in a broader sense – is a type of *inverse problem*.

Non-stationary signals, that is signals with statistical properties that depend on time, are commonly encountered in engineering practice. The vibration responses of structures, such as traffic-excited bridges [Poulimenos and Fassois, 2009b], robotic devices [Petsounis and Fassois, 2000], rotating machinery [Conforto and D'Alessio, 1999b], deployable structures [Xun and Yan, 2008] and so on, constitute typical examples of non-stationary signals (Fig. 1.1). Such structures characterized by properties, either physical or geometrical, that vary with time are referred as Time-Varying (TV) structures. However, non-stationary vibration may also arise in cases of time-invariant structures subject to non-stationary excitation, such as earthquake [Fouskitakis and Fassois, 2002] and turbulence [Mevel et al., 2005], or in the case of structures with inherently nonlinear dynamics [Ben Mrad, 2002].

The final goal of the identification process is to build a mathematical model that will be able to represent the underlying structural dynamics and is, in general, of the form of an appropriate stochastic difference equation. It is tacitly assumed that the measured signal actually obeys a similar (but unknown) mathematical expression, which reflects the underlying structural dynamics and is subsequently referred to as the *actual* or *true* model or representation. The obtained model may subsequently be employed for the non-stationary signal vibration analysis through the extraction of physically meaningful information from the obtained model such as signal moments or more often a form of time-dependent power spectral density function and the time-dependent vibration modes [Petsounis and Fassois, 2000, Poulimenos and Fassois, 2006, Hammond and White, 1996] [Preumont, 1994, ch. 8]. In addition to *analysis*, an obtained model may be also used for purposes of *prediction* [Ben Mrad et al., 1998b], *fault diagnosis* [Poulimenos and Fassois, 2004b], *classification* [Staszewski et al., 1997] and *control* [Niedźwiecki, 1987, Xianya and Evans, 1984].

1.1.1 Non-stationary vibration modelling methods

The modelling of non-stationary vibration is an important and yet challenging problem which has received significant attention in recent years [Poulimenos and Fassois, 2006, Niedźwiecki, 2000, Staszewski and Robertson, 2007, Cohen, 1995, Hammond and White, 1996]. The available non-stationary identification

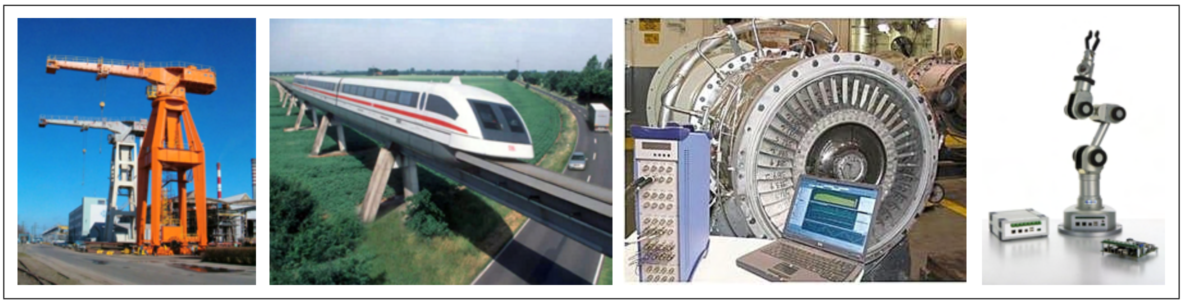

Figure 1.1: Typical examples of time-varying structures.

methods may be broadly classified as *non-parametric* or *parametric*. To date, non-parametric methods have received most of the attention, mainly due to their simplicity. They are based on non-parametrized representations of the vibration signal as a simultaneous function of time and frequency (time-frequency distributions). These methods include the widely used spectrogram based on the Short-Time Fourier Transform (STFT) and its ramifications [Hammond and White, 1996], Priestley's evolutionary spectrum [Priestley, 1988], distributions such as the Wigner-Ville and the Choi-Williams that are unified under the Cohen class of distributions [Cohen, 1995, Hammond and White, 1996], wavelet-based methods [Newland, 1993, Spanos and Failla, 2005] and others.

On the other hand, *parametric methods* are based on parametrized time-dependent representations, mainly of the Time-dependent AutoRegressive Moving Average (TARMA) type or respective Time-dependent State-Space (TSS) types. These representations differ from their conventional, stationary, counterparts in that their parameters are *time-dependent* (for instance see [Poulimenos and Fassois, 2006, Niedźwiecki, 2000]). Thus, a TARMA(n_a, n_c) model, with n_a, n_c designating its AR and MA orders is of the general form:

$$x[t] + \underbrace{\sum_{i=1}^{n_a} a_i[t] \cdot x[t-i]}_{\text{AR part}} = e[t] + \underbrace{\sum_{i=1}^{n_c} c_i[t] \cdot e[t-i]}_{\text{MA part}}, \qquad e[t] \sim \text{NID}(0, \sigma_e^2[t]) \tag{1.1}$$

with t designating normalized discrete time, $x[t]$ the non-stationary vibration signal modelled, $e[t]$ an unobservable uncorrelated (white) innovations (residual) sequence with zero mean and potentially time-dependent variance $\sigma_e^2[t]$, and $a_i[t], c_i[t]$ the model's time-dependent AR and MA parameters, respectively. NID$(\cdot,\cdot)$ stands for Normally Independently Distributed with the indicated mean and variance. Analogously a TSS(n) model of order n is of the general form:

$$\text{State equation}: \boldsymbol{z}[t+1] = \boldsymbol{A}[t] \cdot \boldsymbol{z}[t] + \boldsymbol{K}[t] \cdot e[t] \tag{1.2a}$$

$$\text{Output equation}: x[t] = \boldsymbol{C}[t] \cdot \boldsymbol{z}[t] + e[t], \quad e[t] \sim \text{NID}(0, \sigma_e^2[t]) \tag{1.2b}$$

where $\boldsymbol{z}[t]_{(n\times 1)}$ indicates the model's state vector and $\boldsymbol{A}[t]_{(n\times n)}$, $\boldsymbol{K}[t]_{(n\times 1)}$, $\boldsymbol{C}[t]_{(1\times n)}$ the state-space system, Kalman gain and output matrices, respectively.

In general, contrasted to their non-parametric counterparts, non-stationary methods based on parametrized representations are known to offer a number of potential advantages such as (for instance see [Poulimenos and Fassois, 2006, Petsounis and Fassois, 2000, Conforto and D'Alessio, 1999b, Ben Mrad et al., 1998b, Fouskitakis and Fassois, 2002, Poulimenos and Fassois, 2009a, Zhan and Jardine, 2005a]): (i) Representation parsimony, as models may be potentially specified by a limited number of parameters; (ii) improved accuracy; (iii) improved resolution; (iv) improved tracking of the time-varying dynamics; (v) flexibility in analysis, as parametric methods are capable of "directly" capturing the underlying structural dynamics responsible for the non-stationary behavior; (vi) flexibility in synthesis (simulation) and prediction, as they are more suitable for both purposes; (vii) flexibility in fault diagnosis, as they allow for the use of the broad class of parametric diagnosis techniques; and, (viii) flexibility in control, for which they are also particularly suitable.

1.2 The Focus of the Present Thesis

The focus of the present thesis is on the non-stationary random vibration modelling and analysis based on parametric Functional Series TARMA (FS-TARMA) models.

FS-TARMA models are based on the assumption that their parameters follow a deterministic pattern and thus they may be expanded on properly selected functional subspaces. According to the *classical* approach these functional subspaces are considered to be selected from an ordered set of linearly independent basis functions of a particular family (such as polynomial, trigonometric, wavelets or other). Using this approach, a *classical parametric FS-TARMA*$(n_a, n_c)_{[p_a,p_c,p_s]}$ *model*, with n_a, n_c designating its AR and MA orders, respectively, and p_a, p_c, p_s its AR, MA, and innovations variance functional subspace dimensionalities, is defined as follows [Poulimenos and Fassois, 2006]:

$$x[t] + \sum_{i=1}^{n_a} a_i[t] \cdot x[t-i] = e[t] + \sum_{i=1}^{n_c} c_i[t] \cdot e[t-i], \qquad e[t] \sim \text{NID}(0, \sigma_e^2[t]) \tag{1.3a}$$

$$\begin{gathered}\mathcal{F}_{\text{AR}} = \left\{G_{d_a(1)}[t], \ldots, G_{d_a(p_a)}[t]\right\}, \quad \mathcal{F}_{\text{MA}} = \left\{G_{d_c(1)}[t], \ldots, G_{d_c(p_c)}[t]\right\}, \\ \mathcal{F}_{\sigma_e^2[t]} = \left\{G_{d_s(1)}[t], \ldots, G_{d_s(p_s)}[t]\right\}\end{gathered} \tag{1.3b}$$

$$a_i[t] = \sum_{j=1}^{p_a} a_{i,j} \cdot G_{d_a(j)}[t], \quad c_i[t] = \sum_{j=1}^{p_c} c_{i,j} \cdot G_{d_c(j)}[t], \quad \sigma_e^2[t] = \sum_{j=1}^{p_s} s_j \cdot G_{d_s(j)}[t] \tag{1.3c}$$

with "$\mathcal{F}$" designating functional subspace of the indicated quantity, $d_a(i)$ $(i = 1, \ldots, p_a)$, $d_c(i)$ $(i = 1, \ldots, p_c)$ and $d_s(i)$ $(i = 1, \ldots, p_s)$ the indices of the specific basis functions that are included in each subspace, while $a_{i,j}$, $c_{i,j}$, and s_j stand for the AR, MA, and innovations variance, respectively, *coefficients of projection*. Thus, in this classical approach the complete model parameter vector $\boldsymbol{\theta}$ consists of these coefficients of projection, while considering a specific basis function family the FS-TARMA model structure selection procedure concerns the determination of the AR and MA orders n_a, n_c, and the AR, MA and innovations variance basis functions indices vectors $\boldsymbol{d}_a = [d_{a(1)}, \ldots, d_{a(p_a)}]^T$, $\boldsymbol{d}_c = [d_{c(1)}, \ldots, d_{c(p_c)}]^T$, and $\boldsymbol{d}_s = [d_{s(1)}, \ldots, d_{s(p_s)}]^T$, that is:

$$\boldsymbol{\theta} = [\boldsymbol{\vartheta}_a^T \; \boldsymbol{\vartheta}_c^T \; \boldsymbol{\vartheta}_s^T]^T = [a_{1,1}, \ldots, a_{n_a,p_a} \; c_{1,1}, \ldots, c_{n_c,p_c} \; s_1, \ldots, s_{p_s}]^T \tag{1.3d}$$

$$\mathcal{M} = \{n_a, n_c, \boldsymbol{d}_a, \boldsymbol{d}_c, \boldsymbol{d}_s\} \tag{1.3e}$$

Thus, the basic features of FS-TAR/TARMA models may be summarized as follows:

- They are lumped parameter stochastic models. Stochastic as they include random variables, which reflect the factors of uncertainty that exist in the vibration signal and make the accurate prediction of the model's response impossible, and of lumped parameters as they are described by a finite number of difference equations.
- They are discrete time domain models as they represent the vibration signal in discrete time instants (for instance $t = 1, 2, \ldots, N$), through a relatively small number of parameters.
- They are output-only linear models, that is they represent vibration signals through linear relationships that include past values of response-only signals and random variables.

The *complete FS-TARMA identification problem* may be stated as follows:

"Given N observations of the vibration response, say $x^N = \{x[1] \ldots x[N]\}$ and the FS-TARMA model set:

$$\mathbb{M} \triangleq \left\{ \mathcal{M}(\boldsymbol{\theta}) : \; x[t] + \sum_{i=1}^{n_a} a_i[t,\boldsymbol{\theta}] \cdot x[t-i] = e[t,\boldsymbol{\theta}] + \sum_{i=1}^{n_c} c_i[t,\boldsymbol{\theta}] \cdot e[t-i,\boldsymbol{\theta}]; \right.$$
$$\left. \sigma_e^2[t] = E\left\{e^2[t,\boldsymbol{\theta}]\right\}, \qquad t = 1, \ldots N, \qquad \boldsymbol{\theta} \in \mathfrak{R}^{\dim(\boldsymbol{\theta})} \right\}, \tag{1.4}$$

select an element of $\mathbb{M}$ that best fits the observations".

In this expression $e[t,\boldsymbol{\theta}]$ stands for the model's one-step-ahead prediction error (residual) sequence, which, as in the stationary case, coincides with the model's innovations sequence $e[t]$ [Poulimenos and Fassois, 2006]. The identification may be thus viewed as the problem of determining the model that best "fits" the vibration response observations x^N. Model "fitness" may be judged in terms of various criteria, like the likelihood function or prediction error criteria [Fassois, 2001a]. Both the model structure $\mathcal{M}$ and model parameter vector $\boldsymbol{\theta}$ consisting of the projection coefficients $a_{i,j}, c_{i,j}, s_j$ have to be estimated from the available vibration response.

FS-TARMA models belong to the class of Deterministic Parameter Evolution (DPE) methods as they impose deterministic "structure" upon the evolution of their time-varying parameters. Thus, they may be considered particularly effective for the identification of time-varying engineering structures, which are usually characterized by a deterministic physical mechanism responsible for their variability. Furthermore, FS-TARMA methods are particularly attractive over alternative parametric methods belonging to the classes of Unstructured Parameter Evolution (UPE) or Stochastic Parameter Evolution (SPE) methods, as they [Poulimenos and Fassois, 2006, Conforto and D'Alessio, 1999b, Ben Mrad et al., 1998b, Petsounis and Fassois, 2000, Fouskitakis and Fassois, 2001, Niedźwiecki, 2000]: (a) Impose maximum "structure" on parameter evolution, achieving a high degree of parsimony, (b) are capable of tracking "fast" and "abrupt" variations via proper functional bases and, (c) achieve high modelling accuracy and resolution.

Indeed, UPE methods fail to model the transient phenomena of non-stationary vibration and are suitable only for describing "slow" evolutions in the signal characteristics, involve a trade-off between tracking ability and achievable accuracy, and do not lead to parsimonious representations. SPE methods, on the other hand, offer improved parsimony, but are most suitable for describing random evolutions in the signal's characteristics. Yet, the advantages of FS-TARMA models over alternative non-stationary models (such as segmentation, adaptive, or smoothness priors models), have also been demonstrated via a Monte Carlo comparison study in [Poulimenos and Fassois, 2006]

Despite the long history of FS-TARMA models in non-stationary identification and their successful application in a number of studies, FS-TARMA modelling still remains challenging, mainly due to model structure estimation, including the selection of suitable subspace basis functions. Moreover, practical issues such as the FS-TARMA modelling based on vector random vibration signal measurements, and the development of statistical time series method for the effective solution of the Fault Detection and Identification (FDI) problems in inherently non-stationary structures have hardly been considered.

1.3 Current State-of-the-Art

FS-TARMA models have played an important role in the development and evolution of non-stationary random signal identification and analysis over the last forty years. They were introduced in 1970 by Rao [Rao, 1970] who proposed the truncated Taylor series expansion of a TAR model parameters – this is equivalent to assuming time-dependent parameters that can be described as polynomials of time. Three years later, Mendel [Mendel, 1973] classified the available non-stationary identification methods into the aforementioned three classes (UPE, SPE and DPE) and defined a general FS linear regression model as appropriate for the case in which a set of time-invariant or slowly TV parameters may be distinguished from the rest of the parameters which evolve rapidly with time.

Functional Series models of the pure TAR form with parameters belonging to a subspace spanned by Legendre polynomials were used for first time within the context of random vibration, and more specifically earthquake ground motion, modelling and simulation in an early paper by Kozin in 1977 [Kozin, 1977]. Nevertheless, FS models did not enjoy widespread popularity before the early 1980's, when a number of researchers start studying their properties and examining their potential for accurate non-stationary signal modelling [Grenier, 1983b, Hall et al., 1983, Clergeot, 1984, Charbonnier et al., 1987, Niedźwiecki, 1988].

Since then, FS-TAR/TARMA models have been used in various structural dynamics related applications, such as the modelling and simulation of earthquake ground motion [Fouskitakis and Fassois, 2002], vibration analysis in rotating machinery [Bardou and Sidahmed, 1994, Conforto and D'Alessio, 1999b, Zhang et al., 2010a], the modelling and prediction of power consumption in an automobile active suspension [Ben Mrad et al., 1998b], the modelling and analysis of simulated robot vibration [Petsounis and Fassois, 2000], and the modelling and vibration analysis of a bridge with heavy vehicle type laboratory structure [Poulimenos and Fassois, 2009b]. However, the majority of FS-TARMA studies are limited to the simple *single* vibration response signal (univariate) case. Although the *multiple* vibration response (vector or multivariate) case is much more important from a practical standpoint, it has thus far received limited attention. Yet, vector identification can lead to much more complete descriptions, reduced data acquisition and processing times, improved data set "consistency", and also improved modal parameter accuracy [Fassois, 2001b]. Even if the subclass of Functional Series Vector Time-dependent Autoregressive (FS-VTAR) models has been used in a broader context by Gersch and Kitagawa [Gersch and Kitagawa, 1982] and Sato *et al.* [Sato et al., 2007] for the modelling and analysis of econometric and biomedical time series, respectively, full FS-VTARMA models have not been previously considered.

Regarding the FS-TARMA model structure selection problem, although the significance of the proper functional subspace selection was underlined in many publications within the first twenty years of FS-TARMA models history, it was only in 1993 when Tsatsanis and Giannakis presented a complete model structure selection scheme based on the concept of backward regression [Tsatsanis and Giannakis, 1993]. However, a more systematic examination of the subject has take place over the last decade. For instance, a simplified scheme based on the backward regression concept was proposed in [Poulimenos and Fassois, 2003b] which decomposes the structure selection problem into two subproblems treated in equal phases: i) the model orders (n_a, n_c) selection, and (ii) the functional subspaces selection. The goal of this scheme is to reduce the computational time that is required for the exhaustive search that is done by Tsatsanis and Giannakis scheme. Forward regression procedure based on Gram-Schmidt orthogonalization was also proposed by Wei and Billings in [Wei and Billings, 2002]. Finally, a more automated procedure based on integer optimization and Genetic Algorithm (GA) was proposed in [Poulimenos and Fassois, 2003a].

Most certainly, beyond the model structure selection scheme utilized, the family of basis functions selected for the expansion of the FS model time-dependent parameters is of crucial importance. The bases that have been proposed in the literature include time polynomials of arbitrary order [Liporace, 1975], polynomial basis functions like Chebyshev [Fouskitakis and Fassois, 2002] and Legendre [Kozin, 1977, Grenier, 1983b], trigonometric basis functions [Petsounis and Fassois, 2000, Poulimenos and Fassois, 2009a], discrete prolate spheroidal functions [Grenier, 1983b], various wavelet families [Tsatsanis and Giannakis, 1993, Li et al., 2011], and others. Recently, methods based on multiple basis functions which try to combine the characteristics of two or more bases have also been proposed [Li et al., 2011, Chon et al., 2005].

However, the common characteristic of all the aforementioned studies is that the functional subspaces, either selected arbitrarily or by taking advantage of any prior information regarding the parameter evolution, always consist of basis functions of *fixed form* which are selected from a *pre-selected list*. Hence, the goodness of model fit is heavily dependent on the chosen family of basis functions.

As already mentioned, identified parametric models may be used for a number of purposes with fault diagnosis being one of the most important for reasons related with operational safety and service costs. Within the fault diagnosis context, in recent years, significant attention has been paid to vibration-based methods, which are founded upon the fundamental principle that small changes (faults) in a structure cause discrepancies in the dynamics and consequently on the vibration response, which may be detected and associated with a specific cause (fault type) [Doebling et al., 1998, Farrar et al., 2001]. However, despite the progress achieved for stationary (time-invariant) structures, this is not the case for structures with inherent non-stationarities. Only a small number of studies have been presented up to date in the literature. For instance, a statistical decision framework utilizing the residuals of an FS-TARX model was applied for the on-line damage detection in the aforementioned “bridle-like” structure [Poulimenos and Fassois, 2004b]. In order to assess the impact of a damage on the modal characteristics of a reinforced concrete frame, Huang *et al.* [Huang et al., 2009] also applied FS-TARX modelling on segments of vibrational data. Nevertheless, the main drawback of the aforementioned methods is that they use input-output data. Thus, access to the structure’s excitation, which is usually unavailable in practical applications, is required for their application.

1.4 Thesis Objectives

The specific objectives of the present thesis may be summarized as follows:

(i). Experimental assessment and comparison of the main non-stationary random vibration modelling methods via their application to a benchmark laboratory structure. Discussion of the methods’ main features, operational characteristics and applicability, as well as investigation of their pros and cons.

(ii). The postulation of a vector (multivariate) FS-TARMA method for output-only structural dynamics identification. Development of effective tools for both model parameter estimation and model structure selection. Assessment of the method effectiveness by its application to the output-only identification of a TV “bridge-like” laboratory structure.

(iii). The introduction of a novel class of Adaptable FS-TARMA (AFS-TARMA) models and the development of a method for their effective identification. AFS-TARMA models are adaptable in the sense that they are not based on basis functions of a fixed form, but instead, they use basis functions with a-priori unknown properties that may adapt to the specific random signal characteristics. Validation of the method through its application in numerical and experimental case studies and comparisons with currently available non-stationary signal identification methods.

(iv). The presentation – for first time – of a thorough review on FS-TARMA models covering both theoretical and practical aspects of the subject such as the FS-TARMA model parameter estimation and structure selection problems, with special emphasis being placed on promising new methods that aim at overcoming problems of previous approaches. Detailed comparison and assessment of the reviewed methods based on Monte Carlo experiments and comparisons with alternative non-stationary methods.

(v). The introduction of a statistical method for vibration-based fault detection and identification in inherently non-stationary structures, which utilizes – for first time in an real application – the asymptotic properties of recently introduced multi-stage FS-TAR estimator [Poulimenos and Fassois, 2007]. Application of the introduced method for the fault detection and identification in a TV pick-and-place mechanism consisting of two electromagnetic linear motors. Evaluation of the method’s effectiveness in terms of its fault detection capability under various fault scenarios.

The thesis chapters and their specific contribution are analytically presented in the next section.

1.5 Organization and Contributions of this Thesis

The chapters of the thesis are summarized in Table 1.1:

Table 1.1: Thesis chapters.

Chapter	Title
2	Output-Only Identification and Dynamic Analysis of Time-Varying Mechanical Structures Under Random Excitation: A comparative assessment of parametric methods
3	Parametric Identification of Time-Varying Structures Based on Vector Vibration Response Measurements via FS-VTARMA Models
4	Adaptable FS-TARMA Models for Non-Stationary Signal Modelling
5	Non-Stationary Random Vibration Modelling and Analysis via FS-TARMA Models – A critical survey
6	An FS-TAR Based Statistical Method for the Modelling and Fault Diagnosis in Time-Varying Structures: A pick-and-place mechanism application study

Chapter 2: Output-Only Identification and Dynamic Analysis of Time-Varying Mechanical Structures Under Random Excitation: A comparative assessment of parametric methods

This chapter addresses the problem of parametric time-domain identification and dynamic analysis for TV mechanical structures under unobservable random excitation. The methods presented are based on TARMA models, and are classified according to the mathematical structure imposed on the TV parameter evolution as unstructured parameter evolution, stochastic parameter evolution, and deterministic parameter evolution. The features and relative merits of each class are outlined. A representative method from each is then assessed through its application to the identification and dynamic analysis of a "bridge-like" laboratory TV structure consisting of a beam with a mass moving on it. The results are mutually compared and contrasted to those obtained through "frozen-configuration" (multiple experiment) baseline identification.

Main contributions:

(i). Provides a concise overview of the techniques of TARMA based methods for TV structural identification.

(ii). Comparative assessment of the methods through a case study, pertaining to the modelling and dynamic analysis of the non-stationary random vibration of a time-varying "bridge-like" laboratory structure.

Chapter 3: Parametric Identification of Time-Varying Structures Based on Vector Vibration Response Measurements via FS-VTARMA Models.

The problem of parametric output-only identification of time-varying structures based on vector random vibration signal measurements is considered in this chapter.

Although FS-TARMA models are known to outperform the classes of unstructured and stochastic parameter evolution methods in the simpler univariate case [Poulimenos and Fassois, 2006], they have not been used for multivariate TV structural identification. The *goal* of this chapter is to fill this gap by introducing a Functional Series Vector Time-dependent AutoRegressive Moving Average (FS-VTARMA) method and to provide effective tools for both model parameter estimation and model structure selection problems. The method is also employed for the identification of a "bridge-like" laboratory structure consisting of a beam and a moving mass. The identification is based on three simultaneously measured vibration response signals obtained during a single experiment. The method is judged against baseline modelling based on multiple "frozen-configuration" stationary experiments, and is shown to be effective and capable of accurately tracking the dynamics. The structure was previously identified via univariate FS-TARMA models [Poulimenos and Fassois, 2009a], which offered the possibility of comparisons with the simpler univariate (single response measurement) case. Additional comparisons with a recursive

Pseudo-Linear Regression VTARMA (PLR-VTARMA) method and a Short Time Stochastic Subspace Identification (ST-SSI) method are made in order to demonstrate the method's superior achievable accuracy and model parsimony.

Main contributions:

(i). Extension of the FS-TARMA models to the multivariate case.

(ii). Identification of a time-varying laboratory structure based on the FS-VTARMA models.

(iii). Comparison with alternative multivariate methods.

Chapter 4: Adaptable FS-TARMA Models for Non-Stationary Signal Modelling

The application of FS-TARMA identification still has its difficulties, as model estimation and particularly the model structure selection may be a complicated problem. This is due to the fact that in order to solve this problem effectively numerous multi-branch decisions have to be taken, with the most significant being the choice of a specific family of basis functions and the selection of the optimal functional subspace. To date, the literature on FS-TARMA models has mainly focused on the first problem of functional basis selection, while the equally significant problem of functional subspace selection has been treated thoroughly only in a small number of studies. However, the common characteristic of all the studies on FS-TARMA models is that the functional subspaces, either selected arbitrarily or by taking advantage of any prior information regarding the parameter evolution, is always formed by fixed basis functions belonging to a prescribed set. Hence, the goodness of model fit is heavily dependent on the chosen basis.

The *aim* of this chapter is to approach the FS-TARMA identification problem from a different data-centered perspective. Toward this end, a new class of Adaptable FS-TARMA (AFS-TARMA) models is introduced. AFS-TARMA models are adaptable in the sense that they are not based on basis functions of a fixed form, but instead, they use basis functions with a-priori unknown properties that may adapt to the specific random signal characteristics. This is accomplished via: (a) proper basis function parametrizations which allow their decay rate and frequency (decaying trigonometric functions) or knots (B-splines) to be directly estimated, and (b) a Separable Nonlinear Least Squares (SNLS) type procedure ([Golub and Pereyra, 1973]) that achieves simultaneous estimation of the basis functions and the coefficients of projection through a reduced dimensionality, constrained non-quadratic optimization problem tackled via Particle Swarm Optimization (PSO) and gradient-type refinement. The model structure parameters, that is model orders and the functional subspace dimensionalities, are estimated based on suitable criteria and PSO.

The method's effectiveness is evaluated through numerical and experimental case studies and comparisons between the introduced method, the classical FS-TARMA approach and other existent non-stationary methods.

Main contributions:

(i). Introduction of a novel class of Adaptable FS-TARMA (AFS-TARMA) models.

(ii). Introduction of a novel identification framework for AFS-TARMA models exemplified to two types of adaptable basis functions: B-splines and decaying trigonometric functions.

(iii). Assessment of the methods via Monte Carlo simulations and comparisons with classical counterparts.

(iv). Application of the method to an experimental case study pertaining to the identification of a time-varying pick-and-place mechanism.

Chapter 5: Non-Stationary Random Vibration Modelling and Analysis via FS-TARMA Models – A critical survey

Even though the advantages of FS-TARMA models over alternative non-stationary models (such as segmentation, adaptive, or smoothness priors models), have been demonstrated via a Monte Carlo comparison study in [Poulimenos and Fassois, 2006], there is a number of issues that have hardly been considered. These include the assessment of the various FS-TARMA estimation methods, the comparison of the various model structure selection schemes, and the problem of time-dependent variance estimation. The *aim* of this chapter is to provide a critical overview of the FS-TAR/TARMA methods that have been proposed in the literature and the assessment of these methods via an extended comparison study based on the identification of simulated systems. The estimation methods considered include regression type methods based on the minimization of Prediction Error (PE) criteria, recursive estimation methods, multistage methods and the Maximum Likelihood (ML) method. For the model structure selection problem integer optimization schemes, and schemes based on the concept of backward and forward regression are reviewed.

Finally, the effectiveness of FS-TARMA methods over alternative parametric and non-parametric methods is demonstrated through a critical comparison study based on Monte Carlo experiments on the identification of simulated TAR and TARMA models.

Main contributions:

(i). Presentation of a critical survey on FS-TARMA models and their variants regarding:

- parameter estimation methods
- model structure selection criteria and methods
- innovations time-dependent variance estimation
- variants, alternative methods, applications
- recent advances.

(ii). Comparison study of the main methods for FS-TARMA parameter estimation and structure selection based on Monte Carlo experiments.

Chapter 6: An FS-TAR based method for vibration-response-based fault diagnosis in stochastic time-varying structures: Experimental application to a pick-and-place mechanism.

In recent years, significant attention has been paid to fault detection via vibration based methods. These appear promising and offer potential advantages over alternative fault detection methods, as they require no visual inspection, are "global" (in the sense of covering large areas) and capable of working at a "system level", can be automated, and also tend to be time and cost effective [Fassois and Sakellariou, 2007]. Nevertheless, although there is a large number of studies on the vibration based fault detection for stationary structures this is not the case for non-stationary ones.

The *goal* of this chapter is the introduction of a statistical (parametric) model based method for vibration based fault detection in inherently non-stationary structures. The proposed method is based on non-stationary FS-TAR modelling and a proper statistical decision making scheme which utilizes the asymptotic properties of a Multi-Stage (MS) estimator. The method is validated and its effectiveness is experimentally assessed via its application to fault detection and identification on a pick–and–place mechanism consisting of two industrial type linear motors. Random force excitation is provided via an electromechanical shaker, while the vibration responses are measured at various positions via accelerometers. The fault scenarios considered consist of loosening or removal of bolts from various points of the mechanism and small added masses attached to the structure. The method is shown to achieve effective fault detection and identification based solely on the response signal of the structure acquired by a single sensor.

Main contributions:

(i). Introduction of a statistical (parametric) model based method for vibration-based structural dynamics modelling and fault diagnosis (that is fault detection and identification), in inherently TV structures.

(ii). Application of the introduced statistical time series method in a TV pick-and-place mechanism consisting of two electromagnetic linear motors.

(iii). Assessment of the method in terms of both modelling accuracy and fault detection capability under various fault scenarios considered.

Chapter 2

Output-Only Identification and Dynamic Analysis of Time-Varying Mechanical Structures Under Random Excitation: A comparative assessment of parametric methods

The problem of parametric time-domain identification and dynamic analysis for *Time-Varying* (TV) mechanical structures under unobservable random excitation is addressed in this chapter. The methods presented are based on Time-dependent AutoRegressive Moving Average (TARMA) models, and are classified according to the mathematical structure imposed on the TV parameter evolution as unstructured parameter evolution, stochastic parameter evolution, and deterministic parameter evolution. The features and relative merits of each class are outlined. A representative method from each is then assessed through its application to the identification and dynamic analysis of a laboratory TV structure consisting of a beam with a mass moving on it. The results are mutually compared and contrasted to those obtained through "frozen-configuration" (multiple experiment) baseline identification.

2.1 Introduction

Time-varying (TV), or else *non-stationary*, mechanical structures are those characterized by (mass, stiffness, power dissipation) properties that vary with time. Prime examples include crane and similar structures, robotic and other variable configuration structures, railway bridges, rocket and aircraft structures, rotating structures, vehicle suspensions with adjustable characteristics, deployable space structures, and so on. *Continuously variable configuration* structures, that is structures with geometrical characteristics varying with time, constitute an important subclass of TV structures.

TV structures are often subject to random excitation producing random vibration responses. In contrast to Time-invariant (TI) structures which produce vibration responses with TI (*stationary*) statistical characteristics, the responses of TV structures are characterized by TV (*non-stationary*) statistical characteristics [Bendat and Piersol, 2000, ch. 12], [Poulimenos and Fassois, 2006, Preumont, 1994, Priestley, 1988, Hammond and White, 1996, Kitagawa and Gersch, 1996]. Non-stationary responses may be also produced by TI structures subject to non-stationary excitation (such as earthquakes and atmospheric turbulence), or by structures with inherent nonlinear dynamics. Although these cases may be also treated by the methods presented in the following, our main focus will be on TV structures.

In many cases it is useful to identify a model of a TV structure which may be subsequently used for dynamic analysis [Conforto and D'Alessio, 1999b, Petsounis and Fassois, 2000, Ghanem and Romeo, 2000, Liu and Deng, 2006, Poulimenos and Fassois, 2009a], for the refinement of analytic models [Dimitriadis et al., 2004], for simulation [Fouskitakis and Fassois, 2002], for damage detection and identification [Bardou and Sidahmed, 1994, Poulimenos and Fassois, 2004b, Zhan et al., 2006], as well as for prediction and control [Ben Mrad et al., 1998b]. Oftentimes, this identification has to be based on vibration response-only measurements (the *output-only problem*). This is so because the force excitation may be due to various sources that are difficult or impossible to precisely isolate and measure (this is the case of oscillations in a crane system, a rocket, a railway bridge, and so on). The focus of this chapter is precisely on this case, although the methods may be extended to the observable excitation case as well (for instance see [Dimitriadis et al., 2004, Poulimenos and Fassois, 2004b, Ben Mrad, 2002]). A recent survey on the topic is Ref. [Poulimenos and Fassois, 2006], where the methods surveyed are compared by means of a Monte Carlo study based on a TV suspension model.

The mathematical models for the output-only identification of TV structures may be of the *parametric* or *non-parametric* types. Attention is presently restricted to the former category, which is known to offer a number of potential advantages compared to the category of non-parametric methods [Poulimenos and Fassois, 2006, Hammond and White, 1996, Conforto and D'Alessio, 1999b, Petsounis and Fassois, 2000]. These include (i) representation parsimony, (ii) improved accuracy, (iii) improved frequency resolution, (iv) improved tracking of the time-varying dynamics, and (v) flexibility in analysis, as parametric methods are capable of directly capturing the underlying dynamics responsible for the time-varying behavior. The reader may consult references such as [Hammond and White, 1996, Newland, 1994, Spanos and Failla, 2005] for non-parametric methods.

Parametric mathematical models are of the TARMA type or corresponding state space forms [Liu and Deng, 2006]. TARMA models resemble their conventional, stationary ARMA counterparts [Box et al., 1994, p. 53], with the significant difference being that they allow their parameters to depend upon time [Poulimenos and Fassois, 2006, Petsounis and Fassois, 2000, Niedźwiecki, 2000, Grenier, 1989a, Owen et al., 2001, Cooper and Worden, 2000]. Depending on the nature of the mathematical structure imposed on the time evolution of their parameters, TARMA models may be classified as unstructured parameter evolution, stochastic parameter evolution, and deterministic parameter evolution.

Unstructured parameter evolution TARMA (UPE-TARMA) models impose no mathematical structure on the time evolution of their parameters, which are thus free to change with time. Such a model is thus directly parametrized in terms of its TV parameters. As the complete description of a TV structure requires knowledge of the model parameters at each time instant, UPE-TARMA models are characterized by low parsimony (low model parametrization economy) and are mainly capable of tracking slow evolutions in the dynamics. Due to their simplicity and ease of use, they are frequently used in practice (for instance see [Owen et al., 2001, Cooper and Worden, 2000, Gersch and Brotherton, 1982, Cooper, 1990]).

The class of stochastic parameter evolution TARMA models impose stochastic structure on the time evolution of their parameters. The latter are thus assumed to be autocorrelated random variables allowed to change with time, but with their evolution being subject to certain smoothness constraints. These are often referred to as *smoothness priors constraints*, and the models are thus referred to as *smoothness priors TARMA* (SP-TARMA) models. SP-TARMA models achieve low parsimony, as knowledge of the model parameters at each time instant is still required. At the same time, they may still leave an unnecessarily high number of degrees of freedom in parameter evolution. SP-TARMA models have been used primarily for the modelling and analysis of earthquake ground motion signals (for instance see [Kitagawa and Gersch, 1996, Gersch and Kitagawa, 1985, Kitagawa and Gersch, 1985]).

Finally, deterministic parameter evolution TARMA models impose deterministic structure on the time evolution of their parameters. This is achieved by postulating model parameters as deterministic functions of time belonging to specific *functional subspaces* [Poulimenos and Fassois, 2006, Conforto and D'Alessio, 1999b, Bardou and Sidahmed, 1994], [Niedźwiecki, 2000, ch. 6], [Grenier, 1989a, Ben Mrad et al., 1998a]. These models are specifically referred to as *Functional Series TARMA* (FS-TARMA) models. FS-TARMA models achieve high parsimony, as they use a limited number of parameters. Through proper selection of the functional subspaces, FS-TARMA models may represent various types of evolution in the dynamics, including slow, fast or even discontinuous evolutions [Conforto and D'Alessio, 1999b, Petsounis and Fassois, 2000, Fouskitakis and Fassois, 2002, Ben Mrad et al., 1998b], [Niedźwiecki, 2000, p. 215], [Fouskitakis and Fassois, 2001].

FS-TAR/TARMA models have been used in various structural dynamics related applications, such as the modelling and simulation of earthquake ground motion [Fouskitakis and Fassois, 2002, Kozin, 1977], vibration analysis in rotating machinery [Conforto and D'Alessio, 1999b], the modelling and prediction of power consumption in an automobile active suspension [Ben Mrad et al., 1998b], the modelling and analysis of simulated robot vibration [Petsounis and Fassois, 2000], and the modelling and vibration analysis of a bridge with heavy vehicle type laboratory structure [Poulimenos and Fassois, 2009a].

The aim of the present study is twofold: (i) To provide a concise overview of the techniques of time-dependent ARMA methods for TV structural identification, and (ii) to present an application and comparative assessment of the methods through a case study, pertaining to the modelling and dynamic analysis of the non-stationary random vibration of a time-varying bridge with heavy vehicle type laboratory structure. Comparisons with a "frozen-configuration" baseline model based on multiple stationary experiments are also made.

The remainder of this chapter is organized as follows: The mathematical description of a TV and a continuously variable configuration structure and their connection are discussed in Section 2.2. The parametric models for the output-only identification of TV structures are presented in Section 2.3, while in Section 2.4 the model parameter estimation and model structure selection problems are considered. In Section 2.5 the TV (continuously variable configuration) structure under study is presented. The identification results and the dynamic analysis of the structure based on the identified TARMA models are in the focus of Sections 2.6 and 2.7, respectively. Finally the conclusions of the study are summarized in Section 2.8.

2.2 Time-Varying and Continuously Variable Configuration Structures and Their Response

A lumped parameter model of a TV viscously damped structure is provided by the ordinary differential equation (ODE)

$$\boldsymbol{M}(t)\ddot{\boldsymbol{x}}(t) + \boldsymbol{C}(t)\dot{\boldsymbol{x}}(t) + \boldsymbol{K}(t)\boldsymbol{x}(t) = \boldsymbol{f}(t), \qquad t \in [t_0, t_f], \tag{2.1}$$

with t designating analog time, $\boldsymbol{x}(t)$ the structural displacement response vector, and $\boldsymbol{f}(t)$ the force excitation vector. $\boldsymbol{M}(t)$, $\boldsymbol{C}(t)$, and $\boldsymbol{K}(t)$ stand for the TV mass, viscous damping, and stiffness matrices, respectively, which are responsible for the TV nature of the structure.

By "freezing" the mass, viscous damping, and stiffness matrices successively at each time instant τ ($\tau \in [t_0, t_f]$), one may associate a noncountable sequence of TI structures with the TV structure of Eq. (2.1). Each such *"frozen" structure* is described by the ODE

$$\boldsymbol{M}(\tau)\ddot{\boldsymbol{x}}(t) + \boldsymbol{C}(\tau)\dot{\boldsymbol{x}}(t) + \boldsymbol{K}(\tau)\boldsymbol{x}(t) = \boldsymbol{f}(t), \quad \text{for all } t, \tag{2.2}$$

which is TI for the selected time instant τ. This sequence of TI structures may be thought of as a *"frozen-time" representation* of the TV structure. The knowledge of the frozen-time representation of a TV structure is equivalent to knowledge of the TV structure and vice versa, as it provides the characteristics that the structure would have if it were indeed frozen at each time instant.

As already noted, continuously variable configuration structures characterized by geometrical characteristics that vary with time, form an important subclass of TV structures. Defining a *configuration vector* $\boldsymbol{r}(t)$ that fully describes the geometry of the continuously variable configuration structure at each time instant, the structure matrices of Eq. (2.1) become functions of $\boldsymbol{r}(t)$, that is $\boldsymbol{M}(t) \equiv \boldsymbol{M}(\boldsymbol{r}(t))$, $\boldsymbol{C}(t) \equiv \boldsymbol{C}(\boldsymbol{r}(t))$, and $\boldsymbol{K}(t) \equiv \boldsymbol{K}(\boldsymbol{r}(t))$.

By analogy to the frozen-time representation of a TV structure, the *"frozen-configuration" representation* of a continuously variable configuration structure may be thought of as consisting of a noncountable sequence of TI structures obtained by "freezing" the configuration vector successively at each time instant τ ($\tau \in [t_0, t_f]$). Designating the frozen-configuration vector $\boldsymbol{r}(\tau) = \boldsymbol{\rho}$, each such frozen structure is described by the ODE

$$\boldsymbol{M}(\boldsymbol{\rho})\ddot{\boldsymbol{x}}(t) + \boldsymbol{C}(\boldsymbol{\rho})\dot{\boldsymbol{x}}(t) + \boldsymbol{K}(\boldsymbol{\rho})\boldsymbol{x}(t) = \boldsymbol{f}(t), \quad \text{for all } t, \tag{2.3}$$

and is TI for the selected $\boldsymbol{\rho}$. Obviously, the frozen-time and frozen-configuration representations are equivalent for a continuously variable configuration structure with known time variation of its configuration vector.

A practically important feature of continuously variable configuration structures is that it is often possible to obtain access to a (configuration-vector-discretized) version of its frozen-configuration representation by "freezing" the configuration vector at selected discrete values (say $\boldsymbol{\rho}_1, \boldsymbol{\rho}_2, \ldots, \boldsymbol{\rho}_M$). The dynamics of the structure for each value of $\boldsymbol{\rho}$ are described by Eq. (2.3), and identification of its frozen-configuration representation may be based on data sets obtained from M distinct experiments. This procedure is referred to as *baseline identification* and is used in the present study as well. Its advantage is twofold: Conventional TI identification is used, and the achievable accuracy may be high due to the availability of (large) data sets from M experiments. Yet, its disadvantage is exactly the need for running M distinct experiments and identification cycles. Moreover, TI identification does not directly provide information on the actual non-stationary vibration response.

The above concepts and ideas obviously extend to the discrete-time case. The ODE representation of Eq. (2.1) is then converted into a vector second-order difference equation. When the single excitation single vibration response is considered, the (partial) dynamics may be described by a scalar difference equation

$$x[t] + \sum_{i=1}^{n_a} a_i[t]x[t-i] = \sum_{i=0}^{n_c} c_i[t]f[t-i], \qquad t = 1, \ldots, N, \tag{2.4}$$

in which t designates normalized discrete-time (absolute time normalized by the sampling period), $f[t]$, $x[t]$ the discretized versions of the scalar force and observed vibration displacement response, respectively, $a_i[t]$, $c_i[t]$ the discrete-time TV parameters, n_a, n_c the equation orders, and N the signals' length in samples. The expressions for the discrete-time frozen-time and frozen-configuration representations are analogous to their continuous-time counterparts.

2.3 Parametric Models for the Identification of Time-Varying Structures

Parametric models typically are of the TARMA type or proper extensions (for instance TARMAX models – that is TARMA models with exogenous excitation, which additionally account for measurable force excitations). A TARMA(n_a, n_c) model, with n_a, n_c designating its autoregressive (AR) and moving average (MA) orders, respectively, is thus of the form (compare with Eq. (2.4))

$$\underbrace{x[t] + \sum_{i=1}^{n_a} a_i[t]x[t-i]}_{\text{AR part}} = \underbrace{e[t] + \sum_{i=1}^{n_c} c_i[t]e[t-i]}_{\text{MA part}}, \qquad e[t] \sim \text{NID}(0, \sigma_e^2[t]), \tag{2.5}$$

with t designating normalized discrete time, $x[t]$ the non-stationary vibration response signal, $e[t]$ an unobservable uncorrelated (white) non-stationary *innovations*, or else *residual* signal characterized by zero mean and TV variance $\sigma_e^2[t]$, and $a_i[t]$, $c_i[t]$ the model's TV AR and MA parameters, respectively. NID$(\cdot, \cdot)$ stands for normally independently distributed random variables with the indicated mean and variance.

As already indicated, depending on the nature of the mathematical structure imposed on the time evolution of their parameters, TARMA models may be classified as unstructured parameter evolution, stochastic parameter evolution, and deterministic parameter evolution.

2.3.1 Unstructured parameter evolution TARMA models

Unstructured Parameter Evolution TARMA (UPE-TARMA) models impose no mathematical structure on the time evolution of their parameters, which are thus free to change with time. Such a model is thus directly parametrized in terms of its TV parameters $a_i[t], c_i[t], \sigma_e^2[t]$, and a specific model structure, say $\mathcal{M}_{UPE}$, is defined by the representation orders n_a, n_c, that is:

$$\mathcal{M}_{UPE} \triangleq \{n_\alpha, n_c\} \tag{2.6}$$

2.3.2 Stochastic parameter evolution TARMA models

Stochastic parameter evolution TARMA models impose stochastic structure on the time evolution of their parameters. The latter are thus assumed to be autocorrelated random variables allowed to change with time, but with their evolution being subject to certain smoothness constraints. These are often referred to as *smoothness priors constraints*, and the models are thus referred to as *Smoothness Priors TARMA* (SP-TARMA) models. The smoothness priors constraints typically are stochastic difference equations of the forms

$$\Delta^\kappa a_i[t] = w_{a_i}[t], \quad w_{a_i}[t] \sim \text{NID}(0, \sigma^2_{w_{a_i}}[t]), \tag{2.7a}$$

$$\Delta^\kappa c_i[t] = w_{c_i}[t], \quad w_{c_i}[t] \sim \text{NID}(0, \sigma^2_{w_{c_i}}[t]), \tag{2.7b}$$

acting on each one of the AR and MA parameters. In these expressions κ designates the difference equation order, Δ^κ the κ-th order difference operator ($\Delta^\kappa \triangleq (1-\mathcal{B})^\kappa$; where $\mathcal{B}$ the backshift operator $\mathcal{B}^i x[t] \triangleq x[t-i]$) and $w_{a_i}[t], w_{c_i}[t]$ zero-mean, uncorrelated (white) and mutually uncorrelated, and uncrosscorrelated with $e[t]$, Gaussian sequences with potentially TV variances. The degree of smoothness of the time evolution of each parameter is controlled by the corresponding white sequence variance, and increases for decreasing variance. A specific SP-TARMA model structure is defined by the model orders n_a, n_c and the smoothness constraints order κ (the latter being typically assumed to be common for all AR and MA parameters):

$$\mathcal{M}_{SP} \triangleq \{n_a, n_c, \kappa\} \tag{2.8}$$

2.3.3 Deterministic parameter evolution TARMA models

Deterministic parameter evolution TARMA models impose deterministic structure on the time evolution of their parameters. This is achieved by postulating model parameters as deterministic functions of time belonging to specific *functional subspaces* [Poulimenos and Fassois, 2006, Conforto and D'Alessio, 1999b, Bardou and Sidahmed, 1994], [Niedźwiecki, 2000, ch. 6], [Grenier, 1989a], [Ben Mrad et al., 1998a]. These models are specifically referred to as *Functional Series TARMA* (FS-TARMA) models. Their AR and MA parameters, as well as their innovations variance, are thus expanded on the selected functional subspaces:

$$\mathcal{F}_{AR} \triangleq \left\{G_{d_a(1)}[t],\ \ldots,\ G_{d_a(p_a)}[t]\right\}, \qquad \mathcal{F}_{MA} \triangleq \left\{G_{d_c(1)}[t],\ \ldots,\ G_{d_c(p_c)}[t]\right\},$$

$$\mathcal{F}_{\sigma_e^2} \triangleq \left\{G_{d_s(1)}[t],\ \ldots,\ G_{d_s(p_s)}[t]\right\}$$

Each functional subspace consists of a set of orthogonal *basis functions* selected from a suitable family (such as a polynomial family, a trigonometric family, and so on). The AR, MA, and variance subspace dimensionalities are indicated as p_a, p_c, p_s, respectively, while the indices $d_a(i)$ $(i = 1, \ldots, p_a)$, $d_c(i)$ $(i = 1, \ldots, p_c)$ and $d_s(i)$ $(i = 1, \ldots, p_s)$ designate the specific basis functions of a particular family that are included in each subspace. The TV AR and MA parameters and the innovations variance of an FS-TARMA$(n_a, n_c)_{[p_a,p_c,p_s]}$ model are then expressed as

$$a_i[t] \triangleq \sum_{j=1}^{p_a} a_{i,j} G_{d_a(j)}[t], \qquad c_i[t] \triangleq \sum_{j=1}^{p_c} c_{i,j} G_{d_c(j)}[t], \qquad \sigma_e^2[t] \triangleq \sum_{j=1}^{p_s} s_j G_{d_s(j)}[t],$$

with $a_{i,j}$, $c_{i,j}$, and s_j designating the AR, MA, and innovations variance, respectively, *coefficients of projection*. An FS-TARMA model is thus parametrized in terms of its projection coefficients $a_{i,j}, c_{i,j}, s_j$, while a specific model structure $\mathcal{M}_{FS}$ is defined by the model orders n_a, n_c, and the functional subspaces $\mathcal{F}_{AR}, \mathcal{F}_{MA}, \mathcal{F}_{\sigma_e^2}$.

$$\mathcal{M}_{FS} \triangleq \{n_a, n_c, \mathcal{F}_{AR}, \mathcal{F}_{MA}, \mathcal{F}_{\sigma_e^2}\} \tag{2.9}$$

FS-TARMA models achieve high parsimony, as they use a limited number of parameters. Through proper selection of the functional subspaces, FS-TARMA models may represent various types of evolution in the dynamics, including slow, fast or even discontinuous evolutions [Conforto and D'Alessio, 1999b, Petsounis and Fassois, 2000, Fouskitakis and Fassois, 2002, Ben Mrad et al., 1998b, Fouskitakis and Fassois, 2001], [Niedźwiecki, 2000, p. 215].

2.4 The Identification Problem and Methods

Given a single, N-sample-long, non-stationary vibration response signal $x^N \triangleq \{x[1] \ldots x[N]\}$ and a selected model class (unstructured, stochastic, or deterministic parameter evolution), the TARMA identification problem may be posed as the problem of selecting the corresponding model structure $\mathcal{M}$, the model AR/MA parameter vector $\boldsymbol{\theta}[t] \triangleq [\ a_1[t]\ \ldots\ a_{n_a}[t]\ \vdots\ c_1[t]\ \ldots\ c_{n_c}[t]\ ]^T$ and the innovations variance $\sigma_e^2[t]$ that best "fit" the observed response. *Model "fitness"* may be understood in various ways. In all of them a key role is assigned to the *model predictive ability*, that is the ability of a specific model in providing accurate one-step-ahead predictions.

Based on Eq. (2.5) it is straightforward to verify that the minimum mean square error one-step-ahead prediction $\hat{x}[t|t-1]$ of the signal value $x[t]$ made at time $t-1$ is equal to

$$\hat{x}[t|t-1] = -\sum_{i=1}^{n_a} a_i[t]x[t-i] + \sum_{i=1}^{n_c} c_i[t]e[t-i], \tag{2.10}$$

(note that the hat generally designates estimator/estimate of the indicated quantity). Comparing Eq. (2.10) with the TARMA model of Eq. (2.5) it is also straightforward to verify that the one-step-ahead prediction error $\hat{e}[t|t-1] \triangleq x[t] - \hat{x}[t|t-1]$ is equal to $e[t]$.

Common “fitness” functions include the residual sum of squares (RSS), the Gaussian negative log-likelihood function, and the Bayesian information criterion (BIC) defined as [Box et al., 1994, pp. 200-202], [Ljung, 1999, pp. 505-507]

$$\text{RSS} = \sum_{t=1}^{N} e^2[t], \tag{2.11}$$

$$-\ln \mathcal{L}\left(x^N\right) = \frac{N}{2}\ln 2\pi + \frac{1}{2}\sum_{t=1}^{N}\left(\ln\left(\sigma_e^2[t]\right) + \frac{e^2[t]}{\sigma_e^2[t]}\right), \tag{2.12}$$

$$\text{BIC} = -\ln \mathcal{L}\left(x^N\right) + \frac{\ln N}{2} d, \tag{2.13}$$

respectively. In the BIC expression d designates the number of independently estimated model parameters. Also note that the BIC consists of the superposition of the negative log-likelihood function and a term that penalizes the model size (complexity), thus discouraging model overfitting. For this reason it may be used for both parameter estimation and model structure selection. Nevertheless, it may not be formally used within the context of UPE-TARMA and SP-TARMA models, the parameters of which are (recursively) updated at each time instant. In principle, a model is thus identified as that minimizing a selected “fitness” function.

For purposes of practicality and conceptual simplicity, the identification problem is commonly distinguished into two subproblems: (a) *Model parameter estimation*, and (b) *model structure selection*. Model parameter estimation is subsequently discussed first, as it is an essential part of model structure selection as well.

2.4.1 Model parameter estimation

Model parameter estimation refers to the determination, for a given model form and structure, of the AR/MA parameter vector $\boldsymbol{\theta}[t]$ and the residual variance $\sigma_e^2[t]$ at all time instants $t = 1, \ldots, N$.

2.4.1.1 Unstructured parameter evolution TARMA models

The estimation of UPE-TARMA models is often based on *recursive* methods, which update the parameter vector estimate each time a new signal sample becomes available [Cooper and Worden, 2000], [Ljung, 1999, ch. 11], [Ben Mrad and Fassois, 1991a, Ben Mrad and Fassois, 1991b]. Presently, the *recursive maximum likelihood* (RML) algorithm [Ljung, 1999, p. 372] is used for UPE-TARMA model parameter estimation and the corresponding method is thus referred to as RML-TARMA. A summary of the method is provided in Table 2.1. The quantity λ of these equations is referred to as the *forgetting factor*; its selection is critical and represents the basic trade-off between tracking ability in the dynamics and achievable parameter accuracy.

Following parameter estimation, the innovations (one-step-ahead prediction error) variance $\sigma_e^2[t]$ may be estimated by using a window of length $2K+1$, centered at the time instant t, that slides over the prediction error (residual) sequence, that is

$$\hat{\sigma}_e^2[t] = \frac{1}{2K+1}\sum_{\tau=t-K}^{t+K} \hat{e}^2[\tau|\tau-1] \tag{2.14}$$

2.4.1.2 Stochastic parameter evolution TARMA models

Model parameter estimation for the SP-TARMA models of Eq. (2.7) may be developed by setting the latter, along with the TARMA model expression of Eq. (2.5), into linear state space form.

Table 2.1: RML-TARMA estimation.

Estimator update	$\hat{\boldsymbol{\theta}}[t] = \hat{\boldsymbol{\theta}}[t-1] + \boldsymbol{k}[t]\hat{e}[t\|t-1]$
Prediction error	$\hat{e}[t\|t-1] = x[t] - \hat{x}[t\|t-1] = x[t] - \boldsymbol{\phi}^T[t]\hat{\boldsymbol{\theta}}[t-1]$
Gain:	$\boldsymbol{k}[t] = \frac{\boldsymbol{P}[t-1]\boldsymbol{\psi}[t]}{\lambda+\boldsymbol{\psi}^T[t]\boldsymbol{P}[t-1]\boldsymbol{\psi}[t]}$
"Covariance" update	$\boldsymbol{P}[t] = \frac{1}{\lambda}\left(\boldsymbol{P}[t-1] - \frac{\boldsymbol{P}[t-1]\boldsymbol{\psi}[t]\boldsymbol{\psi}^T[t]\boldsymbol{P}[t-1]}{\lambda+\boldsymbol{\psi}^T[t]\boldsymbol{P}[t-1]\boldsymbol{\psi}[t]}\right)$
Filtering	$\boldsymbol{\psi}[t] + \hat{c}_1[t-1]\boldsymbol{\psi}[t-1] + \ldots + \hat{c}_{n_c}[t-1]\boldsymbol{\psi}[t-n_c] = \boldsymbol{\phi}[t]$
A-posteriori error	$\hat{e}[t\|t] = x[t] - \boldsymbol{\phi}^T[t]\hat{\boldsymbol{\theta}}[t]$

$$\boldsymbol{\phi}[t] \triangleq \Big[-x[t-1]\ \ldots\ -x[t-n_\alpha] \,\vdots\, \hat{e}[t-1|t-1]\ \ldots\ \hat{e}[t-n_c|t-n_c]\Big]^T$$

Initialization: $\hat{\boldsymbol{\theta}}[0] = \mathbf{0}$, $\boldsymbol{P}[0] = \alpha\boldsymbol{I}$ with α designating a "large" positive number. The signal and a-posteriori error initial values are set to zero.

It can be shown that in the general (κ-th order) smoothness constraint SP-TARMA(n_a, n_c) model is expressed as [Poulimenos and Fassois, 2006, Kitagawa and Gersch, 1996]:

$$\boldsymbol{z}[t] = \boldsymbol{F}\cdot\boldsymbol{z}[t-1] + \boldsymbol{G}\cdot\boldsymbol{w}[t], \qquad x[t] = \boldsymbol{h}^T[t, \boldsymbol{z}^{t-1}]\cdot\boldsymbol{z}[t] + e[t] \tag{2.15a}$$

$$\left[\begin{array}{c}\boldsymbol{w}[t]\\ \hline e[t]\end{array}\right] \sim \text{NID}\left(\left[\begin{array}{c}0\\ \vdots\\ 0\end{array}\right], \left[\begin{array}{c|c}\boldsymbol{Q}[t] & \begin{array}{c}0\\ \vdots\\ 0\end{array}\\ \hline 0\ldots0 & \sigma_e^2[t]\end{array}\right]\right), \qquad \boldsymbol{Q}[t] = \sigma_w^2[t]\cdot\boldsymbol{I}_{n_a+n_c} \tag{2.15b}$$

with:

$$\boldsymbol{h}[t, \boldsymbol{z}^{t-1}] \triangleq \Big[-x[t-1]\ldots -x[t-n_a] \,\vdots\, e[t-1, \boldsymbol{z}^{t-1}]\ldots e[t-n_c, \boldsymbol{z}^{t-n_c}] \,\vdots\, 0\ldots0\Big]^T_{\kappa\cdot(n_a+n_c)\times 1} \tag{2.15c}$$

$$\boldsymbol{z}[t] \triangleq \Big[a_1[t]\ldots a_{n_a}[t]\ c_1[t]\ldots c_{n_c}[t] \vdots\ \ldots\ \vdots a_1[t-\kappa+1]\ldots a_{n_a}[t-\kappa+1]\ c_1[t-\kappa+1]\ \ldots\ c_{n_c}[t-\kappa+1]\Big]^T_{\kappa\cdot(n_a+n_c)\times 1} \tag{2.15d}$$

$$\boldsymbol{w}[t] \triangleq \Big[\ w_{a_1}[t]\ w_{a_2}[t]\ \ldots\ w_{a_{n_a}}[t] \,\vdots\, w_{c_1}[t]\ w_{c_2}[t]\ \ldots\ w_{c_{n_c}}[t]\ \Big]^T_{n_a+n_c\times 1} \tag{2.15e}$$

z^t designating a vector containing all state vectors $\boldsymbol{z}[t]$ up to time t, and F, G matrices of the following forms (depending on the value of κ):

$$\kappa = 1: \qquad \boldsymbol{F} \triangleq \boldsymbol{I}_{n_a+n_c}, \qquad \boldsymbol{G} \triangleq \boldsymbol{I}_{n_a+n_c}$$

$$\kappa = 2: \qquad \boldsymbol{F} \triangleq \left[\begin{array}{c|c} 2\cdot\boldsymbol{I}_{n_a+n_c} & -\boldsymbol{I}_{n_a+n_c}\\ \boldsymbol{I}_{n_a+n_c} & \mathbf{0}_{n_a+n_c}\end{array}\right], \qquad \boldsymbol{G} \triangleq \left[\begin{array}{c}\boldsymbol{I}_{n_a+n_c}\\ \mathbf{0}_{n_a+n_c}\end{array}\right]$$

$$\kappa = 3: \qquad \boldsymbol{F} \triangleq \left[\begin{array}{c|c|c} 3\cdot\boldsymbol{I}_{n_a+n_c} & -3\cdot\boldsymbol{I}_{n_a+n_c} & \boldsymbol{I}_{n_a+n_c}\\ \hline \boldsymbol{I}_{n_a+n_c} & \mathbf{0}_{n_a+n_c} & \mathbf{0}_{n_a+n_c}\\ \hline \mathbf{0}_{n_a+n_c} & \boldsymbol{I}_{n_a+n_c} & \mathbf{0}_{n_a+n_c}\end{array}\right], \qquad \boldsymbol{G} \triangleq \left[\begin{array}{c}\boldsymbol{I}_{n_a+n_c}\\ \hline \mathbf{0}_{n_a+n_c}\\ \hline \mathbf{0}_{n_a+n_c}\end{array}\right]$$

and so on,

where $\boldsymbol{I}_n$ and $\mathbf{0}_n$ designate the $n\times n$ dimensional identity and zero matrices, respectively. As indicated by the above expressions, $z[t]$ forms a *state vector* (Eq. (2.15a)), whereas $\boldsymbol{w}[t]$ consists of the scalar innovations entering in each constraint expression.

Table 2.2: Kalman filter and backward smoothing for the estimation of SP-TARMA models (normalized form).

Time update (prediction):

State prediction	$\hat{\boldsymbol{z}}[t\|t-1] = \boldsymbol{F}\hat{\boldsymbol{z}}[t-1\|t-1]$
Prediction error	$\hat{e}[t\|t-1] = x[t] - \boldsymbol{h}^T[t]\hat{\boldsymbol{z}}[t\|t-1]$
"Covariance" update	$\tilde{\boldsymbol{P}}[t\|t-1] = \boldsymbol{F}\tilde{\boldsymbol{P}}[t-1\|t-1]\boldsymbol{F}^T + \boldsymbol{G}\tilde{\boldsymbol{Q}}[t]\boldsymbol{G}^T$

Observation update (filtering):

Gain	$\boldsymbol{k}[t] = \tilde{\boldsymbol{P}}[t\|t-1]\boldsymbol{h}[t]\left(\boldsymbol{h}^T[t]\tilde{\boldsymbol{P}}[t\|t-1]\boldsymbol{h}[t]+1\right)^{-1}$
State update	$\hat{\boldsymbol{z}}[t\|t] = \hat{\boldsymbol{z}}[t\|t-1] + \boldsymbol{k}[t]\hat{e}[t\|t-1]$
"Covariance" update	$\tilde{\boldsymbol{P}}[t\|t] = \left(\boldsymbol{I} - \boldsymbol{k}[t]\boldsymbol{h}^T[t]\right)\tilde{\boldsymbol{P}}[t\|t-1]$

Smoothing:

$$\boldsymbol{A}[t] = \tilde{\boldsymbol{P}}[t|t]\boldsymbol{F}^T\tilde{\boldsymbol{P}}^{-1}[t+1|t]$$
$$\hat{\boldsymbol{z}}[t|N] = \hat{\boldsymbol{z}}[t|t] + \boldsymbol{A}[t]\left(\hat{\boldsymbol{z}}[t+1|N] - \hat{\boldsymbol{z}}[t+1|t]\right)$$
$$\tilde{\boldsymbol{P}}[t|N] = \tilde{\boldsymbol{P}}[t|t] + \boldsymbol{A}[t]\left(\tilde{\boldsymbol{P}}[t+1|N] - \tilde{\boldsymbol{P}}[t+1|t]\right)\boldsymbol{A}^T[t]$$
$$\tilde{\boldsymbol{P}}[t|t] \triangleq \frac{\boldsymbol{P}_{[t|t]}}{\sigma_e^2[t]}, \qquad \tilde{\boldsymbol{P}}[t|t-1] \triangleq \frac{\boldsymbol{P}_{[t|t-1]}}{\sigma_e^2[t]}, \qquad \tilde{\boldsymbol{Q}}[t] \triangleq \frac{\boldsymbol{Q}_{[t]}}{\sigma_e^2[t]} = \underbrace{\frac{\sigma_w^2[t]}{\sigma_e^2[t]}}_{\nu[t]}\boldsymbol{I}_{n_a+n_c}$$

Initialization: $\hat{\boldsymbol{\theta}}[0] = \boldsymbol{0}$, $\boldsymbol{P}[0] = \alpha\boldsymbol{I}$ with α designating a "large" positive number.

The second of Eqs. (2.15a) is a non-linear function of $\boldsymbol{z}[t]$. SP-TARMA parameter estimation may be then based on an extended least squares (ELS)-like algorithm, by replacing the theoretical prediction errors $e[t,\boldsymbol{z}^t]$ in Eq. (2.15c) with their respective posterior estimates $\hat{e}[t|t]$ (which are then treated as measurements). SP-TARMA parameter estimation may be then achieved via the ordinary Kalman filter (KF) algorithm with:

$$\boldsymbol{h}[t] = \left[\, -x[t-1] \;\ldots\; -x[t-n_a] \;\vdots\; \hat{e}[t-1|t-1] \;\ldots\; \hat{e}[t-n_c|t-n_c] \;\vdots\; 0 \;\ldots\; 0 \,\right]^T_{\kappa\cdot(n_a+n_c)\times 1} \tag{2.16}$$

$$\hat{e}[t|t] = x[t] - \boldsymbol{h}^T[t]\cdot\hat{\boldsymbol{z}}[t|t]$$

A summary of a normalized version of the method, including a final backward smoothing phase, is provided in Table 2.2. It should be noted that the ratio $\nu[t]$ of the constraint model innovations variance $\sigma_w^2[t]$ (assumed to be common for all constraints) over the residual variance $\sigma_e^2[t]$, which is for simplicity assumed to be constant ($\nu[t] = \nu$), constitutes a user selected design parameter that controls the equivalent memory of the estimation algorithm (similar to the forgetting factor in the RML-TARMA estimation method). Indeed, $\nu \to 0$ implies a locally deterministic (polynomial) parameter evolution, while $\nu \to \infty$ implies no structure on parameter evolution. Of course, it is also possible to optimize (estimate) ν based on a suitable criterion (such as minimization of the RSS).

Innovations variance estimation may be achieved either via the scheme described in Ref. [Kitagawa and Gersch, 1985], or through that of the previous (RML-TARMA) method (Eq. (2.14)).

2.4.1.3 Deterministic parameter evolution TARMA models

Parameter estimation for FS-TARMA models consists of determining the AR/MA and innovations variance projection coefficient vectors

$$\boldsymbol{\vartheta}_{a|c} \triangleq [\,\boldsymbol{\vartheta}_a^T \mid \boldsymbol{\vartheta}_c^T\,]^T_{(n_a p_a + n_c p_c)\times 1}, \qquad \text{and} \qquad \boldsymbol{\vartheta}_s \triangleq [\,s_1 \ldots s_{p_s}\,]^T_{p_s\times 1}, \tag{2.17}$$

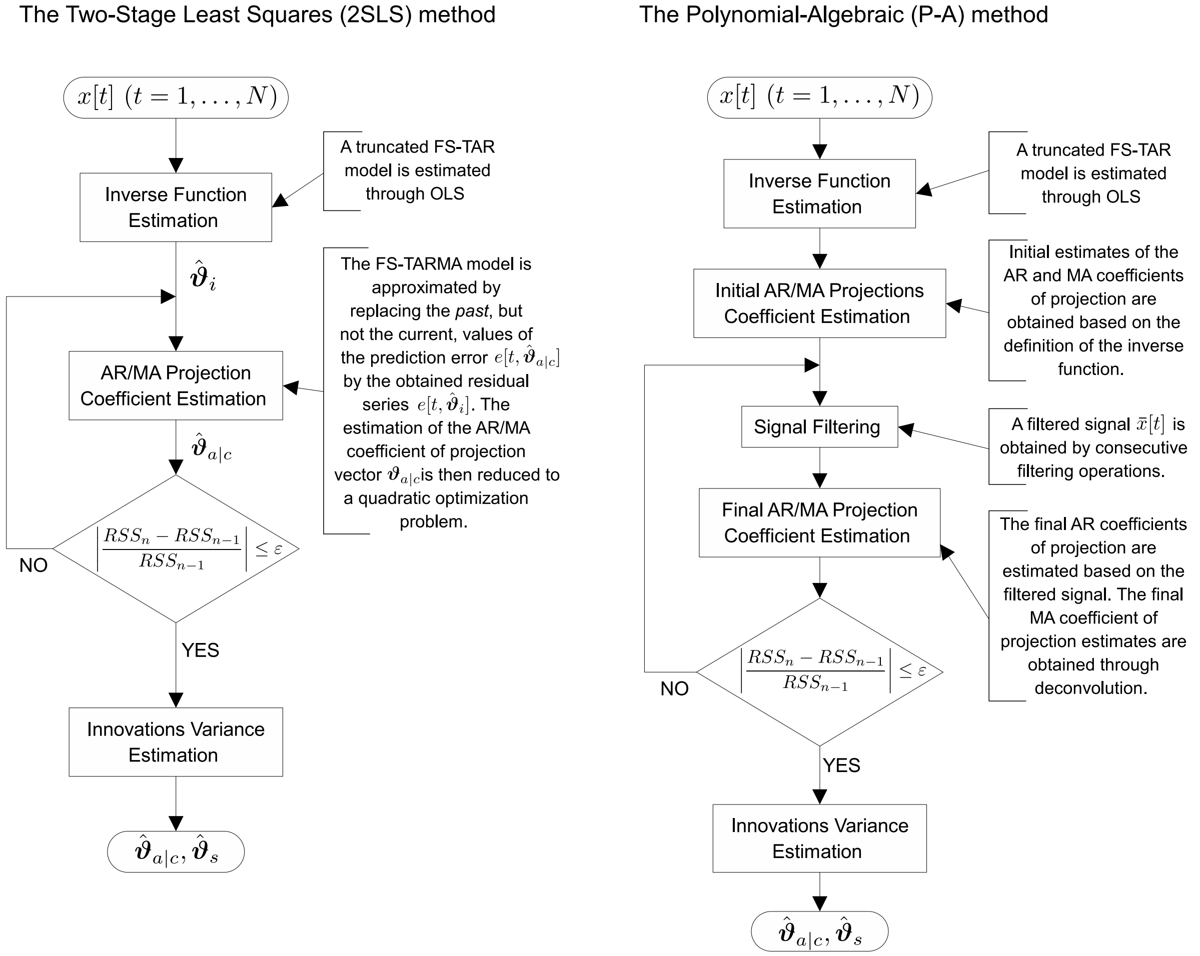

Figure 2.1: Two multistage methods for FS-TARMA model identification.

respectively, with

$$\boldsymbol{\vartheta}_a \triangleq [\, a_{1,1} \dots a_{1,p_a} \mid \ \dots \ \mid a_{n_a,1} \dots a_{n_a,p_a} \,]^T_{(n_a p_a)\times 1}, \quad \boldsymbol{\vartheta}_c \triangleq [\, c_{1,1} \dots c_{1,p_c} \mid \ \dots \ \mid c_{n_c,1} \dots c_{n_c,p_c} \,]^T_{(n_c p_c)\times 1}$$

Estimation of the parameter vector $\boldsymbol{\vartheta}_{a|c}$ may be based on a *prediction error* criterion consisting of the sum of squares of the model's one-step-ahead prediction errors (RSS):

$$\hat{\boldsymbol{\vartheta}}_{a|c} = \arg\min_{\boldsymbol{\vartheta}_{a|c}} \sum_{t=1}^{N} e^2[t, \boldsymbol{\vartheta}_{a|c}] \tag{2.18}$$

It is obvious, that the residual $e[t, \boldsymbol{\vartheta}_{a|c}]$ depends nonlinearly on the MA projection coefficient vector $\boldsymbol{\vartheta}_c$, implying that minimization of a prediction error criterion constitutes a nonquadratic problem that has to be tackled through nonlinear optimization techniques. This necessitates the use of rather accurate initial parameter values, which may be obtained through linear multi stage methods (recursive methods may be also used).

Linear multistage methods attempt to approximate the original prediction error problem by a sequence of subproblems that may be tackled by means of linear techniques. Two such methods, the *two stage least squares* (2SLS) method [Poulimenos and Fassois, 2006, Grenier, 1983b] and the *polynomial-algebraic* (P-A) method [Ben Mrad et al., 1998a] are outlined in Fig. 2.1.

Finally, the estimation of the innovations variance projection coefficients may be achieved by the following procedure. An initial, non-parametric, estimate of the innovations variance may be based on a sliding time window that uses the estimated residual series $e[t, \hat{\boldsymbol{\vartheta}}_{a|c}]$ (as in Eq. (2.14)), and an estimate of the projection coefficient vector $\boldsymbol{\vartheta}_s$ may be subsequently obtained by fitting the estimated variance $\hat{\sigma}_e^2[t]$ to a selected functional subspace $\mathcal{F}_{\sigma_e^2}$. This leads to the overdetermined set of equations

$$\hat{\sigma}_e^2[t] = \sum_{j=1}^{p_s} s_j G_{d_s(j)}[t] = \boldsymbol{g}^T[t]\boldsymbol{\vartheta}_s, \tag{2.19}$$

with $\boldsymbol{g}[t] \triangleq \begin{bmatrix} G_{d_s(1)}[t] & G_{d_s(2)}[t] & \dots & G_{d_s(p_s)}[t] \end{bmatrix}_{p_s\times 1}^T$, which is then solved in a least squares sense.

2.4.2 Model structure selection

Model structure selection refers to the estimation of the proper model structure within a selected model class. The model structure includes the AR and MA orders n_a and n_c, respectively, as well as additional structural parameters that depend on the particular model class considered [see Eqs. (2.6), (2.8), and (2.9) that define the model structure $\mathcal{M}_{UPE}/\mathcal{M}_{SP}/\ \mathcal{M}_{FS}$ for each class].

A search scheme for locating the best "fitness" model, is subsequently discussed for the most general case of FS-TARMA models which have the "richest" structure and are characterized by the maximum number of "structural" parameters. The key characteristic of this scheme is the approximate decomposition of the "structure" selection problem into two subproblems: (i) model order (n_a, n_c) selection, and (ii) functional subspace $[p_a, p_c, p_s, d_a(j), d_c(j), d_s(j)]$ selection.

Phase I: Model Order Selection.

In order to "decouple" the selection of the model orders from that of functional subspaces, their interaction has to be minimized. This may be achieved by ensuring functional subspace adequacy by initially adopting an "extended" (high dimensionality) and "complete" (in the sense of including all consecutive functions up to the subspace dimensionality) functional subspaces. Using them, model order selection may be achieved through trial and error techniques based on the optimization of the fitness function.

Phase II: Functional subspace selection.

The aim of this phase is the optimization of the functional subspaces, in the sense of increasing the representation parsimony without significantly reducing model accuracy. This may be accomplished through trial and error techniques detecting "excess" basis functions by using either the fitness function or the aggregate parameter deviation (APD). The latter constitutes a measure for the aggregate deviation of the parameter trajectories of the current model from those of the initial (phase I) model

$$\text{APD} \triangleq \sum_{i=1}^{n_a} \Delta a_i + \sum_{i=1}^{n_c} \Delta c_i + \Delta s, \tag{2.20}$$

with

$$\Delta q_i \ \triangleq \ \frac{\sum_{t=1}^{N} |q_i^{\circ}[t] - q_i[t]|}{\sum_{t=1}^{N} |q_i^{\circ}[t]|},$$

in which $q_i^{\circ}[t]$ designates the initial model AR/MA/innovations variance parameter trajectories and $q_i[t]$ the respective trajectories of the currently considered model. Basis functions may be thus successively dropped (one at a time) as long as no significant changes in the fitness function or in the APD are produced.

A specific basis function family (such as a proper polynomial or trigonometric family) is generally pre-selected (although not the specific functions that define the model's functional subspaces). This pre-selection may be based on various factors, including physical insight, prior knowledge, or experience. Yet, it should be stressed that, although the pre-selection does affect the final identified model structure (thus the model "size") and parameters, it does *not* critically affect model accuracy. The reason is that essentially any functional family may be used for approximating any given curve with arbitrary accuracy as long as a sufficient number of functions is used [Walter, 1994, p. 77]. In practice a good strategy is to use two or more families, obtain the best (according to the selected "fitness" function) under each one, have them properly validated, and finally select the globally optimum (best) model.

A few words are finally in order regarding model validation: Any identified model should be normally validated. Although such validation may be based on various criteria, which may generally depend on the model's intended use, the Gaussianity and, in particular, the whiteness of the identified model's one-step-ahead prediction error (residual) sequence are parts of standard validation procedures. Due to the TV nature of the model residual variance, the usual residual whiteness tests are not applicable in the present case. Yet, a simple test that may be applied is the residual sign test – see Refs. [Poulimenos and Fassois, 2006], [Draper and Smith, 1998, pp. 192–198].

2.5 The Laboratory Time-Varying Structure and Preliminary Analysis

The laboratory TV structure is shown in Fig. 2.2. It is a bridge with heavy vehicle type structure consisting of a steel beam of dimensions $2670 \times 50 \times 12$ mm $(L \times W \times H)$, clamped close to its both ends on vertical stands, and a steel cylindrical mass of dimension 52.5×75.0 mm $(R \times H)$ sliding on it (being pulled by a DC motor with constant speed u). As the ratio of the two masses is significant ($m/M \approx 0.4$), the structure is clearly TV, with the rate of variation depending on the selected speed u. Evidently, the structure belongs to the subclass of continuously variable configuration structures, and the configuration vector may be defined as pointing at the moving mass position. This structure has been used in a previous study by employing FS-TARMA models [Poulimenos and Fassois, 2009a].

The beam is subject to zero-mean, Gaussian, random force excitation vertically exerted through an electromechanical shaker (MB Dynamics Modal Exciter 50A, max load 225 N) equipped with a stinger. The resulting beam vibration is measured at three selected locations [Fig. 2.2(a); locations 1-3] by piezoelectric accelerometers (PCB 352A10 ICP accelerometers, frequency range $0.003 - 10$ kHz, sensitivity ~ 1.052 mV/m/sec^2), although only that at location 3 is presently used. The measured vibration signals are conditioned and subsequently driven into a 20-42 SigLab data acquisition module (featuring four 20-bit simultaneously sampled A/D, two 16-bit D/A channels, and analog anti-aliasing filters).

In a single experiment the cylindrical mass traverses the beam (from left to right) once, at a constant speed of $u = 33.4$ mm/s. At this speed the structure may be characterized as relatively *slowly* TV. The vertical vibration (acceleration) signal is sampled at $f_s = 128$ Hz and is $N = 10,113$ samples (79.0078 s) long. The study focuses on the $4 - 60$ Hz frequency range, hence the signal is digitally bandpass filtered.

The obtained response signal is shown in Fig. 2.3(a) and is evidently variance non-stationary. Non-parametric time-frequency analysis based on the short-time Fourier transform (STFT; 512-sample-long moving Hamming data window advanced by one sample each time) yields the TV power spectral density (PSD) function of Figs. 2.3(b) and 2.3(c). Evidently, the structure is characterized by three TV vibration modes (three natural frequencies) and the response signal is non-stationary in terms of its spectral content as well.

2.6 Output-Only Identification Results

Model order estimation, which is the part of model structure selection shared by all parametric methods, is based on the successive identification of TARMA(n, n) models of orders $n = 2, \ldots, 12$ and the optimization of a proper "fitness" function – specifically the RSS in the RML-TARMA and SP-TARMA cases, and the BIC in the FS-TARMA case.

In the RML-TARMA case the RSS leads to a UPE-TARMA$(8, 8)$ model estimated with forgetting factor $\lambda = 0.9905$ and initial covariance matrix $10^4\boldsymbol{I}$. Note that this result is optimized with respect to the forgetting factor (an exhaustive search has been implemented). Furthermore, in order to reduce the effects of arbitrary initial conditions in the estimation, three sequential passes (forward, backward, and final forward) are executed over the entire data record.

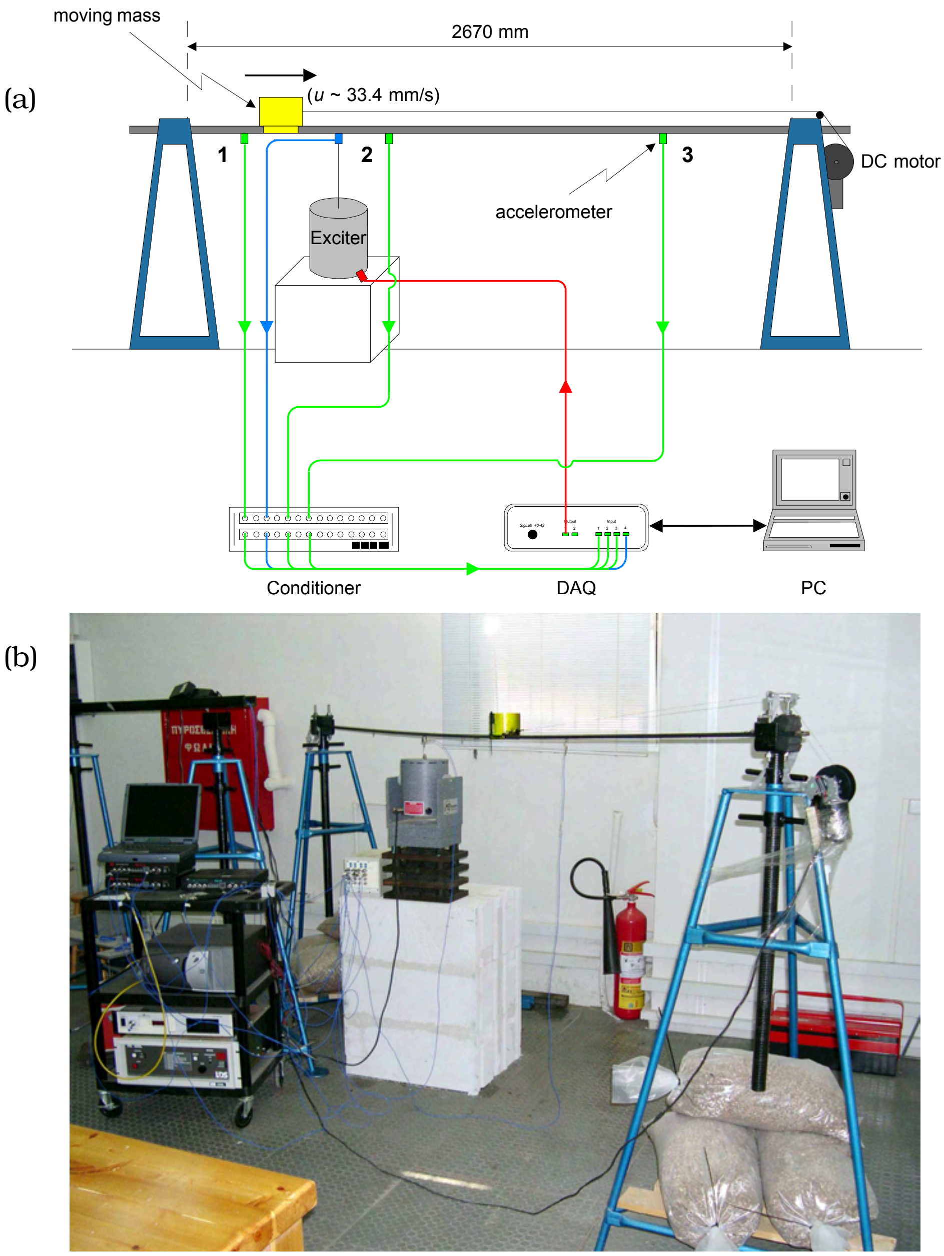

Figure 2.2: The laboratory TV structure. A bridge with heavy vehicle type structure consisting of a steel beam, clamped close to its both ends on vertical stands, and a cylindrical mass sliding on it at a selected speed. (a) Schematic diagram. (b) Photo of the experimental setup [Poulimenos and Fassois, 2009a].

In the SP-TARMA case and for each estimated model, three possible orders are considered for the smoothness priors constraints, namely $\kappa = 1, 2, 3$, while optimization (of the RSS) with respect to ratio of the smoothness priors constraints innovations variance over the residual variance ν is also carried out. Like in the RML-TARMA case, three sequential passes (forward, backward, and a final forward) are executed over the entire data record, while a final backward smoothing algorithm is also applied. For the initialization of the KF algorithm the covariance matrix is set to $10^4\boldsymbol{I}$. The $\kappa = 1, 2$ selections provide reasonable results, with almost identical RSS values for large model orders ($n_a, n_c > 7$; see Fig. 2.4). Yet, the $\kappa = 1$ selection leads to somewhat increased variability in the TV natural frequency and PSD estimates (see also the results in Appendix 2.B.1). The $\kappa = 3$ selection leads to numerical problems as the obtained ν is very small (10^{-16}). Based on the above, the selected model is SP-TARMA$(8, 8)$ with $\kappa = 2$ and $\hat{\nu} = 2.757 \times 10^{-11}$.

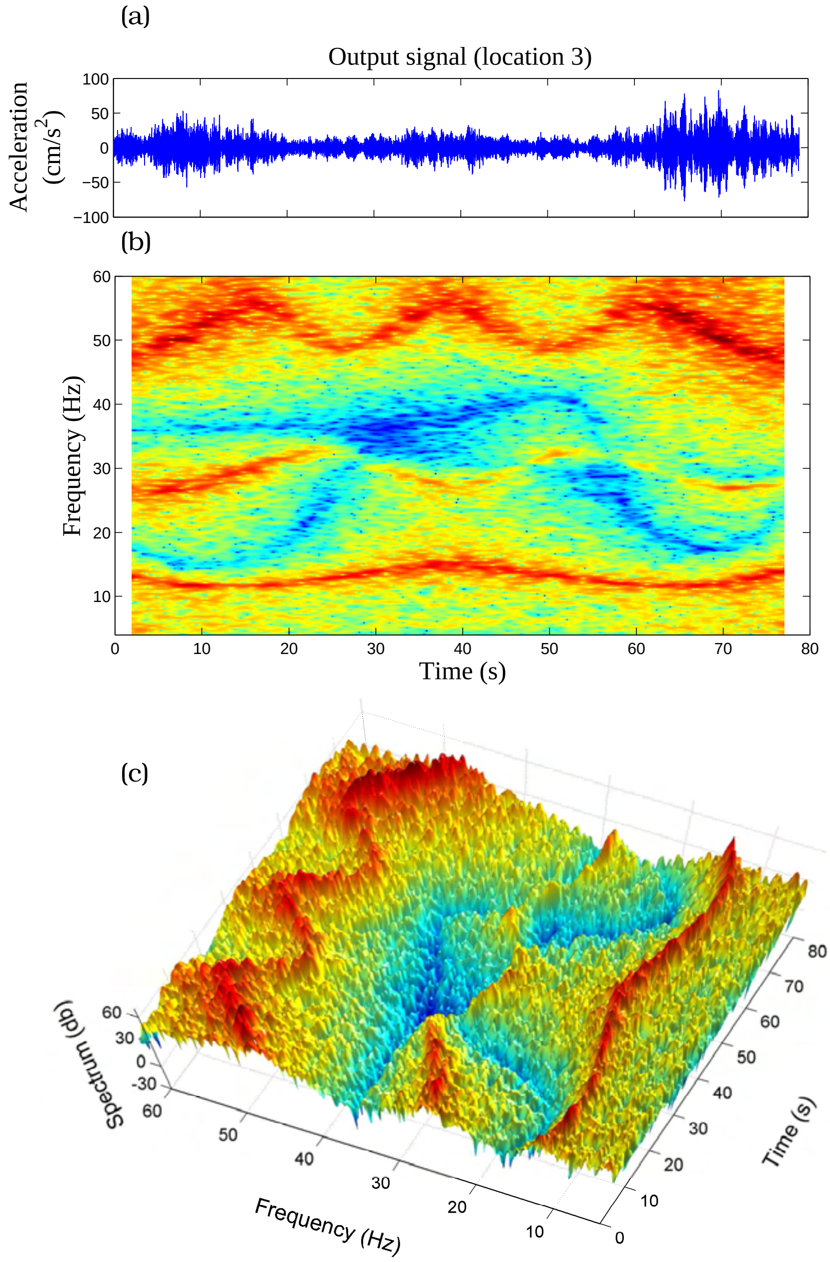

Figure 2.3: The non-stationary vibration response and preliminary analysis: (a) The vibration response signal (sampling frequency $f_s = 128$ Hz, signal length $N = 10,113$ samples or 79.0078 s). (b) 2D plot of the non-parametrically obtained TV PSD estimate (STFT employing a 512-sample-long moving Hamming data window advanced by one sample each time). (c) 3D plot of the non-parametrically obtained TV PSD estimate.

In the FS-TARMA case functional bases spanned by trigonometric functions of the form

$$G_0[t] = 1, \quad G_{2k-1}[t] = \sin\left(\frac{k\pi(t-1)}{N-1}\right), \quad G_{2k}[t] = \cos\left(\frac{k\pi(t-1)}{N-1}\right),$$

with $t = 1, \ldots, N$ and $k = 1, 2, \ldots$ are employed. Their selection is motivated by the non-parametric estimates of Figs. 2.3(b) and 2.3(c). Model order selection is achieved using phase I of the search scheme described in Section 2.4.2, the BIC, and an extended and complete functional subspace of dimensionality 21 ($p_a = p_c = p_s = 21$). An FS-TARMA$(8,8)_{[21,21,21]}$ model is thus initially selected as adequate (see Fig. 2.5(a)). Functional subspace selection is subsequently pursued based on phase II and the APD criterion

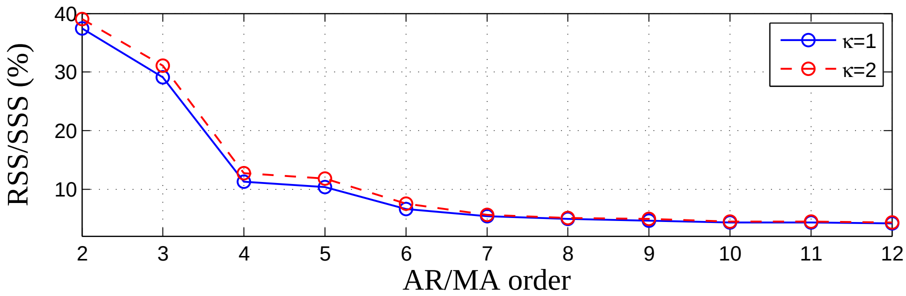

Figure 2.4: SP-TARMA model structure selection. AR/MA order and smoothness constraints order selection based on the RSS/SSS function.

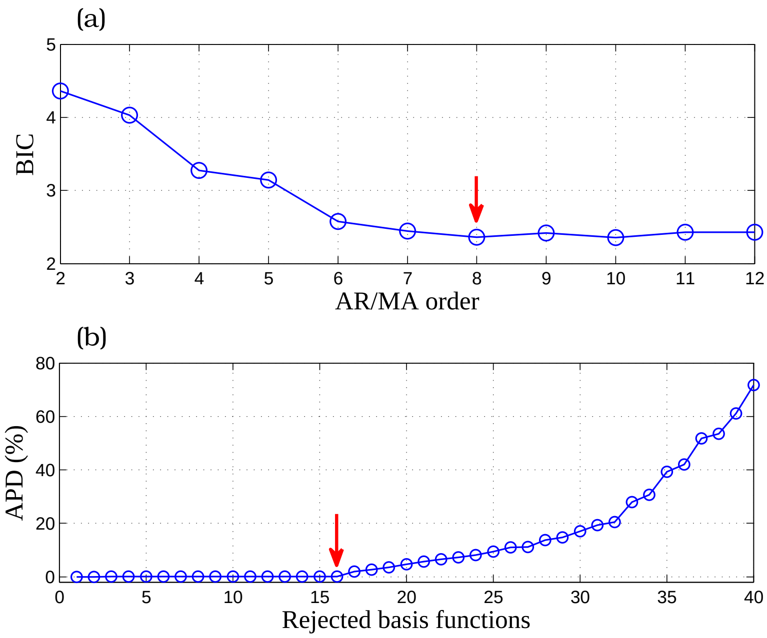

Figure 2.5: FS-TARMA model structure selection: (a) AR/MA order selection based on the BIC using an extended and complete functional subspace ($p_a = p_c = p_s = 21$). (b) Combined AR/MA functional subspace selection. APD values obtained by iteratively rejecting the least significant basis function versus the number of rejected functions. The model just before the first significant increment is selected (16 functions are presently rejected and 26 are maintained in the AR/MA subspaces).

combined with the backward procedure. This leads to the AR/MA functional subspaces (Fig. 2.5(b))

$$\mathcal{F}_{AR} = \{G_0[t], \ldots, G_{10}[t]\}, \qquad \mathcal{F}_{MA} = \{G_0[t], \ldots, G_{14}[t]\},$$

and, similarly, to the innovations variance subspace

$$\mathcal{F}_{\sigma_e^2} = \{G_0[t], \ldots, G_6[t], G_8[t], G_9[t], G_{10}[t], G_{12}[t], G_{13}[t], G_{14}[t], G_{17}[t], G_{19}[t]\}.$$

Hence an FS-TARMA$(8, 8)_{[11,15,15]}$ model is finally selected (further details in [Poulimenos and Fassois, 2009a]).

The three identified TARMA models are validated, whereas their characteristics are summarized in Table 2.3.

The obtained RSS normalized by the series sum of squares (RSS/SSS) and the negative log-likelihood function of the estimated TARMA models are depicted in Fig. 2.6(a). Indicative one-step-ahead signal predictions obtained by the estimated TARMA models are (for a short time segment of the signal) compared to the actual signal values in Fig. 2.6(b). It is observed that all methods provide more or less good

Table 2.3: Identification methods, their characteristics, and the identified models.

Model Class	Identification Method	Method Characteristics	Identified Model
Unstructured Parameter Evolution	RML-TARMA	$\lambda = 0.9905$ $\alpha = 10^4$	UPE-TARMA$(8,8)$
Stochastic Parameter Evolution	SP-TARMA	$\nu = 2.757 \times 10^{-11}$ $\alpha = 10^4$	SP-TARMA$(8,8)_{\kappa=2}$
Deterministic Parameter Evolution	FS-TARMA	Prediction error method Gauss-Newton optimization	FS-TARMA$(8,8)_{[11,15,15]}$

predictions, with the FS-TARMA model achieving the best prediction accuracy (RSS/SSS= 3.255%), followed by the RML-estimated UPE-TARMA model, and, finally, the SP-TARMA model. It should be mentioned that the RSS/SSS and negative log-likelihood function for the SP-TARMA$(8,8)$ model may be reduced somewhat (to 4.893 and 2.336×10^4, respectively) when using first order ($\kappa = 1$) smoothness priors constraints. As already mentioned, this model is nevertheless not selected, as the corresponding natural frequency estimates and the TV PSD exhibit higher variability.

The residual variance estimates for the three TARMA models are compared in Fig. 2.6(c), in which the baseline model innovations variance (although not directly comparable; description in the next paragraph) is presented as well. As it may observed, the FS-TARMA model provides, almost uniformly, the lowest variance, followed by the UPE-TARMA, and finally the SP-TARMA model.

Frozen-configuration baseline identification

In order to establish an additional basis for judging identification accuracy, a space-discretized version of the structure's frozen-configuration representation is obtained by "freezing" the mass at $M = 120$ equispaced locations and performing an equal number of *stationary* experiments. The stationary vibration response at location 3 on the beam is, in each case, obtained ($f_s = 128$ Hz, signal length $N = 3,962$ samples) and a conventional (stationary) ARMA model is identified by using the linear multi stage (LMS) estimation method [Fassois, 2001a] and maximum-likelihood (ML) refinement [Ljung, 1999, pp. 216-217]. This leads to $M = 120$ ARMA$(8,8)$ models which constitute what is henceforth referred to as the *baseline* (frozen-configuration) representation of the structure.

2.7 Model-Based Dynamic Analysis Results

The TV structural dynamics are now recovered based on the identified models. The vibration response signal's frozen-time PSD is obtained as

$$S(\omega, t) = \left| \frac{1 + \sum_{i=1}^{n_c} c_i[t] e^{-j\omega T_s i}}{1 + \sum_{i=1}^{n_a} a_i[t] e^{-j\omega T_s i}} \right|^2 \sigma_e^2[t], \tag{2.21}$$

with the model parameters and innovations variance being replaced by their respective estimates, ω designating frequency in rad/s, T_s the sampling period in s, and j the imaginary unit. The system's frozen-time natural frequencies and damping ratios are computed as

$$\omega_{ni}[t] = \frac{\left|\ln \lambda_i[t]\right|}{T_s} \quad \text{(rad/s)}, \qquad \text{and} \qquad \zeta_i[t] = -\cos\bigl(\arg(\ln \lambda_i[t])\bigr) \tag{2.22}$$

respectively, with $\lambda_i[t]$ designating the i-th TV frozen model pole. The antiresonance natural frequencies and damping ratios are similarly obtained from the frozen model zeros.

The frozen-time PSD estimates corresponding to the three estimated TARMA$(8,8)$ models are contrasted to that obtained from the frozen-configuration baseline modelling in Fig. 2.7. Obviously, all TARMA PSD estimates are in good overall agreement with their baseline counterpart. Yet, smoother, and also clear and informative, estimates are obtained based on the FS-TARMA and SP-TARMA models.

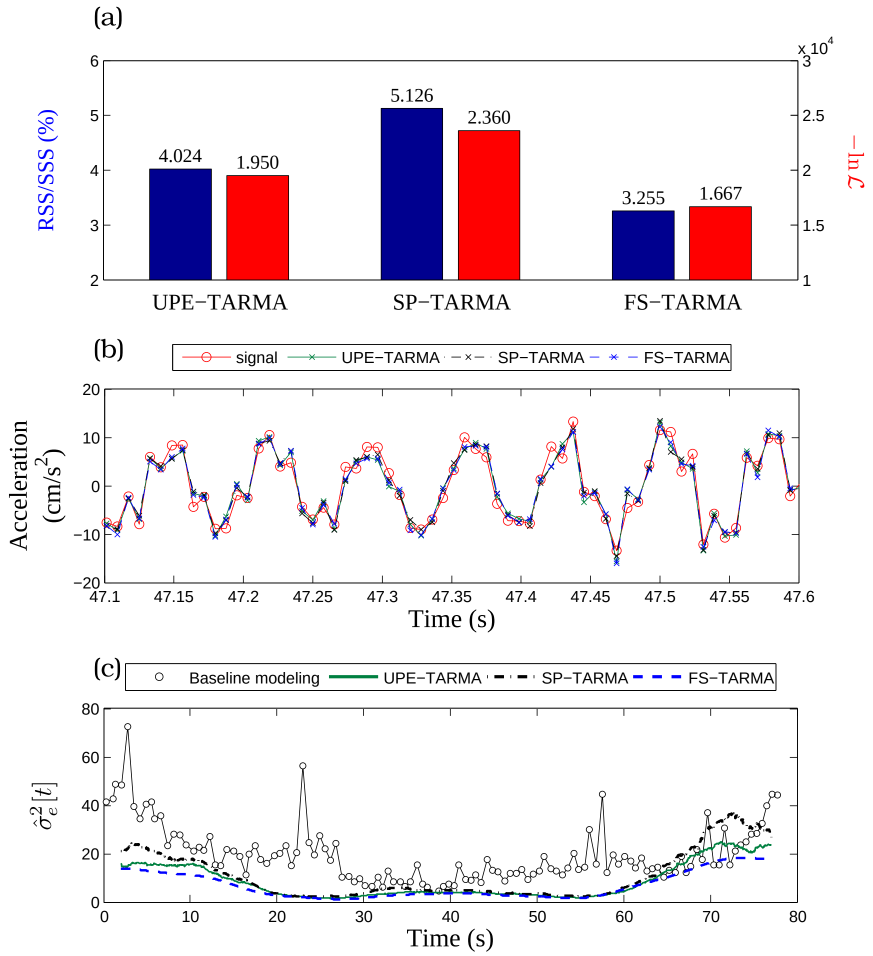

Figure 2.6: Comparative TARMA identification results. (a) The RSS/SSS and the negative log-likelihood function for the estimated TARMA models. (b) Segment of the vibration response signal and TARMA-based one-step-ahead predictions. (c) The residual variance for the estimated TARMA models (although not directly comparable, the “frozen-configuration” innovations variance is also provided).

On the other hand, the estimate obtained based on the UPE-TARMA model exhibits significantly more scatter.

Figure 2.8 depicts the structure’s TV natural frequency estimates along with their baseline model counterparts. Note that non-parametric PSD estimates (Welch-based; 512-sample-long Hamming data window) obtained during baseline identification by using the 120 measured signals are also shown in the background.

The UPE-TARMA estimates track their baseline counterparts adequately well, although with some scatter observed for the second and third natural frequency trajectories. On the other hand, the SP-TARMA estimates appear unable of tracking the second natural frequency during the last 30 s. This is probably due to pole-zero cancellations occurring. A possible remedy could be the increase of the model order to 10 or higher. Such an action, though, introduces false (computational) modes in the time-frequency plane (see Fig. 2.9) which are characterized by damping ratios smaller than 10% and being difficult to distinguish from the true modes. Finally, the excellent tracking of the natural frequencies achieved by the FS-TARMA estimates is certainly worth noting.

Similar comments may be made for the estimated frozen-time antiresonance natural frequencies (Fig. 2.10). The SP-TARMA based estimates seem unable of tracking the evolution of their baseline counterparts for significant periods of time, in contrast to the UPE-TARMA based estimates which exhibit a good overall agreement with them, but also significant scatter. On the other hand, the FS-TARMA based

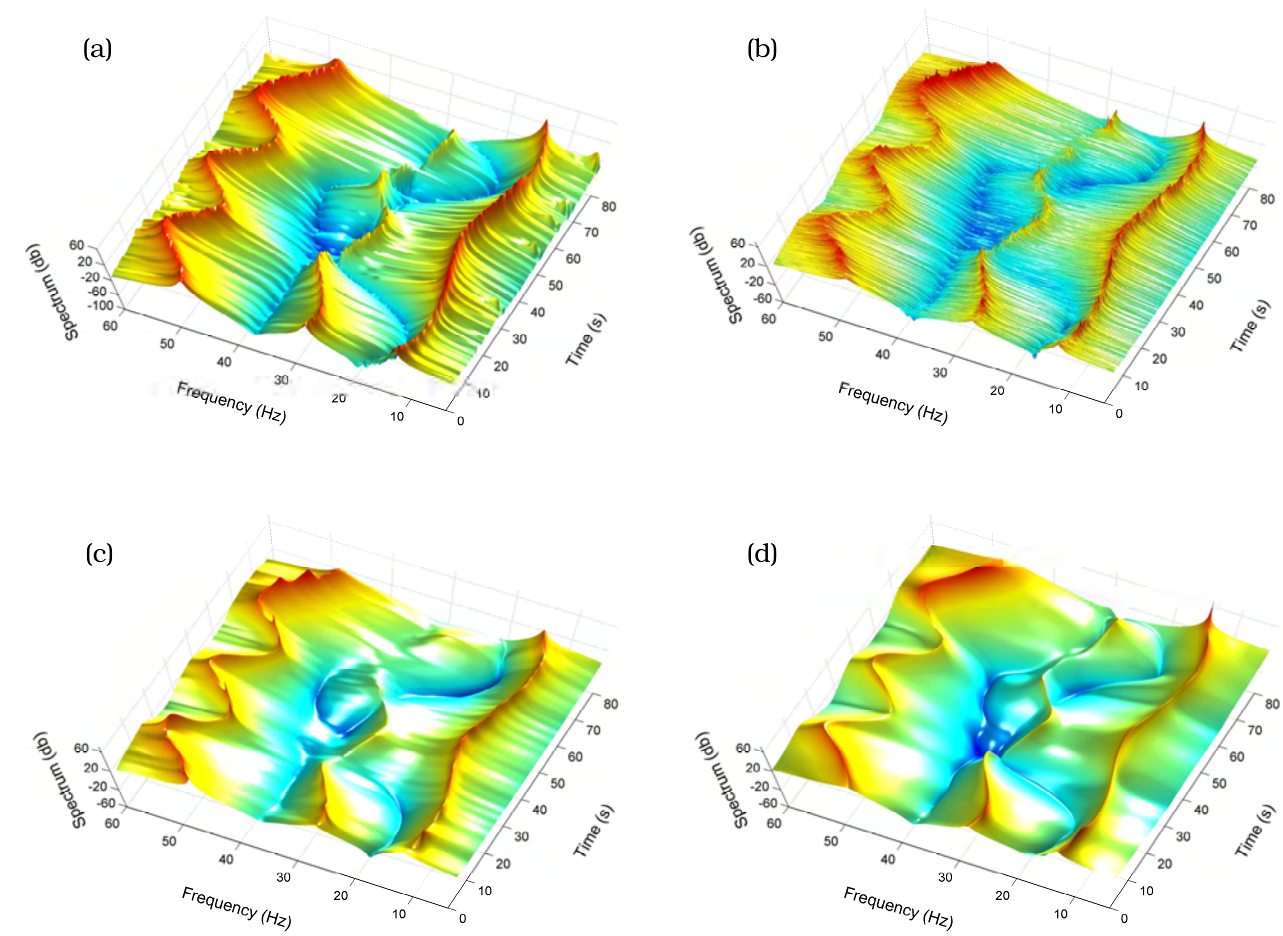

Figure 2.7: Comparison of TV PSD estimates. (a) The "frozen-configuration" baseline estimate. (b) The UPE-TARMA$(8, 8)$ estimate. (c) The SP-TARMA$(8, 8)_{\kappa=2}$ estimate. (d) The FS-TARMA$(8, 8)_{[11,15,15]}$ estimate.

estimates clearly exhibit the best performance (Welch-based non-parametric PSD estimates obtained during baseline identification are also shown in the background).

2.8 Conclusions

An overview and comparative assessment of parametric TARMA methods for the identification and model-based analysis of TV structures under unobservable excitation was presented. The methods were classified according to the mathematical structure imposed on the TV parameter evolution as unstructured parameter evolution, stochastic parameter evolution, and deterministic parameter evolution. A representative identification method (RML-TARMA, SP-TARMA, FS-TARMA) from each class was outlined.

The performance characteristics of the three classes of methods were examined through their application to the problem of identification and model-based dynamic analysis of a laboratory TV (continuously variable configuration) structure consisting of a beam with a mass moving on it. The frozen-configuration (baseline) characteristics of the structure were also extracted and used as an additional basis of comparison.

The three methods were compared to each other in terms of achievable prediction accuracy and model-based analysis. Although the TV structure used is characterized by relatively slowly varying dynamics, the best performance characteristics were achieved by the FS-TARMA method, followed by the RML-TARMA and, finally, the SP-TARMA method. This is also true for the model-based dynamics, including the resonance and antiresonance natural frequencies and the TV PSD of the vibration response,

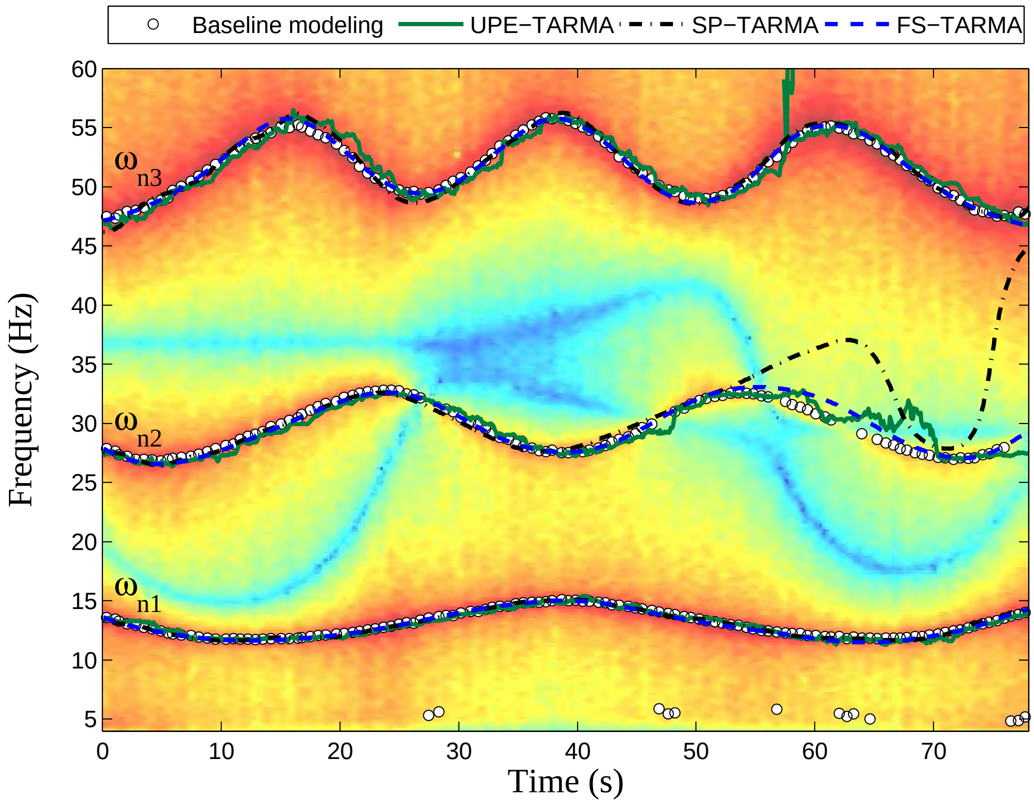

Figure 2.8: Comparison of TV natural frequency estimates. The UPE-TARMA, SP-TARMA, and FS-TARMA based estimates are plotted against the "frozen-configuration" baseline estimates (baseline Welch-based PSD estimates are shown in the background).

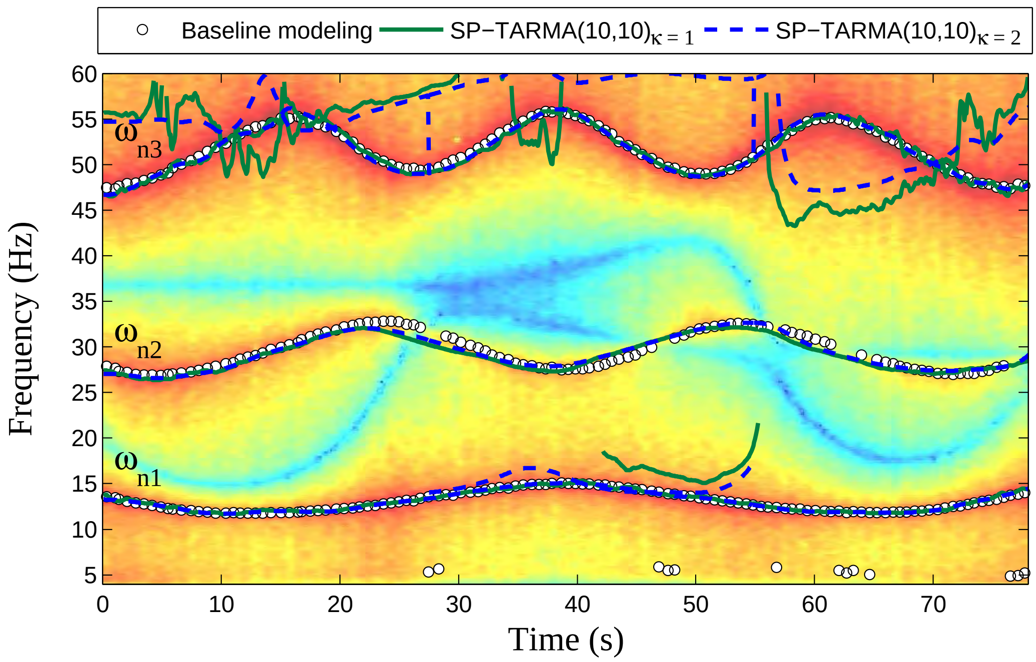

Figure 2.9: Comparison of the SP-TARMA$(10, 10)$ based natural frequency estimates against the "frozen-configuration" baseline estimates (baseline Welch-based PSD estimates are shown in the background).

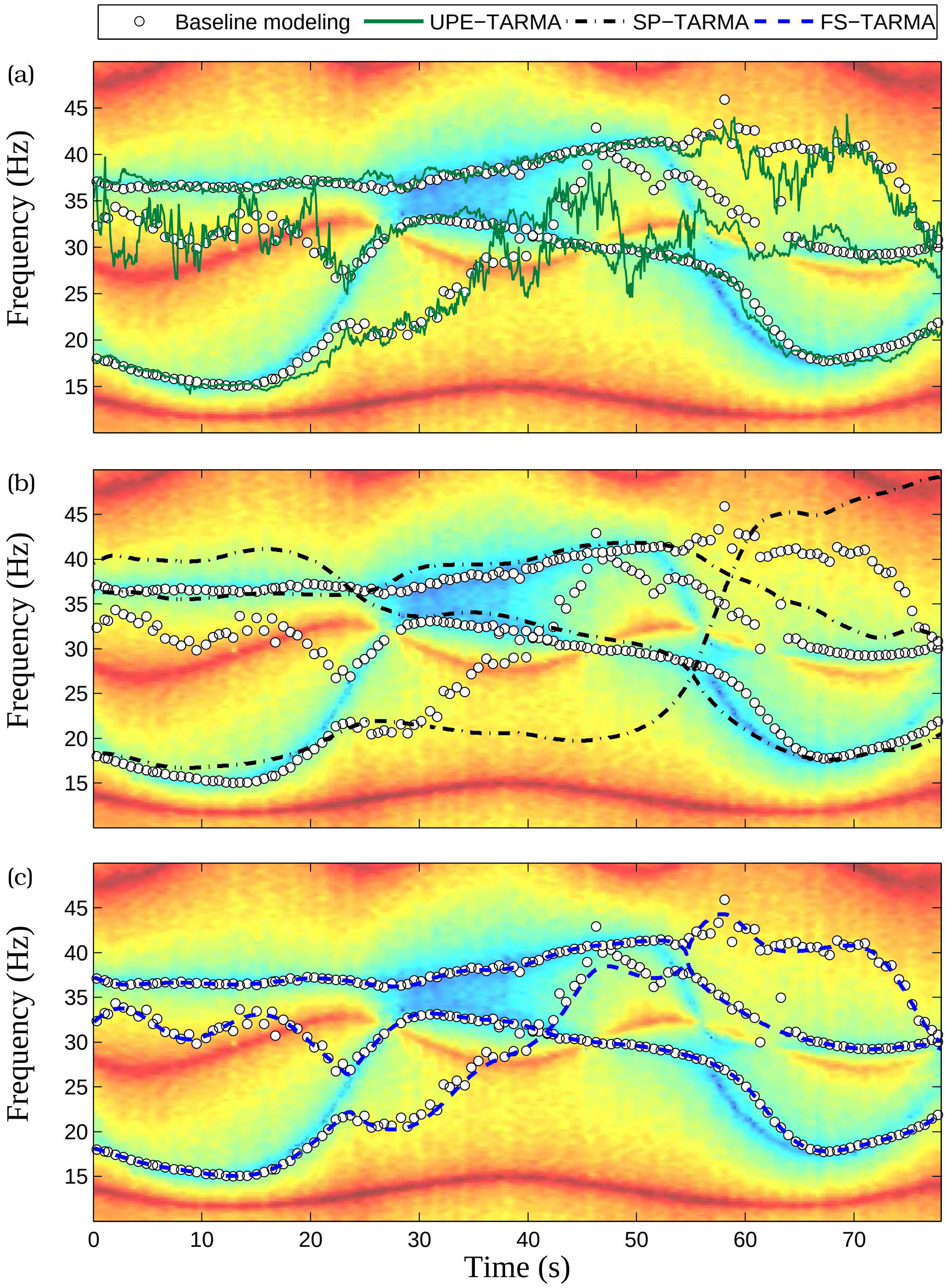

Figure 2.10: Comparison of TV antiresonance natural frequency estimates. (a) The UPE-TARMA, (b) SP-TARMA, and (c) FS-TARMA based estimates plotted against the “frozen-configuration” baseline estimates (baseline Welch-based PSD estimates are shown in the background).

that were most accurately captured by the FS-TARMA method. These results came as no surprise, and, reveal good identification performance, owing to the deterministic nature of the time variation in the structural dynamics which is best reflected in the FS-TARMA models. Overall, the results demonstrate the parametric methods’ applicability, effectiveness, and high potential for parsimonious and accurate identification and dynamic analysis of TV structures under unobservable excitation.

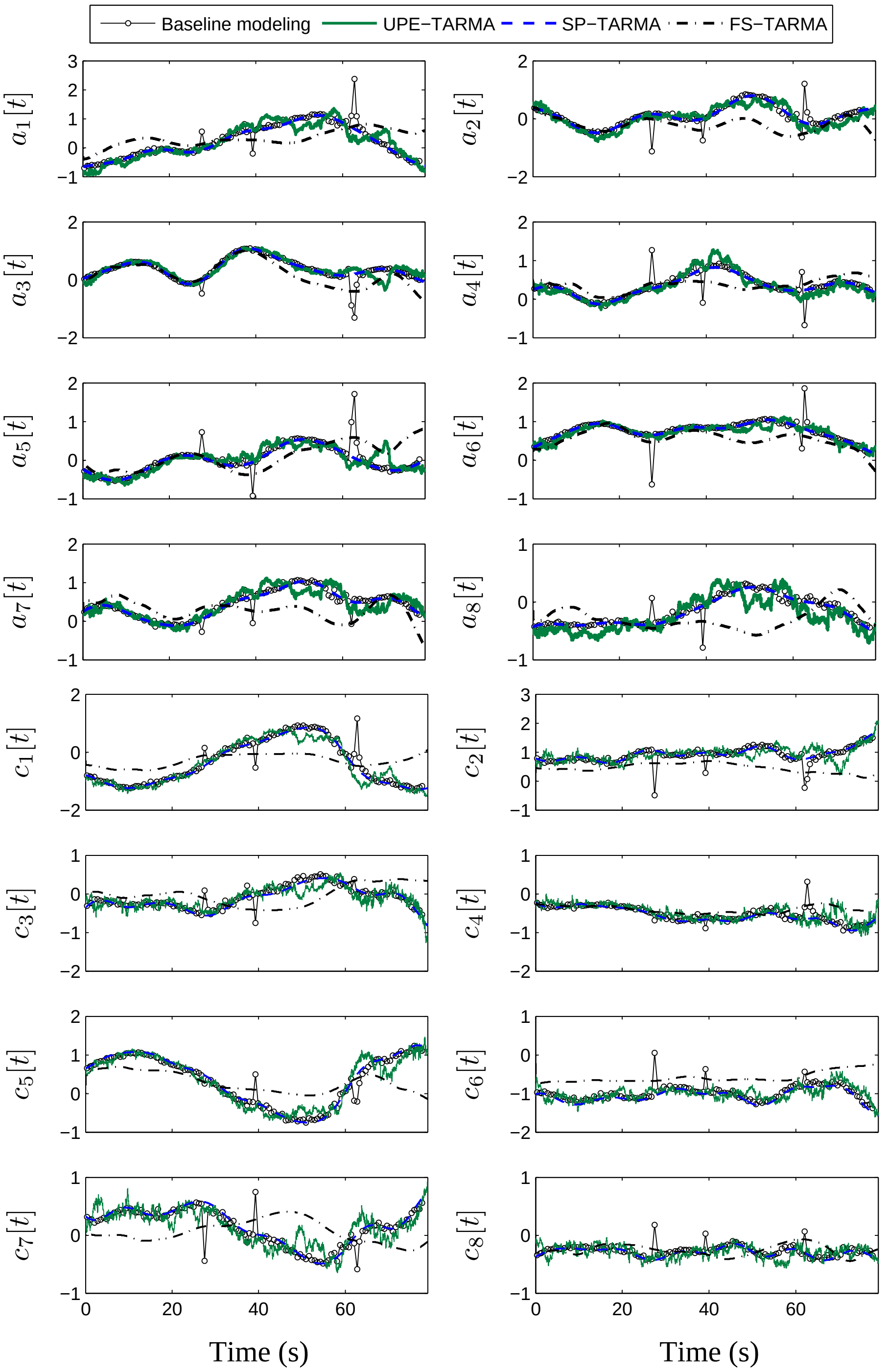

Figure 2.A.1: Comparison of TV AR and MA parameters. The UPE-TARMA, SP-TARMA, and FS-TARMA based estimates are plotted against the "frozen-configuration" baseline estimates.

Appendix 2.A Additional Identification Results

The TARMA$(8,8)$ models parameters estimated through the UPE-TARMA, SP-TARMA and FS-TARMA methods are illustrated along with the corresponding "frozen-configuration" baseline model counterparts in Fig. 2.A.1 (the "time" axis is derived from the correspondence between time and mass position).

It may be noted that the estimated AR parameters are grossly similar in terms of their trajectories while some differences are evident for the parameters of the MA polynomial. However, both AR and MA parameters of the identified models depict comparable variability it terms of their amplitude and

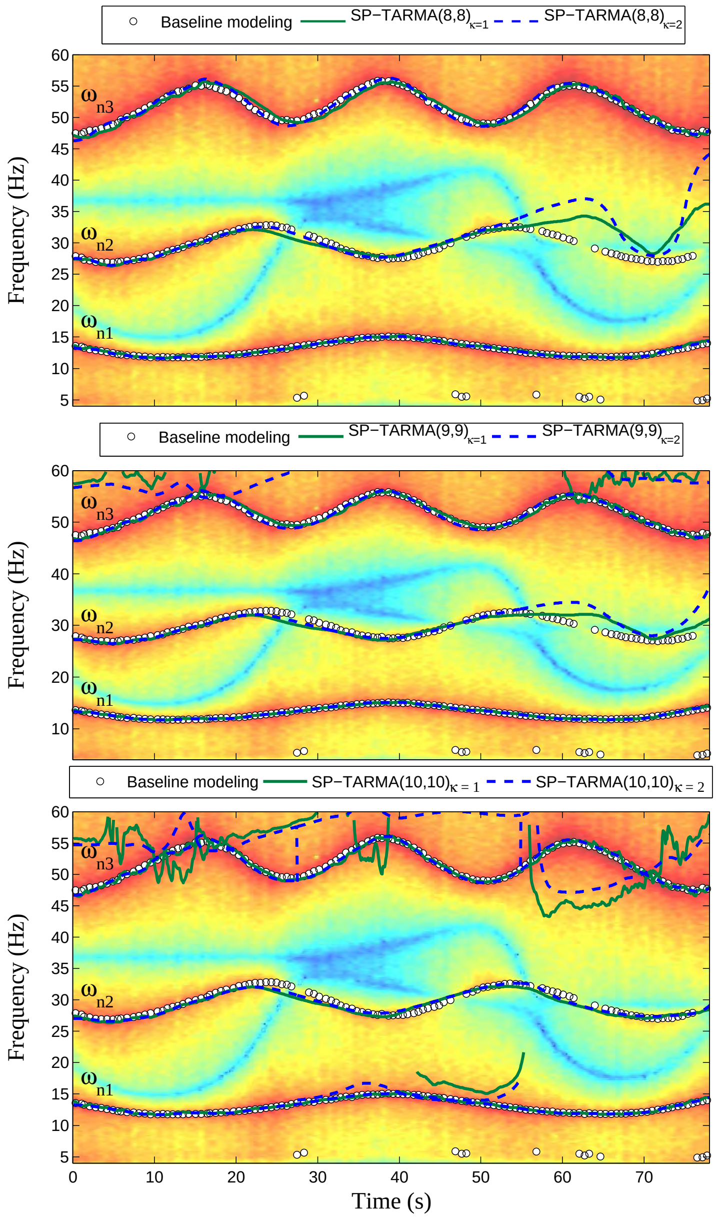

Figure 2.B.1: Comparison of the SP-TARMA$(8, 8)$, SP-TARMA$(9, 9)$, and SP-TARMA$(10, 10)$ based natural frequency estimates against the "frozen-configuration" baseline estimates ($\kappa = 1$ and $\kappa = 2$; baseline Welch-based PSD estimates are shown in the background).

frequency content while only the UPE-TARMA based estimates are shown to be characterized by high frequency variability.

Appendix 2.B Additional Model-Based Dynamic Analysis Results

2.B.1 SP-TARMA based natural frequency estimates

The SP-TARMA based natural frequency estimates are compared against the "frozen-configuration" baseline estimates for $\kappa = 1, 2$ and AR/MA orders $n_a = n_c = 8, 9, 10$ in Fig. 2.B.1. It may be noted, that even if the SP-TARMA$(9, 9)$ and SP-TARMA$(10, 10)$ models provide improved tracking for the second natural frequency, which as already mentioned is the most difficult to track due to pole-zero cancellations that take place after the first 50 s of the experiment, they also introduce spurious modes especially in the higher frequency band (40-60 Hz). Thus, the SP-TARMA$(8, 8)$ is considered more appropriate for the

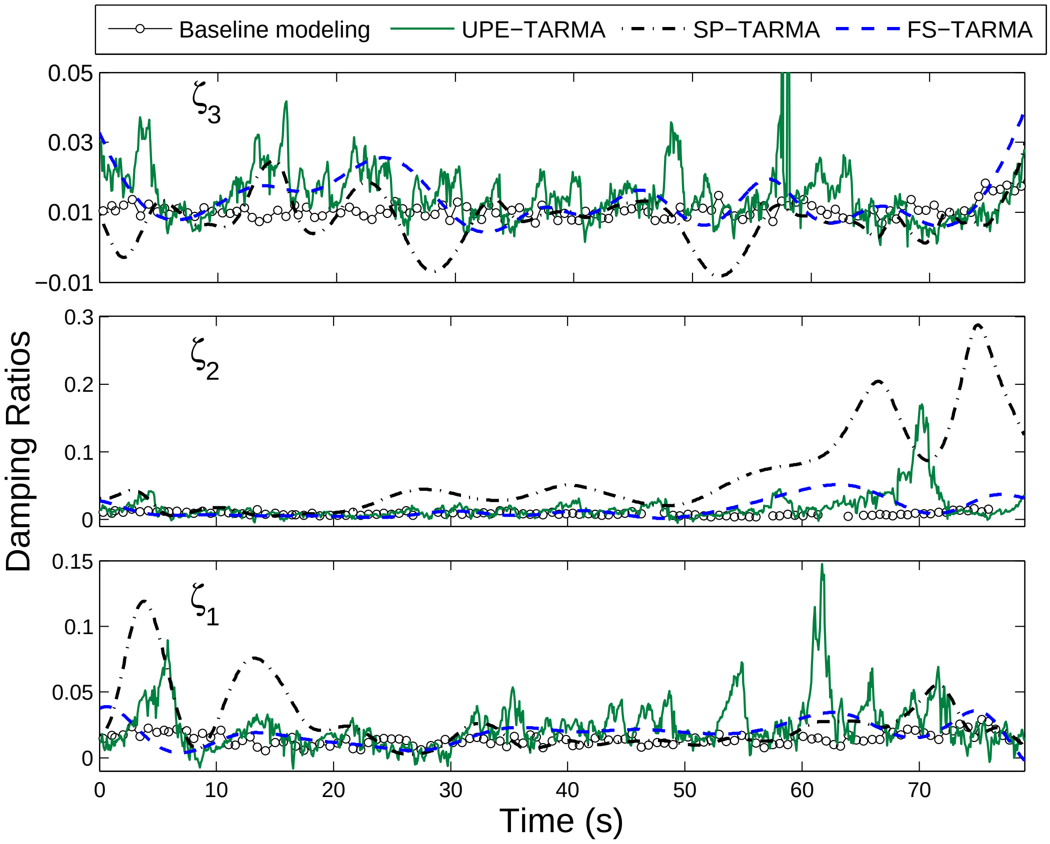

Figure 2.B.2: Comparison of TV damping ratio estimates. The UPE-TARMA, SP-TARMA, and FS-TARMA based estimates are plotted against the "frozen-configuration" baseline estimates.

description of the structural dynamics. At the same time, the increased scatter in the natural frequency estimates that are based on SP-TARMA models with $\kappa = 1$ is apparent in all cases $n_a = n_c = 8, 9, 10$ and thus the SP-TARMA$(8, 8)$ model with $\kappa = 2$ is finally chosen.

2.B.2 Estimated time-dependent damping ratios

The time-dependent "frozen" damping ratio estimates obtained by the TARMA$(8, 8)$ models are contrasted to the "frozen-configuration" baseline modelling counterparts in Fig. 2.B.2. As it may be observed, smooth estimates are obtained based on the FS-TARMA and the SP-TARMA models. However, particularly the SP-TARMA based estimates depict high variability not in accordance with the "frozen-configuration" baseline model estimates which exhibit only small variability. This inconsistency is even more pronounced in the case of the UPE-TARMA estimates.

Chapter 3

Parametric Identification of a Time-Varying Structure Based on Vector Vibration Response Measurements

The problem of parametric output-only identification of a time-varying structure based on vector random vibration signal measurements is considered in this chapter. A Functional Series Vector Time-dependent AutoRegressive Moving Average (FS-VTARMA) method is introduced and employed for the identification of a "bridge-like" laboratory structure consisting of a beam and a moving mass. The identification is based on three simultaneously measured vibration response signals obtained during a single experiment. The method is judged against baseline modelling based on multiple "frozen-configuration" stationary experiments, and is shown to be effective and capable of accurately tracking the dynamics. Additional comparisons with a recursive Pseudo-Linear Regression VTARMA (PLR-VTARMA) method and a Short Time Stochastic Subspace Identification (ST-SSI) method are made and demonstrate the method's superior achievable accuracy and model parsimony.

3.1 Introduction

Many engineering structures, such as traffic-excited bridges [Li et al., 2003, Garibaldi and Marchesiello, 2006], cranes [Kullaa, 2004], robotic devices and flexible mechanisms [Petsounis and Fassois, 2000, Zhou et al., 2007], rotating machinery [Ouyang, 2007, Zhan et al., 2006], variable geometry aerospace structures [Senba and Furuya, 2008] and so on, exhibit characteristics that vary with time. These structures are referred to as *time-varying* (TV) or *non-stationary*. Structures with variability due to changing geometric configuration form an important subclass of TV structures. In case that the geometric configuration changes continuously with time, the term *continuously variable configuration* structure is used. Robotic devices, cranes, and deployable structures constitute primary examples of this subclass.

The problem of TV structural identification involves the determination of a mathematical model representing the underlying time-varying dynamics based on excitation and/or vibration response signals. In contrast to Time-Invariant (TI) structures, which produce *stationary* vibration responses with time-invariant statistical characteristics, the responses of TV structures are *non-stationary*, characterized by time-dependent statistical characteristics [Poulimenos and Fassois, 2006], [Niedźwiecki, 2000, pp. 52-55]. TV structural identification thus is a rather complicated issue, in which non-stationary signal analysis techniques need to be employed [Poulimenos and Fassois, 2006, Niedźwiecki, 2000, Conforto and D'Alessio, 1999b, Liu and Deng, 2006].

In many occasions, such as in railway bridges, aircraft, surface vehicles and so on, controlled testing may not be feasible under realistic operating conditions, so that structural identification is pursued by exclusively using measured vibration response signals. This is the *output-only TV identification problem* which is in the focus of the present study.

Output-only TV structural identification methods are classified as *non-parametric* or *parametric*. The former are based on non-parametric representations of the non-stationary response as a simultaneous function of time and frequency (*time-frequency representations*). The Short Time Fourier Transform (STFT) [Hammond and White, 1996], the Cohen class of distributions [Cohen, 1995], and wavelet based methods [Ghanem and Romeo, 2000] constitute some of the main and most frequently used methods. Non-parametric methods are easy to use, but lack in terms of representation parsimony (economy), frequency resolution, tracking accuracy – especially in cases of fast variations in the dynamics – and flexibility in analysis [Petsounis and Fassois, 2000, Poulimenos and Fassois, 2006, Conforto and D'Alessio, 1999b].

Parametric methods are based on Time-dependent AutoRegressive Moving Average (TARMA) and time-dependent state space models which may be thought of as conceptual extensions of their conventional, stationary, counterparts, in that their parameters are time-dependent (for instance see [Poulimenos and Fassois, 2006, Niedźwiecki, 2000]). Parametric models and the corresponding identification methods may be further classified according to the type of mathematical structure imposed on the evolution of the time-varying model parameters as *unstructured*, *stochastic*, or *deterministic* parameter evolution. The reader is referred to the recent survey by Poulimenos and Fassois [Poulimenos and Fassois, 2006] for a detailed account and assessment of various parametric methods.

The majority of parametric TV structural identification methods are limited to the simple *single* vibration response signal (univariate) case. Although the *multiple* vibration response (vector or multivariate) case is much more important from a practical standpoint, it has thus far received limited attention. Yet, vector identification can lead to much more complete descriptions, reduced data acquisition and processing times, improved data set "consistency", and also improved modal parameter accuracy [Fassois, 2001b].

The majority of available vector parametric output-only methods are of the *unstructured parameter evolution* type, which imposes no mathematical structure upon the evolution of their time-varying parameters. Kirkegaard *et al.* [Kirkegaard et al., 1996] use Recursive Vector TARMA models for the identification of the TV parameters of a simulated reinforced concrete structure under earthquake excitation. A similar identification problem is considered by Yang *et al.* [Yang and Lin, 2005, Yang et al., 2007], who use recursive least squares estimation based on the physical model of the structure and adaptive forgetting factors. Various recursive and short time subspace methods have been also used for vector TV structural identification over the last decade. Although most of them have been limited to the analysis of simulated TV structures (for instance [Shi et al., 2007, Kameyama and Ohsumi, 2007]), Goethals *et al.* [Goethals et al., 2004] and Mevel *et al.* [Mevel et al., 2005] use a recursive and a short time subspace method, respectively, in order to track the time-varying modal characteristics of an aircraft during flutter vibration. Bosse *et al.* [Bosse et al., 1998] consider the identification of a TV truss structure via a recursive subspace based algorithm. A subspace method is also utilized by Liu and Deng [Liu and Deng, 2006] in order to capture the TV dynamics of an axially moving cantilever beam. In contrast to the previously mentioned studies, their analysis requires a significant number of signal realizations (and thus experiments). It should be additionally remarked that unstructured parameter evolution methods may not be suitable for fast varying structures, while also achieving low representation parsimony (economy).

Noticeably fewer studies are available on vector TV structural identification using *stochastic parameter evolution methods*, which impose stochastic mathematical structure upon the evolution of the time-varying model parameters through stochastic smoothness constraints. Kitagawa et al. [Kitagawa and Gersch, 1996, pp. 172-174], [Jiang and Kitagawa, 1993] use such methods for the modelling and analysis of earthquake ground motion signals, while the modelling of wind speed time histories is considered by Chen [Chen, 2005]. Stochastic parameter evolution methods have also been used for the identification of structural variations of a bridge under construction and varying operating conditions [Omenzetter and Brownjohn, 2006], as well as for the identification, analysis and health monitoring of gearboxes [Zhan and Jardine, 2005a, Zhan and Jardine, 2005b]. Stochastic parameter evolution methods may offer improvements in accuracy and tracking over the unstructured parameter evolution methods, but model parsimony remains an issue.

The class of *deterministic parameter evolution methods* is known to offer a number of advantages and improved accuracy and model parsimony in the single signal (univariate) case [Poulimenos and Fassois, 2006], yet it has not been thus far used for vector TV structural identification. These methods impose deterministic evolution on the model parameters by postulating them as deterministic functions of time belonging to specific functional subspaces [Poulimenos and Fassois, 2006, Conforto and D'Alessio, 1999b, Poulimenos and Fassois, 2004a, Fouskitakis and Fassois, 2002, Ben Mrad et al., 1998a]. They are often referred to as Functional Series TARMA (FS-TARMA) methods, and are physically motivated by the fact that the underlying structural dynamics often change with time in a smooth, deterministic, fashion. In a broader context, the subclass of Functional Series Vector Time-dependent Autoregressive (FS-VTAR) models has been used by Gersch and Kitagawa [Gersch and Kitagawa, 1982] and Sato *et al.* [Sato et al., 2007] for the modelling and analysis of econometric and biomedical time series, respectively. Nevertheless, full FS-VTARMA models have not been previously considered.

This study focuses on the Functional Series Vector TARMA (FS-VTARMA) modelling of TV structural dynamics by using response-only (output-only) measurements. The specific *goals* of the study are:

(a) The postulation of a vector (multivariate) Functional Series Vector TARMA method for output-only structural dynamics identification. This may be viewed as an extension of the univariate (scalar) method in [Poulimenos and Fassois, 2006], and is complete, providing effective tools for both model parameter estimation and model structure selection.

(b) The application of the method to the output-only identification of a TV (continuously variable configuration) "bridge-like" laboratory structure based on three non-stationary vibration responses. The structure was previously identified via univariate FS-TARMA models [Poulimenos and Fassois, 2009b], which offers the possibility of comparisons with the simpler, single response (univariate) case.

(c) The detailed assessment of the method via critical comparisons against baseline modelling which is based on multiple "frozen-configuration" stationary experiments, as well as against a recursive Pseudo-Linear Regression VTARMA (PLR-VTARMA) [Soderstrom and Stoica, 1989, pp. 328-334]

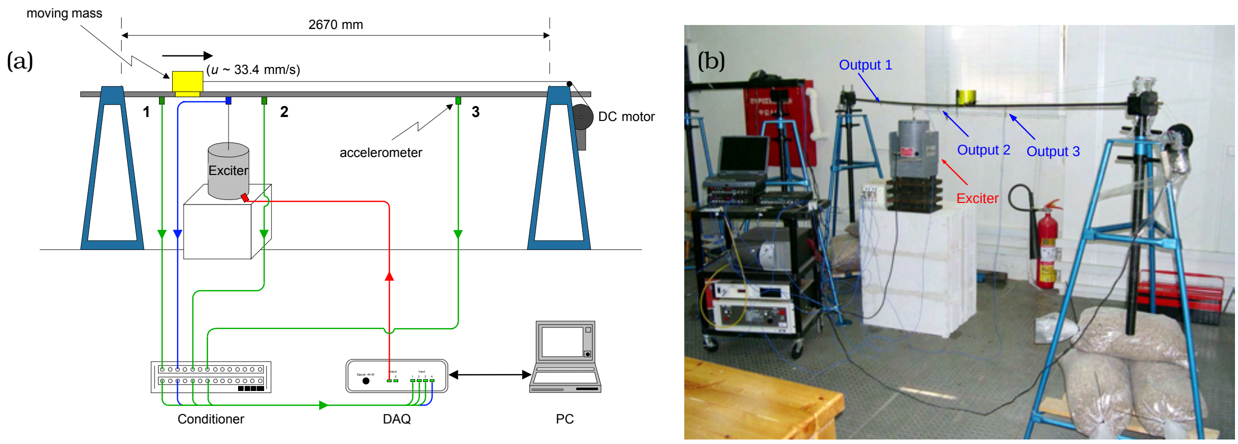

Figure 3.2.1: (a) Schematic diagram, and (b) photo of the TV structure and the experimental setup.

Table 3.1: The main structural characteristics.

Beam				Cylinder		
Length (mm)	Width (mm)	Height (mm)	Mass M (kg)	Radius (mm)	Height (mm)	Mass m (kg)
2670	50	12	13.2	52.5	75	5.2

and a Short Time Stochastic Subspace Identification (ST-SSI) method based on the Canonical Variate Analysis (CVA) algorithm [Overschee and Moor, 1989, pp. 80-81].

The rest of this chapter is organized as follows: The laboratory TV structure, its non-stationary responses, and the determination of the underlying dynamics via multiple “frozen-configuration” stationary experiments (baseline modelling) are presented in Section 3.2. The FS-VTARMA structural identification method, along with brief outlines of the PLR-VTARMA and the ST-SSI methods, is presented in Section 3.3. The identification results and the model based time-varying structural dynamics are presented in Section 3.4, while concluding remarks are summarized in Section 3.5.

3.2 The Laboratory Time-Varying Structure

3.2.1 Description of the structure and the test rig

The laboratory structure is shown in Fig. 3.2.1. It is meant to model a bridge structure with a heavy passing vehicle, and it consists of a fixed-fixed steel beam and a steel cylindrical mass sliding on it, being pulled by a DC motor at a constant speed u. The structure has been used in a recent study by the second author and his co-worker within a univariate (single signal) analysis framework [Poulimenos and Fassois, 2009b]. Its geometry and mass characteristics are summarized in Table 3.1. The structure is clearly time-varying as the ratio of the two masses is significant (m/M = 0.4), while the rate of variation of the dynamics depends upon the selected speed.

In the test rig of Fig. 3.2.1, an electromechanical shaker (MB Dynamics Modal 50A with maximum load of 225 N) equipped with a stinger exerts a vertical zero-mean Gaussian random force excitation to the beam. Lightweight piezoelectric accelerometers (PCB 352A10 ICP accelerometers, frequency range 0.003-10 kHz, sensitivity $\sim$ 1.052 mV/m/s^2, 0.7 gr) are used for the measurement of the resulting vertical random vibration response at three locations (locations 1-3). The measured signals are conditioned and subsequently driven into a SigLab 20-42 data acquisition module (featuring four 20-bit simultaneously sampled A/D channels, two 16-bit D/A channels, and analog 4$^{\text{th}}$-order quasi elliptic anti-aliasing filter).

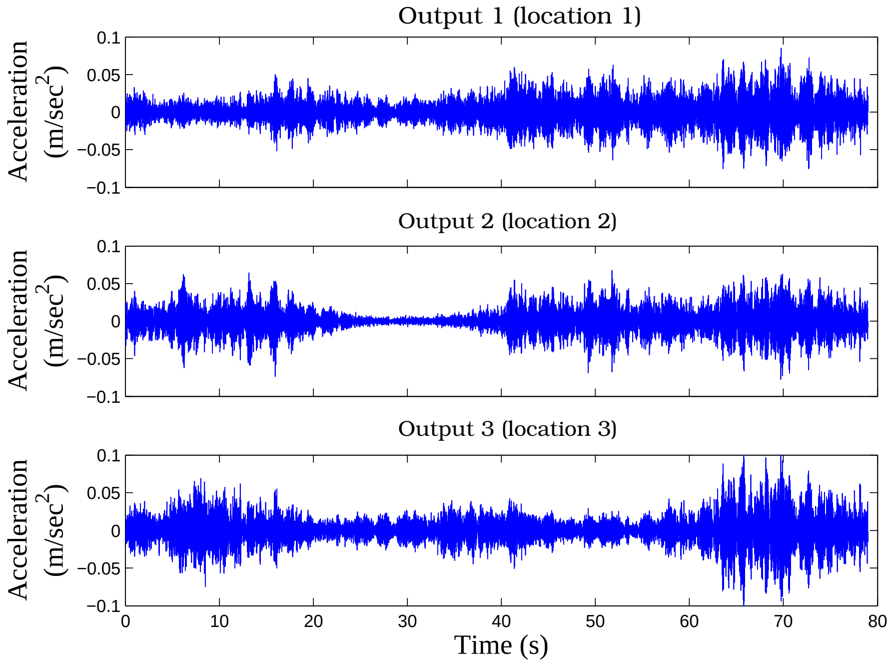

Figure 3.2.2: The non-stationary vibration response signals.

3.2.2 The non-stationary vibration signals and non-parametric analysis

A non-stationary experiment is conducted with the cylindrical mass traversing the beam (from left to right) once, at a constant speed of u=33.4 mm/s. The vertical random vibration (acceleration) signals are 79.0078 s long, sampled at 256 Hz. The study focuses on the 4-60 Hz frequency range (the frequency range of 0-4 Hz is not considered in order to avoid dealing with the exciter nonlinearities). Thus the signals are digitally band-pass filtered (Chebyshev Type I filter; high-pass attenuation 10 dB; low-pass attenuation 30 dB; pass-band ripple 10^{-3} dB) and downsampled to f_s=128 Hz. This produces N=10,113 sample-long versions of the signals.

The obtained signals are depicted in Fig. 3.2.2 and are evidently variance non-stationary. Non-parametric time-frequency analysis based on the sampled continuous Smoothed Pseudo Wigner-Ville (SPWV) distribution [Auger et al., 1996, pp. 69-72] (*tfrspwv* MATLAB function; Blackman data and frequency smoothing windows of 513 samples) yields the time-dependent Power Spectral Density (PSD) matrix $\boldsymbol{S}(\omega, t)$ of Fig. 3.2.3 (ω and t designate frequency and time, respectively). Note that in this figure S_{ii} denotes a diagonal element (the auto spectral density of the i-th response signal), while $S_{ij}(i \neq j)$ denotes an off-diagonal element (the cross spectral density relating the i-th and j-th response signals). The dependence of all spectral densities upon time, and hence the signals non-stationarity, is evident. Moreover, three main time-varying modes of flexural vibration are visible, in the 10-15, 25-35, and 45-55 Hz ranges, respectively.

It should be also noticed from Fig. 3.2.3 that the frequency content of the time-variation of the dynamics is significantly narrower than that of the structural dynamics. Therefore, the structure may, for the particular mass speed of u=33.4 mm/s, be characterized as slowly time-varying.

3.2.3 Baseline modelling of the underlying dynamics via multiple stationary experiments

A TV structure may be associated with an uncountable sequence of TI structures, generated by “freezing” the structure at each time instant. This set of TI structures may be referred to as the *“frozen-time”* representation of the original TV structure. By analogy, a continuously variable configuration structure may be associated with an uncountable sequence of TI structures produced by “freezing” the

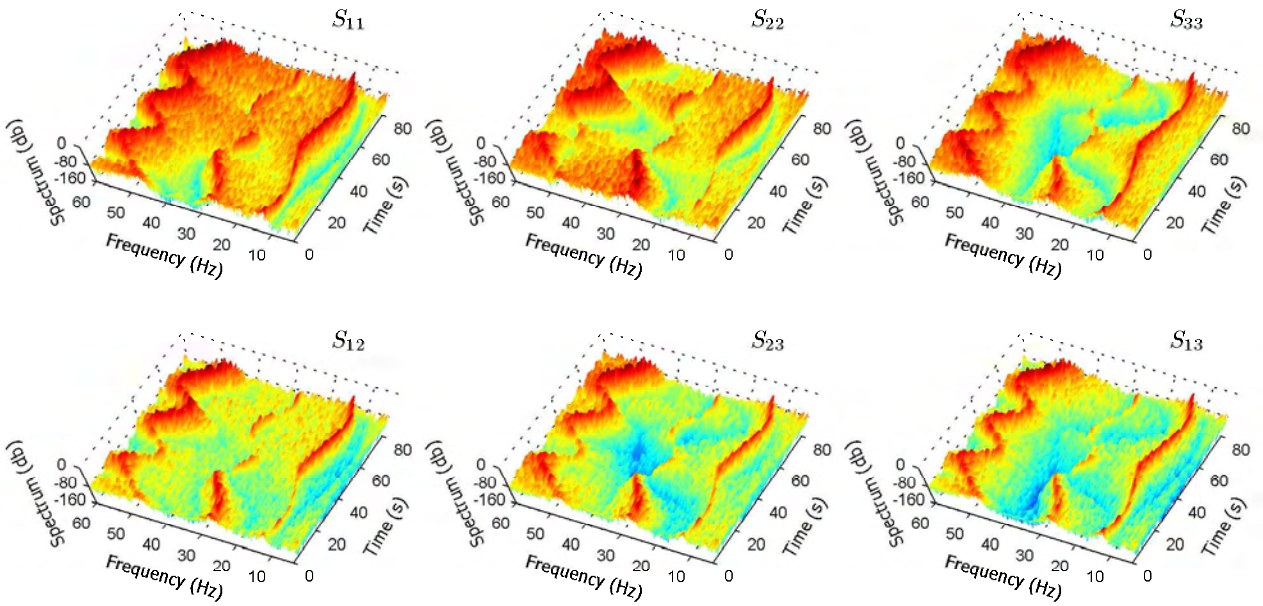

Figure 3.2.3: Non-parametric estimate of the time-dependent PSD matrix: Magnitude of the auto (upper row) and cross (lower row) spectral densities (SPWV method; Blackman time and frequency windows of 513 samples).

configuration (geometrical characteristics) of the structure. This leads to a *"frozen-configuration"* representation of a continuously variable configuration structure. Obviously, for a continuously variable configuration structure characterized by known time-variation of its configuration, "frozen-time" and "frozen-configuration" representations are equivalent (for further details see [Poulimenos and Fassois, 2009b]).

Based on the former observation, and in order to establish a basis for assessing modelling accuracy, the "frozen-configuration" (fixed mass location) structural dynamics are extracted via an exhaustive and accurate, but very time-consuming, baseline modelling procedure. The identification of the baseline model is based on a series of 120 stationary experiments, each one corresponding to distinct and fixed location of the sliding mass. A respective set of 120 stationary trivariate vibration signals (the responses at the three locations) is collected. Similarly to the non-stationary case, these stationary vibration signals are sampled at 256 Hz each one being 28.8438 s long, digitally band-pass filtered in the 4-60 Hz frequency range and downsampled to f_s=128 Hz (final length of N=3,962 samples).

Stationary Vector ARMA (VARMA) [Reinsel, 1993, Papakos and Fassois, 2003] identification is subsequently applied separately to each stationary vector signal. Thus, a sequence of stationary VARMA models, corresponding to the 120 configurations is identified. VARMA parameter estimation is (for a given model order) achieved via the recursive Pseudo-Linear Regression (PLR) estimation method [Soderstrom and Stoica, 1989, pp. 328-334], which is subsequently refined by the off-line Prediction Error (PE) method [Ljung, 1999, pp. 199-203]. Model order estimation is based on minimization of the Bayesian Information Criterion (BIC) [Reinsel, 1993, pp. 92-93].

Model order estimation is achieved via a two-phase procedure:

(i). VARMA(n, n) models for orders $(n = 2, \ldots, 8)$ are estimated, and the proper AR order is selected based on minimization of the BIC criterion (Fig. 3.2.4).

(ii). Following AR order selection, the possibility of MA order reduction is examined in a similar manner.

The VARMA identification procedure leads to a set of 120 VARMA$(4, 4)$ models for representing the dynamics under the various configurations. From this, and the corresponding set of transfer function matrices [Reinsel, 1993, p. 10], the baseline "frozen-configuration" poles and zeros and modal

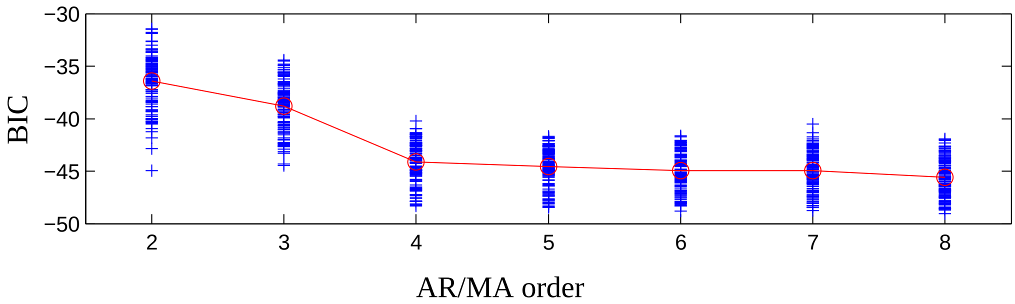

Figure 3.2.4: Baseline VARMA order selection based on minimization of the BIC criterion: BIC values (+) for each AR/MA order considered (120 cases) and their sample means (-o-).

parameters are obtained. The lightly damped (damping ratio < 5%) "frozen-configuration" natural frequency estimates and their corresponding damping ratios are depicted in Fig. 3.2.5 (the "time" axis is derived from the correspondence between time and mass position). As illustrated in Fig. 3.2.5(a) the "frozen-configuration" natural frequency estimates ($\omega_{n1}, \omega_{n2}, \omega_{n3}$; note that the numbering refers to the frequency range considered) coincide with the resonances in the non-stationary SPWV based PSD function $S_{11}(\omega, t)$. Some discontinuities in vibration mode ω_{n2} are probably due to zero-pole cancellations (resonance-antiresonance intersections in Fig. 3.2.3). Furthermore, the initial indication for smooth and periodic curves for the structural time-varying modes obtained from the non-parametrically estimated PSD matrix is confirmed by the "frozen-configuration" natural frequency estimates. On the other hand, the "frozen-configuration" damping ratio estimates (Fig. 3.2.5(b)) exhibit only small variability.

Indicative "frozen-configuration" antiresonant frequency estimates (characterized by damping ratio < 20%) are depicted in Fig. 3.2.6. In particular, the antiresonances corresponding to the elements $(2, 2)$ and $(3, 2)$ of the "frozen-configuration" transfer function matrix are shown in Fig. 3.2.6(a) and (b), respectively.

3.3 Parametric Vector Model Identification Methods

3.3.1 The Functional Series VTARMA model identification method

Functional Series Vector Time-dependent AutoRegressive Moving Average (FS-VTARMA) models constitute conceptual extensions of their conventional (stationary) Vector ARMA counterparts, in that their parameters and the innovations covariance matrix are explicit functions of time, by belonging to functional subspaces spanned by selected functions (*basis functions*). Thus, an FS-VTARMA$(n_a, n_c)_{[p_a,p_c,p_s]}$ model, with n_a, n_c denoting its AutoRegressive (AR) and Moving Average (MA) orders, respectively, p_a, p_c, p_s the AR, MA, and innovations covariance matrix functional basis dimensionalities, respectively, is of the form:

$$\boldsymbol{x}[t] + \sum_{i=1}^{n_a} \boldsymbol{A}_i[t] \cdot \boldsymbol{x}[t-i] \;=\; \boldsymbol{e}[t] + \sum_{i=1}^{n_c} \boldsymbol{C}_i[t] \cdot \boldsymbol{e}[t-i], \qquad \boldsymbol{e}[t] \sim \text{NID}(\boldsymbol{0}, \boldsymbol{\Sigma}[t]) \tag{3.3.1}$$

with t designating normalized discrete time, $\boldsymbol{x}[t]_{(k\times 1)}$ the non-stationary vibration response (vector) signal, and $\boldsymbol{e}[t]_{(k\times 1)}$ the innovations (residual) sequence which is serially uncorrelated and characterized by zero-mean and time-dependent non-singular (and generally non-diagonal) covariance matrix $\boldsymbol{\Sigma}[t]_{(k\times k)}$. $\boldsymbol{A}_i[t]_{(k\times k)}$, $\boldsymbol{C}_i[t]_{(k\times k)}$ are the model's AR and MA time-dependent parameter matrices, respectively, while NID$(\cdot, \cdot)$ stands for Normally Independently Distributed with the indicated mean and covariance.

Using the backshift operator $\mathcal{B}$ ($\mathcal{B}^i \cdot \boldsymbol{x}[t] = \boldsymbol{x}[t-i]$), the VTARMA representation of Eq. (3.3.1) is compactly rewritten as:

$$\boldsymbol{x}[t] + \sum_{i=1}^{n_a} \boldsymbol{A}_i[t] \cdot \mathcal{B}^i \cdot \boldsymbol{x}[t] \;=\; \boldsymbol{e}[t] + \sum_{i=1}^{n_c} \boldsymbol{C}_i[t] \cdot \mathcal{B}^i \cdot \boldsymbol{e}[t] \quad \Longleftrightarrow \quad \boldsymbol{A}[\mathcal{B}, t] \cdot \boldsymbol{x}[t] \;=\; \boldsymbol{C}[\mathcal{B}, t] \cdot \boldsymbol{e}[t], \tag{3.3.2a}$$

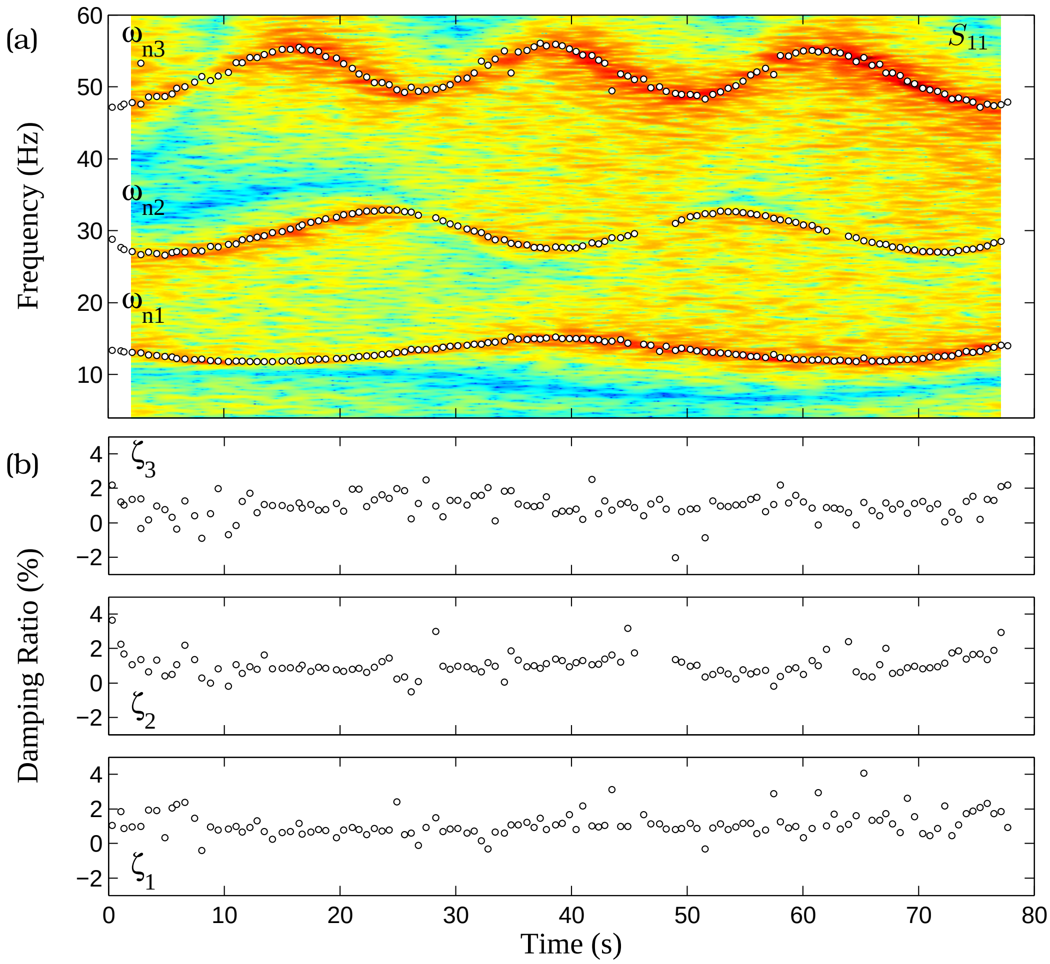

Figure 3.2.5: Baseline "frozen-configuration" VARMA(4, 4) based identification: (a) Natural frequency estimates (○) (only those with damping ratio < 5%) and the $S_{11}(\omega, t)$ SPWV based PSD estimate (background), and, (b) the corresponding damping ratio estimates.

with:

$$\boldsymbol{A}[\mathcal{B}, t] = \boldsymbol{I}_k + \sum_{i=1}^{n_a} \boldsymbol{A}_i[t] \cdot \mathcal{B}^i, \qquad \boldsymbol{C}[\mathcal{B}, t] = \boldsymbol{I}_k + \sum_{i=1}^{n_c} \boldsymbol{C}_i[t] \cdot \mathcal{B}^i, \tag{3.3.2b}$$

designating the AR and MA time-dependent matrix polynomial operators, respectively, while clearly $\boldsymbol{A}_0[t] \equiv \boldsymbol{C}_0[t] \equiv \boldsymbol{I}_k$, with $\boldsymbol{I}_k$ indicating the identity matrix of order k.

The model parameter matrices $\boldsymbol{A}_i[t], \boldsymbol{C}_i[t]$, along with the innovations time-dependent covariance matrix $\boldsymbol{\Sigma}[t]$, belong to functional subspaces with respective bases:

$$\mathcal{F}_{\text{AR}} \triangleq \{ G_{d_a(1)}[t], \ldots, G_{d_a(p_a)}[t] \}, \qquad \mathcal{F}_{\text{MA}} \triangleq \{ G_{d_c(1)}[t], \ldots, G_{d_c(p_c)}[t] \}, \tag{3.3.3a}$$

$$\mathcal{F}_{\boldsymbol{\Sigma}} \triangleq \{ G_{d_s(1)}[t], \ldots, G_{d_s(p_s)}[t] \}, \tag{3.3.3b}$$

where the indices $d_a(i)(i = 1, \ldots, p_a), d_c(i)(i = 1, \ldots, p_c)$, and $d_s(i)(i = 1, \ldots, p_s)$ denote the functions that are included in each basis. These functions may be selected from any properly ordered functional family, including the Chebyshev, Legendre, trigonometric (sine/cosine) and other families. The elements of the time-dependent model parameter matrices, along with the innovations time-dependent covariance matrix, may be thus expressed as:

$$\boldsymbol{A}_i[t]\{a^i_{\ell,m}[t]\} : \; a^i_{\ell,m}[t] = \sum_{j=1}^{p_a} a^{i,j}_{\ell,m} \cdot G_{d_a(j)}[t], \qquad \boldsymbol{C}_i[t]\{c^i_{\ell,m}[t]\} : \; c^i_{\ell,m}[t] = \sum_{j=1}^{p_c} c^{i,j}_{\ell,m} \cdot G_{d_c(j)}[t], \tag{3.3.4a}$$

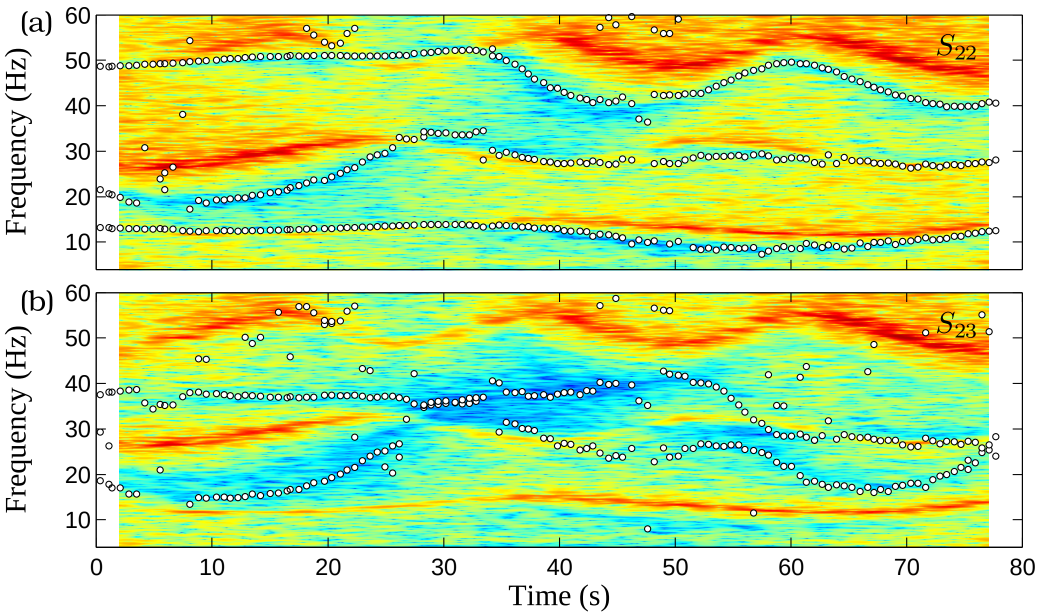

Figure 3.2.6: Baseline “frozen-configuration” VARMA(4, 4) based antiresonant frequency estimates: (a) Antiresonances corresponding to the element (2,2) of the “frozen-configuration” transfer function matrix, and, (b) antiresonances corresponding to the element (3,2) of the “frozen-configuration” transfer function matrix (only those with damping ratio < 20% are depicted; the corresponding elements of the SPWV based PSD matrix estimate are shown in the background).

$$\boldsymbol{\Sigma}[t]\{s_{\ell,m}[t]\} : \; s_{\ell,m}[t] = \sum_{j=1}^{p_s} s_{\ell,m}^{j} \cdot G_{d_s(j)}[t], \tag{3.3.4b}$$

with $\ell, m = 1, \ldots, k$, and $a_{\ell,m}^{i,j}, c_{\ell,m}^{i,j}, s_{\ell,m}^{j}$ designating the AR, MA and innovations covariance matrix coefficients of projection, respectively. An FS-VTARMA model is thus parametrized in terms of the time-invariant projection coefficients $a_{\ell,m}^{i,j}, c_{\ell,m}^{i,j}, s_{\ell,m}^{j}$, while a specific model structure, say $\mathcal{M}$, is defined by the model orders n_a, n_c, and the functional subspaces $\mathcal{F}_{\text{AR}}, \mathcal{F}_{\text{MA}}$ and $\mathcal{F}_{\boldsymbol{\Sigma}}$:

$$\mathcal{M} \triangleq \{n_a, n_c, \mathcal{F}_{\text{AR}}, \mathcal{F}_{\text{MA}}, \mathcal{F}_{\boldsymbol{\Sigma}}\} \tag{3.3.5}$$

The identification may be thus viewed as the problem of determining the model that best “fits” the vibration response observations $\boldsymbol{x}^N = \{\boldsymbol{x}[1] \ldots \boldsymbol{x}[N]\}$. Model “fitness” may be judged in terms of the BIC or other prediction error criteria [Reinsel, 1993, pp. 92-93]. Both the model structure $\mathcal{M}$ and model parameter vector $\boldsymbol{\theta}$ consisting of the projection coefficients $a_{\ell,m}^{i,j}, c_{\ell,m}^{i,j}, s_{\ell,m}^{j}$ have to be estimated from the available vibration response. Yet, for purposes that have to do with practicality and conceptual simplicity, the complete (parameter and model structure) estimation problem is distinguished into two subproblems: (a) *parameter estimation* (for a given model structure $\mathcal{M}$), and (b) the *model structure selection*. These subproblems are discussed in the following subsections.

3.3.1.1 Parameter estimation

Model parameter estimation refers to the determination, for a selected model structure $\mathcal{M}$, of the AR, MA and innovations covariance matrix projection coefficient vectors, $\boldsymbol{\vartheta}_a, \boldsymbol{\vartheta}_c$ and $\boldsymbol{\vartheta}_s$, respectively:

$$\boldsymbol{\theta} = \left[\, \boldsymbol{\vartheta}_{a|c}^T \mid \boldsymbol{\vartheta}_s{}^T \,\right]^T_{k^2(n_a \cdot p_a + n_c \cdot p_c + p_s)\times 1}, \quad \boldsymbol{\vartheta}_{a|c} = \left[\, \boldsymbol{\vartheta}_a{}^T \mid \boldsymbol{\vartheta}_c{}^T \,\right]^T_{k^2(n_a \cdot p_a + n_c \cdot p_c)\times 1}, \quad \boldsymbol{\vartheta}_s = \left[\, s_{1,1}^{1} \; \ldots \; s_{k,k}^{p_s} \,\right]^T_{k^2 \cdot p_s \times 1},$$

$$\boldsymbol{\vartheta}_a = \left[\, a_{1,1}^{1,1}, \; \ldots \; a_{k,1}^{1,1} \mid \; \ldots \; \mid a_{1,k}^{n_a,p_a}, \; \ldots \; a_{k,k}^{n_a,p_a} \,\right]^T_{k^2 \cdot n_a \cdot p_a \times 1},$$

$$\boldsymbol{\vartheta}_c = \left[\, c_{1,1}^{1,1}, \; \ldots \; c_{k,1}^{1,1} \mid \; \ldots \; \mid c_{1,k}^{n_c,p_c}, \; \ldots \; c_{k,k}^{n_c,p_c} \,\right]^T_{k^2 \cdot n_c \cdot p_c \times 1},$$

based on available signal samples $\boldsymbol{x}^N = \{\boldsymbol{x}[1], \ldots, \boldsymbol{x}[N]\}$. The estimation of the AR/MA projection coefficient vector $\boldsymbol{\vartheta}_{a|c}$ is presently based on the Prediction Error (PE) principle [Ljung, 1999, p. 203], according to which a quadratic functional of the model's one-step-ahead prediction error $\boldsymbol{e}[t, \boldsymbol{\vartheta}_{a|c}]$ (residual) sequence (also referred to as Residual Sum of Squares, RSS) is minimized:

$$\hat{\boldsymbol{\vartheta}}_{a|c} = \arg\min_{\boldsymbol{\vartheta}_{a|c}} \sum_{t=1}^{N} \boldsymbol{e}^T[t, \boldsymbol{\vartheta}_{a|c}] \cdot \ \boldsymbol{e}[t, \boldsymbol{\vartheta}_{a|c}] \tag{3.3.6}$$

with $\arg\min$ designating "argument minimizing" and $\boldsymbol{e}[t, \boldsymbol{\vartheta}_{a|c}]$ being obtained as:

$$\boldsymbol{e}[t, \boldsymbol{\vartheta}_{a|c}] \ = \ \boldsymbol{x}[t] + \sum_{i=1}^{n_a} \boldsymbol{A}_i[t, \boldsymbol{\vartheta}_a] \cdot \boldsymbol{x}[t-i] - \sum_{i=1}^{n_c} \boldsymbol{C}_i[t, \boldsymbol{\vartheta}_c] \cdot \boldsymbol{e}[t-i, \boldsymbol{\vartheta}_{a|c}] \tag{3.3.7}$$

The estimation of $\boldsymbol{\vartheta}_{a|c}$ based on the PE criterion of Eq. (3.3.6) constitutes a nonlinear optimization problem due to the nonlinear dependence of the residual vector $\boldsymbol{e}[t, \boldsymbol{\vartheta}_{a|c}]$ on the MA parameters (see Eq. (3.3.7)). Therefore, its estimation has to be handled via iterative optimization techniques which are, nevertheless, amenable to wrong convergence problems which may be due to local minima in the PE criterion [Ljung, 1999, p. 338]. For this reason relatively accurate initial guess parameter values for the AR/MA coefficient of projection are necessary, and this is presently attained via the *Two Stage Least Squares (2SLS)* method [Poulimenos and Fassois, 2006, Grenier, 1983b] outlined in the sequel.

The Two-Stage Least Squares (2SLS) method

The 2SLS method utilizes a (theoretically infinite order) FS-VTAR representation (also referred to as the *inverse function representation*) of the original FS-VTARMA model. The inverse function of an FS-VTARMA model may be obtained by pre-multiplying the latter by $\boldsymbol{C}^{-1}[\mathcal{B}, t]$ (see [Ghosh and Bouthellier, 1993] on the existence of the inverse of a time-varying polynomial operator matrix):

$$\boldsymbol{C}^{-1}[\mathcal{B}, t] \circ \boldsymbol{A}[\mathcal{B}, t] \cdot \boldsymbol{x}[t] \ = \ \boldsymbol{C}^{-1}[\mathcal{B}, t] \circ \boldsymbol{C}[\mathcal{B}, t] \cdot \boldsymbol{e}[t], \quad \Longleftrightarrow \quad \boldsymbol{H}[\mathcal{B}, t] \cdot \boldsymbol{x}[t] = \boldsymbol{e}[t] \tag{3.3.8}$$

with $\boldsymbol{H}[\mathcal{B}, t] \triangleq \boldsymbol{C}^{-1}[\mathcal{B}, t] \circ \boldsymbol{A}[\mathcal{B}, t] = \boldsymbol{I}_k + \sum_{i=1}^{\infty} \boldsymbol{H}_i[t] \cdot \mathcal{B}^i$ denoting the *inverse function matrix* polynomial operator. The symbol "$\circ$" designates a non-commutative ("skew") multiplication operation relationship defined via the expressions $\mathcal{B}^i \circ \mathcal{B}^j = \mathcal{B}^{i+j}$, and $\mathcal{B}^i \circ \boldsymbol{x}[t] = \boldsymbol{x}[t-i] \cdot \mathcal{B}^i$ [Poulimenos and Fassois, 2006, Kamen, 1988].

Stage 1. Inverse Function Estimation.

A truncated n_h-order, inverse function model that corresponds to the representation of Eq. (3.3.8) is considered as follows:

$$\boldsymbol{H}[\mathcal{B}, t, \boldsymbol{\vartheta}_h] \cdot \boldsymbol{x}[t] = \boldsymbol{e}[t, \boldsymbol{\vartheta}_h] \quad \Longleftrightarrow \quad \boldsymbol{x}[t] + \sum_{i=1}^{n_h} \boldsymbol{H}_i[t] \cdot \boldsymbol{x}[t-i] = \boldsymbol{e}[t, \boldsymbol{\vartheta}_h] \quad \Longleftrightarrow$$

$$\Longleftrightarrow \quad \boldsymbol{x}[t] + \sum_{i=1}^{n_h} \begin{bmatrix} \sum_{j=1}^{p_{h_i}} h_{1,1}^{i,j} \cdot G_{d_{h_i}(j)}[t] & \cdots & \sum_{j=1}^{p_{h_i}} h_{1,k}^{i,j} \cdot G_{d_{h_i}(j)}[t] \\ \vdots & \ddots & \vdots \\ \sum_{j=1}^{p_{h_i}} h_{k,1}^{i,j} \cdot G_{d_{h_i}(j)}[t] & \cdots & \sum_{j=1}^{p_{h_i}} h_{k,k}^{i,j} \cdot G_{d_{h_i}(j)}[t] \end{bmatrix} \cdot \boldsymbol{x}[t-i] = \boldsymbol{e}[t, \boldsymbol{\vartheta}_h] \quad \Longleftrightarrow$$

$$\Longleftrightarrow \quad \boldsymbol{x}[t] = \sum_{i=1}^{n_h} \begin{bmatrix} h_{1,1}^{i,1} & \cdots & h_{1,1}^{i,p_{h_i}} & \cdots & h_{1,k}^{i,1} & \cdots & h_{1,k}^{i,p_{h_i}} \\ & \vdots & & \ddots & & \vdots & \\ h_{k,1}^{i,1} & \cdots & h_{k,1}^{i,p_{h_i}} & \cdots & h_{k,k}^{i,1} & \cdots & h_{k,k}^{i,p_{h_i}} \end{bmatrix} \cdot \left(-\boldsymbol{x}[t-i] \otimes \boldsymbol{g}_{d_{h_i}}[t]\right) + \boldsymbol{e}[t, \boldsymbol{\vartheta}_h] \quad \Longleftrightarrow$$

$$\Longleftrightarrow \quad \boldsymbol{x}[t] = \begin{bmatrix} h_{1,1}^{1,1} & \cdots & h_{1,1}^{1,p_{h_1}} & \cdots & h_{1,k}^{n_h,1} & \cdots & h_{1,k}^{n_h,p_{h n_h}} \\ & \vdots & & \ddots & & \vdots & \\ h_{k,1}^{1,1} & \cdots & h_{k,1}^{1,p_{h_1}} & \cdots & h_{k,k}^{n_h,1} & \cdots & h_{k,k}^{n_h,p_{h n_h}} \end{bmatrix} \cdot \begin{bmatrix} -\boldsymbol{x}[t-1] \otimes \boldsymbol{g}_{d_{h_1}}[t] \\ -\boldsymbol{x}[t-2] \otimes \boldsymbol{g}_{d_{h_2}}[t] \\ \vdots \\ -\boldsymbol{x}[t-n_h] \otimes \boldsymbol{g}_{d_{h n_h}}[t] \end{bmatrix} + \boldsymbol{e}[t, \boldsymbol{\vartheta}_h] \quad \Longleftrightarrow$$

$$\iff \quad \mathrm{vec}\left(\boldsymbol{x}[t]\right) = \left(\boldsymbol{\phi}_H^T[t] \otimes I_k\right) \cdot \boldsymbol{\vartheta}_h + \mathrm{vec}\left(\boldsymbol{e}[t, \boldsymbol{\vartheta}_h]\right) \quad \iff$$

$$\iff \quad \boldsymbol{x}[t] = \boldsymbol{\Phi}_H^T[t] \cdot \boldsymbol{\vartheta}_h + \boldsymbol{e}[t, \boldsymbol{\vartheta}_h], \tag{3.3.9}$$

where $\mathrm{vec}(\cdot)$[1] is the column stacking operator (vectorization operator), $\otimes$ the Kronecker product, $\boldsymbol{e}[t, \boldsymbol{\vartheta}_h]$ the model residual vector, $\boldsymbol{\vartheta}_h$ the vector consisting of the truncated inverse function coefficients of projection:

$$\begin{aligned}
\boldsymbol{\vartheta}_h &\triangleq \left[h_{1,1}^{1,1} \ \ldots \ h_{k,1}^{1,1} \mid \ldots \mid h_{1,k}^{n_h, p_{h_{n_h}}} \ \ldots \ h_{k,k}^{n_h, p_{h_{n_h}}}\right]^T_{(\sum_{i=1}^{n_h} p_{h_i})\times 1}, \\
\boldsymbol{\phi}_H[t] &\triangleq \left[\left(-\boldsymbol{x}[t-1] \otimes \boldsymbol{g}_{d_{h_1}}[t]\right)^T \ \left(-\boldsymbol{x}[t-2] \otimes \boldsymbol{g}_{d_{h_2}}[t]\right)^T \ \ldots \ \left(-\boldsymbol{x}[t-n_h] \otimes \boldsymbol{g}_{d_{h_{n_h}}}[t]\right)^T\right]^T_{k\cdot(\sum_{i=1}^{n_h} p_{h_i})\times 1}, \\
\boldsymbol{g}_{d_{h_i}}[t] &\triangleq \left[G_{d_{h_i}(1)}[t] \ \ G_{d_{h_i}(2)}[t] \ \ldots \ G_{d_{h_i}(p_{h_i})}[t]\right]^T_{p_{h_i}\times 1},
\end{aligned}$$

and $\boldsymbol{\Phi}_H[t]$ the corresponding regression matrix. The basis functions $G_{d_{h_i}(j)}[t]$ $(j = 1, \ldots, p_{h_i})$ involved in the above, constitute the p_{h_i}-dimensional inverse function functional subspace $\mathcal{F}_{h_i}$ for each $\boldsymbol{H}_i[t]$ [Poulimenos and Fassois, 2003a].

Since the model residuals (prediction errors) depend linearly on $\boldsymbol{\vartheta}_h$, minimization of the RSS leads to the following Ordinary Least Squares (OLS) estimator:

$$\hat{\boldsymbol{\vartheta}}_h = \left(\frac{1}{N} \cdot \sum_{t=1}^{N} \boldsymbol{\Phi}_H[t] \cdot \boldsymbol{\Phi}_H^T[t]\right)^{-1} \cdot \left(\frac{1}{N} \cdot \sum_{t=1}^{N} \boldsymbol{\Phi}_H[t] \cdot \boldsymbol{x}[t]\right) \tag{3.3.10}$$

Stage 2. AR/MA Projection Coefficient Estimation.

The FS-VTARMA model of Eq. (3.3.2a) may be approximated by replacing the past, but not the current, values of the prediction error $\boldsymbol{e}[t, \boldsymbol{\vartheta}_{a|c}]$ by those obtained in the previous stage (that is $\boldsymbol{e}[t, \hat{\boldsymbol{\vartheta}}_h]$). Thus:

$$\boldsymbol{x}[t] + \sum_{i=1}^{n_a} \boldsymbol{A}_i[t] \cdot \boldsymbol{x}[t-i] = \sum_{i=1}^{n_c} \boldsymbol{C}_i[t] \cdot \boldsymbol{e}[t-i, \hat{\boldsymbol{\vartheta}}_h] + \boldsymbol{e}[t, \boldsymbol{\vartheta}_{a|c}] \quad \iff$$

$$\iff \quad \boldsymbol{x}[t] + \sum_{i=1}^{n_a} \begin{bmatrix} \sum_{j=1}^{p_a} a_{1,1}^{i,j} \cdot G_{d_a(j)}[t] & \cdots & \sum_{j=1}^{p_a} a_{1,k}^{i,j} \cdot G_{d_a(j)}[t] \\ \vdots & \ddots & \vdots \\ \sum_{j=1}^{p_a} a_{k,1}^{i,j} \cdot G_{d_a(j)}[t] & \cdots & \sum_{j=1}^{p_a} a_{k,k}^{i,j} \cdot G_{d_a(j)}[t] \end{bmatrix} \cdot \boldsymbol{x}[t-i] =$$

$$= \sum_{i=1}^{n_c} \begin{bmatrix} \sum_{j=1}^{p_c} c_{1,1}^{i,j} \cdot G_{d_c(j)}[t] & \cdots & \sum_{j=1}^{p_c} c_{1,k}^{i,j} \cdot G_{d_c(j)}[t] \\ \vdots & \ddots & \vdots \\ \sum_{j=1}^{p_c} c_{k,1}^{i,j} \cdot G_{d_c(j)}[t] & \cdots & \sum_{j=1}^{p_c} c_{k,k}^{i,j} \cdot G_{d_c(j)}[t] \end{bmatrix} \cdot \boldsymbol{e}[t-i, \hat{\boldsymbol{\vartheta}}_h] + \boldsymbol{e}[t, \boldsymbol{\vartheta}_{a|c}] \quad \iff$$

$$\iff \quad \boldsymbol{x}[t] = \begin{bmatrix} a_{1,1}^{1,1} & \cdots & a_{1,1}^{1,p_a} & \cdots & c_{1,k}^{n_c,1} & \cdots & c_{1,k}^{n_c,p_c} \\ \vdots & & & \ddots & & & \vdots \\ a_{k,1}^{1,1} & \cdots & a_{k,1}^{1,p_a} & \cdots & c_{k,k}^{n_c,1} & \cdots & c_{k,k}^{n_c,p_c} \end{bmatrix} \cdot \begin{bmatrix} -\boldsymbol{x}[t-1] \otimes \boldsymbol{g}_{d_a}[t] \\ -\boldsymbol{x}[t-2] \otimes \boldsymbol{g}_{d_a}[t] \\ \vdots \\ -\boldsymbol{x}[t-n_a] \otimes \boldsymbol{g}_{d_a}[t] \\ \cdots \\ \boldsymbol{e}[t-1, \hat{\boldsymbol{\vartheta}}_h] \otimes \boldsymbol{g}_{d_c}[t] \\ \boldsymbol{e}[t-2, \hat{\boldsymbol{\vartheta}}_h] \otimes \boldsymbol{g}_{d_c}[t] \\ \vdots \\ \boldsymbol{e}[t-n_c, \hat{\boldsymbol{\vartheta}}_h] \otimes \boldsymbol{g}_{d_c}[t] \end{bmatrix} + \ \boldsymbol{e}[t, \boldsymbol{\vartheta}_{a|c}] \quad \iff$$

[1] $\mathrm{vec}(\boldsymbol{AB}) = (\boldsymbol{B}^T \otimes \boldsymbol{I}_m) \cdot \mathrm{vec}(\boldsymbol{A})$, for matrices $\boldsymbol{A}_{(m\times n)}$ and $\boldsymbol{B}_{(n\times p)}$ [Lütkepohl, 1996, p. 97]

$$\Longleftrightarrow \quad \operatorname{vec}\left(\boldsymbol{x}[t]\right) = \left(\boldsymbol{\phi}^T[t] \otimes I_k\right) \cdot \boldsymbol{\vartheta}_{a|c} + \operatorname{vec}\left(\boldsymbol{e}[t, \boldsymbol{\vartheta}_{a|c}]\right) \quad \Longleftrightarrow$$
$$\Longleftrightarrow \quad \boldsymbol{x}[t] = \boldsymbol{\Phi}^T[t] \cdot \boldsymbol{\vartheta}_{a|c} + \boldsymbol{e}[t, \boldsymbol{\vartheta}_{a|c}] \tag{3.3.11}$$

with:

$$\begin{aligned}
\boldsymbol{\phi}[t] &\triangleq \Big[\left(-\boldsymbol{x}[t-1] \otimes \boldsymbol{g}_{d_a}[t]\right)^T \ \ldots \ \left(-\boldsymbol{x}[t-n_a] \otimes \boldsymbol{g}_{d_a}[t]\right)^T \\
&\qquad \left(\boldsymbol{e}[t-1, \hat{\boldsymbol{\vartheta}}_h] \otimes \boldsymbol{g}_{d_c}[t]\right)^T \ \ldots \ \left(\boldsymbol{e}[t-n_c, \hat{\boldsymbol{\vartheta}}_h] \otimes \boldsymbol{g}_{d_c}[t]\right)^T\Big]^T_{k\cdot(n_a\cdot p_a + n_c \cdot p_c)\times 1} \\
\boldsymbol{g}_{d_a}[t] &\triangleq \left[G_{d_a(1)}[t] \ \ G_{d_a(2)}[t] \ \ldots \ G_{d_a(p_a)}[t]\right]^T_{p_a \times 1} \\
\boldsymbol{g}_{d_c}[t] &\triangleq \left[G_{d_c(1)}[t] \ \ G_{d_c(2)}[t] \ \ldots \ G_{d_c(p_c)}[t]\right]^T_{p_c \times 1}
\end{aligned}$$

and $\boldsymbol{\Phi}[t]$ designating the corresponding regression matrix. As the residual $\boldsymbol{e}[t, \boldsymbol{\vartheta}_{a|c}]$ depends linearly upon the AR/MA projection coefficient vector $\boldsymbol{\vartheta}_{a|c}$, OLS estimation of the latter may be achieved by using the current regression matrix $\boldsymbol{\Phi}[t]$ in the linear OLS estimator of Eq. (3.3.10).

Stage 2 may be (optionally) iterated until a minimum value in the RSS criterion of Eq. (3.3.6) is achieved.

Innovations covariance matrix projection coefficient estimation

The innovations (residual) sequence vector $\boldsymbol{e}[t, \boldsymbol{\vartheta}_{a|c}]$ may be estimated based on the estimated vector $\hat{\boldsymbol{\vartheta}}_{a|c}$ and Eq. (3.3.7). Its covariance matrix may be initially obtained via a moving average filter (sliding time-window) as follows:

$$\widehat{\boldsymbol{\Sigma}}[t] = \frac{1}{2M+1} \sum_{\tau=t-M}^{t+M} \boldsymbol{e}[\tau, \hat{\boldsymbol{\vartheta}}_{a|c}] \cdot \boldsymbol{e}^T[\tau, \hat{\boldsymbol{\vartheta}}_{a|c}] \tag{3.3.12}$$

with $2M+1$ designating the window length. In a second step, its elements are projected onto the corresponding functional subspace $\mathcal{F}_{\boldsymbol{\Sigma}}$:

$$\begin{aligned}
\widehat{\boldsymbol{\Sigma}}[t] &= \begin{bmatrix} s_{1,1}[t] & \cdots & s_{1,k}[t] \\ \vdots & \ddots & \vdots \\ s_{k,1}[t] & \cdots & s_{k,k}[t] \end{bmatrix} = \begin{bmatrix} \sum_{i=1}^{p_s} s_{1,1}^i G_{d_s(i)}[t] & \cdots & \sum_{i=1}^{p_s} s_{1,k}^i G_{d_s(i)}[t] \\ \vdots & \ddots & \vdots \\ \sum_{i=1}^{p_s} s_{k,1}^i G_{d_s(i)}[t] & \cdots & \sum_{i=1}^{p_s} s_{k,k}^i G_{d_s(i)}[t] \end{bmatrix} = \\
&= \begin{bmatrix} s_{1,1}^1 & \cdots & s_{1,1}^{p_s} & \cdots & s_{1,k}^1 & \cdots & s_{1,k}^{p_s} \\ & \vdots & & \ddots & & \vdots & \\ s_{k,1}^1 & \cdots & s_{k,1}^{p_s} & \cdots & s_{k,k}^1 & \cdots & s_{k,k}^{p_s} \end{bmatrix} \cdot \left(\boldsymbol{g}_{d_s}[t] \otimes \boldsymbol{I}_k\right) \quad \Longleftrightarrow \\
&\Longleftrightarrow \quad \operatorname{vec}(\widehat{\boldsymbol{\Sigma}}[t]) = \left(\boldsymbol{g}_{d_s}^T[t] \otimes \boldsymbol{I}_k \otimes \boldsymbol{I}_k\right) \cdot \boldsymbol{\vartheta}_s
\end{aligned} \tag{3.3.13}$$
$$\boldsymbol{g}_{d_s}[t] \triangleq \left[\ G_{d_s(1)}[t] \ \ G_{d_s(2)}[t] \ \ldots \ G_{d_s(p_s)}[t]\ \right]^T_{p_s \times 1}.$$

The projection coefficient vector $\boldsymbol{\vartheta}_s$ is obtained by solving the above in a linear least squares sense (Nk^2 equations for $k^2 p_s$ unknowns) under the covariance matrix positive definiteness constraint. This constraint may be circumvented either by using the Cholesky decomposition or appropriate regularization of the residual covariance matrix. Nevertheless, the constraint is strictly necessary only in the case of non-positive definiteness of the initial (non-parametrically obtained) covariance matrix $\widehat{\boldsymbol{\Sigma}}[t]$.

3.3.1.2 Structure selection

The first step in model structure selection is choosing a proper functional family, such as Chebyshev, Legendre, trigonometric, wavelets, and so on [Weisstein, 1998]. This is mostly done by using physical understanding and the expected form of model parameter variation. Fortunately, for the majority of cases, this is not a critical selection, as any function can be expanded in a space spanned by any set of functions. Just the number of necessary functions included in the various functional subspaces (subspace dimensionalities) shall be generally affected.

Once a functional family has been selected, model structure estimation refers to the estimation of the set of integers:

$$\mathcal{M} = \{n_a, n_c, p_a, p_c, p_s, d_a(j), d_c(j), d_s(j)\}$$

where n_a, n_c, designate the model orders, p_a, p_c and p_s the AR, MA and innovations covariance matrix subspace dimensionalities, respectively, and $d_a(j), d_c(j)$ and $d_s(j)$ the integers indicating the specific functions used in the corresponding subspaces.

Model structure selection may be viewed as a discrete variable selection problem that can be tackled via a hybrid integer optimization method [Poulimenos and Fassois, 2006] consisting of two distinct phases:

Phase I. Coarse ("global") Optimization.
Phase I aims at determining promising subregions of the complete search space within which optimal model structures (either in the local or global sense) might be located. This is achieved via a *Genetic Algorithm (GA)* [Mathworks, 2008] which minimizes the BIC [Reinsel, 1993, pp. 92-93] used as "fitness" function:

$$\text{BIC} = \frac{Nk}{2}\ln 2\pi + \frac{1}{2}\sum_{t=1}^{N}\left(\ln|\boldsymbol{\Sigma}[t,\boldsymbol{\vartheta}_s]| + \boldsymbol{e}^T[t,\boldsymbol{\vartheta}_{a|c}]\cdot\boldsymbol{\Sigma}^{-1}[t,\boldsymbol{\vartheta}_s]\cdot\boldsymbol{e}[t,\boldsymbol{\vartheta}_{a|c}]\right) + \frac{\ln N}{2}\cdot d \qquad (3.3.14)$$

where d stands for the number of independently "adjusted" (estimated) model parameters, k the vibration signal dimensionality, and N its length in samples. The GA starts with the random creation of an initial population of individual solutions, which constitute the first generation. In each subsequent generation, the GA selects the best, in terms of the BIC criterion, individuals to be parents, and uses them to produce the children for the next generation through crossover and mutation rules. In this way the GA evolves toward an optimal solution, imitating the natural selection process of biological evolution.

The population individuals are bit strings whose length depends on the initial search space. For instance, the initial search space for the AR order $n_a \in [0, 15] = [0000_2, 1111_2]$ corresponds to a length of 4 bits for an individual, while 5 bits are needed for the description of an initial search space of the AR functional subspace $\mathcal{F}_{\text{AR}} = \{G_0[t], G_1[t], G_2[t], G_3[t], G_4[t]\}$, with each bit denoting the existence (1) or not (0) of the corresponding basis function in the specific model structure (see Fig. 3.3.1). The outcome of this phase is one or more candidate model structures.

Phase II. Fine ("local") Optimization.
Phase II aims at refining each candidate model structure obtained in phase I and selecting the best structure. It operates in a (suitably defined) neighbourhood of each candidate model structure, and is based on the *backward regression concept* [Haber and Keviczky, 1999, pp. 582-584]. It thus starts with maximum values of the arguments (within the selected neighbourhood) and subsequently reduces either one of the model orders (n_a, n_c), or one of the subspace dimensionalities (p_a, p_c, p_s), until no further reduction in the BIC is achieved. The procedure is repeated for all initial solutions (phase I results), and the model "structure" corresponding to the globally optimum BIC is selected.

3.3.2 The Recursive Pseudo-Linear Regression VTARMA model identification method

Recursive VTARMA models essentially are unstructured parameter evolution models that are estimated via recursive identification techniques [Poulimenos and Fassois, 2006], [Soderstrom and Stoica, 1989, ch. 9], [Ben Mrad and Fassois, 1991a]. They are similar to those of Eq. (3.3.1), with the difference being that their parameters do not have a "structured" time-dependency and thus are "free" to change with time (for more details see the survey of Poulimenos and Fassois [Poulimenos and Fassois, 2006]).

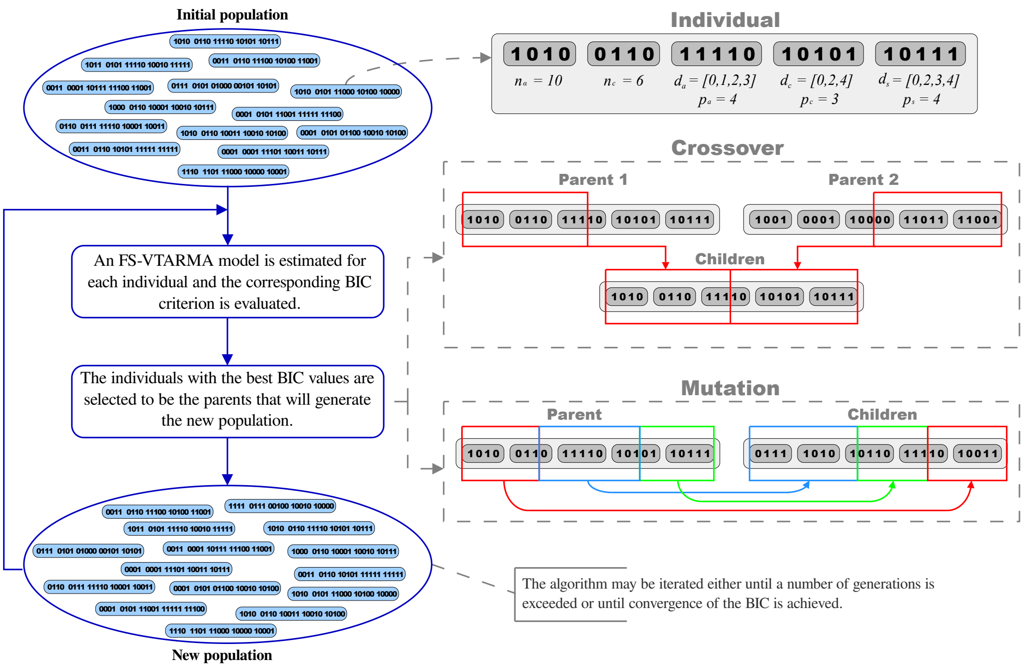

Figure 3.3.1: Flowchart of the FS-VTARMA model structure selection method Phase I based on genetic algorithm.

Overlooking - for a moment - the dependence of the VTARMA model's one-step-ahead prediction error $\boldsymbol{e}[t]$ on the unknown MA parameters, the "unstructured" parameter evolution VTARMA model may be rewritten in a pseudo-linear regression form:

$$\boldsymbol{x}[t] = \boldsymbol{\Phi}^T[t] \cdot \boldsymbol{\vartheta}[t] + \boldsymbol{e}[t] \tag{3.3.15}$$

with

$$\boldsymbol{\vartheta}[t] = \left[\begin{array}{cccccc|cccccc} a^1_{1,1}[t] & a^1_{2,1}[t] & \ldots & a^{n_a}_{k-1,k}[t] & a^{n_a}_{k,k}[t] & & c^1_{1,1}[t] & c^1_{2,1}[t] & \ldots & c^{n_c}_{k-1,k}[t] & c^{n_c}_{k,k}[t] \end{array}\right]^T_{k^2(n_a+n_c)\times 1}$$

being the time-dependent parameter vector, and

$$\boldsymbol{\Phi}[t] = \left[\begin{array}{ccc|c|ccc|c|ccc|c|ccc} -x_1[t-1] & \cdots & 0 & & -x_k[t-n_a] & \cdots & 0 & & e_1[t-1] & \cdots & 0 & & e_k[t-n_c] & \cdots & 0 \\ \vdots & \ddots & \vdots & \cdots & \vdots & \ddots & \vdots & & \vdots & \ddots & \vdots & \cdots & \vdots & \ddots & \vdots \\ 0 & \cdots & -x_1[t-1] & & 0 & \cdots & -x_k[t-n_a] & & 0 & \cdots & e_1[t-1] & & 0 & \cdots & e_k[t-n_c] \end{array}\right]^T_{k^2\cdot(n_a+n_c)\times k}$$

the corresponding regression matrix. The unknown prediction errors in this expression are approximated as $\boldsymbol{e}[t-i] \approx \hat{\boldsymbol{e}}[t, \hat{\boldsymbol{\vartheta}}[t-i-1]]$ (the prediction error estimates obtained at time $t-i$ using the estimated parameters at time $t-i-1$).

At each time instant parameter estimation is accomplished by the Pseudo-Linear Regression (PLR) algorithm [Soderstrom and Stoica, 1989, pp. 328-334] :

$$\text{Estimator update:} \quad \hat{\boldsymbol{\vartheta}}[t] = \hat{\boldsymbol{\vartheta}}[t-1] + \boldsymbol{K}[t] \cdot \hat{\boldsymbol{e}}[t|t-1] \tag{3.3.16a}$$

$$\text{Prediction error:} \quad \hat{\boldsymbol{e}}[t|t-1] = \boldsymbol{x}[t] - \hat{\boldsymbol{x}}[t|t-1] = \boldsymbol{x}[t] - \boldsymbol{\Phi}^T[t] \cdot \hat{\boldsymbol{\vartheta}}[t-1] \tag{3.3.16b}$$

$$\text{Gain:} \quad \boldsymbol{K}[t] = \boldsymbol{P}[t-1] \cdot \boldsymbol{\Phi}[t] \cdot \left\{\lambda \boldsymbol{I}_k + \boldsymbol{\Phi}^T[t] \cdot \boldsymbol{P}[t-1] \cdot \boldsymbol{\Phi}[t]\right\}^{-1} \tag{3.3.16c}$$

$$\text{“Covariance” update:} \quad \boldsymbol{P}[t] = \lambda^{-1}\left\{\boldsymbol{P}[t-1] - \boldsymbol{K}[t] \cdot \boldsymbol{\Phi}^T[t] \cdot \boldsymbol{P}[t-1]\right\} \tag{3.3.16d}$$

Table 3.2: Identification methods, their selected characteristics, and the identified models

Identification Method	Method Characteristics	Identified Model
ST-SSI	$Q = 301,\ q = 10,\ M = 256$	ST-SSI(8)
PLR-VTARMA	$\lambda = 0.985,\ \alpha = 10^4,\ M = 256$	PLR-VTARMA$(4, 4)$
FS-VTARMA	2SLS, $n_h = 8$, 2 iterations, QR implementation of OLS, $M = 256$	FS-VTARMA$(4, 4)_{[16,7,8]}$

with $\hat{\boldsymbol{x}}[t|t-1]$ indicating the one-step-ahead prediction of the vector signal at time t made at time $t-1$, and $\hat{\boldsymbol{e}}[t|t-1] \equiv \boldsymbol{e}[t, \hat{\boldsymbol{\vartheta}}[t-1]]$ the corresponding prediction error vector. λ stands for a forgetting factor which determines how older signal samples are forgotten (diminishing influence on the estimate) by the algorithm, $\boldsymbol{K}$[t] for the adaptation gain, and $\boldsymbol{P}[t]$ for the model parameter "covariance" matrix. For the initialization of the method it is customary to set $\hat{\boldsymbol{\vartheta}}[0] = \mathbf{0}$, $\boldsymbol{P}[0] = \alpha \boldsymbol{I}$, with α designating a "large" positive number.

The innovations covariance matrix $\boldsymbol{\Sigma}[t]$ is subsequently estimated via a moving average filter just as in Eq. (3.3.12). Model order selection may be based on the RSS criterion, as the BIC cannot be formally used with recursive models.

3.3.3 The Short Time Stochastic Subspace Identification method

This method employs unstructured parameter evolution models in state space form, while estimation is not recursive but based on the batch Canonical Variate Analysis (CVA) subspace identification algorithm [Overschee and Moor, 1989, pp. 80-81]. The method operates on a "short" time segment (Q samples long) of the signal at a time. Within this segment the signal may be considered as approximately stationary, and a model is identified that is then associated with the segment's "central" time instant. The operation is repeated for the "next" time segment, produced by an advance of q samples, until the complete signal record is exhausted. The complete method is referred to as ST-SSI.

The output-only state-space model used is of the form:

$$\boldsymbol{z}[t+1] = \boldsymbol{A}\boldsymbol{z}[t] + \boldsymbol{K}\boldsymbol{e}[t] \tag{3.3.17a}$$

$$\boldsymbol{x}[t] = \boldsymbol{C}\boldsymbol{z}[t] + \boldsymbol{e}[t], \quad \boldsymbol{e}[t] \sim \text{NID}(\mathbf{0}, \boldsymbol{\Sigma}) \tag{3.3.17b}$$

with $\boldsymbol{z}[t]_{n\times 1}$ indicating the state vector, $\boldsymbol{x}[t]_{k\times 1}$ the non-stationary signal modelled, $\boldsymbol{e}[t]_{n\times 1}$ the innovations vector, and $\boldsymbol{A}_{n\times n}$, $\boldsymbol{K}_{n\times k}$, $\boldsymbol{C}_{k\times n}$ the state, Kalman gain and output matrices, respectively.

The critical quantities in this method is the segment length Q and the advance q. While a short Q will lead to better time resolution, accuracy will be poorer. On the other hand, a unit advance is best for time resolution, but heavily penalizes the computational effort. Hence reasonable compromises are necessary. The innovations covariance matrix $\boldsymbol{\Sigma}[t]$ is estimated via a moving average filter just as in Eq. (3.3.12).

3.4 TV Structural Dynamics Identification

3.4.1 Parametric identification results

The parametric identification of the time-varying structure is now considered based on the three identification methods presented in the previous section. The selected characteristics of the methods are shown in Table 3.2.

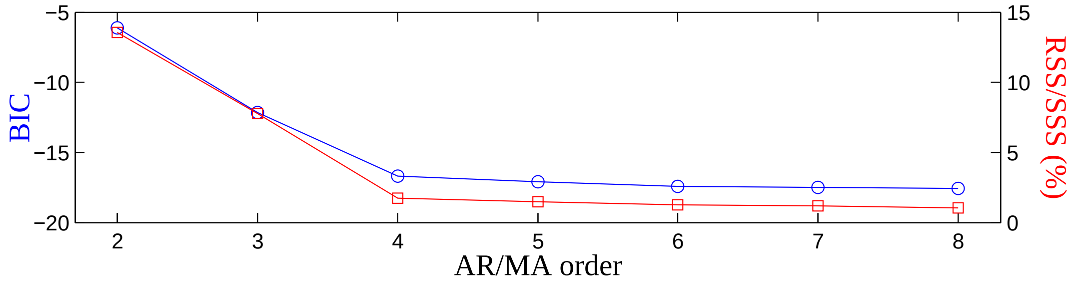

Figure 3.4.1: FS-VTARMA order selection: BIC (-o-) and RSS/SSS (-□-) values versus AR/MA order.

[A] The FS-VTARMA Method

A functional basis spanned by trigonometric (sine and cosine) functions of the form:

$$G_0[t] = 1, \quad G_{2\kappa-1}[t] = \sin\left[\frac{\kappa\,\pi\,(t-1)}{N-1}\right], \quad G_{2\kappa}[t] = \cos\left[\frac{\kappa\,\pi\,(t-1)}{N-1}\right], \quad \kappa = 1, 2, \ldots, \quad t = 1, \ldots, N \tag{3.4.1}$$

(N=10,113) is selected, partly motivated by the approximately periodic nature of the evolution of the dynamics (Figs. 3.2.2 and 3.2.5). For the model structure selection problem, FS-VTARMA(n, n) ($n = 2, \ldots, 8$) models are considered, with the integer optimization scheme of subsection 3.3.1.2 utilized only for the estimation of the AR/MA and innovations covariance matrix functional basis subspace. Thus, for each FS-VTARMA(n, n) model a coarse optimization phase based on a GA (*ga* MATLAB function, population size 100, number of generations equal to 100, crossover fraction equal to 0.8, mutation fraction equal to 0.2) and a fine optimization phase based on the concept of backward regression are used for the estimation of the set $\{p_a, p_c, p_s, d_a(j), d_c(j), d_s(j)\}$. Initial search spaces are set as $\mathcal{F}_{\text{AR}} = \mathcal{F}_{\text{MA}} = \mathcal{F}_{\boldsymbol{\Sigma}} = \{G_0[t], \ldots, G_{19}[t]\}$. The BIC criterion and the RSS normalized by the sum of squares of the signal samples (Series Sum of Squares, SSS) for the obtained FS-VTARMA(n, n) ($n = 2, \ldots, 8$) models are shown in Fig. 3.4.1.

AR/MA order selection is additionally based on the stabilization diagram of the FS-VTARMA(n, n) based "frozen-time" natural frequency estimates depicted in Fig. 3.4.2. Using these, the AR/MA order is selected as $n = 4$, while the obtained AR, MA and innovations covariance matrix functional subspaces are of dimensionalities $p_a = 16$, $p_c = 7$, and $p_s = 8$, respectively, and of the following forms:

$$\mathcal{F}_{\text{AR}} = \{\ G_0[t], \ldots, G_{10}[t], G_{12}[t], G_{13}[t], \ldots, G_{16}[t]\ \}, \qquad \mathcal{F}_{\text{MA}} = \{\ G_0[t], \ldots G_6[t]\ \}$$

$$\mathcal{F}_{\boldsymbol{\Sigma}} = \{\ G_0[t], \ldots, G_7[t]\ \}.$$

[B] The PLR-VTARMA Method

Model order selection is in this case achieved via the RSS criterion and the stabilization plot (see Appendix 3.A.1). The forgetting factor is also optimized based on minimization of the RSS criterion (search space $[0.940, 0.941, \ldots, 0.999]$). For the initialization of the PLR algorithm $\alpha = 10^4$ is used, while three sequential phases (a forward pass, a backward pass, and a final forward pass) are applied in order to reduce the effects of the arbitrary initial conditions. The results suggest a PLR-VTARMA$(4, 4)$ model, with the order being in agreement with that of the selected FS-VTARMA model.

[C] The ST-SSI Method

The segment length and the model order are in this case (*n4sid* MATLAB function) selected based on the RSS criterion, the singular values of the corresponding Hankel matrix [Overschee and Moor, 1989, p. 76], and inspection of the "frozen-time" natural frequency estimates stabilization plot (Appendix 3.A.2). It should be noted that for segment length higher than Q=400 samples, the method seems incapable of tracking the variations in the dynamics. In addition, a lower limit on the segment length is imposed in order to attain sufficient estimation accuracy. The advance is set at q=10 samples (0.078125 s), and the selection procedure has led to a segment length of Q=301 samples and an ST-SSI(8) model.

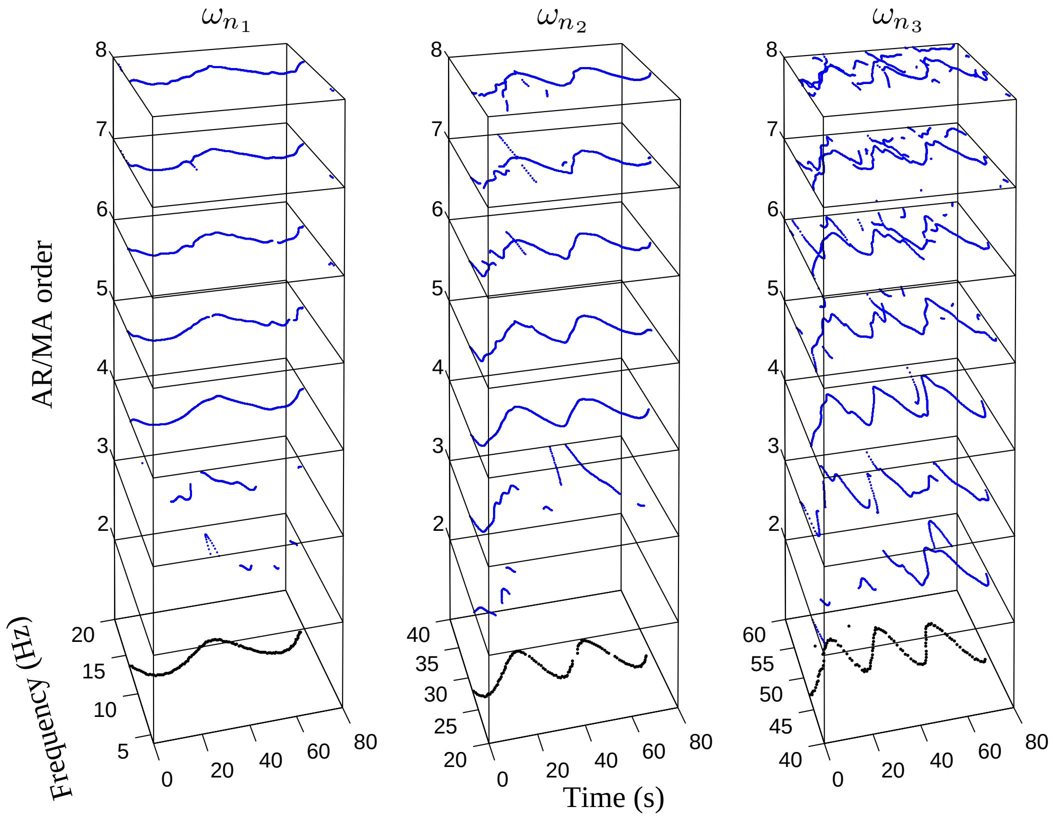

Figure 3.4.2: FS-VTARMA based "frozen-time" natural frequency estimate stabilization plot. The baseline natural frequency estimates are depicted at the bottom level whereas each level above it corresponds to its indicated AR/MA order (only natural frequency estimates with damping ratio $< 5\%$ are depicted).

[D] Comments on the obtained results

The RSS/SSS values for each vibration response signal, as obtained by each one of the three estimated models, are presented in Fig. 3.4.3(a). Evidently, the identified FS-VTARMA model attains better predictions (lower RSS/SSS value) than its ST-SSI and PLR-VTARMA counterparts. It is also worth noting that the FS-VTARMA$(4,4)_{[16,7,8]}$ model provides drastically (by more than an order of magnitude) improved predictions for vibration response 3 (Fig. 3.2.1(a)) over the corresponding predictions attained previously [Poulimenos and Fassois, 2009b] by a univariate (scalar) FS-TARMA$(8,8)_{[11,15,15]}$ model (current RSS/SSS is 0.138$\%$ whereas the previously attained value was 3.210 $\%$).

The normalized processing (CPU) times necessary for the estimation of the non-stationary model parameters (for the selected model structures) are depicted in Fig. 3.4.3(b). These values are indicative of the computational complexity associated with each method, and suggest that the FS-VTARMA method is computationally quite simpler in this respect.

Last but not least is the parametrization parsimony (economy) attained by the FS-VTARMA model as compared to its ST-SSI and PLR-VTARMA counterparts. Indeed, while the FS-VTARMA model is fully described by 900 parameters (coefficients of projection), the ST-SSI and PLR-VTARMA models require 118,822 and 819,153 parameters, respectively. This excessive difference is due to the need of the ST-SSI and PLR-VTARMA models to store their parameter and innovations covariance matrix values for each time instant.

3.4.2 The model based time-varying structural dynamics

The non-stationary vibration response characteristics and the underlying structural dynamics are analyzed based on the estimated parametric models.

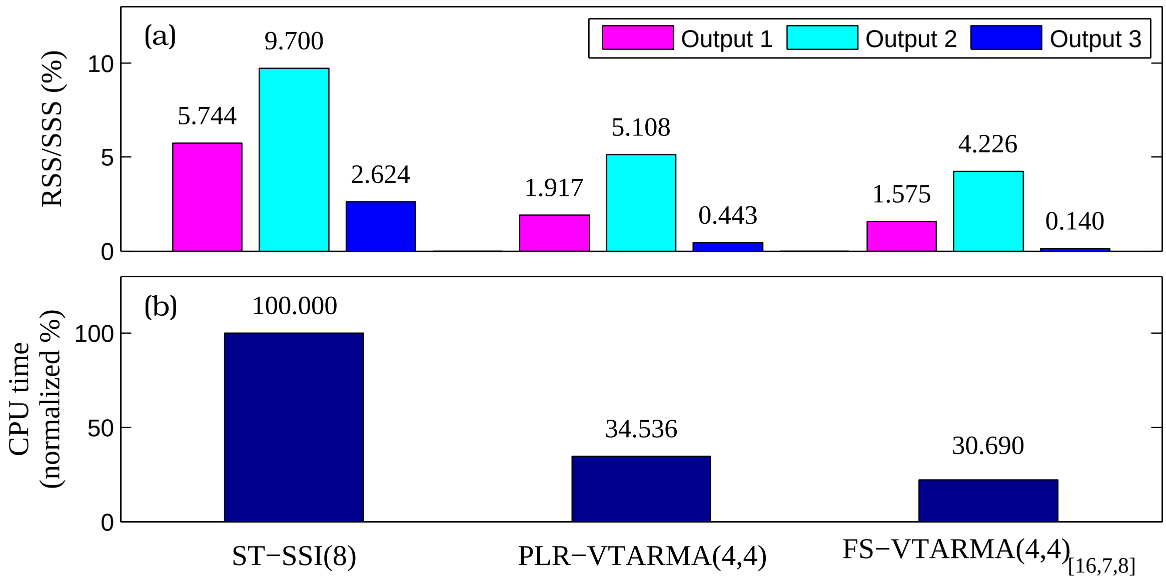

Figure 3.4.3: Comparison of the three estimated non-stationary models: (a) Prediction error (RSS/SSS) values, and (b) normalized processing times required for parameter estimation.

[A] The estimated "frozen-time" PSD matrix

The vibration response "frozen-time" PSD is, for each time instant, obtained as [Reinsel, 1993, p. 34]:

$$\boldsymbol{S}_F(\omega, t) \;=\; \frac{1}{2\pi}\boldsymbol{A}^{-1}[e^{-j\omega T_s}, t]\cdot \boldsymbol{C}[e^{-j\omega T_s}, t]\cdot \boldsymbol{\Sigma}[t]\cdot \boldsymbol{C}^T[e^{-j\omega T_s}, t]\cdot \boldsymbol{A}^{-T}[e^{-j\omega T_s}, t], \qquad t = 1, \ldots, N \quad (3.4.2)$$

in which the model parameter matrices and innovations covariance matrix are replaced by their respective estimates, ω designates frequency in rad/s, T_s the sampling period in s, and j the imaginary unit.

The "frozen-time" PSD matrices corresponding to the estimated ST-SSI(8), PLR-VTARMA$(4,4)$, and FS-VTARMA$(4,4)_{[16,7,8]}$ models are, along with the baseline PSD matrix, presented in Figs. 3.4.4 and 3.4.5. Recall that the baseline result is based on exhaustive modelling using multiple stationary data records, and is therefore considered as an accurate description of the actual "frozen" characteristics. Based on the presented results, the ST-SSI(8) based estimates seem unable to track the sharp antiresonances that are evident in a major portion of the time-frequency plane in the baseline estimates (for instance see the regions highlighted by the transparent frames A, B, C, D and E in Fig. 3.4.4). The frames A, C and E also reveal the difficulty of the ST-SSI model to accurately track the time-varying mode close to 30 Hz in the regions where pole-zero cancellations occur.

On the other hand, although specific elements of the PLR-VTARMA$(4,4)$ model based PSD matrix achieve improved tracking of the antiresonances (especially for the auto spectral densities; see frames F, G and H in Fig. 3.4.5), this is not the case for the cross-spectral density estimates where no significant improvement relatively to the ST-SSI(8) estimates is achieved (see the regions below the I, J, K and L frames in Fig. 3.4.5). For both auto and cross-spectral densities one could say that the PLR-VTARMA model renders the PSD valleys less sharp than those of the baseline estimates. Nevertheless, the effects of pole-zero cancellations in this case are less pronounced compared to the ST-SSI(8) based estimates (compare the regions indicated by the F, H, K frames against those indicated by the A, C and E frames) and the densities are in agreement with their baseline counterparts.

The FS-VTARMA$(4,4)_{[16,7,8]}$ based PSD matrix estimate exhibits very good tracking accuracy (the best among all non-stationary models considered), with respect to both the resonances and antiresonances (for instance see frames M, N, O, P, Q, and S in Fig. 3.4.5). Overall, the identified FS-VTARMA model provides much more clear, smooth and informative PSD estimates than its PLR-VTARMA and ST-SSI counterparts. Somewhat increased variability of the identified modes, which is not in agreement with

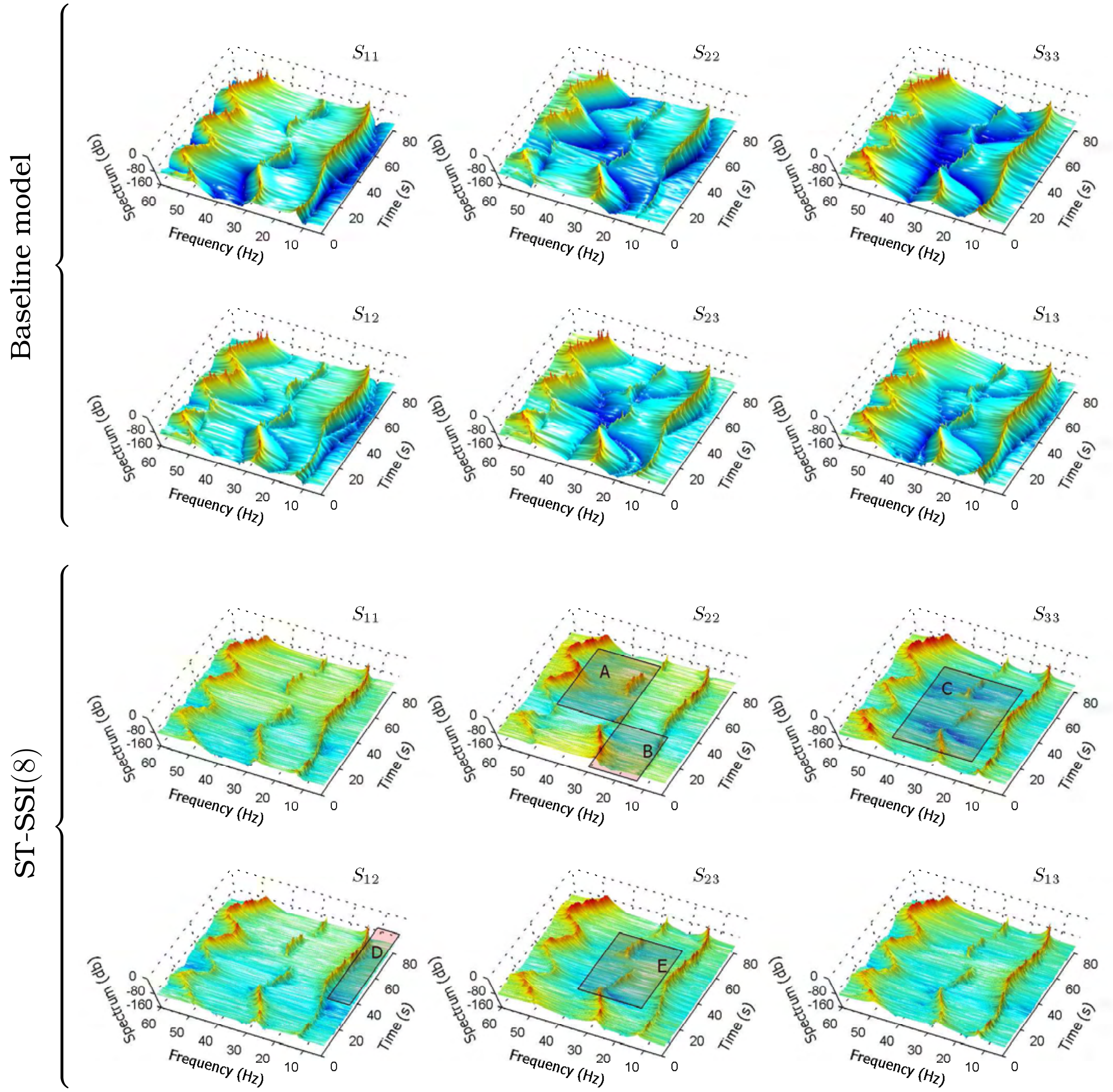

Figure 3.4.4: Baseline "frozen-configuration" VARMA(4,4) based and "frozen-time" ST-SSI(8) based PSD estimates.

the baseline estimates, may be observed for only small regions of the time-frequency plane (such as in frame R in Fig. 3.4.5).

[B] The estimated "frozen-time" modal characteristics

The structure's "frozen-time" global modal parameters (natural frequencies and damping ratios) are obtained as:

$$\omega_{ni}[t] \;=\; \frac{\left|\ln\lambda_i[t]\right|}{T_s} \quad (\text{rad/time unit})\;, \qquad \zeta_i[t] = -\cos\Big(\arg\big(\ln\lambda_i[t]\big)\Big) \tag{3.4.3}$$

with λ_i designating the i-th "frozen-time" model pole.

The "frozen-time" FS-VTARMA$(4,4)_{[16,7,8]}$ based natural frequency estimates (with $\zeta_i[t] < 5\%$) are, along with their ST-SSI(8), PLR-VTARMA$(4,4)$, and baseline counterparts, depicted in Fig. 3.4.6(a).

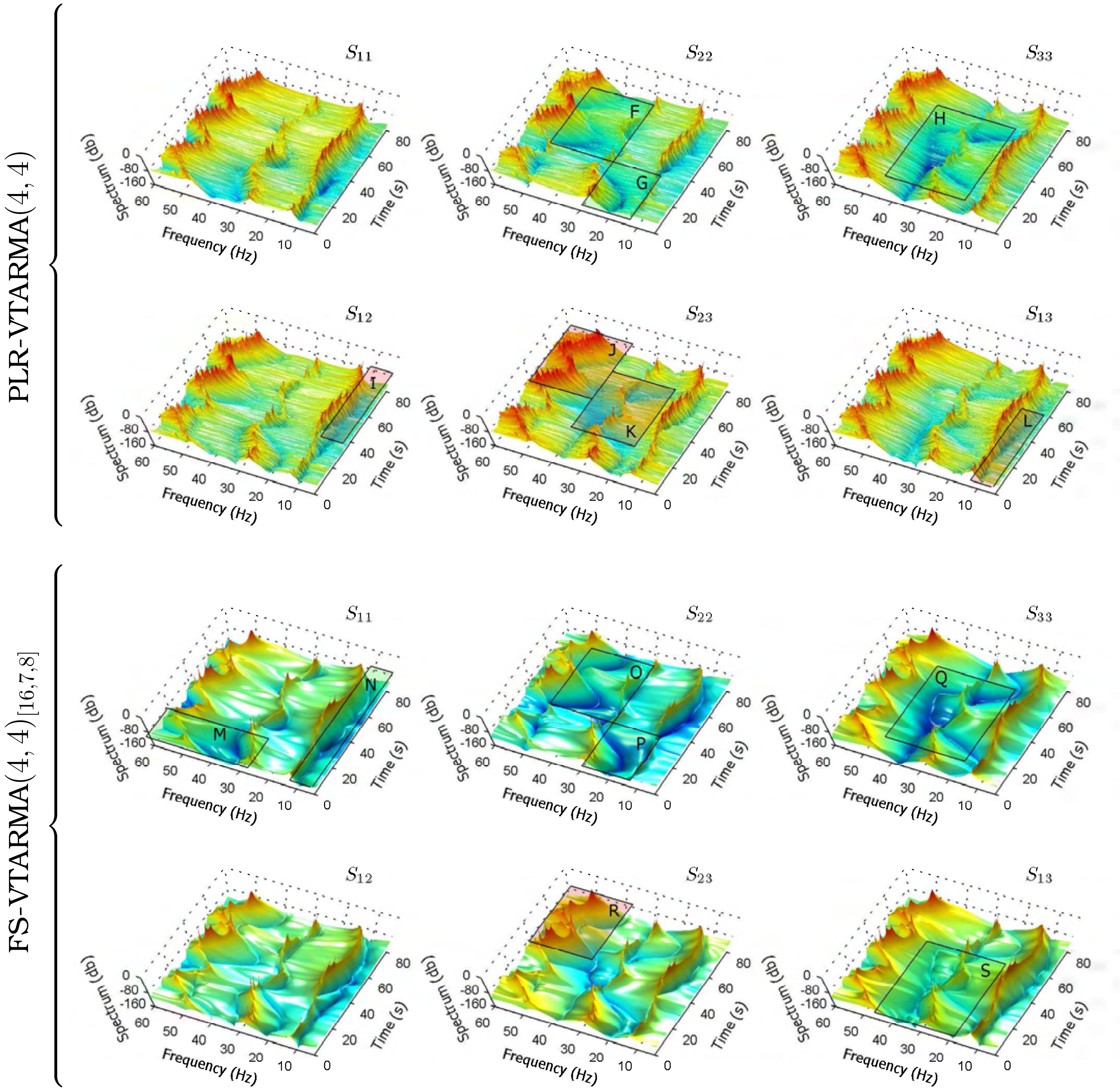

Figure 3.4.5: "Frozen-time" PLR-VTARMA$(4,4)$ and FS-VTARMA$(4,4)_{[16,7,8]}$ based PSD estimates.

Evidently, the FS-VTARMA$(4,4)_{[16,7,8]}$ estimates track the baseline model natural frequency estimates adequately well via smooth curves. The "frozen-time" ST-SSI(8) based natural frequencies also seem to track the three time-varying modes quite well, except for the time regions where pole-zero cancellations occur over the mode ω_{n2}. Finally, the PLR-VTARMA$(4,4)$ based natural frequencies exhibit increased scatter (compared to the smooth evolution of the baseline model estimates), while they provide additional false (computational) modes for extended periods of time. False modes close to the natural frequency ω_{n3} are also provided by the FS-VTARMA$(4,4)_{[16,7,8]}$ and the ST-SSI(8) models, yet only for short time periods.

It is also noted that, compared to the estimates obtained by the univariate FS-TARMA$(8,8)_{[11,15,15]}$ model in [Poulimenos and Fassois, 2009b], the vector (FS-VTARMA$(4,4)_{[16,7,8]}$) model attains better tracking accuracy for the time-varying mode ω_{n2}, although some false modes are introduced in the

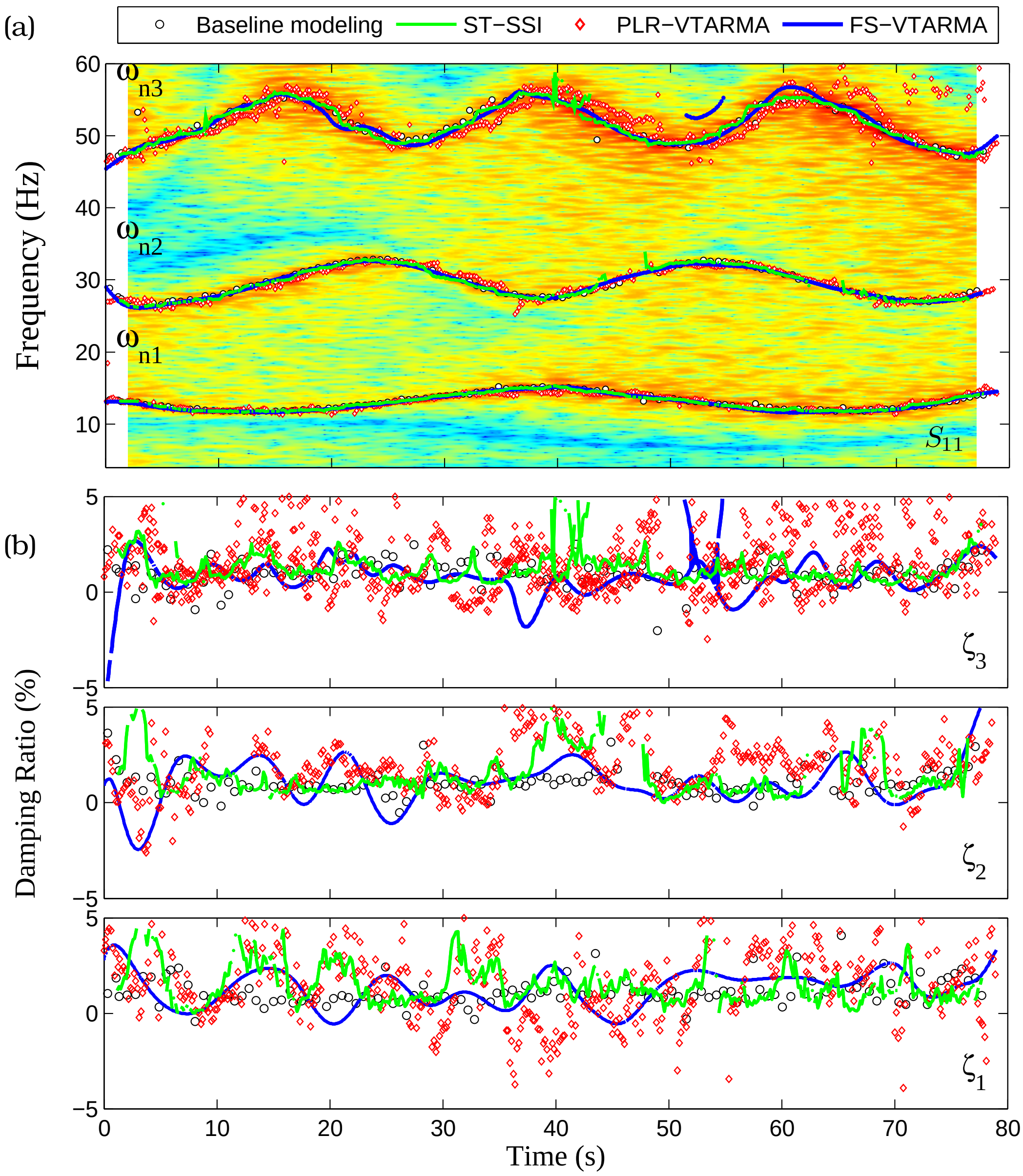

Figure 3.4.6: "Frozen-time" ST-SSI(8), PLR-VTARMA$(4,4)$, and FS-VTARMA$(4,4)_{[16,7,8]}$ based modal parameter estimates against their baseline VARMA$(4,4)$ based counterparts: (a) Natural frequency estimates (○) and the $S_{11}(\omega,t)$ SPWV based PSD estimate (background), and, (b) damping ratio estimates (only natural frequencies with damping ratio < 5% are depicted).

time-frequency area of the structural mode ω_{n3}.

The "frozen-time" damping ratio estimates based on the identified non-stationary models are plotted against their baseline estimates in Fig. 3.4.6(b). In contrast to the natural frequencies, "frozen-time" damping ratio estimates do not seem to follow very smooth curves, but they more likely constitute noisy estimates of the more or less constant over time actual damping ratios. Overall, the ST-SSI(8) and FS-VTARMA$(4,4)_{[16,7,8]}$ models provide better damping ratio estimates (closer to their baseline counterparts and exhibiting lower variability) compared to those of the PLR-VTARMA$(4,4)$ model.

Finally, the results pertaining to the "frozen-time" antiresonant frequency estimates provided by the estimated non-stationary models (Fig. 3.4.7) confirm that (as in the stationary case) their accurate estimation is a rather difficult problem. Nevertheless, the FS-VTARMA$(4,4)_{[16,7,8]}$ based estimates again achieve better tracking of their baseline counterparts.

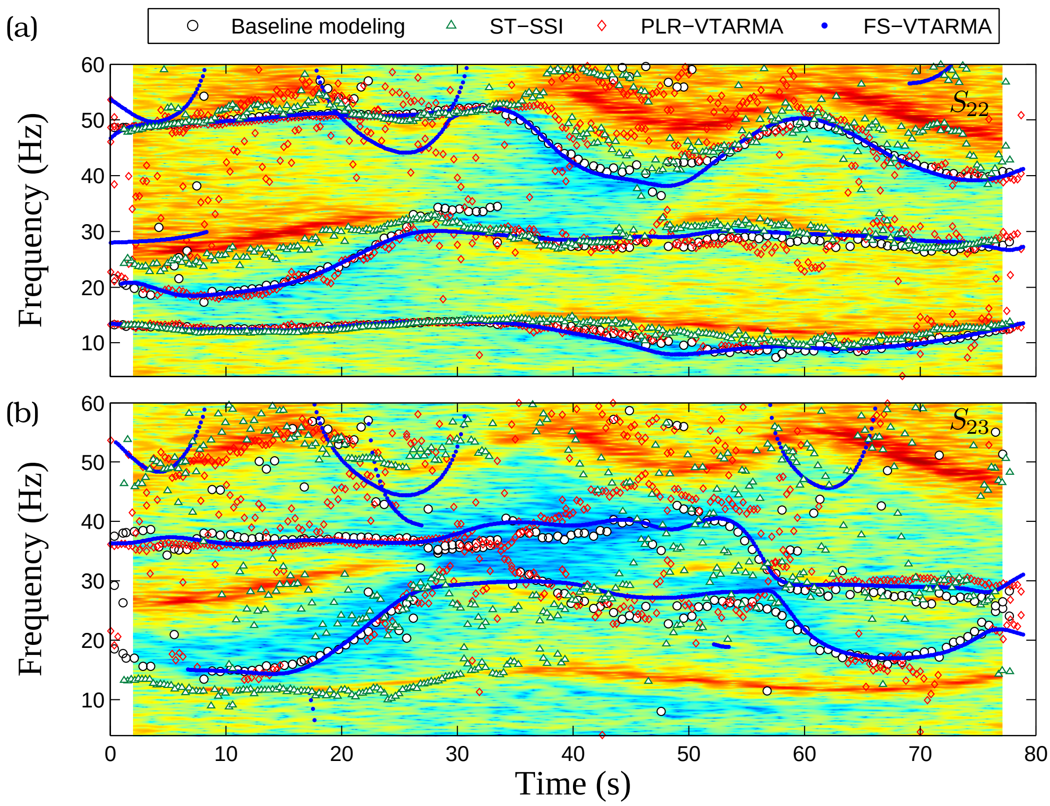

Figure 3.4.7: "Frozen-time" ST-SSI(8), PLR-VTARMA$(4,4)$, and FS-VTARMA$(4,4)_{[16,7,8]}$ based antiresonant frequency estimates against their baseline VARMA$(4,4)$ counterparts: (a) Antiresonances corresponding to the element (2,2) of the "frozen-time" transfer function matrix, and, (b) antiresonances corresponding to the element (3,2) of the "frozen-time" transfer function matrix (only antiresonances with damping ratio < 20% are depicted, while the respective element of the SPWV based PSD matrix estimate is shown in the background).

3.5 Concluding Remarks

A multivariate (vector) FS-VTARMA method for TV structural identification based on vector vibration response measurements was introduced. The method was employed for the identification of a "bridge-like" laboratory structure consisting of a beam and moving mass based on three non-stationary vibration response signals. The identified FS-VTARMA$(4,4)_{[16,7,8]}$ model was contrasted to a baseline model based on multiple "frozen-configuration" stationary experiments, as well as a recursively identified multivariate PLR-VTARMA$(4,4)$ model and an ST-SSI(8) model. The estimated FS-VTARMA$(4,4)_{[16,7,8]}$ model was shown to provide PSD and modal parameter estimates that are in good agreement with those of its baseline counterpart. It was also shown to surpass the PLR-VTARMA and ST-SSI models in terms of predictive ability and tracking accuracy for the "frozen-time" structural dynamics. The identification and model based analysis results demonstrated the ability of the FS-VTARMA method for accurate and parsimonious (economical) output-only multivariate identification of TV structures.

Appendix 3.A Additional Model Structure Selection Results

3.A.1 PLR-VTARMA Method

In the case of PLR-VTARMA method the model order is selected through inspection of the RSS criterion values and the stabilization plot versus AR/MA orders $n_a = n_c = 2, \ldots, 8$, which are shown in Fig. 3.A.1 and 3.A.2, respectively. The results suggest a PLR-VTARMA$(4,4)$ model, with the order being in agreement with that of the selected FS-VTARMA model.

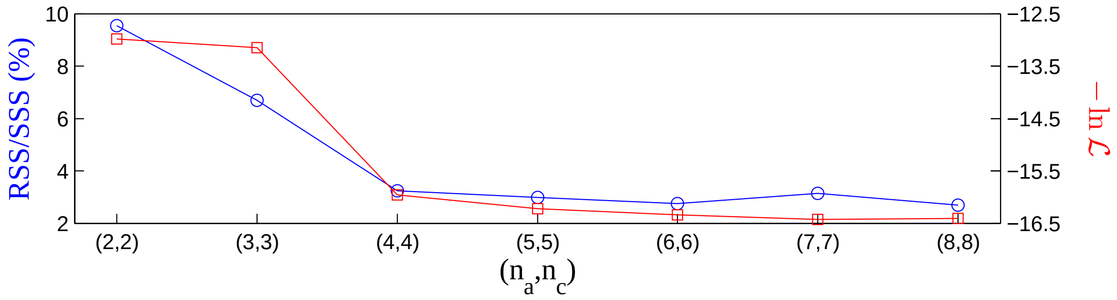

Figure 3.A.1: PLR-VTARMA order selection: RSS/SSS (-o-) and $-\ln\mathcal{L}$ (-□-) values versus AR/MA order.

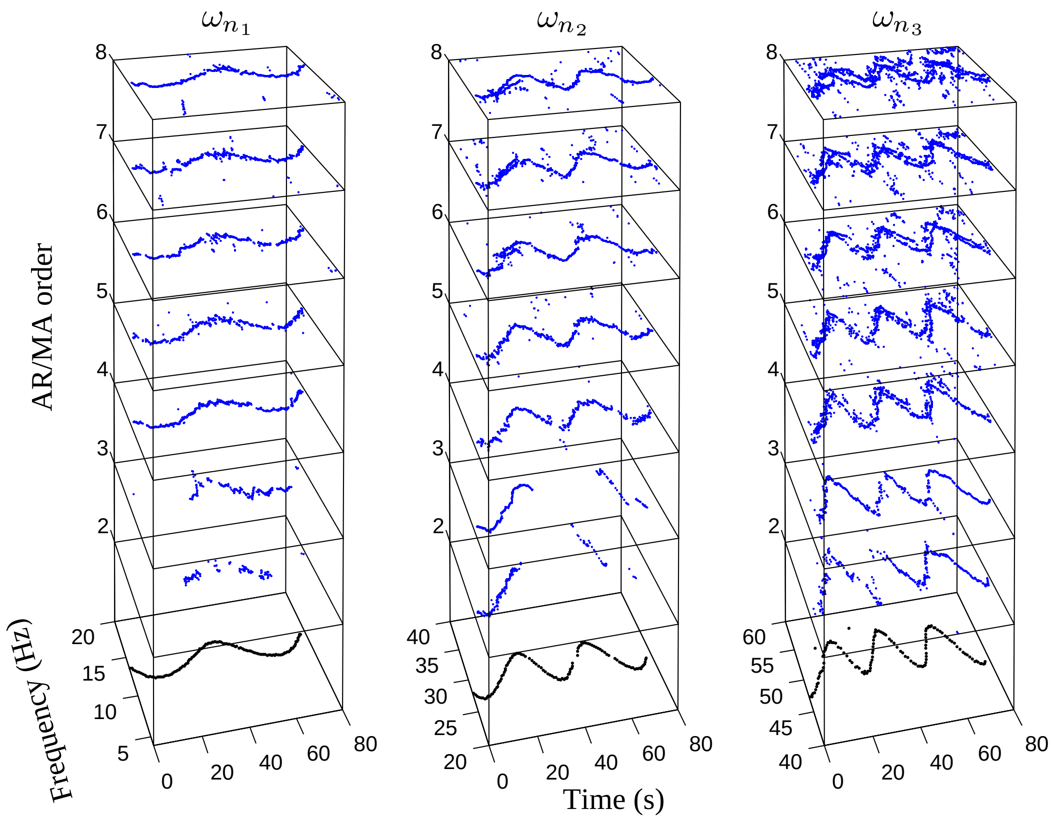

Figure 3.A.2: PLR-VTARMA based “frozen-time” natural frequency estimate stabilization plot. The baseline natural frequency estimates are depicted at the bottom level whereas each level above it corresponds to its indicated AR/MA order (only natural frequency estimates with damping ratio $< 5\%$ are depicted).

3.A.2 ST-SSI Method

For the ST-SSI model structure selection, the RSS criterion values are calculated for a number of estimated models with various orders ($n = 6, \dots, 12$) and windows lengths ($Q = 101, 151, \dots, 551$). The results are plotted in Fig. 3.A.3 and indicate a window of length equal to 301 samples as appropriate for most of the orders considered – trade-off between model tracking ability and statistical reliability is also taken into account for this selection. The final ST-SSI model order is selected by also inspecting the “frozen-time” natural frequency estimates stabilization plot versus state-space model order $n = 6, \dots, 12$ shown in Fig. 3.A.4. The results lead to the selection of a ST-SSI(8) model for the representation of the structural time-varying dynamics, with models of higher order being characterized by spurious modes located at the frequency band between 40 and 60 Hz.

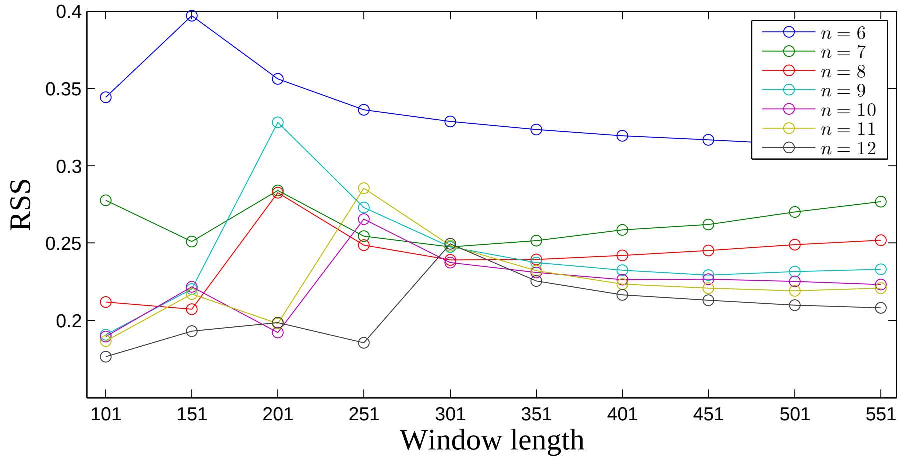

Figure 3.A.3: ST-SSI order and window length selection: RSS values versus window length and state-space model order.

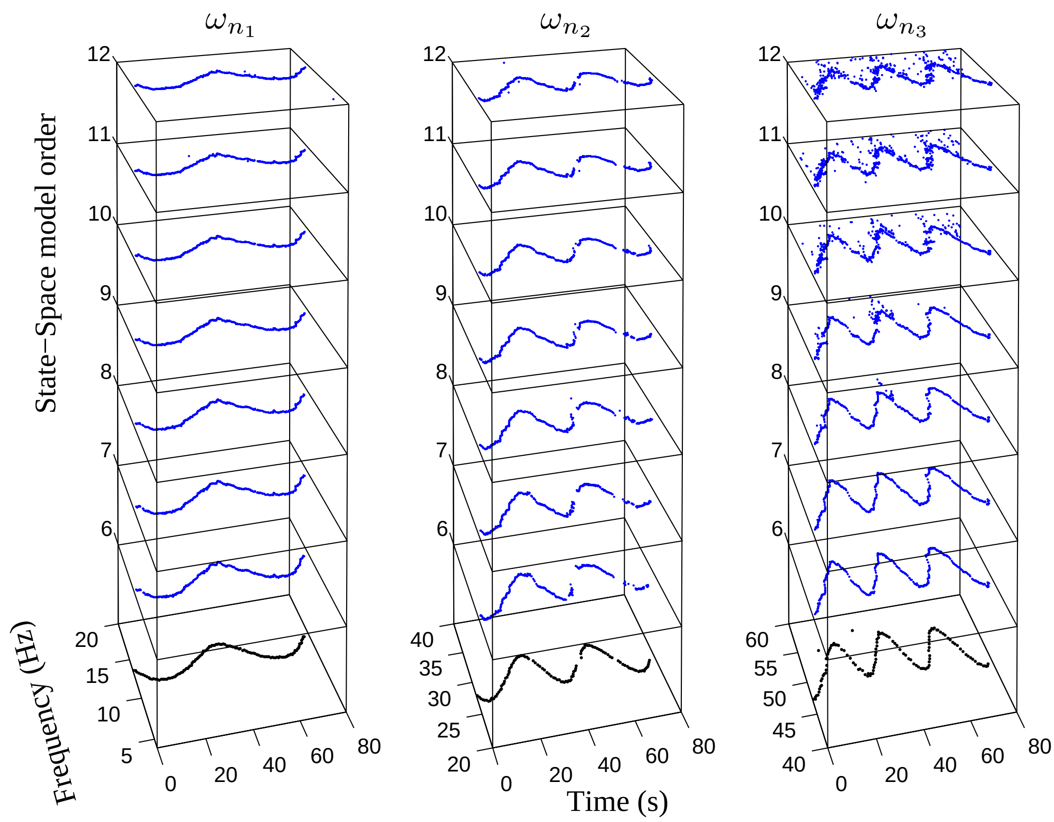

Figure 3.A.4: ST-SSI based “frozen-time” natural frequency estimate stabilization plot. The baseline natural frequency estimates are depicted at the bottom level whereas each level above it corresponds to its indicated state-space model order (only natural frequency estimates with damping ratio $< 5\%$ are depicted).

Chapter 4

Adaptable FS-TARMA Models for Non-Stationary Signal Modelling

Functional Series Time-dependent Autoregressive Moving Average (FS-TARMA) models are effective for representing non-stationary random signals arising in a wide variety of applications. Yet, their identification is challenging as, in addition to coefficient of projection estimation, functional subspace selection is also required. In this study the difficulties arising from the latter problem are alleviated by postulating a new class of Adaptable FS-TARMA (AFS-TARMA) models and a method for their effective identification. The new models are adaptable in the sense that they are based on adaptable basis functions with a-priori unknown characteristics. This is accomplished via proper basis function parametrizations while the AFS-TARMA model identification is based on a Separable Nonlinear Least Squares (SNLS) type procedure which leads to a reduced dimensionality, constrained non-quadratic optimization problem tackled via Particle Swarm Optimization (PSO) and gradient-type refinement. The model orders and subspace dimensionalities are also estimated based on PSO optimization and suitable criteria. The method's effectiveness is demonstrated via Monte Carlo experiments and comparisons with current schemes. An experimental case study pertaining to the identification of a time-varying pick-and-place mechanism is also presented.

4.1 Introduction

Functional Series Time-dependent AutoRegressive Moving Average (FS-TARMA) models, that is ARMA models with time-dependent parameters projected on deterministic basis functions, have been demonstrated to effectively model a wide variety of non-stationary random signals. These range from vibration responses of time-varying structures [Poulimenos and Fassois, 2009a] and earthquake ground motion [Fouskitakis and Fassois, 2002] to biomedical processes [Chon et al., 2005, Li et al., 2011], speech signals [Grenier, 1983b, Kacha et al., 2005], and many others (see [Poulimenos and Fassois, 2006] and the references therein).

The main asset of FS-TARMA models is that they are fully described by time-invariant coefficients of projection of the model parameters onto the selected functional subspaces, while also proper selection of the latter makes them capable of tracking fast or slow evolutions of the non-stationary signal dynamics [Poulimenos and Fassois, 2006]. Yet, the advantages of FS-TARMA models over alternative non-stationary models (such as segmentation, recursive, or smoothness priors models), have been demonstrated via a Monte Carlo comparison study in [Poulimenos and Fassois, 2006] and an experimental study based on the output-only identification of a laboratory “bridge-like” structure in Chapter 2 of this thesis.

However, the price to pay for rendering the estimation of a TARMA model into a time-invariant problem, is the increased complexity of the FS-TARMA model structure problem which, in addition to the model orders, involves the selection of an appropriate family of linearly independent basis functions and the corresponding functional subspaces. With regard to the first problem, several types of functional families have been considered, including time polynomials of arbitrary order [Liporace, 1975], polynomial basis functions [Fouskitakis and Fassois, 2002, Grenier, 1983b, Mukhopadhyay and Sircar, 1997, Kozin, 1977], trigonometric basis functions [Poulimenos and Fassois, 2009a, Hall et al., 1983, Petsounis and Fassois, 2000, Eom, 1999a], uniform B-splines functions (defined on predetermined knot sequences) [Flaherty, 1988, Salcedo et al., 2008], discrete prolate spheroidal functions [Grenier, 1983b, Charbonnier et al., 1987], various wavelet families [Fouskitakis and Fassois, 2002, Li et al., 2011, Tsatsanis and Giannakis, 1993, Wei and Billings, 2002], and others. Recently, methods based on multiple basis functions which try to combine the characteristics of two or more bases have also been proposed. Within this context, Li *et al.* in [Li et al., 2011] propose the simultaneous use of B-spline wavelet functions of various orders along with an appropriate model structure selection scheme, while a method combining the smooth Legendre polynomial functions with the abrupt Walsh functions via a Gram-Schmidt orthogonalization procedure is utilized in [Chon et al., 2005].

Nevertheless, despite the fact that any family may approximate any given curve with arbitrary accuracy, as long as a sufficient number of basis functions is used [Walter, 1994, p. 77], due to reasons of statistical efficiency and model parsimony (economy of representation) the real issue is the selection of a family that may provide the necessary accuracy with a small (or minimal) number of functions. In practice, this problem may shown to be particularly complex when various candidate families of basis functions are considered with the appropriate functional subspaces being searched among a practically infinite set of basis functions.

Although the significance of the proper functional subspace selection has been underlined in many FS-TARMA studies this issue has been treated thoroughly only in a small number of them. Tsatsanis and Giannakis were the first to treat this problem via a complete model structure selection scheme based on the concept of backward regression. More specifically, the researchers proposed a scheme which starts with the construction of an initial FS-TAR or FS-TARMA model of high orders and high subspace dimensionalities in order to assure model adequacy for representing the non-stationary system. Subsequently a statistical hypothesis F-test, or the AIC criterion is used in order to reject insignificant terms (basis functions) and reduce the model dimensionality. The idea of using an inverse “bottom-up” procedure based on forward regression, that is constructing the model by adding basis functions terms to a model of low dimension was also given in the same study and extended in [Tsatsanis, 1995].

The FS-TARMA model structure selection problem has been studied more systematically over the last decade. For instance, a scheme based on the backward regression concept was proposed in [Poulimenos and Fassois, 2003b] which decomposes the structure selection problem into two subproblems treated in equal phases: i) the model orders (n_a, n_c) selection, and (ii) the functional subspaces selection. The goal of this scheme is to reduce the computational time that is required for the exhaustive search that is done by Tsatsanis and Giannakis scheme. Forward regression procedure based on Gram-Schmidt orthogonalization was also proposed by Wei and Billings in [Wei and Billings, 2002]. Finally, a more automated procedure based on integer optimization and Genetic Algorithm (GA) was proposed in [Poulimenos and Fassois, 2003a].

However, the common characteristic of all the aforementioned studies is that the functional subspaces, either selected via one of the aforementioned schemes or by taking advantage of any prior information regarding the parameter evolution, always consist of basis functions of *fixed form* which are selected from a *pre-selected list*. Hence, the goodness of model fit is heavily dependent on the chosen basis functions.

On the other hand, Bakkoury et al. [Bakkoury et al., 2000] in a preliminary study used parametrized basis functions which had to be estimated along with the corresponding coefficients of projection. In this way they tried to adapt basis functions onto a specific identification problem in order to achieve higher tracking accuracy of the time-varying dynamics. However, in this study there is no complete framework developed for the effective identification of the FS models considered. More specifically, there are no conditions defined under which the parametrized basis functions are linearly independent which is of critical importance for the models identifiability. Moreover, although the separability of the basis parameter vector and the coefficient of projection parameter vector was recognised, the estimation method proposed therein is based on suboptimal scheme which does not take into account the interrelationships between these two parameter sets. Thus, and as mentioned by the authors of the study, this identification problem wasn't solved efficiently due to the existence of several local minima in the objective function. For the same reason no results were presented in this study.

The *aim* of the present study is to circumvent the aforementioned difficulties associated with FS-TARMA functional subspace selection and extend the idea of [Bakkoury et al., 2000] by developing a robust identification framework for FS models based on parametrized basis functions. Toward this end, a new class of Adaptable FS-TARMA (AFS-TARMA) models is introduced. AFS-TARMA models are adaptable in the sense that they are not based on basis functions of a fixed form, but instead, they use basis functions with a-priori unknown properties that may adapt to the specific random signal characteristics. This is accomplished via: (a) proper basis function parametrizations which allow their decay rate and frequency (decaying trigonometric functions) or knots (B-splines) to be directly estimated, and (b) a Separable Nonlinear Least Squares (SNLS) type procedure ([Golub and Pereyra, 1973]) that achieves simultaneous estimation of the basis functions and the coefficients of projection through a reduced dimensionality, constrained non-quadratic optimization problem tackled via Particle Swarm Optimization (PSO) and gradient-type refinement. The model structure parameters, that is model orders and the functional subspace dimensionalities, are estimated based on suitable criteria and PSO. The method's effectiveness is examined via a Monte Carlo study and comparisons with current non-stationary signal identification methods are made.

Specifically, the main contributions of this study are:

(i). The introduction of a novel class of Adaptable FS-TARMA (AFS-TARMA) models.

(ii). The introduction of a novel identification framework for AFS-TARMA models exemplified to two types of adaptable basis functions: B-splines and decaying trigonometric.

(iii). The assessment of the methods via Monte Carlo simulations and comparisons with classical methods.

(iv). Application of the method to an experimental case study pertaining to the identification of a time-varying pick-and-place mechanism.

The remaining of this chapter is organized as follows: The class of AFS-TARMA models is presented in Section 4.2 along with the definition of B-splines and the decaying trigonometric basis functions. The problems of AFS-TAR/TARMA parameter estimation and model structure selection are considered in Section 4.3, while the assessment of the introduced method through numerical case studies and the modelling problem of a 2-DOF mechanism through vibration response data are presented in Sections 4.4 and 4.5, respectively. Finally, the conclusions of the study are summarized in Section 4.6.

4.2 Classical and Adaptable FS-TARMA Models

A TARMA(n_a, n_c) model, with n_a, n_c designating its AutoRegressive (AR) and Moving Average (MA) orders, respectively, is of the form:

$$x[t] + \underbrace{\sum_{i=1}^{n_a} a_i[t] \cdot x[t-i]}_{\text{AR part}} = w[t] + \underbrace{\sum_{i=1}^{n_c} c_i[t] \cdot w[t-i]}_{\text{MA part}}, \qquad w[t] \sim \text{NID}(0, \sigma_w^2[t]), \qquad t = 1, \ldots, N \tag{4.2.1}$$

with t designating normalized discrete time, $x[t]$ the non-stationary vibration response signal, $w[t]$ an unobservable uncorrelated (white) non-stationary *innovations*, or else *residual* signal characterized by zero mean and time-varying variance $\sigma_w^2[t]$, and $a_i[t], c_i[t]$ the model's time-varying AR and MA parameters, respectively. NID$(\cdot,\cdot)$ stands for normally independently distributed random variables with the indicated mean and variance.

In the case of Functional Series TARMA (FS-TARMA) models the evolution of the time-dependent AR/MA parameters and innovations standard deviation has a deterministic "structure" reflecting the corresponding nature of the underlying dynamics responsible for the non-stationary behaviour. This is achieved by postulating model parameters as deterministic functions of time, belonging to specific functional subspaces:

$$\mathcal{F}_{\text{AR}} = \left\{G_{a(1)}[t], \; ..., \; G_{a(p_a)}[t]\right\}, \qquad \mathcal{F}_{\text{MA}} = \left\{G_{c(1)}[t], \; ..., \; G_{c(p_c)}[t]\right\}, \qquad \mathcal{F}_{\sigma_w} = \left\{G_{s(1)}[t], \; ..., \; G_{s(p_s)}[t]\right\}$$

where $\mathcal{F}$ designates functional subspace of the indicated part/quantity each one consisting of a set of *basis functions* $G_j[t]$, while p_a, p_c, p_s stand for the AR, MA, and innovations standard deviation functional subspace dimensionalities. In this way, the time-dependent AR,MA parameters and the innovations standard deviation of an FS-TARMA$(n_a, n_c)_{[p_a,p_c,p_s]}$ model may be expressed as:

$$a_i[t] = \sum_{j=1}^{p_a} a_{i,j} \cdot G_{a(j)}[t], \qquad c_i[t] = \sum_{j=1}^{p_c} c_{i,j} \cdot G_{c(j)}[t], \qquad \sigma_w[t] = \sum_{j=1}^{p_s} s_j \cdot G_{s(j)}[t] \tag{4.2.2}$$

with $a_{i,j}$, $c_{i,j}$, and s_j designating the AR, MA, and innovations standard deviation, respectively, *coefficients of projection*. Thus, the problem of FS-TARMA model parameter estimation, reduces to the determination of the time-invariant AR/MA and innovations standard deviation projection coefficient vectors $\boldsymbol{\vartheta}_a$, $\boldsymbol{\vartheta}_c$ and $\boldsymbol{\vartheta}_s$, respectively:

$$\boldsymbol{\vartheta} = [\ \boldsymbol{\vartheta}_a{}^T \mid \boldsymbol{\vartheta}_c{}^T \mid \boldsymbol{\vartheta}_s{}^T\ ]^T = [\ a_{1,1}, \ldots, a_{n_a,p_a} \mid c_{1,1}, \ldots, c_{n_c,p_c} \mid s_1, \ldots, s_{p_s}\ ]^T_{(n_a \cdot p_a + n_c \cdot p_c + p_s)\times 1} \tag{4.2.3}$$

where T designates matrix transposition. It should be noted that, alternatively, the innovations variance $\sigma_w^2[t]$ may be projected onto the selected functional subspace. However, the standard deviation is the square root version of the variance and is thus characterized by lower variability. For this reason, standard deviation normally requires a functional subspace of lower dimensionality for its accurate tracking compared to the one required for tracking the variance.

As already mentioned, the main drawback of the classical FS-TARMA approach is the rather complicated model structure selection related with the choice of a specific family of linearly independent basis functions and the appropriate functional subspaces $\mathcal{F}_{\text{AR}}, \mathcal{F}_{\text{MA}}$, and $\mathcal{F}_{\sigma_w}$. Even if this is only a small price to pay for rendering the estimation of a TARMA model a time-invariant problem, the selection of the appropriate model structure parameters is of crucial importance for accurate modelling. Indeed, despite the fact that theoretically an "extended" (high dimensionality) functional subspace may achieve good tracking of the parameter evolution irrespectively of the selected family of basis functions, this is not true when only a small number of functions has to be selected due to reasons of statistical efficiency and model parsimony (economy of representation).

On the contrary, the advantage of the proposed Adaptable FS-TARMA (AFS-TARMA) approach is that the basis functions are not selected among an essentially infinite number of candidates, but are considered to be fully determined by an a-priori unknown vector of parameters $\boldsymbol{\delta}$ which has also to be estimated along with the coefficients of projection $\boldsymbol{\vartheta}$. In this way, the basis may be automatically adapted on the data in order to track the evolution of the system parameters with the highest possible accuracy. Two different functional families are considered in the sequel: A B-splines family and a decaying trigonometric family. These are collectively capable of effectively modelling a wide variety of parameter evolutions, from slow and smooth to fast and abrupt, but also periodic or quasi-periodic.

For purposes of brevity, the general case of a time-dependent parameter $v[t]$ is considered in the subsequent sections. Thus, substituting $v[t]$ by $a_i[t]$ in the following relationships the case of an AR parameter is obtained, $v[t] \equiv c_i[t]$ for the MA parameters, while $v[t] \equiv \sigma_w[t]$ for the case of the innovations standard deviation.

4.2.1 Adaptable models with B-spline basis functions

In this case we assume that the values of a time-varying parameter $v[t](t =, 1 \ldots, N)$ are data samples drawn from an underlying continuous piecewise polynomial function of order k [de Boor, 2001, Chs. 7-8]. Then, according to the Curry and Schoenberg Theorem [de Boor, 2001, pp. 97-98] a basis of splines (B-splines) may be constructed for the corresponding piecewise polynomial space. This basis is fully defined by an appropriate non-decreasing sequence of points (*knots*) $\boldsymbol{\tau} = [\tau_1, \ldots, \tau_{p+k}] \in [1, N] \subset \Re$ (where p is the basis dimensionality). This theorem leaves open the selection of the first k and last k knots. However, imposing no continuity conditions at the endpoints, $\tau_1 = \ldots = \tau_k = 1$ and $\tau_{p+1} = \ldots = \tau_{p+k} = N$ may be selected. This choice is also consistent with the fact that the constructed basis provides a valid representation only for the interval $[\tau_k, \tau_{p+1}]$, that is $[1, N]$.

Thus, in terms of the above quantities the B-splines of order k may be described by the functional subspace parameter vector $\boldsymbol{\delta} \triangleq [\tau_{k+1}, \ldots, \tau_p]^T$ of dimension $\dim(\boldsymbol{\delta}) = p - k$ consisting of the non-decreasing sequence of the free internal knots. The parameter $v[t] \in [1, N]$ is then expressed as:

$$v[t] = \sum_{j=1}^{p} v_j \cdot G_j^k[t, \boldsymbol{\delta}] \tag{4.2.4}$$

where $G_j^k[t, \boldsymbol{\delta}]$ denotes the sequence of B-splines of order k. Although, there are several ways to define the B-spline functions $G_j[t, \boldsymbol{\delta}]$, a convenient one is by the means of the Cox-de Boor recursion formula for the normalized B-splines [de Boor, 2001, p. 90]

$$G_j^1[t, \boldsymbol{\delta}] = \begin{cases} 1 & \text{if } \tau_j \leq t < \tau_{j+1} \\ 0 & \text{otherwise} \end{cases} \tag{4.2.5a}$$

$$G_j^i[t, \boldsymbol{\delta}] = \xi_{j,i}[t] \cdot G_j^{i-1}[t, \boldsymbol{\delta}] + (1 - \xi_{j,i}[t]) \cdot G_{j+1}^{i-1}[t, \boldsymbol{\delta}], \quad \text{for } 1 < i \leq k \tag{4.2.5b}$$

where

$$\xi_{j,i}[t] = \begin{cases} \frac{t-\tau_j}{\tau_{j+i-1}-\tau_j} & \text{if } \tau_j < \tau_{j+i-1}, \\ 0 & \text{otherwise.} \end{cases} \tag{4.2.5c}$$

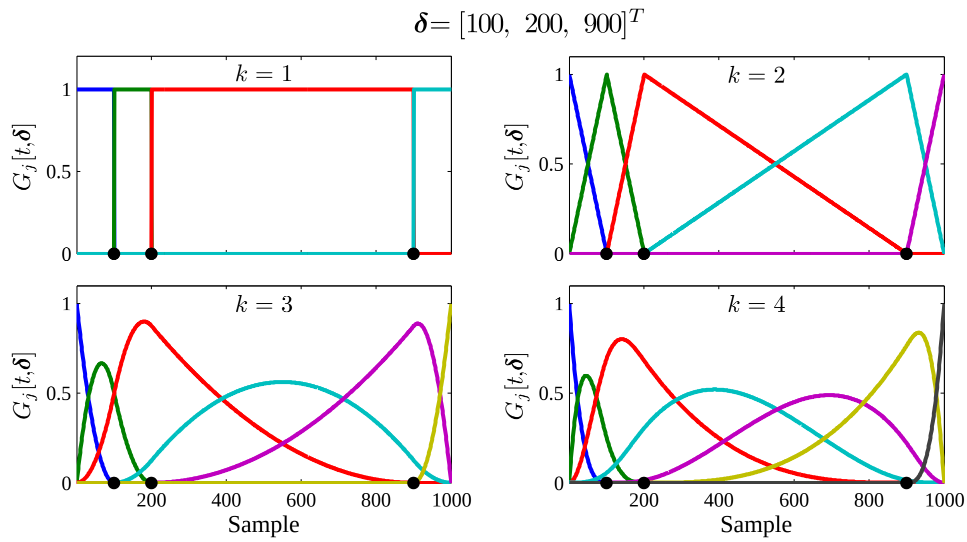

Figure 4.2.1: The B-splines of order $k = 1, 2, 3, 4$ for $N = 1000$ and functional subspace parameter vector $\boldsymbol{\delta} = [100,\ 200,\ 900]^T$.

The B-splines of order $k = 1, 2, 3, 4$ for $N = 1000$ and functional subspace parameter vector $\boldsymbol{\delta} = [100,\ 200,\ 900]^T$ are shown, for purposes of illustration, in Fig. 4.2.1.

B-splines have a number of properties that make them particularly attractive. First, they may achieve various degrees of smoothness depending on k. For instance, for $k = 1$ the basis consists of piecewise constant functions, for $k = 2$ linear B-splines, for $k = 3$ quadratic, for $k = 4$ cubic, and so on (see Fig. 4.2.1). Yet, smoothness may also be controlled by the proximity of knots [de Boor, 2001, Ch. 9].

Another useful property of the B-splines is their local support, that is $G_j^k[t, \boldsymbol{\delta}] \neq 0$ only for $t \in [\tau_j, \tau_{j+k})$. Due to this local support, the resulting basis may consist of splines with various characteristics and therefore may be capable of tracking time-varying parameters with mixed type of evolution, that is alternating patterns of smooth and abrupt changes. Finally, B-splines are locally linear independent, that is they provide a basis for the piecewise polynomial space even for an interval $[\alpha, \beta] \subseteq [\tau_1, \tau_{p+k}]$. A thorough analysis of B-splines and their properties may be found in [de Boor, 2001, Ch. 9].

Remark. Although the time-varying parameters are defined on the discrete time-domain, a continuous time-domain representation via B-splines is presently considered. The advantage of using such a representation is the fact that the derivatives of B-splines with respect to their knots may be computed with relative ease and thus fast optimization schemes, which typically rely on at least first order derivatives may be employed for the estimation of $\boldsymbol{\delta}$ (see Section 4.3).

Constraints on $\boldsymbol{\delta}$. From the above, it is obvious that the internal knots $\tau_{k+1}, \ldots, \tau_p$ are defined in the open set $(1, N)$ while they have also to satisfy an appropriate order relation as they form a non-decreasing sequence of real numbers. Hence, constraints need to be imposed on the parameter vector $\boldsymbol{\delta}$.

In order to come up with reasonably simple forms of constraints, only the case of internal knots with multiplicity one is considered. This is not restrictive in view of the fact that a B-spline with an internal knot of multiplicity $m > 1$ may be approximated by replacing this knot by m simple knots nearby [de Boor, 2001, p. 106].

Thus, an appropriate order relation constraint, suitable for numerical purposes (as it prevents the knots from coalescing when their distance becomes practically equal to zero) is:

$$\tau_j - \tau_{j-1} > \varepsilon, \quad j = k+1, \ldots, p+1, \quad (0 < \varepsilon \ll N)$$

where $\varepsilon > 0$ is a selected, sufficiently small separation parameter.

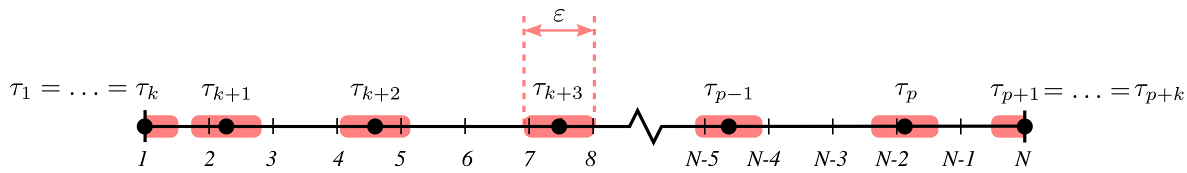

Figure 4.2.2: Constraints imposed on $\boldsymbol{\delta}$ for the case of B-splines. The distance between two internal knots has to be larger than $\varepsilon > 0$. The first and last internal knots, τ_{k+1} and τ_p respectively, have also to be ε away from the endpoints 1 and N, respectively.

Therefore, the following $p-k+1$ inequality constraints are imposed on the parameter vector $\boldsymbol{\delta}$:

$$\left.\begin{aligned} \tau_{k+1}-\tau_k = \tau_{k+1}-1 &\geq \varepsilon \\ \tau_{k+2}-\tau_{k+1} &\geq \varepsilon \\ &\vdots \\ \tau_p-\tau_{p-1} &\geq \varepsilon \\ \tau_{p+1}-\tau_p = N-\tau_p &\geq \varepsilon \end{aligned}\right\} \Longrightarrow \begin{bmatrix} -1 & 0 & \dots & 0 & 0 \\ 1 & -1 & \dots & 0 & 0 \\ \vdots & \vdots & \ddots & \vdots & \vdots \\ 0 & 0 & \dots & 1 & -1 \\ 0 & 0 & \dots & 0 & 1 \end{bmatrix} \cdot \underbrace{\begin{bmatrix} \tau_{k+1} \\ \tau_{k+2} \\ \vdots \\ \tau_{p-1} \\ \tau_p \end{bmatrix}}_{\boldsymbol{\delta}} - \begin{bmatrix} -1-\varepsilon \\ -\varepsilon \\ \vdots \\ -\varepsilon \\ N-\varepsilon \end{bmatrix} \leq 0 \tag{4.2.6}$$

which are also depicted schematically in Fig. 4.2.2.

4.2.2 Adaptable models with decaying trigonometric basis functions

Even though the family of B-splines is capable of accurately representing a wide variety of evolutions, including abrupt and fast changes, a second family of basis functions which may be more effective for the case of periodic or quasi-periodic evolutions is now considered.

For purposes of physical interpretation, it is convenient to begin our analysis by considering that the time-varying parameter $v[t]$ obeys the following homogeneous linear difference equation [Cull et al., 2005, Ch. 2]:

$$v[t] = \psi_1 \cdot v[t-1] + \ldots + \psi_p \cdot v[t-p]$$

with ψ's designating real constant coefficients and p the order of the difference equation. Then, $v[t]$ may be expressed by the means of the general solutions of the above equation as:

$$\begin{aligned} v[t] &= \left[\frac{v_1}{2} + \sqrt{-1}\cdot\frac{v_{q+1}}{2}\right]\cdot\lambda_1^t + \left[\frac{v_1}{2} - \sqrt{-1}\cdot\frac{v_{q+1}}{2}\right]\cdot(\lambda_1^*)^t + \ldots \\ &\quad + \left[\frac{v_q}{2} + \sqrt{-1}\cdot\frac{v_{2q}}{2}\right]\cdot\lambda_q^t + \left[\frac{v_q}{2} - \sqrt{-1}\cdot\frac{v_{2q}}{2}\right]\cdot(\lambda_q^*)^t + v_{2q+1}\cdot\lambda_{2q+1}^t + \ldots + v_{i,p}\cdot\lambda_p^t = \\ &= \sum_{j=1}^{q}\left(v_j r_j^t\cos(\omega_j t) + v_{j+q} r_j^t \sin(\omega_j t)\right] + \sum_{j=1}^{p-2q} v_{j+2q}\rho_j^t = \sum_{j=1}^{p} v_j \cdot G_j[t,\boldsymbol{\delta}] \end{aligned}$$

where

$$G_j[t,\boldsymbol{\delta}] = r_j^t\cos(\omega_j t), \quad G_{j+q}[t,\boldsymbol{\delta}] = r_j^t\sin(\omega_j t), \quad \text{for } j=1,\ldots,q, \text{ and} \tag{4.2.7a}$$

$$G_{j+2q}[t,\boldsymbol{\delta}] = \rho_j^t, \quad \text{for } j=1,\ldots,p-2q \tag{4.2.7b}$$

and q is the number of pairs of complex conjugate roots. In the above relations, $\boldsymbol{\delta} \triangleq [\, r_1,\ldots,r_q,\ \omega_1,\ldots,\omega_q,\ \rho_1,\ldots,\rho_{p-2q}\,]^T$ is the functional subspace parameter vector, r_j and ω_j are the magnitude and phase of the complex root λ_j in polar coordinates, that is $\lambda_j = r_j\cdot[\cos(\omega_j) + i\cdot\sin(\omega_j)]$, with $j=1,\ldots,q$, and $\lambda_{2q+j} \equiv \rho_j \in \Re$, with $j=1,\ldots,p-2q$, are the real roots. The asterisk * indicates complex conjugate. Note that in this study only the case of distinct complex roots is considered while extensions to other cases may be readily obtained.

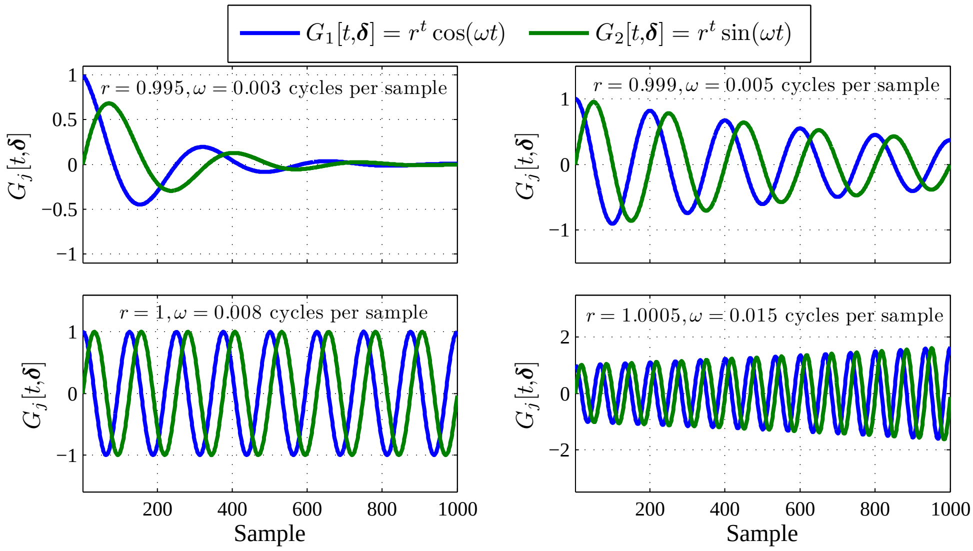

Figure 4.2.3: The decaying trigonometric basis functions $G_1[t, \boldsymbol{\delta}] = r^t \cos(\omega t)$ and $G_2[t, \boldsymbol{\delta}] = r^t \sin(\omega t)$ for $N = 1000$ and various rates of decay and frequencies ($\boldsymbol{\delta} = [r,\ \omega]^T$).

Apparently, the resulting time-invariant parameter vector $\boldsymbol{\delta}$ includes the characteristics of the decaying trigonometric functional basis. In contrast to the trigonometric bases that have been used in the literature, the one just described does not consist of discrete frequency trigonometric functions and thus may achieve accurate estimation of the underlying frequencies. Moreover, the rate of decay makes it more flexible for tracking also piecewise periodic or quasi-periodic evolutions.

The decaying trigonometric basis functions $G_1[t, \boldsymbol{\delta}] = r^t \cos(\omega t)$ and $G_2[t, \boldsymbol{\delta}] = r^t \sin(\omega t)$ for $N = 1000$ and various rates of decay and frequencies are shown in Fig. 4.2.3.

Constraints on $\boldsymbol{\delta}$. The magnitudes r and ρ must be constrained close to unity, that is

$$1 - \frac{\varepsilon}{N} < [r_i, \rho_j] < 1 + \frac{\varepsilon}{N}, \qquad (\text{with } i = 1, \ldots, q, j = 1, \ldots, p - 2q \text{ and } 0 < \varepsilon < N) \tag{4.2.8a}$$

In that way, the corresponding trigonometric functions do not decay or increase too fast and as a result the case of a practically null or infinite basis function is circumvented (i.e. for $\rho_j \ll 1$ the basis ρ_j^t is practically equal to zero for almost every t). Lower bounds should also be placed on the phases ω_j, preventing the corresponding pair of complex roots from falling on the real axis giving again a null basis [for $\omega_j = 0$ the basis $r_j^t \sin(\omega_j t)$ equals to zero $\forall t$]:

$$0 < \omega_{\min} \leq \omega_j \leq \omega_{\max}, \qquad (\text{with } j = 1, \ldots, q) \tag{4.2.8b}$$

Furthermore, as only distinct roots are considered, the distance between two adjacent roots must be constrained by a lower limit d_0. This constraint leads to the following nonlinear inequalities:

$$\begin{aligned}
&\sqrt{(r_j \cos\omega_j - r_i \cos\omega_i)^2 + (r_j \sin\omega_j - r_i \sin\omega_i)^2} \geq d_0 \quad \Longrightarrow \\
&\sqrt{r_i^2 + r_j^2 - r_i r_j \cos(\omega_i - \omega_j)} \geq d_0 \quad \Longrightarrow \\
&r_i^2 + r_j^2 - r_i r_j \cos(\omega_i - \omega_j) - d_0^2 \geq 0, \quad (i, j = 1, \ldots, q; \quad j > i)
\end{aligned} \tag{4.2.8c}$$

and

$$\sqrt{(\rho_j - \rho_i)^2} \geq d_0 \quad \Longrightarrow |\rho_j - \rho_i| - d_0^2 \geq 0, \quad (i, j = 1, \ldots, p - 2q; \quad j > i) \tag{4.2.8d}$$

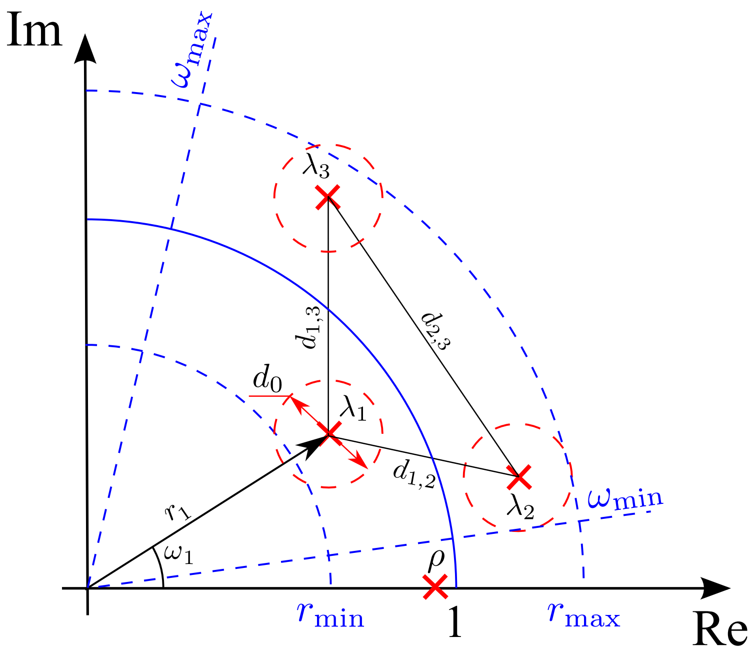

Figure 4.2.4: Constraints imposed on an hypothetical functional subspace parameter vector $\boldsymbol{\delta}$ for the case of decaying trigonometric basis functions. The roots magnitudes have to be in the proximity of the unit circle, the distance between two distinct roots have to be larger than d_0 while also for practical reasons the roots phases are constrained by simple bounds.

Table 4.1: Functional subspace parametrization and constraints.

	$\boldsymbol{\delta}$	$\dim(\boldsymbol{\delta})$	Type of constraints	# of constraint functions
B-splines	τ_j's	$p-k$	Linear inequalities	$p-k+1$
Decaying trigonometric	r_j's, ω_j's, ρ_j's	p	Simple bounds and nonlinear inequalities	$2p+\frac{q(q-1)}{2}+\frac{(p-2q)(p-2q-1)}{2}$

k: B-splines order, q: number of pairs of complex conjugate roots

The total number of constraint functions in this case is $2p+\frac{q!}{2!(q-2)!}+\frac{p-2q!}{2!(p-2q-2)!}=2p+\frac{q(q-1)}{2}+\frac{(p-2q)(p-2q-1)}{2}$, that is $2p$ inequalities for the imposed lower and upper bounds and $\frac{q(q-1)}{2}+\frac{(p-2q)(p-2q-1)}{2}$ nonlinear constraint functions that is all the possible pairs of complex roots and pairs of real roots.

The three types of constraints are represented graphically for a hypothetical set of basis functions in Fig. 4.2.4.

4.2.3 Summary

Two different families of adaptable basis functions were described in the previous paragraphs: a B-splines family characterized by initially unknown knots, and a decaying trigonometric family with initially unknown rates of decay and frequencies. The characteristics of the functional subspace parameter vector $\boldsymbol{\delta}$ for these families are summarized in Table 4.1. In the sequel, the constraints for both cases are expressed as $\boldsymbol{H}(\boldsymbol{\delta}) \leq 0$.

It is reminded that the basis of the AR, MA parts and the innovations standard deviation are described analogously with the corresponding basis functions being determined by the functional subspace parameter vectors $\boldsymbol{\delta}_a$, $\boldsymbol{\delta}_c$ and $\boldsymbol{\delta}_s$, respectively.

4.3 AFS-TARMA Model Identification

The AFS-TARMA model identification problem may be posed as follows:

"Given N observations of the non-stationary signal $\boldsymbol{x}^N \triangleq \{x[1]\ldots x[N]\}$ and the AFS-TARMA model set:

$$\mathbb{M} = \Big\{\mathcal{M}(\boldsymbol{\delta},\boldsymbol{\vartheta}) \;:\; x[t] + \sum_{i=1}^{n_a} a_i[t,\boldsymbol{\delta},\boldsymbol{\vartheta}]\cdot x[t-i] = e[t,\boldsymbol{\delta},\boldsymbol{\vartheta}] + \sum_{i=1}^{n_c} c_i[t,\boldsymbol{\delta},\boldsymbol{\vartheta}]\cdot e[t-i,\boldsymbol{\delta},\boldsymbol{\vartheta}];$$
$$\sigma_e^2[t,\boldsymbol{\delta},\boldsymbol{\vartheta}] = E\{e^2[t,\boldsymbol{\delta},\boldsymbol{\vartheta}]\}, \quad t=1,\ldots,N, \quad \boldsymbol{\delta}\in\Omega\subset\Re^{\dim(\boldsymbol{\delta})}, \quad \boldsymbol{\vartheta}\in\Re^{\dim(\boldsymbol{\vartheta})}\Big\} \tag{4.3.1}$$

select an element of $\mathbb{M}$ that best fits the observations".

In this expression $E\{\cdot\}$ indicates statistical expectation, $\boldsymbol{\delta} = [\ \boldsymbol{\delta}_a^T \mid \boldsymbol{\delta}_c^T \mid \boldsymbol{\delta}_s^T\ ]^T$ the functional subspace parameter vector, $\boldsymbol{\vartheta} = [\ \boldsymbol{\vartheta}_a^T \mid \boldsymbol{\vartheta}_c^T \mid \boldsymbol{\vartheta}_s^T\ ]^T$ the model parameter vector consisting of the projection coefficients $a_{i,j}, c_{i,j}, s_j$, while $e[t,\boldsymbol{\delta},\boldsymbol{\vartheta}]$ stands for the model's one-step-ahead prediction error (residual) sequence, which, as in the stationary case, coincide with the model's innovations sequence $w[t]$ when the true parameter vector responsible for the generation of $x[t]$ is used in Eq. (4.3.1).

For this adaptable approach the complete parameter vector contains the AR, MA, and innovations variance functional subspace parameters and the corresponding coefficients of projection, while the model structure is defined by the model orders n_a, n_c, and the basis dimensionalities p_a, p_c, p_s:

$$\boldsymbol{\theta} = [\boldsymbol{\delta}^T \mid \boldsymbol{\vartheta}^T]^T \tag{4.3.2a}$$

$$\mathcal{M} = \{n_a, n_c, p_a, p_c, p_s\} \tag{4.3.2b}$$

Both $\boldsymbol{\theta}$ and $\mathcal{M}$ need to be estimated from available data with the complete identification problem being usually distinguished into two subproblems: (a) the parameter estimation subproblem (for a given model structure $\mathcal{M}$), and (b) the model structure selection subproblem. These are discussed in the following subsections.

Remark. In the classical FS-TARMA approach the complete parameter vector consists only of the coefficients of projection parameter vectors $\boldsymbol{\theta} = [\ \boldsymbol{\vartheta}_a^T\ \boldsymbol{\vartheta}_c^T\ \boldsymbol{\vartheta}_s^T\ ]^T$ since the functional subspaces are not estimated but are selected from an ordered set of fixed basis functions. At the same time the structure of a classical FS-TARMA model is fully defined by the model orders (n_a, n_c), the functional subspace dimensionalities (p_a, p_c, p_s), and in addition the indeces of the specific basis functions that are included in each functional subspace [Poulimenos and Fassois, 2006].

Comparing the two approaches, classical and adaptable, it becomes clear that in the latter the model structure selection problem is significantly reduced at the price of the increased dimension of the complete parameter vector $\boldsymbol{\theta}$ and the increased algorithmic complexity of the corresponding estimation problem. However, the main advantage of the adaptable approach is that the parametrized basis functions are able to automatically adapt on the data in order to track the evolution of the system parameters with the highest possible accuracy, while in the classical approach the tracking accuracy depends heavily on the selected set of fixed basis functions.

4.3.1 Parameter estimation

4.3.1.1 The AFS-TAR case

Ignoring the MA part of the general AFS-TARMA model of Eq. (4.2.1), the AFS-TAR model may be re-written in the nonlinear regression form:

$$\begin{aligned} x[t] &= -\sum_{i=1}^{n_a}\sum_{j=1}^{p_a} a_{i,j}\cdot G_{a(j)}[t,\boldsymbol{\delta}_a]\cdot x[t-i] + e[t,\boldsymbol{\delta}_a,\boldsymbol{\vartheta}_a] \\ &= -\big(a_{1,1}\cdot G_{a(1)}[t,\boldsymbol{\delta}_a] + \ldots + a_{1,p_a}\cdot G_{a(p_a)}[t,\boldsymbol{\delta}_a]\big)\cdot x[t-1] - \ldots \\ &\quad -\big(a_{n_a,1}\cdot G_{a(1)}[t,\boldsymbol{\delta}_a] + \ldots + a_{n_a,p_a}\cdot G_{a(p_a)}[t,\boldsymbol{\delta}_a]\big)\cdot x[t-n_a] + e[t,\boldsymbol{\delta}_a,\boldsymbol{\vartheta}_a] \Longrightarrow \end{aligned}$$

$$\Longrightarrow x[t] = \underbrace{\begin{bmatrix} -x[t-1]\cdot G_{a(1)}[t,\boldsymbol{\delta}_a] \\ -x[t-1]\cdot G_{a(2)}[t,\boldsymbol{\delta}_a] \\ \vdots \\ -x[t-1]\cdot G_{a(p_a)}[t,\boldsymbol{\delta}_a] \\ \hdashline \vdots \\ \hdashline -x[t-n_a]\cdot G_{a(1)}[t,\boldsymbol{\delta}_a] \\ -x[t-n_a]\cdot G_{a(2)}[t,\boldsymbol{\delta}_a] \\ \vdots \\ -x[t-n_a]\cdot G_{a(p_a)}[t,\boldsymbol{\delta}_a] \end{bmatrix}^T}_{\boldsymbol{\phi}^T[t,\boldsymbol{\delta}_a]_{(n_a\cdot p_a\times 1)}} \cdot \underbrace{\begin{bmatrix} a_{1,1} \\ a_{1,2} \\ \vdots \\ a_{1,p_a} \\ \hdashline \vdots \\ \hdashline a_{n_a,1} \\ a_{n_a,2} \\ \vdots \\ a_{n_a,p_a} \end{bmatrix}}_{\boldsymbol{\vartheta}_{a(n_a\cdot p_a\times 1)}} + e[t,\boldsymbol{\delta}_a,\boldsymbol{\vartheta}_a], \qquad t=1,\ldots,N \tag{4.3.3}$$

Using the stacked signal and innovations sequence vectors $\boldsymbol{x} = \big[x[1],\ldots,x[N]\big]^T$ and $\boldsymbol{e}(\boldsymbol{\delta}_a,\boldsymbol{\vartheta}_a) = \big[e[1,\boldsymbol{\delta}_a,\boldsymbol{\vartheta}_a],\ldots,e[N,\boldsymbol{\delta}_a,\boldsymbol{\vartheta}_a]\big]^T$:

$$\boldsymbol{x} = \boldsymbol{\Phi}(\boldsymbol{\delta}_a)\cdot\boldsymbol{\vartheta}_a + \boldsymbol{e}(\boldsymbol{\delta}_a,\boldsymbol{\vartheta}_a) \tag{4.3.4}$$

where $\boldsymbol{\Phi}(\boldsymbol{\delta}_a) = \big[\boldsymbol{\phi}[1,\boldsymbol{\delta}_a],\ldots,\boldsymbol{\phi}[N,\boldsymbol{\delta}_a]\big]^T$.

The estimation of the model parameter vectors $\boldsymbol{\delta}_a$ and $\boldsymbol{\vartheta}_a$ may be based on the minimization of the Prediction Error (PE) criterion $V(\boldsymbol{\delta}_a,\boldsymbol{\vartheta}_a) = \|\boldsymbol{e}(\boldsymbol{\delta}_a,\boldsymbol{\vartheta}_a)\|^2$ consisting of the sum of squares of the model's one-step-ahead prediction errors, subject to the constraints discussed in the previous section, that is:

$$\begin{aligned} &[\widehat{\boldsymbol{\delta}}_a^T, \widehat{\boldsymbol{\vartheta}}_a^T]^T = \arg\min_{\boldsymbol{\delta}_a,\boldsymbol{\vartheta}_a} V(\boldsymbol{\delta}_a,\boldsymbol{\vartheta}_a) = \arg\min_{\boldsymbol{\delta}_a,\boldsymbol{\vartheta}_a} \|\boldsymbol{e}(\boldsymbol{\delta}_a,\boldsymbol{\vartheta}_a)\|^2 \\ &\text{subject to} \quad \boldsymbol{H}(\boldsymbol{\delta}_a) \leq 0 \end{aligned} \tag{4.3.5}$$

In this relation, $\arg\min$ stands for "argument minimizing", $\boldsymbol{e}(\boldsymbol{\delta}_a,\boldsymbol{\vartheta}_a)$ the model one-step-ahead prediction error, while $\|\cdot\|$ indicates Euclidean norm. The hat designates estimator/estimate of the indicated quantity.

Due to the nonlinear dependence of the basis functions $G_{a(j)}[t,\boldsymbol{\delta}_a]$ on the parameter vector $\boldsymbol{\delta}_a$ the above minimization problem is non-quadratic with linear inequality constraints for the case of the B-splines and nonlinear inequality constraints for the case of the decaying trigonometric functions. This problem may be, in principle, solved through iterative constrained nonlinear optimization schemes with respect to $\dim(\boldsymbol{\vartheta}_a) + \dim(\boldsymbol{\delta}_a) = p_a\cdot n_a + \dim(\boldsymbol{\delta}_a)$ parameters. Interior point methods may be used in this context [Nocedal and Wright, 2006, Ch. 19]. These methods handle inequality constraints through a logarithmic barrier function and have been shown to be particularly effective for large-scale applications [Nocedal and Wright, 2006, pp. 592-593].

Nevertheless, an effective solution may be achieved by taking advantage of the separable nonlinear regression structure of Eq. (4.3.4), that is the fact that the parameters $\boldsymbol{\vartheta}_a$ and $\boldsymbol{\delta}_a$ form two completely disjoint parameter sets. The problem is a Separable Nonlinear Least Squares (SNLS) one that may be solved by the Variable Projection (VP) method introduced by Golub and Pereyra [Golub and Pereyra, 1973], which is based on the fact that $\boldsymbol{\vartheta}_a$ appears linearly in the model. Thus, assuming that the "nonlinear parameter vector" $\boldsymbol{\delta}_a$ is known, a $\boldsymbol{\vartheta}_a$ estimate may be obtained through the Ordinary Least Squares (OLS) estimator:

$$\widehat{\boldsymbol{\vartheta}_a} = \big(\boldsymbol{\Phi}^T(\boldsymbol{\delta}_a)\cdot\boldsymbol{\Phi}(\boldsymbol{\delta}_a)\big)^{-1}\cdot\boldsymbol{\Phi}^T(\boldsymbol{\delta}_a)\cdot\boldsymbol{x} = \boldsymbol{\Phi}^{\dagger}(\boldsymbol{\eta}_a)\cdot\boldsymbol{x} \tag{4.3.6}$$

with † designating pseudo-inverse. Hence, after substituting $\widehat{\boldsymbol{\vartheta}}_a$ in Eq. (4.3.4), the model innovations may be expressed in a VP functional form $e_{\text{VP}}(\boldsymbol{\delta}_a)$ which depends only on $\boldsymbol{\delta}_a$ as follows:

$$\begin{aligned} &\boldsymbol{e}(\boldsymbol{\delta}_a, \widehat{\boldsymbol{\vartheta}_a}) = \boldsymbol{x} - \boldsymbol{\Phi}(\boldsymbol{\delta}_a)\cdot \widehat{\boldsymbol{\vartheta}_a} \implies \boldsymbol{e}_{\text{VP}}(\boldsymbol{\delta}_a) = \boldsymbol{x} - \boldsymbol{\Phi}(\boldsymbol{\delta}_a)\cdot \boldsymbol{\Phi}^\dagger(\boldsymbol{\delta}_a)\cdot \boldsymbol{x} \implies \\ &\boldsymbol{e}_{\text{VP}}(\boldsymbol{\delta}_a) = \big(\boldsymbol{I} - \boldsymbol{\Phi}(\boldsymbol{\delta}_a)\cdot \boldsymbol{\Phi}^\dagger(\boldsymbol{\delta}_a)\big)\cdot \boldsymbol{x} \end{aligned} \tag{4.3.7}$$

and the estimator of Eq. (4.3.5) takes the form:

$$\begin{aligned} &\widehat{\boldsymbol{\delta}}_a = \arg\min_{\boldsymbol{\delta}_a} V_{\text{VP}}(\boldsymbol{\delta}_a) = \arg\min_{\boldsymbol{\delta}_a} \|\boldsymbol{e}_{\text{VP}}(\boldsymbol{\delta}_a)\|^2 = \arg\min_{\boldsymbol{\delta}_a} \|\big(\boldsymbol{I} - \boldsymbol{\Phi}(\boldsymbol{\delta}_a)\cdot \boldsymbol{\Phi}^\dagger(\boldsymbol{\delta}_a)\big)\cdot \boldsymbol{x}\|^2 \\ &\text{subject to} \quad \boldsymbol{H}(\boldsymbol{\delta}_a) \le 0 \end{aligned} \tag{4.3.8}$$

with $V_{\text{VP}}(\boldsymbol{\delta}_a)$ designating the *variable projection* functional. The nonlinear parameter vector $\boldsymbol{\delta}_a$ may be thus estimated by means of iterative constrained nonlinear optimization techniques with only $\dim(\boldsymbol{\delta}_a)$ unknown parameters, while $\boldsymbol{\vartheta}_a$ may be subsequently estimated through linear OLS (Eq. (4.3.6)), after substituting $\boldsymbol{\delta}_a$ by the obtained estimate $\widehat{\boldsymbol{\delta}_a}$. The method is referred to as VP method as the matrix $\big(\boldsymbol{I} - \boldsymbol{\Phi}(\boldsymbol{\delta}_a)\cdot \boldsymbol{\Phi}^\dagger(\boldsymbol{\delta}_a)\big)$ is the projector on the orthogonal complement of the column space of $\boldsymbol{\Phi}(\boldsymbol{\delta}_a)$. A topical review on the VP method and its applications may be found in [Golub and Pereyra, 2003].

This formulation leads to the reduction of the dimensionality of the nonlinear optimization problem, while not affecting the stationary points (minima and maxima) of the original problem. This holds under the rather mild condition of constant (not necessarily maximum) rank of the regression matrix $\boldsymbol{\Phi}(\boldsymbol{\delta}_a)$ over the whole parameter search space of $\boldsymbol{\delta}_a$ ([Golub and Pereyra, 1973, Theorem 2.1]; Appendix 4.A). The constraints described in the previous section in fact guarantee the linear independence for both the B-spline and decaying trigonometric basis functions and thus they define an appropriate parameter space on which $\boldsymbol{\Phi}(\boldsymbol{\delta}_a)$ has constant and full rank.

The cost for reducing the dimension of the nonlinear optimization problem is the increased complexity of the gradient computation for the VP objective function $V_{\text{VP}}(\boldsymbol{\delta}_a)$. Golub and Pereyra [Golub and Pereyra, 1973] have derived the necessary relationships for the differentiation of pseudoinverses and the required gradient of $\Phi^\dagger$ with respect to the nonlinear parameter vector for the general SNLS problem. Approximate solutions which aim at computational time reduction have also been proposed. A comparison and asymptotic analysis study for the three most frequently used algorithms may be found in [Ruhe and Å. Wedin, 1980]. In the present study the original, exact, approach is followed with the resulting gradient being given in 4.B. The algorithmic steps for the estimation of $\boldsymbol{\delta}_a$ and $\boldsymbol{\vartheta}_a$ through the VP method are summarized in Table 4.2.

Estimation of the innovations std parameter vector $[\boldsymbol{\delta}_s^T, \boldsymbol{\vartheta}_s^T]^T$ may also be obtained via the VP method. In particular, based on the normality of the innovations sequence $E\{|e[t]|\} = \sqrt{2/\pi}\cdot\sigma_e[t]$ [Grenier, 1983b] and by utilizing the absolute values of the estimated residual series $e[t, \widehat{\boldsymbol{\delta}_a}, \widehat{\boldsymbol{\vartheta}_a}]$, the following overdetermined set of equations may be obtained

$$|e[t, \widehat{\boldsymbol{\delta}_a}, \widehat{\boldsymbol{\vartheta}_a}]| = \sqrt{\frac{2}{\pi}}\cdot \sum_{j=1}^{p_s} s_j \cdot G_{s(j)}[t, \boldsymbol{\delta}_s] = \boldsymbol{g}_s^T[t, \boldsymbol{\delta}_s]\cdot \boldsymbol{s} \tag{4.3.9}$$

which solved in the least squares sense leads to a constrained SNLS problem of the following VP form:

$$\begin{aligned} &\widehat{\boldsymbol{\delta}}_s = \arg\min_{\boldsymbol{\delta}_s} V_{\text{VP}}(\boldsymbol{\delta}_s) = \arg\min_{\boldsymbol{\delta}_s} \|\big(\boldsymbol{I} - \boldsymbol{G}_s(\boldsymbol{\delta}_s)\cdot \boldsymbol{G}_s^\dagger(\boldsymbol{\delta}_s)\big)\cdot |\boldsymbol{e}(\widehat{\boldsymbol{\delta}_a}, \widehat{\boldsymbol{\vartheta}_a})|\ \|^2 \\ &\text{subject to} \quad \boldsymbol{H}(\boldsymbol{\delta}_s) \le 0 \end{aligned} \tag{4.3.10}$$

In the above $\boldsymbol{g}_s[t, \boldsymbol{\delta}_s] = \sqrt{\frac{2}{\pi}}\cdot \big[G_{s(1)}[t, \boldsymbol{\delta}_s], \ldots, G_{s(p_s)}[t, \boldsymbol{\delta}_s]\big]^T$ and $\boldsymbol{G}_s(\boldsymbol{\delta}_s) = \big[\boldsymbol{g}_s[1, \boldsymbol{\delta}_s], \ldots, \boldsymbol{g}_s[N, \boldsymbol{\delta}_s]\big]^T$. The algorithmic details for the estimation of $\boldsymbol{\delta}_s$ through the VP method are summarized in Table 4.3.

Remark: Gradient-based iterative nonlinear optimization methods are sensitive to initialization, thus may guarantee only local convergence. For this reason rather accurate initial guess parameter values

Table 4.2: AFS-TAR model identification – Algorithm details for $\boldsymbol{\delta}_a$ and $\boldsymbol{\vartheta}_a$ estimation through the variable projection method.

Input: Non-stationary data $\boldsymbol{x}$, AR order n_a, AR functional subspace dimensionality p_a

(1) Choose initial $\boldsymbol{\delta}_a$ appropriately

(2) For $j = 1, 2, \ldots,$ until convergence

(i) Compute $\boldsymbol{e}_{VP}(\boldsymbol{\delta}_a) = \big(\boldsymbol{I} - \boldsymbol{\Phi}(\boldsymbol{\delta}_a) \cdot \boldsymbol{\Phi}^{\dagger}(\boldsymbol{\delta}_a)\big) \cdot \boldsymbol{x}$

(ii) Test for convergence

(iii) Increment $\boldsymbol{\delta}_a^{(j+1)} = \boldsymbol{\delta}_a^{(j)} + \mu^{(j)} \cdot V'_{\mathrm{VP}}(\boldsymbol{\delta}_a)$

(3) Compute $\boldsymbol{\vartheta}_a = \Big(\boldsymbol{\Phi}(\boldsymbol{\delta}_a) \cdot \boldsymbol{\Phi}^T(\boldsymbol{\delta}_a)\Big)^{-1} \cdot \Big(\boldsymbol{\Phi}(\boldsymbol{\delta}_a) \cdot \boldsymbol{x}\Big)$

Ouput: $\widehat{\boldsymbol{\delta}_a}, \widehat{\boldsymbol{\vartheta}_a}$

$\mu^{(j)}$: Step-length

$V'_{\mathrm{VP}}(\boldsymbol{\delta}_a)$: Gradient of the VP functional with respect to $\boldsymbol{\delta}_a$

Table 4.3: AFS-TAR model identification – Algorithm details for $\boldsymbol{\delta}_s$ and $\boldsymbol{\vartheta}_s$ estimation through the variable projection method.

Input: Innovations sequence $\boldsymbol{e}(\widehat{\boldsymbol{\delta}_a}, \widehat{\boldsymbol{\vartheta}_a})$, $\sigma_e[t]$ functional subspace dimensionality p_s

(1) Choose initial $\boldsymbol{\delta}_s$ appropriately

(2) For $j = 1, 2, \ldots,$ until convergence

(i) Compute $\big(\boldsymbol{I} - \boldsymbol{G}_s(\boldsymbol{\delta}_s) \cdot \boldsymbol{G}_s^{\dagger}(\boldsymbol{\delta}_s)\big) \cdot |\boldsymbol{e}(\boldsymbol{\delta}_a, \boldsymbol{\vartheta}_a)|$

(ii) Test for convergence

(iii) Increment $\boldsymbol{\delta}_s^{(j+1)} = \boldsymbol{\delta}_s^{(j)} + \mu^{(j)} \cdot V'_{\mathrm{VP}}(\boldsymbol{\delta}_s)$

(3) Compute $\boldsymbol{\vartheta}_s = \Big(\boldsymbol{G}_s(\boldsymbol{\delta}_s) \cdot \boldsymbol{G}_s^T(\boldsymbol{\delta}_s)\Big)^{-1} \cdot \Big(\boldsymbol{G}_s(\boldsymbol{\delta}_s) \cdot \boldsymbol{x}\Big)$

Ouput: $\widehat{\boldsymbol{\delta}_s}, \widehat{\boldsymbol{\vartheta}_s}$

$\mu^{(j)}$: Step-length

$V'_{\mathrm{VP}}(\boldsymbol{\delta}_s)$: Gradient of the VP functional with respect to $\boldsymbol{\delta}_s$

are normally required. In order to overcome this difficulty, as a first step optimization may be based on a non-gradient probabilistic search algorithm, such as Particle Swarm Optimization (PSO; see Appendix 4.C) followed by refinement through iterative nonlinear optimization methods (interior point methods are presently used in this context [Nocedal and Wright, 2006, Ch. 19]). The proposed estimation procedure is illustrated in the flowchart of Fig. 4.3.1.

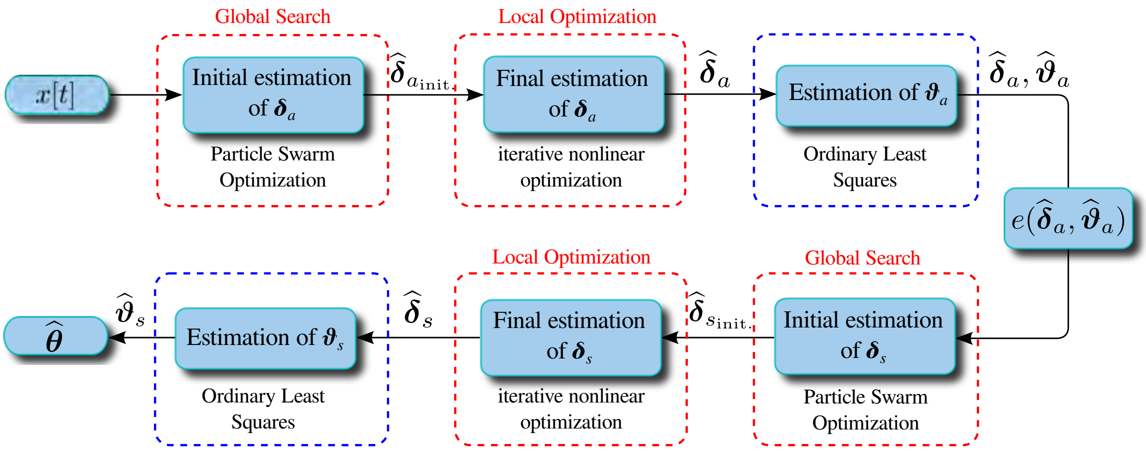

Figure 4.3.1: Flowchart of the AFS-TAR identification method.

4.3.1.2 The AFS-TARMA case

A similar procedure leads to the following nonlinear regression form for the AFS-TARMA model:

$$\Longrightarrow x[t] = \underbrace{\begin{bmatrix} -x[t-1]\cdot G_{a(1)}[t,\boldsymbol{\delta}_a] \\ -x[t-1]\cdot G_{a(2)}[t,\boldsymbol{\delta}_a] \\ \vdots \\ -x[t-n_a]\cdot G_{a(p_a-1)}[t,\boldsymbol{\delta}_a] \\ -x[t-n_a]\cdot G_{a(p_a)}[t,\boldsymbol{\delta}_a] \\ \hdashline e[t-1,\boldsymbol{\delta}_{a|c},\boldsymbol{\vartheta}_{a|c}]\cdot G_{c(1)}[t,\boldsymbol{\delta}_c] \\ e[t-1,\boldsymbol{\delta}_{a|c},\boldsymbol{\vartheta}_{a|c}]\cdot G_{c(2)}[t,\boldsymbol{\delta}_c] \\ \vdots \\ e[t-n_c,\boldsymbol{\delta}_{a|c},\boldsymbol{\vartheta}_{a|c}]\cdot G_{c(p_c-1)}[t,\boldsymbol{\delta}_c] \\ e[t-n_c,\boldsymbol{\delta}_{a|c},\boldsymbol{\vartheta}_{a|c}]\cdot G_{c(p_c)}[t,\boldsymbol{\delta}_c] \end{bmatrix}^T}_{\boldsymbol{\phi}[t,\boldsymbol{\delta}_{a|c},\boldsymbol{\vartheta}_{a|c}]_{(n_a\cdot p_a+n_c\cdot p_c\times 1)}} \cdot \underbrace{\begin{bmatrix} a_{1,1} \\ a_{1,2} \\ \vdots \\ a_{n_a,p_a-1} \\ a_{n_a,p_a} \\ \hdashline c_{1,1} \\ c_{1,2} \\ \vdots \\ c_{n_c,p_c-1} \\ c_{n_c,p_c} \end{bmatrix}}_{\boldsymbol{\vartheta}_{a|c_{(n_a\cdot p_a+n_c\cdot p_c\times 1)}}} + e[t,\boldsymbol{\delta}_{a|c},\boldsymbol{\vartheta}_{a|c}], \qquad t=1,\ldots,N \tag{4.3.11}$$

or, using the stacked signal and innovations sequence vectors:

$$\boldsymbol{x} = \boldsymbol{\Phi}(\boldsymbol{\delta}_{a|c},\boldsymbol{\vartheta}_{a|c})\cdot\boldsymbol{\vartheta}_{a|c} + \boldsymbol{e}(\boldsymbol{\delta}_{a|c},\boldsymbol{\vartheta}_{a|c}) \tag{4.3.12}$$

In these relations $\boldsymbol{\delta}_{a|c} = [\ \boldsymbol{\delta}_a^T \mid \boldsymbol{\delta}_c^T\ ]^T$ designates the AR/MA functional subspace parameter vector and $\boldsymbol{\vartheta}_{a|c} = [\ \boldsymbol{\vartheta}_a^T \mid \boldsymbol{\vartheta}_c^T\ ]^T$ the AR/MA coefficients of projection vector.

Again, the estimation of the parameter vectors $\boldsymbol{\delta}_{a|c}$ and $\boldsymbol{\vartheta}_{a|c}$ may be based on the minimization of the PE criterion $V(\boldsymbol{\delta}_{a|c},\boldsymbol{\vartheta}_{a|c}) = \|\boldsymbol{e}(\boldsymbol{\delta}_{a|c},\boldsymbol{\vartheta}_{a|c})\|^2$ subject to the constraints $\boldsymbol{H}(\boldsymbol{\delta}_a)\leq 0$ and $\boldsymbol{H}(\boldsymbol{\delta}_c)\leq 0$, that is:

$$\begin{aligned} [\widehat{\boldsymbol{\delta}}_{a|c}^T, \widehat{\boldsymbol{\vartheta}}_{a|c}^T]^T &= \arg\min_{\boldsymbol{\delta}_{a|c},\boldsymbol{\vartheta}_{a|c}} V(\boldsymbol{\delta}_{a|c},\boldsymbol{\vartheta}_{a|c}) = \arg\min_{\boldsymbol{\delta}_{a|c},\boldsymbol{\vartheta}_{a|c}} \|\boldsymbol{e}(\boldsymbol{\delta}_{a|c},\boldsymbol{\vartheta}_{a|c})\|^2 \\ \text{subject to} &\quad \boldsymbol{H}(\boldsymbol{\delta}_a)\leq 0 \text{ and } \boldsymbol{H}(\boldsymbol{\delta}_c)\leq 0 \end{aligned} \tag{4.3.13}$$

Nevertheless, this cost function does not have an equivalent VP functional form due to the presence of the unknown residuals $e[t,\boldsymbol{\delta}_{a|c},\boldsymbol{\vartheta}_{a|c}]$, which depend on both $\boldsymbol{\delta}_{a|c}$ and $\boldsymbol{\vartheta}_{a|c}$, in the regression matrix $\boldsymbol{\Phi}(\boldsymbol{\delta}_{a|c},\boldsymbol{\vartheta}_{a|c})$. Thus in this case, the solution may be based solely on the full functional form of Eq. (4.3.13). However, the nature of the PE criterion along with the high dimensionality of the optimization problem ($\dim(\boldsymbol{\delta}_{a|c})+\dim(\boldsymbol{\vartheta}_{a|c}) = \dim(\boldsymbol{\delta}_a)+\dim(\boldsymbol{\delta}_c)+n_ap_a+n_cp_c$) renders optimization difficult[1]. Simu-

[1]To draw a clearer picture, an AFS-TARMA$(6,6)_{[5,5,5]}$ model with parameters expanded on decaying trigonometric functions involves 10 AR/MA functional subspace parameters and 60 AR/MA coefficients of projection, that is in total 70 parameters.

lations have shown that such problems are very sensitive to initial parameter values, so the minimization procedure is very likely to converge to a local minimum when arbitrary or inaccurate initial values are utilized. Yet, the minimization of the PE criterion has been shown to be of increased complexity even for the simpler classical FS-TARMA approach and for problems of much smaller dimensionality [Ben Mrad et al., 1998a].

Therefore, before dealing with the optimization of the full functional problem of Eq. (4.3.13) a suboptimal two-stage pseudo-SNLS procedure is employed in order to obtain good initial estimates. This method is based on a long (of high AR order) AFS-TAR model which is meant to approximate the inverse function representation of the original AFS-TARMA model of Eq. (4.2.1). Theoretically, the inverse function representation is an AFS-TAR model of infinite order [Poulimenos and Fassois, 2006]. The two-stage method is briefly described in the sequel.

Two Stage Variable Projection (2SVP) method

In order to approximate the minimization problem of Eq. (4.3.13) by a pseudo-SNLS problem, the unknown residuals $e[t, \boldsymbol{\delta}_{a|c}, \boldsymbol{\vartheta}_{a|c}]$ of the regression matrix $\boldsymbol{\Phi}(\boldsymbol{\delta}_{a|c}, \boldsymbol{\vartheta}_{a|c})$ have to be replaced by respective estimates. The method consists of the following stages:

Stage 1: Inverse function estimation. A truncated, n_q-order, inverse function model that approximates the infinite order inverse function representation of an AFS-TARMA model is considered as follows:

$$x[t] - \sum_{i=1}^{n_q} \sum_{j=1}^{p_q} q_{i,j} \cdot G_{q(j)}[t, \boldsymbol{\delta}_q] \cdot x[t-i] + e[t, \boldsymbol{\delta}_q, \boldsymbol{\vartheta}_q] \tag{4.3.14}$$

with $n_q \gg \max(n_a, n_c)$. The identification of this long AFS-TAR model based on the minimization of the PE criterion is a SNLS problem which (as previously shown) may be solved by the VP method. Consequently, estimates of the model residuals $e[t, \widehat{\boldsymbol{\delta}}_q, \widehat{\boldsymbol{\vartheta}}_q]$ may be readily obtained.

Stage 2: AR/MA parameter vector estimation. The AFS-TARMA model is approximated by replacing the past, but not the current, values of the prediction error $e[t, \boldsymbol{\delta}_{a|c}, \boldsymbol{\vartheta}_{a|c}]$ by the previously obtained estimates $e[t, \widehat{\boldsymbol{\delta}}_q, \widehat{\boldsymbol{\vartheta}}_q]$ in Eq. (4.3.12)

$$\boldsymbol{x} = \boldsymbol{\Phi}(\boldsymbol{\delta}_{a|c}, \widehat{\boldsymbol{\delta}}_q, \widehat{\boldsymbol{\vartheta}}_q) \cdot \boldsymbol{\vartheta}_{a|c} + \boldsymbol{e}(\boldsymbol{\delta}_{a|c}, \boldsymbol{\vartheta}_{a|c}) \tag{4.3.15}$$

and solving the resultant SNLS problem utilizing the VP functional. The final residual sequence is estimated based on the estimate $[\, \widehat{\boldsymbol{\delta}}_{a|c}^T, \widehat{\boldsymbol{\vartheta}}_{a|c}^T \,]^T$ and the TARMA model expression of Eq. (4.2.1), while its standard deviation may be estimated via the procedure described in the AFS-TAR case.

Remarks: (i) The second stage of the 2SVP method may be iterated, replacing in every iteration the past values of the prediction error $e[t, \boldsymbol{\delta}_{a|c}, \boldsymbol{\vartheta}_{a|c}]$ by the most recent estimates $e[t, \widehat{\boldsymbol{\delta}}_{a|c}, \widehat{\boldsymbol{\vartheta}}_{a|c}]$, until a minimum value of the Residual Sum of Squares (RSS) criterion is achieved. (ii) The 2SVP method is also realized via a hybrid optimization scheme combining global search through PSO and local optimization through iterative gradient based nonlinear techniques. (iii) After obtaining the 2SVP estimates, the minimization of the original full functional problem may be viewed as a subsequent (potential) refinement stage . (iv) Usually n_q is selected as $n_q = (2, \ldots, 5) \cdot \max(n_a, n_c)$. Yet, its value may also be optimized based on the model structure selection scheme of the following section.

4.3.2 Model structure selection

For a selected functional family (B-splines of order k or decaying trigonometric functions) model structure selection for the full AFS-TARMA case refers to the estimation of the set of integers:

$$\mathcal{M} = \{n_a; n_c; p_a; p_c; p_s\}$$

where n_a, n_c, designate the model orders, p_a, p_c and p_s the AR, MA and innovations standard deviation basis dimensionalities, respectively.

Table 4.4: AFS-TARMA model identification – Algorithm details for $\boldsymbol{\delta}_{a|c}$ and $\boldsymbol{\vartheta}_{a|c}$ estimation through the 2SVP method.

Input: Non-stationary data $\boldsymbol{x}$, initial innovation sequence estimate $\boldsymbol{e}(\widehat{\boldsymbol{\delta}_q}, \widehat{\boldsymbol{\vartheta}_q})$, AR order n_a, MA order n_c, AR functional subspace dimensionality p_a, MA functional subspace dimensionality p_c

(1) Choose initial $\boldsymbol{\delta}_{a|c}$ appropriately

(2) For $j = 1, 2, \ldots,$ until convergence

(i) Compute $\boldsymbol{e}_{VP}(\boldsymbol{\delta}_{a|c}) = \big(\boldsymbol{I} - \boldsymbol{\Phi}(\boldsymbol{\delta}_{a|c}, \widehat{\boldsymbol{\delta}_q}, \widehat{\boldsymbol{\vartheta}_q}) \cdot \boldsymbol{\Phi}^{\dagger}(\boldsymbol{\delta}_{a|c}, \widehat{\boldsymbol{\delta}_q}, \widehat{\boldsymbol{\vartheta}_q})\big) \cdot \boldsymbol{x}$

(ii) Test for convergence

(iii) Increment $\boldsymbol{\delta}_{a|c}^{(j+1)} = \boldsymbol{\delta}_{a|c}^{(j)} + \mu^{(j)} \cdot V'_{\text{VP}}(\boldsymbol{\delta}_{a|c})$

(3) Compute $\boldsymbol{\vartheta}_{a|c} = \Big(\boldsymbol{\Phi}(\boldsymbol{\delta}_{a|c}, \widehat{\boldsymbol{\delta}_q}, \widehat{\boldsymbol{\vartheta}_q}) \cdot \boldsymbol{\Phi}^{T}(\boldsymbol{\delta}_{a|c}, \widehat{\boldsymbol{\delta}_q}, \widehat{\boldsymbol{\vartheta}_q})\Big)^{-1} \cdot \Big(\boldsymbol{\Phi}(\boldsymbol{\delta}_{a|c}, \widehat{\boldsymbol{\delta}_q}, \widehat{\boldsymbol{\vartheta}_q}) \cdot \boldsymbol{x}\Big)$

Ouput: $\widehat{\boldsymbol{\delta}_{a|c}}, \widehat{\boldsymbol{\vartheta}_{a|c}}$

$\mu^{(j)}$: Step-length

$V'_{\text{VP}}(\boldsymbol{\delta}_{a|c})$: Gradient of the VP functional with respect to $\boldsymbol{\delta}_{a|c}$

The optimal way to solve such a problem is to use a combinatorial approach [Gill et al., 1981, pp. 282-283] by estimating an AFS-TARMA model for every possible combination of the values that the integer variables can assume and selecting as best the AFS-TARMA model which minimizes a suitable "fitness" function. However, such an approach is practical only when each variable can take only a small number of values, say less than three.

Unfortunately, even for a moderate number of possible values for each variable, the combinatorial approach becomes to expensive computationally as the number of possible cases grows extremely large very quickly. Moreover, usually there is no or little knowledge regarding the values that some of these variables may take. In order to solve the AFS-TARMA model structure selection problem more effectively and render the whole AFS-TARMA identification more automated, a two phase model structure selection scheme is presently proposed, which in its first phase treats the integer variables as continuous in order to locate a promising region of the initial discrete search space [Gill et al., 1981, p. 283]. This solution may serve as a guide to the likely values of the integer variables, while in the second phase a combinatorial approach may be utilized for a more thorough search within a suitably selected neighbourhood of the first phase solution.

Phase I. Coarse search. For this first phase, the model structure selection is embodied within the global search procedure. More particularly, the PSO algorithm explores a combined parameter space defined by the aforementioned set of integers and the parameter space of $\boldsymbol{\delta}$, that is $[n_a; n_c; p_a; p_c; p_s; \boldsymbol{\delta}_a^T; \boldsymbol{\delta}_c^T; \boldsymbol{\delta}_s^T]^T$, trying to minimize a suitable "fitness" function – presently the the Bayesian Information Criterion (BIC) [Poulimenos and Fassois, 2006]:

$$\text{BIC} = -\ln \mathcal{L}(\mathcal{M}(\boldsymbol{\theta}|\boldsymbol{x}^N)) + d \cdot \frac{\ln N}{2} = \frac{1}{2} \cdot \sum_{t=1}^{N} \left(\ln\left(\left(\boldsymbol{g}^T[t, \boldsymbol{\delta}_s] \cdot \boldsymbol{\vartheta}_s \right)^2 \right) + \frac{e^2[t, \boldsymbol{\vartheta}_{a|c}, \boldsymbol{\delta}_{a|c}]}{\left(\boldsymbol{g}^T[t, \boldsymbol{\delta}_s] \cdot \boldsymbol{\vartheta}_s \right)^2} \right) + d \cdot \frac{\ln N}{2} \tag{4.3.16}$$

where $\ln \mathcal{L}$ designates the model log-likelihood and $d = \dim(\boldsymbol{\theta})$ the number of independently "adjusted" (estimated) model parameters.

The proposed approach is illustrated through a paradigm of a hypothetical AFS-TAR model structure selection problem. Specifically, the case of searching for an appropriate AFS-TAR model with order $n_a \in [6, 10]$ and AR functional subspace consisting of at most five decaying trigonometric functions is considered. The initial search space in which the PSO is called to look for the optimal solution,

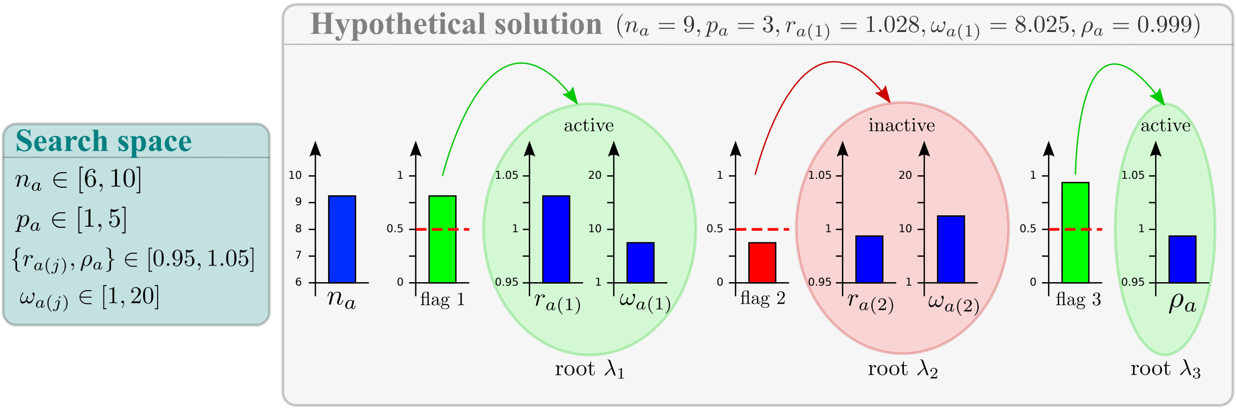

Figure 4.3.2: The search space and a potential solution for the case of an hypothetical AFS-TAR model structure selection problem with respect to the model order n_a, the basis dimensionality p_a and the functional subspace parameter vector $\boldsymbol{\delta}_a$.

and a solution that could have been obtained are depicted in Fig. 4.3.2. Two main points should be noted: First, as long as the basis dimensionality p_a is treated as a variable the dimension of the corresponding functional subspace parameter vector $\boldsymbol{\delta}_a$ would be of variable length. To overcome this hindrance, additional threshold activation variables (flags) are introduced. These variables determine the participation (flag ≥ 0.5) or not (flag < 0.5) of a specific root in a candidate solution with the p_a being finally obtained by the total number of the active roots. Secondly, the integer variable n_a is treated as a continuous one in order to avoid a more complicated mixed-variable optimization approach. Thus, the n_a estimate is obtained by rounding to the nearest integer.

Following these two rules, the potential solution depicted in Fig. 4.3.2 corresponds to an AFS-TAR model of order $n_a = 9$ with only three basis functions (note that the second complex root is inactive due to the low flag 2 value) and the characteristics of these basis functions are $r_{a(1)} = 1.028, \omega_{a(1)} = 8.025$ and $\rho_a = 0.999$. Analogously, the model structure parameter vector could be extended to include the MA order n_c and the MA functional subspace parameters and/or the innovations standard deviation functional subspace parameters for the case of an AFS-TARMA model structure selection problem. For the case of B-splines an activation variable (flag) should be connected which each internal knot variable.

Phase II. Fine ("local") Optimization. This second phase aims at refining the results of phase I and selecting the globally optimum "structure" based on a combinatorial approach. It thus operates in a neighbourhood of phase I solution and estimates an AFS-TARMA model for each possible combination of a confined space of the integer variables. The procedure is repeated for all initial solutions (phase I results), and the model "structure" corresponding to the globally optimum BIC is selected.

Remarks. (i) The pre-selection of the basis function family may be based on prior knowledge regarding the evolution of the underlying time-varying dynamics. In case of lack of prior information, B-splines of order k equal to three or four may be considered, as this family is capable of tracking a wide range of evolutions. (ii) The aforementioned scheme offers the possibility of fixing certain structural parameters in case they happen to be a priori known.

4.4 Performance Assessment via Monte Carlo Studies

The performance characteristics of the introduced AFS-TARMA identification method are first examined via Monte Carlo experiments. Specifically, the identification problem of three TAR(6) models with abrupt parameter evolution of different kinds is considered. The goal of this test case studies is to demonstrate the effectiveness and applicability of the introduced general purpose method even for the difficult problem of identifying a model with parameters characterized by abrupt changes in their evolution.

For the purposes of comparison and in order to evaluate the effectiveness of the introduced method with respect to available non-stationary identification methods the classical FS-TAR method based on fixed basis functions, the Smoothness Priors TAR (SP-TAR) method [Kitagawa and Gersch, 1996] and finally a Recursive Least Squares TAR (RLS-TAR) method with variable forgetting factor (suitable for tracking abrupt parameter changes) [Paleologu et al., 2008] are also employed.

AFS-TAR identification method. Within the context of the AFS-TAR models as long as no prior information with respect to the time-varying parameter evolution is taken into consideration, quadratic B-splines functions ($k = 3$), which as already mentioned are capable of tracking various types of evolution, are employed. Only distinct knots are considered and thus a knot proximity constraint is introduced ($\varepsilon = 20$ samples). Regarding the configuration of the PSO algorithm typical values are chosen for its parameters, that is inertia weight $w = 1$, individual confidence factor $c_1 = 1.45$, and swarm confidence factor $c_2 = 1.45$ [Perez and Behdinan, 2007], while the population size is set equal to 200. The PSO convergence criteria, that is the stall generation limit and the tolerance of the fitness function (BIC) are set equal to 20 and 10^{-6}, respectively. An interior point optimization algorithm that combines line search and trust region steps is employed for the constrained nonlinear optimization (termination rules are shown in Table 4.5).

Classical FS-TAR identification method. For the classical FS-TAR method, which is based on fixed basis functions, the appropriate functional subspaces are sought among three functional bases: the Discrete Cosine Transform (DCT) basis functions, Chebyshev type I polynomial functions, and Haar functions (see Appendix A). More specifically, in each test case and for every functional basis a model structure selection scheme based on Genetic Algorithm (GA) [Poulimenos and Fassois, 2006] and the minimization of the BIC is searching for the appropriate functional subspace among the first 50 basis functions of each family. The best overall, in terms of the BIC, model structure is selected. The estimation of the FS-TAR model coefficients of projection is based on the minimization of the PE criterion and the OLS estimator.

SP-TAR identification method. Regarding the SP-TAR case three possible orders are considered for the smoothness priors constraints, namely $\kappa = 1, 2, 3$ while optimization (of the BIC) with respect to ratio of the smoothness priors constraints innovations variance over the residual variance ν is also carried out. For the initialization of the Kalman filter algorithm the diagonal elements of the covariance matrix are also set equal to 10^4. In order to reduce the effects of arbitrary initial conditions in the estimation, three sequential passes (forward, backward, and final forward) are executed over the entire data record, while a final backward smoothing algorithm is also applied.

RLS-TAR identification method. In the RLS-TAR case the exponential window parameters K_a and K_b are set equal to 2 and 10 respectively, while the threshold ratio γ between the a-priori and the a-posteriori prediction error sequence variance is set equal to 1.5. The maximum value of the forgetting factor $\lambda_{\max}$ is set equal to 0.99. For the algorithm initialization the initial parameter vector is set equal to zero while the diagonal elements of the initial covariance matrix are set equal to 10^4, while like in the SP-TAR case, three sequential passes (forward, backward, and a final forward) are executed over the entire data record in order to reduce the effects of arbitrary initial conditions.

Innovations variance estimation method. For fair comparison, for all the identification methods considered the innovations variance is estimated non-parametrically through a moving time-window of length equal to 129 samples advanced by one sample.

The estimation method characteristics and implementation details for all methods considered are summarized in Table 4.5.

For the subsequent analysis and in order to quantify the achievable time-varying parameter tracking accuracy, percentage accumulated parameter errors are computed as:

$$\mathrm{err}_{a_i[t]} \triangleq 100 \times \frac{\| \widehat{a}_i[t] - a_i[t] \|^2}{\| a_i[t] \|^2} \% \tag{4.4.1}$$

Moreover, the Residual Sum of Squares normalized by the Series Sum of Squares (RSS/SSS) criterion is employed as a measure of model fit. The RSS/SSS criterion is given by the following relationship:

$$\mathrm{RSS/SSS} \triangleq 100 \times \frac{\| \widehat{e}[t, \widehat{\boldsymbol{\delta}}_a, \widehat{\boldsymbol{\vartheta}}_a] \|^2}{\| x[t] \|^2} \% \tag{4.4.2}$$

Table 4.5: Characteristics of the identification methods.

Method	Parameter estimation details	Model structure and algorithmic parameters (search space)	Model structure selection scheme (criterion)
AFS-TAR	VP (Interior point method; MATLAB *fmincon* function) TolFun = 10^{-6}, TolX = 10^{-9}, TolCon = 10^{-6}, B-splines (order $k=3$), $\varepsilon = 0.01 \cdot N = 20$ samples	basis dimensionality p_a ($p_a = 4, \ldots, 10$)	PSO (MATLAB *pso* function) population size = 200, stall generation limit = 50, w = 1, c_1 = 1.45, c_2 = 1.45, TolFun = 10^{-6}, (BIC)
Classical FS-TAR	OLS (QR factorization; MATLAB *mldivide* function)	functional basis (discrete cosine transform functions, Chebyshev polynomials, Haar functions) functional subspace b_a ($b_a = \{0, \ldots, 49\}$)	Genetic Algorithm (MATLAB *ga* function) population size = 100, stall generation limit = 20, crossover fraction = 0.8, mutation rate = 0.2, elite children = 5, (BIC)
SP-TAR	three passes followed by a backward smoothing pass,	smoothness constraints order κ ($\kappa = 1, 2, 3$) variance ratio ν ($\nu = 10^{-12}, 10^{-11}, \ldots, 10^{-1}$)	trial & error (BIC)
RLS-TAR	three passes (forward-backward-forward) $K_a = 2, K_b = 10$ $\gamma = 1.5, \lambda_{\max} = 0.99$	—	—
Innovations variance	moving time-window (window length = 129 samples, advance = 1 sample,)	—	—

Table 4.6: Signal details for Test Case I.

Time	$a_1[t]$	$a_2[t]$	$a_3[t]$	$a_4[t]$	$a_5[t]$	$a_6[t]$
$1 \leq t \leq 770$	-0.30	-0.25	0.14	-0.26	-0.19	0.88
$771 \leq t \leq 2000$	-1.31	0.77	-0.49	0.68	-1.13	0.88
$\sigma_w^2[t] = 1$						
Signal length: $N = 2000$ samples						
Number of Monte Carlo experiments: 500						

where $\widehat{e}[t, \widehat{\boldsymbol{\delta}}_a, \widehat{\boldsymbol{\vartheta}}_a]$ designate the estimated model residuals and $x[t]$ the simulated signal under study.

4.4.1 Test case I – TAR Model with piecewise constant time-varying parameters

A TAR(6) model with piecewise constant parameters is considered in this test case. The true AR parameters are given in Table 4.6 and are shown in Fig. 4.4.1(a). The driving noise sequence variance is constant and equal to unity ($\sigma_w^2 = 1$), while 500 realizations were generated by using different seed numbers. One of these realizations is shown in Fig. 4.4.1(b).

At a first stage, and in order to assess the performance of the proposed model structure selection scheme, no information regarding the true model order and the evolution of the model parameters is considered as available. Thus, the analysis begins with the first phase of the model structure selection scheme described in Section 4.3.2 and the PSO algorithm being employed for the estimation of the appropriate AR model orders and the AR functional subspace dimensionalities for each signal realization. The initial search space is $n_a \in [2, 10]$ and $p_a \in [3, 13]$, that is the dimension of the functional subspace parameter vector is varying from zero to ten ($\dim(\boldsymbol{\delta}_a) = p_a - k \in [0, 10]$).

The results of the Monte Carlo experiments for this phase are depicted in Fig. 4.4.2 and give the correct AR model order ($n_a = 6$) for 73.4 % of the cases, while also indicating that a functional subspace dimensionsionality between six and eight is adequate. The second phase of the model structure selection scheme based on the combinatorial approach for the integer sets $n_a \in [6, 7]$ and $p_a \in [6, 8]$ indicates that an AFS-TAR$(6)_{[6]}$ model is, with respect to the BIC, the most adequate for representing the system under study. Thus, an AFS-TAR$(6)_{[6]}$ model is identified for each one of the 500 realizations with the mean estimate of the AR functional subspace parameter vector being $\widehat{\boldsymbol{\delta}}_a = [750.2,\ 770.7,\ 791.9]^T$. The

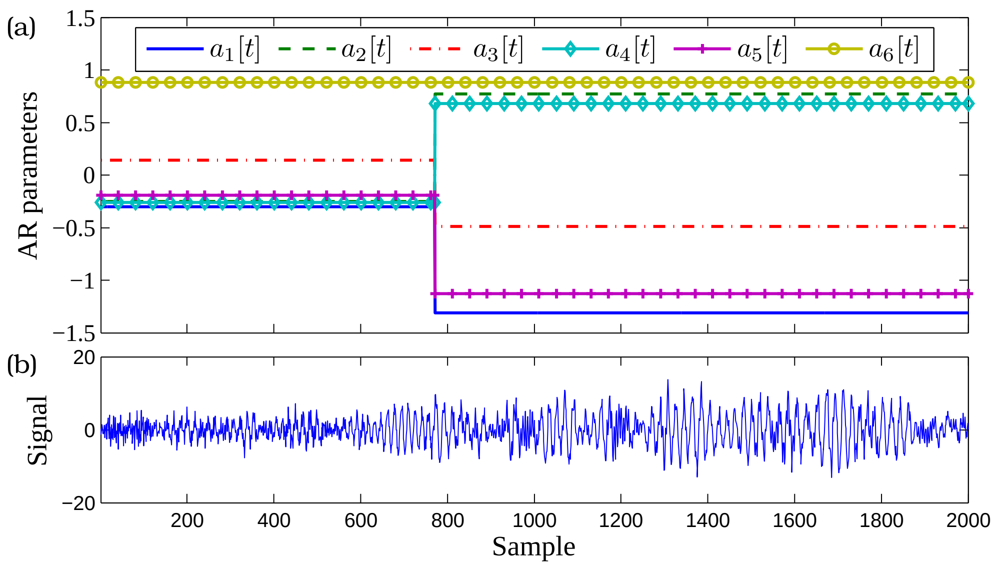

Figure 4.4.1: True model for Test Case I: (a) AR parameters, and (b) signal realization.

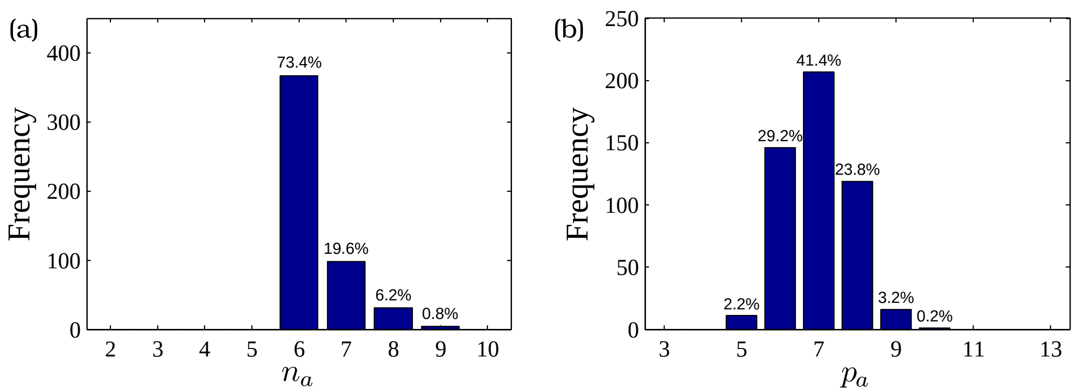

Figure 4.4.2: Test Case I – Phase I of the AFS-TAR model structure selection scheme results based on PSO (500 realizations): (a) AR order estimation, and (b) functional subspace dimensionality estimation.

AR basis functions constructed based on this parameter vector are shown in Fig. 4.4.3.

TAR models of the true order ($n_a = 6$) are also estimated and for the rest of the methods considered. The finally selected model structure parameters for all methods are summarized in Table 4.7.

Indicative comparison results regarding the tracking of model parameters as obtained from a single realization are shown in Fig. 4.4.4, while a clearer picture is drawn by the sample mean over 500 realizations estimated parameters trajectories for a short time window centred at the sample where the discontinuity takes place (Fig. 4.4.5). Clearly, in regard to the tracking of the time-varying AR parameters the introduced AFS-TAR outperforms its candidates. Specifically, the AFS-TAR method successfully adapts to the given data and detects accurately the discontinuity in the parameters. Regarding the innovations sequence variance the AFS-TAR based estimate is much closer to the true constant variance while the estimates based on the rest of the models show large changes in their values within a small

Table 4.7: Selected model structure parameters.

Method	Test Case I	Test Case II	Test Case III
SP-TAR	$\kappa = 1, \nu = 9 \times 10^{-5}$	$\kappa = 2, \nu = 1 \times 10^{-8}$	$\kappa = 1, \nu = 7 \times 10^{-9}$
Classical FS-TAR	Haar, $b_a = [0, 1, 2, 5, 44]$	DCT, $b_a = [0, 1, 2, 3, 6]$	Haar, $b_a = [0, 6, 12, 25]$
AFS-TAR	$p_a = 6$ (3 internal knots)	$p_a = 6$ (3 internal knots)	$p_a = 7$ (4 internal knots)

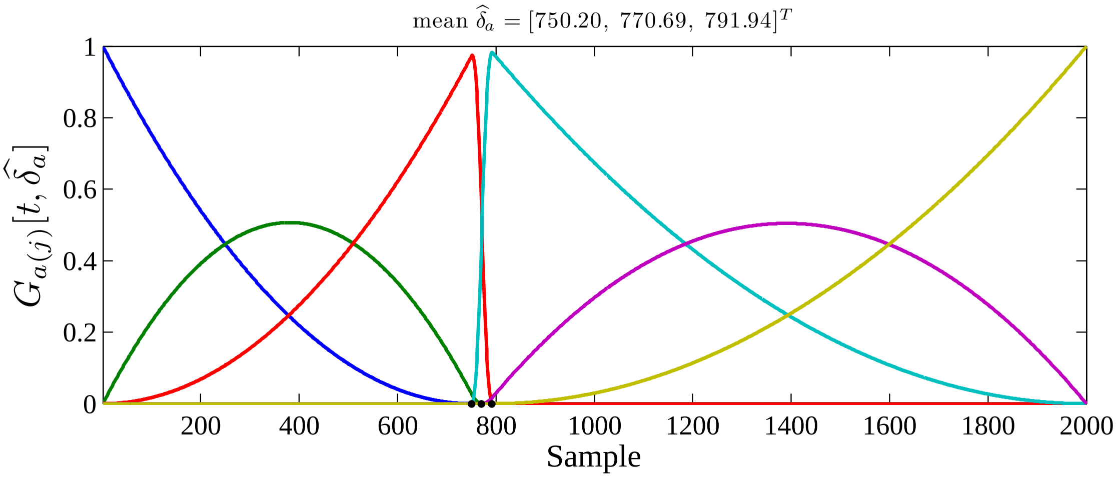

Figure 4.4.3: Test Case I – AR basis functions constructed based on the mean $\boldsymbol{\delta}_a$ estimate. (The respective internal knots are indicated by black dots on the x-axis.)

region of the time axis. Note that variance estimates are available only for $t = 65, 130 \ldots, 1936$ since they are based on a centred moving time-window of length equal to 129 samples.

In the case of the classical FS-TAR approach, a functional subspace consisting of five Haar functions is selected as most appropriate for tracking time-varying parameters with abrupt evolution. However, no basis function in the selected functional subspace depicts a change in the same instant with that of the true AR parameters. Therefore, even if a discontinuity is clearly detected its exact instant (771^{th} sample) is not accurately estimated. This example, highlights the drawback of the fixed basis approach which is heavily dependent on the selected functional basis and the model structure selection procedure.

On the other hand, SP-TAR method fails to detect the jump and depicts a big transition zone between the piecewise constant values. This fact could be accredited to the constant ratio ν between the variance of the parameters and the variance of the innovations sequence which permits the model to track smooth evolutions or evolutions of high variability but not mixed types with alternating patterns.

Finally, the RLS-TAR method even if detects precisely and without delay the existence of an abrupt change in the first five AR parameters it fails to track parameter $a_6[t]$ detecting a big discontinuity even if this parameter is constant through time.

Monte Carlo results of the parameter tracking error $\text{err}_{a_i[t]}$ and the RSS/SSS criterion are depicted in Fig. 4.4.6 and provide further support to the previous comments. Indeed, the mean parameter tracking errors for the AFS-TAR models with parameters expanded on adaptable basis functions lie between 0.15 and 1.5%, that is up to six times lower than the errors achieved by the rest of the methods for some of the time-varying parameters. Moreover, the AFS-TAR method gives the best mean RSS/SSS value. Second best with respect to its parameter tracking accuracy is the classical FS-TAR method while it is worth noting that the errors obtained by the RLS-TAR and SP-TAR models not only are of higher mean value but also depict high variability among the 500 realizations.

4.4.2 Test case II – TAR model with piecewise polynomial parameters

This test case concerns a TAR(6) model with fourth order polynomial parameters that have piecewise constant coefficients. That is, each AR parameter follows the relation:

$$a_i[t] = \ell_{i,1}[t] \cdot \left(\frac{t}{N}\right) + \ell_{i,2}[t] \cdot \left(\frac{t}{N}\right)^2 + \ell_{i,3}[t] \cdot \left(\frac{t}{N}\right)^3 + \ell_{i,4}[t] \cdot \left(\frac{t}{N}\right)^4 \tag{4.4.3}$$

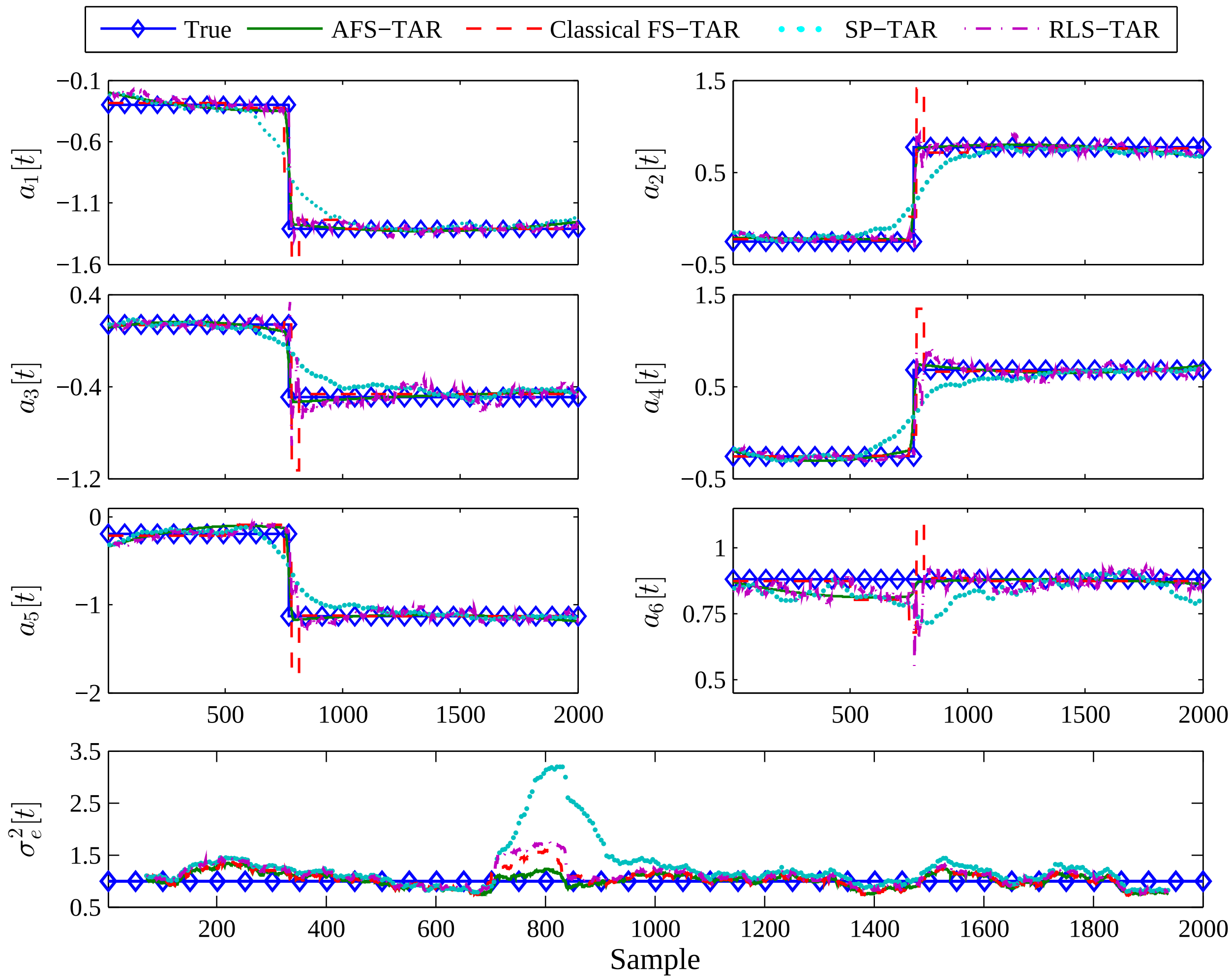

Figure 4.4.4: Test Case I. True and estimated by various methods AR parameter and $\sigma_e^2[t]$ trajectories (single experiment).

Table 4.8: Signal details for Test Case II.

	$j=1$			$j=2$			$j=3$			$j=4$		
	A	B	C	A	B	C	A	B	C	A	B	C
$\ell_{1,j}$	-0.79	136.51	-1.06	-2.07	-1274.08	-7.49	0.61	3996.46	12.38	3.84	-4199.07	-5.09
$\ell_{2,j}$	0.27	-176.11	-1.34	4.51	1682.36	23.29	-1.48	-5373.11	-38.10	-7.40	5715.71	15.84
$\ell_{3,j}$	-0.15	156.90	3.10	-4.84	-1527.04	-31.64	1.36	4928.74	61.54	8.57	-5272.07	-21.53
$\ell_{4,j}$	0.21	163.10	-1.34	4.13	1560.03	-21.83	-1.33	-4986.17	-35.70	-6.80	5305.57	14.85
$\ell_{5,j}$	-0.58	123.67	-0.83	-1.83	-1153.52	-6.66	0.52	3618.43	11.01	3.41	-3801.15	-4.53
$\ell_{6,j}$	0.81	0.81	0.81	0.00	0.00	0.00	0.00	0.00	0.00	0.00	0.00	0.00

$\sigma_w^2[t]=1$
Signal length: $N=2000$ samples
Number of Monte Carlo experiments: 500

with

$$\ell_{i,j}[t] = \begin{cases} \ell_{i,j}^A & \text{for } t = 1, \dots, 771 \\ \ell_{i,j}^B & \text{for } t = 772, \dots, 779 \\ \ell_{i,j}^C & \text{for } t = 800, \dots, 2000 \end{cases}$$

The true $\ell_{i,j}$ values are summarized in Table 4.8 while the resulting time-varying AR parameters are illustrated in Fig. 4.4.7(a). Again constant variance is considered for the driving noise sequence $\sigma_w^2 = 1$.

The first phase of the model structure selection scheme for the AFS-TAR method gives similar results

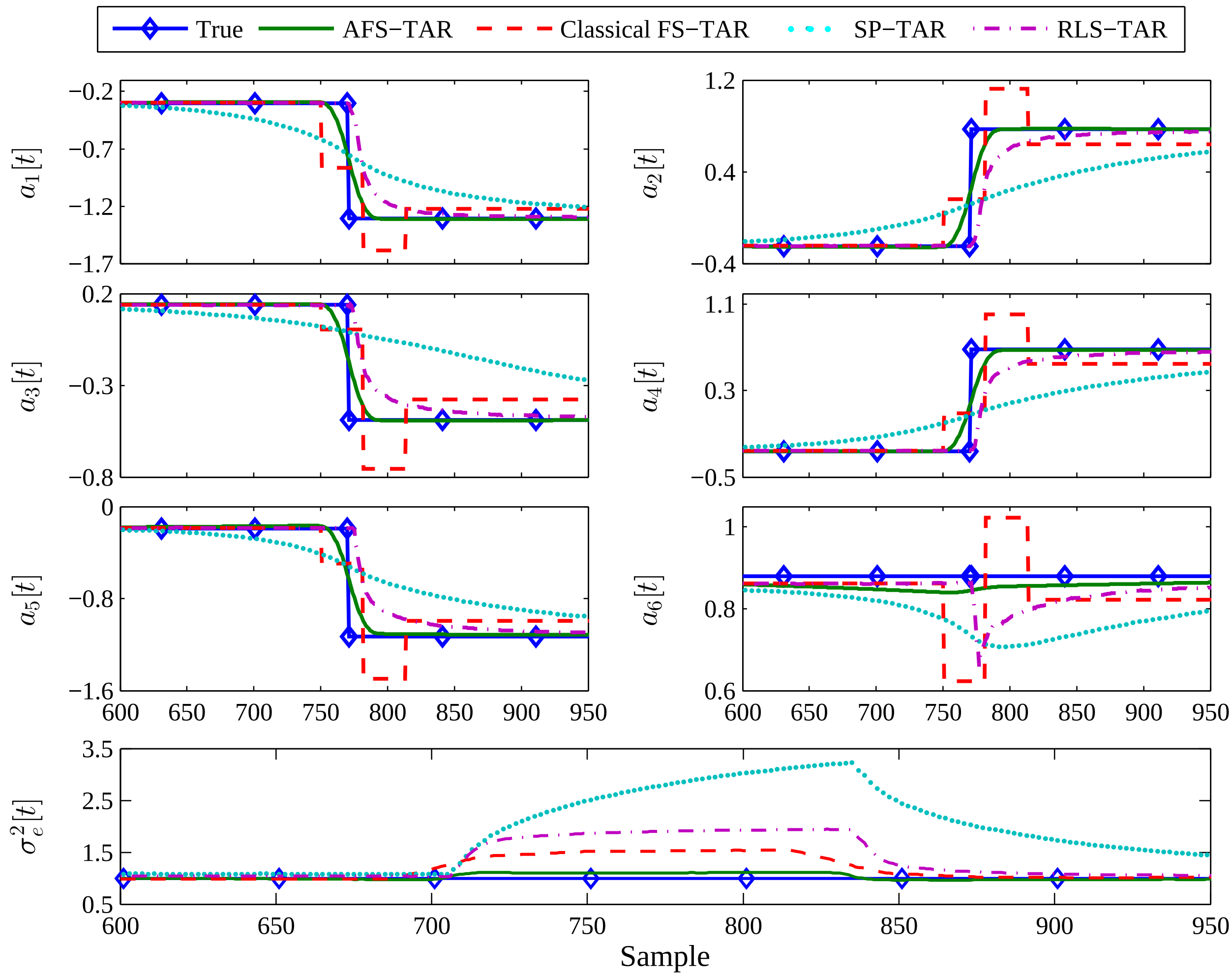

Figure 4.4.5: Test Case I. True and mean estimated by various methods AR parameter and $\sigma_e^2[t]$ trajectories (500 experiments).

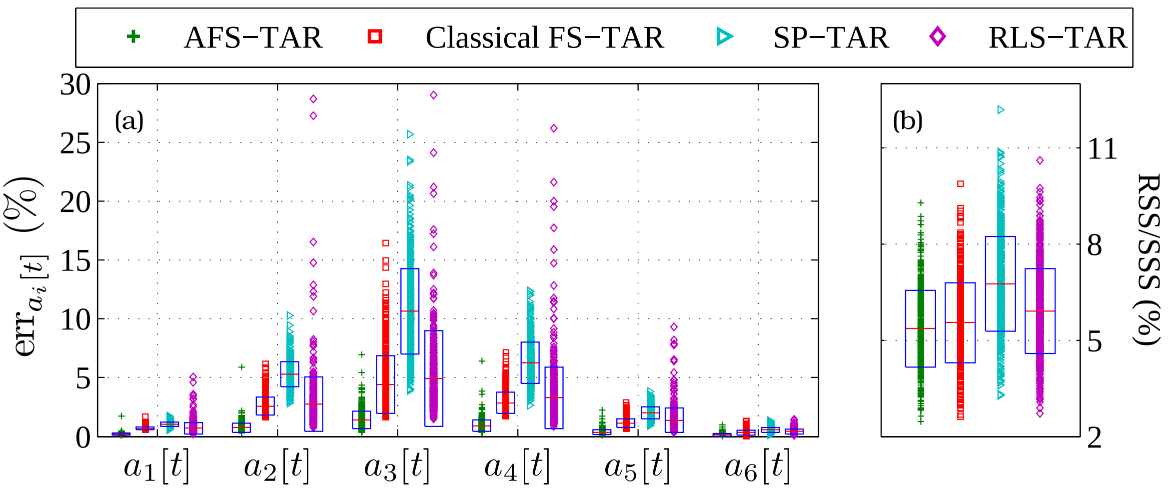

Figure 4.4.6: Test Case I. (a) AR parameter estimation errors and (b) RSS/SSS for the various estimated models (sample mean ± std also shown via boxes; 500 Monte Carlo experiments).

with those in Test Case I (see Fig. 4.4.8). More specifically, the correct order $n_a = 6$ is selected 372 times out of 500 (74.4 %) while a basis dimensionality between five and eight seems to be adequate for

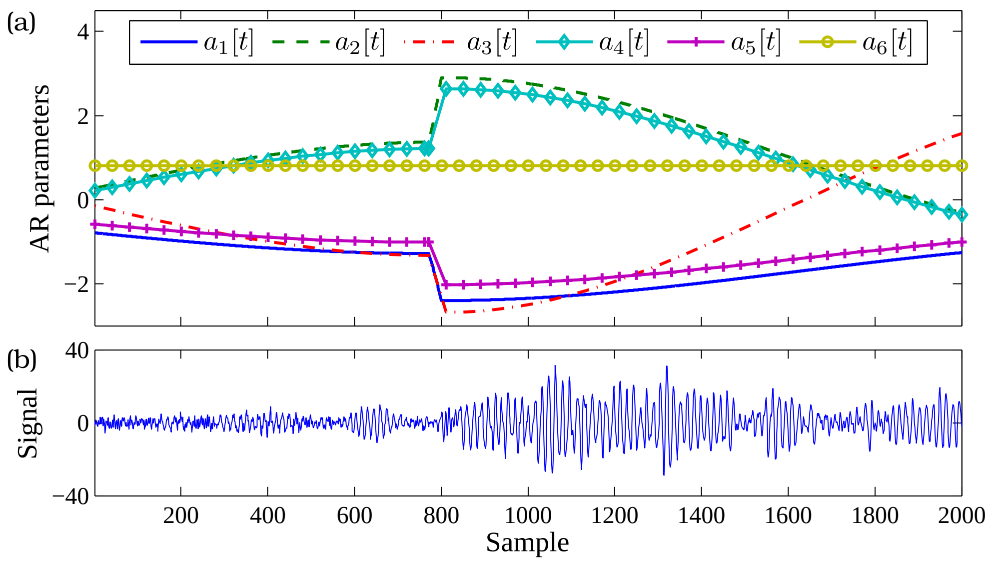

Figure 4.4.7: True model for Test Case II: (a) AR parameters, and (b) signal realization.

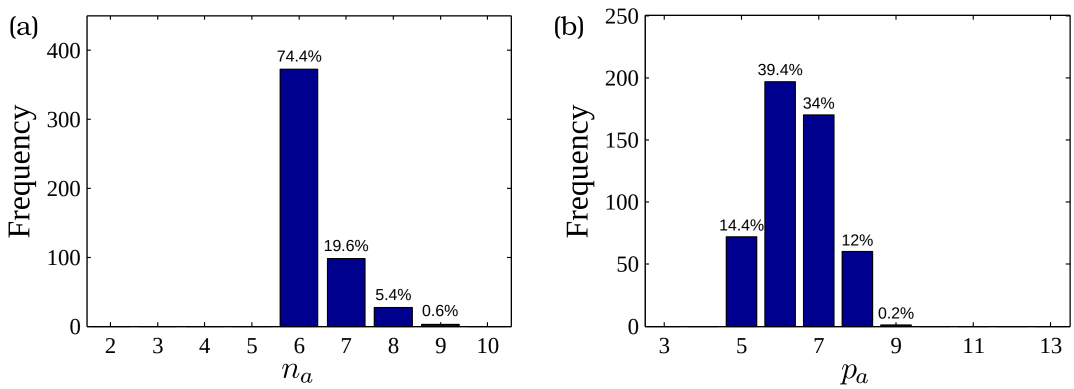

Figure 4.4.8: Test Case II – Phase I of the AFS-TAR model structure selection scheme results based on PSO (500 realizations): (a) AR order estimation, and (b) functional subspace dimensionality estimation.

the specific identification problem. A FS-TAR$(6)_{[6]}$ model is finally selected based on the BIC criterion and the second phase of the scheme (see Table 4.7). The mean estimate of the AR functional subspace parameter vector for this test case is $\widehat{\boldsymbol{\delta}}_a = [760.84,\ 786.24,\ 813.83]^T$ while the corresponding AR basis functions are shown in Fig. 4.4.9.

The true parameters and the model estimates as obtained from a single realization and the four non-stationary identification methods considered are depicted in Fig. 4.4.10, while the mean estimated values are shown in Fig. 4.4.11. The AFS-TAR method estimates based on parametrized B-splines again track almost perfectly the time-varying parameters giving a clear indication of the mixed type of evolution, that is transitions between smooth and abrupt changes.

The rest of the identified models show a delay of several samples and barely track the parameters during their fast transition between the 772$^{\text{th}}$ and 799$^{\text{th}}$ sample. The RLS-TAR models, although they adequately well detect the abrupt change in the parameters, depict high variability in the estimated parameter values even for the time-regions within which the true model parameters evolve smoothly. Moreover, again they are not capable of tracking with accuracy the parameter $a_6[t]$ which is actually constant through time. Finally, the AFS-TAR based innovations variance estimate again is very close to unity and almost constant for the complete time-axis, in contrast to the estimates based on the rest of the models.

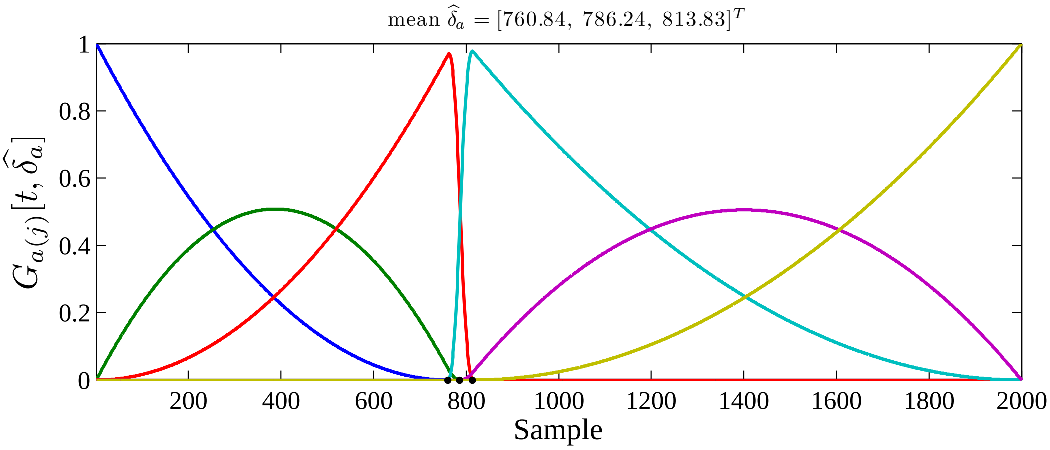

Figure 4.4.9: Test Case II – AR basis functions constructed based on the mean $\boldsymbol{\delta}_a$ estimate. (The respective internal knots are indicated by black dots on the x-axis.)

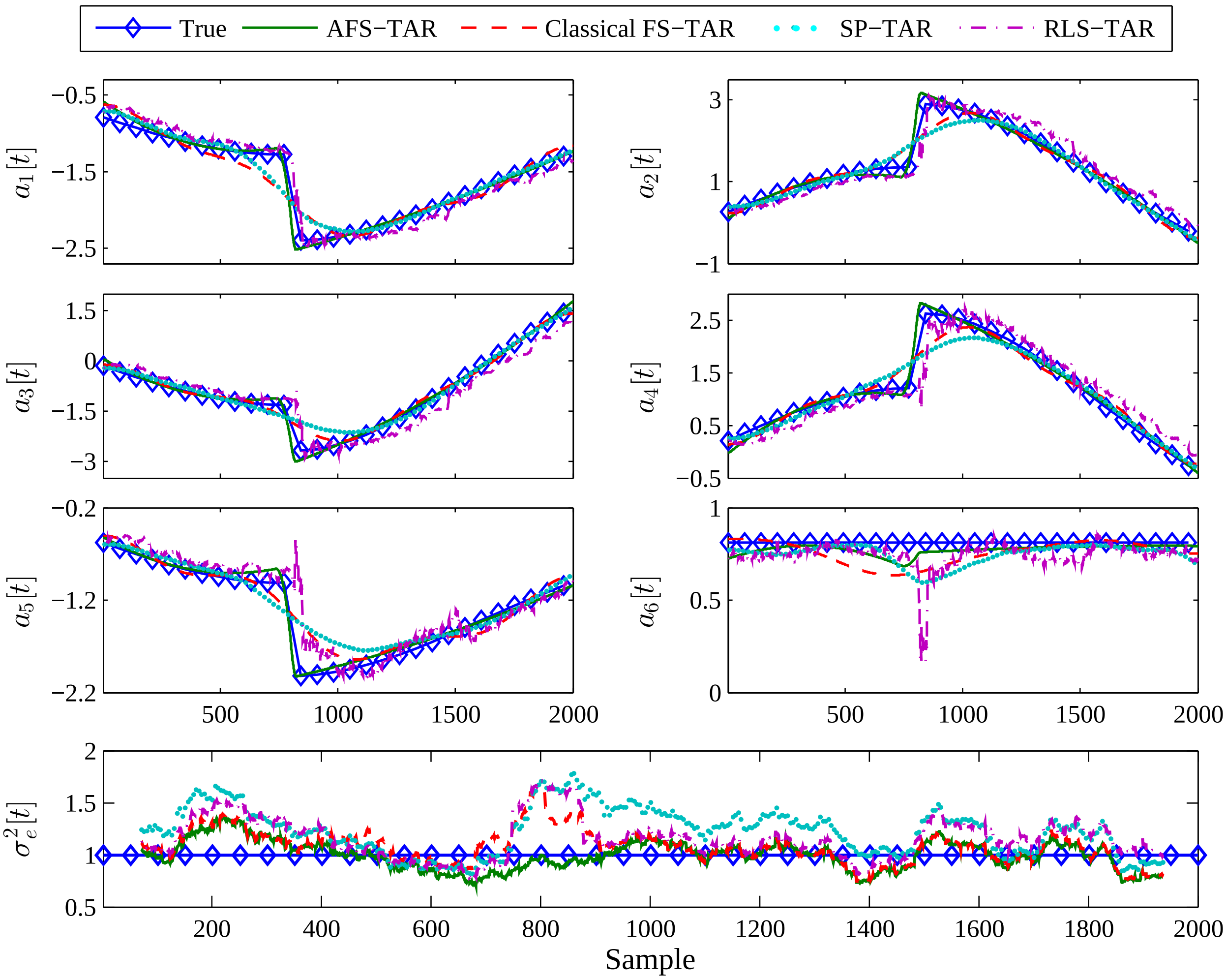

Figure 4.4.10: Test Case II. True and estimated by various methods AR parameter and $\sigma_e^2[t]$ trajectories (single experiment).

Note also that the classical FS-TAR models with parameters expanded on DCT basis functions are not capable of tracking parameters with inhomogeneous evolution. Most certainly, an increased number

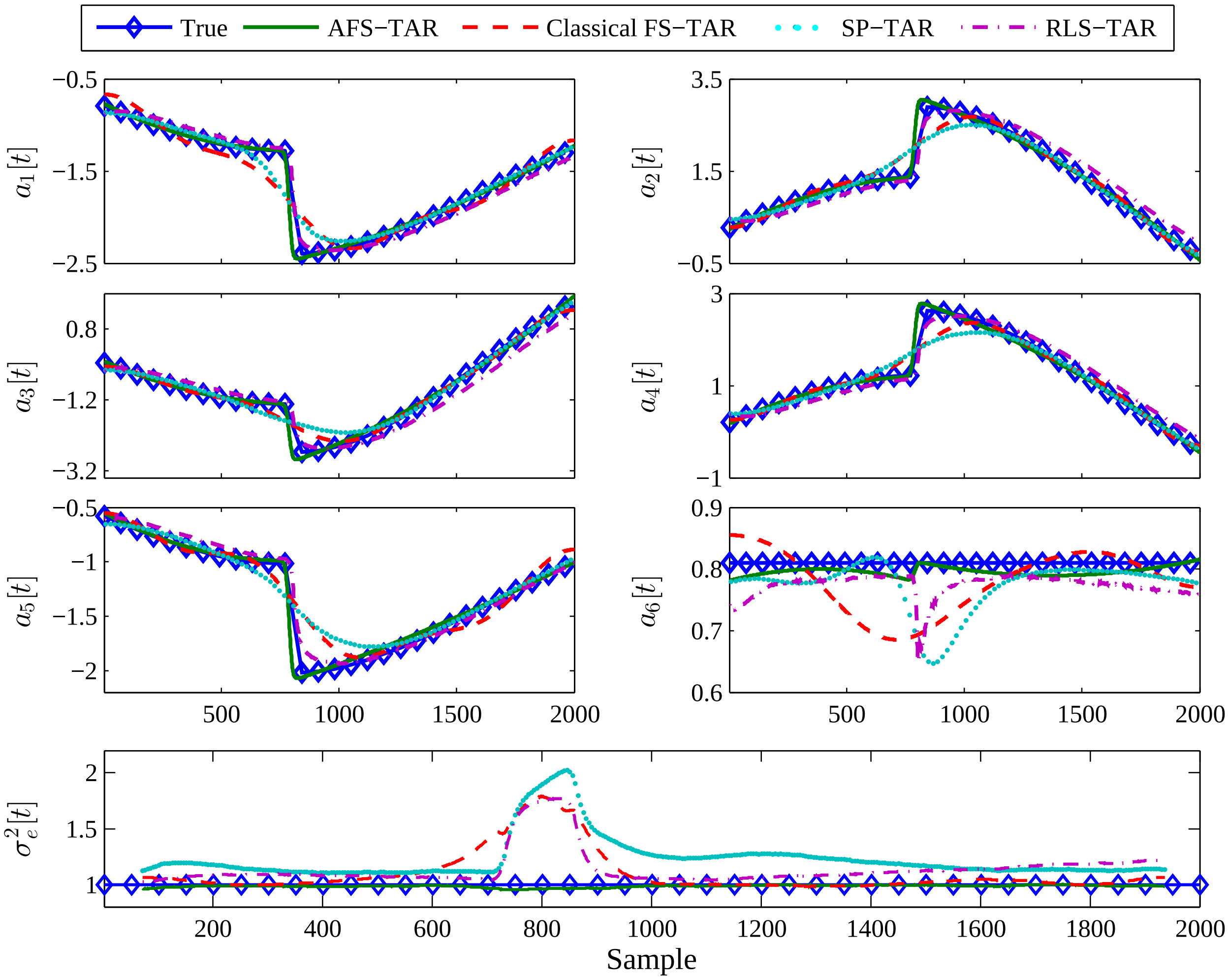

Figure 4.4.11: Test Case II. True and mean estimated by various methods AR parameter and $\sigma_e^2[t]$ trajectories (500 experiments).

of basis functions may improve the models' tracking ability, however at the price of reduced model parsimony. On the other hand, the AFS-TAR model involves only three nonlinear parameters and six basis functions.

The parameter tracking errors $\text{err}_{a_i[t]}$ and the RSS/SSS criterion (Fig. 4.4.12) confirm the big difference in the performance of the AFS-TAR method compared to its counterparts. Note that the parameter tracking errors for the AFS-TAR method lie between 0 and 2 %, that is up to five times better than the values achieved by the rest of the methods.

4.4.3 Test case III – TAR Model with parameters exhibiting short-term variability

The AR model parameters of this test case depict variability only within a small partition of the time axis (between samples 1100 and 1200) while remain constant for the rest of the axis. More specifically, the AR parameters follow a Gaussian function of the form:

$$a_i[t] = \ell_{i,1} + \frac{\ell_{i,2}}{18\sqrt{2\pi}} \cdot \exp\left(-\frac{t-1155}{648}\right), \quad t = 1, \ldots, 2000 \tag{4.4.4}$$

with ℓ_i's given in Table 4.9. A realization used for the model identification and the true time-varying parameters are depicted in Fig. 4.4.13. Also in this case $\sigma_w^2 = 1$.

The model structure selection phase I results (Fig. 4.4.14) indicate in a percentage of 67.8 % the correct AR model order and in 24.8 % n_a equal to seven. However, the second phase of the proposed

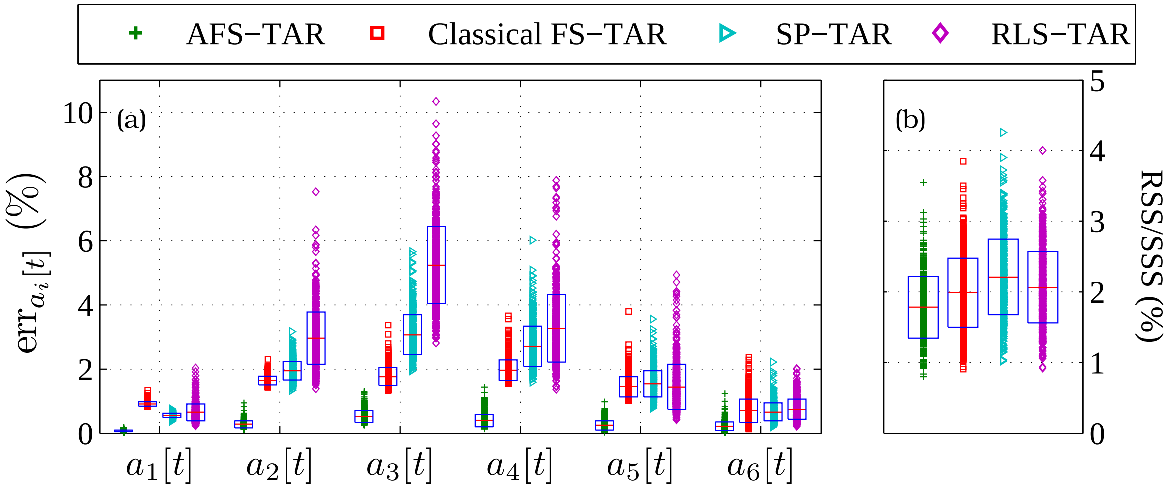

Figure 4.4.12: Test Case II. (a) AR parameter estimation errors and (b) RSS/SSS for the various estimated models (sample mean $\pm$ std also shown via boxes; 500 Monte Carlo experiments).

Table 4.9: Signal details for Test Case III.

	$i=1$	$i=2$	$i=3$	$i=4$	$i=5$	$i=6$
$\ell_{i,1}$	-1.40	0.92	-0.50	0.79	-1.13	0.81
$\ell_{i,2}$	75	-65	20	-60	70	0
$\sigma_w^2[t]=1$						
Signal length: $N=2000$ samples						
Number of Monte Carlo experiments: 500						

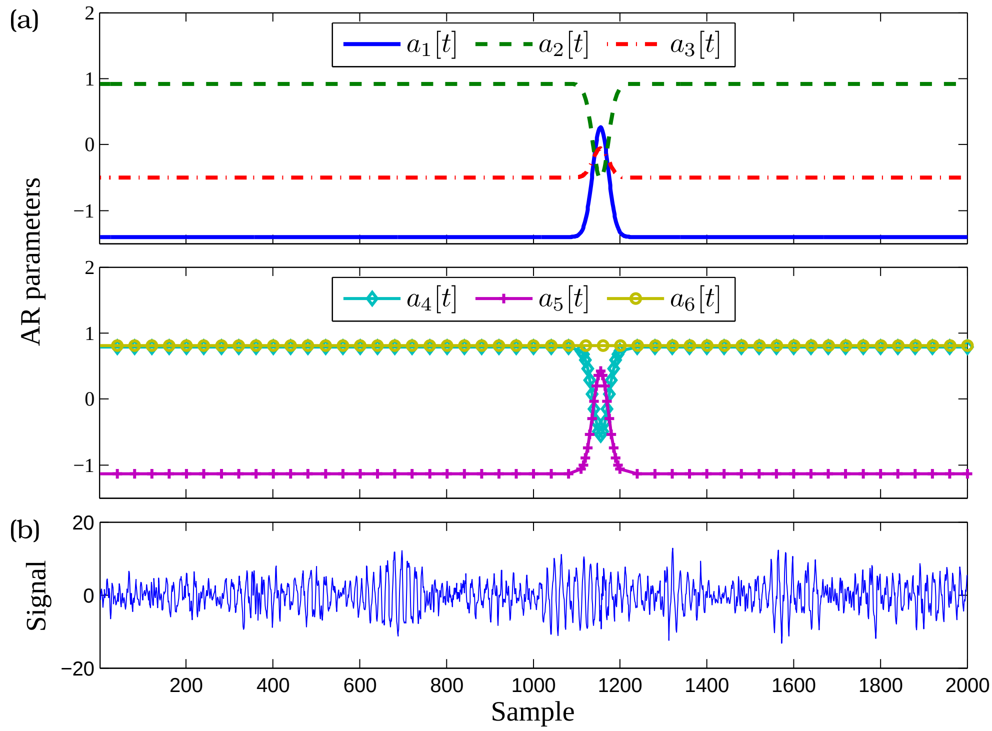

Figure 4.4.13: True model for Test Case III: (a) AR parameters, and (b) signal realization.

scheme leads to the correct AR order and a FS-TAR$(6)_{[7]}$ model as the most appropriate (sample mean over 500 realizations $\widehat{\boldsymbol{\delta}}_a = [1094.50,\ 1135.99,\ 1168.20,\ 1206.68]^T$, Fig. 4.4.15).

The fast evolution of the time-varying parameters in a short time region makes this problem chal-

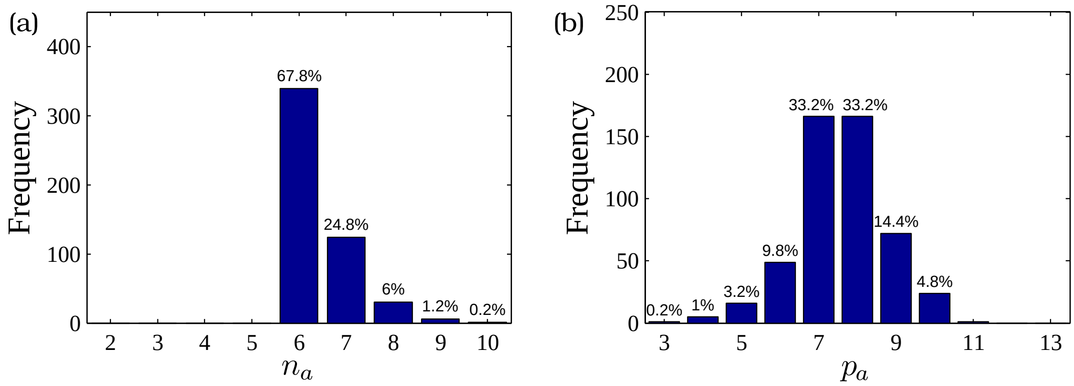

Figure 4.4.14: Test Case III – Phase I of the AFS-TAR model structure selection scheme results based on PSO (500 realizations): (a) AR order estimation, and (b) functional subspace dimensionality estimation.

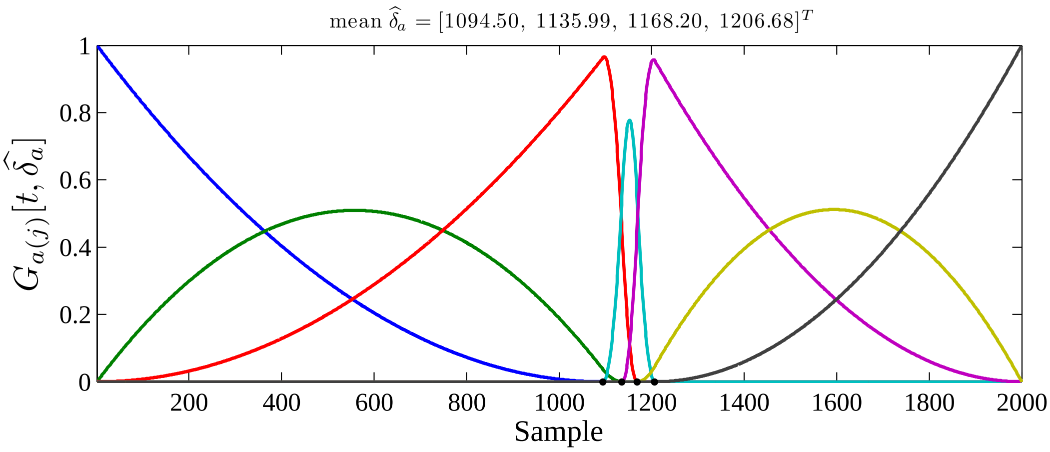

Figure 4.4.15: Test Case III – AR basis functions constructed based on the mean $\boldsymbol{\delta}_a$ estimate. (The respective internal knots are indicated by black dots on the x-axis.)

lenging for all the non-stationary identification methods considered in this study. This is apparent from the results that concern the estimated parameter tracking accuracy shown in Figs. 4.4.16, 4.4.17, and 4.4.18. The novel AFS-TAR method, even for this demanding problem, attains exceptional results, while the classical FS-TAR method with Haar basis functions achieves rather good results. However, the problem of the fixed basis approach is also evident in this case, since the classical FS-TAR model parameter estimates approximate the Gaussian curves by the square shaped Haar functions.

Finally, the recursive methods (RLS-TAR and SP-TAR) seem inadequate of tracking the time-varying parameters. They both show large convergence times and difficulty in tracking the parameter trajectories during the fast transition region.

4.5 Experimental Case Study

4.5.1 The experimental setup and the non-stationary vibration signal

The structure under study is a 2-DOF pick-and-place mechanism consisting of two coaxially aligned linear motors (LinMot P01-37×120) that carry prismatic links (arms) connected to their ends, with the whole mechanism being clamped on an aluminium base (Fig. 4.1(a)). The motors are electromagnetic drives able to generate linear motion with no intermediary mechanical transmission. They are made up of two parts: the slider, that is a high-precision stainless steel tube containing neodymium magnets and

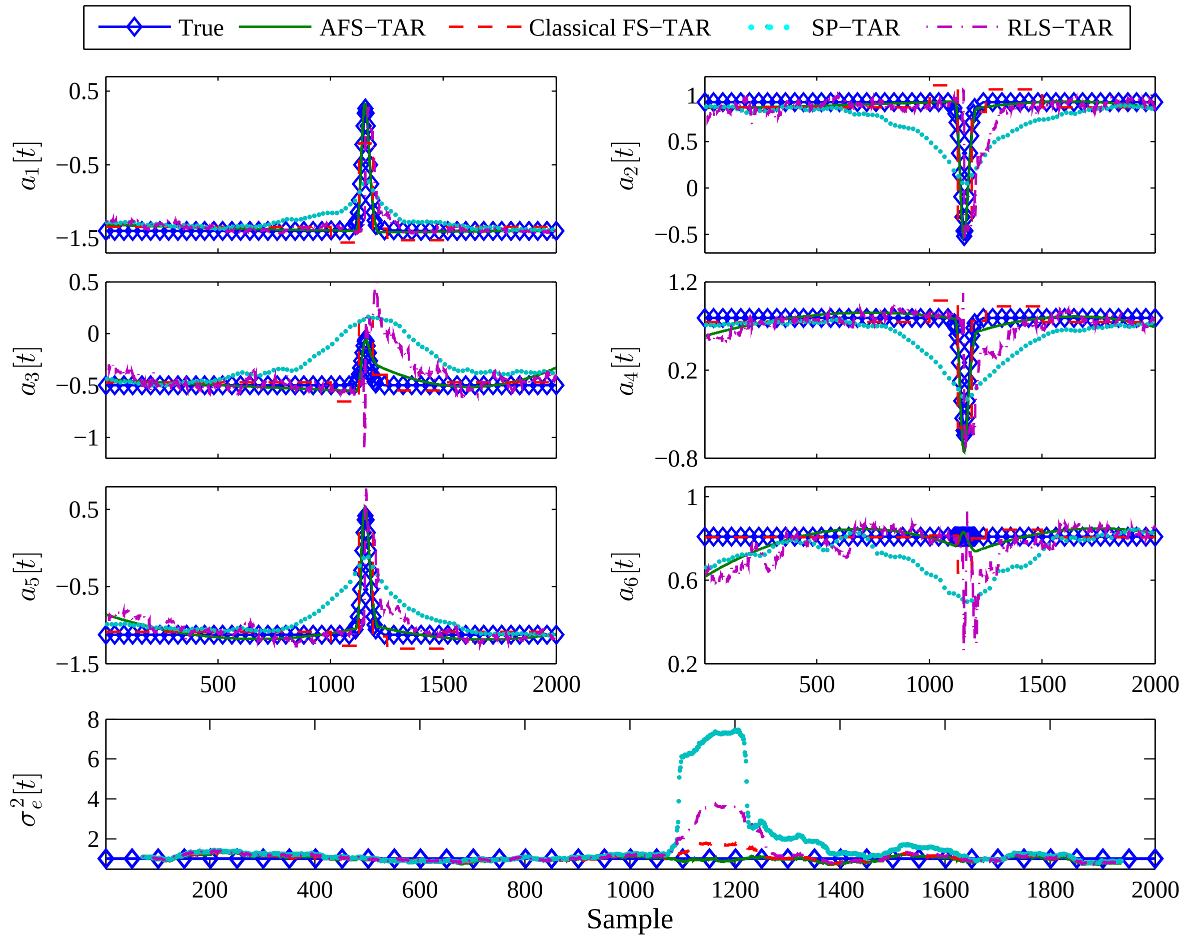

Figure 4.4.16: Test Case III. True and estimated by various methods AR parameter and $\sigma_e^2[t]$ trajectories (single experiment).

the stator that contains the motor windings, slider bearings, position sensors, temperature monitoring, and a microprocessor circuitry. The stators are enclosed in linear guides (LinMot HS01-37x166-GF) that are used for mounting the prismatic links, while they also provide resistance to external forces, rotational and bending moments, contributing in this way to the precise positioning of the stator. A four channel servo controller (LinMot E400-AT) is used to control and measure the position of both motors which may move independently on preselected motion profiles. Note that in this case, in contrast to what their name suggests, the sliders are fixed at one of their ends with the stators sliding on them.

The structure is subject to zero-mean Gaussian random force excitation which is vertically (with respect to the base) exerted via an electromechanical shaker (LDS V201, max load 17.8 N, useful frequency range 5-13,000 Hz) equipped with a stinger (Figs. 4.1(a) and (b)). The vertical (with respect to the base) vibration of the structure is measured at six selected locations (locations 1-6; Fig. 4.1(b)) via lightweight piezoelectric accelerometers (PCB 352C22 ICP accelerometers, frequency range 1 - 10,000 Hz, sensitivity $\sim$ 1.0 mV/m/s^2, weight 0.5 g). The measured vibration signals are conditioned and subsequently driven into SigLab 20-42 data acquisition modules (featuring four 20-bit simultaneously sampled A/D, two 16-bit D/A channels, and 4th-order quasi elliptic analog anti-aliasing filters).

The motion scenario considered is the movement of the motors from their leftmost to their rightmost position and back (Fig. 4.5.2(a); A1–B1 $\rightarrow$ A2–B2 $\rightarrow$ A1–B1) following a reference position profile (Fig. 4.5.2(b); dashed line). The exact position of motor B is measured by embodied magnetic (Hall) sensors with a sampling period of 39.2 ms (Fig. 4.5.2(b); continuous line). The error between the reference and actual position during the experiment is depicted in Fig. 4.5.2(c). The vibration (acceleration) signals are

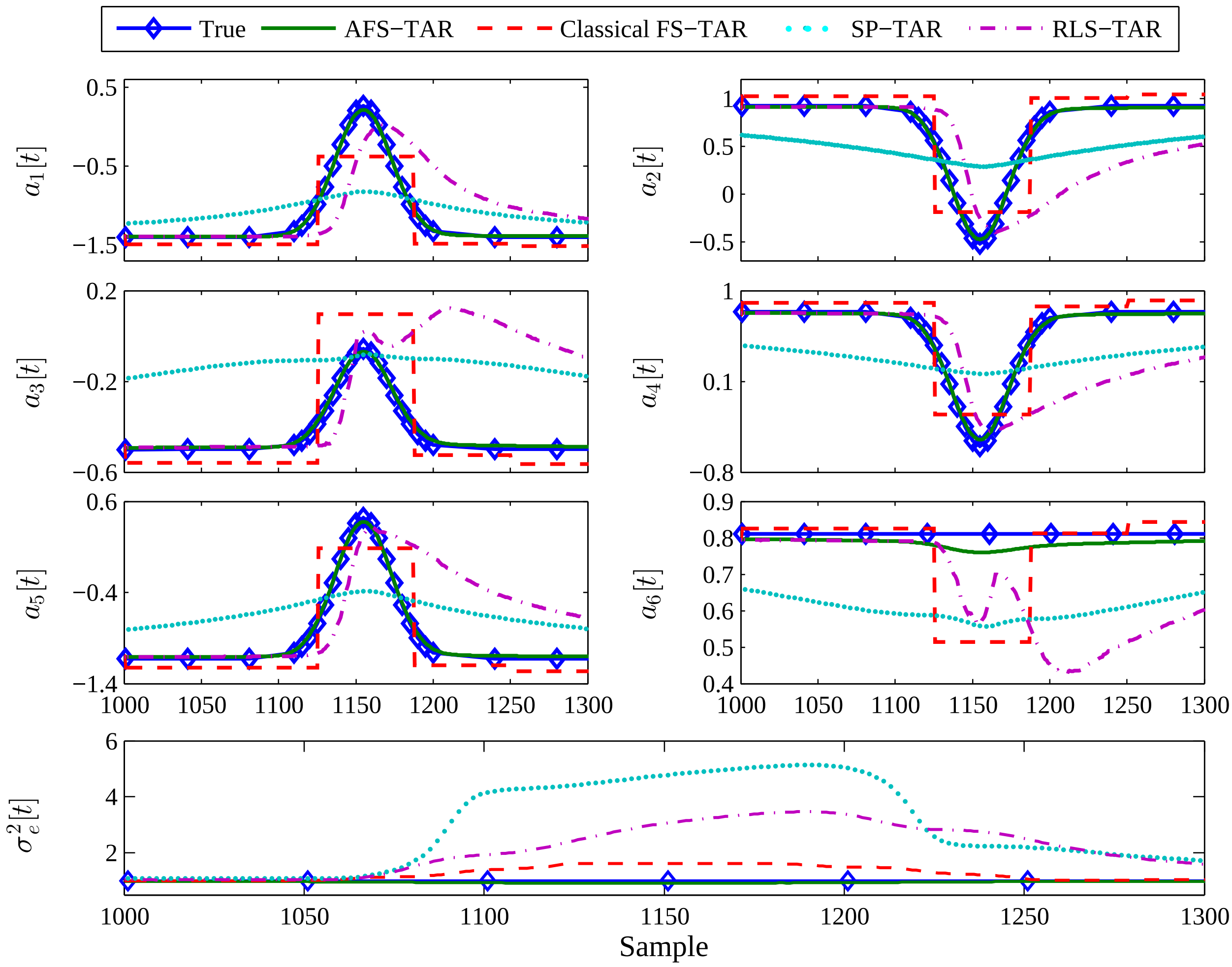

Figure 4.4.17: Test Case III. True and mean estimated by various methods AR parameter and $\sigma_e^2[t]$ trajectories (500 experiments).

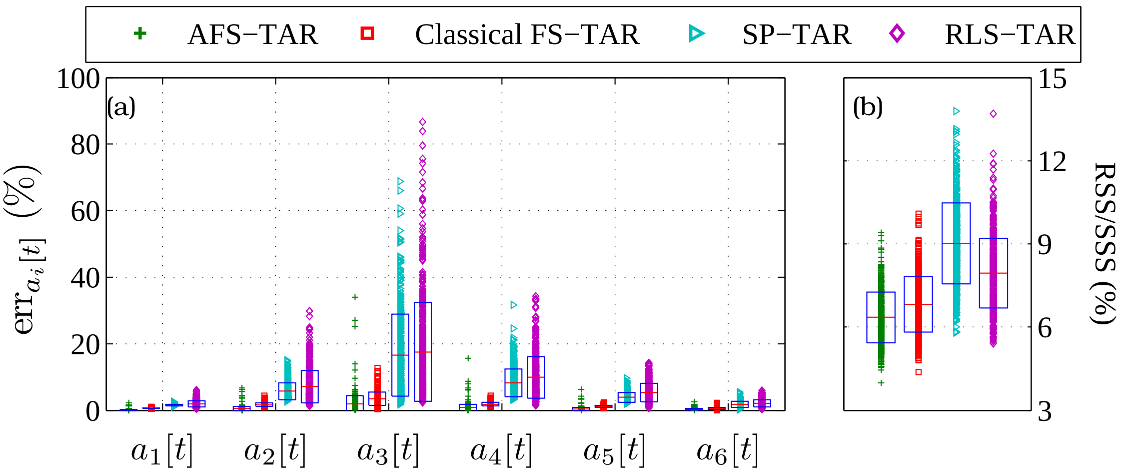

Figure 4.4.18: Test Case III. (a) AR parameter estimation errors and (b) RSS/SSS for the various estimated models (sample mean ± std also shown via boxes; 500 Monte Carlo experiments).

sampled at f_s = 512 Hz, each one being 10 s long. However, the study focuses on the 5 - 125 Hz range, thus the signals are lowpass filtered (Chebyshev II filter of order n = 27 with cut-off frequency of 125 Hz)

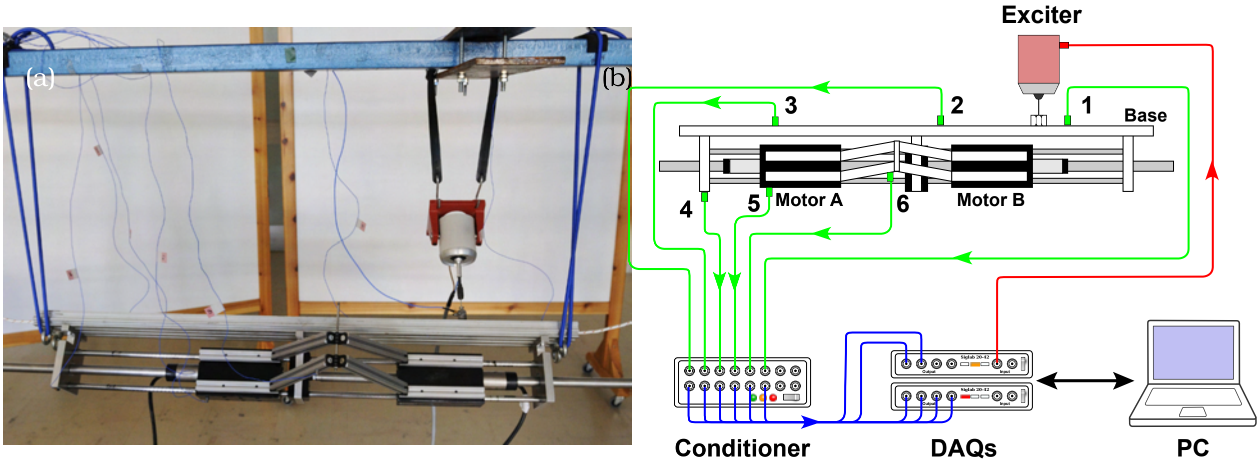

Figure 4.5.1: The pick–and–place mechanism and the experimental setup: (a) photo, (b) schematic diagram.

Table 4.10: Experimental set-up and vibration signal details.

Pick-and-place mechanism	
Linear motors:	LinMot P01-37×120
Linear guides:	LinMot HS01-37x166-GF
Servo controller:	LinMot E400-AT
Excitation	
Excitation signal:	Gaussian white noise
Actuator:	LDS V201 electromechanical shaker
Excitation signal amplifier:	LDS PA500L-CE
Vibration response	
Sensors:	PCB 352C22 lightweight piezoelectric accelerometers
Response signal amplifier:	PCB F482A20
Data acquisition device:	Spectral Dynamics Siglab 20-42
Analysis bandwidth:	5 - 125 Hz
Sampling frequency:	f_s = 128 Hz (downsampled from 512 Hz)
Lowpass filter:	Chebyshev II filter, order n = 27, cut-off frequency = 125 Hz)
Signal length:	$N = 2560$ samples ($= 10$ s)

and downsampled by a factor of two, resulting into N = 2,560 sample long versions. The experimental and vibration signal details are summarized in Table 4.10.

The present identification and analysis of the mechanism time-varying dynamics is based on the non-stationary vibration response measured at location 4 (Fig. 4.1(b)). The signal employed is depicted in Fig. 4.5.3(a). A rough estimate of its time-varying Power Spectral Density (PSD) is obtained through non-parametric time-frequency analysis based on the Short-Time Fourier Transform (STFT) [Hammond and White, 1996] from which non-stationary behaviour is evident (Fig. 4.5.3(b); MATLAB *spectrogram* function, Hamming moving data window of 256 samples advanced by one sample and 256 samples zero-padding).

4.5.2 Structural identification and analysis results

The AFS-TARMA modelling of the time-varying mechanism is presently considered. Again the effectiveness of the introduced method is judged in comparison with available non-stationary identification methods, namely the Smoothness Priors TARMA (SP-TARMA) method [Kitagawa and Gersch, 1996] and a Short-Time version of a Stochastic Subspace Identification (ST-SSI) method based on the Canonical

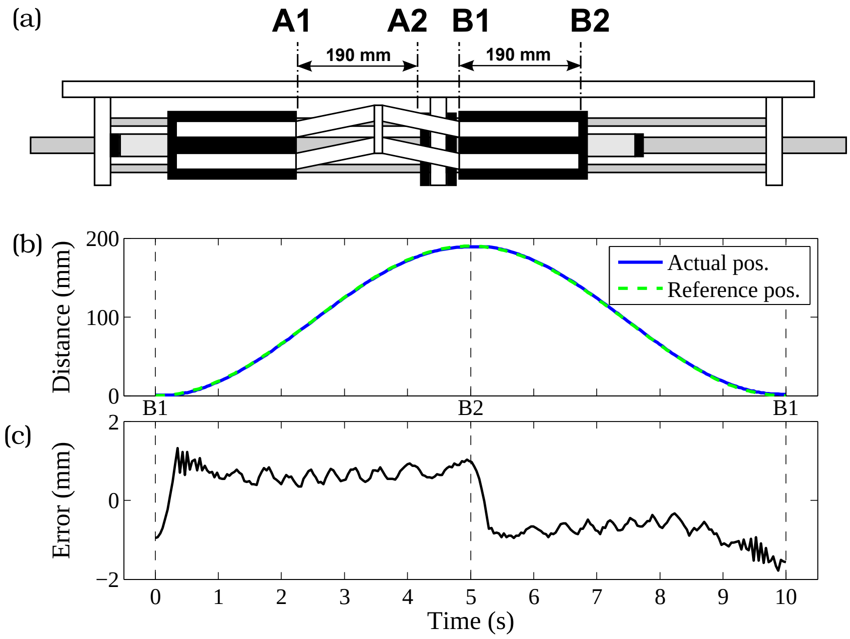

Figure 4.5.2: (a) The pick-and-place mechanism and the motor end positions, (b) the actual and reference position of motor B during the experiment, (c) motor B position error.

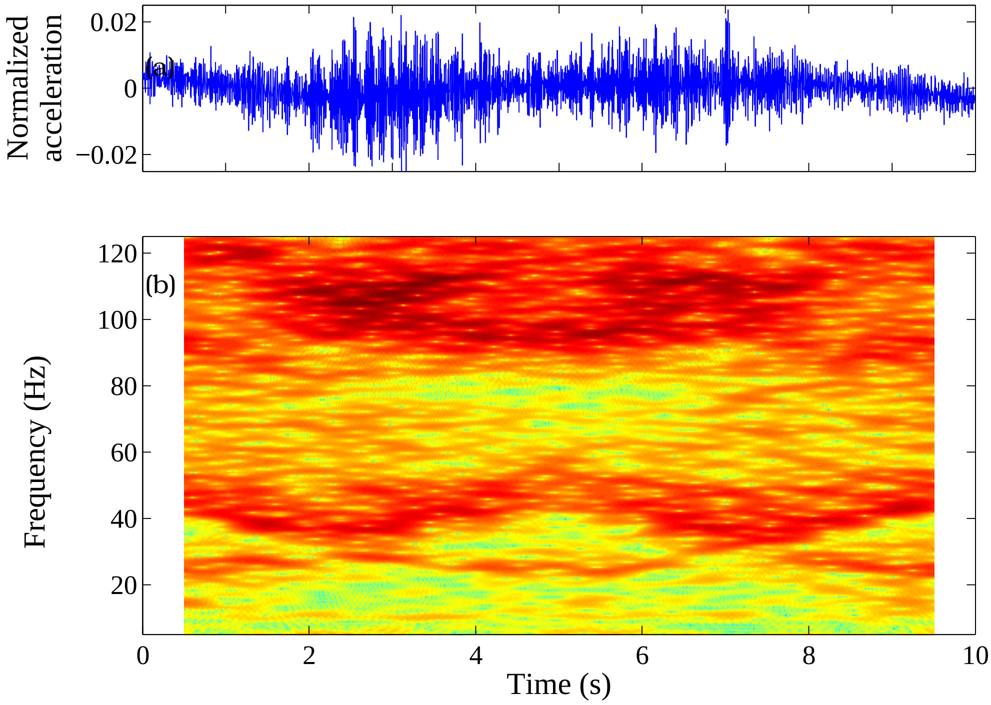

Figure 4.5.3: (a) The non–stationary normalized acceleration signal measured at location 4, and (b) its Short Time Fourier Transform (STFT) based time-varying PSD estimate.

Variate Analysis (CVA) algorithm [Overschee and Moor, 1989, pp. 80-81].

AFS-TARMA identification method. Motivated by the periodic motion profile of the linear motors, functional subspaces consisting of decaying trigonometric basis functions are considered for this case. The 2SVP method is utilized for the AFS-TARMA model parameter estimation initialized by the residual estimates of an AFS-TAR$(23)_{[5]}$ model, with the structure of the latter being selected through the minimization of the BIC criterion.

The AFS-TARMA model structure selection scheme is started off with an initial search space consisting of AR/MA model orders $n_a = n_c = 2, \ldots, 20$ and functional subspace dimensionalities $p_a = 1, \ldots, 9,$

Table 4.11: Characteristics of the identification methods utilized for the identification of the pick-and-place mechanism.

Method	Parameter estimation details	Model structure and algorithmic parameters (search space)	Model structure selection scheme (criterion)
AFS-TARMA	2SVP (Interior point method; MATLAB *fmincon* function; Initial residuals provided by an AFS-TAR$(23)_{[5]}$ model) TolFun = 10^{-6}, TolX = 10^{-9}, TolCon = 10^{-6}, decaying trigonometric basis functions, $r_{\min} = 1 - 5/N = 0.998$, $r_{\max} = 1 + 5/N = 1.002$, $\omega_{\min} = 1/N \simeq 0.0004$ rad/sample, $\omega_{\max} = 20/N \simeq 0.008$ rad/sample, $d_0 = 10^{-4}$	AR/MA orders n_a, n_c ($n_a = n_c = 2, \ldots, 20$), basis dimensionalities p_a, p_c, p_s ($p_a = 1, \ldots, 9$, $p_c = 1, \ldots, 9$, $p_s = 1, \ldots, 9$)	PSO (MATLAB *pso* function) population size = 500, stall generation limit = 50, w = 1, c_1 = 1.45, c_2 = 1.45, TolFun = 10^{-9}, (BIC)
SP-TARMA	three passes followed by a backward smoothing pass,	smoothness constraints order κ ($\kappa = 1, 2, 3$) variance ratio ν ($\nu = 10^{-12}, 10^{-11}, \ldots, 10^{1}$)	trial & error (BIC)
ST-SSI	MATLAB *n4sid* function $q = 10$	model order n $(6, \ldots, 20)$ data segment length Q $(101, 151, 201, \ldots, 551$ samples)	trial & error (RSS)

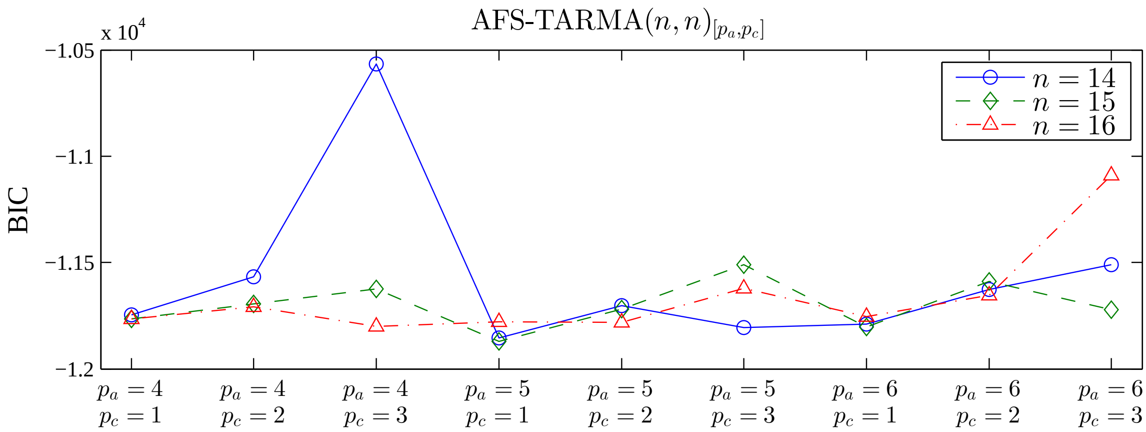

Figure 4.5.4: AFS-TARMA model structure selection (second phase): BIC values attained by the estimated models utilizing the combinatorial approach for $n_a = n_c \in [14, 16]$, $p_a \in [4, 6], p_c \in [1, 3]$ ($p_s = 5$ for all models).

$p_c = 1, \ldots, 9$, and $p_s = 1, \ldots, 9$. Note that for this test case and for purposes of simplicity equal AR and MA orders, and functional bases with at most one single real root (for odd basis dimensionality) are considered. The constraints imposed for the rates of decay ($\{r_a(j), \rho_a, r_c(j), \rho_c, r_s(j), \rho_s\}$), the frequencies ($\{\omega_a(j), \omega_c(j), \omega_s(j)\}$), and the distance between two close roots are selected as shown in Table 4.11. The 2SVP, PSO and the interior point optimization configuration parameters are also indicated in Table 4.11.

The first phase of the model structure selection scheme leads to an AFS-TARMA$(15, 15)_{[5,2,5]}$ model while the combinatorial approach of the second phase with $n_a = n_c \in [14, 16]$, $p_a \in [4, 6]$, $p_c \in [1, 3]$, and $p_s = [4, 6]$ leads to a AFS-TARMA$(15, 15)_{[5,1,5]}$ model as the most appropriate, with respect to the BIC criterion, for the description of the mechanism time-varying dynamics. The estimated functional subspace parameter vectors are given in Table 4.12, while the corresponding AR and MA basis functions are illustrated in Fig. 4.5.5.

SP-TARMA identification method. Regarding the SP-TARMA method, minimization of the BIC with respect to ratio of the smoothness priors constraints innovations variance over the residual variance ν and the smoothness priors constraints is carried out. For the initialization of the Kalman filter algorithm

Table 4.12: Estimated functional subspace parameters vectors of the AFS-TARMA$(15,15)_{[5,1,5]}$ model (frequencies ω_j are given in rad/sample).

$\boldsymbol{\delta}_a$		$\boldsymbol{\delta}_c$		$\boldsymbol{\delta}_s$	
$r_{a(1)}$	0.99987	ρ_c	0.99994	$r_{s(1)}$	1.00140
$\omega_{a(1)}$	0.00199			$\omega_{s(1)}$	0.00363
$r_{a(2)}$	0.99999			$r_{s(2)}$	1.00011
$\omega_{a(2)}$	0.00531			$\omega_{s(2)}$	0.00667
ρ_a	0.99991			ρ_s	0.99987

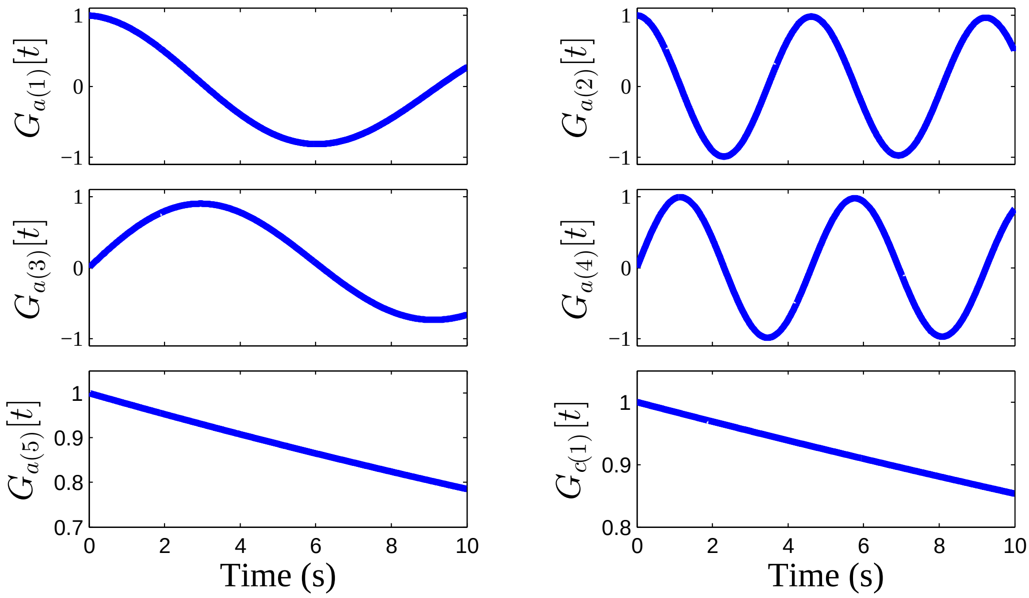

Figure 4.5.5: The estimated AR and MA basis functions of the identified AFS-TARMA$(15,15)_{[5,1,5]}$ model.

the diagonal elements of the covariance matrix are also set equal to 10^4 while also in this case the algorithm is applied in sequential passes over the data record (Table 4.11).

The trial and error model structure selection scheme based on the BIC criterion leads to an SP-TARMA(15,15) model with $\kappa = 1$ and $\nu = 11.6$ for the representation of the mechanism time-varying dynamics. The innovations variance in this case is estimated non-parametrically through a moving time-window of length equal to 201 samples advanced by one sample.

ST-SSI identification method. This method employs a model in state space form, while estimation is based on the batch CVA stochastic subspace identification algorithm. The method operates on a “short” data segment (Q samples long) of the signal at a time. Within this segment the signal may be considered as approximately stationary, and a model is identified. The operation keeps repeated for the “next” segment, produced by an advance of q samples, until the complete signal record is exhausted.

The critical quantities in this method are the segment length Q and the order of the state space model (considered constant for all time segments). Both quantities are selected based on the RSS criterion while compromise between the model order and the segment length is also taken into account for reasons related with statistical efficiency. A trial and error approach searching for the appropriate model order within $n = 6, \ldots, 20$ and segment length $Q = 201, 251, \ldots, 701$ is employed for the selection of these parameters which results in Q equal to 351 samples and n equal to 15. The advancement of the time segments is pre-selected as $q = 10$ (see Table 4.11).

The model structure details for all the identified models considered are summarized in Table 4.13. Finally, some of the AR and MA parameters of the estimated SP-TARMA(15,15) and AFS-TARMA$(15,15)_{[5,1,5]}$ are contrasted in Fig. 4.5.6.

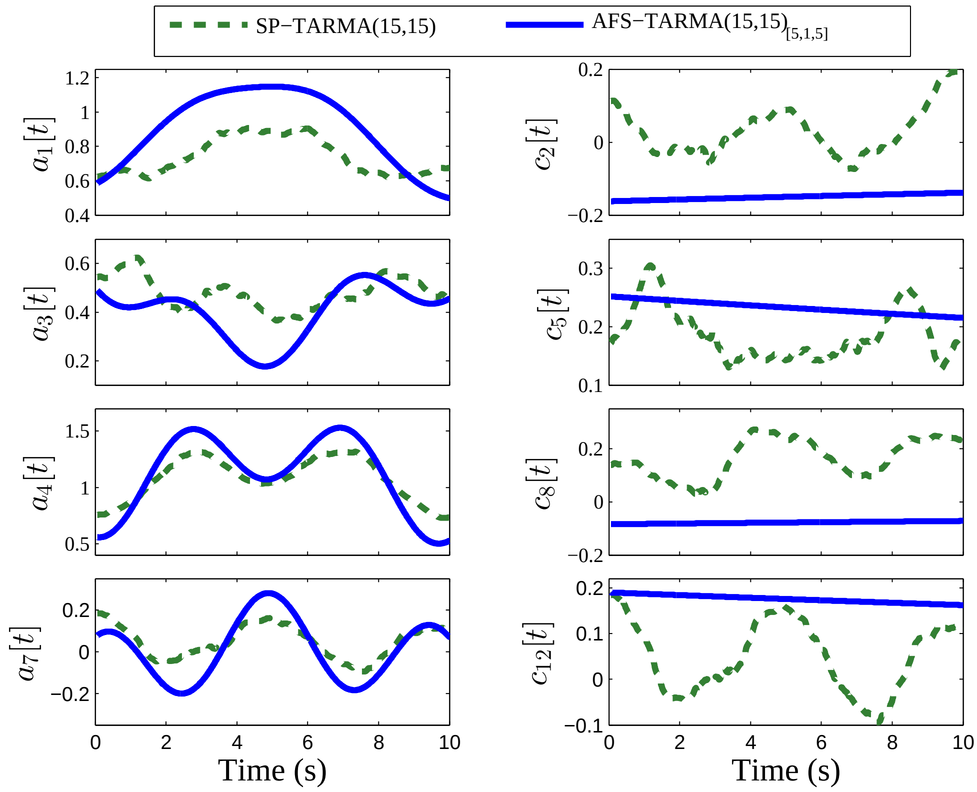

Figure 4.5.6: Comparison of the estimated SP-TARMA(15,15) and AFS-TARMA(15,15)$_{[5,1,5]}$ model parameters.

Table 4.13: Identified model structure parameters.

Method	
ST-SSI	$n = 15, Q = 351, q = 10$
SP-TARMA	$n_a = n_c = 15, \kappa = 1, \nu = 11.6$
AFS-TARMA	deacying trigonometric basis functions, $n_a = n_c = 15, p_a = 5, p_c = 1, p_s = 5$

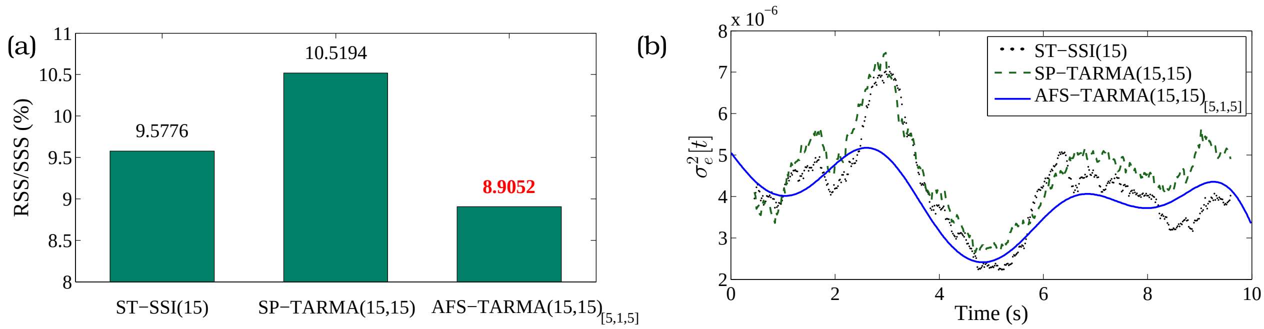

Figure 4.5.7: Predictive ability of the estimated models: (a) RSS/SSS and (b) the residual variance for the various estimated models (a sliding window of 201 samples is used for variance estimation in the case of ST-SSI and SP-TARMA models).

4.5.3 Discussion

The RSS/SSS values attained by the estimated models are provided in Fig. 4.5.7(a). As it may be observed, the estimated AFS-TARMA model attains the best predictive performance, while the worst RSS/SSS value is obtained by the SP-TARMA model. The estimated time-varying variance of the AFS-TARMA model residual is also lower than those obtained by all other models (Fig. 4.5.7(b)).

The AFS-TARMA$(15, 15)_{[5,1,5]}$ based "frozen-time" time-varying PSD estimate [Poulimenos and Fas-

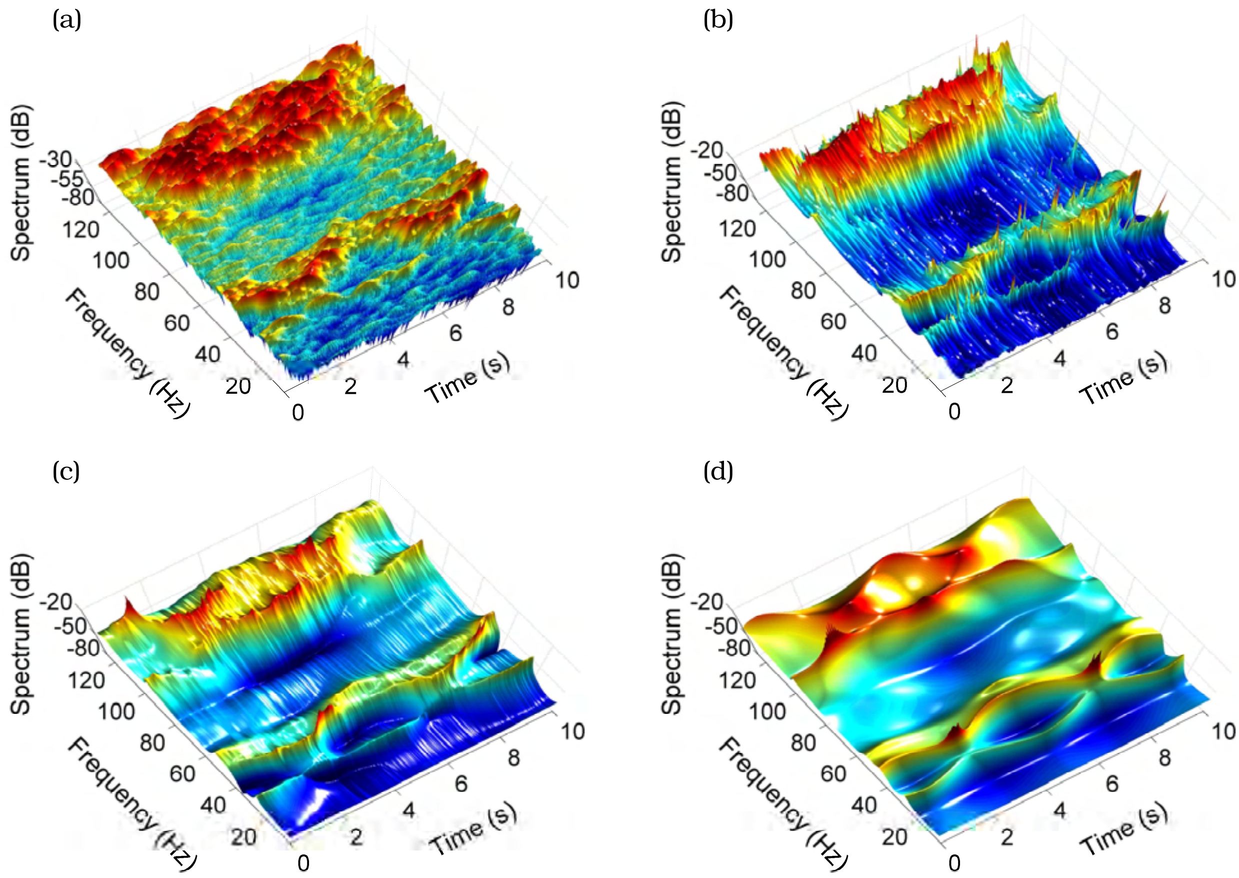

Figure 4.5.8: Comparison of the “frozen-time” time-varying PSD estimates: (a) Non-parametric STFT estimate, (b) ST-SSI(15) estimate, (c) SP-TARMA(15,15) estimate, and (d) AFS-TARMA(15,15)$_{[5,1,5]}$ estimate.

sois, 2006] is also contrasted to those obtained by the SP-TARMA$(15, 15)$ and ST-SSI(15) models and the non-parametric STFT method in Fig. 4.5.8. The AFS-TARMA$(15, 15)_{[5,1,5]}$ estimate is in good overall agreement with the STFT estimate, but of course much more clear, smooth and informative due to the functional structure of the model and in accordance with the smooth variation of the structural geometry. The estimate obtained by the identified SP-TARMA(15,15) model shows very good tracking of the underlying dynamics. On the contrary, the subspace ST-SSI estimate exhibits significant scatter and seems incapable of tracking the time-varying dynamics for specific time periods; this could not be alleviated through higher model orders or different data segments.

The model-based “frozen-time” natural frequency estimates are depicted in Fig. 4.5.9(a). As it may be observed, the agreement of the AFS-TARMA(15,15)$_{[5,1,5]}$ with the non-parametric resonant natural frequency estimates (shown in the background) is very good. SP-TARMA(15,15) based estimates are also good, however higher frequencies depict increased variability. Most of all, the sixth natural frequency estimate varying between 100 and 120 Hz is not symmetric with respect to the mid-time, in opposition to the symmetric nature of the underlying time-varying dynamics. The problem of ST-SSI model to track the time-varying dynamics is even more pronounced in this case. The problem may be attributed to the short length of the data segments, however longer segments lead to estimates incapable of following the rather quickly varying dynamics.

Finally, the model-based “frozen-time” antiresonance natural frequency estimates are depicted in Fig. 4.5.9(b). It is worth noting that the almost constant antiresonance frequency estimates provided by the AFS-TARMA(15,15)$_{[5,1,5]}$ model also agree with the SP-TARMA estimates, despite the fact that the MA parameters of the latter depict a much higher variability compared to that of the former (Fig. 4.5.6). Both

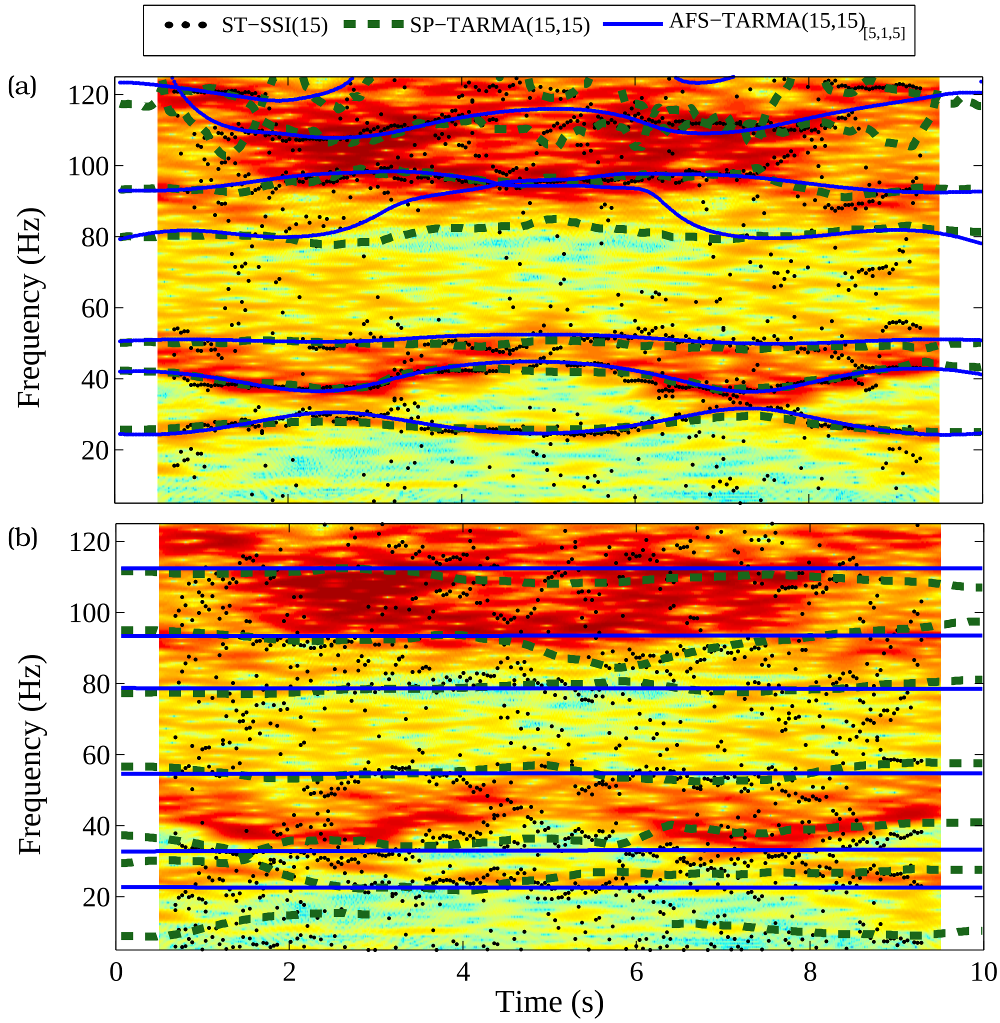

Figure 4.5.9: Comparison of the estimated “frozen-time” modal characteristics: (a) resonance and (b) antiresonance natural frequency estimates (STFT-based time-varying PSD estimate in the background).

models seem to provide spurious antiresonant frequencies but this fact is not totally unexpected since the MA order was constrained and not selected to be equal to the AR model order, and thus probably higher than the true model order.

Summing up, the identified AFS-TARMA model, followed by its SP-TARMA counterpart, seems to exhibit the best tracking of the mechanism dynamics, while also attaining the best predictive ability.

4.6 Conclusions

The class of AFS-TARMA models with adaptable basis functions and an appropriate identification method which achieves simultaneous estimation of coefficient of projection and functional subspace parameters were introduced. The method has been based on proper basis function parametrizations and a SNLS type procedure which leads to a reduced dimensionality, constrained, non-quadratic optimization problem tackled via PSO and gradient-type refinement. The model orders and subspace dimensionalities are estimated based on suitable criteria and PSO. The method's effectiveness was examined via Monte Carlo studies employing TAR model characterized by *abrupt* parameter evolution and an experimental case study pertaining to the identification of a time-varying pick-and-place mechanism. Comparisons with the classical FS-TARMA method and non-stationary identification methods were also performed.

The results of both the numerical and experimental case studies demonstrated the excellent performance and improved accuracy of the proposed method, which is shown to be capable of automatically, and yet effectively, estimating the functional subspaces and coefficients of projection for specified AFS-TAR/TARMA models.

Appendix 4.A Correspondence Between Full and Reduced Functional

The following theorem [Golub and Pereyra, 1973, Theorem 2.1] defines the conditions under which the transformation of the full functional into the VP functional is feasible and the equivalence of the two forms with respect to their stationary points (see [Golub and Pereyra, 1973] for the proof):

Theorem. *Let $V(\boldsymbol{\delta}_a, \boldsymbol{\vartheta}_a)$ and $V_{vp}(\boldsymbol{\delta}_a)$ be defined as in Section 4.3.1.1. The constant rank $r \leq \min(N, \dim(\boldsymbol{\vartheta}_a))$ of $\boldsymbol{\Phi}(\boldsymbol{\delta}_a)$ is assumed within the open set $\boldsymbol{\Omega} \subset \mathbb{R}^{\dim(\boldsymbol{\delta}_a)}$.*

(1) If $\widehat{\boldsymbol{\vartheta}}_a$ is a critical point (or a global minimizer in $\boldsymbol{\Omega}$) of $V_{vp}(\boldsymbol{\delta}_a)$, and

$$\widehat{\boldsymbol{\vartheta}}_a = \boldsymbol{\Phi}^{\dagger}(\widehat{\boldsymbol{\delta}}_a) \cdot \boldsymbol{x} \tag{4.A.1}$$

then $(\widehat{\boldsymbol{\delta}}_a, \widehat{\boldsymbol{\vartheta}}_a)$ is a critical point of $V(\boldsymbol{\delta}_a, \boldsymbol{\vartheta}_a)$ (or a global minimizer for $\boldsymbol{\delta}_a \in \boldsymbol{\Omega}$) and $V(\widehat{\boldsymbol{\delta}}_a, \widehat{\boldsymbol{\vartheta}}_a) = V_{vp}(\widehat{\boldsymbol{\delta}}_a)$.

(2) If $(\widehat{\boldsymbol{\delta}}_a, \widehat{\boldsymbol{\vartheta}}_a)$ is a global minimizer of $V(\boldsymbol{\delta}_a, \boldsymbol{\vartheta}_a)$, for $\boldsymbol{\delta}_a \in \boldsymbol{\Omega}$, then $\widehat{\boldsymbol{\delta}}_a$ is a global minimizer of $V_{vp}(\boldsymbol{\delta}_a)$ in $\boldsymbol{\Omega}$ and $V(\widehat{\boldsymbol{\delta}}_a, \widehat{\boldsymbol{\vartheta}}_a) = V_{vp}(\widehat{\boldsymbol{\delta}}_a)$. Furthermore, if there is an unique $\widehat{\boldsymbol{\vartheta}}_a$ among the minimizing pairs of $V(\boldsymbol{\delta}_a, \boldsymbol{\vartheta}_a)$, then $\widehat{\boldsymbol{\vartheta}}_a$ must satisfy Eq. (4.A.1).

Appendix 4.B Objective Function Gradient

4.B.1 FS-TAR case

4.B.1.1 Full functional

The gradient of the PE criterion with respect to the complete AR parameter vector $[\boldsymbol{\delta}_a^T, \boldsymbol{\vartheta}_a^T]^T$ may be calculated as follows:

$$\begin{aligned} V'(\boldsymbol{\delta}_a, \boldsymbol{\vartheta}_a) &= \begin{bmatrix} \frac{\partial V(\boldsymbol{\delta}_a, \boldsymbol{\vartheta}_a)}{\partial \boldsymbol{\delta}_a} \\ \frac{\partial V(\boldsymbol{\delta}_a, \boldsymbol{\vartheta}_a)}{\partial \boldsymbol{\vartheta}_a} \end{bmatrix} = \begin{bmatrix} \frac{\partial \|\boldsymbol{e}(\boldsymbol{\delta}_a, \boldsymbol{\vartheta}_a)\|^2}{\partial \boldsymbol{\delta}_a} \\ \frac{\partial \|\boldsymbol{e}(\boldsymbol{\delta}_a, \boldsymbol{\vartheta}_a)\|^2}{\partial \boldsymbol{\vartheta}_a} \end{bmatrix} = \begin{bmatrix} \frac{\partial (\sum_{t=1}^N e[t, \boldsymbol{\delta}_a, \boldsymbol{\vartheta}_a]^2)}{\partial \boldsymbol{\delta}_a} \\ \frac{\partial (\sum_{t=1}^N e[t, \boldsymbol{\delta}_a, \boldsymbol{\vartheta}_a]^2)}{\partial \boldsymbol{\vartheta}_a} \end{bmatrix} = \\ &= \sum_{t=1}^{N} \begin{bmatrix} \frac{\partial (e[t, \boldsymbol{\delta}_a, \boldsymbol{\vartheta}_a]^2)}{\partial \boldsymbol{\delta}_a} \\ \frac{\partial (e[t, \boldsymbol{\delta}_a, \boldsymbol{\vartheta}_a]^2)}{\partial \boldsymbol{\vartheta}_a} \end{bmatrix} = 2 \cdot \sum_{t=1}^{N} e[t, \boldsymbol{\delta}_a, \boldsymbol{\vartheta}_a] \cdot \begin{bmatrix} \frac{\partial e[t, \boldsymbol{\delta}_a, \boldsymbol{\vartheta}_a]}{\partial \boldsymbol{\delta}_a} \\ \frac{\partial e[t, \boldsymbol{\delta}_a, \boldsymbol{\vartheta}_a]}{\partial \boldsymbol{\vartheta}_a} \end{bmatrix} \end{aligned}$$

where

$$\begin{aligned} \frac{\partial e[t, \boldsymbol{\delta}_a, \boldsymbol{\vartheta}_a]}{\partial \boldsymbol{\delta}_a} &= \frac{\partial \left(x[t] - \boldsymbol{\phi}^T[t, \boldsymbol{\delta}_a] \cdot \boldsymbol{\vartheta}_a \right)}{\partial \boldsymbol{\delta}_a} = -\frac{\partial \boldsymbol{\phi}^T[t, \boldsymbol{\delta}_a]}{\partial \boldsymbol{\delta}_a} \cdot \boldsymbol{\vartheta}_a = \\ &= -\begin{bmatrix} -x[t-1] \cdot \frac{\partial G_{a(1)}[t, \boldsymbol{\delta}_a]}{\partial \delta_{a(1)}} & \ldots & -x[t-n_a] \cdot \frac{\partial G_{a(p_a)}[t, \boldsymbol{\delta}_a]}{\partial \delta_{a(1)}} \\ -x[t-1] \cdot \frac{\partial G_{a(1)}[t, \boldsymbol{\delta}_a]}{\partial \delta_{a(2)}} & \ldots & -x[t-n_a] \cdot \frac{\partial G_{a(p_a)}[t, \boldsymbol{\delta}_a]}{\partial \delta_{a(2)}} \\ \vdots & \ddots & \vdots \\ -x[t-1] \cdot \frac{\partial G_{a(1)}[t, \boldsymbol{\delta}_a]}{\partial \delta_{a(\dim(\boldsymbol{\delta}_a))}} & \ldots & -x[t-n_a] \cdot \frac{\partial G_{a(p_a)}[t, \boldsymbol{\delta}_a]}{\partial \delta_{a(\dim(\boldsymbol{\delta}_a))}} \end{bmatrix} \cdot \boldsymbol{\vartheta}_a \end{aligned}$$

with the derivatives $\frac{\partial G_{a(j)}[t, \boldsymbol{\delta}_a]}{\partial \delta_{a(i)}}$ for the B-splines and the decaying trigonometric basis functions being given in 4.B.2 and 4.B.3, respectively, and:

$$\frac{\partial e[t, \boldsymbol{\delta}_a, \boldsymbol{\vartheta}_a]}{\partial \boldsymbol{\vartheta}_a} = \frac{\partial \left(x[t] - \boldsymbol{\phi}^T[t, \boldsymbol{\delta}_a] \cdot \boldsymbol{\vartheta}_a \right)}{\partial \boldsymbol{\vartheta}_a} = -\boldsymbol{\phi}[t, \boldsymbol{\delta}_a]$$

4.B.1.2 Variable projection functional

$$V'_{\text{VP}}(\boldsymbol{\delta}_a) \;=\; \frac{\partial\left(\|\boldsymbol{e}_{\text{VP}}(\boldsymbol{\delta}_a)\|^2\right)}{\partial\boldsymbol{\delta}_a} = 2\cdot\underbrace{\frac{\partial\boldsymbol{e}^T_{\text{VP}}(\boldsymbol{\delta}_a)}{\partial\boldsymbol{\delta}_a}}_{\boldsymbol{J}}\cdot\boldsymbol{e}_{\text{VP}}(\boldsymbol{\delta}_a) \tag{4.B.1}$$

The Jacobian of $V'_{\text{VP}}(\boldsymbol{\delta}_a)$ with respect to any of the scalar variables $\delta_{a(i)}$ can be derived by the following manipulations [Golub and Pereyra, 1973] (the dependence on $\boldsymbol{\delta}_a$ is omitted for the sake of notational simplicity) :

$$\begin{aligned}
\frac{\partial\boldsymbol{e}_{\text{VP}}}{\partial\delta_{a(i)}} &= \frac{\partial\left[(\boldsymbol{I}-\boldsymbol{\Phi}\boldsymbol{\Phi}^\dagger)\boldsymbol{x}\right]}{\partial\delta_{a(i)}} = -\frac{\partial\boldsymbol{\Phi}}{\partial\delta_{a(i)}}\boldsymbol{\Phi}^\dagger\boldsymbol{x} - \boldsymbol{\Phi}\frac{\partial\boldsymbol{\Phi}^\dagger}{\partial\delta_{a(i)}}\boldsymbol{x} = \\
&= -\frac{\partial\boldsymbol{\Phi}}{\partial\delta_{a(i)}}\boldsymbol{\Phi}^\dagger\boldsymbol{x} - \boldsymbol{\Phi}\frac{\partial\left[\left(\boldsymbol{\Phi}^T\boldsymbol{\Phi}\right)^{-1}\boldsymbol{\Phi}\right]}{\partial\delta_{a(i)}}\boldsymbol{x} = \\
&= -\frac{\partial\boldsymbol{\Phi}}{\partial\delta_{a(i)}}\boldsymbol{\Phi}^\dagger\boldsymbol{x} - \boldsymbol{\Phi}\left(\boldsymbol{\Phi}^T\boldsymbol{\Phi}\right)^{-1}\left[\frac{\partial\boldsymbol{\Phi}}{\partial\delta_{a(i)}}^T\boldsymbol{\Phi} + \boldsymbol{\Phi}^T\frac{\partial\boldsymbol{\Phi}}{\partial\delta_{a(i)}}\right]\left(\boldsymbol{\Phi}^T\boldsymbol{\Phi}\right)^{-1}\boldsymbol{\Phi}^T\boldsymbol{x} = \\
&= -\left[\frac{\partial\boldsymbol{\Phi}}{\partial\delta_{a(i)}} - (\boldsymbol{\Phi}^\dagger)^T\left(\frac{\partial\boldsymbol{\Phi}}{\partial\delta_{a(i)}}\right)^T\boldsymbol{\Phi} + \boldsymbol{\Phi}\boldsymbol{\Phi}^\dagger\frac{\partial\boldsymbol{\Phi}}{\partial\delta_{a(i)}}\right]\boldsymbol{\Phi}^\dagger\boldsymbol{x}
\end{aligned}$$

where $\frac{\partial\boldsymbol{\Phi}(\boldsymbol{\delta}_a)}{\partial\delta_{a(i)}} = \left[\frac{\partial\boldsymbol{\phi}[1,\boldsymbol{\delta}_a]}{\partial\delta_{a(i)}},\ldots,\frac{\partial\boldsymbol{\phi}[N,\boldsymbol{\delta}_a]}{\partial\delta_{a(i)}}\right]^T$

4.B.2 Derivative of B-splines with respect to a knot

Given the B-splines $G^k_j[t,\boldsymbol{\delta}]$ of order k defined over the knot vector $\boldsymbol{\tau} = [\tau_1,\ldots,\tau_{p+k}]^T$ (where τ_i is a knot of multiplicity less than k and $\boldsymbol{\delta} = [\tau_{k+1},\ldots,\tau_p]^T$), the derivative $\frac{\partial G^k_j[t,\boldsymbol{\delta}]}{\partial\delta_i}$ for $1\le i\le p-k$ is given by the following relation [Piegl and Tiller, 1998]:

$$\frac{\partial G^k_j[t,\boldsymbol{\delta}]}{\partial\delta_i} = \begin{cases}
0, & j=1,\ldots,i-1\\[2mm]
\frac{\overline{G}^k_{i+1}[t,\boldsymbol{\delta}]}{\tau_{i+k}-\tau_{i+1}}, & j=i\\[2mm]
\frac{\overline{G}^k_{j+1}[t,\boldsymbol{\delta}]}{\tau_{j+k}-\tau_{j+1}} - \frac{\overline{G}^k_{j}[t,\boldsymbol{\delta}]}{\tau_{j+k-1}-\tau_{j}}, & j=i+1,\ldots,i+k-1\\[2mm]
-\frac{\overline{G}^k_{i+k}[t,\boldsymbol{\delta}]}{\tau_{i+2k-1}-\tau_{i+k}}, & j=i+k\\[2mm]
0, & j=i+k+1,\ldots,p
\end{cases} \tag{4.B.2}$$

where $\overline{G}^k_j[t,\boldsymbol{\delta}]$ denotes the basis functions of order k corresponding to the knot vector $\boldsymbol{\tau}' = \boldsymbol{\tau}\cup\tau_i = [\tau_1,\ldots,\tau_{i-1},\tau_i,\tau_i,\tau_{i+1}\ldots,\tau_{p+k}]^T$.

4.B.3 Derivatives of a decaying trigonometric function with respect to its parameters

Given the decaying trigonometric function $G_j[t]$ defined by the parameter vector $\boldsymbol{\delta} = [r_1, \dots, r_q, \omega_1, \dots, \omega_q, \rho]^T$ and Eq. (4.2.7), its derivative $\frac{\partial G_j[t,\boldsymbol{\delta}]}{\partial \delta_i}$ may be readily obtained as follows:

$$\frac{\partial G_j[t,\boldsymbol{\delta}]}{\partial \delta_i} = \begin{cases} t \cdot r_i^{t-1} \cdot \cos(\omega_i t), & j = i = 1, \dots, q \\ t \cdot r_i^{t-1} \cdot \sin(\omega_i t), & j = q+1, \dots, 2q, i = 1, \dots, q \\ -t \cdot r_{i-q}^{t} \cdot \sin(\omega_{i-q} t), & j = 1, \dots, q, i = q+1, \dots, 2q \\ t \cdot r_{i-q}^{t} \cdot \cos(\omega_{i-q} t), & j = q+1, \dots, 2q, i = q+1, \dots, 2q \\ t \cdot \rho^{t-1}, & j = i = p, \text{ if } p \text{ is odd} \end{cases} \tag{4.B.3a}$$

with

$$q_a = \begin{cases} \frac{p}{2} & \text{for } p \text{ even} \\ \frac{p-1}{2} & \text{for } p \text{ odd} \end{cases} \tag{4.B.3b}$$

Appendix 4.C Particle Swarm Optimization (PSO) Algorithm

The idea of PSO has emerged from the observation of swarming behaviors of birds flocks, schools of fish, swarm of bees, etc that adjust their physical movements to avoid predators and seek the best food sources [Engelbrecht, 2006, Perez and Behdinan, 2007]. PSO is a non-gradient probabilistic based search algorithm which has been shown to have a number of advantages compared to other evolutionary optimization algorithms, mainly due to the effective sharing of information among its particles.

According to the PSO algorithm, a set of candidate parameter vectors $\boldsymbol{\chi}$ (the "swarm") is moving over the $\dim(\boldsymbol{\chi})$-dimensional search space seeking for the global minima of the objective function. The position of each particle i at iteration $j+1$ is updated as

$$\boldsymbol{\chi}_i^{j+1} = \boldsymbol{\chi}_i^{j} + \boldsymbol{u}_i^{j+1} \tag{4.C.1}$$

where $\boldsymbol{u}_i^{j+1}$ is the corresponding updated velocity vector. The velocity vector, which determines the movement of each particle of the swarm, is determined by three factors: (i) the particle's inertia, (ii) the particle's memory and (iii) the swarm's memory. Thus, the velocity update rule is expressed by the following equation

$$\boldsymbol{u}_i^{j+1} = w\boldsymbol{u}_i^{j} + c_1 r_1(\boldsymbol{p}_i^{j} - \boldsymbol{\chi}_i^{j}) + c_2 r_2(\boldsymbol{p}_g^{j} - \boldsymbol{\chi}_i^{j}) \tag{4.C.2}$$

where r_1 and r_2 are random numbers uniformly distributed in the interval $[0, 1]$, $\boldsymbol{p}_i^{j}$ represents the best ever particle position of particle i, and $\boldsymbol{p}_g^{j}$ corresponds to the global best position in the swarm up to iteration j. The coefficients w, c_1 and c_2 are user defined parameters and represent the weights on the aforementioned factors that affect the velocity of a particle. Specifically, w is the inertia weight, c_1 is a "trust" factor representing the confidence that a particle has in itself (and its memory), and c_2 is a "trust" factor representing the confidence that a particle has in the swarm.

A detailed description of the PSO and its derivatives may be found in [Engelbrecht, 2006, Part III]. Interesting details regarding the performance of the algorithm (e.g. convergence and stability analysis, relation of the algorithm with gradient-based methods) may also be found in [Perez and Behdinan, 2007].

Appendix 4.D Monte Carlo Study on the AFS-TAR Identification of a Simulated FS-TAR Model

The performance characteristics of the introduced AFS-TAR models are also examined via Monte Carlo experiments on the identification of a simulated classical FS-TAR model. Specifically, the identification

Table 4.D.1: True DCT FS-TAR$(6)_{[5]}$ model coefficients of projection.

	$j=1$	$j=2$	$j=3$	$j=4$	$j=5$
$a_{1,j}$	-1.62	0.26	0.41	-0.05	-0.05
$a_{2,j}$	1.31	0.03	-0.83	0.19	0.01
$a_{3,j}$	-0.88	-0.36	0.95	-0.23	0.05
$a_{4,j}$	1.17	0.01	-0.74	0.14	-0.02
$a_{5,j}$	-1.27	0.25	0.30	-0.07	-0.02
$a_{6,j}$	0.76	-0.01	0.02	0.03	-0.02

$\sigma_w^2[t] = 1$

Signal length: $N = 2000$ samples

Number of Monte Carlo experiments: 500

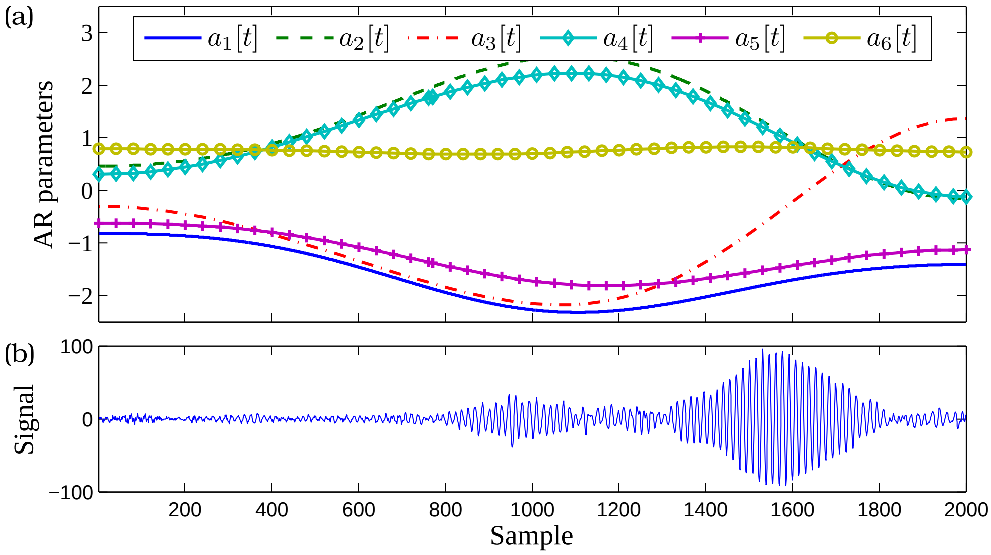

Figure 4.D.1: True classical DCT FS-TAR$(6)_{[5]}$ model: (a) AR parameters, and (b) signal realization.

problem of an FS-TAR$(6)_{[5]}$ model with parameters expanded on DCT basis functions through the AFS-TAR and the classical FS-TAR method is presently considered. The goal of this test case study is to demonstrate the effectiveness of the introduced method even when they are disfavored against their counterparts.

For this purpose, the true AR functional subspace consisting of the first five DCT basis functions is preselected for the classical FS-TAR approach, while within the context of the AFS-TAR models no prior information with respect to the time-varying parameter evolution is taken into consideration, and thus quadratic B-splines functions ($k = 3$) are employed. In this way, no model structure selection is involved for the classical approach, while the appropriate dimensionality and characteristics of the adaptable B-splines functions used for the AFS-TAR models are sought by using the two-phase model structure selection method described in Section 4.3.2. The estimation method characteristics and implementation details are selected just as the test cases considered in Section 4.4 (see Table 4.5).

The true AR coefficients of projection of the simulated FS-TAR model are given in Table 4.D.1 with the corresponding TV AR parameters being depicted in Fig. 4.D.1(a). The driving noise sequence variance is again considered constant and equal to unity ($\sigma_w^2 = 1$), while 500 realizations were generated by using different seed numbers. One of these realizations is shown in Fig. 4.D.1(b).

The AFS-TAR model structure selection scheme based on the PSO algorithm and the combinatorial approach for $p_a \in [4, 10]$ indicates that an AFS-TAR$(6)_{[6]}$ model is, with respect to the BIC, the most adequate for representing the true DCT FS-TAR model – the correct AR order is assumed a-priori known.

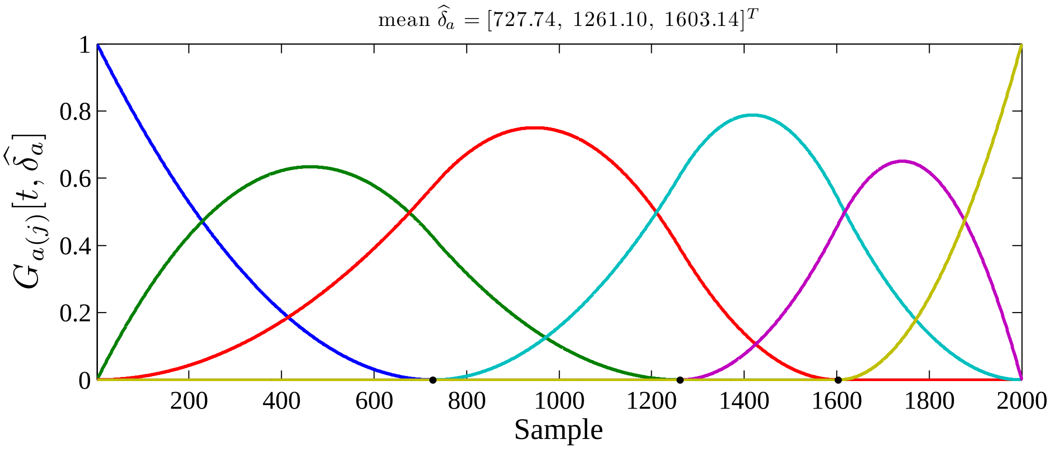

Figure 4.D.2: True classical DCT FS-TAR$(6)_{[5]}$ model identified by the AFS-TAR method. Adaptable basis functions constructed based on the mean $\boldsymbol{\delta}_a$ estimate. (The respective internal knots are indicated by black dots on the x-axis.)

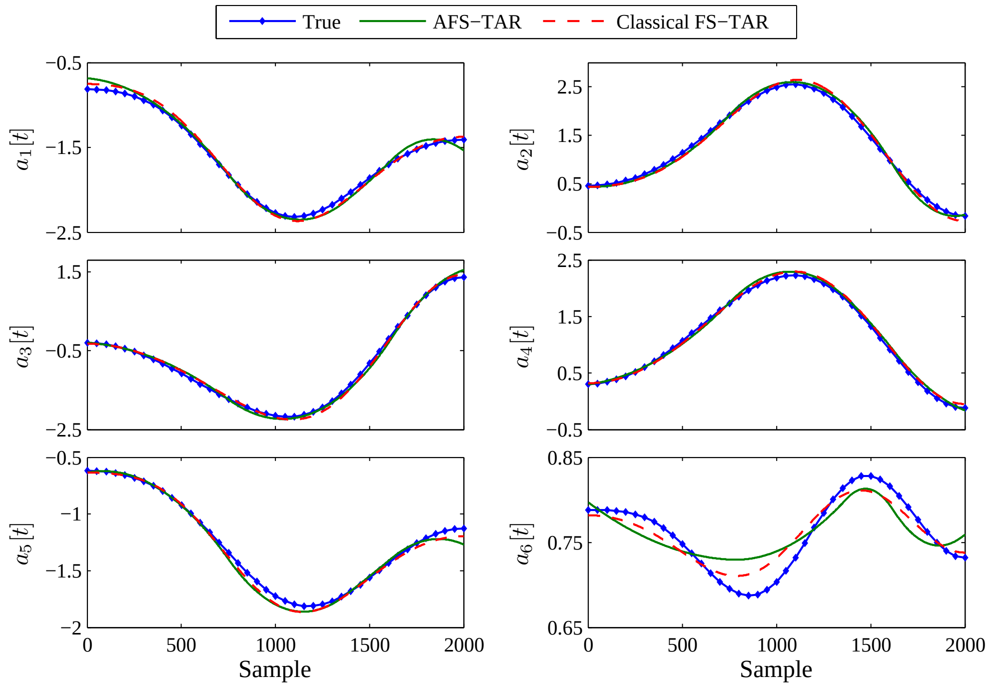

Figure 4.D.3: True classical DCT FS-TAR$(6)_{[5]}$ model identified by the AFS-TAR method. True and estimated AR parameters (single experiment).

Thus, an AFS-TAR$(6)_{[6]}$ model is identified for each one of the 500 realizations with the mean estimate of the AR functional subspace parameter vector being $\widehat{\boldsymbol{\delta}}_a = [727.74,\ 1261.10,\ 1603.14]^T$. The AR basis functions constructed based on this parameter vector are shown in Fig. 4.D.2.

Indicative comparison results regarding the tracking of the TV model parameters as obtained from a single realization are shown in Fig. 4.D.3, while the sample mean over 500 realizations estimated parameters trajectories are depicted in Fig. 4.D.4. Clearly, the AFS-TAR estimates are very close to the true TV parameters and only slightly worse than the corresponding classical FS-TAR estimates for which the true AR functional subspace was preselected. It should be also noted that these results could also be further improved if adaptable decaying trigonometric basis functions were used instead of the B-splines.

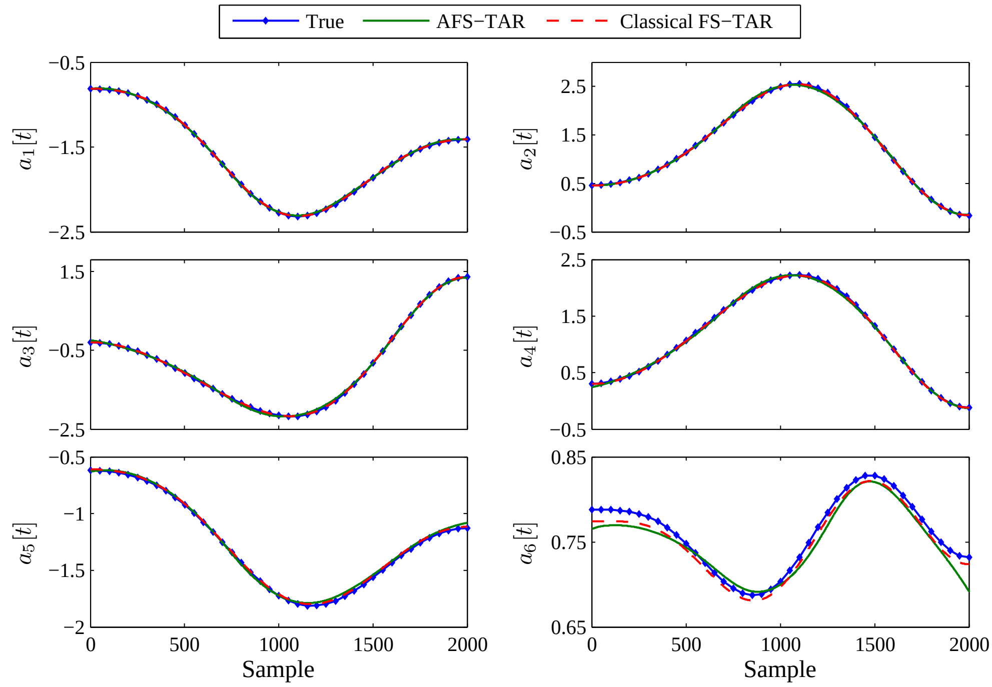

Figure 4.D.4: True classical DCT FS-TAR$(6)_{[5]}$ model identified by the AFS-TAR method. True and estimated AR parameters (500 experiments).

Monte Carlo results of the parameter tracking error $\mathrm{err}_{a_i[t]}$ and the RSS/SSS criterion are depicted in Fig. 4.D.5 and provide further support to the previous comments. Particularly, the mean parameter tracking errors for the AFS-TAR models with parameters expanded on adaptable basis functions lie below 0.5% while the errors achieved by the FS-TAR method lie below 0.3%. Moreover, the AFS-TAR and the classical FS-TAR method give almost equal RSS/SSS values.

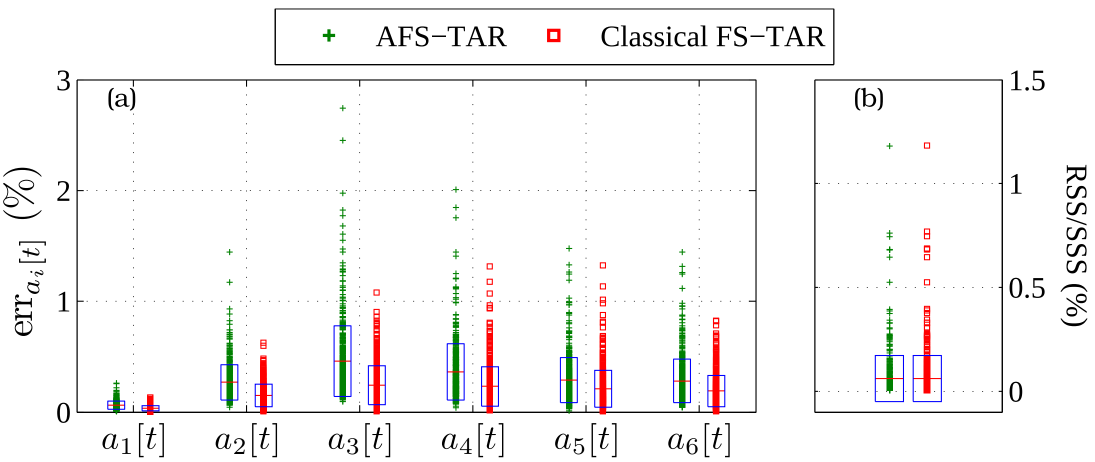

Figure 4.D.5: True classical DCT FS-TAR$(6)_{[5]}$ model identified by the AFS-TAR method. (a) AR parameter estimation errors and (b) RSS/SSS for the classical FS-TAR and AFS-TAR estimated models (sample mean ± std also shown via boxes; 500 Monte Carlo experiments).

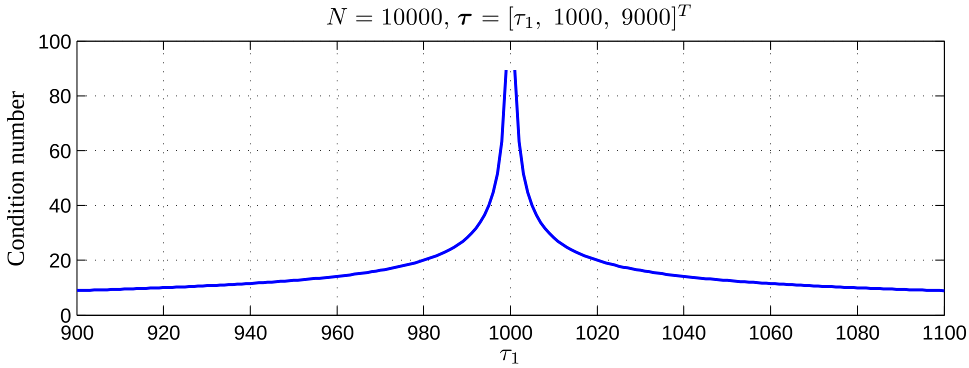

Figure 4.E.1: Numerical reliability problems arising in the case of coalescing knots.

Appendix 4.E Numerical Reliability Problems When No Constraints are Applied

The numerical reliability problems that may arise when no constraints are applied on the parameters of the B-splines or the decaying trigonometric functional basis are illustrated through two simple paradigms in the sequel.

At first, let us assume the case of a B-splines functional basis with $k = 1$ consisting of four basis functions $G_1[t,\boldsymbol{\delta}],\dots,G_4[t,\boldsymbol{\delta}]$, that is three internal knots or else $\boldsymbol{\delta} = [\tau_1, \tau_2, \tau_3]^T$. Two of these knots are considered fixed ($\tau_2 = 1000, \tau_3 = 9000$) while τ_1 varies between 900 and 1100 ($N = 10000$). For each discrete value of τ_1 the basis functions are obtained by using Eq. (4.2.5) and the regression matrix $\boldsymbol{G}(\boldsymbol{\delta}) = \big[\boldsymbol{g}[1,\boldsymbol{\delta}],\dots,\boldsymbol{g}[N,\boldsymbol{\delta}]\big]^T$, where $\boldsymbol{g}[t,\boldsymbol{\delta}] = [G_1[t,\boldsymbol{\delta}],\dots,G_4[t,\boldsymbol{\delta}]]^T$, if formed. This matrix could be used for any SNLS problem such as the one that emerges when trying to project the innovations sequence standard deviation of an AFS-TARMA model onto an a-priori unknown functional basis (see Eq. (4.3.10)). As already mentioned, according to the theorem of Golub and Pereya [Golub and Pereyra, 1973, Theorem 2.1], such a problem may be solved through the VP method only for $\boldsymbol{G}(\boldsymbol{\delta})$ with constant rank over the complete parameter space. However, from Fig. 4.E.1 which illustrates the condition number of $\boldsymbol{G}(\boldsymbol{\delta})$ as a function of τ_1, is evident that when τ_1 coalesces with τ_2 the condition number becomes infinite since the corresponding basis function is zero everywhere reducing automatically the rank of the regression matrix – due to the local support property of B-splines, that is $G_2[t,\boldsymbol{\delta}] \neq 0$ only for $t \in [\tau_1, \tau_2)$. Thus, in order to assure the solvability of the corresponding SNLS problem through the VP method the distance between two sequential knots must be constrained.

Analogous rank deficiencies problems arise also in the case of the decaying trigonometric functional basis with unconstrained functional subspace parameters. In Fig. 4.E.2(a) the condition number of $\boldsymbol{G}(\boldsymbol{\delta})$ consisting of three basis functions $G_1[t,\boldsymbol{\delta}] = r^t\cos(\omega t)$, $G_2[t,\boldsymbol{\delta}] = r^t\sin(\omega t)$ and $G_3[t,\boldsymbol{\delta}] = \rho^t$, with $t = 1,\dots,10000, \omega = 0.001$ rad/sample, $\rho = 0.999$, and unfixed r is given as a function of r. Apparently, the condition number of the regression matrix is of low value only within a neighbourhood of r near unity. Particularly for $r > 1$, the condition number grows rapidly (note the logarithmic scale of the y-axis) as the $G_3[t,\boldsymbol{\delta}]$ basis function, which is always close to unity, becomes insignificant compared to $G_1[t,\boldsymbol{\delta}]$ and $G_2[t,\boldsymbol{\delta}]$.

For a similar decaying trigonometric functional basis consisting of the same tree basis functions $G_1[t,\boldsymbol{\delta}] = r^t\cos(\omega t)$, $G_2[t,\boldsymbol{\delta}] = r^t\sin(\omega t)$ and $G_3[t,\boldsymbol{\delta}] = \rho^t$, but with fixed $r = 1$ and unknown ω varying between 0 and 0.0001 rad/sample, the rank of the corresponding regression matrix is changing from two (for ω very close to zero) to three as ω moves toward infinity. This is due to the fact that $G_2[t,\boldsymbol{\delta}] = r^t\sin(\omega t)$ becomes zero everywhere for ω close to zero. This situation is demonstrated in Fig. 4.E.2(b).

Finally, for a functional basis consisting of five functions $G_1[t,\boldsymbol{\delta}] = r_1^t\cos(\omega_1 t)$, $G_2[t,\boldsymbol{\delta}] = r_1^t\sin(\omega_1 t)$, $G_3[t,\boldsymbol{\delta}] = r_2^t\cos(\omega_2 t)$, $G_4[t,\boldsymbol{\delta}] = r_2^t\sin(\omega_2 t)$ and $G_5[t,\boldsymbol{\delta}] = \rho^t$ is evident that $G_1[t,\boldsymbol{\delta}]$ and $G_2[t,\boldsymbol{\delta}]$ become

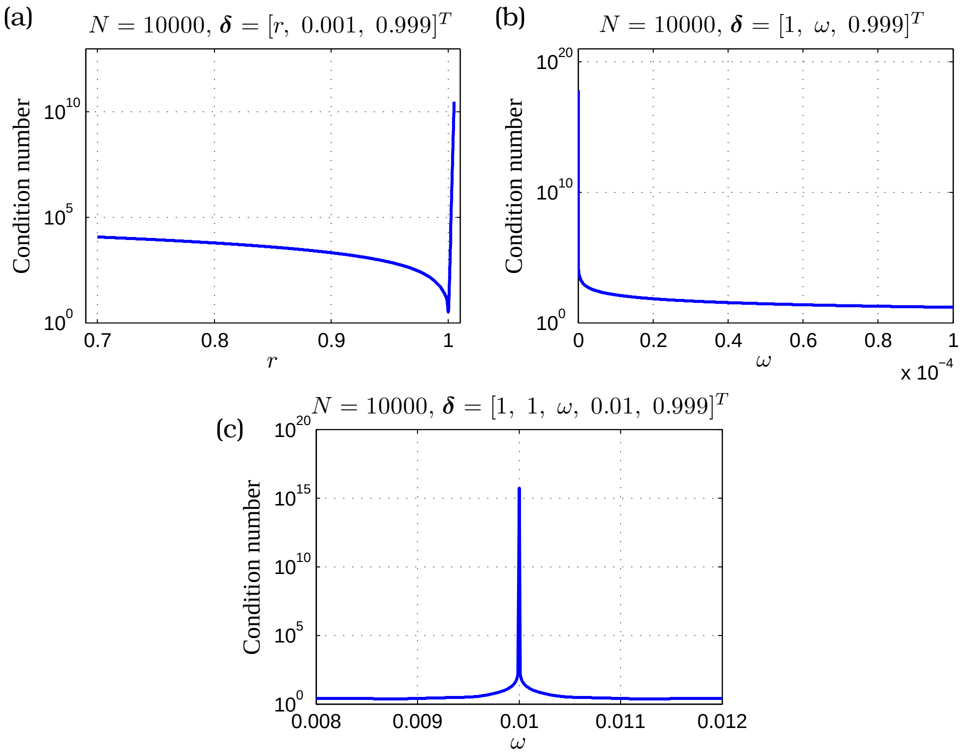

Figure 4.E.2: Numerical reliability problems arising in the case of: (a) too small or too large rate of decay, (b) frequency ω tending to zero, and (c) the distance between two complex roots tends to zero.

linearly dependent to $G_3[t, \boldsymbol{\delta}]$ and $G_4[t, \boldsymbol{\delta}]$ when the pair of parameter values $[r_1, \omega_1]$ gets to close to that of $[r_2, \omega_2]$ leading also to a bad condition number and rank deficiency problems (see Fig. 4.E.2(c)). Of course this obstacle could be overcome by considering a multiple homogeneous linear difference equation root. However, in the present study only discrete roots are considered.

Chapter 5

Non-Stationary Vibration Modelling and Analysis via FS-TARMA Models – A critical survey

In this chapter a review of the Functional Series Time-dependent AutoRegressive Moving Average (FS-TARMA) models for the identification of non-stationary signals is presented. The study contains a critical review of the past and recent developments in non-stationary signal modelling through Functional Series models while also focuses on the applications of FS-TARMA models for the identification and dynamic analysis of time-varying structures based on random vibration data. The objective is to present some of the main approaches that have been proposed, to illustrate them using numerical case studies, to highlight their assets and limitations and to identify future directions.

5.1 Introduction

Non-stationary signals, that is signals with statistical properties that depend on time, are commonly encountered in engineering practice. The vibration responses of structures, such as traffic-excited bridges [Poulimenos and Fassois, 2009b], robotic devices [Petsounis and Fassois, 2000], rotating machinery [Conforto and D'Alessio, 1999b], deployable structures [Xun and Yan, 2008] and so on, constitute typical examples of non-stationary signals. Such structures characterized by properties, either physical or geometrical, that vary with time are referred as Time-Varying (TV) structures. However, non-stationary vibration may also arise in cases of time-invariant structures subject to non-stationary excitation, such as earthquake [Fouskitakis and Fassois, 2002] and turbulence [Mevel et al., 2005], or in the case of structures with inherently nonlinear dynamics [Ben Mrad, 2002].

Unlike the stationary case, non-stationary random vibration signals are characterized by time-dependent statistical properties [Poulimenos and Fassois, 2006, Niedźwiecki, 2000]. For instance, the mean of a non-stationary signal is in general a function of time [Bendat and Piersol, 2000, Ch. 12]:

$$\mu(t) = \mathrm{E}\left\{x(t)\right\} = \int_{-\infty}^{\infty} x(t) \cdot f(x(t)) \cdot dx(t) \tag{5.1.1}$$

while its autocovariance is a function of two considered time instants, that is:

$$\gamma(t_1, t_2) = \mathrm{E}\left\{x(t_1) \cdot x(t_2)\right\} = \int_{-\infty}^{\infty}\int_{-\infty}^{\infty} x(t_1) \cdot x(t_2) \cdot f(x(t_1), x(t_2)) \cdot dx(t_1) \cdot dx(t_2) \tag{5.1.2}$$

with $x(t)$ designating the random vibration signal which is a function of analog time t, $\mathrm{E}\left\{\cdot\right\}$ statistical expectation and $f(\cdot)$ the probability density function. Yet, these first two moments completely define the probability distribution in the Gaussian case which is on the focus of this study.

Usually, and this is also followed in the present study, the case of non-stationary random vibration characterized by *zero-mean* but non-stationary and *continually evolving autocovariance function* is considered. This is due to the fact that in many random vibration analysis problems the mean is either zero or it may be readily estimated and subtracted from the signal by means of curve fitting or high pass signal filtering in case of time-dependency [Augusti et al., 1984, Sec. 8.3]. On the other hand, the continual evolution assumption for the autocovariance function is adopted because this is the typical case in vibration analysis, where a continual evolution of the dynamics is encountered.

The general problem that this study deals with is the non-stationary vibration *modelling* (identification) and *analysis* based upon *equispaced* in time *digital* sampled vibration signal measurements $x[t]$, of finite length N obtained from a single realization. The final goal of the identification process is to build a mathematical model that will be able to represent the underlying structural dynamics. The obtained model may subsequently be employed for the non-stationary signal vibration analysis through the extraction of physically meaningful information from the obtained model such as signal moments or more often a form of time-dependent Power Spectral Density (PSD) function and the time-dependent vibration modes [Petsounis and Fassois, 2000, Poulimenos and Fassois, 2006, Hammond and White, 1996] [Preumont, 1994, ch. 8].

The modelling of non-stationary vibration is an important and yet challenging problem which has received significant attention in recent years [Poulimenos and Fassois, 2006, Niedźwiecki, 2000, Staszewski and Robertson, 2007, Cohen, 1995, Hammond and White, 1996]. The available non-stationary identification methods may be broadly classified as *non-parametric* or *parametric*. To date, non-parametric methods have received most of the attention, mainly due to their simplicity. They are based on non-parametrized representations of the vibration signal as a simultaneous function of time and frequency (time-frequency representations). These methods include the widely used spectrogram based on the Short-Time Fourier Transform (STFT) and its ramifications [Hammond and White, 1996], distributions such as the Wigner-Ville and the Choi-Williams that are unified under the Cohen class of distributions [Cohen, 1995, Hammond and White, 1996], wavelet-based methods [Newland, 1993, Spanos and Failla, 2005] and others.

On the other hand, *parametric methods* are based on parametrized time-dependent representations, mainly of the Time-dependent AutoRegressive Moving Average (TARMA) type or respective Time-dependent State-Space (TSS) types. These representations differ from their conventional, stationary, counterparts in that their parameters are *time-dependent* [Poulimenos and Fassois, 2006, Niedźwiecki, 2000]. Thus, a TARMA(n_a, n_c) model, with n_a, n_c designating its AR and MA orders is of the general form:

$$x[t] + \sum_{i=1}^{n_a} a_i[t] \cdot x[t-i] = e[t] + \sum_{i=1}^{n_c} c_i[t] \cdot e[t-i], \qquad e[t] \sim \mathrm{NID}(0, \sigma_e^2[t]) \tag{5.1.3}$$

with t designating normalized discrete time, $x[t]$ the non-stationary vibration signal modelled, $e[t]$ an unobservable uncorrelated (white) innovations (residual) sequence with zero mean and potentially time-dependent variance $\sigma_e^2[t]$, and $a_i[t], c_i[t]$ the model's time-dependent AR and MA parameters, respectively. $\mathrm{NID}(\cdot, \cdot)$ stands for Normally Independently Distributed with the indicated mean and variance. Analogously a TSS(n) model of order n is of the general form:

$$\text{State equation} : \boldsymbol{z}[t+1] = \boldsymbol{A}[t] \cdot \boldsymbol{z}[t] + \boldsymbol{K}[t] \cdot e[t] \tag{5.1.4a}$$

$$\text{Output equation} : x[t] = \boldsymbol{C}[t] \cdot \boldsymbol{z}[t] + e[t], \quad e[t] \sim \mathrm{NID}(0, \sigma_e^2[t]) \tag{5.1.4b}$$

where $\boldsymbol{z}[t]_{(n\times 1)}$ indicates the model's state vector and $\boldsymbol{A}[t]_{(n\times n)}$, $\boldsymbol{K}[t]_{(n\times 1)}$, $\boldsymbol{C}[t]_{(1\times n)}$ the state-space system, Kalman gain and output matrices, respectively. The general model forms of Eqs. (5.1.3) and (5.1.4) correspond to scalar output-only models while extensions to the multivariate and/or input-output case may be readily obtained.

In general, contrasted to their non-parametric counterparts, non-stationary methods based on parametrized representations are known to offer a number of potential advantages. These include representation parsimony, improved tracking of the time-varying dynamics, that is translated into improved representation accuracy, and improved resolution [Petsounis and Fassois, 2000, Conforto and D'Alessio, 1999b, Ben Mrad et al., 1998b]. Moreover, they also offer flexibility in analysis as they are particularly suitable not only for vibration model-based analysis but also for purposes of prediction (simulation) [Fouskitakis and Fassois, 2002, Ben Mrad et al., 1998b], fault diagnosis [Poulimenos and Fassois, 2004b], classification [Bardou and Sidahmed, 1994, Eom, 1999b, Paulik et al., 1992] and control applications [Xianya and Evans, 1984, Niedźwiecki, 1987].

According to the classification proposed by Mendel [Mendel, 1973, Ch. 6] and followed by many authors [Poulimenos and Fassois, 2006, Niedźwiecki, 2000, Grenier, 1983b], parametric non-stationary identification methods may be divided in three main classes: a) the class of Unstructured Parameter Evolution (UPE) methods [Ljung and Soderstrom, 1983, Ljung, 1999, Lin et al., 2005, Verboven et al., 2004], b) the class of Stochastic Parameter Evolution (SPE) methods [Kitagawa and Gersch, 1996, Kitagawa and Gersch, 1985, Gersch and Kitagawa, 1985], and finally c) the class of Deterministc Parameter Evolution (DPE) methods [Poulimenos and Fassois, 2006, Grenier, 1983b, Tsatsanis and Giannakis, 1993]. This classification concerns the "structure" that methods impose on the evolution of the time-varying parameters. Thus, methods of the UPE class impose no-structure on their model parameters which are thus free to change with time. They are usually based on the assumption that the TV characteristics of the system to be identified evolve slowly with time and they thus employ stationary methods in windowed versions of the signal, within which the stationarity assumption is approximately valid. Typical methods of this class include short-time ARMA or SS models [Niedźwiecki, 2000, Ch. 3], that is stationary models applied on short segments of the non-stationary signal, and recursive methods that employ exponential windows in order to estimate their parameters based only on recent values of the non-stationary signal [Ljung and Soderstrom, 1983, Ljung, 1999]. UPE methods are characterized by conceptual and algorithmic simplicity, however due to the quasi-stationarity assumption are appropriate mainly for the identification of systems with slowly evolving parameters. In addition they are characterized by low parsimony as the complete description of a non-stationary signal requires knowledge of the model parameters at each time instant.

On the other hand, SPE methods rely on non-stationary models with a stochastic "structure" imposed on the time evolution of their parameters [Kitagawa and Gersch, 1996]. More specifically, the latter are considered as being random variables allowed to change with time, but with their evolution being subject to stochastic smoothness constraints. These constraints are often referred to as *smoothness priors constraints* and the models are referred to as *smoothness priors* models. SPE methods have been shown to be particularly effective for specific problems, such as the modelling of earthquake ground motion [Gersch and Kitagawa, 1985, Kitagawa and Gersch, 1985] or biomedical signals [Kitagawa and Gersch, 1996]. However, in general they leave an unnecessarily high number of degrees of freedom in the parameter evolution, particularly when the physical mechanism responsible for the time-variation is deterministic, which is the case for a plethora of engineering applications [Poulimenos and Fassois, 2006].

Actually, this is the advantage of the DPE methods, which consider a structured deterministic pattern for their model parameter evolutions. DPE methods for non-stationary identification through random vibration data records are mainly based on Functional Series TARMA (FS-TARMA) models [Rao, 1970, Grenier, 1983b, Tsatsanis and Giannakis, 1993, Poulimenos and Fassois, 2006]. The parameters of these models depend explicitly upon time being projected on specific functional subspaces that are described by deterministic basis functions $G_j[t]$ (for instance polynomial or trigonometric) as follows:

$$a_i[t] = \sum_{j=1}^{p_a} a_{i,j} \cdot G_j[t], \qquad c_i[t] = \sum_{j=1}^{p_c} c_{i,j} \cdot G_j[t] \tag{5.1.5}$$

where p_a and p_c stand for the AR and MA functional subspace dimensionalities, respectively. Therefore, an FS-TARMA model is fully parametrized by the corresponding time-invariant coefficients of projection $a_{i,j}$ and $c_{i,j}$ which may be estimated through well established stationary methods adjusted to the specific model form. However, significant differences are caused by the fact that the innovations variance is also time-dependent and for this reason distinction should be made between *parametric* FS-TARMA models with innovations variance expanded on basis functions, that is $\sigma_e^2[t] = \sum_{j=1}^{p_s} s_j \cdot G_j[t]$, and those which are based on non-parametrized expression of the time-dependent variance $\sigma_e^2[t]$ leading to a *semi-parametric* FS-TARMA type of model.

The price to pay for rendering the estimation of a TARMA model into a time-invariant problem, is the increased complexity of the FS-TARMA model structure problem which, in addition to the model orders n_a, n_c, involves the selection of an appropriate family of linearly independent basis functions and the corresponding functional subspaces. Actually and despite the fact that any family may approximate any given curve with arbitrary accuracy, as long as a sufficient number of basis functions is used [Walter, 1994, p. 77], due to reasons of statistical efficiency and model parsimony (economy of representation) the real issue is the selection of a family that may provide the necessary accuracy with a small (or minimal) number of functions. In practice, this problem may shown to be particularly complex when various candidate families of basis functions are considered with the appropriate functional subspaces being searched among a practically infinite set of basis functions.

Besides the difficulties that arise within their parameter and structure estimation, FS-TARMA models have been shown to be particularly effective for non-stationary random vibration modelling and analysis. Yet, the advantages of FS-TARMA models over alternative non-stationary models (such as segmentation, recursive, or smoothness priors models), have been demonstrated via a Monte Carlo comparison study in [Poulimenos and Fassois, 2006]. However, despite their long history in non-stationary identification and their successful application in a number of studies, issues such as structure selection, asymptotic properties, and the postulation of efficient estimation methods, have only recently been studied in a systematic way. For instance, a novel method that offers important improvements in overcoming the drawbacks of the functional subspace selection by simultaneously estimating both the characteristics of the appropriate basis function along with the corresponding coefficients of projection has just been developed (Chapter 4). Thus, in contrast to the *classical* FS-TARMA approach, in this new *adaptable* approach the basis functions are not prescribed but are adapted to the data in order to form functional subspaces that provide the highest achievable accuracy.

Moreover, the asymptotic properties of the FS-TAR/TARMA models that were studied thoroughly in [Poulimenos and Fassois, 2007, Poulimenos and Fassois, 2009a] have provided the necessary framework for the understanding of the statistical properties of the estimators and have also led to the development of alternative statistically efficient estimation schemes. Hence, multi-stage methods which overcome the problems related with the nonlinear optimization of Maximum Likelihood (ML) estimation have also been proposed in these studies.

These advancements along with the accumulated experience of forty years of research and development constitute FS-TARMA models today a ripe tool for non-stationary identification. Nonetheless, up to date there is no study offering a holistic view on the subject. The present work aims to fill this gap by presenting a thorough review on FS-TARMA models covering both theoretical and practical aspects on the subject. Toward this end, a critical overview of the available methods for the FS-TARMA model parameter estimation and structure selection problems is presented while special emphasis is placed on promising new methods that aim at overcoming problems of previous approaches.

The detailed comparison and assessment of the main methods based on Monte Carlo experiments is also performed. More specifically, the main methods for FS-TARMA parameter estimation and model structure selection are employed for the identification of simulated models. Several families of basis functions and various model structure selection criteria are also compared. Finally, comparisons with alternative non-stationary methods are also performed. These include methods of the UPE and SPE families based on both TARMA and TSS models. The results of the study demonstrate the effectiveness and improvements offered by the new methods over previous counterparts, as well as the FS-TARMA approach overall accuracy and effectiveness.

Summarizing, the main contributions of the present study are:

a) The presentation of a critical survey on FS-TARMA models and their variants regarding their parameter estimation methods, model structure selection criteria and methods, innovations time-dependent variance estimation, applications and recent advances.

b) The comparison study of the main methods for FS-TARMA parameter estimation and structure selection based on Monte Carlo experiments.

The work may be viewed as an extension and update of the survey paper of [Poulimenos and Fassois, 2006] the comparison study of Chapter 2, and the more focused overview of deterministic parameter evolution models of [Spiridonakos and Fassois, 2009b]. The univariate (scalar) case is currently treated – for multivariate (vector) methods the reader is referred to [Spiridonakos and Fassois, 2009c, Sato et al., 2007, Kacha et al., 2008, Jachan et al., 2009].

The remaining of this chapter is organized as follows: An overview of the FS-TARMA models literature is given in Section 5.2, while the FS-TARMA models and their variants are presented in Section 5.3. The methods for FS-TARMA model parameter estimation and structure selection are discussed in Sections 5.4 and 5.5 respectively. The application of the main FS-TAR model estimation and structure selection methods for the identification of a simulated TAR model is presented in Section 5.6, while a respective TARMA problem is examined in Section 5.7. Finally, the concluding remarks of the study and a brief outlook are summarized in Section 5.8.

5.2 Overview of the Literature

FS-TARMA models have played an important role in the development and evolution of non-stationary stochastic signal identification and analysis over the last forty years. They were introduced in 1970 by Rao [Rao, 1970] who proposed the truncated Taylor series expansion of a TAR model parameters – this is equivalent to assuming time-dependent parameters that can be described as polynomials of time. Three years later, Mendel [Mendel, 1973] classified the available non-stationary identification methods into the aforementioned three classes (UPE, SPE and DPE) and defined a general FS linear regression model as appropriate for the case in which a set of time-invariant or slowly TV parameters may be distinguished from the rest of the parameters which evolve rapidly with time.

Functional Series models of the pure TAR form with parameters belonging to a subspace spanned by Legendre polynomials were used for first time within the context of random vibration, and more specifically earthquake ground motion, modelling and simulation in an early paper by Kozin in 1977 [Kozin, 1977]. Nevertheless, FS-TARMA models did not enjoy widespread popularity before the early 1980's, when a number of researchers start studying their properties and examining their potential for accurate non-stationary signal modelling. One of the researchers who contributed significantly to the development of FS models is Grenier who extended FS models for the TARMA case and examined a number of theoretical issues such as the existence of a TARMA representation for a non-stationary system and the uniqueness of such a representation [Grenier, 1983b]. The ML and the Two-Stage Least Squares (2SLS) estimators for an FS-TARMA model were also derived in this pioneering study, while in the following years Grenier and his colleagues published a number of papers on FS model variants and speech modelling applications based on such models [Grenier, 1983a, Grenier, 1984, Chevalier et al., 1985, Grenier, 1986, Lima-Veiga and Grenier, 1991].

Niedźwiecki also contributed to the understanding of the properties and capabilities of FS-TARMA models with a series of studies in the late 1980's and early 1990's – probably he is the first to use the term "functional series modelling" to describe TAR models with parameters expanded on functional basis [Niedźwiecki, 1988]. In the latter study, the invariance of the family of basis functions selection in contrast to the importance of choosing the correct functional subspace was highlighted by the means of a theorem. Moreover, studying the issue of non-stationary signal modelling under the prism of a control application Niedźwiecki proposed the Recursive Least Squares (RLS) for the on-line estimation of FS models with varying coefficients of projection, referred to as "localized" FS model [Niedźwiecki, 1990]. In addition he examined the estimation accuracy of the recursive FS-TAR estimator when utilized for the identification of a TI system in order to assess the applicability of the method in such problems or in case in which non-stationarity is in question.

FS-TARMA models with eXogenous input (FS-TARMAX) [Tsatsanis and Giannakis, 1993], FS Time-dependent Finite Impulse Response (FS-TFIR) models [Tsatsanis and Giannakis, 1996b, Tsatsanis and Giannakis, 1996a] and a number of issues regarding the properties and the efficient estimation of these types of models were considered by Tsatsanis and Giannakis. These issues were including the identifiability of an FS-TFIR model, the PE estimation of FS-TARMAX models, the validity of various criteria for the FS model structure selection problem while these authors were also the first to propose a complete model structure selection scheme [Tsatsanis and Giannakis, 1993].

Ben Mrad *et al.* in 1998 [Ben Mrad et al., 1998a] introduced a multi-stage method for the estimation of an FS-TARMA model and applied for first time an FS-TARMA model for the modelling of a real world engineering application, that is the power consumption of an active suspension vehicle [Ben Mrad et al., 1998b]. Comparisons with the simpler FS-TAR models were also performed in this study. However a critical comparison between FS-TAR and FS-TARMA models applied for the modelling of a simulated planar manipulator was presented in [Petsounis and Fassois, 2000]. The comparison was made in terms of the achievable time-dependent spectrum accuracy, resolution, and tracking, as well as on estimated modal parameter accuracy and the FS-TARMA models were shown to outperform their counterparts.

A number of studies investigating the properties of FS-TAR and FS-TARMA models and their estimators have been presented by Poulimenos and Fassois over the last decade. The functional subspace of the inverse function of an FS-TARMA model with known AR and MA functional subspaces was on focus in [Poulimenos and Fassois, 2003a]. The inverse function representation of an FS-TARMA model is used within the 2SLS and P-A multi-stage methods that are widely used for FS-TARMA parameter estimation. The same authors also recently introduced an appropriate asymptotic analysis framework for the FS-TAR/FS-TARMA models in which is recognised the dependency of the "true" generating process of a non-stationary signal on the number of samples [Poulimenos and Fassois, 2007, Poulimenos and Fassois, 2009a]. In these studies the consistency of the class of Weighted Least Squares (WLS) estimators was proved and the properties under which asymptotic efficiency is attained were also examined.

Relations for the asymptotic distributions of the WLS estimators were also derived.

Although the majority of FS-TARMA estimation methods rely in time-domain estimators there also few studies concerned with time-frequency domain methods. These are based on the fitting error minimization of an FS model on a non-parametrically obtained time-frequency representation of the signal under study. Toward this end, the evolutionary spectrum was considered in [Abdrabbo, 1979], the evolutionary periodogram in [Kaderli and Kayhan, 2001] and a time-frequency cepstrum estimate in [Jachan et al., 2007].

The first steps regarding the rather complex FS-TAR/TARMA model structure selection problem were taken by Kozin and Nakajima who studied the applicability of the Akaike Information Criterion (AIC) for the selection of the AR order of a FS-TAR model [Kozin and Nakajima, 1980] under the restrictive assumption of known and fixed AR basis dimensionality. However, although the significance of the proper functional subspace selection was underlined in many publications within the first twenty years of FS-TARMA models history, it was only in 1993 when Tsatsanis and Giannakis presented a complete model structure selection scheme based on the concept of backward regression. More specifically, the researchers proposed a scheme which starts with the construction of an initial FS-TAR or FS-TARMA model of high orders and high subspace dimensionalities in order to assure model adequacy for representing the non-stationary system. Subsequently a statistical hypothesis F-test is used in order to reject insignificant terms (basis functions) and reduce the model dimensionality. Recognising the drawback related with the necessity for selecting a threshold and the subjectivity of such a selection, authors alternatively proposed the use of the AIC or the Final Prediction Error (FPE) criterion instead of the F-test. In this case, terms whose removal causes reduction in the criterion values are rejected until the minimum is achieved. The idea of using an inverse "bottom-up" procedure based on forward regression, that is constructing the model by adding basis functions terms to a model of low dimension was also given in the same study and extended in [Tsatsanis, 1995].

The FS-TARMA model structure selection problem has been studied more systematically over the last decade. For instance, a scheme based on the backward regression concept was proposed in [Poulimenos and Fassois, 2003b] which decomposes the structure selection problem into two subproblems treated in equal phases: i) the model orders (n_a, n_c) selection, and (ii) the functional subspaces selection. The goal of this scheme is to reduce the computational time that is required for the exhaustive search that is done by Tsatsanis and Giannakis scheme. Forward regression procedure based on Gram-Schmidt orthogonalization was also proposed by Wei and Billings in [Wei and Billings, 2002]. Finally, a more automated procedure based on integer optimization and Genetic Algorithm (GA) was proposed in [Poulimenos and Fassois, 2003a].

Most certainly, beyond the model structure selection scheme utilized the family of basis functions selected for the expansion of the FS model time-dependent parameters is of crucial importance. The bases that have been proposed in the literature include time polynomials of arbitrary order [Liporace, 1975], polynomial basis functions like Chebyshev [Mukhopadhyay and Sircar, 1997, Ben Mrad et al., 1994, Fouskitakis and Fassois, 2002], Legendre [Kozin, 1977, Grenier, 1983b] and Jacobi [Poulimenos and Fassois, 2003a], trigonometric basis functions [Hall et al., 1983, Petsounis and Fassois, 2000, Poulimenos and Fassois, 2009a, Eom, 1999a], discrete prolate spheroidal functions [Grenier, 1983b, Charbonnier et al., 1987], various wavelet families [Tsatsanis and Giannakis, 1993, Wei and Billings, 2002, Fouskitakis and Fassois, 2002, Li et al., 2011], and others. Complex exponential basis functions have also been used for the FS modelling of complex signals or analytic representations of real valued signals, (for instance see [Tsatsanis and Giannakis, 1996a, Funaki et al., 1998a, Jachan et al., 2007]). Recently, methods based on multiple basis functions which try to combine the characteristics of two or more bases have also been proposed. Within this context, Li *et al.* in [Li et al., 2011] propose the simultaneous use of B-spline wavelet functions of various orders along with an appropriate model structure selection scheme, while a method combining the smooth Legendre polynomial functions with the abrupt Walsh functions via a Gram-Schmidt orthogonalization procedure is utilized in [Chon et al., 2005].

The FS-TFIR modelling of a cyclostationary signal with parameters expanded on exponential functions whose frequencies are estimated from the signal's higher order statistics was also considered in [Tsatsanis and Giannakis, 1996b]. This study may be considered as a first attempt to adapt basis functions on a specific problem while a similar approach was followed in [Bakkoury et al., 2000]. A similar study on the adaptation of sigmoidal basis functions for the modelling of signals with medium rate transition between two stationary states was also presented in [Kaipio and Karjalainen, 1997]. Even though in both this paradigms the solutions proposed may be considered as ad-hoc as they were heavily based on prior knowledge regarding the evolution of the parameters – periodicity in the first case and transition between two states at an approximately known time instant in the second – both of them aimed at reducing the basis dimensionality by using this knowledge. On the other hand, a more advanced method for the simultaneous estimation of both the functional subspaces and the corresponding coefficients of projection has been introduced in Chapter 4.

Regarding FS-TARMA application on vibration modelling and analysis, Bardou and Sidahmed in 1994 considered the problem of fault detection in a reciprocating compressor [Bardou and Sidahmed, 1994]. To this end, authors utilized Principal Component Analysis (PCA) for extracting an appropriate feature vector from the FS-TAR coefficients of projection parameters estimated from vibration signals and subsequently employed neural networks in order to classify the various faults considered. Conforto and D'Alessio also employ FS-TAR models for the identification and vibrational analysis of rotors with increasing rotational speed and compared the estimated "frozen" power spectral density with those obtained by non-parametric methods based on the Short-Time Fourier Transform (STFT) and the Choi-Williams distribution [Conforto and D'Alessio, 1999b]. In a more recent study Zhang *et al.* [Zhang et al., 2010a] applied FS-TAR modelling on rotor vibration during start up under four operating conditions: i) normal, ii) unbalance, iii) looseness, and iv) rub and they examine the potential of using images of the estimated PSD for purposes of damage detection.

A number of applications for the identification and dynamic analysis in various laboratory structures and mechanisms have been performed by the second author and his co-workers during the last decade. Particularly, in [Poulimenos and Fassois, 2009b] FS-TARMA models were applied for the identification of a benchmark TV laboratory structure consisting of a beam with moving mass, which is used to simulate a bridge-like structure with a moving vehicle. The significant advantage of this set-up is that an accurate baseline model obtained by "freezing" the moving mass at many positions along the beam was also identified. This baseline model provided a basis for the assessment of the identified non-stationary models. For this reason this set-up was also used in Chapter 2 for the comparison of FS-TARMA with alternative non-stationary methods, while multivariate FS-TARMA models were introduced and used for the same problem in Chapter 3. A finite element model used to represent this structure was also updated through FS-TARX models in [Dimitriadis et al., 2004]. The identification and dynamic analysis of a deployable prismatic link structure through FS-TARMA models is on the focus of the studies [Spiridonakos and Fassois, 2009a,Spiridonakos and Fassois, 2009b] while the identification of adaptable FS-TARMA which achieves simultaneous estimation of both functional subspaces and coefficients of projection is introduced and applied for the dynamic analysis of a pick-and-place mechanism in Chapter 4 of the present thesis.

Within the context of vibration-based damage detection, a statistical decision framework utilizing the residuals of an FS-TARX model was applied for the on-line damage detection in the aforementioned "bridle-like" structure [Poulimenos and Fassois, 2004b]. A similar framework based on a multivariate FS-TARX model and the likelihood ratio test was proposed and applied for the fault detection in an expandable prismatic link laboratory structure in [Spiridonakos and Fassois, 2009d], while a framework based on the AR coefficients of projection and the asymptotic properties of a multi-stage estimator were utilized for the damage detection and identification in a time-varying pick-and-place mechanism in [Spiridonakos and Fassois, 2012]. In order to assess the impact of a damage on the modal characteristics of a reinforced concrete frame, Huang *et al.* [Huang et al., 2009] also applied FS-TARX modelling on segments of vibrational data.

The modelling, analysis and simulation of earthquake ground motion signal records based on FS-TAR and FS-TARMA models has also been studied in [Fouskitakis and Fassois, 2002], while FS-TARMA models have been used also for the identification of automobile subsystems. Particularly, Ben Mrad and his colleagues worked on the FS-TARMA modelling of the power consumption of an active suspension vehicle [Ben Mrad et al., 1998b, Ben Mrad and Farag, 2002] based on acceleration signals.

Beyond non-stationary vibration modelling applications, FS-TARMA models have been also utilized in a number of disciplines. For instance, in 1980's FS-TARMA models found fertile ground in the field of speech signal analysis as a competitor of the widely used short-time approach and a number of application studies were presented [Hall et al., 1983, Chevalier et al., 1985, Grenier, 1986, Boudaoud and Chaparro, 1987, Flaherty, 1988], while similar studies are performed up to date [Nathan et al., 1991, Tsatsanis and Giannakis, 1993, Akan and Chaparro, 1994, Ha and Ann, 1995, Funaki et al., 1998b, Conforto and D'Alessio, 1999a, Funaki, 2001, Kacha et al., 2005, Evers and Hopgood, 2007, Schnell and Lacroix, 2007]. The main advantage that FS models offered within this application area is the high compression rates as they are characterized only by a small number of parameters. Beyond speech signals, FS-TARMA modelling has been applied also on various acoustic signals. For instance, the FS-TAR and FS-TARMA modelling of bat echolocation calls is performed in [Grenier, 1985] and [Jachan et al., 2007], respectively, while dolphins whistle sounds are analysed by time-varying notch filters based on FS-TARMA models of a special form in [Johansson and White, 2008]. Finally, the "frozen" characteristics of identified FS-TAR models are used for the classification of vehicle acoustic signatures through neural networks in [Eom, 1999a].

Furthermore, even though the modelling of biomedical signals, and more specifically ElectroEncephaloGram (EEG) signals, that is recordings of the electrical activity along the scalp of human subjects, was one of the first FS-TAR applications on real data [Gersch et al., 1983], the interest of the biomedical scientific community on FS-TARMA models was rekindled during the last fifteen years. Beyond studies on EEG analysis [Kaipio and Karjalainen, 1997, Juntunen et al., 1998, Hiltunen et al., 1999, Sato et al., 2007, Kacha et al., 2008, Salcedo et al., 2008, Pachori and Sircar, 2008, Zhang et al., 2010b, Li et al., 2011], FS-TARMA models have also been applied for the modelling of heart rate and blood velocity signals [Thonet and Vesin, 1997, Girault et al., 2000, Zou et al., 2003, Chon et al., 2005, Chon et al., 2008, Yang and Chon, 2010], electromyographic signals [Korosec, 2000, Zhang et al., 2010c] the modelling of the respiratory airflow [Ciftci and Kahya, 2008], modelling of the human elbow dynamic stiffness [Sanyal et al., 2005] and data acquired during an experiment of functional magnetic resonance imaging [Salcedo et al., 2008]. The aim of these studies is the detection of diseases or disorders through the classification of biomedical processes signals acquired from healthy and unhealthy subjects.

Finally, besides the aforementioned applications, models of the FS-TARMA class have also been utilized for the modelling of the nonlinear process of mass air flow going into an automobile engine [Ben Mrad, 2002], the modelling of communication channels [Jachan and Matz, 2005, Zheng et al., 2001b], the analysis of financial data [Hinich and Roll, 1981, Gersch and Kitagawa, 1982, Salcedo et al., 2008], for purposes of classification of objects through contour images [Paulik et al., 1992, Eom, 2000], the modelling of sunspot data and the identification of a flight vehicle experimental simulator [Wei and Billings, 2002], for the reliability analysis of railway vehicles based on the modelling of times between failures series [Stavropoulos and Fassois, 2000], and others.

5.3 FS-TARMA Identification Problem Statement

The goal of the present section is to provide a more complete description of the FS-TARMA models, report on the various extensions and variants and classify them putting together all the different pieces.

FS-TARMA models are based on the assumption that their parameters follow a deterministic pattern and thus they may be expanded on properly selected functional subspaces. According to the *classical* approach these functional subspaces are considered to be selected from an ordered set of linearly independent basis functions of a particular family (such as polynomial, trigonometric, wavelets or other). In early FS-TARMA studies this subspace was formed by consecutive basis functions up to a maximum index – note that for purposes of simplicity this notation was also used in Eq. (5.1.5). Nevertheless, more economic representations may be obtained by using an appropriate model structure selection method in order to pick out only the most significant non-consecutive basis functions.

Using this approach, a *classical parametric FS-TARMA*$(n_a, n_c)_{[p_a,p_c,p_s]}$ *model*, with n_a, n_c designating its AR and MA orders, respectively, and p_a, p_c, p_s its AR, MA, and innovations variance functional subspace dimensionalities, is defined as follows [Poulimenos and Fassois, 2006]:

$$x[t] + \sum_{i=1}^{n_a} a_i[t] \cdot x[t-i] = e[t] + \sum_{i=1}^{n_c} c_i[t] \cdot e[t-i], \qquad e[t] \sim \mathrm{NID}(0, \sigma_e^2[t]) \tag{5.3.1a}$$

$$\begin{gathered}\mathcal{F}_{\mathrm{AR}} = \left\{G_{d_a(1)}[t], \ldots, G_{d_a(p_a)}[t]\right\}, \quad \mathcal{F}_{\mathrm{MA}} = \left\{G_{d_c(1)}[t], \ldots, G_{d_c(p_c)}[t]\right\}, \\ \mathcal{F}_{\sigma_e^2[t]} = \left\{G_{d_s(1)}[t], \ldots, G_{d_s(p_s)}[t]\right\}\end{gathered} \tag{5.3.1b}$$

$$a_i[t] = \sum_{j=1}^{p_a} a_{i,j} \cdot G_{d_a(j)}[t], \quad c_i[t] = \sum_{j=1}^{p_c} c_{i,j} \cdot G_{d_c(j)}[t], \quad \sigma_e^2[t] = \sum_{j=1}^{p_s} s_j \cdot G_{d_s(j)}[t] \tag{5.3.1c}$$

with "$\mathcal{F}$" designating functional subspace of the indicated quantity, $d_a(i)$ $(i = 1, \ldots, p_a)$, $d_c(i)$ $(i = 1, \ldots, p_c)$ and $d_s(i)$ $(i = 1, \ldots, p_s)$ the indices of the specific basis functions that are included in each subspace, while $a_{i,j}$, $c_{i,j}$, and s_j stand for the AR, MA, and innovations variance, respectively, *coefficients of projection*. Thus, in this classical approach the complete model parameter vector $\boldsymbol{\theta}$ consists of these coefficients of projection, while considering a specific basis function family the FS-TARMA model structure selection procedure concerns the determination of the AR and MA orders n_a, n_c, and the AR, MA and innovations variance basis functions indices vectors $\boldsymbol{d}_a = [d_{a(1)}, \ldots, d_{a(p_a)}]^T$, $\boldsymbol{d}_c = [d_{c(1)}, \ldots, d_{c(p_c)}]^T$, and $\boldsymbol{d}_s = [d_{s(1)}, \ldots, d_{s(p_s)}]^T$, that is:

$$\boldsymbol{\theta} = [\boldsymbol{\vartheta}_a^T \ \boldsymbol{\vartheta}_c^T \ \boldsymbol{\vartheta}_s^T]^T = [a_{1,1}, \ldots, a_{n_a,p_a} \ c_{1,1}, \ldots, c_{n_c,p_c} \ s_1, \ldots, s_{p_s}]^T \tag{5.3.1d}$$

$$\mathcal{M} = \{n_a, n_c, \boldsymbol{d}_a, \boldsymbol{d}_c, \boldsymbol{d}_s\} \tag{5.3.1e}$$

Apparently in this case, the functional subspace dimensionalities are given by the length of the basis indices vectors, that is $p_a = \dim(\boldsymbol{d}_a), p_c = \dim(\boldsymbol{d}_c)$ and $p_s = \dim(\boldsymbol{d}_s)$, where $\dim(\cdot)$ indicates the dimension of the indicated vector. A *classical semi-parametric FS-TARMA*$(n_a, n_c)_{[p_a,p_c]}$ *model* may be obtained when the innovations variance is not expanded on basis functions, either because its estimation is not of direct interest or for the purposes of simplification as in this case there is no need for estimating the parameters s_j and $\boldsymbol{d}_s$.

In contrast to the classical, an alternative Adaptable FS-TARMA (AFS-TARMA) approach considers functional subspaces which are not selected from a prescribed set of basis functions, but uses parametrized basis functions which are fully determined by an a-priori unknown vector of parameters $\boldsymbol{\delta}$ (Chapter 4). The latter has also to be estimated along with the coefficients of projection vector $\boldsymbol{\vartheta}$ and in this way the basis functions may be automatically adapted to the data in order to track the evolution of the system parameters with the highest possible accuracy. A *parametric AFS-TARMA*$(n_a, n_c)_{[p_a,p_c,p_s]}$ *model* is defined as follows:

$$x[t] + \sum_{i=1}^{n_a} a_i[t] \cdot x[t-i] = e[t] + \sum_{i=1}^{n_c} c_i[t] \cdot e[t-i], \qquad e[t] \sim \mathrm{NID}(0, \sigma_e^2[t]) \tag{5.3.2a}$$

$$\begin{gathered}\mathcal{F}_{\mathrm{AR}} = \left\{G_{a(1)}[t, \boldsymbol{\delta}_a], \ldots, G_{a(p_a)}[t, \boldsymbol{\delta}_a]\right\}, \quad \mathcal{F}_{\mathrm{MA}} = \left\{G_{c(1)}[t, \boldsymbol{\delta}_c], \ldots, G_{c(p_c)}[t, \boldsymbol{\delta}_c]\right\}, \\ \mathcal{F}_{\sigma_e^2[t]} = \left\{G_{s(1)}[t, \boldsymbol{\delta}_s], \ldots, G_{s(p_s)}[t, \boldsymbol{\delta}_s]\right\}\end{gathered} \tag{5.3.2b}$$

$$a_i[t] = \sum_{j=1}^{p_a} a_{i,j} \cdot G_{a(j)}[t, \boldsymbol{\delta}_a], \quad c_i[t] = \sum_{j=1}^{p_c} c_{i,j} \cdot G_{c(j)}[t, \boldsymbol{\delta}_c], \quad \sigma_e^2[t] = \sum_{j=1}^{p_s} s_j \cdot G_{s(j)}[t, \boldsymbol{\delta}_s] \tag{5.3.2c}$$

Table 5.3.1: Types of FS-TARMA models.

	Classical Model	Adaptable Model
Semi-parametric	FS-TARMA$(n_a, n_c)_{[p_a,p_c]}$ $\boldsymbol{\theta} = [\boldsymbol{\vartheta}_a^T \ \boldsymbol{\vartheta}_c^T]^T$ $\mathcal{M} = \{n_a, n_c, \boldsymbol{d}_a, \boldsymbol{d}_c\}$	AFS-TARMA$(n_a, n_c)_{[p_a,p_c]}$ $\boldsymbol{\theta} = [\boldsymbol{\vartheta}_a^T \ \boldsymbol{\vartheta}_c^T \ \boldsymbol{\delta}_a^T \ \boldsymbol{\delta}_c^T]^T$ $\mathcal{M} = \{n_a, n_c, p_a, p_c\}$
Parametric	FS-TARMA$(n_a, n_c)_{[p_a,p_c,p_s]}$ $\boldsymbol{\theta} = [\boldsymbol{\vartheta}_a^T \ \boldsymbol{\vartheta}_c^T \ \boldsymbol{\vartheta}_s^T]^T$ $\mathcal{M} = \{n_a, n_c, \boldsymbol{d}_a, \boldsymbol{d}_c, \boldsymbol{d}_s\}$	AFS-TARMA$(n_a, n_c)_{[p_a,p_c,p_s]}$ $\boldsymbol{\theta} = [\boldsymbol{\vartheta}_a^T \ \boldsymbol{\vartheta}_c^T \ \boldsymbol{\vartheta}_s^T \ \boldsymbol{\delta}_a^T \ \boldsymbol{\delta}_c^T \ \boldsymbol{\delta}_s^T]^T$ $\mathcal{M} = \{n_a, n_c, p_a, p_c, p_s\}$

$\boldsymbol{\theta}$: complete model parameter vector
$\mathcal{M}$: set of model structure parameters

where $\boldsymbol{\delta}_a, \boldsymbol{\delta}_c$, and $\boldsymbol{\delta}_s$ indicate the AR, MA, and innovations variance functional subspace parameter vector, respectively. For this adaptable approach the model structure is defined by the model orders n_a, n_c, and the basis dimensionalities p_a, p_c, p_s, while the complete parameter vector now contains also the functional subspace parameters:

$$\boldsymbol{\theta} = [\boldsymbol{\vartheta}_a^T \ \boldsymbol{\vartheta}_c^T \ \boldsymbol{\vartheta}_s^T \ \boldsymbol{\delta}_a^T \ \boldsymbol{\delta}_c^T \ \boldsymbol{\delta}_s^T]^T \tag{5.3.2d}$$

$$\mathcal{M} = \{n_a, n_c, p_a, p_c, p_s\} \tag{5.3.2e}$$

Comparing Eq. (5.3.2e) with Eq. (5.3.1e) is observed that in the adaptable approach the model structure selection problem is significantly reduced at the price of the increased dimension of the complete parameter vector $\boldsymbol{\theta}$.

As already mentioned two different families of adaptable basis functions have been proposed (Chapter 4): A B-splines family characterized by initially unknown control points (knots), and a decaying trigonometric family with initially unknown rates of decay and frequencies. However, within this context several other families of adaptable basis functions could be proposed such as orthogonal polynomials generated by a recurrence relation with initially unknown coefficients, wavelets with initially unknown scaling and shifting parameters, and others. It should be noticed that in all the aforementioned cases constraints apply on the functional subspace parameter vectors $\boldsymbol{\delta}$'s which for example in the case of non-uniform B-splines with a-priori unknown knots have to do with the limits imposed by the time axis limits ($t \in [1, N]$) while additional constraints may apply if only distinct knots are considered (for more details see Chapter 4).

Apparently, also in this case a *semi-parametric AFS-TARMA*$(n_a, n_c)_{[p_a,p_c]}$ *model* may be obtained by ignoring the parametric representation of the innovations variance of Eq. (5.3.2c). The types of FS-TARMA models outlined in the preceding paragraphs are summarized in Table 5.3.1.

Remarks:

(i) In case of known input the FS-TARMA model may be readily extended to the FS-TARMA with eXogenous input (FS-TARMAX) model [Ben Mrad, 2002, Niedźwiecki, 2000, Tsatsanis and Giannakis, 1993, Zheng et al., 2001a]:

$$x[t] + \sum_{i=1}^{n_a} a_i[t] \cdot x[t-i] = \sum_{i=n_d}^{n_b} b_i[t] \cdot u[t-i] + e[t] + \sum_{i=1}^{n_c} c_i[t] \cdot e[t-i], \qquad e[t] \sim \text{NID}(0, \sigma_e^2[t]) \tag{5.3.3}$$

where $u[t]$ designates the input signal, n_b the corresponding order and n_d the excitation delay, with the time-dependent parameters $b_i[t]$ being also expanded on selected or estimated functional subspace depending on which approach is followed, classical or adaptable. Of course, FS-TARX models may also be obtained by omitting the MA part [Niedźwiecki, 1990, Tsatsanis, 1995, Bakkoury et al., 2000, Poulimenos and Fassois, 2004b], while omitting both the AR and MA parts results in an FS-TFIR model [Niedźwiecki, 1988, Tsatsanis and Giannakis, 1996a]. Although this study focuses on the output-only FS-TAR and FS-TARMA models, the methods described in the sequel may also be adapted to the identification of the aforementioned input-output types of models.

(ii) A more general FS-TARMA model may be defined by considering uncommon functional subspaces for the AR and MA parameters, that is $\mathcal{F}_{\text{AR}} = \left\{\mathcal{F}_{a_1[t]}, \ldots, \mathcal{F}_{a_{n_a}[t]}\right\}$ and $\mathcal{F}_{\text{MA}} = \left\{\mathcal{F}_{c_1[t]}, \ldots, \mathcal{F}_{c_{n_c}[t]}\right\}$. However, for the purposes of notational simplicity common functional subspaces have been considered in the above definitions.

(iii) In this study the most widely used "shifted" TARMA model form in which the model parameters are not "synchronized" with the lagged variables $x[t-i]$ and $e[t-i]$ is adopted. However, a "synchronous" TARMA model of the following form:

$$x[t] + \sum_{i=1}^{n_a} a_i[t-i] \cdot x[t-i] = e[t] + \sum_{i=1}^{n_c} c_i[t-i] \cdot e[t-i] \tag{5.3.4}$$

may also be used [Grenier, 1983b, Grenier, 1989b]. Even though the distinction between the two forms is only superficial, the "shifted" form is conceptually simpler and easily connected to the "frozen-time" concept that is often used during model-based analysis [Grenier, 1989b, pp. 156-157].

(iv) It should be noted that, alternatively, the innovations standard deviation $\sigma_e[t]$ may be projected onto the selected functional subspace, that is $\sigma_e[t] = \sum_{j=1}^{p_s} s_j \cdot G_{d_s(j)}[t]$. In this case $\boldsymbol{\vartheta}_s$ represents the innovations standard deviation coefficient of projection vector. Yet, this choice leads to more economic representations since the standard deviation depicts lower variability than its squared version (variance) and normally requires less basis functions for its accurate description.

(v) In the majority of FS-TARMA studies the innovations sequence is considered to be a stationary process, that is its variance is constant through time $\sigma_e[t] = c$, which of course constitutes a special case of the general model of Eq. (5.3.1). Stationary innovation sequences following non-Gaussian distributions have also been considered in [Funaki et al., 1998b, Zheng et al., 2001b, Bakrim et al., 1994, Sanubari and Tokuda, 1997].

5.3.1 The identification problem

The *complete FS-TARMA/AFS-TARMA identification problem* may be stated as follows:
Definition. *"Given N observations of the vibration response, say $x^N = \{x[1] \ldots x[N]\}$ and the FS-TARMA or AFS-TARMA model set:*

$$\mathbb{M} \triangleq \left\{ \mathcal{M}(\boldsymbol{\theta}) : \; x[t] + \sum_{i=1}^{n_a} a_i[t,\boldsymbol{\theta}] \cdot x[t-i] = e[t,\boldsymbol{\theta}] + \sum_{i=1}^{n_c} c_i[t,\boldsymbol{\theta}] \cdot e[t-i,\boldsymbol{\theta}]; \right.$$
$$\left. \sigma_e^2[t] = E\left\{e^2[t,\boldsymbol{\theta}]\right\}, \qquad t = 1, \ldots N, \qquad \boldsymbol{\theta} \in \Theta \subseteq \mathfrak{R}^{\dim(\boldsymbol{\theta})} \right\}, \tag{5.3.5}$$

select an element of $\mathbb{M}$ that best fits the observations".

In this expression $\boldsymbol{\theta}$ designates the complete model parameter vector, Θ the parameter space defined by the parameter constraints ($\Theta \equiv \mathfrak{R}^{\dim(\boldsymbol{\theta})}$ for the classical FS-TARMA approach), while $e[t,\boldsymbol{\theta}]$ stands for the model's one-step-ahead prediction error (residual) sequence, which, as in the stationary case, coincides with the model's innovations sequence $e[t]$ [Poulimenos and Fassois, 2006].

The parameter vector $\boldsymbol{\theta}$ and the model structure $\mathcal{M}$ have to be estimated from available data. These quantities are given in Table 5.3.1 for each FS-TARMA type. The complete problem is usually distinguished into two subproblems: (a) the parameter estimation subproblem (for a given model structure $\mathcal{M}$), and (b) the model structure selection subproblem. These are discussed in the following sections.

5.4 Parameter Estimation Methods

The estimation of the model parameter vector $\boldsymbol{\theta}$ based on a given, N-sample long, non-stationary signal record x^N and a selected specific model "structure" $\mathcal{M}$ is presently considered.

5.4.1 The Maximum Likelihood (ML) method

Semi-Parametric Models. The ML estimator of $\boldsymbol{\theta}$ may be obtained through the maximization of the log-likelihood function, which for the *semi-parametric* FS-TARMA/AFS-TARMA model and under the Gaussian assumption for the innovations sequence is given as [Poulimenos and Fassois, 2006, Poulimenos and Fassois, 2007, Poulimenos and Fassois, 2009a, Tsatsanis and Giannakis, 1993]:

$$\ln \mathcal{L}(\boldsymbol{\theta}, \boldsymbol{\sigma}_e | x^N) = -\frac{N}{2} \cdot \ln 2\pi - \frac{1}{2} \cdot \sum_{t=1}^{N} \left(\ln \left(\sigma_e^2[t] \right) + \frac{e^2[t, \boldsymbol{\theta}]}{\sigma_e^2[t]} \right) \tag{5.4.1}$$

with $\boldsymbol{\sigma}_e = \left[\sigma_e^2[1], \ldots, \sigma_e^2[N]\right]^T$ constituting a nuisance parameter vector of high dimensionality while $\boldsymbol{\theta}$ is a parameter vector of low dimensionality. In such cases, the nuisance parameter vector may be "profiled out" from the log-likelihood function by considering the Conditional Maximum Likelihood (CML) estimate of $\widehat{\boldsymbol{\sigma}}_e$ for known $\boldsymbol{\theta}$ and substituting it into Eq. (5.4.1). Toward this end,

$$\frac{\partial \ln \mathcal{L}}{\partial \sigma_e^2[t]} = 0 \implies -\frac{1}{2} \cdot \left[\frac{1}{\sigma_e^2[t]} - \frac{e^2[t, \boldsymbol{\theta}]}{\sigma_e^4[t]} \right] = 0 \implies \widehat{\sigma}_e^2[t] = e^2[t, \boldsymbol{\theta}], \quad \text{for } t = 1, \ldots, N \tag{5.4.2}$$

This estimate indeed leads to a maxima of the conditional log-likelihood function as:

$$\frac{\partial^2 \ln \mathcal{L}}{\partial (\sigma_e^2[t])^2} \bigg|_{\sigma_e^2[t] = e^2[t, \boldsymbol{\theta}]} = -\frac{1}{2} \cdot \left[\frac{-1}{\sigma_e^4[t]} + \frac{2e^2[t, \boldsymbol{\theta}]}{\sigma_e^6[t]} \right]_{\sigma_e^2[t] = e^2[t, \boldsymbol{\theta}]} = -\frac{1}{2} \cdot \left[\frac{2}{\sigma_e^4[t]} - \frac{1}{\sigma_e^4[t]} \right] = -\frac{1}{2\sigma_e^4[t]} < 0 \tag{5.4.3}$$

From the above it follows that:

$$\widehat{\boldsymbol{\theta}} = \arg \max_{\boldsymbol{\theta}} \left\{ \ln \mathcal{L} \left(\boldsymbol{\theta}, \widehat{\boldsymbol{\sigma}}_e | x^N \right) \right\} = \arg \max_{\boldsymbol{\theta}} \left\{ -\frac{1}{2} \sum_{t=1}^{N} \ln e^2[t, \boldsymbol{\theta}] \right\} \tag{5.4.4}$$

$\widehat{\boldsymbol{\theta}}$ is actually a pseudo-likelihood estimator which however leads to the same point estimate with the original ML estimator of $\boldsymbol{\theta}$ and $\boldsymbol{\sigma}_e$ [Garthwaite et al., 2002, p. 55]. Profile likelihood is one of the several modifications of the likelihood, collectively known as pseudo-likelihoods, which are based on a derived likelihood for a subset of parameters [Garthwaite et al., 2002]. The derived maximization problem is a non-quadratic one which has to be solved through nonlinear optimization techniques for both FS-TAR/AFS-TAR and FS-TARMA/AFS-TARMA cases. Note that in the adaptable approach constraints apply for the $\boldsymbol{\delta}_a, \boldsymbol{\delta}_c$ parameter vectors and thus appropriate methods have to be applied for $\boldsymbol{\theta}$ estimation (for instance interior point methods may be used in this context [Nocedal and Wright, 2006, Ch. 19]).

Parametric Classical Models. In the fully parametrized classical FS-TARMA approach ($\boldsymbol{\theta} = [\boldsymbol{\vartheta}_a^T \ \boldsymbol{\vartheta}_c^T \ \boldsymbol{\vartheta}_s^T]^T = [\boldsymbol{\vartheta}_{a|c}^T \ \boldsymbol{\vartheta}_s^T]^T$), and under Gaussian innovations, the log-likelihood function is:

$$\ln \mathcal{L}(\boldsymbol{\theta} | x^N) = -\frac{N}{2} \cdot \ln 2\pi - \frac{1}{2} \cdot \sum_{t=1}^{N} \left(\ln \left(\sigma_e^2[t, \boldsymbol{\vartheta}_s] \right) + \frac{e^2[t, \boldsymbol{\vartheta}_{a|c}]}{\sigma_e^2[t, \boldsymbol{\vartheta}_s]} \right) \tag{5.4.5}$$

In this case, the derivation of the profile likelihood function does not lead to a simplified form while the dimension of the innovations variance parameter vector $\boldsymbol{\vartheta}_s$ is usually much lower than the dimension of $\boldsymbol{\vartheta}_{a|c}$. Finally, it must be added that also in this case, and even for the simpler FS-TAR model, the log-likelihood function is still non-quadratic in terms of $\boldsymbol{\vartheta}_s$.

Parametric Adaptable Models. The $\boldsymbol{\theta}$ ML estimator for a parametric AFS-TARMA model ($\boldsymbol{\theta} = [\boldsymbol{\vartheta}_{a|c}^T \; \boldsymbol{\vartheta}_s^T \; \boldsymbol{\delta}_{a|c}^T \; \boldsymbol{\delta}_s^T]^T$) may be obtained from the maximization of the following equation:

$$\ln \mathcal{L}(\boldsymbol{\theta}|x^N) = -\frac{N}{2} \cdot \ln 2\pi - \frac{1}{2} \cdot \sum_{t=1}^{N} \left(\ln\left(\sigma_e^2[t, \boldsymbol{\vartheta}_s, \boldsymbol{\delta}_s]\right) + \frac{e^2[t, \boldsymbol{\vartheta}_{a|c}, \boldsymbol{\delta}_{a|c}]}{\sigma_e^2[t, \boldsymbol{\vartheta}_s, \boldsymbol{\delta}_s]} \right) \tag{5.4.6}$$

subject to the constraints that apply for the functional subspace parameter vectors $\boldsymbol{\delta}_a, \boldsymbol{\delta}_c, \boldsymbol{\delta}_s$. This optimization problem has to be handled via appropriate constrained nonlinear optimization techniques.
Remarks:

- ***(i)*** The ML estimation problem in all of the aforementioned cases has to be handled via iterative optimization techniques. Normally, these techniques require rather accurate initial estimates in order to overcome potential local maxima. These initial estimates may be provided by regression type methods, a summary of which is outlined in the subsequent sections.
- ***(ii)*** When stationary innovation sequence is considered the ML estimator coincides with the Weighted Least Squares (WLS) estimator [Tsatsanis and Giannakis, 1993, Eom, 1999b].

5.4.2 Regression type methods for classical models

In general, regression type methods are based on a regression-type model representation:

$$\begin{aligned} x[t] &= -\sum_{i=1}^{n_a}\sum_{j=1}^{p_a} a_{i,j} \cdot G_{d_{a(j)}}[t] \cdot x[t-i] + \sum_{i=1}^{n_c}\sum_{j=1}^{p_c} c_{i,j} \cdot G_{d_{c(j)}}[t] \cdot e[t-i, \boldsymbol{\vartheta}_{a|c}] + e[t, \boldsymbol{\vartheta}_{a|c}] = \\ &= -\left(a_{1,1} \cdot G_{d_{a(1)}}[t] + \ldots + a_{1,p_a} \cdot G_{d_{a(p_a)}}[t]\right) \cdot x[t-1] - \ldots \\ &\quad + \left(c_{n_c,1} \cdot G_{d_{c(1)}}[t] + \ldots + c_{n_c,p_c} \cdot G_{d_{c(p_c)}}[t]\right) \cdot e[t-n_c, \boldsymbol{\vartheta}_{a|c}] + e[t, \boldsymbol{\vartheta}_{a|c}] \Longrightarrow \end{aligned}$$

$$\Longrightarrow x[t] = \underbrace{\begin{bmatrix} -x[t-1] \cdot G_{d_{a(1)}}[t] \\ -x[t-1] \cdot G_{d_{a(2)}}[t] \\ \vdots \\ -x[t-n_a] \cdot G_{d_{a(p_a-1)}}[t] \\ -x[t-n_a] \cdot G_{d_{a(p_a)}}[t] \\ \hdashline e[t-1, \boldsymbol{\vartheta}_{a|c}] \cdot G_{d_{c(1)}}[t] \\ e[t-1, \boldsymbol{\vartheta}_{a|c}] \cdot G_{d_{c(2)}}[t] \\ \vdots \\ e[t-n_c, \boldsymbol{\vartheta}_{a|c}] \cdot G_{d_{c(p_c-1)}}[t] \\ e[t-n_c, \boldsymbol{\vartheta}_{a|c}] \cdot G_{d_{c(p_c)}}[t] \end{bmatrix}^T}_{\boldsymbol{\phi}[t, \boldsymbol{\vartheta}_{a|c}]} \cdot \underbrace{\begin{bmatrix} a_{1,1} \\ a_{1,2} \\ \vdots \\ a_{n_a,p_a-1} \\ a_{n_a,p_a} \\ \hdashline c_{1,1} \\ c_{1,2} \\ \vdots \\ c_{n_c,p_c-1} \\ c_{n_c,p_c} \end{bmatrix}}_{\boldsymbol{\vartheta}_{a|c}} + e[t, \boldsymbol{\vartheta}_{a|c}] \tag{5.4.7}$$

or, using the stacked signal and innovations sequence vectors $\boldsymbol{x} = \left[x[1], \ldots, x[N]\right]^T$ and $\boldsymbol{e}(\boldsymbol{\vartheta}_{a|c}) = \left[e[1, \boldsymbol{\vartheta}_{a|c}], \ldots, e[N, \boldsymbol{\vartheta}_{a|c}]\right]^T$:

$$\boldsymbol{x} = \boldsymbol{\Phi}(\boldsymbol{\vartheta}_{a|c}) \cdot \boldsymbol{\vartheta}_{a|c} + \boldsymbol{e}(\boldsymbol{\vartheta}_{a|c}) \tag{5.4.8}$$

where $\boldsymbol{\Phi}(\boldsymbol{\vartheta}_{a|c}) = \left[\boldsymbol{\phi}[1, \boldsymbol{\vartheta}_{a|c}], \ldots, \boldsymbol{\phi}[N, \boldsymbol{\vartheta}_{a|c}]\right]^T$ is the regression matrix. It may be observed that this model form may be used only for the estimation of the AR/MA coefficients of projection parameter vector $\boldsymbol{\vartheta}_{a|c}$, while $\boldsymbol{\vartheta}_s$, if it is of interest (parametric FS-TARMA model type), may be subsequently estimated based on the model's one-step-ahead prediction error (residual) sequence $e[t, \widehat{\boldsymbol{\vartheta}}_{a|c}]$.

Thus, within the context of regression type methods, the estimation of the parameter vectors $\boldsymbol{\vartheta}_{a|c}$ and $\boldsymbol{\vartheta}_s$ is achieved in distinct sequential phases. More specifically, for the more general parametric

FS-TARMA model type each regression method includes at least the following phases: (a) Estimation of $\boldsymbol{\vartheta}_{a|c}$ based on the minimization of a suitable Prediction Error (PE) criterion and (b) estimation of $\boldsymbol{\vartheta}_s$ based on $e[t, \widehat{\boldsymbol{\vartheta}}_{a|c}]$ obtained from the first phase.

5.4.2.1 Phase A: Estimation of AR/MA coefficients of projection parameter vector

The estimation of the coefficients of projection parameter vector $\boldsymbol{\vartheta}_{a|c}$ is in general based on the minimization of the *Weighted Least Squares (WLS)* criterion:

$$\widehat{\boldsymbol{\vartheta}}_{a|c} = \arg\min_{\boldsymbol{\vartheta}_{a|c}} \left\{ \sum_{t=1}^{N} \frac{e^2[t, \boldsymbol{\vartheta}_{a|c}]}{w^2[t]} \right\} = \arg\min_{\boldsymbol{\vartheta}_{a|c}} \left\{ \boldsymbol{e}(\boldsymbol{\vartheta}_{a|c})^T \cdot \boldsymbol{W} \cdot \boldsymbol{e}(\boldsymbol{\vartheta}_{a|c}) \right\} \tag{5.4.9}$$

where $w^2[t]$ is a user defined weighting sequence and $\boldsymbol{W} = \text{diag}\{1/w^2[1], \ldots, 1/w^2[N]\}$ the respective $N \times N$ diagonal weighting matrix. Poulimenos and Fassois in their recent studies on asymptotic analysis of FS-TAR [Poulimenos and Fassois, 2007, Theorem 1] and FS-TARMA [Poulimenos and Fassois, 2009a] model estimators have proven that any weighting sequence $w^2[t]$ being bounded uniformly in t, that is $0 < \underline{w^2} \leq w^2[t] \leq \overline{w^2} < \infty$ (for every t), leads to a consistent estimator of the true parameter vector $\boldsymbol{\vartheta}^o_{a|c}$. The consistency of the WLS estimator is valid under some rather mild regularity conditions with respect to model stability and of course under the condition that the candidate model to be estimated has the same structure $\mathcal{M}$ with the true model that generated the non-stationary signal under study [Poulimenos and Fassois, 2007, Poulimenos and Fassois, 2009a]. Note that the weighting sequence bounding condition is equivalent with the condition for a positive definite weighing matrix $\boldsymbol{W}$.

However, despite consistency is guaranteed for any positive definite weighting sequence $w^2[t]$, an asymptotically efficient estimator, that is the WLS estimator with the smallest asymptotic covariance matrix, is achieved when the weighting sequence utilized is proportional to the true innovations variance $w[t] = c \cdot \sigma^2_e[t]$ [Poulimenos and Fassois, 2007, Poulimenos and Fassois, 2009a]. Yet, the true innovations variance is a-priori unknown and has to be replaced by an appropriate estimate $\widehat{\sigma}^2_e[t]$, and thus multi-stage methods including both Phase A and Phase B methods must be employed.

Apparently, depending on the specific weighting sequence employed various $\boldsymbol{\vartheta}_{a|c}$ estimation methods may be proposed. The most important of them are described in the sequel. However, before proceeding with them it must be noted that due to the dependence of the model residual on the model parameter vector $\boldsymbol{\vartheta}_{a|c}$ the regression model of Eq. (5.4.8) is nonlinear in the full FS-TARMA case but linear for the simpler FS-TAR case ($\boldsymbol{x} = \boldsymbol{\Phi} \cdot \boldsymbol{\vartheta}_a + \boldsymbol{e}(\boldsymbol{\vartheta}_a)$). This significant difference between FS-TAR and FS-TARMA models makes the separate examination of the corresponding estimation methods imperative.

The FS-TAR case

The Weighted Least Squares (WLS) method. The linear dependence of the innovations sequence $e[t, \boldsymbol{\vartheta}_a]$ on the parameter vector $\boldsymbol{\vartheta}_a$ leads to a linear WLS estimator for the latter:

$$\widehat{\boldsymbol{\vartheta}}_a = \left(\boldsymbol{\Phi}^T \cdot \boldsymbol{W} \cdot \boldsymbol{\Phi}\right)^{-1} \cdot \left(\boldsymbol{\Phi}^T \cdot \boldsymbol{W} \cdot \boldsymbol{x}\right) \tag{5.4.10}$$

independently of the weighting matrix $\boldsymbol{W}$ utilized.

The Ordinary Least Squares (OLS) method. As long as the true innovations variance $\sigma^2_e[t]$ is a-priori unknown and consistency is guaranteed for any uniformly bounded weighting sequence, the simplest and obvious choice for $w^2[t]$ is to set it equal to unity. In this case, estimation of $\boldsymbol{\vartheta}_a$ is achieved through the *Ordinary Least Squares (OLS)* estimator:

$$\widehat{\boldsymbol{\vartheta}}_a = \left(\boldsymbol{\Phi}^T \cdot \boldsymbol{\Phi}\right)^{-1} \cdot \left(\boldsymbol{\Phi}^T \cdot \boldsymbol{x}\right) \tag{5.4.11}$$

Nevertheless, it is reminded that this choice is suboptimal with respect to the achieved asymptotic efficiency [Poulimenos and Fassois, 2007].

The Recursive Least Squares (RLS) method. The OLS estimator may be also realized recursively through the classic *Recursive Least Squares (RLS)* scheme [Niedźwiecki, 2000, pp. 203-205] [Niedźwiecki and Klaput, 2002]. The RLS method was initially proposed for on-line applications [Xianya and Evans, 1984, Niedźwiecki, 1990] and/or the problem of slowly varying coefficients of projection $\boldsymbol{\vartheta}_a[t]$ [Boudaoud and Chaparro, 1987, Charbonnier et al., 1987]. For the latter case the RLS method may be based on an exponentially weighed PE criterion introduced through a suitably selected forgetting factor λ. However, it should be stressed that problems related to the selection of λ arise in this case while also FS-TAR models with only *partially* structured parameter evolution are obtained as long as the coefficient of projection vector has to be stored for every time instant $t = 1, \ldots, N$.

On the other hand, when batch processing and TI coefficients of projection are considered, the RLS estimation method must be (recursively) applied to the data record, with the final AR coefficient of projection estimate $\widehat{\boldsymbol{\vartheta}}_a[N]$ being maintained. In this case, improved RLS estimates may be obtained by applying the method in sequential phases (for instance a forward pass, a backward pass and a final forward pass over the data) in order to reduce the effects of arbitrary initial conditions.

The Multi-Stage (MS) method. A Multi-Stage (MS) method which approximates the optimal, in terms of asymptotic efficiency WLS estimator has been introduced in [Poulimenos and Fassois, 2007]. The MS method consists of three stages:

Stage 1. Initial AR projection coefficient vector estimation: In this stage an initial estimation of the AR projection coefficient vector is obtained through the OLS estimator (Eq. (5.4.11)).

Stage 2. Innovations variance projection coefficient vector estimation: Estimation of the innovations variance parameter vector $\boldsymbol{\vartheta}_s$, is achieved by maximizing the conditional log-likelihood function with respect to $\boldsymbol{\vartheta}_s$ replacing the innovations $e[t, \boldsymbol{\vartheta}_a]$ by their respective estimates $e[t, \widehat{\boldsymbol{\vartheta}_a}] = x[t] - \boldsymbol{\phi}^T[t] \cdot \widehat{\boldsymbol{\vartheta}_a}$ in Eq. (5.4.5). This stage is described in more detail in Section 5.4.2.2 where Phase B of regression methods dealing with estimation of $\boldsymbol{\vartheta}_s$ is discussed.

Stage 3. Final AR projection coefficient vector estimation: Final estimation of the AR projection coefficient vector is obtained by the WLS estimator of Eq. (5.4.10) by utilizing the innovations standard deviation CML estimate for the weighting sequence, that is $w^2[t] = \widehat{\sigma}_e^2[t] = \sum_{j=1}^{p_s} \widehat{s}_j \cdot G_{d_s(j)}[t]$.

Stages 2 and 3 of the MS method may be iterated until a convergence criterion with respect to the estimated parameters and/or the PE criterion is met. Further simplification may be achieved by relaxing the requirement for a ML estimator of $\boldsymbol{\vartheta}_s$ which as shown in Section 5.4.2.2 necessitates the use of nonlinear optimization techniques. In such a case a “relaxed” version of the aforementioned MS method may be derived (Relaxed Multi-Stage; RMS). Yet, the RMS method does not share the same asymptotic properties with the MS.

The FS-TARMA case

The WLS and OLS methods. Distinction should be made again between the simple $w^2[t] = 1$ case leading to an OLS estimator and the general WLS estimator for any other weighting sequence. However, as already mentioned, in the case of FS-TARMA models the innovations are nonlinearly dependent on the MA coefficients of projection vector $\boldsymbol{\vartheta}_c$ (Eq. (5.4.7)), and thus minimization of the PE criterion is a non-quadratic optimization problem regardless of the weighting sequence $w^2[t]$ utilized [Poulimenos and Fassois, 2006]. Such problems may be tackled via common iterative nonlinear optimization techniques – usually the Gauss-Newton or the Levenberg-Marquardt algorithm [Nocedal and Wright, 2006, Ch. 10] – utilizing the Jacobian matrix of the model innovations with respect to the AR/MA coefficients of projection vector $\boldsymbol{\vartheta}_{a|c}$. A detailed description of the Jacobian matrix construction may be found in [Ben Mrad et al., 1998a].

Yet, nonlinear least squares techniques are sensitive to the initial parameter values and if no accurate estimates are available the minimization procedure is very likely to converge to a local minima. The minimization of the PE criterion through OLS estimation has been shown to be of increased complexity even for problems of low dimensionality [Ben Mrad et al., 1998a]. Due to the potential wrong convergence problems when arbitrary initial estimates are utilized, suboptimal multi-stage methods such as the *Two*

Stage Least Squares (*2SLS*; [Grenier, 1983b, Poulimenos and Fassois, 2006]) or the *Polynomial-Algebraic* (*P-A*; [Ben Mrad et al., 1998a, Fouskitakis and Fassois, 2001, Poulimenos and Fassois, 2006]) may be used either as suboptimal solutions or just in order to provide initial estimates to be refined via iterative techniques.

The Two Stage Least Squares (2SLS) method. The main idea behind this method is the approximation of the nonlinear OLS problem by a pseudo-linear problem through the replacement of the unknown innovations $e[t, \boldsymbol{\vartheta}_{a|c}]$ of the regression matrix $\boldsymbol{\Phi}(\boldsymbol{\vartheta}_{a|c})$ (Eq. (5.4.8)) by respective estimates. The 2SLS method consists of the following stages:

Stage 1. Inverse function estimation. A long (of high AR order) FS-TAR$(n_q)_{[p_q]}$ model which is meant to approximate the inverse function representation of the original FS-TARMA model is considered as follows (see [Poulimenos and Fassois, 2006] on the existence and the properties of such a representation):

$$x[t] - \sum_{i=1}^{n_q} \sum_{j=1}^{p_q} q_{i,j} \cdot G_{q(j)}[t] \cdot x[t-i] + e[t, \boldsymbol{\vartheta}_q] \tag{5.4.12}$$

with $n_q \gg \max(n_a, n_c)$. The identification of this long FS-TAR model based on the minimization of the PE criterion is a linear optimization problem which (as previously shown) may be solved by the OLS method. Consequently, estimates of the model innovations $e[t, \widehat{\boldsymbol{\vartheta}}_q]$ may be readily obtained.

Stage 2: AR/MA projection coefficient estimation. The FS-TARMA model is approximated by replacing the past, but not the current, values of the prediction error $e[t, \boldsymbol{\vartheta}_{a|c}]$ by the previously obtained estimates $e[t, \widehat{\boldsymbol{\vartheta}}_q]$ in Eq. (5.4.8):

$$\boldsymbol{x} = \boldsymbol{\Phi}(\widehat{\boldsymbol{\vartheta}}_q) \cdot \boldsymbol{\vartheta}_{a|c} + \boldsymbol{e}(\boldsymbol{\vartheta}_{a|c}) \tag{5.4.13}$$

and solving the resultant linear regression problem in the OLS sense. The final residual sequence is estimated based on the estimate $\widehat{\boldsymbol{\vartheta}}_{a|c}$ and the TARMA model expression of Eq. (5.1.3).

Remarks:

(i) The second stage of the 2SLS method may be iterated, replacing in every iteration the past values of the prediction error $e[t, \boldsymbol{\vartheta}_{a|c}]$ by the most recent estimates $e[t, \widehat{\boldsymbol{\vartheta}}_{a|c}]$, until a minimum value of the PE criterion is achieved.

(ii) Usually selecting n_q between two and five times of $\max(n_a, n_c)$ is adequate, however its value may also be optimized based on an appropriate model structure selection scheme (see Section 5.5).

(iii) Theoretically, the inverse function representation is an FS-TAR model of infinite order [Poulimenos and Fassois, 2006], while its TV parameters are expanded onto functional subspaces that stem from the combination of the subspaces of the initial FS-TARMA model [Poulimenos and Fassois, 2003a]. However, these functional subspaces may, in certain cases (for instance in cases of high MA subspace dimensionalities), become of quite high dimensionalities. This may lead to statistically unreliable estimates if the ratio of the number of available signal samples over the number of projection coefficients to be estimated is smaller than, say, 20. In such a case it is preferable to use truncated functional subspaces for the inverse function parameters.

(iv) A Two Stage Weighted Least Squares (2SWLS) method is obtained if the estimation of the AR/MA coefficients of projection vector taking place at the second stage of the method, is achieved by solving the approximate linear regression model $\boldsymbol{x} = \boldsymbol{\Phi}(\widehat{\boldsymbol{\vartheta}}_q) \cdot \boldsymbol{\vartheta}_{a|c} + \boldsymbol{e}(\boldsymbol{\vartheta}_{a|c})$ in the WLS sense. An estimate of the innovations variance based on the residuals $e[t, \widehat{\boldsymbol{\vartheta}_q}]$ may be utilized for this purpose.

(v) 2SLS, 2SWLS and P-A methods do not lead to consistent estimators.

The Recursive Extended Least Squares (RELS) method. The OLS estimator may be also approximated through the *Recursive Extended Least Squares (RELS)* method [Niedźwiecki, 2000, pp. 136-137]. In this method, at a given time instant t the unknown innovations $e[t-i, \boldsymbol{\vartheta}_{a|c}]$ that appear in the regression matrix of Eq. (5.4.8) are replaced by the respective a-posteriori one-step ahead predictions of the algorithm obtained during the previous time instant $t-1$. This estimation method is (recursively) applied

Table 5.4.1: RELS estimation method.

Estimator update	$\widehat{\boldsymbol{\vartheta}}_{a\|c}[t] = \widehat{\boldsymbol{\vartheta}}_{a\|c}[t-1] + \boldsymbol{k}[t] \cdot \left(x[t] - \boldsymbol{\phi}^T[t] \cdot \widehat{\boldsymbol{\vartheta}}_{a\|c}[t-1] \right)$
Gain*:	$\boldsymbol{k}[t] = \dfrac{\boldsymbol{P}[t-1] \cdot \boldsymbol{\phi}[t]}{\lambda + \boldsymbol{\phi}^T[t] \cdot \boldsymbol{P}[t] \cdot \boldsymbol{\phi}[t]}$
Covariance" update*	$\boldsymbol{P}[t] = \dfrac{1}{\lambda} \cdot \left(\boldsymbol{P}[t-1] - \dfrac{\boldsymbol{P}[t-1] \cdot \boldsymbol{\phi}[t] \cdot \boldsymbol{\phi}^T[t] \cdot \boldsymbol{P}[t-1]}{\lambda + \boldsymbol{\phi}^T[t] \cdot \boldsymbol{P}[t] \cdot \boldsymbol{\phi}[t]} \right)$
A-posteriori error	$\hat{e}[t\|t] = x[t] - \boldsymbol{\phi}^T[t] \cdot \widehat{\boldsymbol{\vartheta}}_{a\|c}[t]$

$$\boldsymbol{\phi}[t] \triangleq \Big[-G_{d_a(1)}[t] \cdot x[t-1] \ \ldots \ -G_{d_a(p_a)}[t] \cdot x[t-n_a] \ \vdots \ G_{d_c(1)}[t] \cdot \hat{e}[t-1|t-1] \ \ldots \ G_{d_c(p_c)}[t] \cdot \hat{e}[t-n_c|t-n_c] \Big]^T$$

$^*\lambda = 1$ for time-invariant coefficients of projection.

Initialization: $\widehat{\boldsymbol{\vartheta}}_{a|c}[0] = \mathbf{0}$, $\boldsymbol{P}[0] = \alpha \boldsymbol{I}$ with α designating a "large" positive number. The signal and a-posteriori error initial values are set to zero.

to the data record, with the final AR/MA coefficient of projection estimate being equal to $\widehat{\boldsymbol{\vartheta}}_{a|c}[N]$. The method is presented in Table 5.4.1. To reduce the effects of arbitrary initial conditions, recursions on the available signal may be applied in sequential phases (for instance a forward pass, a backward pass and a final forward pass).

Similarly with the RLS algorithm in the FS-TAR case, a forgetting factor λ may be introduced into the method for tracking a time-dependent projection coefficient vector $\boldsymbol{\vartheta}_{a|c}[t]$. However, the same problems related to the selection of λ and the partially structured parameter evolution also apply in this case.

Finally it is noted that RELS is just an approximation of the original OLS method and thus may not be connected with asymptotic consistency.

The Multi-Stage (MS) method. As in the FS-TAR case [Poulimenos and Fassois, 2009a], the WLS estimator with the smallest asymptotic covariance matrix, is achieved for $w^2[t] = c{\cdot}\sigma_e^2[t]$. Since again $\sigma_e^2[t]$ is a-priori unknown a Multi-Stage (MS) method which approximates the optimal, in terms of asymptotic efficiency, WLS estimator may be implemented as follows [Poulimenos and Fassois, 2007]:

Stage 1. Initial AR/MA projection coefficient vector estimation: Initial estimation of $\boldsymbol{\vartheta}_{a|c}$ obtained through the OLS method.

Stage 2. Innovations variance projection coefficient vector estimation: Estimation of the innovations variance parameter vector $\boldsymbol{\vartheta}_s$ achieved by maximizing the conditional log-likelihood function with respect to $\boldsymbol{\vartheta}_s$ replacing the innovations $e[t, \boldsymbol{\vartheta}_{a|c}]$ with their respective estimates $e[t, \widehat{\boldsymbol{\vartheta}}_{a|c}]$ in Eq. (5.4.5).

Stage 3. Final AR/MA projection coefficient vector estimation: Final estimation of the AR/MA projection coefficient vector obtained by the WLS estimator by utilizing $w^2[t] = \widehat{\sigma}_e^2[t] = \sum_{j=1}^{p_s} \widehat{s}_j{\cdot}G_{d_s(j)}[t]$ as estimated from the second stage.

It is reminded that both OLS and WLS estimation methods of Stages 1 and 3, lead to non-quadratic optimization problems, while also the $\boldsymbol{\vartheta}_s$ ML estimate of Stage 2 has to be obtained through nonlinear optimization techniques. A family of "Relaxed" MS (RMS) methods may be realized by substituting the nonlinear stages of MS by respective linear ones. Indicatively, such a method may be realized as shown schematically in Fig. 5.4.1. However, RMS methods do not share the same asymptotic properties with the original MS method.

5.4.2.2 Phase B: Estimation of innovations variance coefficients of projection parameter vector

The estimation of the parameter vector $\boldsymbol{\vartheta}_s$ for the fully parametrized classical FS-TARMA model may be based on one of the following methods.

The Moving Window (MW) method [Poulimenos and Fassois, 2006]. An initial smoothed non-parametric estimate of the variance is obtained via a window of length, say $2K + 1$, centred at the

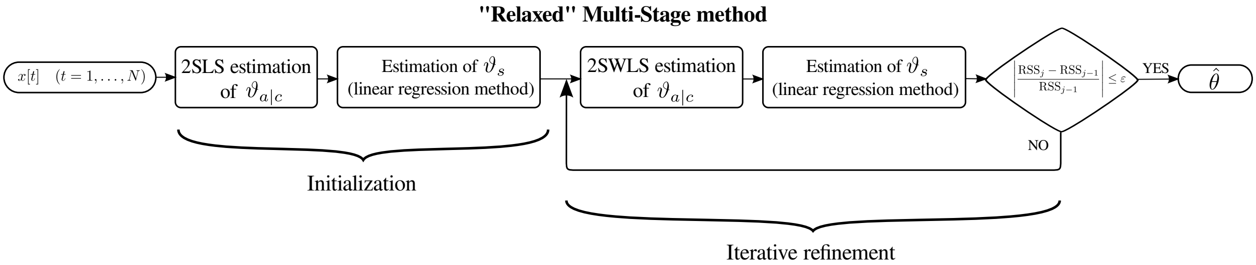

Figure 5.4.1: Flowchart of an indicative "Relaxed" Multi-Stage (RLS) method for FS-TARMA model estimation.

time instant t, that slides over the innovation sequence, that is:

$$\widehat{\sigma}_e^2[t] = \frac{1}{2K+1} \cdot \sum_{\tau=t-K}^{t+K} e^2[\tau, \widehat{\boldsymbol{\vartheta}}_{a|c}] \tag{5.4.14}$$

An estimate of the projection coefficient vector $\boldsymbol{\vartheta}_s$ may be then obtained by fitting the non-parametrically obtained variance $\widehat{\sigma}_e^2[t]$ to a selected functional subspace $\mathcal{F}_{\sigma_e^2[t]}$. This leads to the overdetermined set of equations:

$$\widehat{\sigma}_e^2[t] = \sum_{j=1}^{p_s} s_j \cdot G_{d_s(j)}[t] = \boldsymbol{g}_s^T[t] \cdot \boldsymbol{\vartheta}_s \tag{5.4.15}$$

which solved in an OLS sense gives:

$$\widehat{\boldsymbol{\vartheta}}_s = \left(\boldsymbol{G}_s^T \cdot \boldsymbol{G}_s\right)^{-1} \cdot \left(\boldsymbol{G}_s^T \cdot \widehat{\boldsymbol{\sigma}}_e\right) \tag{5.4.16}$$

where $\boldsymbol{g}_s[t] = \left[G_{d_s(1)}[t], \ldots G_{d_s(p_s)}[t]\right]^T$, $\boldsymbol{G}_s = \left[\boldsymbol{g}_s[1], \ldots, \boldsymbol{g}_s[N]\right]^T$ and $\widehat{\boldsymbol{\sigma}}_e = \left[\widehat{\sigma}_e^2[1], \ldots, \widehat{\sigma}_e^2[N]\right]^T$.

The main disadvantage of this method is the necessity for the additional selection of an appropriate window length parameter K. This parameter consists a trade-off between the statistical accuracy and the tracking ability of the non-parametric variance estimator, so it should be deliberately selected.

The Instantaneous Variance (IV) method [Boudaoud and Chaparro, 1987]. According to the definition of the general TARMA model of Eq. (5.1.3), the innovation sequence $e[t]$ is white with zero mean and time-dependent variance $\sigma_e^2[t]$. Therefore, a reasonable estimator for $\sigma_e^2[t]$ is the squared innovation $e^2[t, \widehat{\boldsymbol{\vartheta}}_{a|c}]$ - actually the unbiasedness of $e^2[t, \widehat{\boldsymbol{\vartheta}}_{a|c}]$ as an estimator of $\sigma_e^2[t]$ was also proved in Eq. (5.4.2). Therefore, an estimate for $\boldsymbol{\vartheta}_s$ is obtained by solving the following equation:

$$e^2[t, \widehat{\boldsymbol{\vartheta}}_{a|c}] = \sum_{j=1}^{p_s} s_j \cdot G_{d_s(j)}[t] = \boldsymbol{g}_s^T[t] \cdot \boldsymbol{\vartheta}_s \tag{5.4.17}$$

in the OLS sense.

The Instantaneous Standard Deviation (ISD) method [Grenier, 1983b]. In this case the innovations standard deviation $\sigma_e[t]$ is projected onto the selected functional subspace. In particular, based on the fact that $E\{|e[t]|\} = \sqrt{2/\pi} \cdot \sigma_e[t]$, with $E\{\cdot\}$ designating statistical expectation, the following is solved for $\boldsymbol{\vartheta}_s$ again in the OLS sense

$$|e[t, \widehat{\boldsymbol{\vartheta}_a}]| = \sqrt{\frac{2}{\pi}} \cdot \sum_{j=1}^{p_s} s_j \cdot G_{b_s(j)}[t] = \sqrt{\frac{2}{\pi}} \cdot \boldsymbol{g}_s^T[t] \cdot \boldsymbol{\vartheta}_s \tag{5.4.18}$$

The Conditional Maximum Likelihood (CML) [Poulimenos and Fassois, 2006]. In regression type methods estimation of $\boldsymbol{\vartheta}_s$ may be achieved by maximizing the *conditional* log-likelihood function $\ln \mathcal{L}(\boldsymbol{\vartheta}_s | \widehat{\boldsymbol{\vartheta}}_{a|c}, x^N)$ of Eq. (5.4.5) with respect to $\boldsymbol{\vartheta}_s$, treating the estimated innovation sequence $e[t, \widehat{\boldsymbol{\vartheta}}_{a|c}]$

provided by Phase A as measurements. This estimation constitutes a nonlinear optimization problem of low dimensionality (p_s) that may be tackled via iterative optimization techniques. An estimator of $\boldsymbol{\vartheta}_s$ based on the previous methods may be used for the initialization of this nonlinear optimization procedure.

Remarks:

(i) The estimation of the innovations variance or standard deviation coefficients of projection is actually a constrained optimization problem as long as these statistical quantities are by definition positive. Hence, the estimation of $\boldsymbol{\vartheta}_s$ should be subject to the constraints $\sum_{j=1}^{p_s} s_j \cdot G_{b_s(j)}[t] > 0$, for every t. This fact is usually overlooked in the literature, probably because violation of this constraint rarely occurs in practical problems. Nonetheless, if such a difficulty occurs, constrained optimization may be avoided by adding a constant mean value to the innovations sequence before estimating $\boldsymbol{\vartheta}_s$. Of course this mean value has to be subtracted from the final estimate.

(ii) The smoothed non-parametric estimate of the variance obtained through a moving window, that is the first step of the MW method, may also provide a smoothed estimate of the innovations variance for the semi-parametric FS-TARMA type of mode.

(iii) One could argue that the instantaneous estimates of the innovations variance or standard deviation are inaccurate and therefore of limited practical value. Notwithstanding, these instant values are unbiased estimates and the collection of a large number of them makes the corresponding methods reliable. Yet, instantaneous estimates of higher order statistics have also been successfully applied for the estimation of the coefficients of projection of FS-FIR models [Tsatsanis, 1995, Tsatsanis and Giannakis, 1996a, Tsatsanis and Giannakis, 1997].

5.4.3 Regression type methods for adaptable models

Regression type methods for AFS-TARMA models are based on an equivalent to Eq. (5.4.7) regression model form:

$$x[t] \;=\; \underbrace{\begin{bmatrix} -x[t-1]\cdot G_{a(1)}[t,\boldsymbol{\delta}_a] \\ -x[t-1]\cdot G_{a(2)}[t,\boldsymbol{\delta}_a] \\ \vdots \\ -x[t-n_a]\cdot G_{a(p_a-1)}[t,\boldsymbol{\delta}_a] \\ -x[t-n_a]\cdot G_{a(p_a)}[t,\boldsymbol{\delta}_a] \\ \hdashline e[t-1,\boldsymbol{\vartheta}_{a|c}]\cdot G_{c(1)}[t,\boldsymbol{\delta}_c] \\ e[t-1,\boldsymbol{\vartheta}_{a|c}]\cdot G_{c(2)}[t,\boldsymbol{\delta}_c] \\ \vdots \\ e[t-n_c,\boldsymbol{\vartheta}_{a|c}]\cdot G_{c(p_c-1)}[t,\boldsymbol{\delta}_c] \\ e[t-n_c,\boldsymbol{\vartheta}_{a|c}]\cdot G_{c(p_c)}[t,\boldsymbol{\delta}_c] \end{bmatrix}^T}_{\boldsymbol{\phi}[t,\boldsymbol{\delta}_{a|c},\boldsymbol{\vartheta}_{a|c}]} \cdot \underbrace{\begin{bmatrix} a_{1,1} \\ a_{1,2} \\ \vdots \\ a_{n_a,p_a-1} \\ a_{n_a,p_a} \\ \hdashline c_{1,1} \\ c_{1,2} \\ \vdots \\ c_{n_c,p_c-1} \\ c_{n_c,p_c} \end{bmatrix}}_{\boldsymbol{\vartheta}_{a|c}} + e[t,\boldsymbol{\delta}_{a|c},\boldsymbol{\vartheta}_{a|c}] \tag{5.4.19}$$

or, using the stacked signal and innovations sequence vectors:

$$\boldsymbol{x} = \boldsymbol{\Phi}(\boldsymbol{\delta}_{a|c},\boldsymbol{\vartheta}_{a|c})\cdot\boldsymbol{\vartheta}_{a|c} + \boldsymbol{e}(\boldsymbol{\delta}_{a|c},\boldsymbol{\vartheta}_{a|c}) \tag{5.4.20}$$

Similarly with the regression type methods for classical FS-TARMA models the estimation of the parameter vectors $\boldsymbol{\delta}_{a|c}, \boldsymbol{\vartheta}_{a|c}$ and $\boldsymbol{\delta}_s, \boldsymbol{\vartheta}_s$ is achieved in distinct sequential phases.

5.4.3.1 Phase A: Estimation of AR/MA functional subspace and coefficients of projection parameter vectors

This phase is based on the minimization of the general WLS criterion:

$$[\widehat{\boldsymbol{\delta}}_{a|c}^T, \widehat{\boldsymbol{\vartheta}}_{a|c}^T]^T = \arg\min_{\boldsymbol{\delta}_{a|c}, \boldsymbol{\vartheta}_{a|c}} \left\{ \sum_{t=1}^{N} \frac{e^2[t, \boldsymbol{\delta}_{a|c}, \boldsymbol{\vartheta}_{a|c}]}{w^2[t]} \right\} = \arg\min_{\boldsymbol{\delta}_{a|c}, \boldsymbol{\vartheta}_{a|c}} \left\{ \boldsymbol{e}(\boldsymbol{\delta}_{a|c}, \boldsymbol{\vartheta}_{a|c})^T \cdot \boldsymbol{W} \cdot \boldsymbol{e}(\boldsymbol{\delta}_{a|c}, \boldsymbol{\vartheta}_{a|c}) \right\} \tag{5.4.21}$$

with various methods obtained depending on the weighting sequence $w^2[t]$ selected. However, no asymptotic properties have been derived for the methods of this recently introduced type of models.

The simpler AFS-TAR case is characterized by a nonlinear regression model special form $\boldsymbol{x} = \boldsymbol{\Phi}(\boldsymbol{\delta}_a) \cdot \boldsymbol{\vartheta}_a + \boldsymbol{e}(\boldsymbol{\delta}_a, \boldsymbol{\vartheta}_a)$ in which the parameter vectors $\boldsymbol{\vartheta}_a$ and $\boldsymbol{\delta}_a$ form two completely disjoint parameter sets. This special form makes the estimation of the parameter vectors involved simpler compared to that of the complete AFS-TARMA model, and hence the two cases are examined separately.

The AFS-TAR case

The WLS and OLS methods. Due to the nonlinear dependence of the basis functions $G_{a(j)}[t, \boldsymbol{\delta}_a]$ on the parameter vector $\boldsymbol{\delta}_a$ the AFS-TAR estimation problem based on the minimization of the PE criterion constitutes a nonlinear optimization problem independently of the weighting sequence $w^2[t]$ utilized. This problem may be, in principle, solved through iterative constrained nonlinear optimization methods with respect to $\dim(\boldsymbol{\vartheta}_a) + \dim(\boldsymbol{\delta}_a) = p_a \cdot n_a + \dim(\boldsymbol{\delta}_a)$ parameters. However, again this optimization problem is usually of high dimensionality and wrong convergence problems may arise when arbitrary or inaccurate estimates are used for its initialization.

The Separable Nonlinear Least Squares (SNLS) method. An effective approach for minimizing the PE criterion is to take advantage of the separable nonlinear regression structure of Eq. (5.4.19), that is the fact that the parameters $\boldsymbol{\vartheta}_a$ and $\boldsymbol{\delta}_a$ form two completely disjoint parameter sets. Such special structure regression problems may be solved through the Separable Nonlinear Least Squares (SNLS) method and more specifically by the Variable Projection (VP) algorithm introduced by Golub and Pereyra [Golub and Pereyra, 1973]. This algorithm is based on the fact that $\boldsymbol{\vartheta}_a$ appears linearly in the model and thus, assuming that the nonlinear parameter vector $\boldsymbol{\delta}_a$ is known, an $\boldsymbol{\vartheta}_a$ estimate may be obtained through the linear OLS estimator:

$$\widehat{\boldsymbol{\vartheta}}_a = \left(\boldsymbol{\Phi}^T(\boldsymbol{\delta}_a) \cdot \boldsymbol{\Phi}(\boldsymbol{\delta}_a)\right)^{-1} \cdot \boldsymbol{\Phi}^T(\boldsymbol{\delta}_a) \cdot \boldsymbol{x} = \boldsymbol{\Phi}^\dagger(\boldsymbol{\delta}_a) \cdot \boldsymbol{x} \tag{5.4.22}$$

where † denotes pseudo-inverse. Hence, the model innovations may be obtained by a functional form which depends solely on $\boldsymbol{\delta}_a$, that is:

$$\boldsymbol{e}(\boldsymbol{\delta}_a, \boldsymbol{\vartheta}_a) = \boldsymbol{x} - \boldsymbol{\Phi}(\boldsymbol{\delta}_a) \cdot \widehat{\boldsymbol{\vartheta}}_a \implies \boldsymbol{e}_{\text{VP}}(\boldsymbol{\delta}_a) = \boldsymbol{x} - \boldsymbol{\Phi}(\boldsymbol{\delta}_a) \cdot \boldsymbol{\Phi}^\dagger(\boldsymbol{\delta}_a) \cdot \boldsymbol{x} \Longrightarrow \boldsymbol{e}_{\text{VP}}(\boldsymbol{\delta}_a) = \left(\boldsymbol{I} - \boldsymbol{\Phi}(\boldsymbol{\delta}_a) \cdot \boldsymbol{\Phi}^\dagger(\boldsymbol{\delta}_a)\right) \cdot \boldsymbol{x} \tag{5.4.23}$$

Thus, the estimator of Eq. (5.4.21) for $w^2[t] = 1$ takes the form:

$$\widehat{\boldsymbol{\delta}}_a = \arg\min_{\boldsymbol{\delta}_a} \left\{ \boldsymbol{e}_{\text{VP}}(\boldsymbol{\delta}_a)^T \cdot \boldsymbol{e}_{\text{VP}}(\boldsymbol{\delta}_a) \right\} = \arg\min_{\boldsymbol{\delta}_a} \left\| \left(\boldsymbol{I} - \boldsymbol{\Phi}(\boldsymbol{\delta}_a) \cdot \boldsymbol{\Phi}(\boldsymbol{\delta}_a)^\dagger\right) \cdot \boldsymbol{x} \right\|^2 \tag{5.4.24}$$

The nonlinear parameter vector $\boldsymbol{\delta}_a$ may be thus estimated by means of iterative constrained nonlinear optimization techniques with only $\dim(\boldsymbol{\delta}_a)$ unknown parameters, while $\boldsymbol{\vartheta}_a$ may be subsequently estimated through linear OLS (Eq. (5.4.22)), after substituting $\boldsymbol{\delta}_a$ by the obtained estimate $\widehat{\boldsymbol{\delta}_a}$.

This formulation leads to the reduction of the dimensionality of the nonlinear optimization problem, while not affecting the stationary points (minima and maxima) of the original problem. This holds under the rather mild condition of constant (not necessarily maximum) rank of the regression matrix $\boldsymbol{\Phi}(\boldsymbol{\delta}_a)$ over the whole parameter search space of $\boldsymbol{\delta}_a$ ([Golub and Pereyra, 1973, Theorem 2.1]). The cost for reducing the dimension of the nonlinear optimization problem is the increased complexity of the gradient computation for the innovation sequence $e_{\text{VP}}(\boldsymbol{\delta}_a)$ that is required for the construction of the Jacobian matrix (see Chapter 4 for more details on the subject).

The Separable Nonlinear Weighted Least Squares (SNWLS) method. The SNLS method is readily extended to a SNWLS method for any uniformly bounded weighting sequence $w^2[t]$ (that is $0 < \underline{w^2} \leq w^2[t] \leq \overline{w^2} < \infty$ for every t). In this case the weighting matrix $\boldsymbol{W}$ is positive definite and may be written as $\boldsymbol{W} = \boldsymbol{D}^T \cdot \boldsymbol{D}$, where $\boldsymbol{D}$ is an invertible $(N \times N)$ matrix. Hence, the OLS estimator of Eq. (5.4.22) may be substituted by the WLS estimator of the following equation:

$$\begin{aligned} \widehat{\boldsymbol{\vartheta}_a} &= \left(\boldsymbol{\Phi}(\boldsymbol{\delta}_a)^T \cdot \boldsymbol{W} \cdot \boldsymbol{\Phi}(\boldsymbol{\delta}_a)\right)^{-1} \left(\boldsymbol{\Phi}(\boldsymbol{\delta}_a)^T \cdot \boldsymbol{W} \cdot \boldsymbol{x}\right) \\ &= \left(\boldsymbol{\Phi}(\boldsymbol{\delta}_a)^T \cdot \boldsymbol{D}^T \cdot \boldsymbol{D} \cdot \boldsymbol{\Phi}(\boldsymbol{\delta}_a)\right)^{-1} \cdot \left(\boldsymbol{\Phi}(\boldsymbol{\delta}_a)^T \cdot \boldsymbol{D}^T \cdot \boldsymbol{D} \cdot \boldsymbol{x}\right) = \widetilde{\boldsymbol{\Phi}}(\boldsymbol{\eta}_a)^\dagger \cdot \tilde{\boldsymbol{x}} \end{aligned} \tag{5.4.25}$$

where $\widetilde{\boldsymbol{\Phi}}(\boldsymbol{\eta}_a) = \boldsymbol{D} \cdot \boldsymbol{\Phi}(\boldsymbol{\eta}_a)$ and $\tilde{\boldsymbol{x}} = \boldsymbol{D} \cdot \boldsymbol{x}$. Therefore, the model innovations may be obtained as

$$\tilde{\boldsymbol{e}}(\boldsymbol{\delta}_a, \boldsymbol{\vartheta}_a) = \tilde{\boldsymbol{x}} - \widetilde{\boldsymbol{\Phi}}(\boldsymbol{\delta}_a) \cdot \widehat{\boldsymbol{\vartheta}}_a \implies \tilde{\boldsymbol{e}}_{\text{VP}}(\boldsymbol{\delta}_a) = \tilde{\boldsymbol{x}} - \widetilde{\boldsymbol{\Phi}}(\boldsymbol{\delta}_a) \cdot \widetilde{\boldsymbol{\Phi}}(\boldsymbol{\delta}_a)^\dagger \cdot \tilde{\boldsymbol{x}} \Longrightarrow \tilde{\boldsymbol{e}}_{\text{VP}}(\boldsymbol{\delta}_a) = \left(\boldsymbol{I} - \widetilde{\boldsymbol{\Phi}}(\boldsymbol{\delta}_a) \cdot \widetilde{\boldsymbol{\Phi}}(\boldsymbol{\delta}_a)^\dagger\right) \cdot \tilde{\boldsymbol{x}} \tag{5.4.26}$$

and the estimator of $\boldsymbol{\delta}_a$ is given from the following minimization problem:

$$\widehat{\boldsymbol{\delta}}_a = \arg\min_{\boldsymbol{\delta}_a} \left\{\tilde{\boldsymbol{e}}_{\text{VP}}(\boldsymbol{\delta}_a)^T \cdot \tilde{\boldsymbol{e}}_{\text{VP}}(\boldsymbol{\delta}_a)\right\} = \arg\min_{\boldsymbol{\delta}_a} \|\left(\boldsymbol{I} - \widetilde{\boldsymbol{\Phi}}(\boldsymbol{\delta}_a) \cdot \widetilde{\boldsymbol{\Phi}}(\boldsymbol{\delta}_a)^\dagger\right) \cdot \tilde{\boldsymbol{x}}\|^2 \tag{5.4.27}$$

Remark. A corresponding with that of the classical FS-TAR case MS method consisting of the same three stages may be also derived.

The AFS-TARMA case

The WLS and OLS methods. Once more the WLS method constitutes a nonlinear optimization problem independently of the weighting sequence $w^2[t]$ utilized and yet of increased dimension since $\dim(\boldsymbol{\vartheta}_{a|c}) + \dim(\boldsymbol{\delta}_{a|c}) = p_a \cdot n_a + p_c \cdot n_c + \dim(\boldsymbol{\delta}_{a|c})$ parameters have to be estimated.

Moreover, the nonlinear regression model of Eq. (5.4.20) does not have a separable structure due to the presence of the unknown innovations $e[t, \boldsymbol{\delta}_{a|c}, \boldsymbol{\vartheta}_{a|c}]$, which depend on both $\boldsymbol{\delta}_{a|c}$ and $\boldsymbol{\vartheta}_{a|c}$, in the regression matrix $\boldsymbol{\Phi}(\boldsymbol{\delta}_{a|c}, \boldsymbol{\vartheta}_{a|c})$. Thus, the SNLS method may not be used in order to reduce the number of parameters that have to be estimated through nonlinear optimization. To overcome this obstacle a suboptimal two-stage pseudo-SNLS procedure, analogous to the 2SLS method for the classical FS-TARMA model parameter estimation, may be employed.

The Two Stage Separable Nonlinear Least Squares (2SSNLS) method. The two-stage method consists of the following stages:

Stage 1: Inverse function estimation. A truncated, n_q-order, inverse function model that approximates the infinite order inverse function representation of an AFS-TARMA model is considered as follows:

$$x[t] - \sum_{i=1}^{n_q} \sum_{j=1}^{p_q} q_{i,j} \cdot G_{q(j)}[t, \boldsymbol{\delta}_q] \cdot x[t-i] + e[t, \boldsymbol{\delta}_q, \boldsymbol{\vartheta}_q] \tag{5.4.28}$$

with $n_q \gg \max(n_a, n_c)$. The identification of this long AFS-TAR model based on the minimization of the PE criterion is a SNLS problem which (as previously shown) may be solved by the SNLS method. Consequently, estimates of the model innovations $e[t, \widehat{\boldsymbol{\delta}}_q, \widehat{\boldsymbol{\vartheta}}_q]$ may be readily obtained.

Stage 2: AR/MA parameter vector estimation. The FS-TARMA model is approximated by replacing the past, but not the current, values of the prediction error $e[t, \boldsymbol{\delta}_{a|c}, \boldsymbol{\vartheta}_{a|c}]$ by the previously obtained estimates $e[t, \widehat{\boldsymbol{\delta}}_q, \widehat{\boldsymbol{\vartheta}}_q]$.

$$\boldsymbol{x} = \boldsymbol{\Phi}(\boldsymbol{\delta}_{a|c}, \widehat{\boldsymbol{\delta}}_q, \widehat{\boldsymbol{\vartheta}}_q) \cdot \boldsymbol{\vartheta}_{a|c} + \boldsymbol{e}(\boldsymbol{\delta}_{a|c}, \boldsymbol{\vartheta}_{a|c}) \tag{5.4.29}$$

and solving the resultant separable nonlinear regression problem through the SNLS method. The final innovation sequence is estimated based on the estimates $\widehat{\boldsymbol{\delta}}_{a|c}, \widehat{\boldsymbol{\vartheta}}_{a|c}$ and the TARMA model expression of Eq. (5.1.3).

Remarks:

(i) The second stage of the 2SSNLS method may be iterated, replacing in every iteration the past values of the prediction error $e[t, \boldsymbol{\delta}_{a|c}, \boldsymbol{\vartheta}_{a|c}]$ by the most recent estimates $e[t, \widehat{\boldsymbol{\delta}}_{a|c}, \widehat{\boldsymbol{\vartheta}}_{a|c}]$, until a minimum value of the PE criterion is achieved.

(ii) After obtaining the 2SSNLS estimates, minimization of the original full functional problem may be viewed as a subsequent (potential) refinement stage.

(iii) A positive definite weighting matrix $\boldsymbol{W}$ may also be used during the stage of the 2SSNLS method leading to a 2SSNWLS.

5.4.3.2 Phase B: Estimation of innovations variance functional subspace and coefficients of projection parameter vectors

The estimation of the innovations variance parameter vectors $\boldsymbol{\delta}_s$ and $\boldsymbol{\vartheta}_s$ for the parametric AFS-TARMA model may also be obtained via the VP algorithm and one of the following methods.

The Moving Window (MW) method. An initial smoothed non-parametric estimate of the variance is obtained via a window of length, say $2K+1$, centred at the time instant t, that slides over the innovation sequence, that is:

$$\widehat{\sigma}_e^2[t] = \frac{1}{2K+1} \cdot \sum_{\tau=t-K}^{t+K} e^2[\tau, \widehat{\boldsymbol{\delta}}_{a|c}, \widehat{\boldsymbol{\vartheta}}_{a|c}] \tag{5.4.30}$$

An estimate of the functional subspace parameter vector $\boldsymbol{\delta}_s$ and the projection coefficient vector $\boldsymbol{\vartheta}_s$ may be then obtained by fitting the obtained variance $\widehat{\sigma}_e^2[t]$ to the a-priori unknown functional subspace as follows:

$$\widehat{\sigma}_e^2[t] = \sum_{j=1}^{p_s} s_j \cdot G_{s(j)}[t, \boldsymbol{\delta}_s] = \boldsymbol{g}_s^T[t, \boldsymbol{\delta}_s] \cdot \boldsymbol{\vartheta}_s \tag{5.4.31}$$

which solved in the SNLS sense with respect to the functional subspace parameter vector $\boldsymbol{\delta}_s$:

$$\widehat{\boldsymbol{\delta}_s} = \arg\min_{\boldsymbol{\delta}_s} \|\big(\boldsymbol{I} - \boldsymbol{G}_s(\boldsymbol{\delta}_s) \cdot \boldsymbol{G}_s(\boldsymbol{\delta}_s)^\dagger\big) \cdot \widehat{\boldsymbol{\sigma}}_e\|^2 \tag{5.4.32}$$

subject to the constraints of the functional subspace parameter vector $\boldsymbol{\delta}_s$. In the above $\boldsymbol{g}_s[t, \boldsymbol{\delta}_s] = \big[G_{s(1)}[t, \boldsymbol{\delta}_s], \ldots, G_{s(p_s)}[t, \boldsymbol{\delta}_s]\big]^T$, $\boldsymbol{G}_s(\boldsymbol{\delta}_s) = \big[\boldsymbol{g}_s[1, \boldsymbol{\delta}_s], \ldots, \boldsymbol{g}_s[N, \boldsymbol{\delta}_s]\big]^T$ and $\boldsymbol{\sigma}_e = \big[\widehat{\sigma}_e^2[1], \ldots, \widehat{\sigma}_e^2[N]\big]^T$. The coefficient of projection vector $\boldsymbol{\vartheta}_s$ is subsequently obtained by the linear OLS estimator:

$$\widehat{\boldsymbol{\vartheta}}_s = \big(\boldsymbol{G}_s(\boldsymbol{\delta}_s)^T \cdot \boldsymbol{G}_s(\boldsymbol{\delta}_s)\big)^{-1} \cdot \big(\boldsymbol{G}_s(\boldsymbol{\delta}_s)^T \cdot \widehat{\boldsymbol{\sigma}}_e\big) \tag{5.4.33}$$

The necessity for the additional selection of an appropriate window length parameter K is again noted.

The Instantaneous Variance (IV) method. Using the estimated from Phase A innovations sequence as an initial rough estimate of the instantaneous variance, the parameter vectors $\boldsymbol{\delta}_s$ and $\boldsymbol{\vartheta}_s$ may be estimated by the projection of the adaptable basis functions as:

$$e^2[t, \widehat{\boldsymbol{\delta}}_{a|c}, \widehat{\boldsymbol{\vartheta}}_{a|c}] = \sum_{j=1}^{p_s} s_j \cdot G_{s(j)}[t, \boldsymbol{\delta}_s] = \boldsymbol{g}_s^T[t, \boldsymbol{\delta}_s] \cdot \boldsymbol{s} \tag{5.4.34}$$

which solved in the SNLS sense gives:

$$\widehat{\boldsymbol{\delta}_s} = \arg\min_{\boldsymbol{\delta}_s} \|\big(\boldsymbol{I} - \boldsymbol{G}_s(\boldsymbol{\delta}_s) \cdot \boldsymbol{G}_s(\boldsymbol{\delta}_s)^\dagger\big) \cdot \boldsymbol{e}_s(\widehat{\boldsymbol{\delta}}_{a|c}, \widehat{\boldsymbol{\vartheta}}_{a|c})\ \|^2 \tag{5.4.35}$$

subject to the constraints to the functional subspace parameter vector $\boldsymbol{\delta}_s$. In the above $\boldsymbol{g}_s[t, \boldsymbol{\delta}_s] = \big[G_{s(1)}[t, \boldsymbol{\delta}_s], \ldots G_{s(p_s)}[t, \boldsymbol{\delta}_s]\big]^T$, $\boldsymbol{G}_s(\boldsymbol{\delta}_s) = \big[\boldsymbol{g}_s[1, \boldsymbol{\delta}_s], \ldots, \boldsymbol{g}_s[N, \boldsymbol{\delta}_s]\big]^T$ and $\boldsymbol{e}_s(\widehat{\boldsymbol{\delta}}_{a|c}, \widehat{\boldsymbol{\vartheta}}_{a|c}) = \big[e^2[1, \widehat{\boldsymbol{\delta}}_{a|c}, \widehat{\boldsymbol{\vartheta}}_{a|c}], \ldots, e^2[N, \widehat{\boldsymbol{\delta}}_{a|c}, \widehat{\boldsymbol{\vartheta}}_{a|c}]\big]^T$. Of course, constraints on the functional subspace parameter vector $\boldsymbol{\delta}_s$ also apply in this case.

As before Phase B is completed by the estimation of the coefficient of projection vector $\boldsymbol{\vartheta}_s$ through the linear OLS estimator:

$$\widehat{\boldsymbol{\vartheta}}_s = \left(\boldsymbol{G}_s(\boldsymbol{\delta}_s)^T \cdot \boldsymbol{G}_s(\boldsymbol{\delta}_s)\right)^{-1} \cdot \left(\boldsymbol{G}_s(\boldsymbol{\delta}_s)^T \cdot \boldsymbol{e}_s(\widehat{\boldsymbol{\delta}}_{a|c}, \widehat{\boldsymbol{\vartheta}}_{a|c})\right) \tag{5.4.36}$$

The Instantaneous Standard Deviation (ISD) method. Based on the normality of the innovations sequence $E\{|e[t]|\} = \sqrt{2/\pi} \cdot \sigma_e[t]$ and by utilizing the absolute values of the estimated innovation series $e[t, \widehat{\boldsymbol{\delta}}_{a|c}, \widehat{\boldsymbol{\vartheta}}_{a|c}]$, the following overdetermined set of equations may be obtained

$$\left|e[t, \widehat{\boldsymbol{\delta}}_{a|c}, \widehat{\boldsymbol{\vartheta}}_{a|c}]\right| = \sqrt{\frac{2}{\pi}} \cdot \sum_{j=1}^{p_s} s_j \cdot G_{s(j)}[t, \boldsymbol{\delta}_s] = \boldsymbol{g}_s^T[t, \boldsymbol{\delta}_s] \cdot \boldsymbol{s} \tag{5.4.37}$$

which solved in the SNLS sense:

$$\widehat{\boldsymbol{\delta}}_s = \arg\min_{\boldsymbol{\delta}_s} \|\left(\boldsymbol{I} - \boldsymbol{G}_s(\boldsymbol{\delta}_s) \cdot \boldsymbol{G}_s(\boldsymbol{\delta}_s)^{\dagger}\right) \cdot |\boldsymbol{e}(\widehat{\boldsymbol{\delta}}_{a|c}, \widehat{\boldsymbol{\vartheta}}_{a|c})| \ \|^2 \tag{5.4.38}$$

subject to the constraints to the functional subspace parameter vector $\boldsymbol{\delta}_s$. In the above $\boldsymbol{g}_s[t, \boldsymbol{\delta}_s] = \sqrt{\frac{2}{\pi}} \cdot \left[G_{s(1)}[t, \boldsymbol{\delta}_s] \ldots G_{s(p_s)}[t, \boldsymbol{\delta}_s]\right]^T$ and $\boldsymbol{G}_s(\boldsymbol{\delta}_s) = \left[\boldsymbol{g}_s[1, \boldsymbol{\delta}_s], \ldots, \boldsymbol{g}_s[N, \boldsymbol{\delta}_s]\right]^T$.

Finally, the $\boldsymbol{\vartheta}_s$ estimator is obtained by the following equation:

$$\widehat{\boldsymbol{\vartheta}}_s = \left(\boldsymbol{G}_s(\boldsymbol{\delta}_s)^T \cdot \boldsymbol{G}_s(\boldsymbol{\delta}_s)\right)^{-1} \cdot \left(\boldsymbol{G}_s(\boldsymbol{\delta}_s)^T \cdot |\boldsymbol{e}(\widehat{\boldsymbol{\delta}}_{a|c}, \widehat{\boldsymbol{\vartheta}}_{a|c})|\right) \tag{5.4.39}$$

The Conditional Maximum Likelihood (CML) method. In regression type methods, estimation of the parameter vectors $\boldsymbol{\delta}_s$ and $\boldsymbol{\vartheta}_s$ may be achieved by maximizing the *conditional* log-likelihood function $\ln \mathcal{L}(\boldsymbol{\delta}_s, \boldsymbol{\vartheta}_s | \widehat{\boldsymbol{\delta}}_{a|c}, \widehat{\boldsymbol{\vartheta}}_{a|c}, x^N)$ of Eq. (5.4.6) with respect to $\boldsymbol{\delta}_s$ and $\boldsymbol{\vartheta}_s$, treating the estimated innovation sequence $e[t, \widehat{\boldsymbol{\delta}}_{a|c}, \widehat{\boldsymbol{\vartheta}}_{a|c}]$ provided by Phase A as measurements. The CML estimation also constitutes a constrained nonlinear optimization problem. Estimators of $\boldsymbol{\delta}_s$ and $\boldsymbol{\vartheta}_s$ based on the previous methods may be used for the initialization of this nonlinear optimization procedure.

Remarks: The same comments as in the estimation of the innovations variance coefficients of projection for the classical fully parametrized FS-TARMA model approach also apply in this case.

The estimation methods described in the preceding paragraphs are summarized in Table 5.4.2.

5.4.4 Model validation

Once a model has been obtained, it must be validated with respect to the assumptions behind the identification method used [Fassois, 2001a]. Although such validation may be based on various criteria depending on the model's intended use, the Gaussianity and in particular the whiteness of the identified model's one-step-ahead prediction error (innovations) sequence are parts of standard validation procedures. However, due to the TV nature of the model innovations variance, the usual innovation whiteness tests are not applicable. Although this hindrance may be overcome by standardizing the random sequence of $e[t]$ to $\epsilon[t]$ as follows [Fouskitakis and Fassois, 2002]:

$$\epsilon[t] = \frac{e[t]}{\sigma_e[t]}, \qquad \epsilon[t] \sim \mathrm{NID}(0, 1) \tag{5.4.40}$$

this procedure is heavily dependent on the accuracy of the innovations time-dependent variance estimation.

Alternatively, a relatively simple test based on the number of sign changes in the innovation sequence may be applied (residual sign test) [Poulimenos and Fassois, 2006], [Draper and Smith, 1998, pp. 192-198]. This test is based on the number of observed "runs", that is groups of sequential innovations with common sign (+ and −) in the estimated innovations sequence and examines whether the pattern of

Table 5.4.2: Parameter estimation methods.

	Classical Models				Adaptable Models			
	FS-TAR	**FS-TARMA**	**Innovations Variance or Std** parametric	**Innovations Variance or Std** non-parametric	**AFS-TAR**	**AFS-TARMA**	**Innovations Variance or Std** parametric	**Innovations Variance or Std** non-parametric
Maximum Likelihood	**ML** Maximum Likelihood	**ML** Maximum Likelihood	✓ (included)	✓ (included)	**ML** Maximum Likelihood	**ML** Maximum Likelihood	✓ (included)	✓ (included)
Regression methods	OLS Ordinary Least Squares	**OLS** Ordinary Least Squares	MW/IV/ISD/**CML**	MW/CML	**OLS** Ordinary Least Squares	**OLS** Ordinary Least Squares	**MW/IV/ISD/CML**	MW/CML
	RLS Recursive Least Squares	RELS Recursive Extended Least Squares	MW/IV/ISD/**CML**	MW/CML	**SNLS** Separable Nonlinear Least Squares	**2SSNLS** Two Stage SNLS	**MW/IV/ISD/CML**	MW/CML
		2SLS Two-Stage Least Squares	MW/IV/ISD/**CML**	MW/CML	**WLS** Weighted Least Squares	**WLS** Weighted Least Squares	**MW/IV/ISD/CML**	MW
	WLS Weighted Least Squares	**WLS** Weighted Least Squares	MW/IV/ISD/**CML**	MW	**SNWLS** Separable Nonlinear Weighted Least Squares	**2SSNWLS** Two Stage Separable Nonlinear Weighted Least Squares	**MW/IV/ISD/CML**	MW
	MS Multi Stage	**MS** Multi Stage	**CML** (included)	n/a[1]	**MS** Multi Stage	**MS** Multi Stage	**CML** (included)	n/a[1]
	RMS Relaxed Multi Stage	RMS Relaxed Multi Stage	MW/IV/ISD	MW				

n/a: not applicable.

[1] MS method concerns only the fully parametrized model forms.

Note: *the methods that include nonlinear optimization techniques are indicated in bold.*

Note: *a complete regression method is denoted as [Phase A method (initialization method if applicable)– Phase B method (initialization method if applicable)].*

runs is “unusual” for a zero-mean uncorrelated series or not. The test is based on a distribution-free hypothesis testing procedure.

Remarks: The typical validation procedure in stationary stochastic methods is based on the cross-validation principle, and presumes the availability of an additional data set, referred to as the validation set. This is usually obtained by splitting the data into estimation and validation sets, with the former used exclusively for estimation and the latter for validation [Fassois, 2001a]. However, such an approach is not applicable to non-stationary modelling as long as a model represents the underlying system or process only within the timespan for which it is identified.

5.5 Model Structure Selection Methods

5.5.1 Main ideas and criteria

Model structure selection is an optimization procedure according to which models corresponding to various candidate “structures” are estimated (via the methods of the previous section), and the one providing the *“best fitness”* to the non-stationary signal is selected.

Model “fitness” may be judged in terms of various criteria with the Residual Sum of Squares (RSS) [Boudaoud and Chaparro, 1987, Liporace, 1975]:

$$\text{RSS} = \sum_{t=1}^{N} e^2[t] \tag{5.5.1}$$

or the equivalent Mean Squared Error (MSE $=$ RSS$/N$), the negative Gaussian log-likelihood function (Eq. (5.4.1)), the Akaike Information Criterion (AIC) [Kozin and Nakajima, 1980, Clergeot, 1984]:

$$\text{AIC} = -2 \cdot \ln \mathcal{L}(\boldsymbol{\theta}|x^N) + 2 \cdot k \tag{5.5.2}$$

and the Bayesian Information Criterion (BIC) [Petsounis and Fassois, 2000, Thonet and Vesin, 1997]:

$$\text{BIC} = -\ln \mathcal{L}(\boldsymbol{\theta}|x^N) + \frac{\ln N}{2} \cdot k \tag{5.5.3}$$

being the more widely used. In the relations above k designates the number of independently adjusted model parameters, that is $k = \dim(\boldsymbol{\theta})$. The problem with the negative Gaussian log-likelihood function and the criteria related with the model's predictive ability (RSS and MSE) is that they may monotonically decrease with increasing model structure (that is models of higher orders and/or subspace dimensionalities), and as a result lead to overfitting. For this reason, criteria such as the AIC and the BIC are often preferred as they include a term that penalizes the model size (structural complexity) and thus they discourage model overfitting. It must be also noticed that the RSS and MSE criteria do not depend on $\boldsymbol{\vartheta}_s$ (and $\boldsymbol{\delta}_s$ for the AFS-TARMA model type) in contrast to the rest of the aforementioned criteria.

Although, one or more of the criteria just described may be used for the final model selection, the candidate models should also be checked in terms of statistical and numerical reliability. A criterion that is usually used as an indication of the statistical reliability is the Samples Per Parameter (SPP) criterion, that is the ratio of the number of samples N to the number of estimated parameters. For the latter issue of numerical reliability and for the regression type methods which usually include the inversion of a regression matrix, the condition number, that is the ratio of the maximum to the minimum eigenvalue of the matrix inverted should always be checked.

In general, FS-TARMA model structure selection is an intricate procedure; especially for the classical approach which is characterized by the maximum number of “structural” parameters. The main difficulty stems from the fact that except from the estimation of the AR and MA orders (which is necessary even for the simple stationary ARMA case), the model structure procedure involves the choice of a specific family of linearly independent basis functions and the appropriate functional subspaces $\mathcal{F}_{\text{AR}}$, $\mathcal{F}_{\text{MA}}$, and

$\mathcal{F}_{\sigma_e^2[t]}$. Even if this is only a small price to pay for rendering the estimation of a TARMA model into a time-invariant problem, the selection of the appropriate model structure parameters is of crucial importance for accurate modelling. This fact has been ignored by the majority of the studies on FS-TARMA models, which utilize either no model structure selection procedure or are based on heuristic procedures.

Despite the fact that theoretically an "extended" (of high dimensionality) functional subspace may achieve good tracking of the parameter evolution irrespectively of the selected family of basis functions [Walter, 1994, p. 77], this is not true when, due to reasons of statistical efficiency and model parsimony (economy of representation) only a small number of functions has to be selected. Therefore, an appropriate functional basis that will be able to describe the TV evolution of the model parameters adequately with the smallest possible number of basis functions, that is with the smallest appropriate subspace dimensionality, must be initially selected. Thus, every FS-TARMA model structure procedure begins with the choice of an appropriate family of basis functions.

In general, the selection of the basis function family may be based on prior knowledge regarding the evolution of the time-varying model parameters or physical understanding of the system to be identified. For instance, a trigonometric basis should normally be selected when periodic or quasi-periodic evolutions are expected while wavelets or Walsh functions should be chosen for the identification of a system characterized by abrupt changes in its properties. A first, however usually rough picture, of the TV parameters evolution that could potentially facilitate the choice of a specific basis functions family may also be provided by a non-parametric estimation of the Power Spectral Density (PSD) of the non-stationary signal under study (such as the spectrogram or the scalogram [Hammond and White, 1996]).

In cases where no-prior information is available or no indication stems from the use of an non-parametric PSD estimate, a good strategy is to use two or more families, obtain the best (according to the selected "fitness" function) under each one and finally select the globally optimum (best) model.

Once a specific family of basis functions for the expansion of the TV parameters has been selected, the remaining model structure selection procedure for a parametric FS-TARMA model concerns the determination of the set of $p_a+p_c+p_s+2$ integers ($\mathcal{M}=\{n_a,n_c,\boldsymbol{d}_a,\boldsymbol{d}_c,\boldsymbol{d}_s\}$) for obtaining the best fitting model or p_a+p_c+2 integers ($\mathcal{M}=\{n_a,n_c,\boldsymbol{d}_a,\boldsymbol{d}_c\}$) for a semi-parametric. The corresponding model structure for a parametric AFS-TARMA model and a given family of adaptable basis functions concerns the set of five integers ($\mathcal{M}=\{n_a,n_c,p_a,p_c,p_s\}$) or four ($\mathcal{M}=\{n_a,n_c,p_a,p_c\}$) for the semi-parametric case. Thus, in general model structure selection may be viewed as a discrete optimization problem that may be tackled via one of the following schemes.

5.5.2 Integer optimization scheme

This is a hybrid optimization scheme consisting of two distinct phases [Poulimenos and Fassois, 2003b, Poulimenos and Fassois, 2006].

Phase I. Coarse ("global") Optimization. Phase I aims at determining promising subregions of the complete search space within which optimal model "structures" (either in the local or global sense) might be located. This is achieved via a *Genetic Algorithm* [Coley, 1999] which minimizes the AIC/BIC ("fitness" function).

GA starts with the random creation of an initial population of individual solutions, which constitute the first generation. At each generation GA selects the best, in terms of the "fitness" function criterion, individuals to be parents, and uses them to produce the children (individuals) for the next generation through crossover and mutation rules. In this way GA evolves toward an optimal solution, imitating the natural selection process of biological evolution.

Phase II. Fine ("local") Optimization. Phase II aims at refining the results of phase I and selecting the globally optimum "structure" based on the concept of *backward regression*. It thus operates in a neighbourhood of phase I solution and reduces either one of the model orders (n_a,n_c), or one of the subspace dimensionalities (p_a,p_c,p_s), until no further reduction in the AIC/BIC is achieved. The procedure is repeated for all initial solutions (phase I results), and the model "structure" corresponding

to the globally optimum AIC/BIC is selected.
Remarks:

(i) The most important advantage of the scheme is that it is automated. Yet, at the same time and depending upon the occasion, this may be a disadvantage as the search is exclusively based upon the "fitness" function and may lead to overparameterizations.

(ii) Even though GAs are capable of solving difficult optimization problems with local extrema, their configuration necessities the selection of a number of algorithmic characteristics (such as crossover and mutation ratios, and the number of elite children [Coley, 1999]), which highly affect their performance. Moreover, problems of premature convergence to local extrema may also be observed in cases of high dimensional search spaces. In such cases, the adoption of more exhaustive search schemes is proposed; for instance optimal "structural" parameters may be sought for each selected model orders pair (n_a, n_c), with the overall optimal model being finally selected.

(iii) The population individuals are bit strings whose length depends on the initial search space. For instance, four bits are required in order to describe an initial search space of $n_a \in \{1, \ldots, 16\}$ since this set of integers may be assigned to the set of bit strings $\{0000_2, \ldots, 1111_2\}$ which consists of the same number of elements. Respectively, for the AFS-TARMA model structure selection problem the initial search space of the AR functional subspace dimensionality $p_a \in \{1, \ldots, 8\}$ would require three bits for its description.

In the FS-TARMA case, and for the hypothetical scenario of searching for the AR functional subspace among the first five functional basis of an appropriate family, that is initial search space $\{G_0[t], G_1[t], G_2[t], G_3[t], G_4[t]\}$, five bits will be required for its description with each bit denoting the existence (1) or not (0) of the corresponding basis function in the specific model structure.

(iv) A similar scheme that may be used within the AFS-TARMA approach is proposed in Chapter 4. According to this a Particle Swarm Optimization (PSO) algorithm [Engelbrecht, 2006, Part III] is employed in order to search simultaneously for both the functional subspace parameters ($\boldsymbol{\delta}$'s) and the model structure parameters $\mathcal{M}$ in a combined search space.

5.5.3 Regression schemes

A number of model structure selection methods proposed in the literature are based on the regression concept. These may be divided in two main categories: a) those based on the concept of *backward regression* and b) those based on the inverse concept of *forward regression*. Methods of the former category start by considering an initial FS-TAR/FS-TARMA (or AFS-TAR/AFS-TARMA) model of high orders and high subspace dimensionalities in order to assure model adequacy for representing the non-stationary signal. Subsequently, they attempt to reduce the model dimensionality by rejecting (one at a time) the insignificant terms (basis functions). On the contrary, methods based on the forward regression concept start with a low dimension model and construct the final model structure by adding one at a time the significant terms. In both cases, the significance of a specific term may be judged by various criteria while various schemes have been proposed for the reduction or augmentation of the initial model.

5.5.3.1 Backward regression schemes

The first method based on the backward regression concept was proposed by Tsatsanis and Giannakis [Tsatsanis and Giannakis, 1993]. According to the procedure they proposed the reduction of the basis functions is realized by the means of an appropriate F-test that actually compares, in a statistical sense, the RSS values obtained by a model that includes a specific basis function and by a second one obtained by the removal of the latter accounting also for the dimensionality of the candidate models. In the same study the use of the AIC or the Final Prediction Error (FPE) criterion instead of the F-test was proposed, since the drawback related with the selection of an appropriate threshold, and the subjectivity of such a selection, that is required for the F-test was recognised by the authors. In the AIC or FPE based scheme, terms whose removal causes reduction in the criterion values are rejected until the minimum is achieved.

This scheme is exhaustive as it considers uncommon functional subspaces for the time-dependent parameters with the whole procedure being very time-consuming particularly for initial models of high initial orders and large functional subspaces. A simplified scheme that attempts to approximately decompose the "structure" selection problem into two subproblems: (i) the *model orders* (n_a, n_c) selection, and (ii) the *functional subspaces* selection $[\boldsymbol{d}_a, \boldsymbol{d}_c, \boldsymbol{d}_s]$ was proposed in [Poulimenos and Fassois, 2006, Poulimenos and Fassois, 2009a]. This scheme consists of two phases as follows:

Phase I. Model Orders Selection. In order to "decouple" the selection of the model orders from that of functional subspaces, their interaction has to be minimized. This may be achieved by ensuring functional subspace adequacy by initially adopting an "extended" (high dimensionality) and "complete" (in the sense of including all consecutive functions up to the subspace dimensionality) functional subspaces. Using them, model order selection may be achieved through trial and error techniques based on the optimization of the fitness function (typically the AIC or the BIC).

Phase II. Functional Subspace Selection. The aim of this phase is the optimization of the "extended" (redundant) functional subspaces, in the sense of increasing the representation parsimony without significantly reducing model accuracy. This may be accomplished via trial and error techniques detecting "excess" basis functions by using the "fitness" function (the AIC or the BIC). Basis functions may be thus consecutively dropped (one at a time) as long as no significant values of the criterion employed are produced.

Remarks:

(i) From a practical standpoint the simplified two-phase scheme is effective, as it is simple to implement, of low computational complexity, and "flexible" in accounting for user provided "structural" information. However both backward regression method may be considered as suboptimal, in the sense that it may not provide the globally optimal model "structure". Their main limitation is associated with the use of models with "extended" and "complete" functional subspaces. These will typically be highly overparameterized, and the estimation of the associated high number of coefficients of projection may pose statistical difficulties (in the sense that the number of available signal samples may be inadequate for this purpose).

(ii) For the implementation of the second phase of the scheme, that is the detection of the "excess" basis functions, the use of a measure for the aggregate deviation of the parameter trajectories has also been proposed [Poulimenos and Fassois, 2006]. However, as in the F-test case the main limitation of this approach is the additional requirement for the subjective selection of appropriate threshold.

5.5.3.2 Forward regression scheme

This scheme introduced by Wei and Billings [Wei and Billings, 2002] was initially proposed for the equally complicated structure selection problem of stochastic nonlinear ARMAX models [Chen et al., 1989]. Is based on the orthogonal least squares algorithm in order to transform al linear regression model into an auxiliary model given as

$$\boldsymbol{x} = \boldsymbol{\Psi} \cdot \boldsymbol{\eta} + \boldsymbol{e}(\boldsymbol{\eta}) \tag{5.5.4}$$

where $\boldsymbol{\Psi}$ is a transformed regressor matrix consisting of orthogonal columns such as $\boldsymbol{\psi}_i \cdot \boldsymbol{\psi}_j = 0$ for $i \neq j$ and $i, j = 1, \dots, n_a p_a + n_c p_c$, while $\boldsymbol{\eta}$ is the corresponding transformed coefficients of parameter vector. The orthogonalization of the initial regression model may be realized by applying the Gram-Schmidt procedure as described in [Chen et al., 1989].

The orthogonality of the transformed regressors permits estimating the novel parameters η_i one at a time. As a consequence, the significance of each regressor term towards the reduction in the total mean square error may be quantified through the Error Reduction Ratio (ERR):

$$\mathrm{ERR}_i = \frac{\hat{\eta}_i^2 \left(\boldsymbol{\psi}_i^T \cdot \boldsymbol{\psi}_i\right)}{\sum_{t=1}^{N} x^2[t]} \tag{5.5.5}$$

The larger the value of ERR, the more significant the term will be in the final model, while terms with low ERR values may be excluded as trivial.

Nevertheless, simply orthogonalizing candidate terms in an arbitrary order may result in incorrect information regarding the significance of terms, since the ERR values depend on the order in which candidate terms are orthogonalized. In order to overcome this problem, the Orthogonal Forward Regression (OFR) algorithm [Chen et al., 1989] may be utilized. OFR arranges the candidate model terms in the order of significance and provides a simple method of selecting the most relevant model terms. The selection procedure is completed when:

$$1 - \sum_{i=1}^{N_r} \mathrm{ERR}_i < \rho \tag{5.5.6}$$

where $\rho (0 < \rho \leq 1)$ is a desired tolerance, and N_r the number of the finally selected regressors.
Remarks:

- ***(i)*** The ideal tolerance ρ is case dependent and not known a-priori. Thus, its value has to be found by trial and error.
- ***(ii)*** The termination criterion of Eq. (5.5.6) does not take into account model complexity. Alternatively, criteria such as the AIC or BIC could be employed with significant model terms being added to the final model as long as their inclusion entails a reduction of these criteria.
- ***(iii)*** The forward regression method builds FS models with uncommon functional subspaces. But in contrast to the backward regression methods this is not accomplished at the price of increased computational times.
- ***(iv)*** For the FS-TARMA case OFR algorithm may be used only within the second stage of the 2SLS method as long as the initial regressor $\boldsymbol{\Phi}$ must be given. For the AFS-TAR it may be used only after the estimation of the functional subspace parameter vector $\boldsymbol{\delta}_a$ and the formation of the regressor matrix $\boldsymbol{\Phi}(\boldsymbol{\delta}_a)$. Respectively, for the AFS-TARMA case it may be used only within the 2SSNLS method and after the estimation of the functional subspace parameter vectors $\boldsymbol{\delta}_a$ and $\boldsymbol{\delta}_c$ and the formation of the regressor matrix $\boldsymbol{\Phi}(\boldsymbol{\delta}_{a|c}, \widehat{\boldsymbol{\delta}}_q, \widehat{\boldsymbol{\vartheta}}_q)$.
- ***(v)*** The idea of using an inverse "bottom-up" procedure based on forward regression, that is constructing the model by adding basis functions terms to a model of low dimension was also proposed by Tsatsanis and Giannakis in [Tsatsanis and Giannakis, 1993] and extended in [Tsatsanis, 1995].
- ***(vi)*** A similar scheme has been proposed by Zou et al. in [Zou et al., 2003] who also try to find the linearly independent regressors from a pool of candidate vectors. However, they test the candidate terms in an arbitrary order, so their approach could be characterized as suboptimal.

5.6 The TAR Case: A Monte Carlo Study and Comparison

The FS-TAR model parameter estimation and structure selection methods reviewed in Sections 5.4 and 5.5 are presently applied to the identification problem of a TAR(6) model with piecewise polynomial TV parameters. For this purpose 200 Monte Carlo experiments are performed based on an equal number of realizations of the model's response. The methods performance is judged in terms of various criteria regarding tracking of the TV parameters, time-frequency representation accuracy, predictive ability and others.

5.6.1 The signals

The true TV parameters of the considered TAR(6) model were selected pointwisely and depict variability characterized by transitions between smooth and abrupt changes of their values (Fig. 5.6.1).

The model's "frozen-time" PSD and the corresponding global modal characteristics (natural frequencies and damping ratios) are illustrated in Fig. 5.6.2. The simulated model is characterized by three almost equally strong TV modes with their damping ratios taking values between 0.01 and 0.05.

The identification of the true model is based on 4000-sample long realizations of its responses. For each Monte Carlo run a different realization is used which is produced by different excitation signals – different seed numbers are used to produce stationary white noise sequences which are subsequently multiplied by the true time-dependent standard deviation of the model. A typical response signal realization is depicted in Fig. 5.6.3.

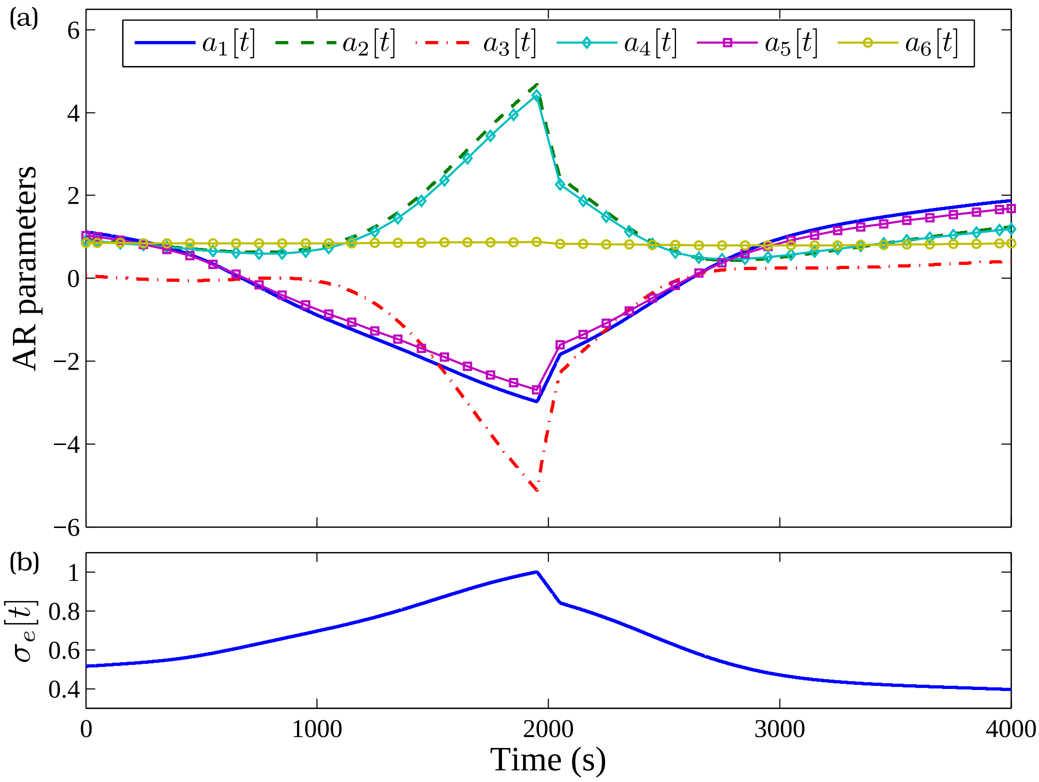

Figure 5.6.1: The true TAR(6) model parameters: (a) AR and (b) innovations standard deviation.

5.6.2 Identification results

The main FS-TAR identification results are now presented. Special emphasis is placed on model structure selection by using the schemes outlined in Section 5.5. The true AR model order and the type of parameters evolution are considered unknown. For this reason the correct AR order is searched within the range $n_a \in [5, 12]$ while various families of basis functions are considered. Specifically, for the classical FS-TAR approach the Discrete Cosine Transform (DCT) basis functions, Legendre polynomials, uniform B-splines of order equal to three, and Haar functions are utilized (see Appendix A). Non-uniform B-splines with a-priori unknown knots are utilized for the AFS-TAR models, while in both cases parametric models are considered. Relations for the construction of the bases used are given in A.6.

The algorithmic details for the model structure selection methods presently used are indicated in Table 5.6.1. All methods are based on the BIC criterion, while the OLS-ISD regression method is used for the estimation of the coefficients of projection parameter vectors $\boldsymbol{\vartheta}_a$ and $\boldsymbol{\vartheta}_s$ of the FS-TAR models,

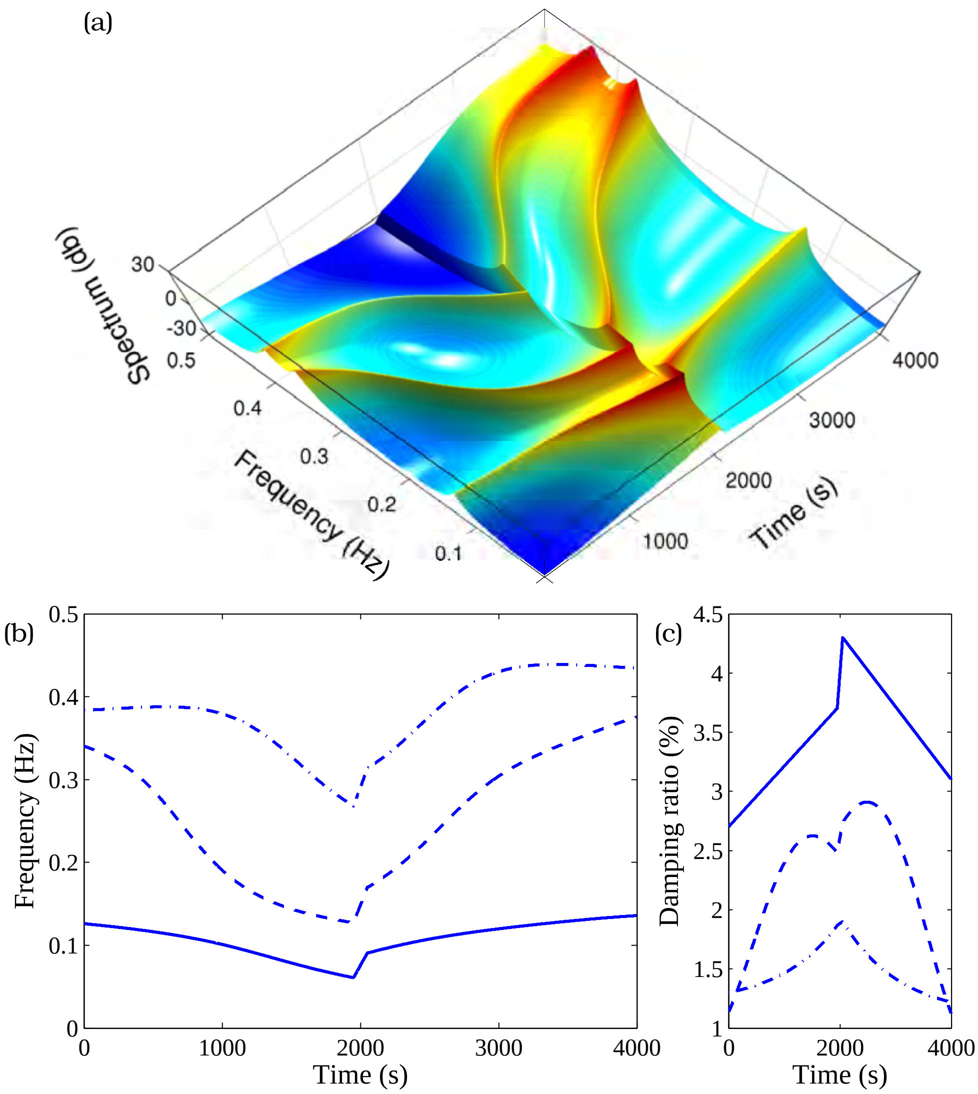

Figure 5.6.2: "Frozen-time" analysis of the true TAR(6) model: (a) power spectral density, (b) natural frequencies and (c) damping ratios.

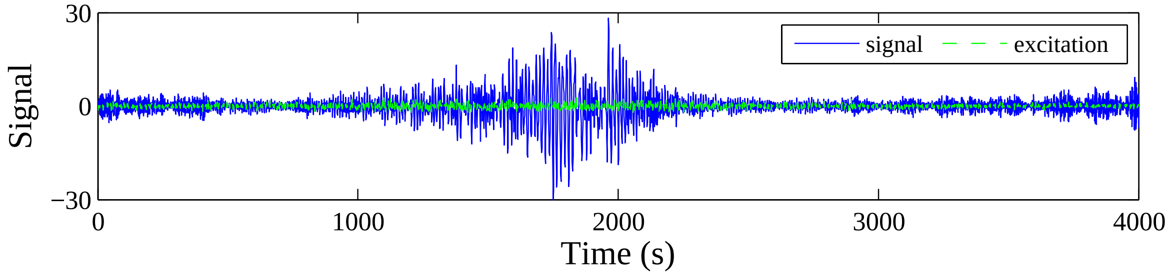

Figure 5.6.3: A single realization of the non-stationary response signal of the true TAR(6) model.

while the SNLS-ISD regression method is used for the estimation of the functional subspace parameter vectors $\boldsymbol{\delta}_a, \boldsymbol{\delta}_s$ and the corresponding coefficients of projection vectors $\boldsymbol{\vartheta}_a, \boldsymbol{\vartheta}_s$ of the AFS-TAR models. The algorithms, the MATLAB functions and the termination rules used for the optimization problems that the aforementioned estimation methods and the methods used in the sequel involve are summarized in Table 5.6.2.

Model structure selection. Starting with the simplified model structure selection scheme based on

Table 5.6.1: Model structure selection methods and algorithmic details.

	Method	Functional basis	Algorithmic details
FS-TAR	Integer Optimization	Discrete Cosine Transform (DCT) functions Legendre polynomials Uniform B-splines (order $k = 3$) Haar functions	Genetic Algorithm (MATLAB *ga* function), population size = 100, elite children = 5, crossover fraction = 0.8, mutation rate = 0.2, stall generation limit = 20
	Backward Regression		
	Forward Regression		
AFS-TAR	Integer Optimization	Non-uniform B-splines (order $k = 3$)	Particle Swarm Optimization (MATLAB *pso* function), population size = 100, inertia weight w = 1, cognitive parameter c_1 = 1.45, social parameter c_2 = 1.45, stall generation limit = 20

Table 5.6.2: Optimization method details.

Optimization method	Optimization algorithm	Termination rules $\lVert\hat{\boldsymbol{\vartheta}}_i - \hat{\boldsymbol{\vartheta}}_{i-1}\rVert$	$\lVert f(\hat{\boldsymbol{\vartheta}}_i) - f(\hat{\boldsymbol{\vartheta}}_{i-1})\rVert^{\dagger}$
Linear Least Squares	QR implementation (Matlab *mldivide* function)	–	–
Nonlinear Least Squares	Levenberg-Marquardt method (Matlab *lsqnonlin* function)	$< 10^{-9}$	$< 10^{-6}$
ML	BFGS Quasi-Newton method (Matlab *fminunc* function)	$< 10^{-8}$	$< 10^{-3}$
CML	BFGS Quasi-Newton method (Matlab *fminunc* function)	$< 10^{-12}$	$< 10^{-6}$

$^{\dagger}\boldsymbol{\vartheta}$: parameter vector to be estimated, $f(\cdot)$: nonlinear cost function, $\lVert\cdot\rVert$: Euclidian norm, i: iteration number
BFGS: Broyden-Fletcher-Goldfarb-Shanno method

the concept of backward regression and for the classical FS-TAR model, initial "extended" functional subspaces dimensionalities p_a and p_c equal to 21 are selected for its first phase. The mean, over 200 runs, values of the BIC, AIC, and the RSS/SSS obtained by the estimated FS-TAR$(n_a)_{[21,21]}$ $(n_a = 5, \ldots, 12)$ models are depicted in Fig. 5.6.4. In the same figure the mean condition numbers of the regressor matrix $\mathbf{\Phi}$ – whose inversion is involved during OLS estimation – are also shown. It must be noted that the SPP value for the FS-TAR$(12)_{[21,21]}$ models which are characterized by the maximum number of parameters among the models considered ($k = n_a \cdot p_a + p_s = 12 \cdot 21 + 21 = 273$) equals to 14.65. This value may be considered as low but not prohibitive with respect to the statistical reliability of the estimators.

Evidently, with these "extended" subspaces, the models with parameters expanded on one of the first three families attain more or less the same performance, while those with parameters expanded on Haar basis functions show inferior performance. This result, confirms practically the fact that the modelling accuracy of an FS model depends on the choice of the subspace and not on the particular choice of the basis functions family. Thus, bases with similar characteristics, in the particular case basis functions characterized by smooth evolution, and "extended" subspace dimensionality offer the same potential for accurate modelling. On the other hand, the square-shaped Haar functions do not seem capable of good tracking of the TV parameters, despite the fact that the latter show an abrupt change for a small region of time.

Nonetheless, irrespectively of the basis function family considered, the FS-TAR$(6)_{[21,21]}$ model achieves the minimum BIC. Even though in general AIC is known to suffer from the problem of overfitting, in this case study the AIC also indicates the correct AR order. On the other hand, as expected the RSS/SSS

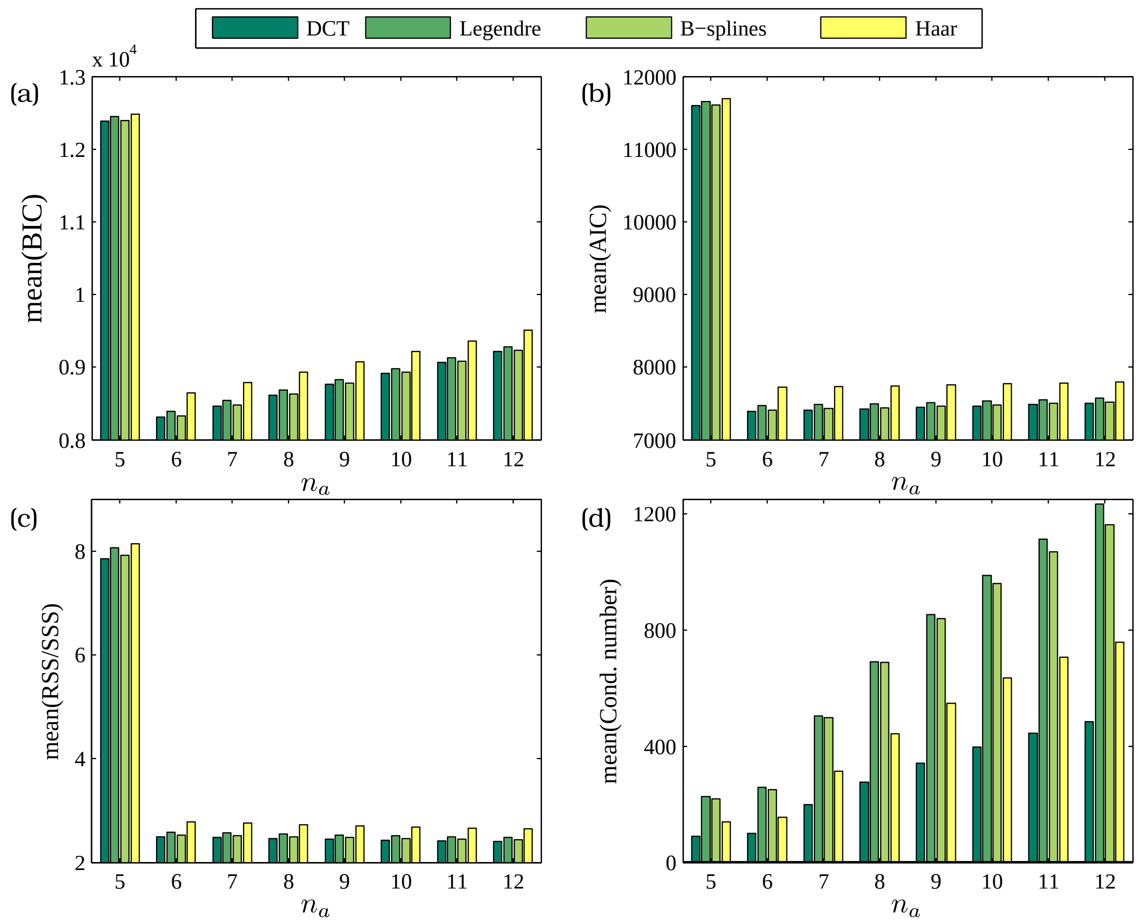

Figure 5.6.4: FS-TAR model structure selection (backward regression search scheme – phase I). Mean values of the (a) BIC, (b) AIC, (c) RSS/SSS and (d) condition number of the regressor matrix $\mathbf{\Phi}$ versus AR order for OLS-ISD estimated FS-TAR$(n_a)_{[21,21]}$ models and various functional families (the first 21 functions of each family are used $p_a = p_s = 21$).

criterion depicts a descending trend for increasing AR orders. It must be noted that special concern should be given to the selection of the "extended" subspaces used in the first phase of the backward regression scheme. An excessive number of basis functions may lead to a regressor matrix with large condition number and thus numerical problems.

After the selection of the appropriate AR order ($n_a = 6$), the second phase of the model structure selection scheme focuses on the reduction of the functional subspaces by rejecting the basis functions whose removal entails reduction of the BIC. The procedure is repeated for every run and leads to 200 models FS-TAR$(6)_{[p_a,p_s]}$ for every family of basis functions. The BIC values obtained by the estimated models during this phase are shown in Fig. 5.6.5. The results lead to the selection of the DCT functional basis. In Fig. 5.6.6 the frequency of observations for the AR and innovations standard deviation subspaces dimensionality p_a and p_s respectively, and the corresponding frequency of existence of the functional basis into the finally selected subspaces are shown. According to these results an FS-TAR$(6)_{[10,6]}$ with parameters expanded on subspaces defined by DCT basis functions with indices $\boldsymbol{d}_a = [1,\ldots,10]^T, \boldsymbol{d}_s = [1,\ldots,5,7]^T$ should be selected as the most appropriate to model the system under study. It must be noted that, even if the FS-TAR$(6)_{[p_a,p_s]}$ models with parameters expanded on Haar functions attain better RSS/SSS values, that is better predictive ability, this is achieved by using the initial extended functional subspace of 21 basis functions as none of the candidate functions is rejected during the second phase of the scheme.

On the contrary, the forward regression scheme based on the BIC employed for the selection of the

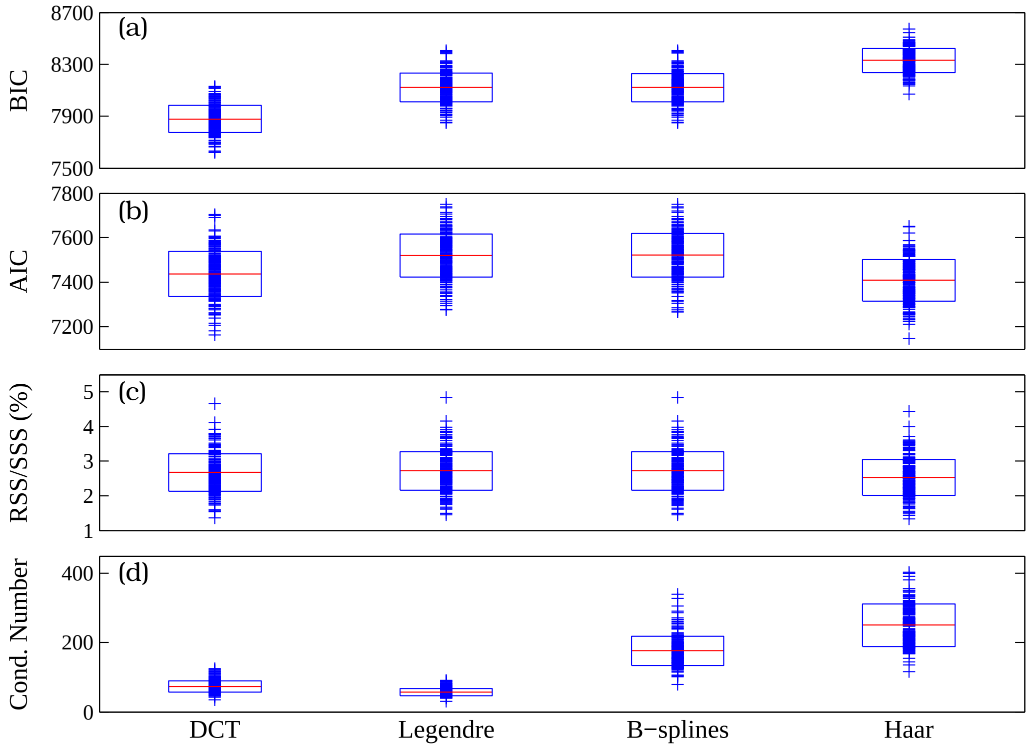

Figure 5.6.5: FS-TAR model structure selection (backward regression search scheme – phase II): (a) BIC, (b) AIC, (c) RSS/SSS, and (d) regressor condition number values of the models identified during the second phase of the method for OLS-ISD estimated FS-TAR(6) models and various families of basis functions (Mean $\pm$ one std values of the criteria are shown with boxes).

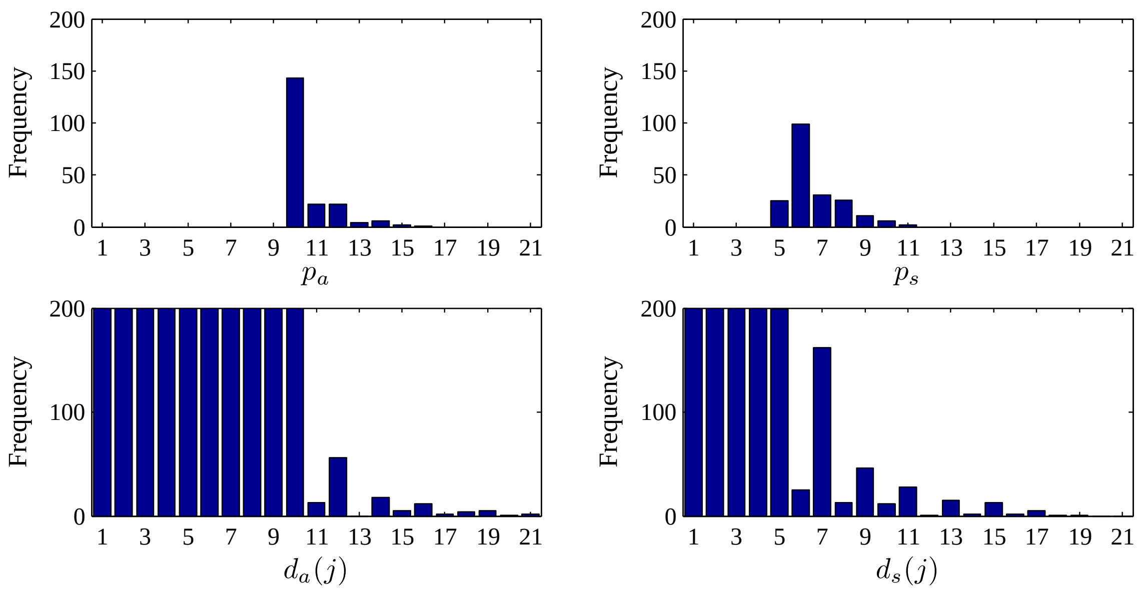

Figure 5.6.6: FS-TAR model structure selection (backward regression search scheme – phase II): The frequency of observations for the AR and innovations standard deviation subspace dimensionalities and the corresponding basis indices (DCT basis functions).

most significant terms from the regressor matrix of an initial FS-TAR$(12)_{[21,21]}$ model was not capable of correctly estimating the true AR order $n_a = 6$ for any of the functional bases considered (Fig. 5.6.7). Specifically in percentages over 90 % the specific model structure method selects as significant regressors

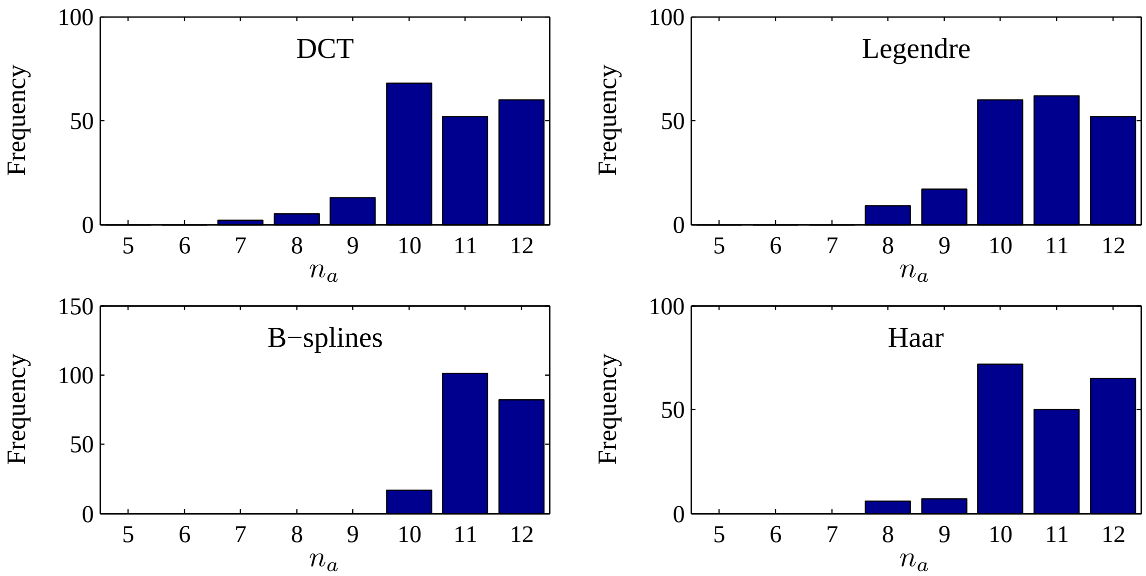

Figure 5.6.7: FS-TAR model structure selection (forward regression scheme): AR orders frequency of observations for each family of basis functions considered.

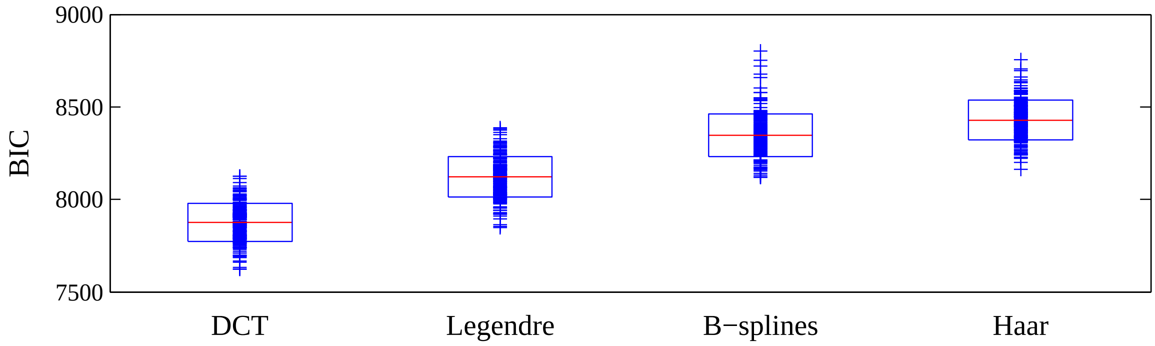

Figure 5.6.8: FS-TAR model structure selection (integer optimization scheme): BIC values of the models obtained for OLS-ISD estimated FS-TAR(6) models and various functional families.

that correspond to AR orders between 10 and 12.

However, for an initial FS-TAR$(6)_{[21,21]}$ model the method estimates similar functional subspaces with those obtained by the previous method. The results were worse when the criterion of Eq. (5.5.6) based on ERR was used.

Figure 5.6.8 depicts the results of the integer optimization based model structure selection. The scheme is based on a genetic algorithm and the OLS-ISD method for each family of basis functions considered in order to find the optimal AR order and functional subspaces. The initial search space for the AR order is as before $n_a \in [5, \ldots, 12]$ while the optimal functional subspaces are searched among the first 21 basis function of each family. The obtained BIC values shown in Fig. 5.6.9 agree with those of the previous analysis as the minimum BIC is achieved by the DCT FS-TAR models, while the histograms with the frequency of observations indicate the same functional subspaces as more appropriate (Fig. 5.6.8). It is also noted that the correct AR order is selected 199 times for the DCT and Legendre bases, 165 times for the B-splines basis and 200 times out of 200 for the Haar.

An integer optimization scheme based on the PSO algorithm is also employed for the model structure selection problem in the case of AFS-TAR models with parameters expanded on non-uniform B-spline basis functions with a-priori unknown internal knots. It is reminded that for this approach the model structure is defined only by the model orders n_a, and the basis dimensionalities p_a, p_s, since for a given basis dimension the corresponding functions are not selected but constructed based on the estimates

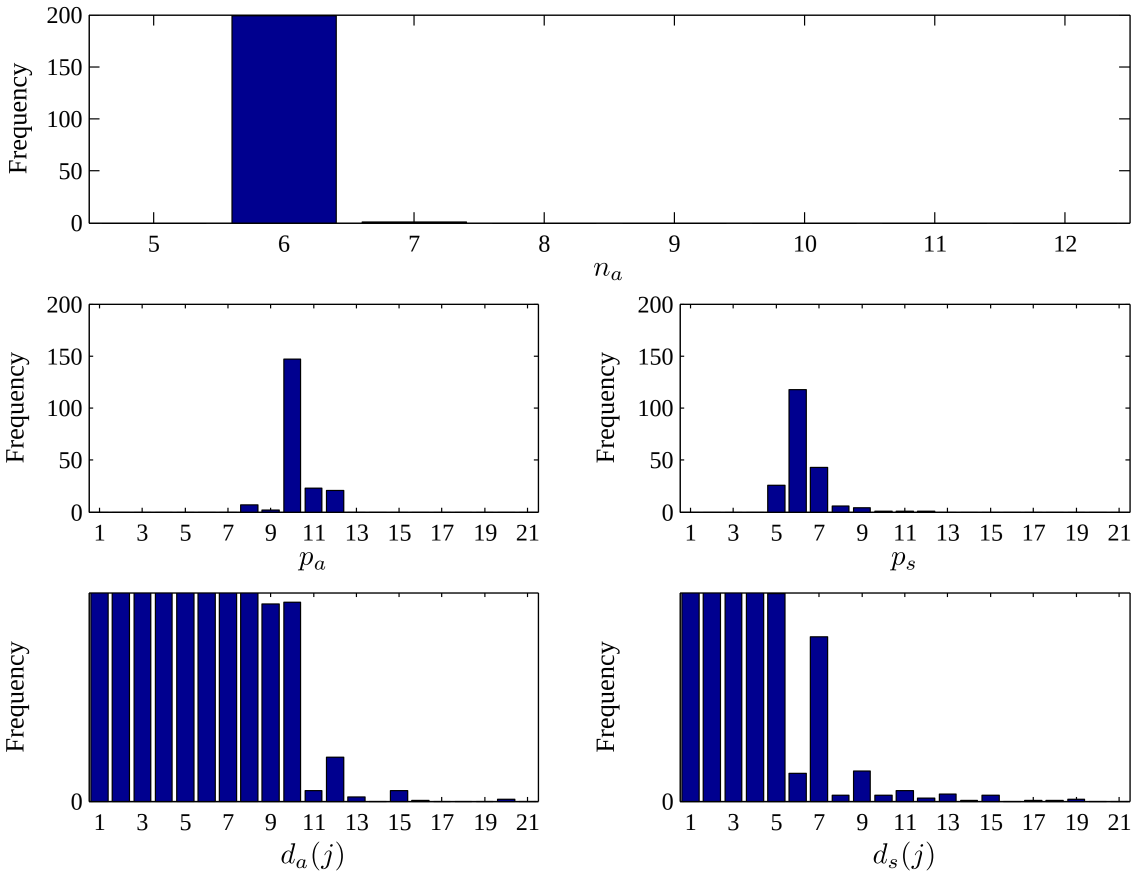

Figure 5.6.9: FS-TAR model structure selection (integer optimization scheme): The frequency of observations for the AR order, the AR and the innovations standard deviation subspace dimensionalities and the corresponding basis indices (DCT basis functions).

of the functional subspace parameter vectors $\boldsymbol{\delta}_a$ and $\boldsymbol{\delta}_s$. The results for the estimated n_a, and p_a, p_s in this case depict a higher variability (Fig. 5.6.10). Although, the correct AR order is the most frequently selected while a second phase based on the backward regression finally leads to an AFS-TAR$(6)_{[8,8]}$ model for all the test cases. This model is compared to the DCT FS-TAR$(6)_{[10,6]}$ model selected by the previous schemes in the subsequent analysis and the model parameter estimation results.

Model parameter estimation. Firstly, a comparison of the methods for the estimation of the innovations variance coefficient of projection vector $\boldsymbol{\vartheta}_s$ within the context of classic FS-TAR models is performed. Particularly, the MW, IV, ISD and CML(ISD) methods are applied on the residuals of the OLS estimated DCT FS-TAR$(6)_{[10,p_s]}$ models. The mean BIC values achieved are presented in Fig. 5.6.11(a). It must be noted that the functional subspaces for the MW method and the IV method in which the innovations variance is expanded on functional basis are also selected based on the integer optimization model structure selection scheme. The obtained functional subspace consists of 12 basis functions ($\boldsymbol{d}_s = [1, \ldots, 9, 11, 13, 15]^T$), that is the double number of basis functions compared to those selected for the ISD method ($\boldsymbol{d}_s = [1, \ldots, 5, 7]^T$). This result comes as no surprise since the variance depicts higher variability than its square root, that is the standard deviation and normally this higher variability will require more basis functions for its accurate description. For this reason, the ISD method achieves lower BIC values, while this value is of course improved when the CML nonlinear optimization is employed for the refinement of the parameter vector $\boldsymbol{\vartheta}_s$. For this reason, the ISD method is preferred in the sequel, while the CML(ISD) method is used for ML refinement of $\boldsymbol{\vartheta}_s$ whenever this is required.

It is reminded that the necessity for window length (K) selection for the MW is an additional potential drawback for this method (an optimization procedure based on BIC presently leads to $K = 250$ which

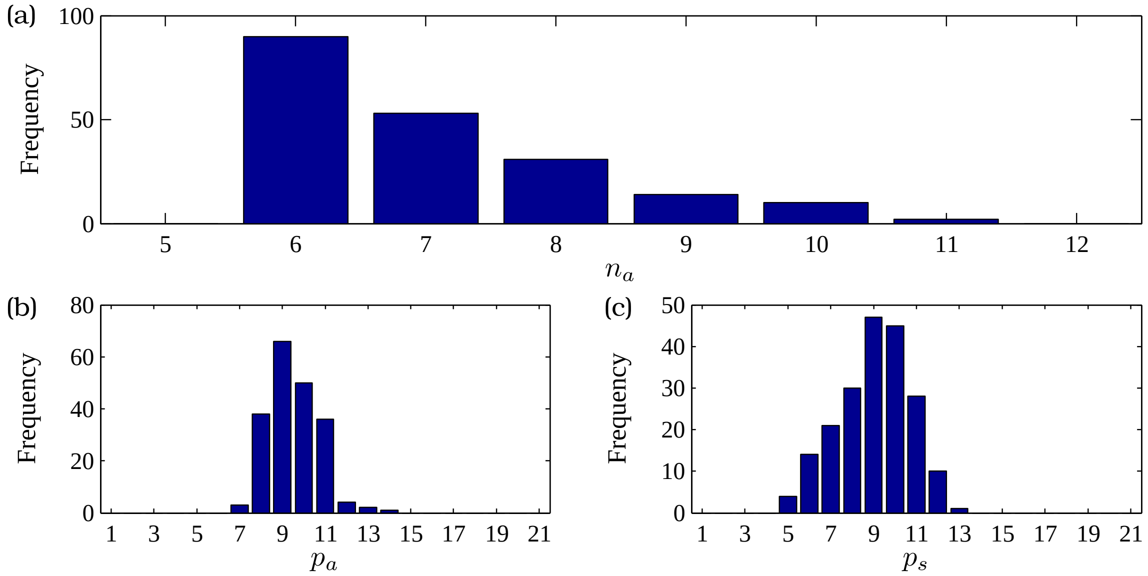

Figure 5.6.10: AFS-TAR model structure selection (integer optimization scheme based on PSO algorithm; non-uniform B-splines basis functions): The frequency of observations for (a) the AR order, (b) the AR functional subspaces dimensionality, and (c) the innovations standard deviation functional subspace dimensionality.

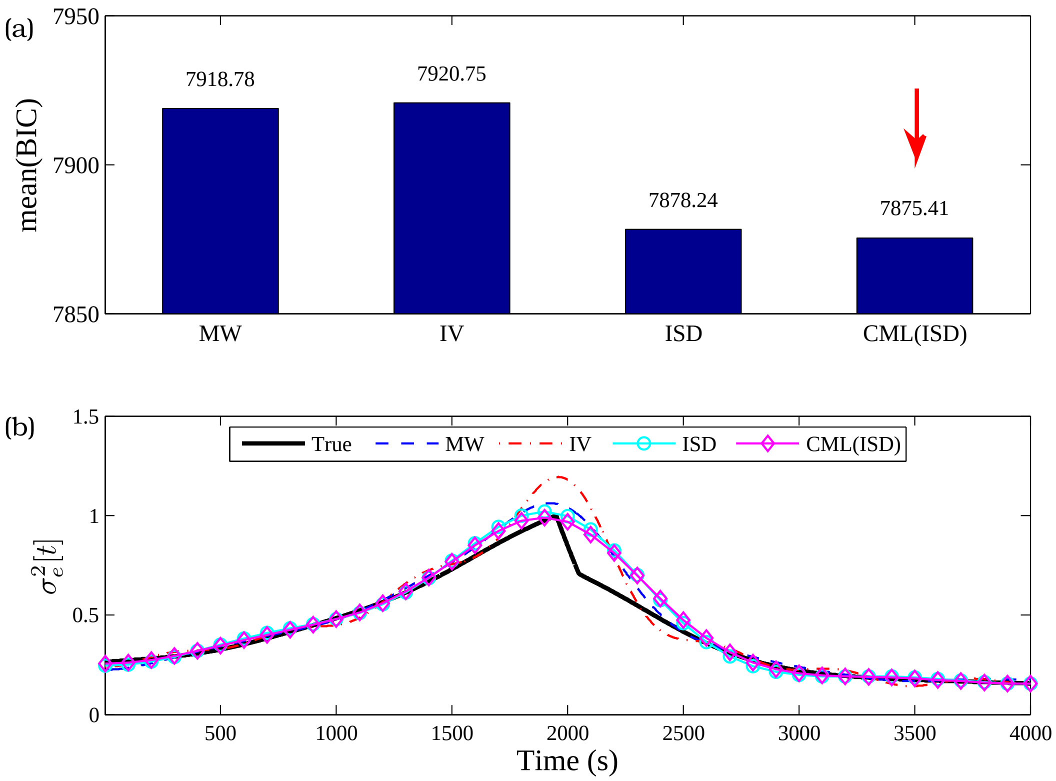

Figure 5.6.11: Comparison of methods for innovations variance coefficient of projection estimation: (a) mean BIC values, and (b) mean estimated innovations variance versus time contrasted to the true variance of the model's excitation (OLS estimated DCT FS-TAR$(6)_{[10,p_s]}$ models; $p_s = 12$ for MW and IV and $p_s = 6$ for ISD and CML).

was used for the methods compared; see Fig. 5.6.12).

The performance of the various FS-TAR estimation methods considered for the parameter estimation

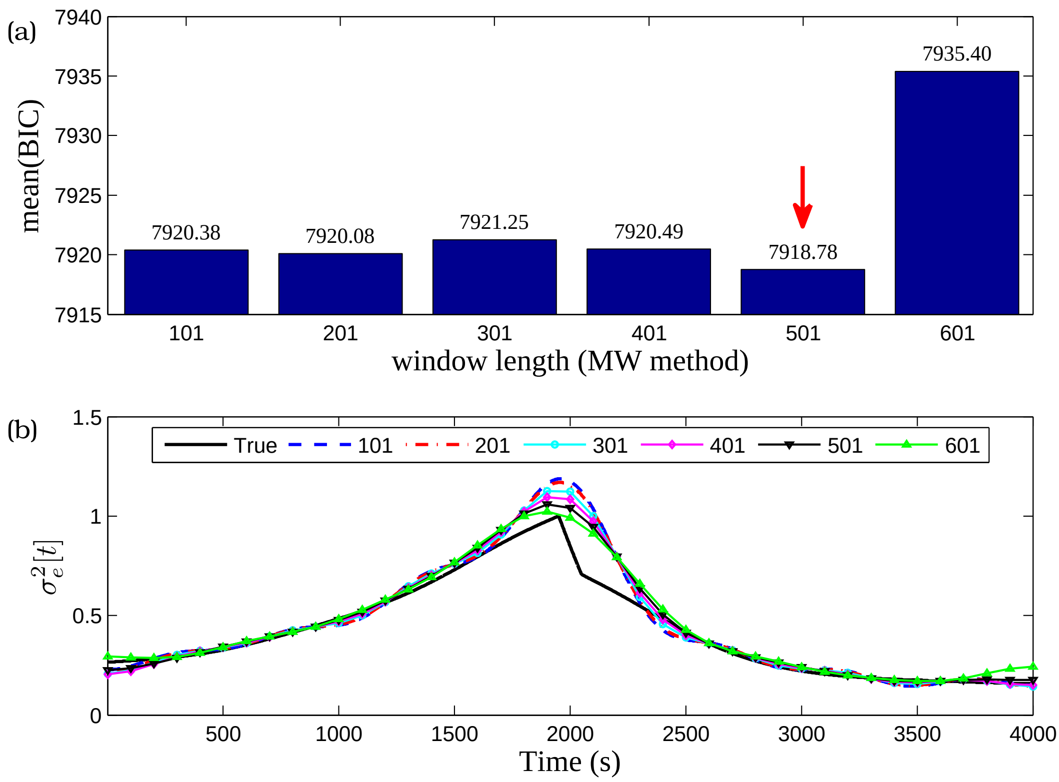

Figure 5.6.12: Optimization procedure for the selection of the window length parameter K (MW method for the coefficient of projection estimation): (a) mean BIC values, and (b)mean estimated innovations variance versus time for the various windows considered contrasted to the true variance of the system's driving noise. (DCT FS-TAR$(6)_{[10,12]}$ models; OLS estimation).

of a DCT FS-TAR$(6)_{[10,6]}$ model and a non-uniform B-splines AFS-TAR$(6)_{[8,8]}$ model is judged in terms of BIC, RSS/SSS and normalized execution times in Fig. 5.6.13 (it is reminded that the RSS/SSS doesn't depend on ϑ_s and ϑ_s). As it may be observed, the SNLS-ISD estimated AFS-TAR models with parameters expanded on the adaptable basis functions outperform their DCT counterparts. However, the estimation of the functional subspace parameters is achieved at the price of increased computational complexity as the adaptable approach includes additional nonlinear least squares stages for the SNLS method.

For the classical FS-TAR$(6)_{[10,6]}$ models the OLS-ISD estimation method normally achieves the best predictive performance while the MS, ML(OLS-ISD), and ML(WLS-ISD) methods achieve the best BIC. Thus, the theoretical analysis concerning the statistical efficiency of the MS method is confirmed while the MS has the additional advantage of smaller execution time (5 and 3 times faster in mean computational time value than the ML(OLS-ISD) and ML(WLS-ISD) methods, respectively). It is also worth noting that the ML method initialized with the parameter estimates provided by the OLS-ISD regression method needs many more iterations and computational time in order to converge compared to the case of initialization by WLS-ISD estimates. At this point it should be mentioned that the ML converges to local minima when arbitrary initial values are used (for instance, see the results in Appendix 5.A). This results may be attributed to the highly nonlinear nature of the log-likelihood function and they high dimensionality $(n_a \cdot p_a + p_s)$ of the corresponding optimization problem.

The estimated FS-TAR models were also validated using a distribution-free sign test [Poulimenos and Fassois, 2006] [Draper and Smith, 1998, pp. 192-198]. Validation results are presented in Fig. 5.6.14.

The superior performance of the novel AFS-TAR approach is even more pronounced by the comparison of Figs. 5.6.15 and 5.6.16 where the MS estimated (DCT FS-TAR$(6)_{[10,6]}$ models) and SNLS-ISD estimated (non-uniform B-splines AFS-TAR$(6)_{[8,8]}$ models) time-dependent AR parameters and innovations standard deviation are illustrated. Clearly the functional subspaces provided by the adaptable

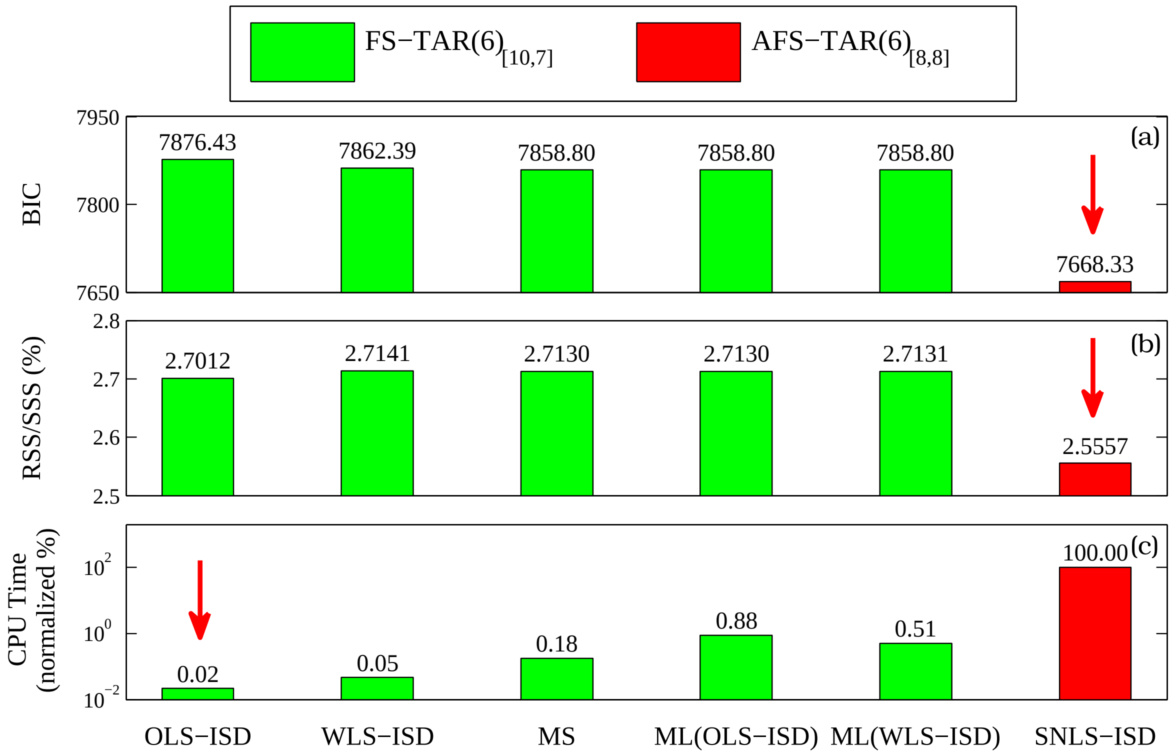

Figure 5.6.13: Performance comparison for various FS-TAR and AF-TAR models estimated by various methods: Mean (a) BIC, (b) RSS/SSS, and (c) normalized execution times.

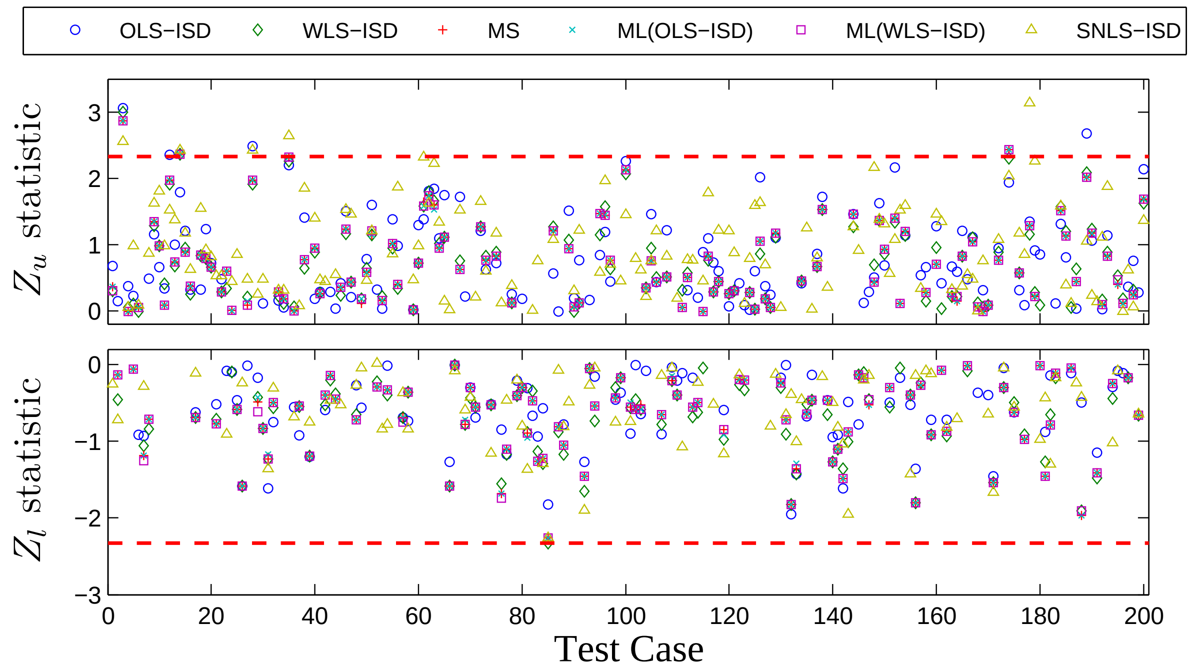

Figure 5.6.14: FS-TAR models validation through the residual sign test at the $\alpha = 0.01$ risk level (the model is accepted if the test statistic is within the critical limits): DCT FS-TAR$(6)_{[10,6]}$ models estimated through various methods and AFS-TAR$(6)_{[8,8]}$ models estimated through SNLS-ISD method.

B-splines functions increase the potential for excellent tracking of the parameters even for the regions where transitions between smooth and abrupt changes take place. On the contrary, the DCT FS-TAR$(6)_{[10,6]}$ based estimates smooth out the abrupt change and barely track the parameters during their

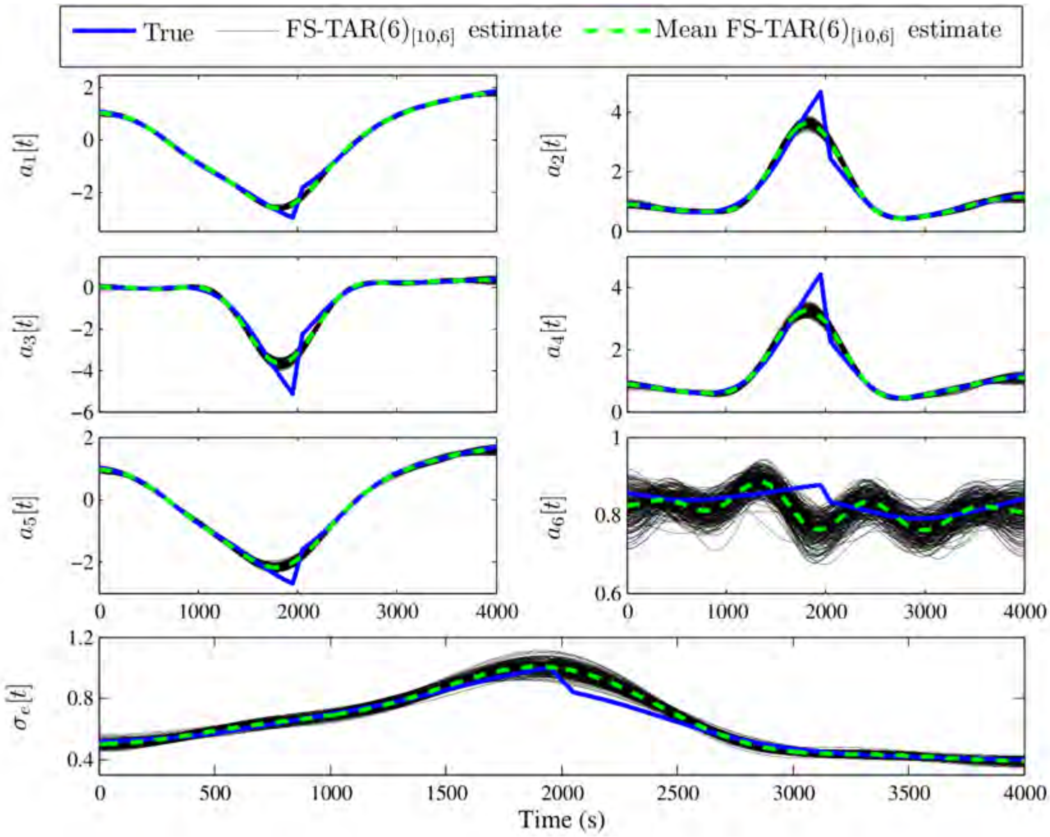

Figure 5.6.15: True TAR(6) model parameter trajectories and estimated values based on the DCT FS-TAR$(6)_{[10,6]}$ models (MS method).

fast transition at the middle of the time axis span. Both models fail to track the sixth TV AR parameter which is characterized by small variability compared to the rest of the parameters.

In order to quantify the achievable TV parameter tracking accuracy, percentage accumulated parameter errors are computed as:

$$\mathrm{err}_{a_i[t]} \triangleq 100 \times \frac{\| \widehat{a}_i[t] - a_i[t] \|^2}{\| a_i[t] \|^2} \% \tag{5.6.1a}$$

and

$$\mathrm{err}_{\sigma_e[t]} \triangleq 100 \times \frac{\| \widehat{\sigma}_e[t] - \sigma_e[t] \|^2}{\| \sigma_e[t] \|^2} \% \tag{5.6.1b}$$

The parameter tracking errors $\mathrm{err}_{a_i[t]}$ and $\mathrm{err}_{\sigma_e[t]}$ (Fig. 5.6.17) confirm the big difference in the performance of the AFS-TAR models compared to the classical. Note that the mean parameter tracking errors for the AFS-TAR method lie between 0.2 and 0.8 %, that is two to five times better than the values achieved by the MS estimated FS-TAR models.

Similar results are obtained for the estimates of the global modal characteristics. The “frozen-time” natural frequencies and damping ratios as estimated via the MS method for the DCT FS-TAR$(6)_{[10,6]}$ and the SNLS-ISD method for the non-uniform B-splines FS-TAR$(6)_{[8,8]}$ models are shown in Figs. 5.6.18 and 5.6.19, respectively. The mean over 200 runs values are also depicted in these figures. The corresponding accumulated tracking error computed by relations similar to those of Eq. (5.6.1) are depicted in Fig. 5.6.20. Despite the good tracking of the time-dependent natural frequencies the corresponding damping ratios are tracked with an accumulated error which exceeds 20% for the case of DCT FS-TAR$(6)_{[10,6]}$ models and is bigger than 8% for all damping ratios ζ_i. Nevertheless, the difficulty in estimating the true damping ratios is a well known problem even in the stationary case.

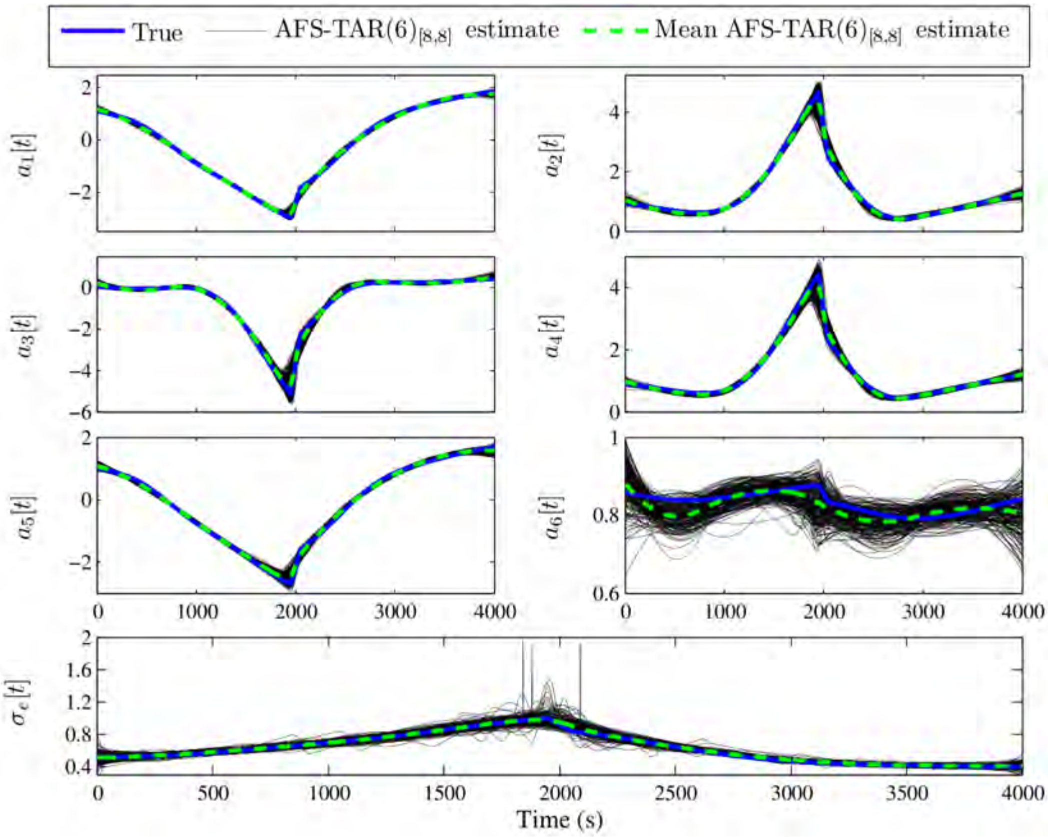

Figure 5.6.16: True TAR(6) model parameter trajectories and estimated values based on the non-uniform B-splines AFS-TAR$(6)_{[8,8]}$ models (SNLS-ISD method).

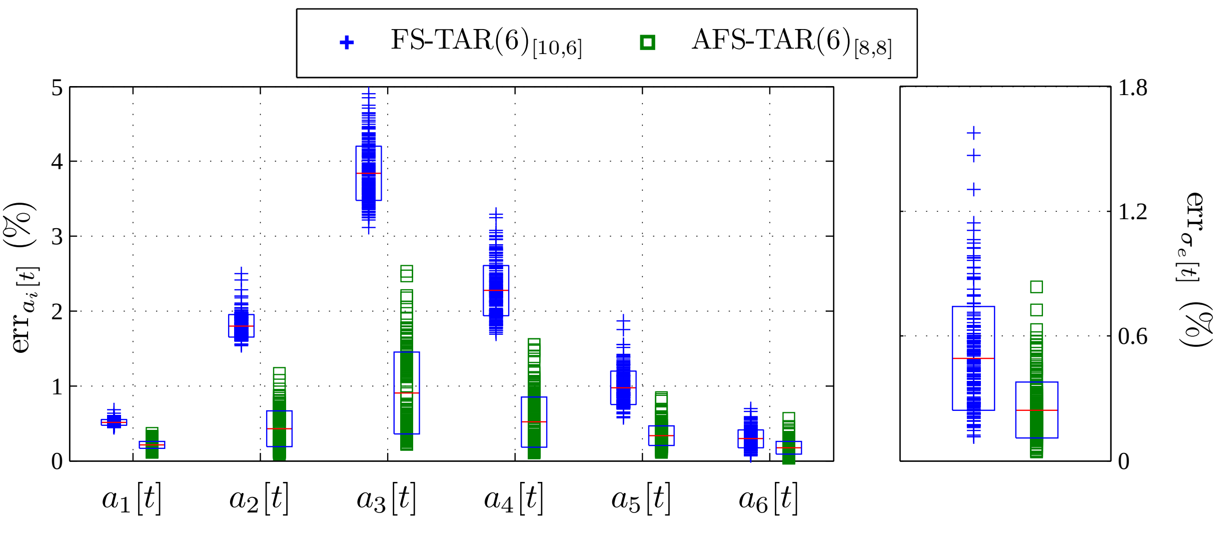

Figure 5.6.17: Accumulated parameter tracking errors for the MS estimated DCT FS-TAR$(6)_{[10,6]}$ models and the SNLS-ISD estimated non-uniform B-splines AFS-TAR$(6)_{[8,8]}$ models. (Mean $\pm$ one std values of the percentage errors are shown with boxes).

Finally, the mean values of the "frozen-time" PSD estimates along with the mean absolute errors for each point of the time-frequency plane are illustrated in Fig. 5.6.21. These estimates are calculated for a grid of 1000×1000 points. The absolute error is in general of small magnitude but again the adaptable model-based estimates are closer to the true "frozen-time" PSD.

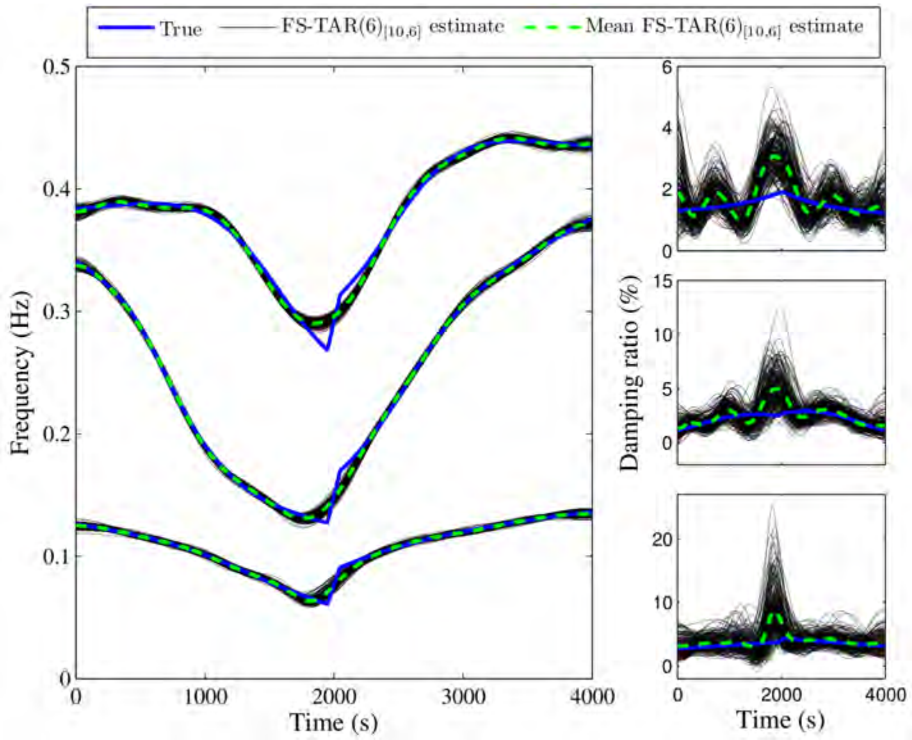

Figure 5.6.18: True TAR(6) model “frozen-time” natural frequency and damping ratios and estimated values based on the DCT FS-TAR$(6)_{[10,6]}$ models (MS method).

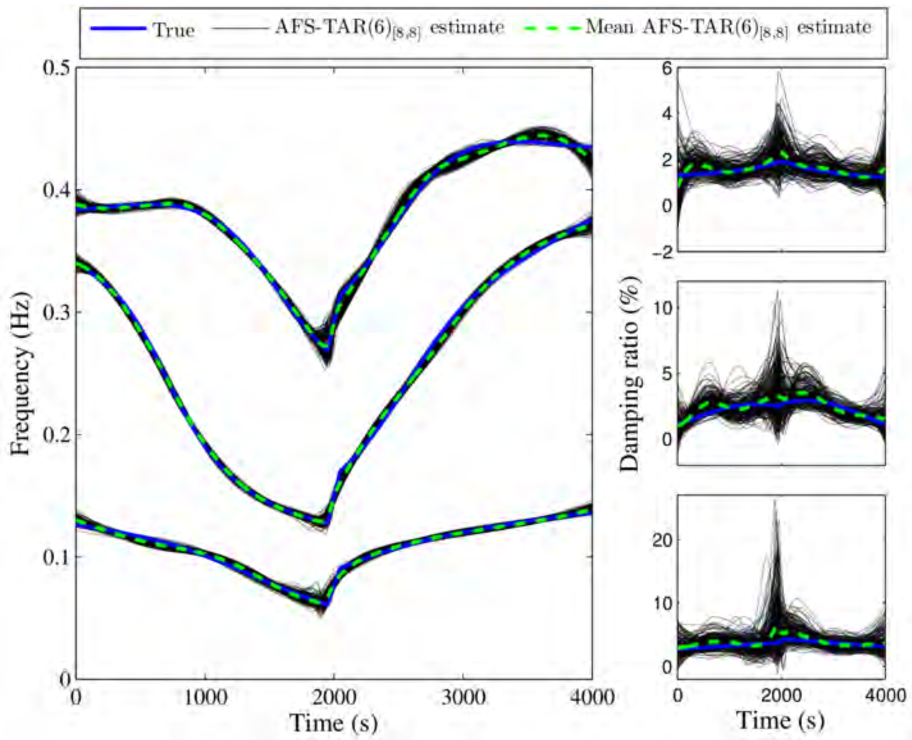

Figure 5.6.19: True TAR(6) model “frozen-time” natural frequency and damping ratios and estimated values based on the non-uniform B-splines AFS-TAR$(6)_{[8,8]}$ models (SNLS-ISD method).

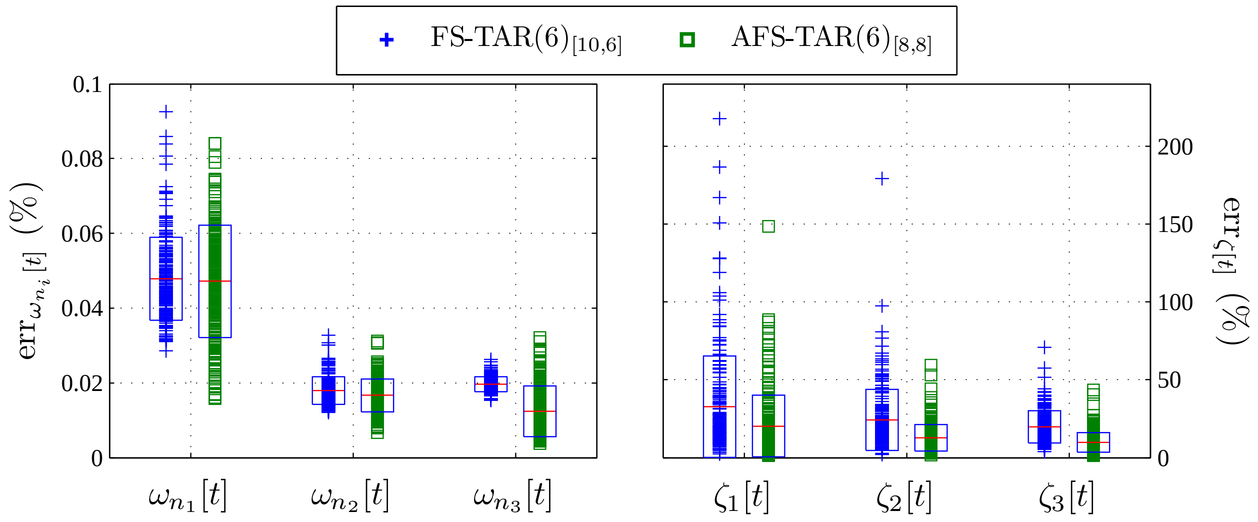

Figure 5.6.20: Accumulated modal parameter tracking errors for the MS estimated DCT FS-TAR$(6)_{[10,6]}$ models and the SNLS-ISD estimated non-uniform B-splines AFS-TAR$(6)_{[8,8]}$ models. (Mean $\pm$ one std values of the percentage errors are shown with boxes).

5.6.3 Discussion

The discussion on the FS-TAR models estimated by the various methods focuses on the following issues:

(a) Achievable overall modelling accuracy in terms of model-based one-step-ahead predictions. The achievable overall modelling accuracy is presently judged in terms of models predictive ability quantified by the one-step-ahead ahead predictions of the models considered. Summary results, taking into account all 200 Monte Carlo runs, and expressed in terms of the RSS normalized by the Series Sum of Squares (SSS), are for all methods, provided in Figure 5.6.13(b). It is observed that all models provide excellent predictions, with the AFS-TAR (SNLS-ISD) being the best followed by the OLS-ISD estimated FS-TAR models.

(b) Achievable time-dependent parameter tracking accuracy. The achievable model parameter tracking accuracy of the AFS-TAR models was shown to be superior compared to that of the classic FS-TAR models. The latter even though they may accurately track model parameters with either smooth or abrupt evolution in the model parameters they normally need excessive functional subspaces in order to track parameters with inhomogeneous type of evolution. On the other hand the adaptable approach along with the use of non-uniform B-splines was shown to provide a basis with mixed characteristics capable of tracking the model parameters accurately.

(c) Achievable time-dependent power spectral density and modal parameter accuracy, resolution and tracking. The true model "frozen-time" natural frequencies are also tracked with higher accuracy by the SNLS-ISD estimated AFS-TAR$(6)_{[8,8]}$ model and yet the 200 estimates depict small variability. This is not the case for the corresponding damping ratios which are estimated with large errors. The fact of large uncertainties in the damping ratio estimates even for the stationary case is a well known issue. However, the mean estimates of the AFS-TAR models are again better than those obtained by the MS estimated FS-TAR models.

Finally, the "frozen-time" PSD mean estimate obtained by the AFS-TAR model is of higher accuracy with mean absolute errors lower that 5 dB for the 99.8% of the time-frequency grid consisting of 1000×1000 points. The largest mean absolute error is of 10.7 dB and is observed in the time-region where fast transitions take place. The performance attained by the classic FS-TAR model estimated through the MS method is slightly reduced. In this case the mean absolute error is lower of 5 dB within the 98.49 % of the total surface and the maximum mean absolute error value is equal to 16.8 dB.

(d) Computational simplicity. As indicated in Fig. 5.6.13(c), which provides relative computer execution (CPU) times for the various methods considered the computational burden of the SNLS-ISD

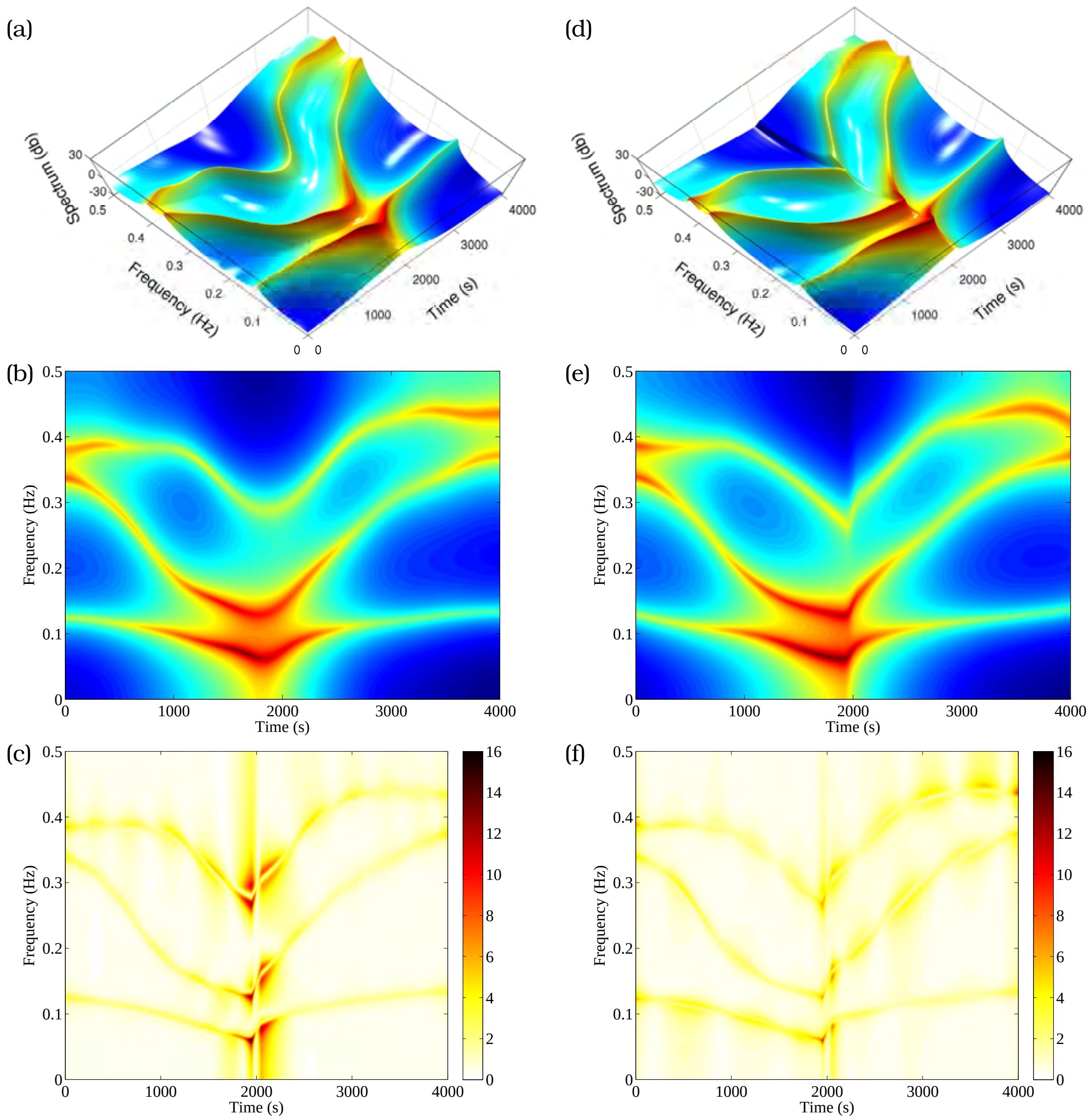

Figure 5.6.21: "Frozen-time" PSD mean estimates and mean absolute errors: (a) 3d-view of the mean PSD estimate, (b) 2d-view of the mean PSD estimate, and (c) mean absolute error as obtained by the DCT FS-TAR$(6)_{[10,6]}$ models (MS method). (d) 3d-view of the mean PSD estimate, (e) 2d-view of the mean PSD estimate, and (f) mean absolute error as obtained by the non-uniform B-splines AFS-TAR$(6)_{[8,8]}$ models (SNLS-ISD method).

estimation method is particularly high compared to the rest estimation methods considered for the classical FS-TAR models (observe that the scale on the vertical axis is logarithmic). In fact, the computationally simplest method is the OLS-ISD method with the WLS-ISD and MS methods being close. It is also worth observing that the ML estimation method is computationally quite expensive compared to the regression type methods due to the nonlinear optimization method required for the estimation of both $\boldsymbol{\vartheta}_a$ and $\boldsymbol{\vartheta}_s$.

(e) Ease of use. The classic FS-TAR models estimation methods may be considered as particularly simple even for the inexperienced user while this is not valid for the adaptable models. This is due to the fact that even the simplest SNLS-ISD method includes constrained nonlinear optimization problems,

while the respective OLS-ISD method for the classic models is a linear problem of low complexity. However, in both cases the model structure selection is a task requiring caution and expertise. Although it may be automated to a certain degree (see Section 5.5), some user familiarity is still necessary. Also, the selection of the method parameters and characteristics, as well as the interpretation of the method's behavior or results, may require attention.

5.7 The TARMA Case: A Monte Carlo Study and Comparison

The identification problem of a true TARMA$(6, 5)$ model with piecewise polynomial TV parameters is presently addressed. Also in this case study 200 Monte Carlo experiments are performed based on an equal number of realizations of the model's response. For the purposes of comparison except from the various FS-TARMA and AFS-TARMA methods considered the true model is also identified by the means of alternative estimation methods belonging to the classes of UPE and SPE methods. The methods' performance is judged in terms of various criteria regarding tracking of the TV parameters, time-frequency representation accuracy, predictive ability and others.

5.7.1 The signals

The true TV parameters of the considered TARMA$(6, 5)$ simulated model are depicted in Fig. 5.7.1. It should be mentioned that the simulated TARMA model is created pointwisely and it is partly based on the identified characteristics of a laboratory deployable link structure as these were identified through an experimental vibration-based modelling and analysis study [Spiridonakos and Fassois, 2009a]. However, for this hypothetical scenario the case of a deployable link structure which extends, is then loaded with a linearly increasing mass and finally retracts back to its initial position is considered.

The model's "frozen-time" PSD, natural frequencies and damping ratios are illustrated in Fig. 5.7.2. The non-stationarity of the simulated models is evident in their theoretical "frozen" time-frequency characteristics. The model is characterised by three almost equally strong TV modes and two antiresonant modes.

The identification of the true model is based on 4000-sample long realizations of its response. For each Monte Carlo run a different realization is used which is produced by different excitation signals. A typical response signal realization is depicted in Fig. 5.7.3.

5.7.2 Identification results

For the reasons outlined in Section 5.4, the FS-TARMA modelling problem is much more complicated than the corresponding FS-TAR. It must be added that except the potential existence of local minima, instability problems often arise when ML or WLS methods are utilized with inaccurate initial values. These methods require the use of nonlinear optimization techniques which have to be started off from a feasible solution.

In addition, in many cases, an "excess" MA functional subspace leads to algorithmic instability, that results in excessive residual estimates. As a consequence, in such cases the model estimation cannot even be completed. For instance, this kind of problem may be confronted during the backward regression search scheme for FS-TARMA model selection which considers functional subspaces of high dimensionality in its first phase in order to determine the appropriate model orders.

It is also reminded that the forward regression scheme may be utilized only in cases of a given initial regression matrix. For this reason it may be used along the 2SLS estimation method, with this method being in general a good choice for the implementation of the model structure selection schemes as it is significantly faster that the rest of the methods. Nevertheless, its accuracy is highly dependent on the inverse function approximation, that is the long FS-TAR model which provides approximate estimates for the innovations residuals. The order and the functional subspaces of this inverse representation have to be selected with caution.

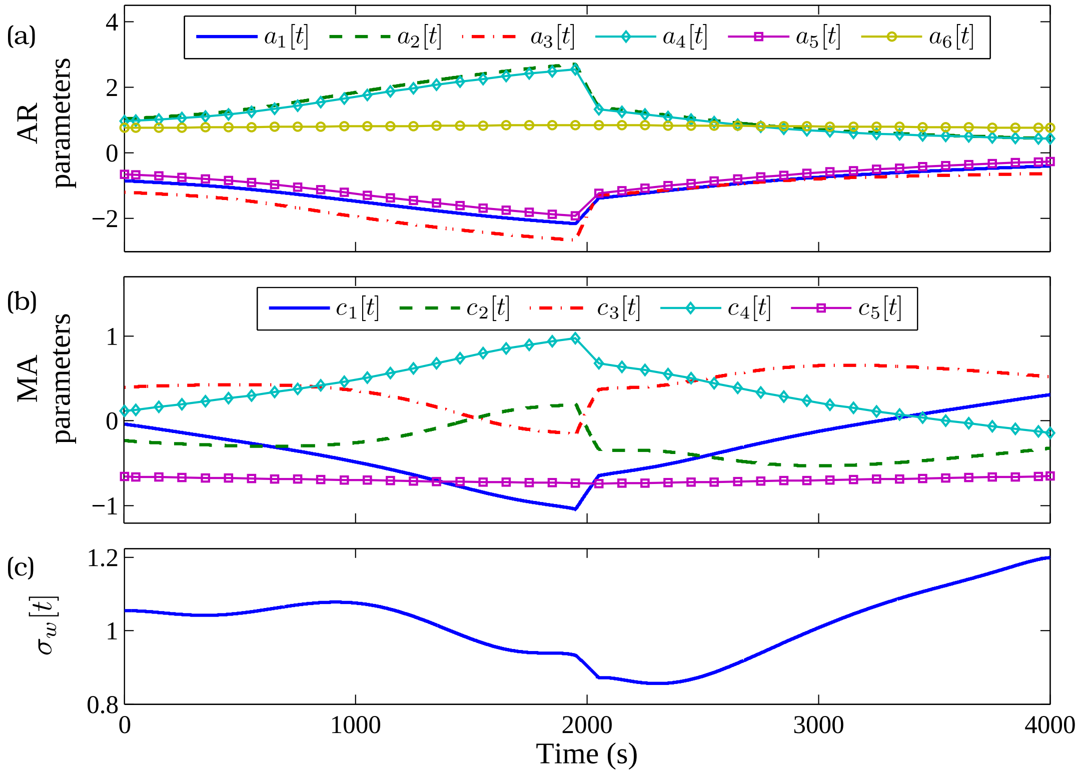

Figure 5.7.1: The true TARMA(6,5) model parameters: (a) AR, (b) MA, and (c) innovations standard deviation.

For the TARMA modelling problem under study and regarding the classical FS-TARMA models, the model structure selection schemes of Section 5.5 utilized for the selection of the appropriate functional subspaces, considering known the true AR and MA orders, lead to the selection of a DCT FS-TARMA$(6,5)_{[7,4,4]}$ model with $\boldsymbol{d}_a = [1,\ldots,6,8]^T$, $\boldsymbol{d}_c = [1,\ldots,4]^T$, and $\boldsymbol{d}_s = [1,3,4,9]^T$ (2SLS-ISD estimation) and non-uniform B-splines AFS-TARMA$(6,5)_{[6,6,6]}$ model (2SSNLS-ISD estimation). The inverse function representation was approximated by OLS estimated DCT FS-TAR$(20)_{[12]}$ models for the classical FS-TARMA models and SNLS estimated non-uniform B-splines AFS-TAR$(20)_{[9]}$ for the AFS-TARMA models. The functional subspaces of this long FS-TAR models were selected by the BIC.

The performance of the finally obtained FS-TARMA and AFS-TARMA models and the various estimation methods considered is judged in terms of the BIC, RSS/SSS and normalized execution times in Fig. 5.7.4. With regard to the FS-TARMA estimation methods, it may be observed that the RELS method does not attain good results when only one pass over the data is performed. This may attributed primarily to the zero initial conditions and secondly to the abrupt change of the TV parameters taking place at the middle of the time axis which is reflected to a change of the optimal coefficients of projection (see Fig. 5.7.5). However, the estimates are improved when three passes are performed (RELS$_3$ method; RELS applied on the non-stationary signal in a forward, backward and final forward pass). In general, the RELS$_3$ method has been shown to be a robust solution for FS-TARMA model estimation while it also has the additional assets of minimal user expertise and small execution times.

Regarding the 2SLS method, the importance of an accurate approximation of the FS-TARMA inverse function representation, that is the long FS-TAR model used during the first stage of the 2SLS, is highlighted by the results of Fig. 5.7.4. Apparently, the results obtained by the 2SLS method with initial innovation estimates provided by an FS-TAR$(20)_{[12]}$ model are significantly improved compared to that obtained when the innovation estimates are provided by an FS-TAR$(9)_{[12]}$ model. The RMS method is implemented as shown in Fig. 5.4.1 and doesn't seem to provide any significant improvement compared to the simpler 2SLS-ISD method.

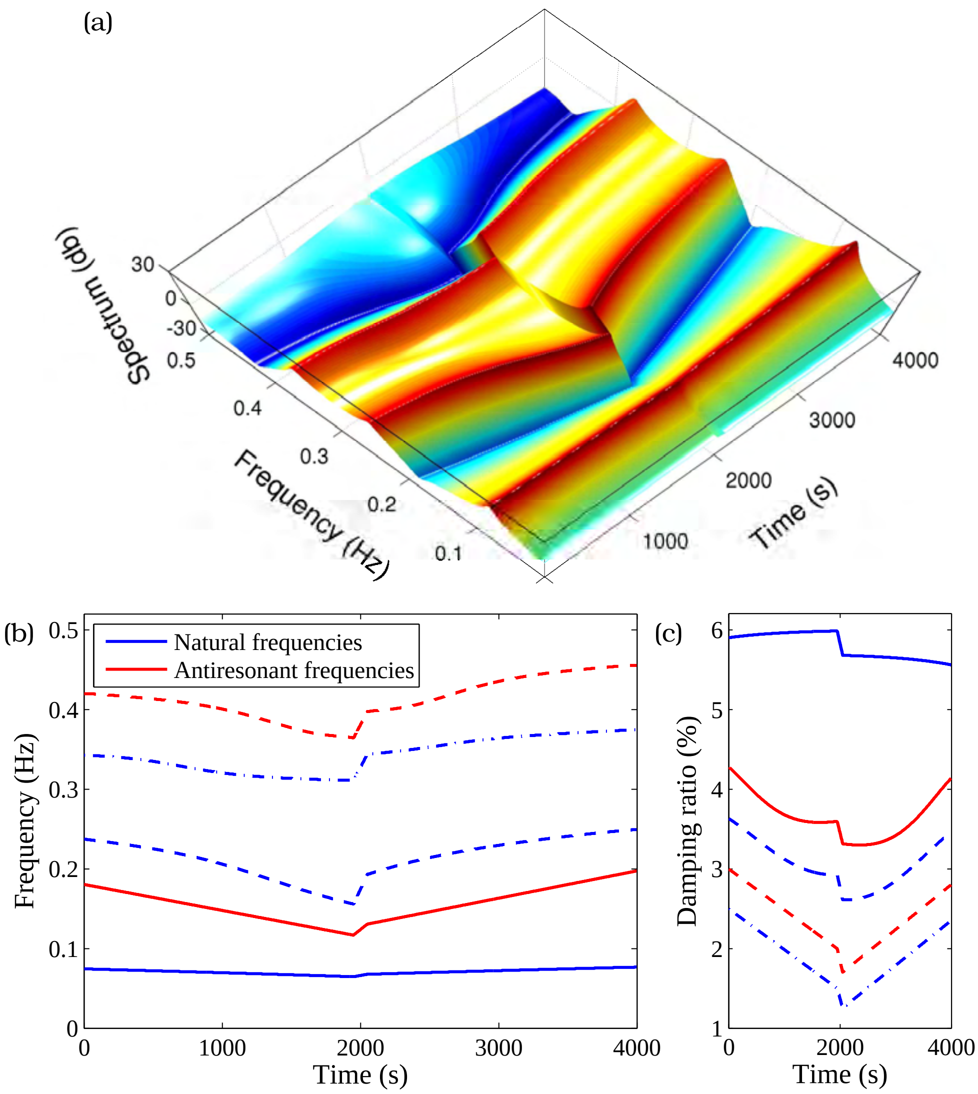

Figure 5.7.2: "Frozen-time" analysis of the true TARMA$(6, 5)$ model: (a) power spectral density, (b) natural frequencies, and (c) damping ratios.

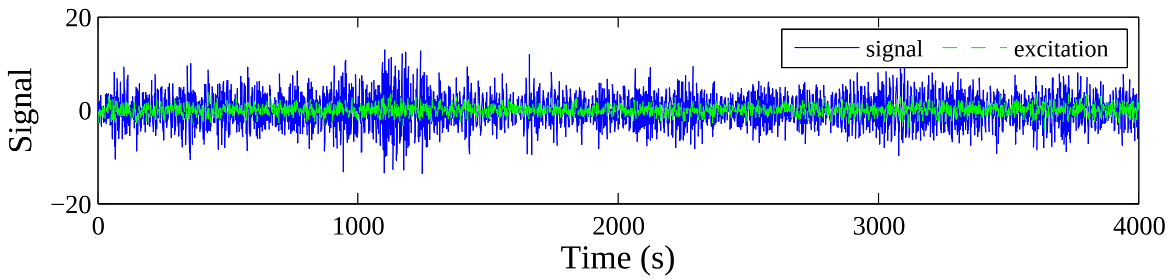

Figure 5.7.3: A single realization of the non-stationary response signal of the true TARMA$(6, 5)$ model.

Yet, the best results in terms of the BIC and RSS/SSS are attained by the OLS-ISD and MS methods (irrespectively of the parameter estimation method used for its initialization since similar results are obtained when estimates based on RELS_3 are utilized).

Finally, note that the AFS-TARMA models with parameters expanded on non-uniform B-splines again outperform those that use fixed DCT basis. For this reason the former is maintained for the subsequent model-based analysis. However, before proceeding with this analysis the results of the identification of the TARMA model through alternative non-stationary methods are presented in the next section.

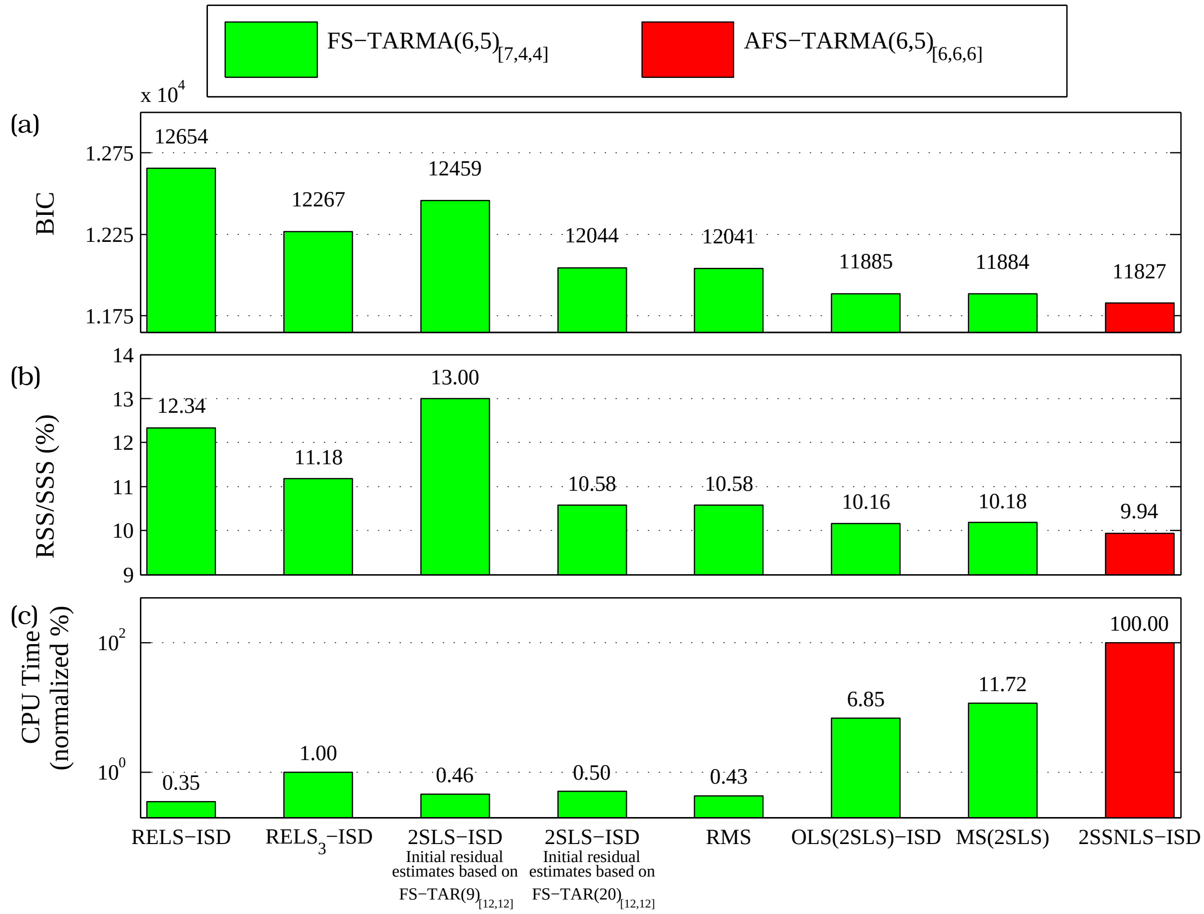

Figure 5.7.4: Performance comparison for various FS-TARMA and AFS-TARMA models estimated by various methods: Mean (a) BIC, (b) RSS/SSS, and (c) normalized execution times.

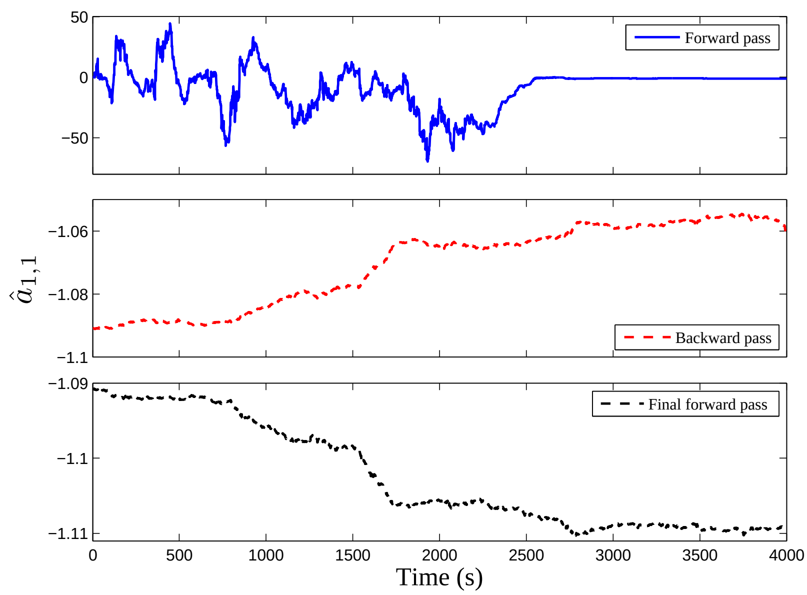

Figure 5.7.5: Estimation of the $a_{1,1}$ coefficient of projection parameter through the RELS method applied in three sequential passes over the non-stationary signal (DCT FS-TARMA$(6,5)_{[7,4,4]}$).

Table 5.7.1: Identification methods, their characteristics, and the identified models.

Model Class	Identification Method	Method Characteristics	Identified Model
Unstructured Parameter Evolution	Canonical Variate Analysis (CVA) (MATLAB *n4sid* function)	$Q = 401$, $q = 10$	ST-SS(6)
	Recursive Maximum Likelihood (RML) (MATLAB *rarmax* function)	$\lambda = 0.989$ $\alpha = 10^4$	RML-TARMA$(6, 5)$
Stochastic Parameter Evolution	Kalman Filter (KF)	$\kappa = 1, \nu = 7.9 \times 10^{-5}$ $\alpha = 10^4$	SP-TARMA$(6, 5)$

5.7.3 Comparisons with UPE and SPE methods

The alternative identification methods used, their characteristics, as well as the finally obtained models are summarized in Table 5.7.1.

Regarding the ST-SS model, the case of overlapping segments is considered with the active segment being forwarded by q=10 samples. The segment length and the model order are selected based on the RSS criterion and the singular values of the corresponding Hankel matrix. It should be noted that for data segments of more than 500 samples, the method seems incapable of tracking the variations of the true system variability. Obviously, depending on the model order, a lower limit of the segments length is imposed by the requirement for statistically reliability. The selection procedure has suggested a data segment of 401 samples and a ST-SS(6) model.

In the case of RML method the true model orders are considered ($n_a = 6, n_c = 5$) while the forgetting factor is optimized based on the minimization of the RSS criterion (search space $[0.950, 0.951, \ldots, 0.999]$). For the initialization of the RML algorithm the covariance matrix was selected equal to $10^4\boldsymbol{I}$, while three sequential phases (a forward pass, a backward pass and a final forward pass) are applied in order to reduce the effects of the arbitrary initial conditions.

In the SP-TARMA case the selected stochastic smoothness constraints and the ratio of the constraint model innovations variance over the residual variance ν was optimized based on minimization of the BIC for a model with $n_a = 6, n_c = 5$. The finally obtained model is an SP-TARMA$(6, 5)$ with $\kappa = 1$ and variance ratio $\hat{\nu} = 7.9 \times 10^{-5}$. For the initialization of the Kalman filter the covariance matrix was selected equal to $10^4\boldsymbol{I}$ and three sequential passes (forward, backward, forward and a final backward smoothing pass) were executed.

5.7.4 Discussion

The discussion on the FS-TAR models estimated by the various methods focuses on the following issues:

(a) Achievable overall modelling accuracy in terms of model-based one-step-ahead predictions. The obtained mean RSS/SSS values achieved by the estimated TARMA and ST-SS models are depicted in Fig. 5.7.6(a). Indicative one-step-ahead signal predictions obtained by the estimated models are (for a short time segment of the signal) compared to the actual signal values for a single realization in Fig. 5.7.6(b). It is observed that the AFS-TARMA model achieves the best prediction accuracy (mean RSS/SSS $= 9.59\%$), followed by the RML-TARMA models, while SP-TARMA and ST-SS models attain equally bad performance with mean RSS/SSS values around 12.5%.

(b) Achievable time-dependent parameter tracking accuracy. The TV AR, MA and innovation standard deviation estimates obtained by the AFS-TARMA$(6, 5)_{[6,6,6]}$, SP-TARMA$(6, 5)$, and RML-TARMA$(6, 5)$ models are compared with the true ones in Figs. 5.7.7, 5.7.8 and 5.7.9, respectively. For fair comparison in all cases the innovations standard deviation was estimated non-parametrically through a moving time-window of length equal to 401 samples advanced by one sample (for this reason standard deviation estimates are available for $t = 201, 202 \ldots, 3800$).

As it may be observed, the AFS-TARMA model estimates provide the highest tracking accuracy followed by those obtained by the RML-TARMA models which however depict high variability even for the

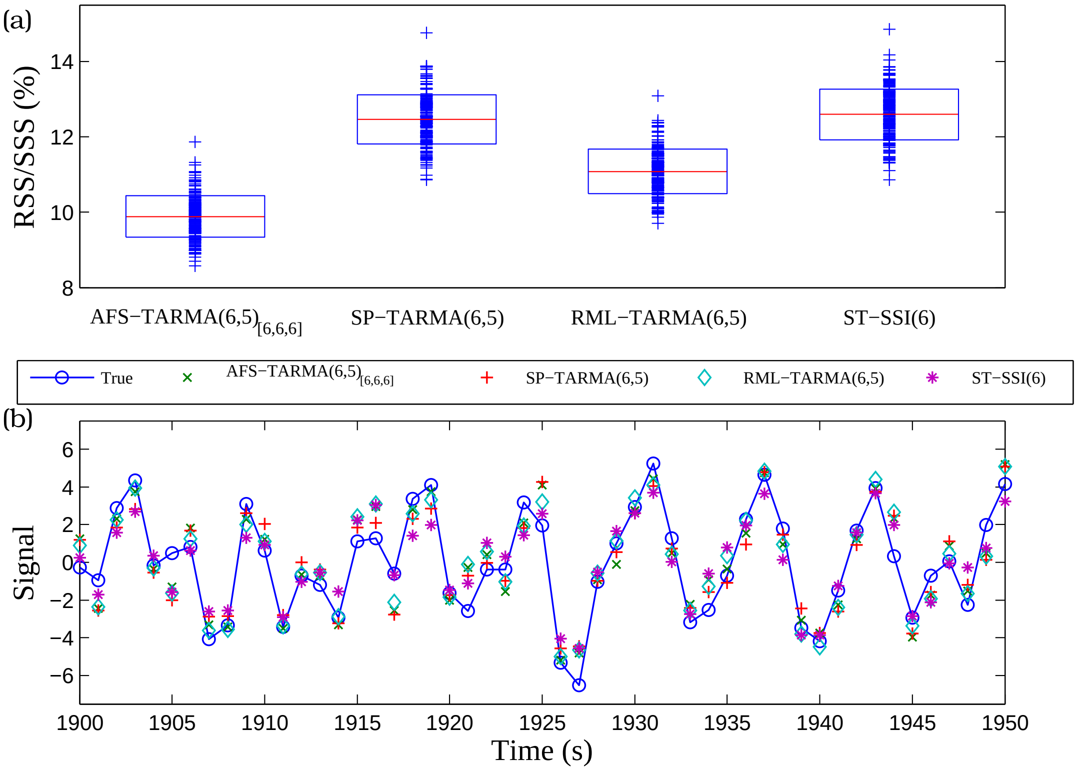

Figure 5.7.6: Estimated models predictive ability: (a) RSS/SSS values as calculated for the 200 Monte Carlo experiments (mean $\pm$ one std are also shown with boxes), and (b) the true signal corresponding to a single realization and the corresponding one-step-ahead predictions based on the FS-TARMA$(6,5)_{[6,6,6]}$, the SP-TARMA$(6,5)$, the RML-TARMA$(6,5)$, and the ST-SS(6) models.

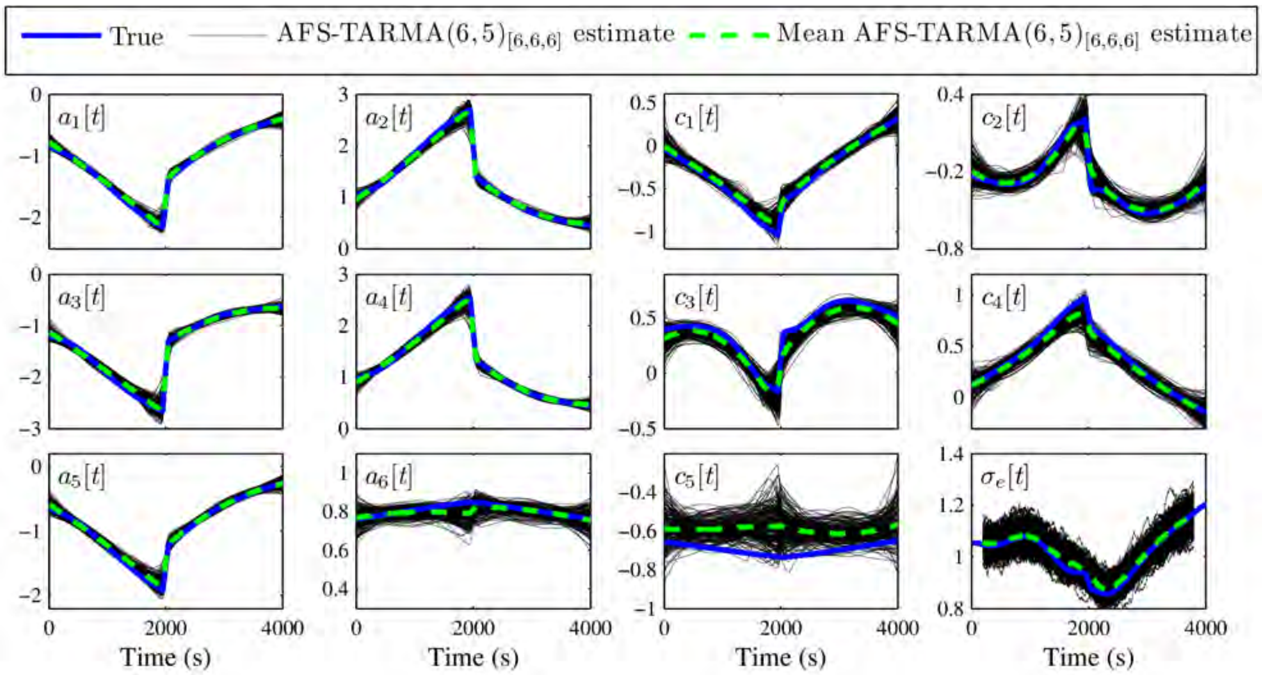

Figure 5.7.7: True TARMA$(6,5)$ model parameter trajectories and estimated values based on the AFS-TARMA$(6,5)_{[6,6,6]}$ models.

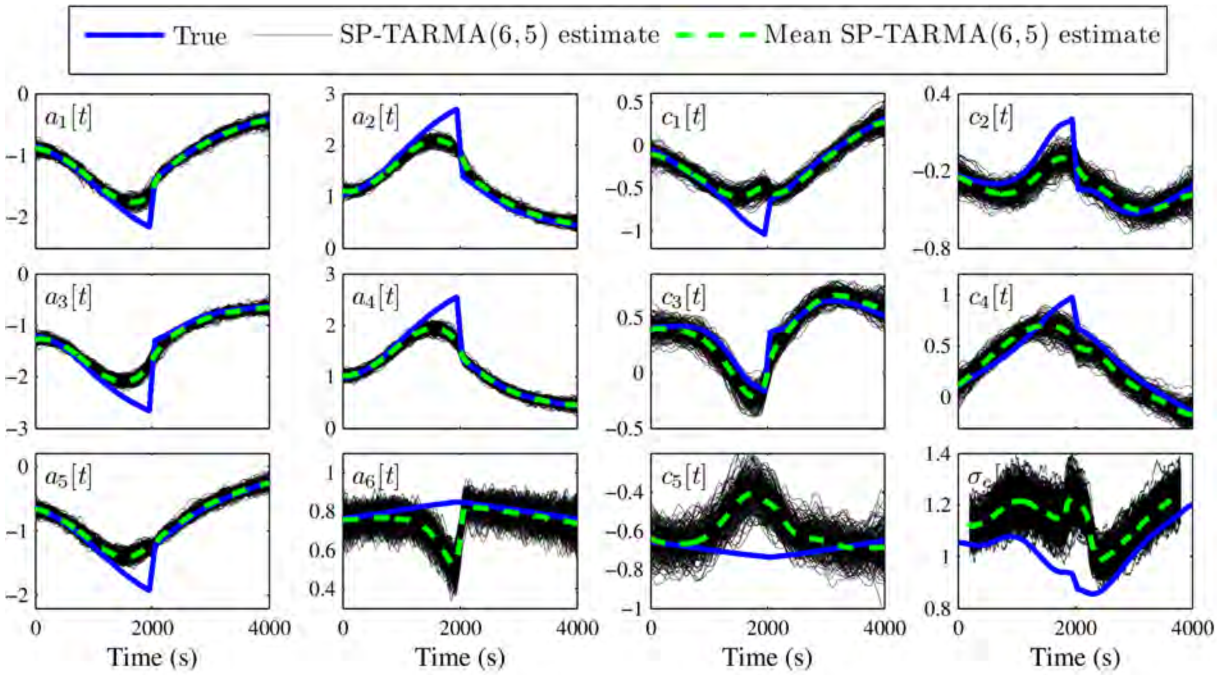

Figure 5.7.8: True TARMA$(6, 5)$ model parameter trajectories and estimated values based on the SP-TARMA$(6, 5)$ models.

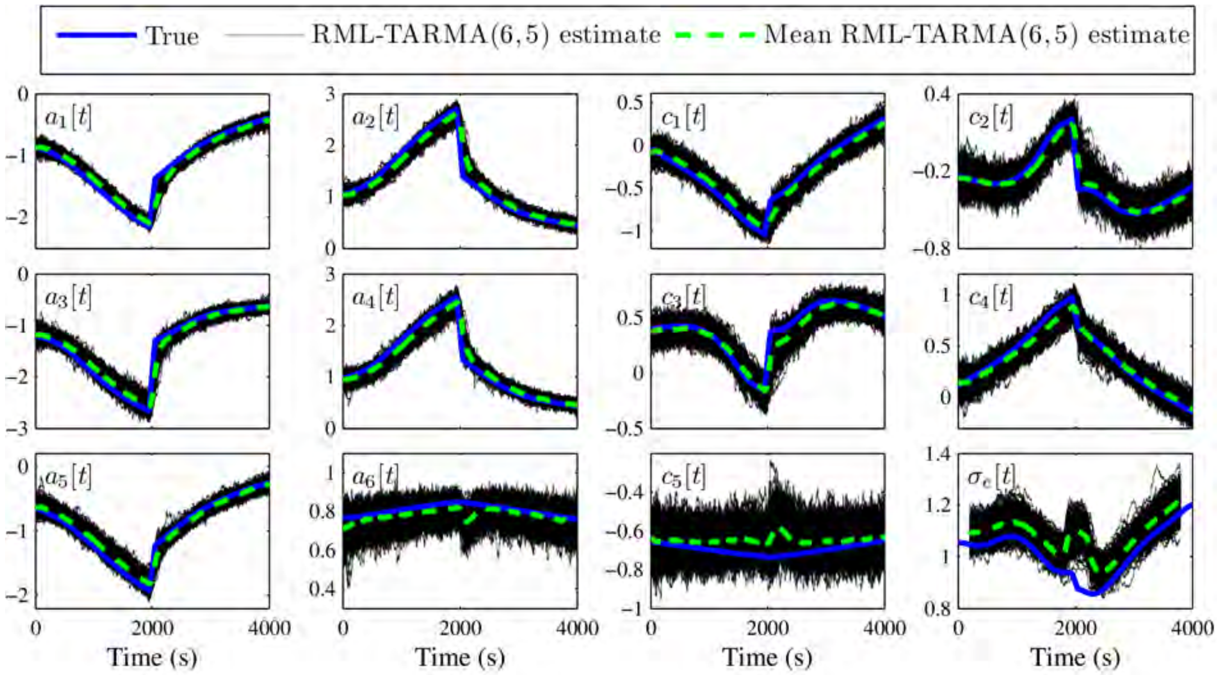

Figure 5.7.9: True TARMA$(6, 5)$ model parameter trajectories and estimated values based on the RML-TARMA$(6, 5)$ models.

regions of time where the parameters evolve smoothly. However, the mean values provided by the RML-TARMA model estimates track very well the TV parameters. On the contrary SP-TARMA models fails to track the TV parameters during the time region where fast changes take place, that is between samples 1950 and 2050. This fact may be attributed to the constant variance ratio between the parameter variance and the innovations variance (ν) which makes the model inflexible for tracking inhomogeneous types of evolution.

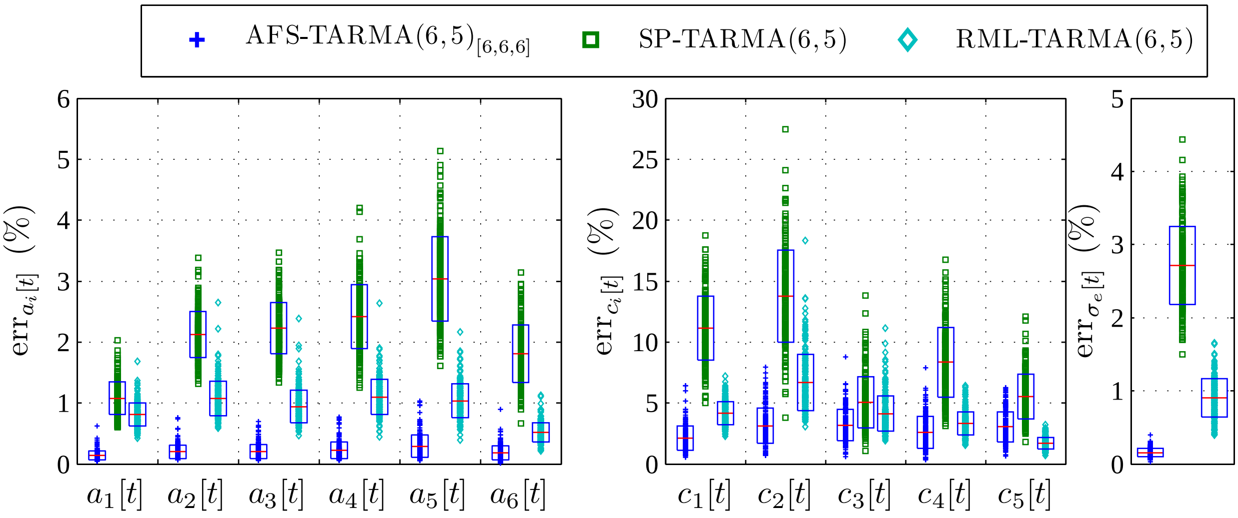

Figure 5.7.10: Mean percentage accumulated parameter errors for the FS-TARMA$(6,5)_{[7,4,4]}$, the SP-TARMA$(6,5)$ and RML-TARMA$(6,5)$ models.

The parameter tracking errors obtained through Eq. (5.6.1) shown in Fig. 5.7.10 give an even clearer picture regarding the estimated models tracking accuracy. The AFS-TARMA model outperforms its counterparts with error less than 5% in all cases and yet below 1% for the AR parameters and the innovations standard deviation. Only, the MA parameter $c_5[t]$ is tracked with higher accuracy by the RML-TARMA model which depicts also good tracking performance. It is noted that the parameters of the ST-SS model may not be directly compared as they correspond to different type of model.

(c) Achievable time-dependent power spectral density and modal parameter accuracy, resolution and tracking. The "frozen-time" AFS-TARMA$(6,5)_{[6,6,6]}$ natural frequency, antiresonant frequency, and damping ratio estimates are, along with true TARMA$(6,5)$ model values depicted in Fig. 5.7.11. Corresponding figures for the SP-TARMA$(6,5)$, RML-TARMA$(6,5)$ and the ST-SS(6) model-based estimates are shown in Figs. 5.7.12, 5.7.13, and 5.7.14, respectively. It must be noted that the modal characteristic are estimated for the time instants for which ST-SS models were estimated, that is $t = 201, 211, 221, \ldots, 3791$.

Overall, the AFS-TARMA$(6,5)_{[6,6,6]}$ models provide very good estimates (closer to the true values and exhibiting lower variability) compared to those obtained by the rest of the models. On the contrary the SP-TARMA and ST-SS models fail to track in accuracy the antiresonant frequencies even in their mean value estimates. This observation is made more clear by the accumulated parameter tracking errors obtained through similar relationships with those of Eq. (5.6.1) shown in Fig. 5.7.15. Clearly, again the AFS-TARMA model outperforms its counterparts with error less than 0.2% for the natural and antiresonant frequencies. The largest errors are obtained by the SP-TARMA$(6,5)$ models followed by the ST-SS(6). It is worth noting that the RML-TARMA$(6,5)$ based estimates depict very good performance. Nevertheless, as in the TAR case study the damping ratios are estimated with large deviations.

The frozen-time PSD mean estimates corresponding to the AFS, SP and RML TARMA$(6,5)$ and the ST-SS(6) models are depicted in Fig. 5.7.16. In the same figure the plots of the mean absolute error between the true and the estimated PSDs are illustrated. The non-parametric estimates of the innovations standard deviation are utilized for the calculation of the PSD estimation, while these estimates are calculated for a grid of 360 points along the time axis ($t = 201, 211, 221, \ldots, 3791$) and 500 points for the frequency axis ($\omega = 0.001, 0.002, 0.003, \ldots, 0.5$ Hz). The points on the time-axis are those on which the ST-SS model was estimated.

Obviously, the AFS-TARMA based PSD mean estimate attains the smallest mean error with the largest errors occurring between 0.1 and 0.2 Hz due to its incapability of estimating in accuracy the sharpness of the first valley (antiresonant frequency). Second is the RTM-TARMA model based mean estimate with some difficulty on the representation of the sharp transition that takes places at the

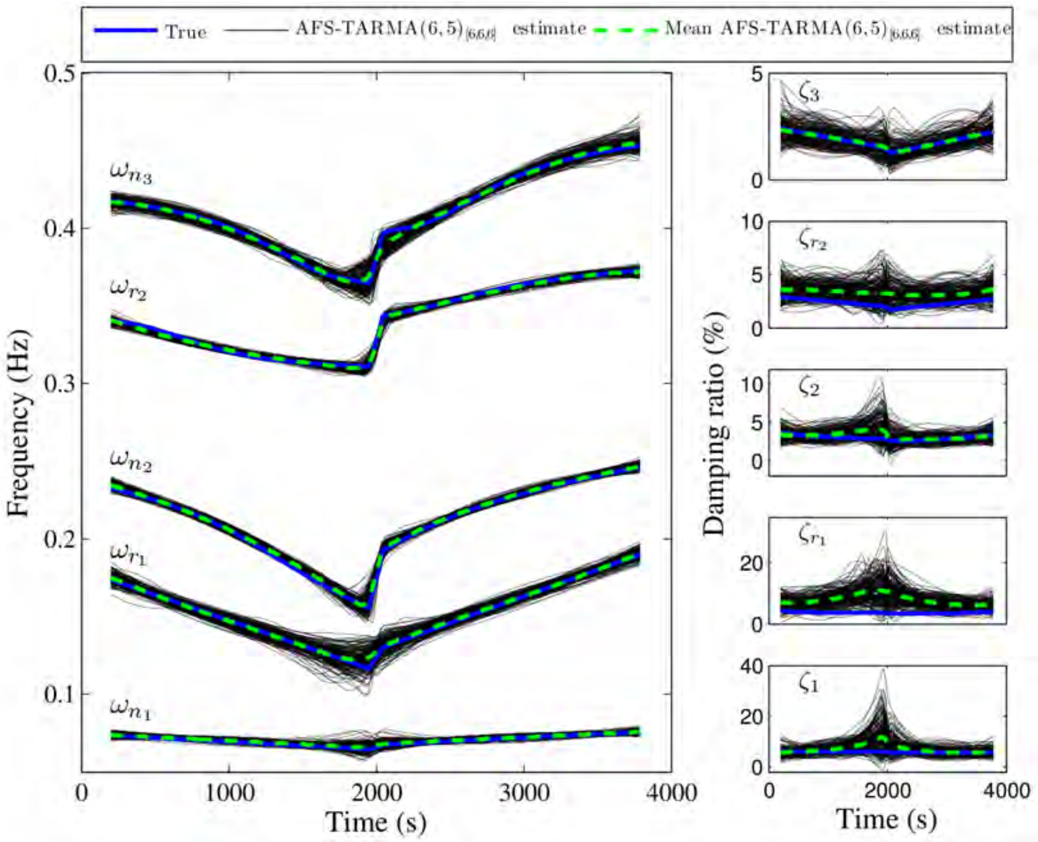

Figure 5.7.11: True TARMA$(6, 5)$ "frozen-time" global modal characteristics and estimated values based on the AFS-TARMA$(6, 5)_{[6,6,6]}$ models.

mid span of the time axis. Regarding the performance of the SP-TARMA models, even though their tracking performance may be judged as satisfactory for the resonant modes this is not true for the antiresonant ones corresponding to the values of the spectrum. The problem is much more intense for the regions where modes and antiresonances close in. Similar deficiencies had been observed in experimental comparison study based on the identification of a TV bridge-like laboratory structure for various TARMA based methods (Chapter 2). Finally, ST-SS models seem not only to be incapable of tracking the antiresonant modes but also overestimate the spectrum magnitude and thus the sharpness of the identified peaks and valleys that exist in the PSD.

(d) Ease of use. Both FS-TARMA and AFS-TARMA estimation methods may be considered as particularly complicated when compared to the rest of the non-stationary methods considered. This is due to the fact that most of them involve nonlinear optimization problems and a lot of algorithmic parameters that have to be selected. However, the 2SLS and RELS methods, which are of comparable algorithmic and computational complexity with respect to the CVA, RML, and KF methods, may provide adequate estimates.

At the same time, the FS model structure selection procedure usually necessitates user expertise and a lot of decisions have to be taken with respect to the family of basis functions to be used, the specific structure selection method and the tuning of these methods. On the contrary the number of structural parameters that have to be selected for methods belonging to the UPE and SPE classes are usually significantly less.

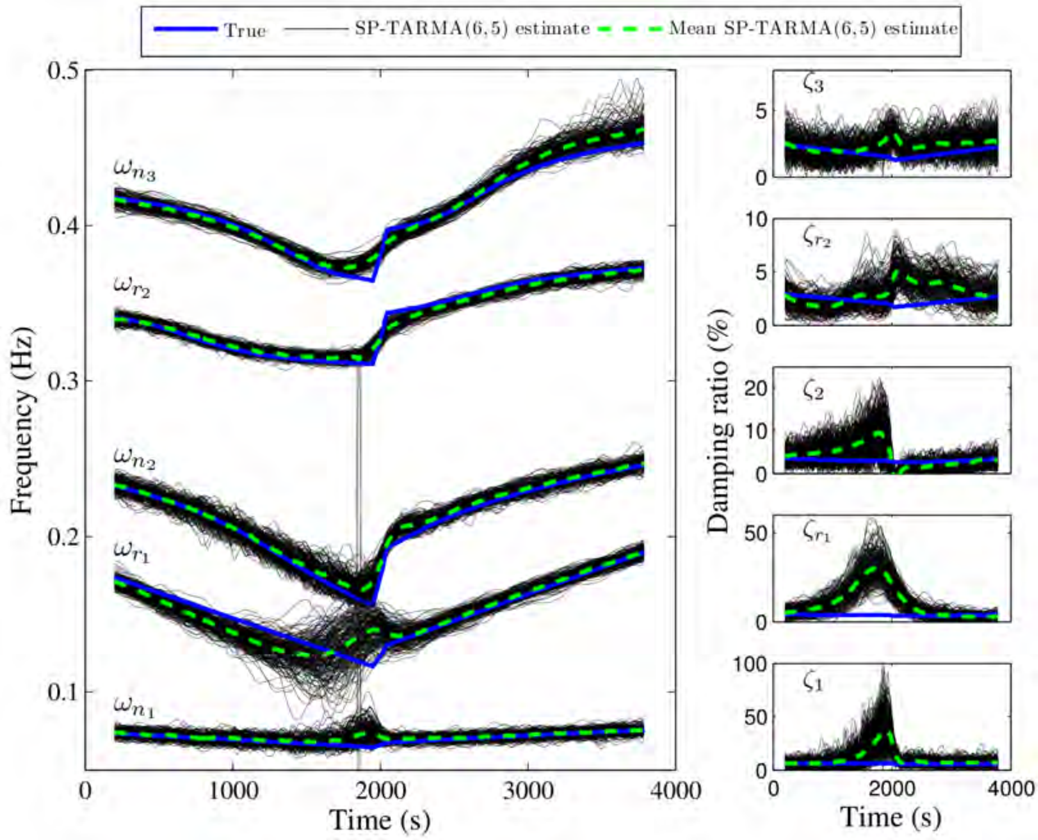

Figure 5.7.12: True TARMA$(6,5)$ "frozen-time" global modal characteristics and estimated values based on the SP-TARMA$(6,5)$ models.

5.8 Concluding Remarks and Outlook

The problem of non-stationary random vibration modelling and analysis via Functional Series TARMA models was addressed. An overview of the various identification methods was presented, and a comparative assessment study focusing on the identification of simulated systems was performed.

More specifically, the main FS-TARMA and AFS-TARMA estimation methods for both parametric and semi-parametric type of models were summarized. The methods were distinguished in Maximum Likelihood and regression type methods with emphasis given to both theoretical and practical issues.

FS-TARMA model structure selection methods were also reviewed and classified in two major categories: the integer optimization methods and those based on the concept of regression (backward or forward). The advantages and disadvantages of each method and the various parameters that are required for the realization of each method were discussed, while the performance of four model structure selection methods was examined via their application to the problem of FS-TAR model structure selection for the identification of a simulated TAR(6) model. For the same identification problem various FS-TAR and AFS-TAR estimation methods were employed and their results were compared in terms of achieved predictive ability, model parameter tracking accuracy, model-based analysis, computational simplicity and ease of use.

The performance characteristics of various FS-TARMA and AFS-TARMA estimation methods were also examined via their application to the problem of modelling and analysis of a simulated TARMA model via Monte Carlo experiments. Alternative non-stationary identification methods belonging to the classes of SPE and UPE methods were also employed for this problem and the various models estimated were also compared in terms of various criteria. The simulated non-stationary model is characterized by inhomogeneous evolution of its parameters, that is they are characterized by transitions between

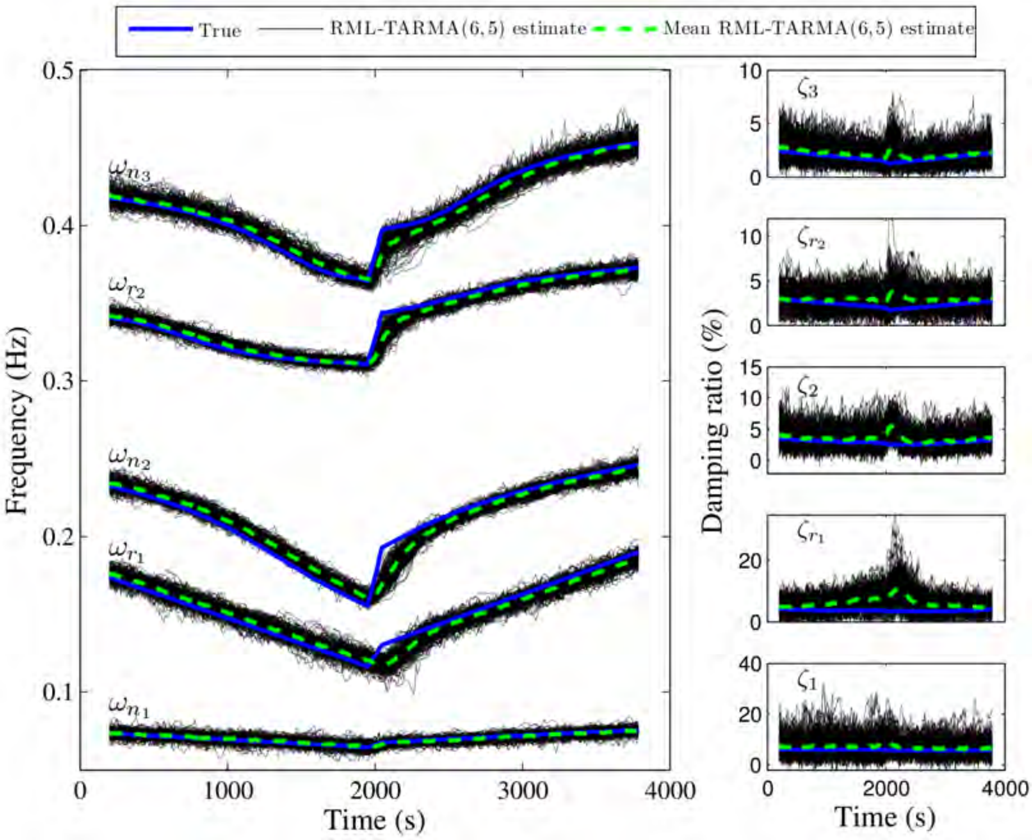

Figure 5.7.13: True TARMA$(6,5)$ “frozen-time” global modal characteristics and estimated values based on the RML-TARMA$(6,5)$ models.

smooth and abrupt changes in their values, and its identification was found to be particularly difficult for most of the methods considered. However, the best (in fact excellent) performance characteristics were achieved by AFS-TARMA models followed by RML-TARMA.

Some of the conclusions drawn from the study are:

(i) Model structure and basis functional family selection play an important role in achieving high modelling accuracy. The adaptable approach based on parametrized functional subspaces offers, at the price of increased computational complexity, significant improvement particularly for cases of inhomogeneous evolution of the time-dependent parameters.

(ii) The MS method was found to be superior to its counterparts for classic FS-TAR model estimation, while also of reduced computational complexity when compared to the ML estimates. Yet, the OLS method was found to be the best choice as long as predictive ability and simplicity are of interest.

(iii) Regarding classical FS-TARMA model estimation again the MS method provided the best results, however the best trade-off between computational complexity and achievable accuracy was provided by the 2SLS method.

(iv) AFS-TARMA models with parameters expanded on adaptable non-uniform B-spline basis functions were shown to be able to track parameters with inhomogeneous type of evolution, in contrast with the fixed bases which are used for the classical FS model types.

Despite the progress achieved thus far and the increasing number of successful applications, FS-TARMA model based non-stationary vibration analysis remains somewhat challenging for the newcomer. This is due to the elaborate model structure selection procedures, the complexity of the identification cost functions and the potential existence of local extrema, as well as problems related to estimated

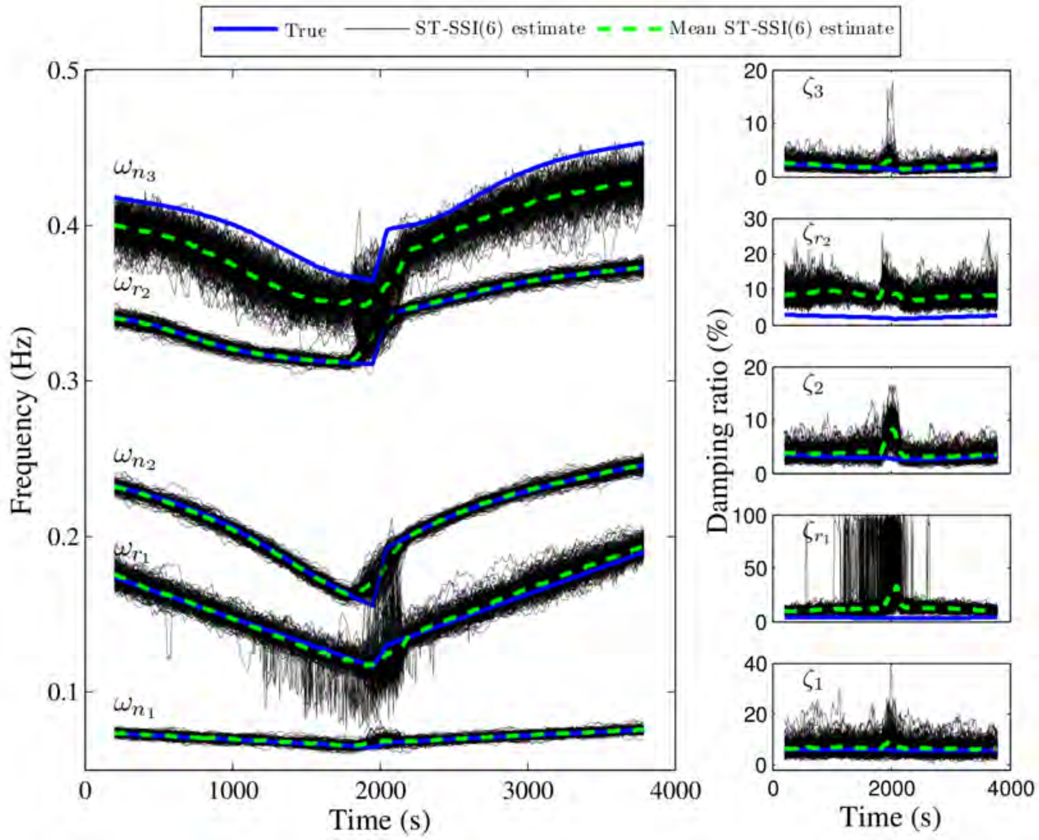

Figure 5.7.14: True TARMA$(6,5)$ "frozen-time" global modal characteristics and estimated values based on the ST-SS(6) models.

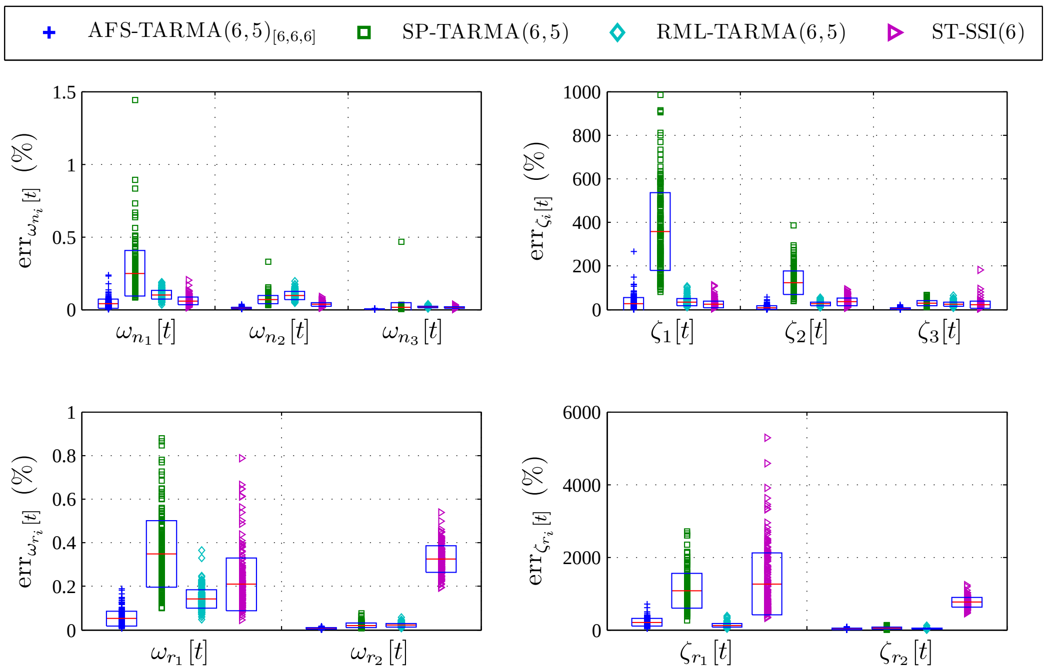

Figure 5.7.15: Mean percentage modal parameter errors for the FS-TARMA$(6,5)_{[7,4,4]}$, the SP-TARMA$(6,5)$ and RML-TARMA$(6,5)$ models.

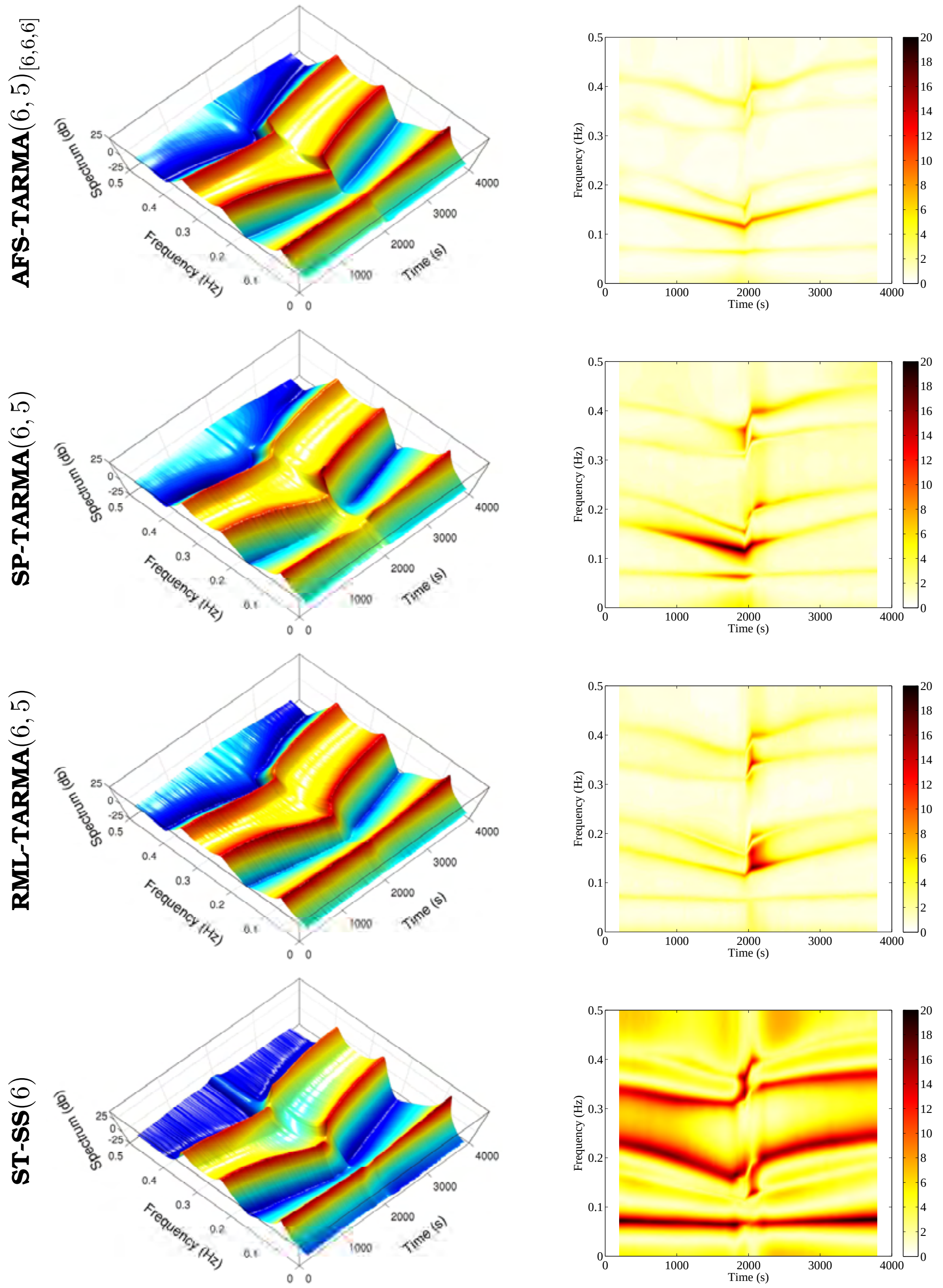

Figure 5.7.16: Mean values of the estimated through the AFS-TARMA, SP-TARMA, RML-TARMA, and ST-SS methods (left column) and the corresponding mean absolute errors (right column).

model stability and invertibility and the difficulties these may pose to both estimation and analysis. These problems need to be resolved or significantly alleviated in order to further foster practical use and applications. In spite of the remaining difficulties, the FS-TARMA models present a number of wonderful possibilities and lead to very interesting and useful results in non-stationary vibration analysis!

Appendix 5.A FS-TAR$(6)_{[10,6]}$ ML Estimates with Arbitrary Initial Values

The effectiveness of the ML estimation method initialized by random arbitrary values (normally distributed $\mathcal{N}(0,1)$) is presently examined. The first ten AR coefficient of projection estimates for 200 Monte Carlo runs and the corresponding negative log-likelihood function values are compared with those ob-

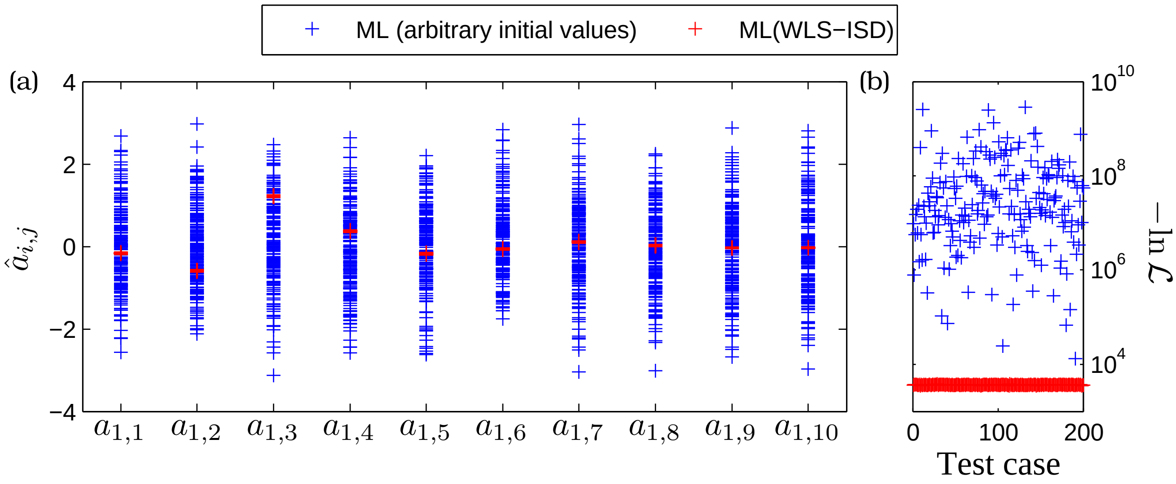

Figure 5.A.1: Performance comparison for FS-TAR ML estimation initialized by random arbitrary values (normally distributed $\mathcal{N}(0,1)$) and by estimates provided by the WLS-ISD method (DCT FS-TAR$(6)_{[10,6]}$ models): (a) the first 10 AR coefficient of projection estimates, and (b) the negative log-likelihood function values obtained.

tained by the ML method initialized by WLS-ISD estimates. As it may readily observed the ML method initialized by arbitrary values converges in all cases to a local minima while the large variability of the obtained values is an indication for the multi-modality of the log-likelihood function.

Chapter 6

An FS-TAR Based Statistical Method for the Modelling and Fault Diagnosis in Time-Varying Structures: A pick-and-place mechanism application study

The problem of vibration-response-based fault diagnosis, that is fault detection and identification, in stochastic time-varying structures is considered via a statistical time series method. The method is based on stochastic Functional Series Time-dependent AutoRegressive (FS-TAR) modelling of the structural dynamics, as well as on an appropriate statistical decision making scheme for fault diagnosis. It is an output-only method, capable of operating with a minimal number of random vibration response signals, even of limited time duration and frequency bandwidth, under normal operating conditions, and in a potentially automated way. The method is applied to the problem of fault diagnosis in a pick-and-place mechanism based on a single vibration response signal. Its performance characteristics are thus confirmed using various fault scenarios and a number of experimental test cases.

6.1 Introduction

Structures characterized by properties, either physical or geometric, that vary with time are referred as Time-Varying (TV), or else non-stationary. Such structures are widely used in a significant number of applications, such as robotics and mechanisms, variable geometry structures in aerospace technology, bridges with passing heavy vehicles, crane systems, rotating machinery, wind turbines, and so on. In a significant number of cases the TV structures operate endlessly on a repeating basis following a prescribed pattern, so their in-operation inspection based on automated decision making is of critical importance.

In recent years, significant attention has been paid to structural fault detection and identification, collectively referred to as fault diagnosis, via vibration-based methods. These are founded upon the fundamental principle that small changes (faults) in a structure cause discrepancies in the dynamics and consequently on the vibration response, which may be detected and associated with a specific cause (fault type) [Doebling et al., 1998, Farrar et al., 2001]. Vibration-based methods for fault diagnosis offer a number of potential advantages, as they require no visual inspection, are "global" (in the sense of covering large areas) and capable of working at a "system level", can operate in an automated mode during normal use/operation of the structure, and also tend to be time and cost effective [Doebling et al., 1998, Fassois and Sakellariou, 2007].

Statistical time series methods form an important category within the vibration-based fault diagnosis methods [Doebling et al., 1998, Farrar et al., 2001]. They utilize random vibration signals under healthy and potentially faulty structural states, identification of suitable time series models describing the dynamics under each structural state, and extraction of a statistical characteristic quantity Q characterizing the structural state in each case (baseline phase). Fault diagnosis is then accomplished via statistical decision making consisting of comparing, in a statistical sense, the current characteristic quantity Q_u with that of each potential state as pre-determined in the baseline phase (inspection phase). Statistical time series methods offer a number of advantages, including no requirement for physics based or finite element models, no requirement for complete modal models, no need to interrupt normal operation, effective treatment of uncertainties, and statistical decision making with specified performance characteristics. For an extended overview of the principles and also descriptions of the main methods the interested reader is referred to [Fassois and Sakellariou, 2007, Fassois and Sakellariou, 2009].

The aforementioned advantages render statistical time series fault diagnosis methods particularly attractive for TV structures. Yet, despite the progress achieved for stationary (time-invariant) structures (for instance see [Doebling et al., 1998, Fassois and Sakellariou, 2007, Carden and Fanning, 2004] and the references therein), this is not the case for non-stationary (TV) ones. A main difficulty encountered when dealing with TV structures is that their vibration responses are non-stationary, that is they are characterized by time-dependent statistical properties [Poulimenos and Fassois, 2006, Niedźwiecki, 2000]. This fact renders TV structural modelling a complicated issue, requiring the use of non-stationary modelling and analysis techniques [Poulimenos and Fassois, 2006, Staszewski and Robertson, 2007].

Depending on the nature of model used, non-stationary statistical time series methods may be broadly classified as *non-parametric* and *parametric*. Non-parametric are those methods that are based on non-parametric time-frequency representations, such as the Short-Time Fourier Transform (STFT) [Wang and McFadden, 1993], the Wigner-Ville distribution [Staszewski et al., 1997, Chengdong et al., 2008] or wavelet-based methods [Staszewski and Robertson, 2007, Peng and Chu, 2004]. Even though such methods have been extensively applied for fault diagnosis (mainly in rotating machinery), they are rarely based on statistical decision making. Hitherto, these methods rely either on visual inspection of certain characteristics (such as a time-frequency diagram) on part of the user, or more often, on classification and pattern recognition techniques capable of detecting the "fingerprint" of, say, nonlinear vibration behaviour often caused by a defect [Staszewski and Robertson, 2007]. Yet, the selection (and often the required compression) of a feature vector to be used for effective classification usually requires prior knowledge regarding the regions of the time-frequency plane in which the changes due to the defect are more pronounced, while user expertise is also required for the training phase of pattern recognition methods. Additional problems arise due to the limited achievable accuracy (including the trade-off between time and frequency resolution) of non-parametric time-frequency representations [Staszewski and Robertson, 2007].

On the other hand, parametric statistical time series methods, even though they are known to offer potentially increased modelling accuracy and resolution when compared to their non-parametric counterparts [Poulimenos and Fassois, 2006,Conforto and D'Alessio, 1999b], have, thus far, been seldom used for fault diagnosis in non-stationary (TV) structures. The problem that has somewhat more been studied is that in which a stationary structure operates under non-stationary environment or operating conditions, in which case the problem of interest is that of distinguishing changes in the dynamics (say model parameters) caused by a fault from those caused by the non-stationary environment [Basseville et al., 2007]. This is a totally different problem from (and should not be confused with) the one considered in the present study, in which the structure itself is non-stationary (TV) irrespectively of environmental or operating conditions.

An early fault detection study for inherently TV structures based on a parametric time series method has been developed by the second author and a co-worker [Poulimenos and Fassois, 2004b]. The method is based on statistical decision making utilizing the residuals of a Functional Series Time Dependent Autoregressive with eXogenous excitation (FS-TARX) model and was successively applied for the on-line fault detection in a "bridle-like" laboratory structure. A similar method based on a multivariate FS-TARX model and likelihood ratio hypothesis testing has been recently introduced and applied to the problem of fault detection in an expandable prismatic link laboratory structure [Spiridonakos and Fassois, 2009a]. In both of these studies fault diagnosis is based on availability (measurement) of both excitation (input) and response (output) signals. Yet, as in many practical applications (for instance wind turbines) excitation measurement is normally unavailable, it is important to have methods capable of achieving fault diagnosis based on response measurement(s) alone (the output-only case).

Additional statistical parametric model based methods have been utilized within the context of fault diagnosis in rotating machinery, for instance see [Zhan and Jardine, 2005a, Zhan and Jardine, 2005b, Wang et al., 2008]. However, such methods are developed for a special form of non-stationarity, specifically *cyclostationarity* which originates from the periodic motion of rotating machinery. These methods take advantage of the cyclic statistics and use synchronous average versions of the vibration signals obtained during a number of successive cycles of operation. For this reason, the methods are considered as special purpose and cannot be applied to any inherently TV structure, and/or when a decision has to be based on vibration signals acquired during a single operational cycle of the structure.

The *goal* of the present study is the introduction of a parametric statistical time series method for the effective fault diagnosis in inherently non-stationary (TV) structures with prescribed time-varying evolution. The introduced method is *output-only* and capable of operating with a *minimal number* of random vibration response signals (minimal number of sensors – presently a single signal) measured under *normal operation*, and of *limited time duration* (that may be as short as a single operational cycle, leading to limited signal duration and prompt diagnosis capability) and *frequency bandwidth*. Its normal operation (in the inspection phase) may be *automated*, requiring no human intervention.

The method is presently formulated such as to employ a single (scalar) random vibration response signal from the structure in its healthy state, as well as from a number of potential faulty states during a single operation cycle, identifying suitable non-stationary Functional Series Time-Dependent AutoRegressive (FS-TAR) statistical time series models describing the structure in each state. The AR coefficients of projection parameter vector is subsequently extracted and utilized as the characteristic quantity representing the structural state in each case (baseline phase). In its normal operation, fault detection and identification is accomplished via statistical decision making consisting of comparing, in a statistical sense, the current characteristic quantity (obtained from a fresh signal record) with that of each potential state as determined in the baseline phase (inspection phase).

The effectiveness of the method is assessed by its application to a laboratory pick-and-place mechanism which is a TV structure consisting of two electromagnetic linear motors that follow prescribed motion profiles. To this end, a number of test cases (experiments) are considered, each one correspond-

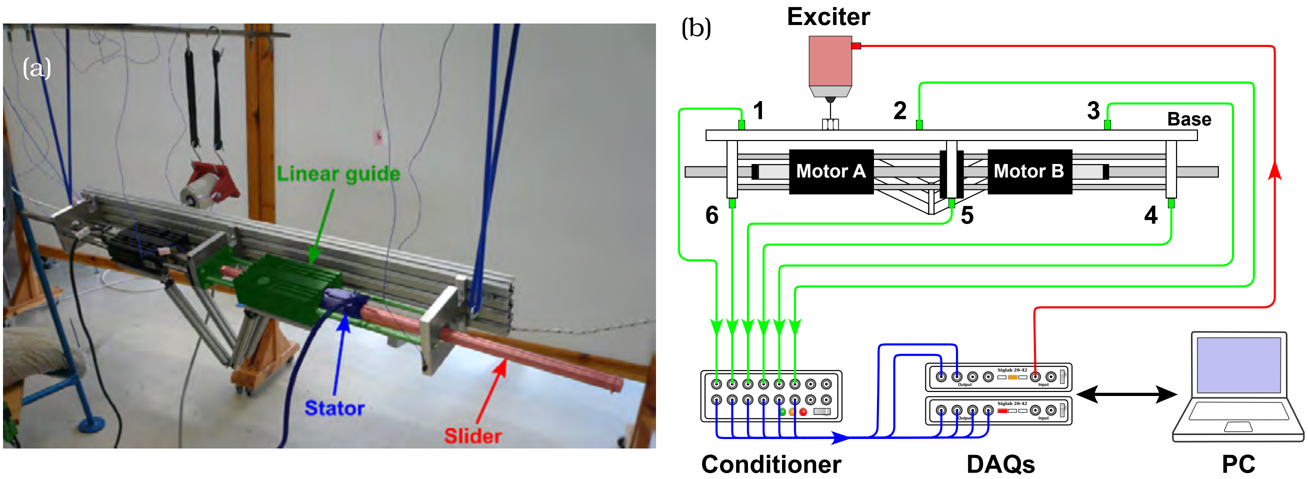

Figure 6.2.1: The pick-and-place mechanism and the experimental setup: (a) photo, (b) schematic diagram.

ing either to the nominal (healthy) state of the mechanism or to a specific fault scenario (loosening or removing one or more bolts from various parts of the mechanism or adding small mass on the slider of a motor). It is worth mentioning that linear motors, due to their advantages over rotary-motors [Yao and Xu, 2002] (less friction and no backlash, no mechanical limitations on achievable accelerations and velocities, higher reliability, longer lifetime) are met in a number of industrial applications such as manufacturing, packaging, in parallel kinematic machines, and others [Howe, 2000].

The remaining of this chapter is organized as follows: The pick-and-place mechanism, the experimental set-up, the fault scenarios, and the non-stationary experiments are presented in Section 6.2. The structural identification (modelling) of the nominal (healthy) TV dynamics is presented in Section 6.3, while the fault diagnosis method is introduced in Section 6.4. Identification results for the healthy mechanism are presented in Section 6.5, while fault detection and identification results are provided in Section 6.6. The conclusions of the study are finally summarized in Section 6.7.

6.2 The Mechanism, the Experimental Set-Up and the Faults

6.2.1 The mechanism

The system under study is a 2-DOF pick-and-place mechanism consisting of two coaxially aligned linear motors (LinMot P01-37×120) that carry prismatic links (arms) connected to their ends, with the whole mechanism being clamped on an aluminum base (Fig. 6.1(a)). The motors are electromagnetic drives able to generate linear motion with no intermediary mechanical transmission. They are made up of two parts: the slider, that is a high-precision stainless steel tube containing neodymium magnets and the stator that contains the motor windings, slider bearings, position sensors, temperature monitoring, and a microprocessor circuitry. The stators are enclosed in linear guides (LinMot HS01-37x166-GF) that are used for mounting the prismatic links, while they also provide resistance to external forces, rotational and bending moments, contributing in this way to the precise positioning of the stator. A four channel servo controller (LinMot E400-AT) is used to control and measure the position of both motors which may move independently on preselected motion profiles. Note that in this case, in contrast to what their name suggests, the sliders are fixed at one of their ends with the stators sliding on them.

6.2.2 The experimental set-up and the fault scenarios

The mechanism is suspended through two bungee cords from a long rigid beam sustained by two heavy-type stands. The suspension is designed in a way as to exhibit a pendulum rigid body mode below the

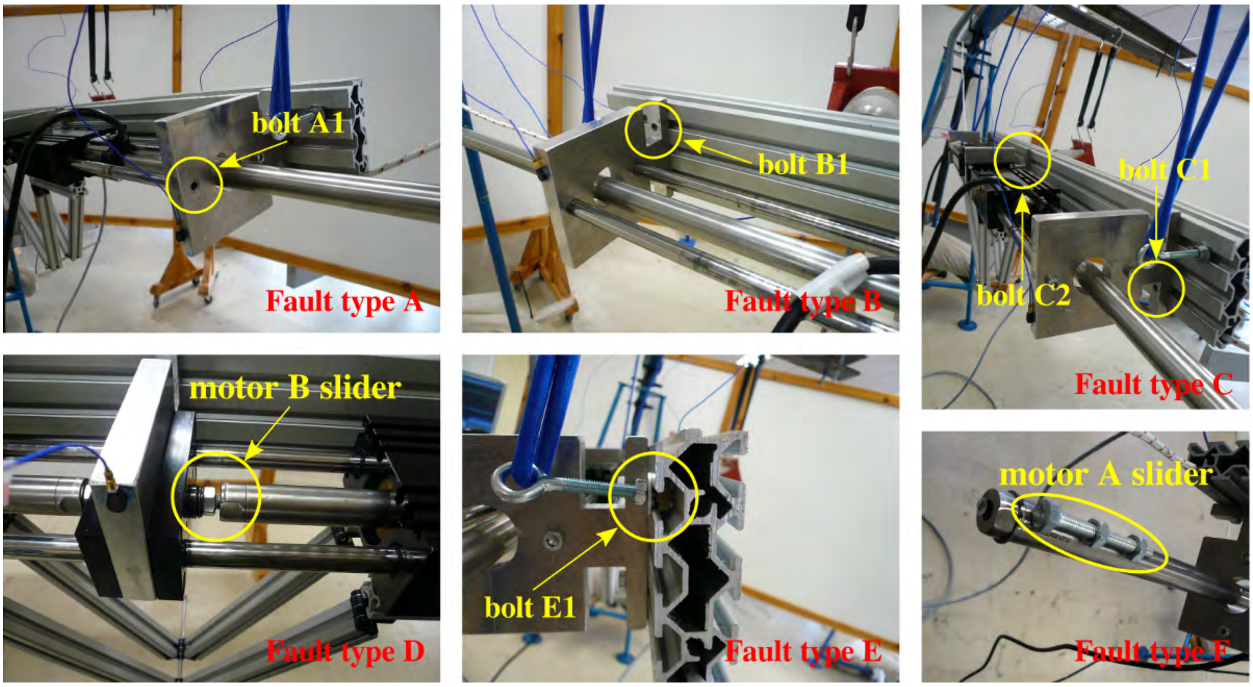

Figure 6.2.2: The considered fault types (A, B, C, D, E and F).

frequency range of interest, as the boundary conditions are free-free.

The excitation is a zero-mean Gaussian random stationary force which is vertically (with respect to the base) exerted via an electromechanical shaker (LDS V201, max load 17.8 N, useful frequency range 5-13,000 Hz) equipped with a stinger (Figs. 6.1(a) and (b)). The vertical with respect to the base vibration of the mechanism is measured at six selected locations (locations 1-6; Fig. 6.1(b)) via lightweight piezoelectric accelerometers (PCB 352C22 ICP accelerometers, frequency range 1 - 10,000 Hz, sensitivity $\sim$ 1.0 mV/m/s^2, mass 0.5 g). The measured vibration signals are conditioned and subsequently driven into SigLab 20-42 data acquisition modules (featuring four 20-bit simultaneously sampled A/D, two 16-bit D/A channels, and 4th-order quasi elliptic analog anti-aliasing filters).

The fault scenarios utilized for the purpose of assessing the effectiveness of the method correspond to the loosening or removal of various bolts at different points of the mechanism, loosening the slider of motor B, and adding a mass at the free end of the slider of motor A. In total, six distinct fault scenarios (types) are considered (Fig. 6.2.2): The first, referred to as fault type A, corresponds to the removal of bolt A1 joining one of the horizontal bars of motor B linear guide to the rightmost vertical stand of the aluminium base. The second, referred to as damage type B, corresponds to the removal of one of the two bolts joining together the leftmost vertical stand with the horizontal element of the base. The third, referred to as damage type C, corresponds to the removal of bolts C1 and C2 joining together the horizontal element of the base with two of the vertical stands. The fourth, referred to as damage type D, corresponds to the loosening of the motor B slider. The fifth, fault type E, corresponds to the loosening of the hook bolt through which the right bungee cord passes. Finally, the sixth, referred to as damage type F, corresponds to attaching a bolt to the motor A slider near its free end – the added mass is equal to 44.7 g. Note that these fault scenarios are, of course, not exhaustive, as the objective is the assessment of the effectiveness of the method. All fault types considered are summarized in Table 6.2.1.

6.2.3 The non-stationary experiments

The assessment of the statistical time series method with respect to the fault detection and identification subproblems is based on 40 experiments for the healthy and 40 experiments for each considered fault state of the mechanism (fault types $A, B, \ldots, F$ – see Table 6.2.1). However, an additional experiment

Table 6.2.1: The considered fault types, number of experiments, and vibration signal details.

Structural State	Description	Added mass[†] (g)	Total number of fault diagnosis experiments
Healthy	—	—	40
Fault Type A	removal of bolt A1	-5.1	40
Fault Type B	removal of bolt B1	-4.9	40
Fault Type C	removal of bolts C1 and C2	-9.8	40
Fault Type D	loosening of motor B slider	—	40
Fault Type E	loosening of bolt E1	—	40
Fault Type F	adding a mass on motor A slider	$+\,44.7$	40
Analysis bandwidth:	5–200 Hz		
Sampling frequency:	$f_s = 512$ Hz		
Signal length:	$N = 5{,}120$ samples ($= 10$ s)		

[†]The total mass of the mechanism is 14.5 kg

with the mechanism under its healthy state and one for each faulty state (fault types $A, B, \ldots, F$) are executed for the modelling of the mechanism (baseline phase).

During a single experiment the linear motors move from their rightmost to their leftmost position and back (Fig. 6.2.3(a); from endpoints A_1–B_1 to A_2–B_2 and back to A_1–B_1) following a reference position profile lasting 10 s (Figs. 6.2.3(b) and (c); dashed lines). The exact positions of the motors are measured by embodied magnetic Hall sensors with a sampling period of 39.2 ms (Figs. 6.2.3(b) and (c); continuous thick lines). The error between the reference and actual position in all test cases varies stochastically between -2 and 2 mm, introducing in this way an additional uncertainty. The position error curve obtained during the healthy baseline experiment is also depicted in Figs. 6.2.3(b) and (c) (continuous thin lines).

The frequency range of interest is selected as 5–200 Hz, with the lower limit set in order to avoid instrument dynamics and rigid body modes. Thus, the vibration (acceleration) signals are sampled at f_s = 512 Hz, resulting to N = 5,120 samples long (10 s) signals, with each signal subsequently being sample mean corrected (Table 6.2.1). The modelling and fault diagnosis of the time-varying mechanism is presently based on the non-stationary vibration response measured at location 4 (Fig. 6.1(b)). Of course, other locations could be alternatively used with largely similar (although not identical) results. The important fact is the use of a single response signal, which also is of limited bandwidth; characteristics that render the fault diagnosis problem challenging!

The signal employed for the modelling of the healthy TV structural dynamics of the mechanism, is depicted in Fig. 6.2.4(a). A rough estimate of its TV Power Spectral Density (PSD) obtained through the Short-Time Fourier Transform (STFT) [Hammond and White, 1996] employing a 512-sample-long moving Gaussian data window advanced by five samples (MATLAB *spectrogram* function) is depicted in Figs. 6.2.4(b) and (c). Even though the low resolution of this non-parametric representation does not permit the extraction of safe conclusions regarding the precise number of vibration modes and the way they evolve with time, it is apparent that the spectral content of the mechanism is concentrated in three frequency zones: (i) from 20 to 50 Hz, (ii) from 90 to 130 Hz, and (iii) from 140 to 190 Hz, with each zone including at least two modes.

6.3 Modelling the TV Structural Dynamics

The modelling of the TV structural dynamics is presently based on scalar FS-TAR models [Poulimenos and Fassois, 2006]. Extensions to vector models are, of course, possible (see Chapter 3). FS-TAR models constitute conceptual extensions of their conventional (stationary) AR counterparts, in that their parameters are explicit functions of time, by belonging to functional subspaces spanned by selected

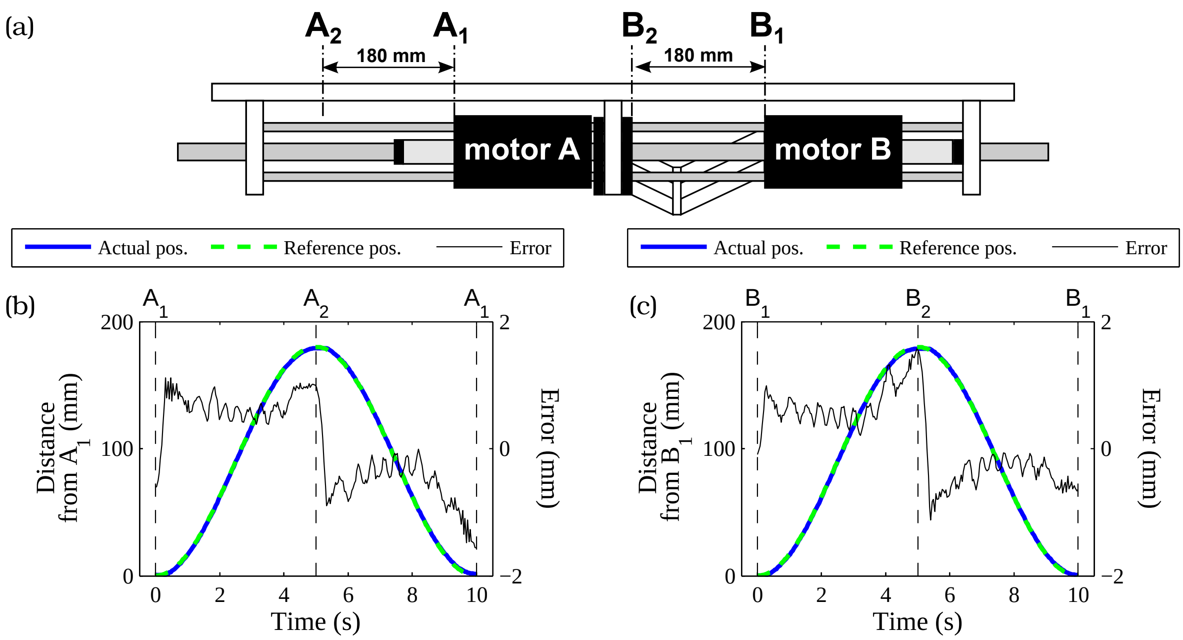

Figure 6.2.3: (a) The pick-and-place mechanism and the motor end positions, (b) actual, reference and corresponding error position of motor A, and (c) actual, reference and corresponding error position of motor B during the healthy baseline experiment.

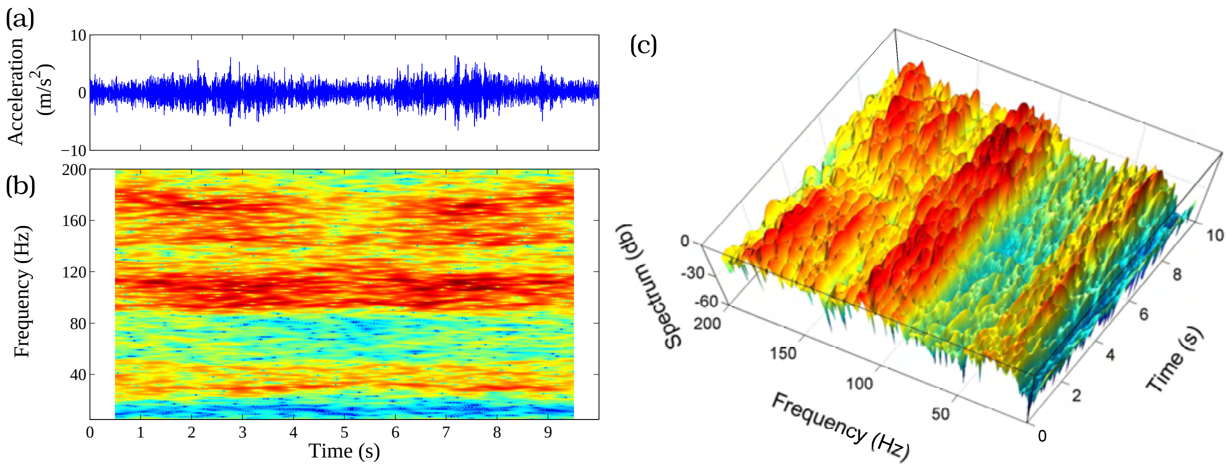

Figure 6.2.4: The healthy baseline non-stationary vibration response and preliminary analysis: (a) The vibration response signal, (b) 2D plot of the non-parametrically obtained TV PSD estimate (Short-Time Fourier Transform employing a 512-sample-long moving Gaussian data window advanced by five samples), (c) 3D plot of the non-parametrically obtained TV PSD estimate.

basis functions. They belong to the class of *deterministic parameter evolution* methods as they impose deterministic structure on the time evolution of their parameters [Poulimenos and Fassois, 2006].

An FS-TAR$(n_a)_{[p_a,p_s]}$ model, with n_a denoting its AutoRegressive (AR) order, p_a and p_s the AR and innovations standard deviation functional basis dimensionalities, respectively, is of the form:

$$x[t] + \sum_{i=1}^{n_a} a_i[t] \cdot x[t-i] = e[t], \qquad e[t] \sim \text{NID}(0, \sigma_e^2[t]), \qquad t = 1, \ldots, N \tag{6.3.1}$$

with t designating discrete time normalized by the sampling period, $x[t]$ the non-stationary response signal, and $e[t]$ the corresponding innovations (residual) sequence which is characterized by zero-mean and time-dependent standard deviation $\sigma_e[t]$. NID(·) stands for Normally Independently Distributed with the indicated mean and variance.

Let, $\mathcal{F}_{AR} \triangleq \{G_{d_a(1)}[t], \ldots, G_{d_a(p_a)}[t]\}$ and $\mathcal{F}_{\sigma_e} \triangleq \{G_{d_s(1)}[t], \ldots, G_{d_s(p_s)}[t]\}$ designate the AR and innovations standard deviation functional subspaces, respectively, where the indices $d_a(j)(j = 1, \ldots, p_a)$ and $d_s(j)(j = 1, \ldots, p_s)$ designate the functions included in each basis. Then, the FS-TAR model time-dependent parameters, along with the innovations time-dependent standard deviation, may be expressed as:

$$a_i[t] \triangleq \sum_{j=1}^{p_a} a_{i,j} \cdot G_{d_a(j)}[t], \qquad \sigma_e^2[t] \triangleq \sum_{j=1}^{p_s} s_j \cdot G_{d_s(j)}[t] \tag{6.3.2}$$

An FS-TAR model is thus parametrized in terms of its time-invariant projection coefficients $a_{i,j}, s_j$, while a specific model structure, say $\mathcal{M}$, is defined by the AR model order n_a and the functional subspaces $\mathcal{F}_{AR}, \mathcal{F}_{\sigma_e}$.

The model parameter vector and the model structure are both estimated from available vibration response data. The complete problem is distinguished into (a) the parameter estimation subproblem (for a given model structure), and (b) the model structure selection subproblem.

6.3.1 Model parameter estimation

The estimation of the projection coefficient vector $\boldsymbol{\theta}$, consisting of the AR and innovations standard deviation vectors, $\boldsymbol{\vartheta}_a$ and $\boldsymbol{\vartheta}_s$, respectively (the subscripts to brackets designate vector dimension):

$$\boldsymbol{\theta} \triangleq [\, \boldsymbol{\vartheta}_a^T \mid \boldsymbol{\vartheta}_s^T \,]^T, \quad \boldsymbol{\vartheta}_a \triangleq [\, a_{1,1} \ldots a_{1,p_a} \mid \; \ldots \; \mid a_{n_a,1} \ldots a_{n_a,p_a} \,]^T_{(n_a p_a)\times 1}, \quad \text{and} \quad \boldsymbol{\vartheta}_s \triangleq [\, s_1 \ldots s_{p_s} \,]^T_{p_s \times 1}, \tag{6.3.3}$$

is based on available vibration response signal (from a single non-stationary experiment) $X \triangleq \{x[1], x[2], \ldots, x[N]\}$ and a selected specific model structure $\mathcal{M}$.

In the present study the estimation of the parameter vector $\boldsymbol{\theta}$ is based on the Multi-Stage (MS) method which has been proven to provide consistent and asymptotically efficient estimates, that is the asymptotic covariance matrix of the MS estimator achieves the Cramér-Rao lower bound [Poulimenos and Fassois, 2007]. The MS method is implemented in three stages which are very briefly presented below.

Stage 1. Initial AR projection coefficient vector estimation: In this stage an initial estimation of the AR projection coefficient vector $\boldsymbol{\vartheta}_a$ is obtained through the Ordinary Least Squares (OLS) estimator:

$$\widehat{\boldsymbol{\vartheta}}_a^{\text{OLS}} = \left[\frac{1}{N} \sum_{t=1}^{N} \boldsymbol{\phi}[t] \cdot \boldsymbol{\phi}^T[t] \right]^{-1} \cdot \left[\frac{1}{N} \sum_{t=1}^{N} \boldsymbol{\phi}[t] \cdot x[t] \right] \tag{6.3.4}$$

where $\boldsymbol{\phi}[t] \triangleq [\, -G_{d_a(1)}[t] \cdot x[t-1], \ldots, -G_{d_a(p_a)}[t] \cdot x[t-n_a] \,]^T$.

Stage 2. Innovations standard deviation projection coefficient vector estimation: Estimation of the innovations standard deviation vector $\boldsymbol{\vartheta}_s$, is achieved by maximizing the log-likelihood of the FS-TAR model with respect to $\boldsymbol{\vartheta}_s$:

$$\widehat{\boldsymbol{\vartheta}}_s^{\text{ML}} = \arg\min_{\boldsymbol{\vartheta}_s} \left[-\ln \mathcal{L}\left(\mathcal{M}(\boldsymbol{\theta}) \mid X \right) \right] = \arg\min_{\boldsymbol{\vartheta}_s} \frac{1}{N} \sum_{t=1}^{N} \left[\ln\left(\left(\boldsymbol{g}_s^T[t] \cdot \boldsymbol{\vartheta}_s \right)^2 \right) + \frac{e^2[t, \widehat{\boldsymbol{\vartheta}}_a^{\text{OLS}}]}{\left(\boldsymbol{g}_s^T[t] \cdot \boldsymbol{\vartheta}_s \right)^2} \right] \tag{6.3.5}$$

where $\mathcal{L}\left(\mathcal{M}(\boldsymbol{\theta}) \mid X \right)$ indicates the likelihood function of the model $\mathcal{M}(\boldsymbol{\theta})$ given the vibration response data X, while $\boldsymbol{g}_s[t] \triangleq \left[G_{d_s(1)}[t] \quad G_{d_s(2)}[t] \;\ldots\; G_{d_s(p_s)}[t] \right]^T_{p_s \times 1}$. The prediction errors $e[t, \widehat{\boldsymbol{\vartheta}}_a^{\text{OLS}}]$ are obtained by the relation $e[t, \widehat{\boldsymbol{\vartheta}}_a^{\text{OLS}}] = x[t] - \boldsymbol{\phi}^T[t] \cdot \widehat{\boldsymbol{\vartheta}}_a^{\text{OLS}}$. Estimation of $\boldsymbol{\vartheta}_s$ based on Eq. (6.3.5) constitutes a nonlinear optimization problem, usually of low dimensionality (p_s), that may be tackled via iterative optimization techniques.

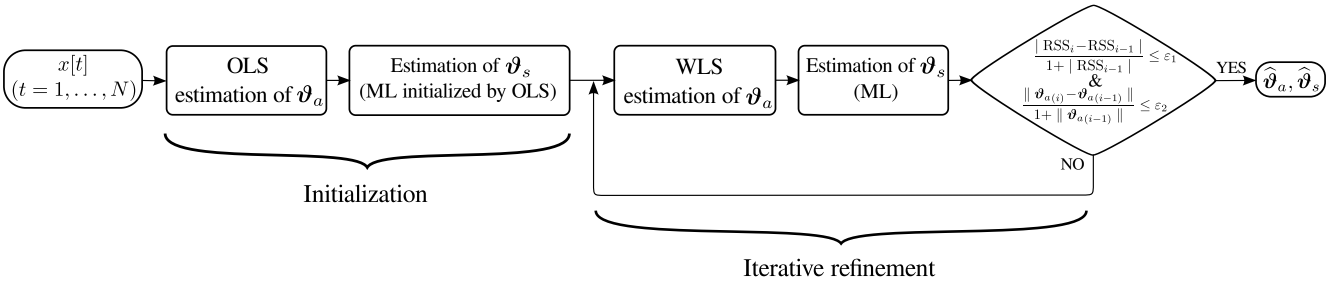

Figure 6.3.1: Flowchart of the Multi-Stage estimation method. Convergence criteria with respect to the estimated parameters and the value of the RSS are used for the termination of the iterative refinement.

Stage 3. Final AR projection coefficient vector estimation: Final estimation of the AR projection coefficient vector ϑ_a is obtained by a Weighted Least Squares (WLS) estimator by utilizing the innovations standard deviation projection coefficient vector $\widehat{\vartheta}_s^{\mathrm{ML}}$ for the weighting sequence:

$$\widehat{\vartheta}_a = \left[\frac{1}{N}\sum_{t=1}^{N}\frac{\phi[t]\cdot\phi^T[t]}{\left(g_s^T[t]\cdot\widehat{\vartheta}_s^{\mathrm{ML}}\right)^2}\right]^{-1}\cdot\left[\frac{1}{N}\sum_{t=1}^{N}\frac{\phi[t]\cdot x[t]}{\left(g_s^T[t]\cdot\widehat{\vartheta}_s^{\mathrm{ML}}\right)^2}\right] \quad (6.3.6)$$

Remarks. (a) An OLS estimator of ϑ_s is used for the initialization of the nonlinear optimization procedure of Stage 2. This is obtained by using the innovation sequence based on $\widehat{\vartheta}_a^{\mathrm{OLS}}$ and the normality of the residual sequence $e[t, \widehat{\vartheta}_a^{\mathrm{OLS}}]$, as follows [Grenier, 1983b]:

$$\widehat{\vartheta}_s^{\mathrm{OLS}} = \sqrt{\frac{\pi}{2}}\cdot\left[\sum_{t=1}^{N} g_s[t]\cdot g_s^T[t]\right]^{-1}\cdot\left[\sum_{t=1}^{N} g_s[t]\cdot\left|e[t, \widehat{\vartheta}_a^{\mathrm{OLS}}]\right|\right] \quad (6.3.7)$$

(b) Stages 2 and 3 may be iterated until a convergence criterion with respect to the estimated parameters and/or the value of a suitable prediction error function, such as the Residual Sum of Squares (RSS $= \sum_{t=1}^{N} e^2[t, \widehat{\vartheta}_a]$), is achieved. Presently, the convergence of the iterative procedure is considered with respect to both the aforementioned criteria. A flowchart of the complete MS method is depicted in Fig. 6.3.1.

6.3.2 Model structure estimation

Given a basis function family, model structure estimation refers to the estimation of the set of integers $\mathcal{M} = \{n_a, p_a, p_s, d_a(j), d_s(j)\}$ for obtaining the best fitting model. Thus, model structure selection may be viewed as a discrete variable selection problem that may be tackled via a two-phase procedure based on the concept of backward regression [Poulimenos and Fassois, 2006]. The key characteristic of this scheme is the approximate decomposition of the "structure" selection problem into two subproblems: (i) the model order (n_a) selection subproblem, and (ii) the functional subspaces selection subproblem $\{p_a, p_s, d_a(j), d_s(j)\}$.

Thus, in the first phase, in order to "isolate" the selection of the model orders from that of the functional subspaces, their interaction has to be minimized. For this reason, FS-TAR models of various orders with "extended" (high) and "complete" (in the sense of including all consecutive functions up to the selected subspace dimensionality) functional subspaces are estimated, with the appropriate AR order being selected based on the minimization of the Bayesian Information Criterion (BIC) [Poulimenos and Fassois, 2006]:

$$\mathrm{BIC} = -\ln\mathcal{L}(\mathcal{M}(\theta)|X) + d\cdot\frac{\ln N}{2} = \frac{N}{2}\cdot\ln 2\pi + \frac{1}{2}\cdot\sum_{t=1}^{N}\left(\ln\left(\left(g_s^T[t]\cdot\vartheta_s\right)^2\right) + \frac{e^2[t,\vartheta_a]}{\left(g_s^T[t]\cdot\vartheta_s\right)^2}\right) + d\cdot\frac{\ln N}{2} \quad (6.3.8)$$

where $d = n_a \cdot p_a + p_s$ is the number of independently "adjusted" (estimated) model parameters.

The second phase focuses on the optimization of the functional subspaces, in the sense of increasing the representation parsimony without significantly reducing model accuracy. This is accomplished by successively dropping (one at a time) basis functions whose removal leads to the reduction of the BIC. In each iteration the specific basis function whose removal leads to the largest decrease of the BIC is dropped while the procedure is repeated until no further reduction of the BIC is possible.

6.4 The Fault Diagnosis Method

The fault diagnosis method consists of two phases: (a) The *baseline phase*, which includes the modelling of the TV dynamics of the mechanism based on the baseline measured response signals, and (b) the *inspection phase* that is performed periodically or on demand during the mechanism's service cycle. This second phase utilizes the current vibration response signal – with the mechanism being under its current (unknown) state – and performs fault diagnosis through statistical decision making tests.

More specifically, let S_o designate the mechanism in its nominal (healthy) state and S_u the mechanism in an unknown (to be determined) state. Furthermore, let $S_A, S_B, \ldots, S_F$ designate the mechanism under fault of type $A, B, \ldots, F$, respectively. The complete response signals obtained during the baseline phase are analogously designated as $X_o, X_A, X_B, \ldots, X_F$, while the data record X_u, corresponding to an unknown (to be determined) structural state, is obtained and analyzed in the inspection phase.

The obtained signals are subsequently used for parametric modelling following the method described in Section 6.3. From each estimated FS-TAR model, the corresponding MS estimate of the AR coefficients of projection parameter vector $\boldsymbol{\vartheta}_a$ is extracted ($\widehat{\boldsymbol{\vartheta}}_{a_o}, \widehat{\boldsymbol{\vartheta}}_{a_A}, \widehat{\boldsymbol{\vartheta}}_{a_B}, \ldots, \widehat{\boldsymbol{\vartheta}}_{a_F}$ in the baseline phase; $\widehat{\boldsymbol{\vartheta}}_{a_u}$ in the inspection phase).

Fault detection is then based on testing for statistically significant changes in the parameter vector $\boldsymbol{\vartheta}_a$ between the nominal and current state of the TV mechanism through the hypothesis testing problem [Fassois and Sakellariou, 2007]:

$$\begin{array}{lll} H_0 & : & \delta\boldsymbol{\vartheta}_a = \boldsymbol{\vartheta}_{a_o} - \boldsymbol{\vartheta}_{a_u} = 0 \qquad \text{(null hypothesis – healthy mechanism)} \\ H_1 & : & \delta\boldsymbol{\vartheta}_a = \boldsymbol{\vartheta}_{a_o} - \boldsymbol{\vartheta}_{a_u} \neq 0 \qquad \text{(alternative hypothesis – faulty mechanism)} \end{array} \tag{6.4.1}$$

For sufficiently long signals the $\boldsymbol{\vartheta}_a$ MS estimator is (under mild conditions [Poulimenos and Fassois, 2007]; Appendix 6.A) Gaussian distributed with mean equal to its true value $\mathring{\boldsymbol{\vartheta}}_a$ and covariance matrix [Poulimenos and Fassois, 2007]:

$$\boldsymbol{P} = \frac{1}{N} \cdot \left\{ \frac{1}{N} \sum_{t=1}^{N} \frac{\boldsymbol{\phi}[t] \cdot \boldsymbol{\phi}^T[t]}{\left(\boldsymbol{g}_s^T[t] \cdot \widehat{\boldsymbol{\vartheta}}_s^{\mathrm{ML}}\right)^2} \right\}^{-1} \cdot \left\{ \frac{1}{N} \sum_{t=1}^{N} \frac{\sigma_e^2[t] \cdot \boldsymbol{\phi}[t] \cdot \boldsymbol{\phi}^T[t]}{\left(\boldsymbol{g}_s^T[t] \cdot \widehat{\boldsymbol{\vartheta}}_s^{\mathrm{ML}}\right)^4} \right\} \cdot \left\{ \frac{1}{N} \sum_{t=1}^{N} \frac{\boldsymbol{\phi}[t] \cdot \boldsymbol{\phi}^T[t]}{\left(\boldsymbol{g}_s^T[t] \cdot \widehat{\boldsymbol{\vartheta}}_s^{\mathrm{ML}}\right)^2} \right\}^{-1} \tag{6.4.2}$$

Hence,

$$\boldsymbol{\vartheta}_a \sim \mathcal{N}(\mathring{\boldsymbol{\vartheta}}_a, \boldsymbol{P}) \tag{6.4.3}$$

The difference between the two parameter vector estimators also follows Gaussian distribution [Fassois and Sakellariou, 2007], that is

$$\delta\widehat{\boldsymbol{\vartheta}}_a = \widehat{\boldsymbol{\vartheta}}_{a_o} - \widehat{\boldsymbol{\vartheta}}_{a_u} \sim \mathcal{N}(\delta\boldsymbol{\vartheta}_a, \delta\boldsymbol{P}) \tag{6.4.4}$$

with $\delta\boldsymbol{\vartheta}_a = \boldsymbol{\vartheta}_{a_o} - \boldsymbol{\vartheta}_{a_u}$ and $\delta\boldsymbol{P} = \boldsymbol{P}_o + \boldsymbol{P}_u$, where $\boldsymbol{P}_o, \boldsymbol{P}_u$ designate the corresponding covariance matrices. Under the null (H_0) hypothesis $\delta\widehat{\boldsymbol{\vartheta}}_a = \widehat{\boldsymbol{\vartheta}}_{a_o} - \widehat{\boldsymbol{\vartheta}}_{a_u} \sim \mathcal{N}(0, 2\boldsymbol{P}_o)$ and the quantity

$$\chi^2_{\boldsymbol{\vartheta}_a} = \delta\widehat{\boldsymbol{\vartheta}}_a^T \cdot \delta\boldsymbol{P}^{-1} \cdot \delta\widehat{\boldsymbol{\vartheta}}_a \tag{6.4.5}$$

with $\delta\boldsymbol{P} = 2\boldsymbol{P}_o$ follows χ^2 distribution with $n_a p_a$ (parameter vector $\boldsymbol{\vartheta}_a$ dimensionality) degrees of freedom [Fassois and Sakellariou, 2007], [Ljung, 1999, p. 558]. As the covariance matrix $\boldsymbol{P}_o$ corresponding to the healthy structure is unavailable, its estimated version $\widehat{\boldsymbol{P}}_o$ is used, obtained from Eq. (6.4.2) substituting

Table 6.4.1: Statistical hypothesis testing problems for the fault detection and identification tasks.

Fault Detection	
$H_0 : \boldsymbol{\vartheta}_{a_u} \sim \boldsymbol{\vartheta}_{a_o}$	null hypothesis – healthy state
$H_1 : \boldsymbol{\vartheta}_{a_u} \nsim \boldsymbol{\vartheta}_{a_o}$	alternative hypothesis – faulty state
Fault Identification	
$H_A : \boldsymbol{\vartheta}_{a_u} \sim \boldsymbol{\vartheta}_{a_A}$	hypothesis A – fault type A
$H_B : \boldsymbol{\vartheta}_{a_u} \sim \boldsymbol{\vartheta}_{a_B}$	hypothesis B – fault type B
$\vdots$	$\vdots$

$\sigma_e^2[t]$ by $\left(\boldsymbol{g}_s^T[t] \cdot \widehat{\boldsymbol{\vartheta}}_s^{\text{ML}}\right)^2$. Then, the following test is constructed at the α (type I) risk level (that is the probability of rejecting the null hypothesis H_0 although it is true, or else the false alarm probability):

$$\begin{aligned} &\chi^2_{\boldsymbol{\vartheta}_a} \leq \chi^2_{1-\alpha}(n_a p_a) && \Longrightarrow && H_0 \text{ is accepted (healthy mechanism)} \\ &\text{Else} && \Longrightarrow && H_1 \text{ is accepted (faulty mechanism)} \end{aligned} \tag{6.4.6}$$

with $\chi^2_{1-\alpha}(n_a p_a)$ designating the χ^2 distribution's $1-\alpha$ critical point.

Fault identification may be based on the hypotheses testing problems of Table 6.4.1 comparing the parameter vector $\boldsymbol{\vartheta}_{a_u}$ belonging to the current state of the structure to those corresponding to different fault types $\boldsymbol{\vartheta}_{a_A}, \boldsymbol{\vartheta}_{a_B}, \ldots, \boldsymbol{\vartheta}_{a_F}$. The complete fault diagnosis framework is depicted in Fig. 6.4.1. It should be noted that the fault identification is presently based on successive binary hypothesis tests – as opposed to multiple hypothesis tests [Fassois and Sakellariou, 2007].

6.4.1 Brief summary of the method

Baseline Phase

Step 1. *Modelling of the healthy structural dynamics.* Use a vibration response signal X_o (sample mean subtracted) from the healthy structure to estimate an appropriate FS-TAR model using the procedure of Sections 3.1 and 3.2 (Eqs. (4)-(8)).

Step 2. *Modelling of the structural dynamics for each fault type.* If fault identification is desired, repeat Step 1 as necessary, each time using a vibration response signal X_A or X_B or ... or X_F (sample mean subtracted) from the structure under each one of the faults A or B or ... or F, respectively.

Inspection Phase

Step 3. *Modelling of the current structural dynamics using the healthy model structure.* Use a fresh response signal X_u (sample mean subtracted) from the current (in unknown state) structure to estimate an FS-TAR model of order and subspaces identical to that of the healthy baseline model estimated in Step 1 using the procedure of Section 3.1 (Eqs. (4)-(7); no model structure selection procedure implemented here).

Step 4. *Fault detection.* Compare the current model to its baseline phase counterpart (obtained in Step 1) via the statistical hypothesis testing procedure of Eqs. (9)-(10), (12)-(14) and decide (at a selected α risk level) whether the structure is healthy or faulty.

Step 5. If the structure is healthy the method terminates. Otherwise proceed to Step 6.

Step 6. *Modelling of the current structural dynamics using the various fault type model structures.* Use the same fresh response signal X_u (sample mean subtracted) and the procedure of Step 3 to estimate current FS-TAR models of identical (in each fault type case) orders and functional subspaces to those determined in the baseline phase (Step 2) using the procedure of Section 3.1 (Eqs. (4)-(7); no model structure selection implemented here).

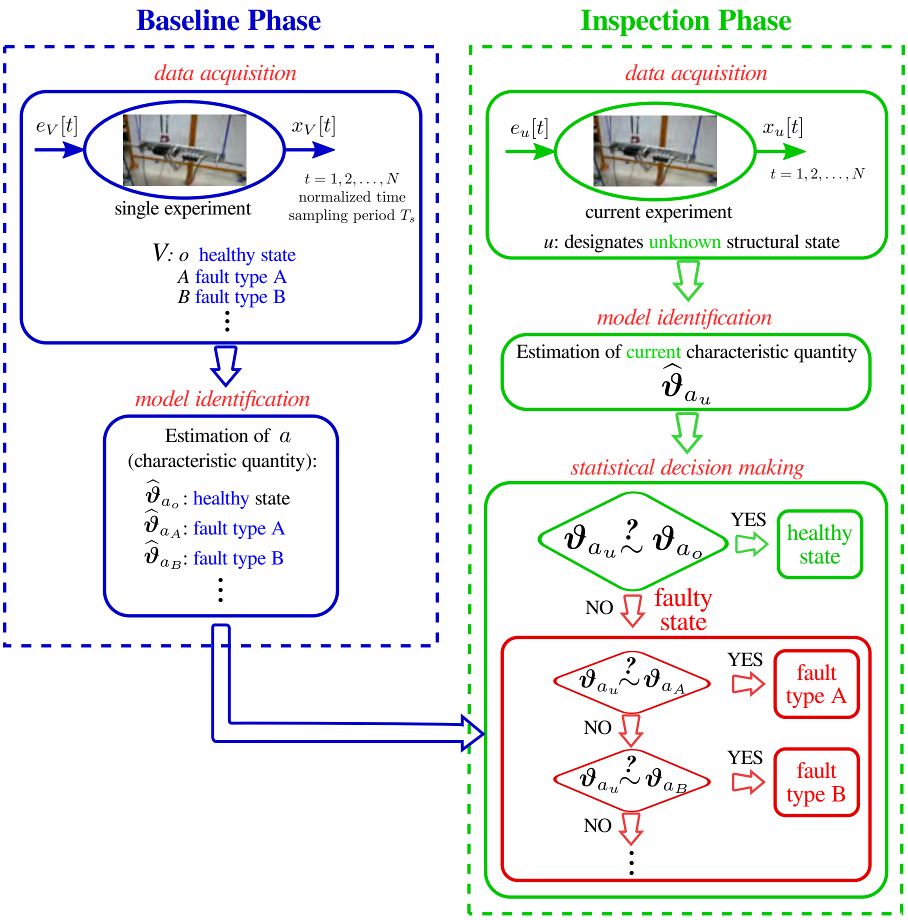

Figure 6.4.1: Flowchart of the fault diagnosis method.

Step 7. *Fault identification.* Compare the current FS-TAR model (corresponding to fault type A and obtained in Step 6) to its baseline phase counterpart (obtained in Step 2) via the statistical hypothesis testing procedure of Eqs. (9)-(10), (12)-(14) to decide (at a selected α risk level) whether the structure is under fault type A. If not, then repeat for each additional fault type ($B, C, \ldots, F$) until the fault type is determined.

6.5 Modelling Results for the Healthy TV Structural Dynamics

The FS-TAR modelling of the TV mechanism dynamics under its healthy (nominal) structural state is presently considered. A functional basis spanned by the Discrete Fourier Transform (DFT) functions:

$$G_0[t] = 1, \quad G_{2\kappa-1}[t] = \cos\left[\frac{2\kappa\,\pi\,(t-1)}{N-1}\right], \quad G_{2\kappa}[t] = \sin\left[\frac{2\kappa\,\pi\,(t-1)}{N-1}\right], \text{ with } \kappa = 1, 2, \ldots, \text{ and } t = 1, \ldots, N \tag{6.5.1}$$

is adopted, prescribed by the periodic nature of the linear motors motion profile. The model structure selection is achieved using the search scheme described in Section 6.3.2. Thus, at first an extended and complete functional subspaces of dimensionality equal to 13 ($p_a = p_s = 13$) is employed and FS-TAR$(n_a)_{[13,13]}$ models with $n_a = 10, \ldots, 30$ are estimated, with the optimal AR order being selected based on the BIC. The initial functional subspaces are subsequently reduced based on the BIC and the backward regression procedure.

The BIC values for the obtained FS-TAR$(n_a)_{[13,13]}$ ($n_a = 10, \ldots, 30$) are shown in Fig. 6.5.1(a). The optimal AR order is selected as $n_a = 21$, while the finally obtained AR and innovations standard deviation functional subspaces are of dimensionalities $p_a = 3$ ($\mathcal{F}_{\text{AR}} = \{G_0[t], G_1[t], G_3[t]\}$) and $p_s = 4$

Table 6.5.1: Parameter estimation method implementation details.

OLS	MATLAB *mldivide* function (Householder transformation)
$\boldsymbol{\vartheta}_a$ MS estimation	termination rules: $\dfrac{\mid \text{RSS}_i - \text{RSS}_{i-1} \mid}{1+ \mid \text{RSS}_{i-1} \mid} \leq 10^{-8}$ and $\dfrac{\parallel \boldsymbol{\vartheta}_{a(i)} - \boldsymbol{\vartheta}_{a(i-1)} \parallel}{1+ \parallel \boldsymbol{\vartheta}_{a(i-1)} \parallel} \leq 10^{-8}$
$\boldsymbol{\vartheta}_s$ ML nonlinear optimization	MATLAB *fminsearch* function (Nelder-Mead simplex method), termination rules: $\dfrac{\mid (\ln \mathcal{L})_i - (\ln \mathcal{L})_{i-1} \mid}{1+ \mid (\ln \mathcal{L})_{i-1} \mid} \leq 10^{-8}$ and $\dfrac{\parallel \boldsymbol{\vartheta}_{s(i)} - \boldsymbol{\vartheta}_{s(i-1)} \parallel}{1+ \parallel \boldsymbol{\vartheta}_{s(i-1)} \parallel} < 10^{-12}$

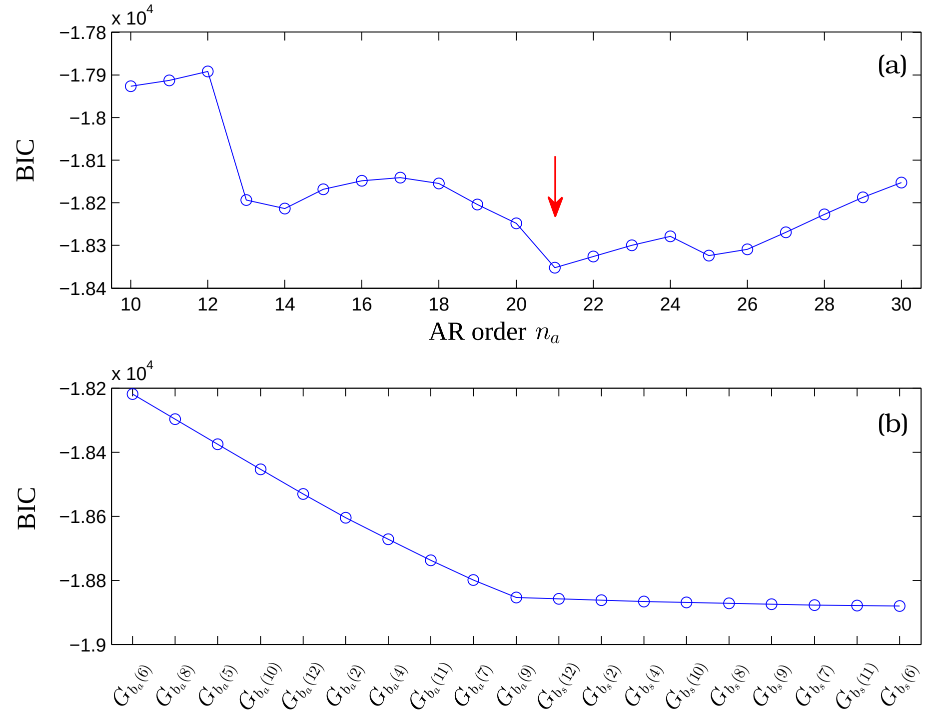

Figure 6.5.1: Baseline Phase: FS-TAR model structure selection for the healthy structural dynamics. (a) AR order selection based on the BIC using an extended and complete functional subspace ($p_a = p_s = 13$), and (b) BIC values obtained by sequentially dropping each of the indicated basis functions until no further reduction is possible.

($\mathcal{F}_{\sigma_e^2[t]} = \{G_0[t], G_1[t], G_3[t], G_5[t]\}$), respectively (Fig. 6.5.1(b)). The implementation details for the parameter estimation method are summarized in Table 6.5.1, while as shown in Fig. 6.5.2 the finally estimated FS-TAR model is successfully validated (at the 0.01 risk level) using a distribution-free sign test [Poulimenos and Fassois, 2006] [Draper and Smith, 1998, pp. 192-198].

It must be noticed that the AR functional subspace consists of the basis functions $G_0[t] = 1, G_1[t] = \cos\left[\frac{2\pi(t-1)}{N-1}\right]$ and $G_3[t] = \cos\left[\frac{4\pi(t-1)}{N-1}\right]$, that is the constant function and the first two cosine functions of the DFT basis. The time-dependent basis functions correspond to frequencies $f_1 = 0.1$ Hz and $f_2 = 0.2$ Hz, or else and as shown in Fig. 6.5.3(a) are cosine functions with one and two periods, respectively, during the complete non-stationary experiment. In the same figure, the motors passage from the rightmost endpoints A_1-B_1, the midpoints A_m-B_m, and the leftmost endpoints A_2-B_2 of the motors motion trajectories are associated with time and indicated by dot-dashed vertical lines which may provide a guide for illustrating the relationship of f_1 and f_2 with the motion of the motors and the geometry of the mechanism. More specifically, the fact that each motor returns to its initial position following sinusoidal motion profiles is reflected in f_1 (it is reminded that the motors move from A_1-B_1 to A_2-B_2 and back to A_1-B_1). To illustrate the connection of f_2 with the evolution of the underlying TV

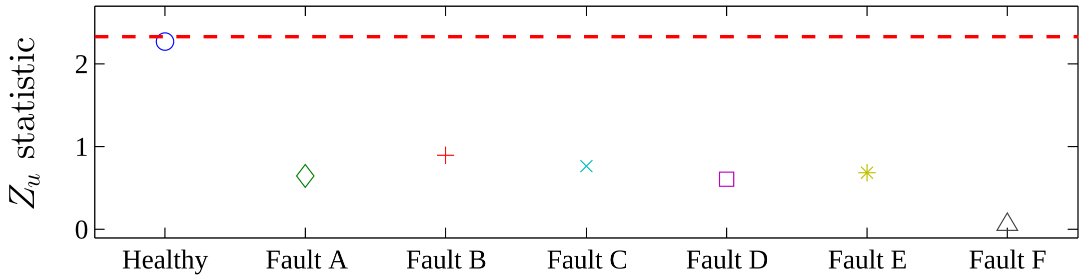

Figure 6.5.2: Baseline Phase: FS-TAR model validation through the residual sign test (risk level $\alpha = 0.01$; a model is successfully validated if the test statistic is below the critical limit designated by the dashed horizontal line).

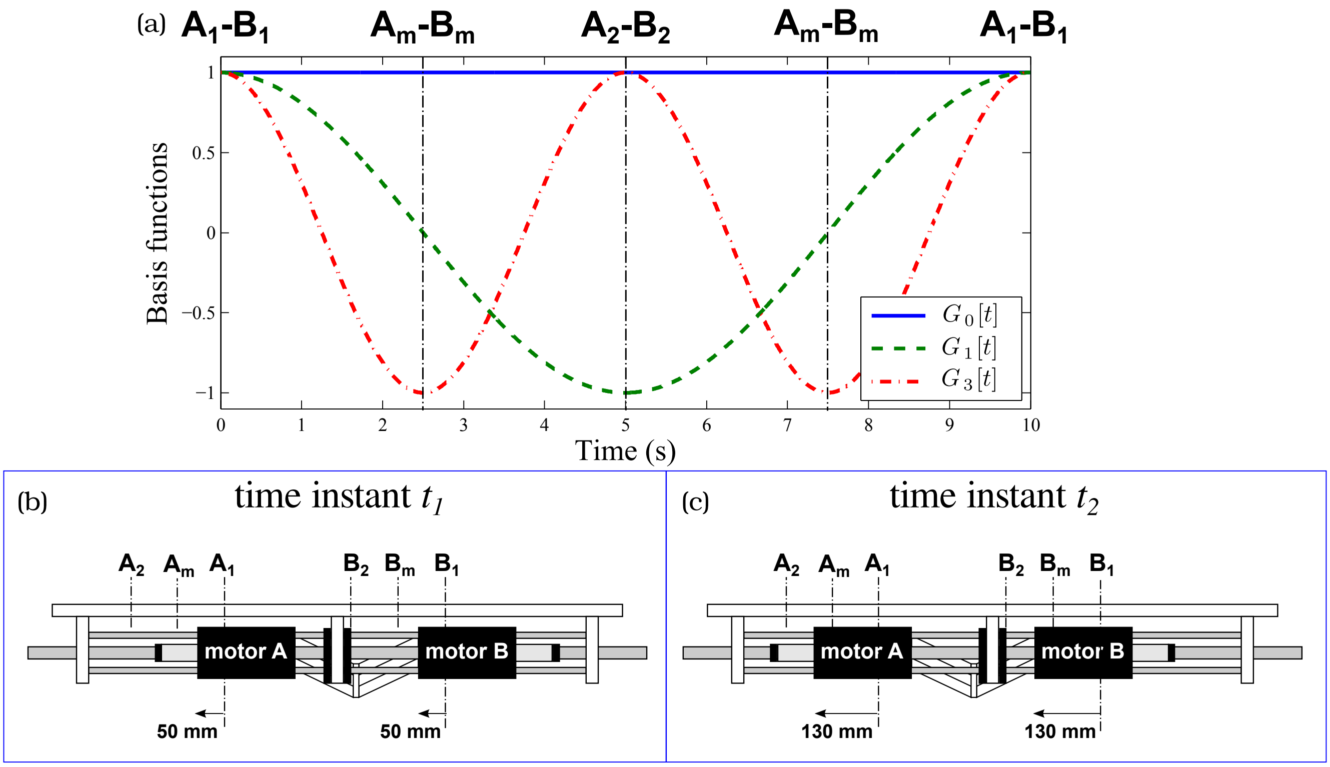

Figure 6.5.3: (a) The basis functions $G_0[t]$, $G_1[t]$ and $G_3[t]$, (b) the "frozen" configuration of the mechanism with the motors having covered a distance of 50 mm from their initial position A_1-B_1, and (c) the "frozen" configuration of the mechanism with the motors having covered a distance of 130 mm from their initial positions A_1-B_1.

structural dynamics, let consider the time instants t_1 and t_2 with the motors having covered 50 mm and 130 mm, respectively, from their initial positions (rightmost endpoints A_1-B_1). On the contrary, at time instant t_1 the distance of the motors from their leftmost endpoints A_2-B_2 is 130 mm while at t_2 is 50 mm. As shown in Figs. 6.5.3(b) and (c) the "frozen" configuration of the mechanism at t_1 is a reflected image of the respective configuration of the mechanism at t_2. As a consequence the global characteristics of the mechanism TV structural dynamics, which are represented by the time-dependent AR parameters, will be the same for these two time instants. Thus, there is an additional symmetry with respect to the midpoints A_m-B_m which is directly related with f_2.

The accuracy of the FS-TAR model representing the mechanism under its healthy state is also judged in terms of the model-based analysis of the mechanism TV dynamics. For this purpose, the vibration

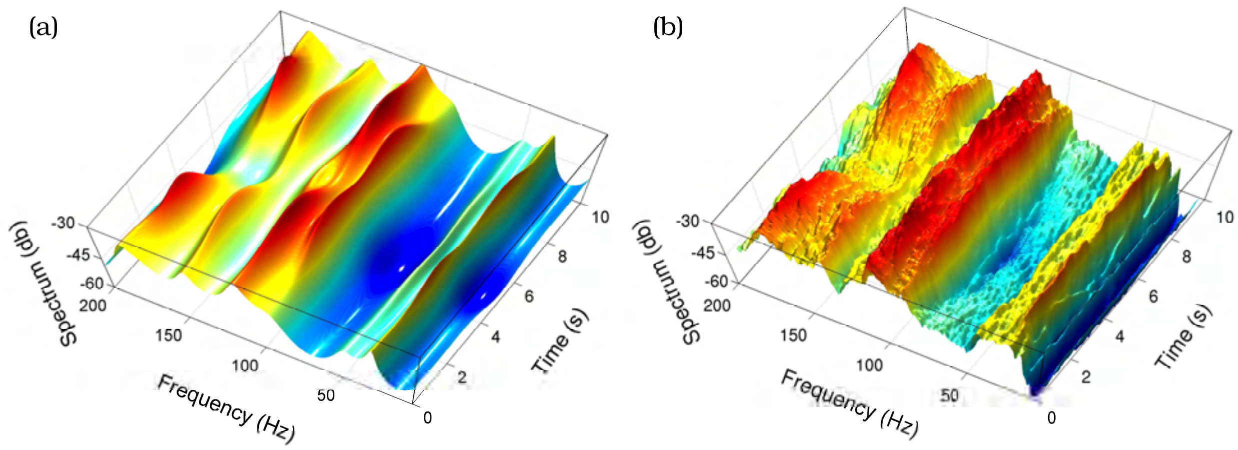

Figure 6.5.4: Healthy baseline dynamics: (a)"Frozen-time" TV-PSD estimate based on the FS-TAR$(21)_{[3,4]}$ model, and (b) sample mean spectrogram obtained from the total of 41 non-stationary experiments.

response signal's "frozen-time" PSD is obtained as [Poulimenos and Fassois, 2006]:

$$S(\omega, t) = \frac{\sigma_e^2[t]}{\left|1 + \sum_{i=1}^{n_a} a_i[t] e^{-j\omega T_s i}\right|^2}, \tag{6.5.2}$$

with the model parameters and innovations variance being replaced by their respective estimates, ω designating frequency in rad/s, T_s the sampling period in s, and j the imaginary unit, while the system's "frozen-time" natural frequencies and damping ratios are also computed by the TV frozen model poles.

The "frozen-time" PSD estimated based on the FS-TAR$(21)_{[3,4]}$ model is depicted in Fig. 6.5.4. The model-based PSD estimate is contrasted to the sample mean spectrogram obtained from the 41 non-stationary experiments with the mechanism being under its healthy state. As it may be observed the FS-TAR based estimate is in good agreement with its non-parametric counterpart but much more clear smooth and informative. This result is indicative of the potential of non-stationary parametric based methods for accurate modelling and the advantages that they offer contrasted to their non-parametric counterparts with respect to the achievable resolution.

The corresponding "frozen-time" natural frequency estimates are illustrated in Fig. 6.5.5 (with the sample mean spectrogram shown in the background) along with the corresponding damping ratios. In total, eight natural frequencies are identified in the analyzed bandwidth which, as already indicated from the preprocessing analysis of Section 6.2.3, are concentrated in three distinct frequency zones (20-50 Hz, 90-130 Hz, and 140-190 Hz). Most of these modes are characterized by low damping ratios ($< 10\%$), while all of them depict high variability characterized by the f_1 and f_2 frequencies of the AR basis functions.

6.6 Fault Diagnosis Results

6.6.1 Baseline phase

The FS-TAR model parameter and structure estimation procedure described in Section 6.3 is subsequently employed for the estimation of the remaining baseline models, each one corresponding to each fault type (scenario), that is $A, B, \ldots, F$. The model structure details for the estimated models are summarized in Table 6.6.1 (the model structure selection results are given in Appendix 6.B), while the finally estimated FS-TAR models are also successfully validated (see Fig. 6.5.2).

Summary results expressed in terms of various performance criteria are, for all baseline models, provided in Fig. 6.6.1. It is observed that in all cases baseline models attain similar predictive performance (RSS/SSS values) except from the baseline models representing the mechanism under fault states C

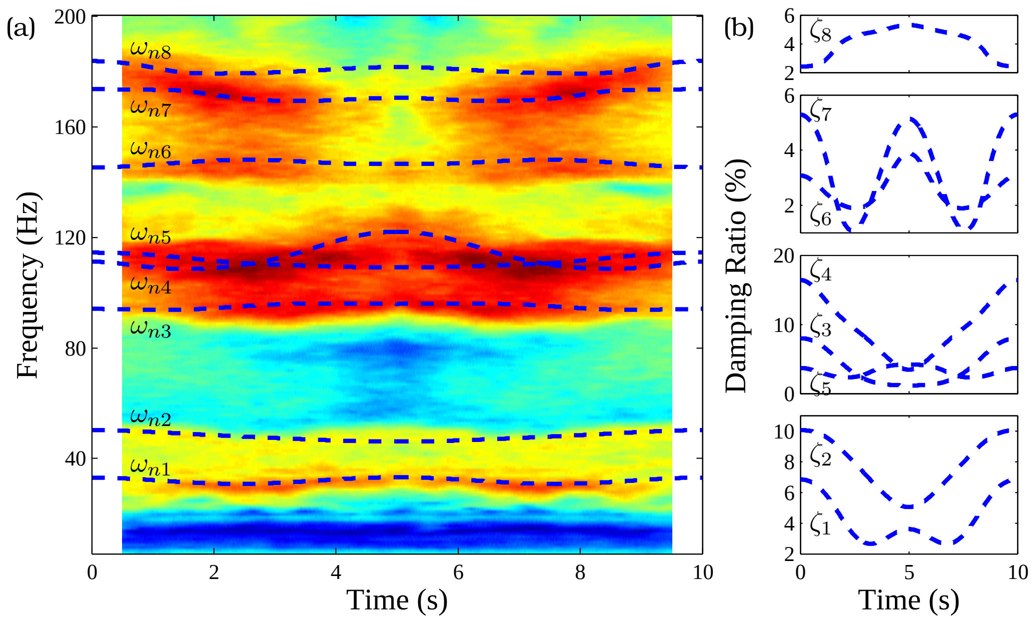

Figure 6.5.5: Healthy baseline dynamics based on the FS-TAR$(21)_{[3,4]}$ model: (a) "Frozen-time" natural frequency estimates (sample mean spectrogram shown in the background), and (b) the corresponding "frozen-time" damping ratios.

Table 6.6.1: Model structure details for the identified baseline FS-TAR models.

Structural State	n_a	d_a	p_a	d_s	p_s
Healthy	21	[0 1 3]	3	[0 1 3 5]	4
Fault Type A	22	[0 1 3]	3	[0 1 3 5]	4
Fault Type B	22	[0 1 3]	3	[0 3 5 7]	4
Fault Type C	21	[0 1 3]	3	[0 3 5 9 11 12]	6
Fault Type D	22	[0 1 3]	3	[0 1 3]	3
Fault Type E	21	[0 1 3]	3	[0 1 3]	3
Fault Type F	22	[0 1 3]	3	[0 3]	2

and D. Therefore, these baseline models may be considered as less capable of representing the faulty mechanism dynamics. On the other hand, the good Samples Per Parameters (SPP) values and the low regression matrix conditions numbers indicate good statistical and numerical reliability for all estimated models.

The "frozen-time" natural frequency and damping ratio estimates obtained by the baseline FS-TAR models representing the mechanism under fault states C and E are also illustrated in Figs. 6.6.2 and 6.6.3, respectively. Although, when compared to the corresponding healthy model based estimates (Fig. 6.5.5) small changes are observed in the case of fault E, this is not true for fault C, with the changes being more pronounced in the modes above 100 Hz. The increased sensitivity of the higher modes to local damage has also been observed in a number of previous studies (see [Salawu, 1997] and the references therein). Similar comments apply to faults B and D, while smaller changes are observed for faults A and F. These results constitute an indication for the severity of each fault and are in agreement with the RSS/SSS values attained by the identified baseline models, which constitute a model fitting criterion.

At this point it must be noted, that the symmetries of the mechanism which in the health case are reflected by f_1 and f_2 are only approximately valid for the fault cases since faults do not occur in a symmetric way. Thus, it is expected that more severe faults will cause increased deviation from symmetry and FS-TAR models with parameters expanded on DFT basis functions, which are by definition

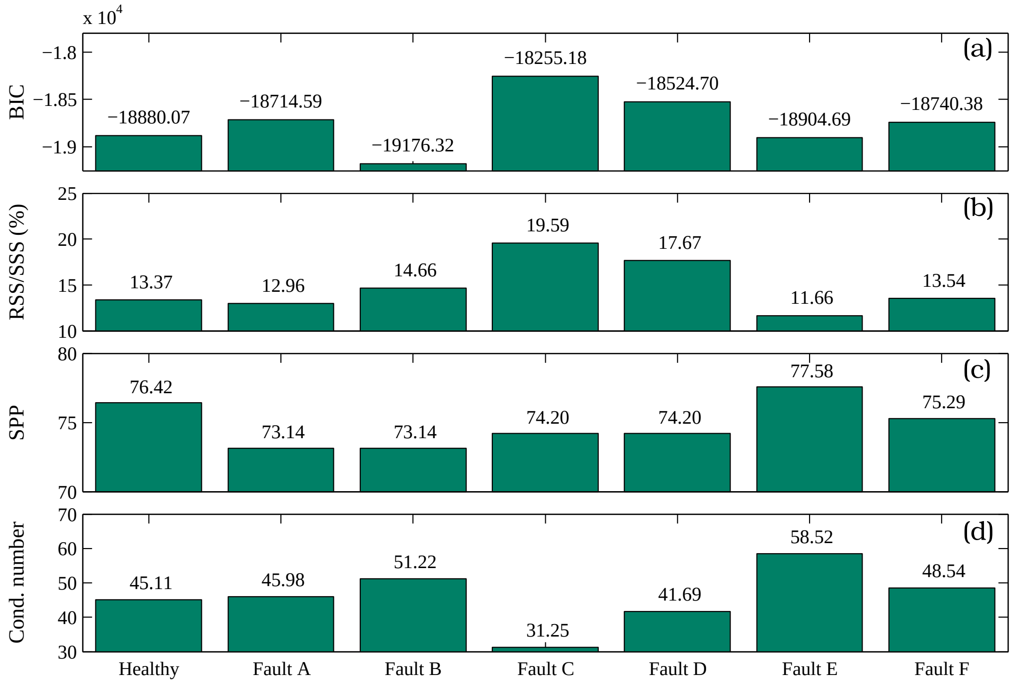

Figure 6.6.1: Baseline FS-TAR models performance criteria: (a) BIC, (b) RSS normalized by the Series Sum of Squares (RSS/SSS), (c) Samples Per Parameters (SPP), and (d) the condition number of the regression matrix.

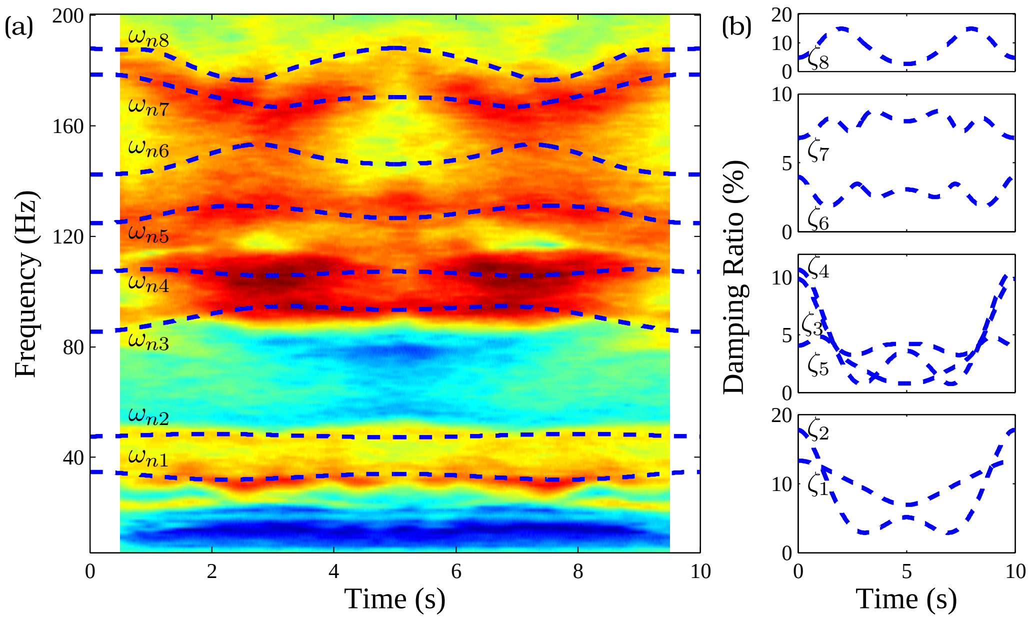

Figure 6.6.2: Baseline dynamics under fault C based on the FS-TAR$(21)_{[3,6]}$ model: (a) "Frozen-time" natural frequency estimates (sample mean spectrogram shown in the background), and (b) the corresponding "frozen-time" damping ratios.

symmetric, will be less capable of accurately describing the TV structural dynamics of the mechanism. However, this is a disadvantage only as long as modelling of the faulty mechanism is considered, but actually consists an asset for fault diagnosis.

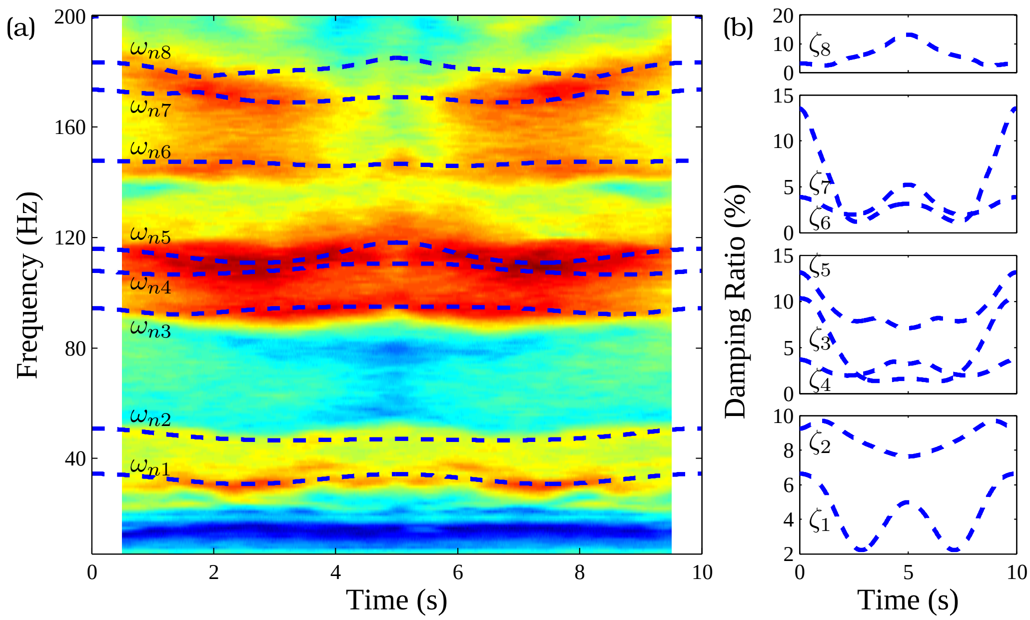

Figure 6.6.3: Baseline dynamics under fault E based on the FS-TAR$(21)_{[3,3]}$ model: (a) "Frozen-time" natural frequency estimates (sample mean spectrogram shown in the background), and (b) the corresponding "frozen-time" damping ratios.

6.6.2 Inspection phase

As already mentioned the fault diagnosis method is based on the vibration response of a single accelerometer (Fig. 6.2.1 - location 4) along with the FS-TAR$(21)_{[3,4]}$ model identified in the baseline phase. In addition, corresponding FS-TAR models are identified in each test case using the current response signal (inspection phase).

Figure 6.6.4 presents the fault detection results. The test statistics corresponding to the healthy mechanism are shown in circles (40 experiments), while the test statistics corresponding to the various fault types are presented with symbols of different color (different for each fault type). Evidently, correct detection is obtained in each test case, as the test statistic is shown not to exceed the critical limit (at the $\alpha = 10^{-8}$ risk level) in the healthy cases, while it exceeds it in all fault cases (note the logarithmic scale at the vertical axis in Fig. 6.6.4). It should be added, that in each test case (experiment) the motion profiles considered in Fig. 6.2.3 (a) and (b) is only approximately followed by the linear motors of the mechanism. It is thus evident that the method effectively accounts for such stochastic effects and inherent variabilities. The "global" fault detection capability of the method is also worth noting. This is to say that both "local" and "remote" (with respect to the proximity of the fault location to the sensor) are effectively handled (for instance faults of both A and B types; Fig. 6.2.2.

Similarly, fault identification is based on the mechanism vibration response of accelerometer at location 4 and the baseline FS-TAR models identified for each faulty case. The fault identification results for all 240 test cases related to a faulty state are presented in Figs. 6.6.5(a) - 6.6.5(f). Evidently, for fault types A to D correct identification is obtained as the test statistics are shown not to exceed the critical point for the fault type considered, while the test cases corresponding to the other fault types exceed it. Note the logarithmic scale on the vertical axis which indicates significant difference between the correct fault type statistics and the rest fault types statistics. It is reminded that faults A to C correspond to the removal of various bolts from specific parts of the mechanism, while fault type D corresponds to the loosening of the slider of motor B.

On the other hand, the fault identification results for fault cases E and F, that is loosening the bolt E1 connecting the right bungee cord hook with the aluminium base and adding a mass at the free end of the motor A slider respectively (see Fig. 6.2.2), depicted in Fig. 6.6.5 show that there is a small

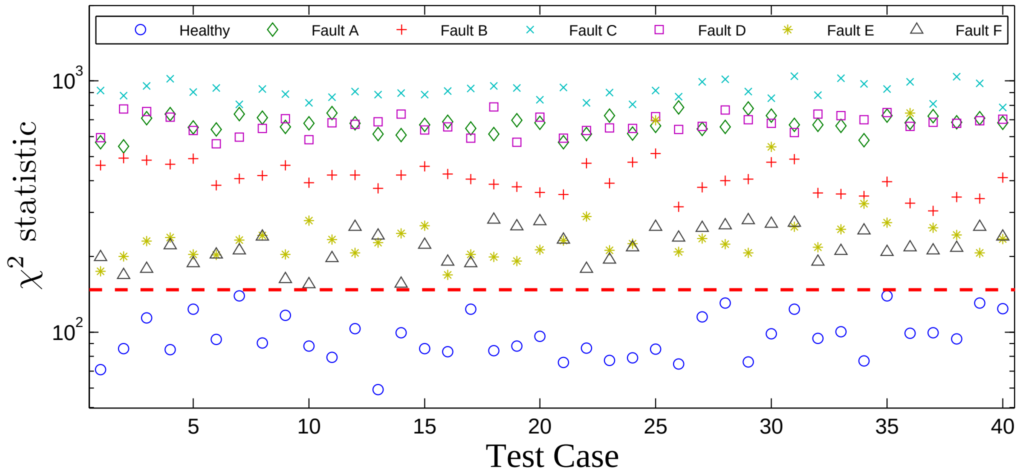

Figure 6.6.4: Inspection phase: Fault detection results for all 280 test cases (risk level $\alpha = 10^{-8}$; a fault is detected if the test statistic exceeds the critical limit designated by the dashed horizontal line.

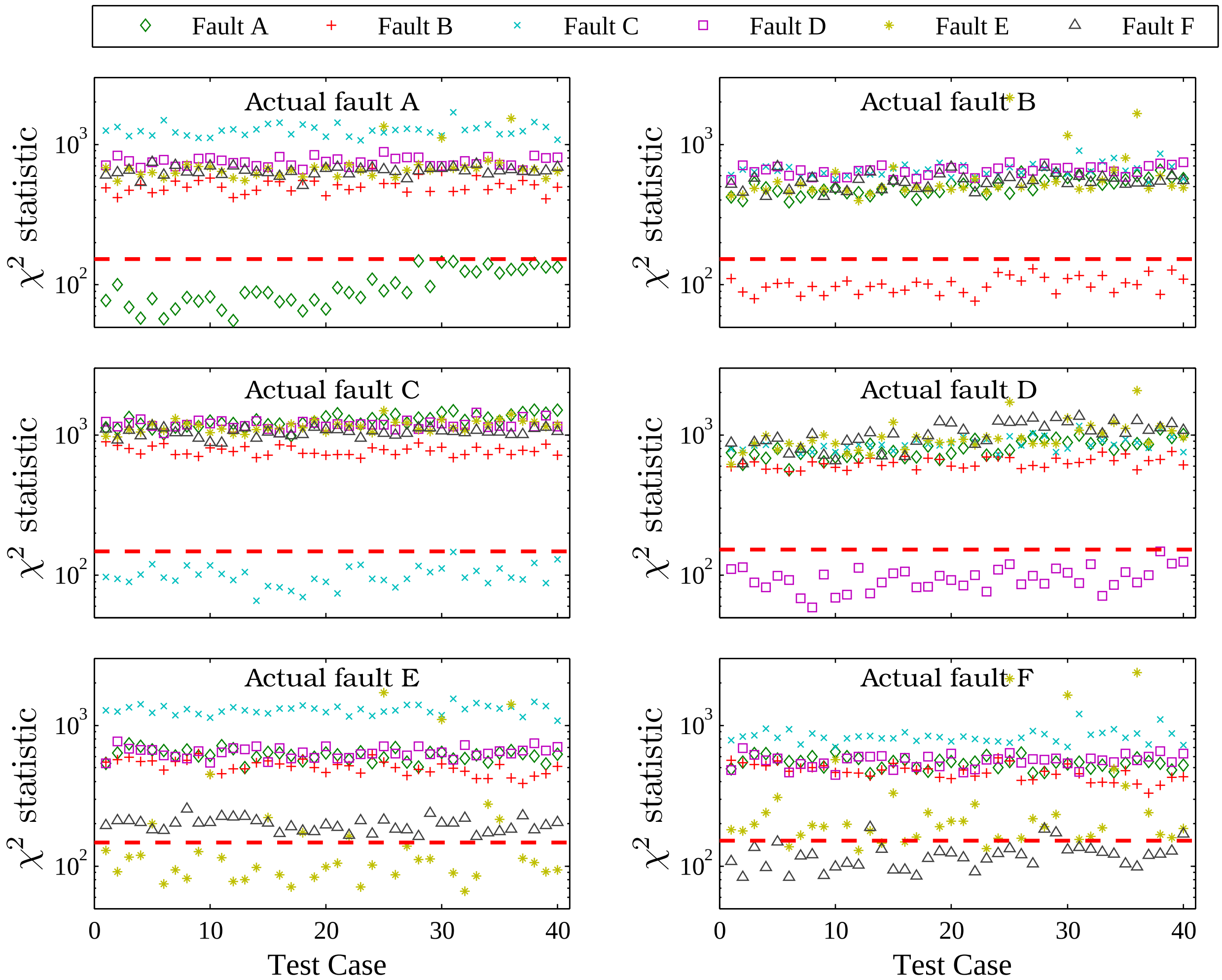

Figure 6.6.5: Inspection Phase: Fault identification results (240 test cases) with the actual fault being of the indicated type (risk level $\alpha = 10^{-8}$).

number of fault misclassifications in these cases. Summary fault detection and identification results are presented in Table 6.6.2.

Table 6.6.2: Inspection phase: Summary of the fault detection and identification results.

Fault Detection						
False Alarms	Missed Faults					
Healthy	Fault A	Fault B	Fault C	Fault D	Fault E	Fault F
0/40	0/40	0/40	0/40	0/40	0/40	0/40
Fault Identification (misclassifications)						
—	Fault A	Fault B	Fault C	Fault D	Fault E	Fault F
—	0/240	0/240	0/240	0/240	10/240	9/240

6.7 Conclusions

A statistical time series vibration-response-based method for fault diagnosis in inherently TV structures was introduced. The method is based on non-stationary Functional Series AutoRegressive (FS-TAR) models and a proper statistical decision making scheme. It is an output-only method, capable of operating with a minimal number of random vibration response signals which may be of limited time duration and frequency bandwidth, under normal operating conditions, and in a potentially automated way. It is of general applicability, but particularly suitable for TV structures that work repeatedly on an operational cycle characterized by prescribed evolution of their time-varying properties (physical or geometrical).

The method was applied to the problem of fault diagnosis in a pick-and-place mechanism based on a single vibration response signal. Various fault scenarios were employed along with a number of case studies (experiments). The method's very good performance characteristics were confirmed, as no false alarms or missed faults occurred, while the fault identification (classification) performance was also very good.

Appendix 6.A Regularity Conditions

The asymptotic analysis framework, based on which the covariance matrix of the AR coefficients of projection vector is derived, is valid under some general regularity conditions which the true FS-TAR data generating process should follow [Poulimenos and Fassois, 2007]:

CD 1: The innovations standard deviation is bounded, uniformly in t, as follows:

$$0 < \underline{\sigma_e} \leq \boldsymbol{g}_s^T[t] \cdot \mathring{\boldsymbol{\vartheta}}_s \leq \overline{\sigma_e} < \infty, \quad \forall t. \tag{6.A.1a}$$

CD 2: The basis functions are linearly independent and bounded, uniformly in t, that is:

$$\max_{i,j} \left(|G_{d_a(i)}[t]|, |G_{d_s(j)}[t]| \right) \leq \overline{g} < \infty, \quad \forall t. \tag{6.A.1b}$$

CD 3: The impulse response polynomial operators of the FS-TAR data generating process are absolutely summable, uniformly in t, that is:

$$\sum_{r=0}^{\infty} \sup_t \left| h_r[t, \mathring{\boldsymbol{\vartheta}}_a] \right| = \overline{h} < \infty. \tag{6.A.1c}$$

where $h_r[t, \mathring{\boldsymbol{\vartheta}}_a] = -\mathring{a}_r[t] - \sum_{j=1}^{r-1} \mathring{a}_j[t] \cdot h_{r-j}[t-j, \mathring{\boldsymbol{\vartheta}}_a], \quad r = 1, 2, \ldots,$ with $\mathring{a}_i[t] \equiv 0$ for $i > n_a$.

In the above relations $\mathring{\boldsymbol{\vartheta}}_a$ and $\mathring{\boldsymbol{\vartheta}}_s$ designate the true AR and innovations sequence standard deviation coefficients of projection vector, respectively. Conditions *CD 1,2* are quite natural. Condition *CD 3* may be seen as a stability condition, since Eq. (6.A.1c) suffices for the Bounded Input Bounded Output (BIBO) stability of the FS-TAR models.

6.A.1 A-posteriori validation of the regularity conditions

The a-posteriori validation of the regularity conditions that are used in the derivation of the asymptotic properties of the MS estimator (Eqs. (6.A.1)) is presently considered for the FS-TAR$(21)_{[3,4]}$ baseline model representing the mechanism under its healthy state. As it may be observed in Fig. 6.A.1 the estimated standard deviation and the functional basis are uniformly bounded while also the impulse response polynomial operators of the identified FS-TAR model are absolutely summable uniformly in t.

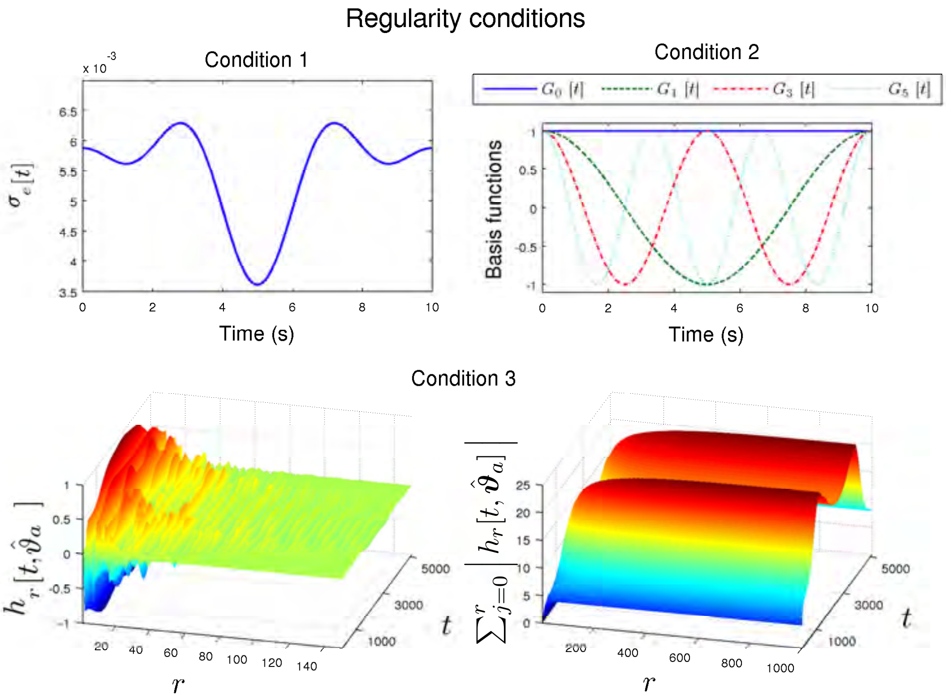

Figure 6.A.1: A-posteriori validation of the regularity conditions. The estimated standard deviation and the functional basis are uniformly bounded while also the impulse response polynomial operators of the identified FS-TAR model are absolutely summable, uniformly in t.

Appendix 6.B Model Structure Selection Details

The BIC, RSS/SSS, SPP, and regression matrix condition number values obtained by the candidate baseline models estimated during the model structure selection procedure are shown in Figs. 6.B.1 - 6.B.7 (healthy and faulty cases $A, B, \ldots, F$). For each baseline model extended and complete functional subspaces of dimensionality equal to 13 ($p_a = p_s = 13$) are employed and FS-TAR$(n_a)_{[13,13]}$ models with $n_a = 10, \ldots, 30$ are estimated, with the optimal AR order being selected based on the BIC (Phase A). The initial functional subspaces are subsequently reduced based again on the BIC and a backward regression procedure (Phase B). It is noted that only the values obtained by the candidate models during the reduction of the AR functional subspace are depicted in these figures.

Appendix 6.C Coefficients of Projection and Time-Dependent Parameters

The coefficients of projection of the MS estimated FS-TAR$(21)_{[3,4]}$ model representing the structure under its healthy state are given in Table 6.C.1. The standard deviation values of the estimated parameters are also given in this table while the corresponding time-dependent parameters are depicted in Fig. 6.C.1.

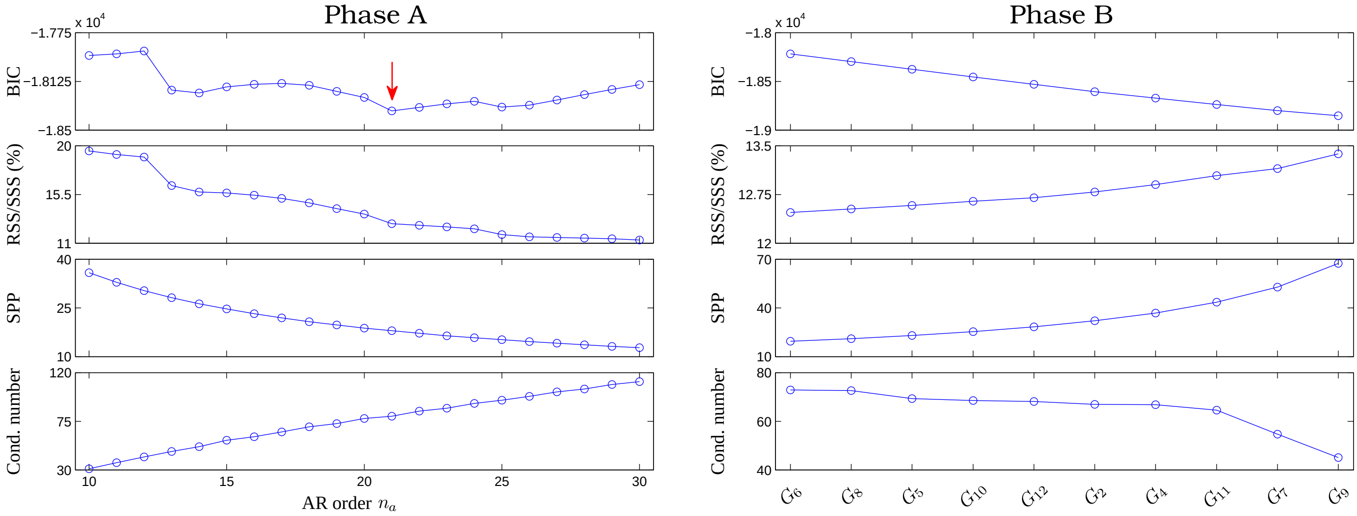

Figure 6.B.1: Healthy baseline FS-TAR model structure selection. Phase A: AR order selection based on the BIC using an extended and complete functional subspace $p_a = p_s = 13$. Phase B: BIC values obtained by sequentially dropping the indicated basis functions until no further reduction is possible. The Residual Sum of Squares (RSS), Sample Per Parameters (SPP) and the condition number of the regression matrix of the identified models are also illustrated.

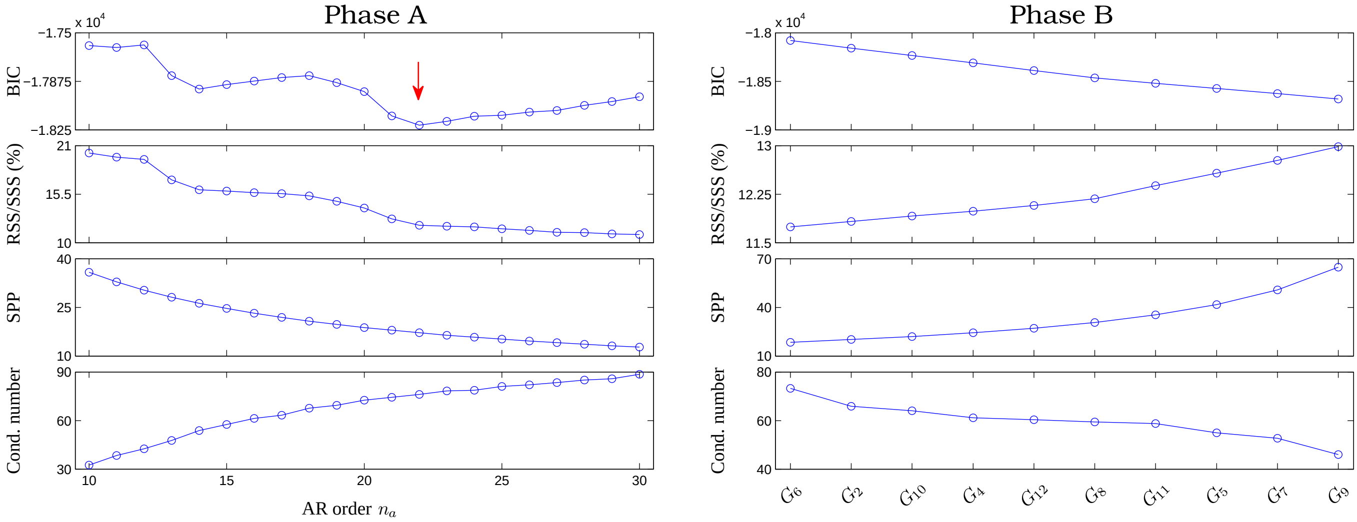

Figure 6.B.2: Fault A baseline FS-TAR model structure selection. Phase A: AR order selection based on the BIC using an extended and complete functional subspace $p_a = p_s = 13$. Phase B: BIC values obtained by sequentially dropping the indicated basis functions until no further reduction is possible. The Residual Sum of Squares (RSS), Sample Per Parameters (SPP) and the condition number of the regression matrix of the identified models are also illustrated.

Appendix 6.D One-Step-Ahead Signal Predictions

Indicative one-step-ahead signal predictions obtained by the estimated baseline FS-TAR models are (for a short time segment of the signals) compared to the actual signal values in Fig. 6.D.1. It is observed that all models provide more or less good predictions with RSS normalized by the Series Sum of Squares (RSS/SSS) values varying between 11.66% (fault case E) and 19.58% (fault case C).

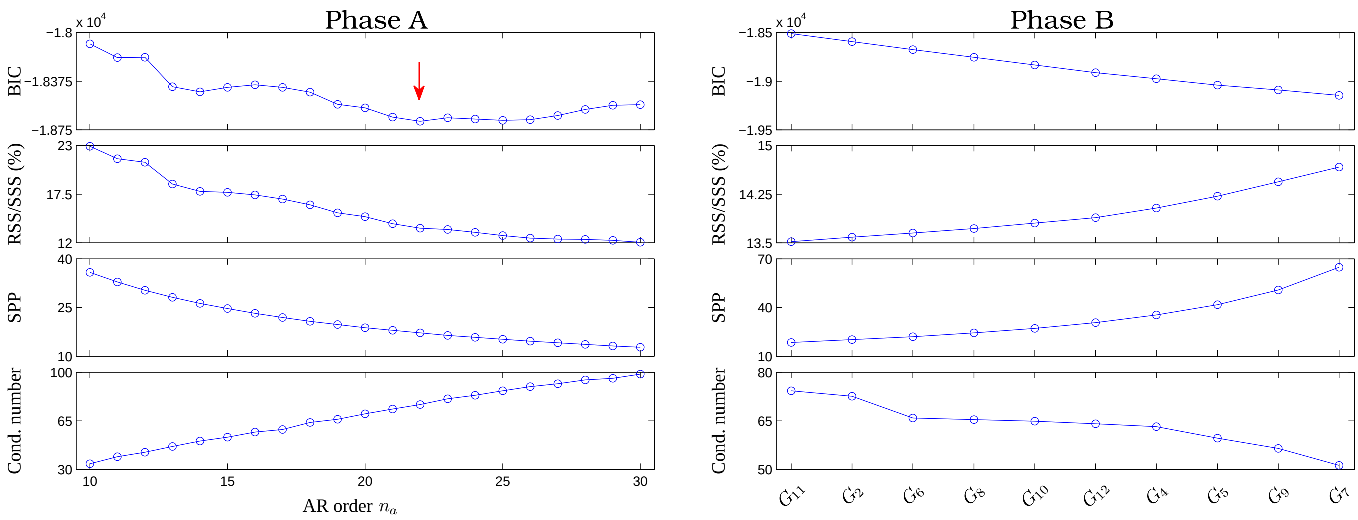

Figure 6.B.3: Fault B baseline FS-TAR model structure selection. Phase A: AR order selection based on the BIC using an extended and complete functional subspace $p_a = p_s = 13$. Phase B: BIC values obtained by sequentially dropping the indicated basis functions until no further reduction is possible. The Residual Sum of Squares (RSS), Sample Per Parameters (SPP) and the condition number of the regression matrix of the identified models are also illustrated.

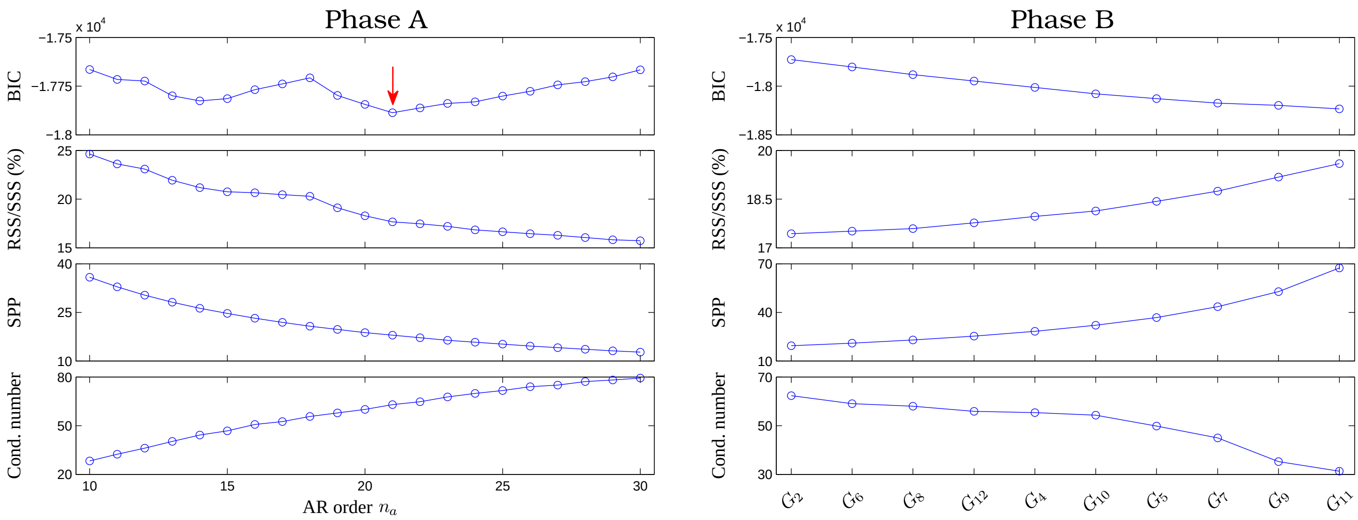

Figure 6.B.4: Fault C baseline FS-TAR model structure selection. Phase A: AR order selection based on the BIC using an extended and complete functional subspace $p_a = p_s = 13$. Phase B: BIC values obtained by sequentially dropping the indicated basis functions until no further reduction is possible. The Residual Sum of Squares (RSS), Sample Per Parameters (SPP) and the condition number of the regression matrix of the identified models are also illustrated.

Appendix 6.E Fault Diagnosis Based on a Reduced Dimensionality Coefficient of Projection Vector

Fault detection results utilizing Principal Component Analysis (PCA [Jolliffe, 2002]; MATLAB *pcacov* function) for the reduction of the parameter vector space are summarized in Table 6.E.1. Various percentages of the explained variance and respective compression of the parameter spaces are examined (Fig. 6.E.1). The results indicate that for a percentage of almost 70% of the initial parameter space, which corresponds to 99% of the explained variance, the fault detection results are almost the same (one missed fault instead of zero missed faults) with those obtained by using the initial full length parameter

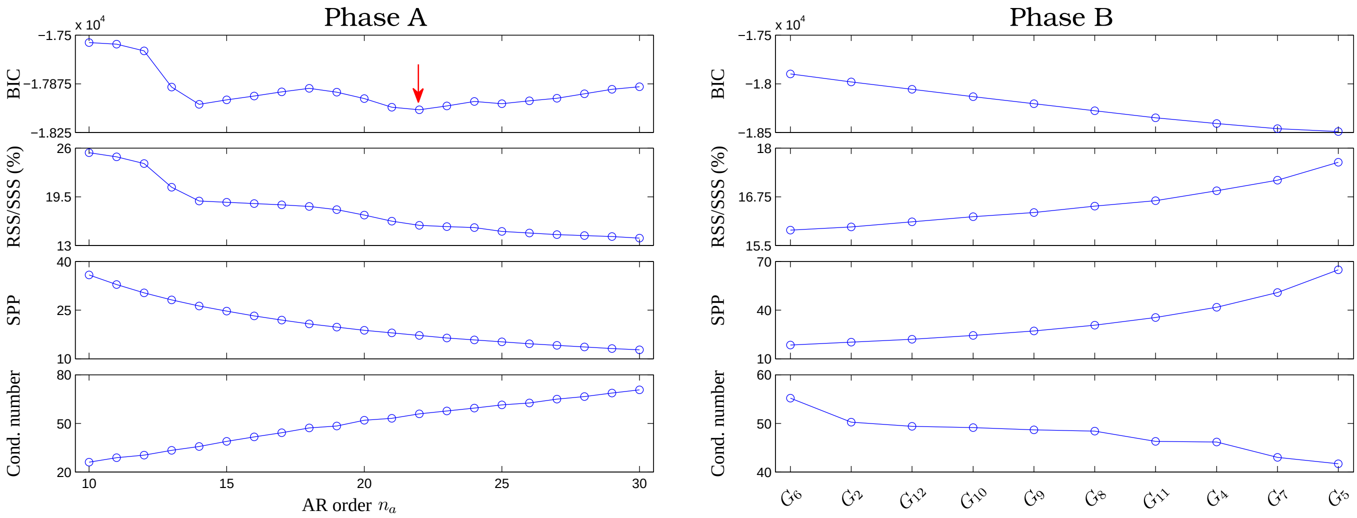

Figure 6.B.5: Fault D baseline FS-TAR model structure selection. Phase A: AR order selection based on the BIC using an extended and complete functional subspace $p_a = p_s = 13$. Phase B: BIC values obtained by sequentially dropping the indicated basis functions until no further reduction is possible. The Residual Sum of Squares (RSS), Sample Per Parameters (SPP) and the condition number of the regression matrix of the identified models are also illustrated.

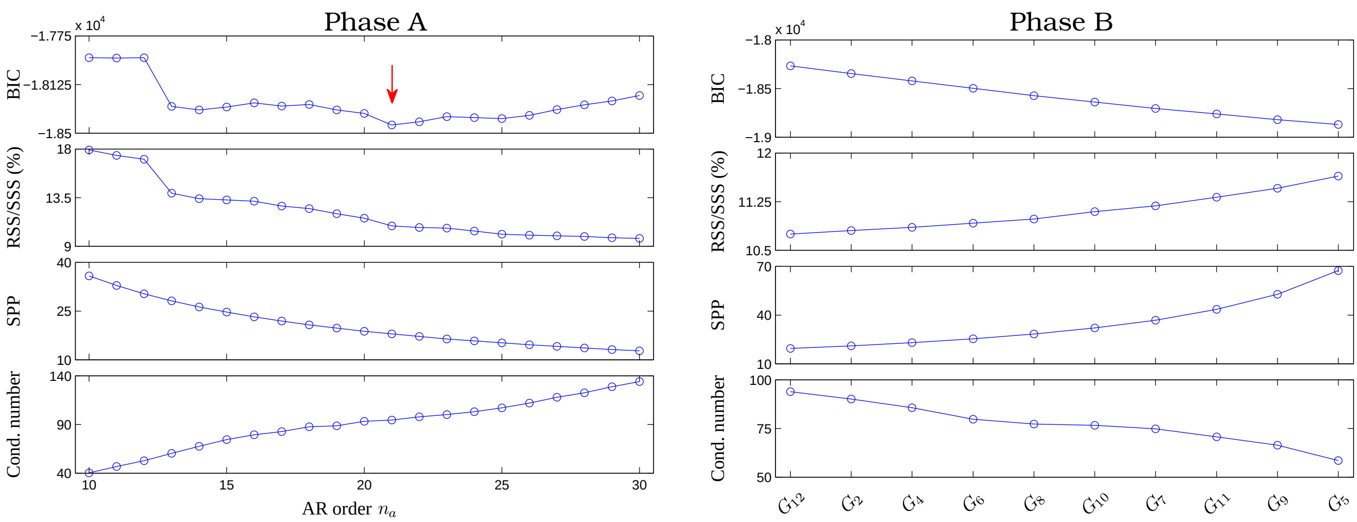

Figure 6.B.6: Fault E baseline FS-TAR model structure selection. Phase A: AR order selection based on the BIC using an extended and complete functional subspace $p_a = p_s = 13$. Phase B: BIC values obtained by sequentially dropping the indicated basis functions until no further reduction is possible. The Residual Sum of Squares (RSS), Sample Per Parameters (SPP) and the condition number of the regression matrix of the identified models are also illustrated.

vector $\widehat{\boldsymbol{\vartheta}}_{a_o}$.

Fault identification results using the principal components which explain 99% of the variance are summarized in Table 6.E.2. Even if a decreased number of misclassifications is obtained for Fault E, the corresponding misclassifications for Fault F are more than double compared to those obtained by using the initial full length parameter vectors $\widehat{\boldsymbol{\vartheta}}_{a_V}$ (with $V = A, B, \ldots, F$), while at the same time 8 misclassifications for Fault A and 1 for Fault D arise. Concluding, although in this case study the identified baseline models consists of AR coefficients of projection parameter vectors of low dimensionality (63 parameters for the healthy case, the faulty case C and the faulty case E, and 66 for the rest of the cases) and the compression is not of critical importance, PCA may be particularly helpful in cases of

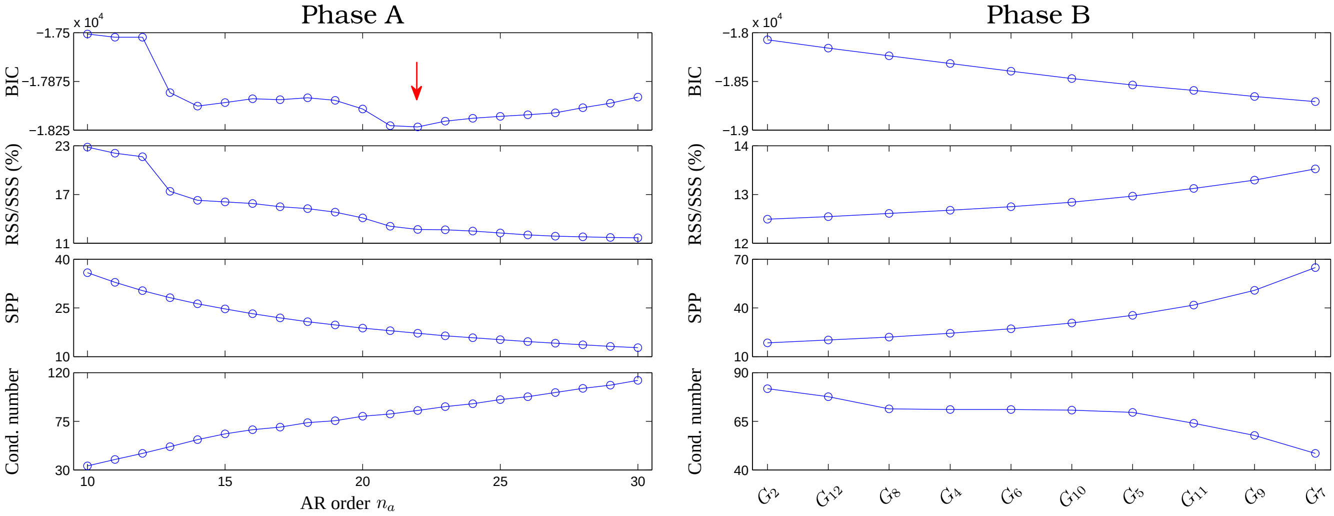

Figure 6.B.7: Fault F baseline FS-TAR model structure selection. Phase A: AR order selection based on the BIC using an extended and complete functional subspace $p_a = p_s = 13$. Phase B: BIC values obtained by sequentially dropping the indicated basis functions until no further reduction is possible. The Residual Sum of Squares (RSS), Sample Per Parameters (SPP) and the condition number of the regression matrix of the identified models are also illustrated.

Table 6.C.1: Coefficients of projection $\pm$ one standard deviation of the estimated baseline FS-TAR$(21)_{[3,4]}$ model representing the mechanism under its healthy state.

i	$a_{i,1} \pm \text{std}(a_{i,1})$	$a_{i,2} \pm \text{std}(a_{i,2})$	$a_{i,3} \pm \text{std}(a_{i,3})$
1	-0.124 ± 0.014	0.003 ± 0.021	0.073 ± 0.019
2	1.073 ± 0.014	-0.108 ± 0.021	-0.127 ± 0.019
3	-0.552 ± 0.021	-0.066 ± 0.029	0.236 ± 0.028
4	0.464 ± 0.023	0.061 ± 0.032	-0.294 ± 0.030
5	-0.702 ± 0.024	-0.007 ± 0.033	0.372 ± 0.032
6	0.293 ± 0.026	0.042 ± 0.035	-0.237 ± 0.035
7	0.079 ± 0.026	-0.012 ± 0.035	0.341 ± 0.035
8	0.674 ± 0.026	-0.247 ± 0.034	-0.294 ± 0.035
9	0.098 ± 0.027	-0.025 ± 0.035	0.237 ± 0.036
10	0.251 ± 0.027	-0.246 ± 0.034	-0.211 ± 0.035
11	-0.503 ± 0.027	0.184 ± 0.033	0.108 ± 0.034
12	-0.165 ± 0.027	0.036 ± 0.034	-0.121 ± 0.035
13	-0.475 ± 0.027	0.200 ± 0.034	0.102 ± 0.035
14	0.000 ± 0.026	-0.061 ± 0.033	-0.062 ± 0.034
15	-0.025 ± 0.026	-0.028 ± 0.033	0.073 ± 0.034
16	0.188 ± 0.025	-0.130 ± 0.033	-0.124 ± 0.033
17	-0.259 ± 0.023	-0.007 ± 0.031	0.085 ± 0.031
18	-0.150 ± 0.022	-0.021 ± 0.030	-0.087 ± 0.029
19	-0.421 ± 0.020	0.123 ± 0.028	0.074 ± 0.028
20	-0.151 ± 0.014	0.071 ± 0.020	-0.041 ± 0.019
21	-0.246 ± 0.014	0.060 ± 0.020	0.060 ± 0.019

$s_1 \pm \text{std}(s_1)$	$s_2 \pm \text{std}(s_2)$	$s_3 \pm \text{std}(s_3)$	$s_4 \pm \text{std}(s_4)$
$5.480 \cdot 10^{-3} \pm 5.536 \cdot 10^{-5}$	$6.634 \cdot 10^{-4} \pm 7.401 \cdot 10^{-5}$	$-7.365 \cdot 10^{-5} \pm 7.891 \cdot 10^{-5}$	$4.712 \cdot 10^{-4} \pm 7.739 \cdot 10^{-5}$

baseline models of high AR orders and extended functional subspaces.

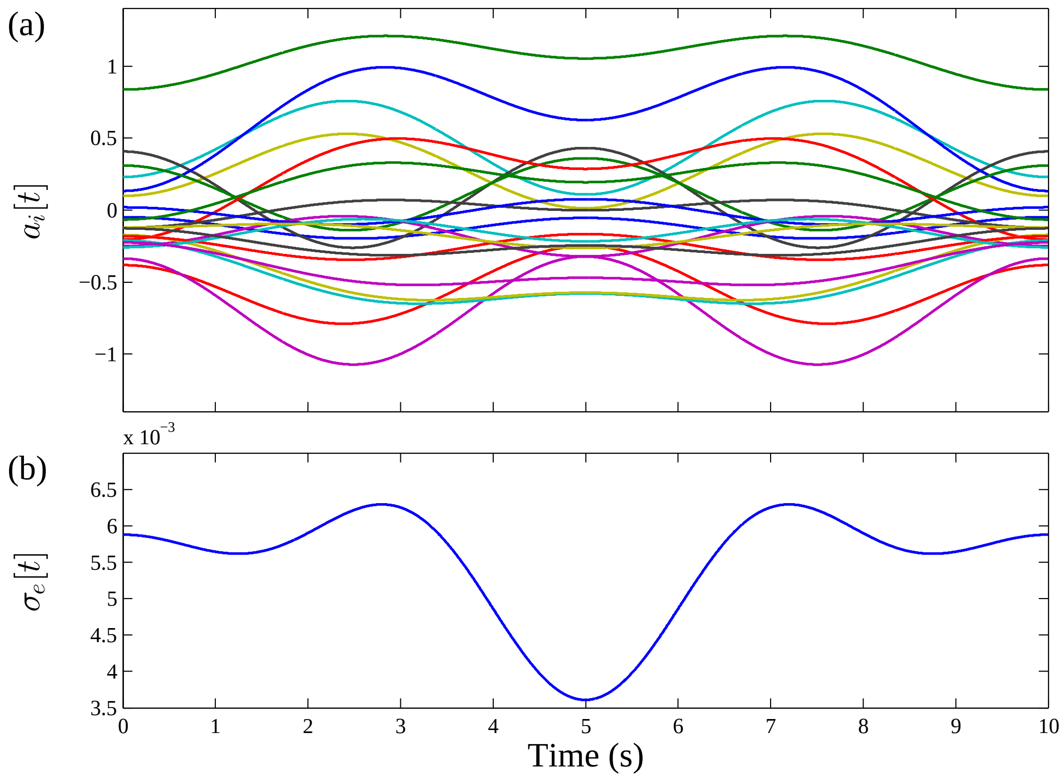

Figure 6.C.1: The time-varying parameters of the identified FS-TAR$(21)_{[3,4]}$ model representing the mechanism under its healthy state: (a) AR parameters and (b) innovations sequence standard deviation.

Table 6.E.1: Fault detection results based on reduced dimensionality coefficient of projection vectors.

Variance explained (%)	Number of PCs	False Alarms Healthy	Missed Faults Fault A	Fault B	Fault C	Fault D	Fault E	Fault F
80	14/63 (22.22 %)	1/40	22/40	39/40	12/40	0/40	13/40	12/40
90	21/63 (33.33 %)	0/40	4/40	19/40	0/40	0/40	5/40	7/40
95	28/63 (44.44 %)	0/40	0/40	7/40	0/40	0/40	6/40	6/40
97.5	35/63 (55.56 %)	0/40	0/40	0/40	0/40	0/40	5/40	5/40
99	44/63 (69.84 %)	0/40	0/40	0/40	0/40	0/40	0/40	1/40

Table 6.E.2: Fault identification (misclassifications) results based on the reduced dimensionality coefficient of projection vectors which explain 99% of the variance.

Fault A	Fault B	Fault C	Fault D	Fault E	Fault F
8/239	0/239	0/239	1/239	5/239	23/239

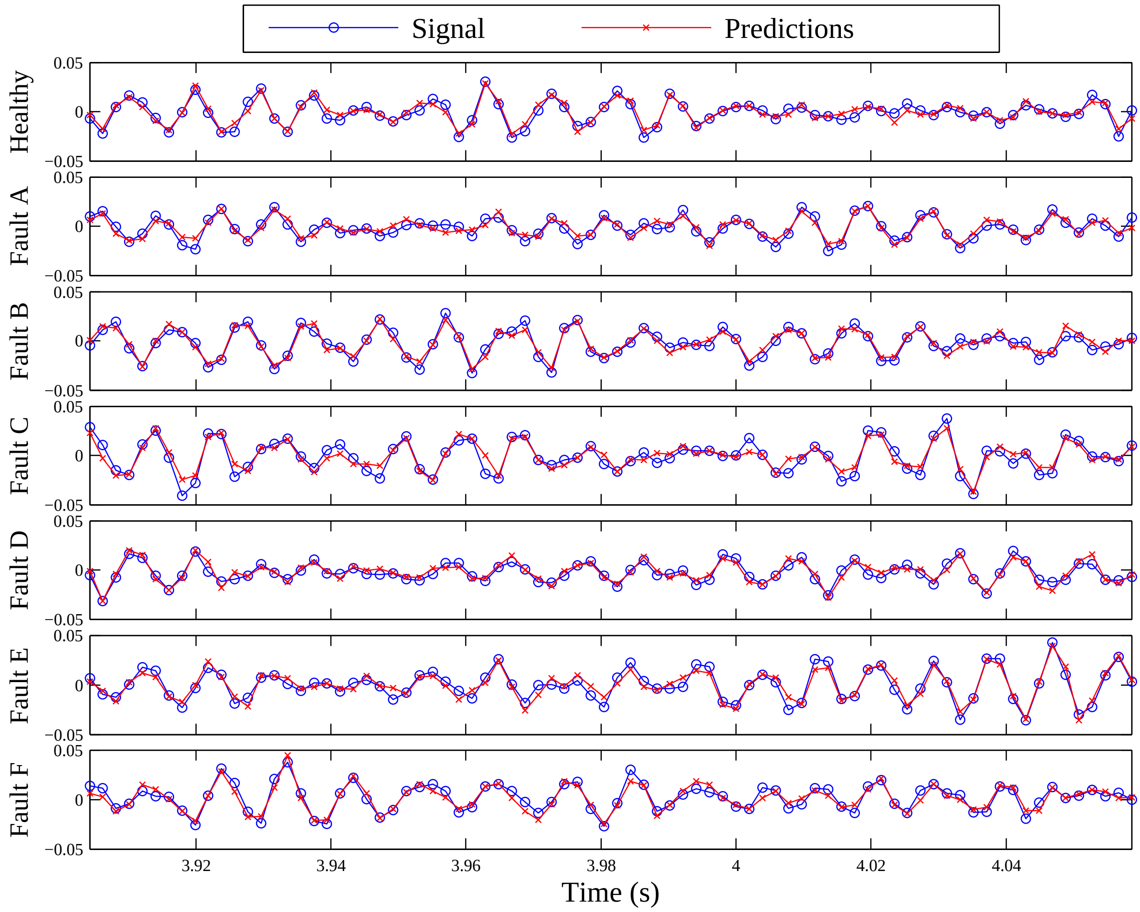

Figure 6.D.1: Segment of the vibration response signals acquired during the baseline experiments with the mechanism under the states considered and the corresponding one-step-ahead predictions obtained by the identified baseline FS-TAR models (see Table 6.6.1).

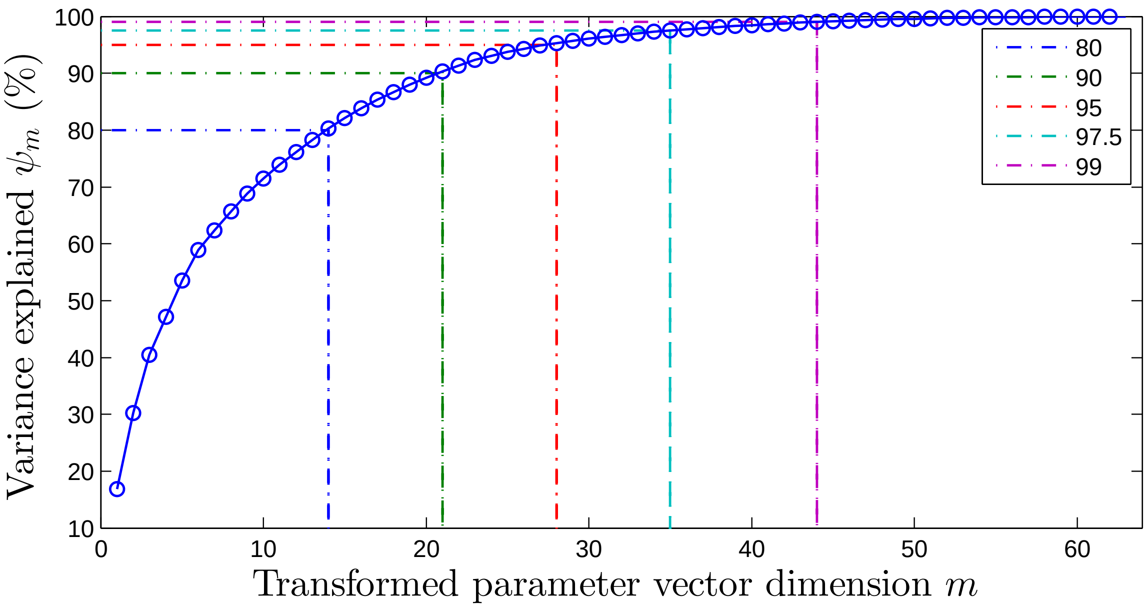

Figure 6.E.1: The percentage of the explained variance versus the dimension of the transformed parameter vector, that is the number of principal components.

Appendix 6.F Residual-Based Methods for Fault Diagnosis (Inspection Phase)

6.F.1 Method A: Using the likelihood function

In this method, fault detection is based upon the likelihood function under the null (H_0) hypothesis of a healthy mechanism (see [Gertler, 1998, pp. 119-120]). The hypothesis testing problem considered is:

$$H_0\colon \boldsymbol{\theta}_o = \boldsymbol{\theta}_u \quad \text{(null hypothesis – healthy mechanism)}$$
$$H_1\colon \boldsymbol{\theta}_o \neq \boldsymbol{\theta}_u \quad \text{(alternative hypothesis – faulty mechanism)}$$

with $\boldsymbol{\theta}_o$ and $\boldsymbol{\theta}_u$ designating the healthy and current structure's complete parameter vectors, respectively. Assuming independence of the innovations sequence, the Gaussian likelihood function for the data X is given as [Poulimenos and Fassois, 2006]:

$$\ln \mathcal{L}\left(\mathcal{M}(\boldsymbol{\theta}) \mid X\right) = \ln \mathrm{f}\left(X \mid \mathcal{M}(\boldsymbol{\theta})\right) = \ln \prod_{t=1}^{N} \mathrm{f}\left(e[t,\boldsymbol{\theta}]\right) = -\sum_{t=1}^{N}\left(\ln\left(\sigma_e^2[t,\boldsymbol{\vartheta}_s]\right) + \frac{e^2[t,\boldsymbol{\vartheta}_a]}{\sigma_e^2[t,\boldsymbol{\vartheta}_s]}\right) \tag{6.F.1}$$

with $\mathrm{f}(\cdot)$ designating the Gaussian probability density function. Under the null (H_0) hypothesis, the residual series $e_u[t,\boldsymbol{\vartheta}_{a_o}]$ generated by driving the current signal through the nominal model $\mathcal{M}(\boldsymbol{\theta}_o)$ is (just like the healthy baseline model residual sequence $e_o[t,\boldsymbol{\vartheta}_{a_o}]$) normally independently distributed with zero mean and variance $\sigma^2_{e_o}[t,\boldsymbol{\vartheta}_{s_o}]$. Decision making may be then based upon the likelihood function under H_0 evaluated for the current data, by requiring it to be larger or equal to a threshold ℓ (which is to be selected) in order for the null (H_0) hypothesis to be accepted, that is:

$$\begin{array}{lll} \ln \mathcal{L}\left(\mathcal{M}(\boldsymbol{\theta}_o) \mid X_u\right) \geq \ell & \Longrightarrow & H_0 \text{ is accepted (healthy mechanism)} \\ \text{Else} & \Longrightarrow & H_1 \text{ is accepted (faulty mechanism)} \end{array} \tag{6.F.2}$$

The evaluation of the log-likelihood $\ln \mathcal{L}\left(\mathcal{M}(\boldsymbol{\theta}_o) \mid X_u\right)$ requires knowledge of the true innovations variance $\sigma^2_{e_o}[t,\boldsymbol{\vartheta}_{s_o}]$. If this quantity is known, or may be estimated with very good accuracy in the baseline phase (which is reasonable for estimation based upon a large number of samples N) so that it may be treated as a fixed quantity of negligible variability, the condition for the acceptance of the null hypothesis may be written as:

$$\ln \mathcal{L}\left(\mathcal{M}(\boldsymbol{\theta}_o) \mid X_u\right) \geq \ell \Longrightarrow -\sum_{t=1}^{N}\left(\ln\left(\left(\boldsymbol{g}_s^T[t]\cdot\boldsymbol{\vartheta}_{s_o}\right)^2\right) + \frac{e_u^2[t,\boldsymbol{\vartheta}_{a_o}]}{\left(\boldsymbol{g}_s^T[t]\cdot\boldsymbol{\vartheta}_{s_o}\right)^2}\right) \geq \ell \Longrightarrow \sum_{t=1}^{N}\frac{e_u^2[t,\boldsymbol{\vartheta}_{a_o}]}{\left(\boldsymbol{g}_s^T[t]\cdot\boldsymbol{\vartheta}_{s_o}\right)^2} \leq \ell^*$$

where $\ell^* = \ell + \sum_{t=1}^{N} \ln\left(\left(\boldsymbol{g}_s^T[t]\cdot\boldsymbol{\vartheta}_{s_o}\right)^2\right)$, since the projected innovations standard deviation $(\boldsymbol{g}_s^T[t]\cdot\boldsymbol{\vartheta}_{s_o})$ as already mentioned is considered as constant after its estimation. Thus, the decision-making rule of Eq. (6.F.2) may be re-expressed as:

$$\begin{array}{lll} \sum_{t=1}^{N}\frac{e_u^2[t,\boldsymbol{\vartheta}_{a_o}]}{\left(\boldsymbol{g}_s^T[t]\cdot\boldsymbol{\vartheta}_{s_o}\right)^2} \leq \ell & \Longrightarrow & H_0 \text{ is accepted (healthy mechanism)} \\ \text{Else} & \Longrightarrow & H_1 \text{ is accepted (faulty mechanism)} \end{array} \tag{6.F.3}$$

The fault detection results based on the above likelihood-based test with ℓ^* selected equal to $5,800$ are illustrated in Fig. 6.F.1. As shown the statistic attains similar values for the healthy case and the faulty cases of type B and E and as a result gives a high percentage of missed faults $(81/240)$.

6.F.2 Method B: Using the innovations standard deviation coefficients of projection parameter vector

In this method the characteristic quantity Q used for the fault detection and identification problems is the innovation standard deviation coefficients of projection parameter vector $\boldsymbol{\vartheta}_s$ of the identified FS-TAR models.

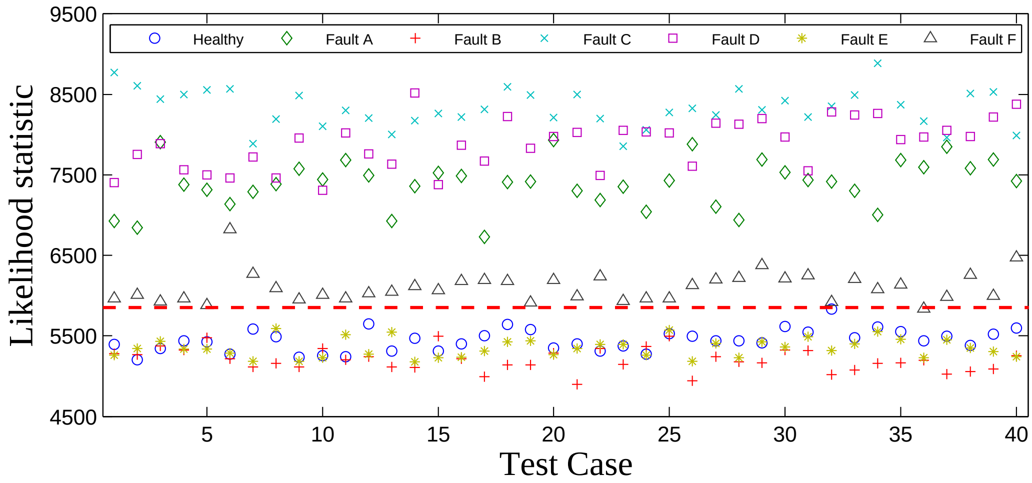

Figure 6.F.1: Fault detection results based on the likelihood statistic. A fault is detected if the test statistic exceeds the critical user-defined limit ℓ^* (— — —).

Let $\mathcal{M}(\boldsymbol{\theta}_o)$, $e_o[t, \boldsymbol{\vartheta}_{a_o}]$,and $\boldsymbol{\vartheta}_{s_o}$ represent the healthy baseline model, the corresponding residual sequence and the residuals standard deviation coefficients of projection vector, respectively, obtained in the baseline modelling phase. Also, let $e_u[t, \boldsymbol{\vartheta}_{a_o}]$ and $\boldsymbol{\vartheta}_{s_u}$ represent the current residual sequence and the corresponding standard deviation coefficients of projection vector, respectively, obtained by using the baseline model and the current available vibration response signals (with the mechanism being in its current unknown state). The latter is estimated through the maximization of the log-likelihood function of Eq. (6.3.5) conditional to the innovations sequence $e_u[t, \boldsymbol{\vartheta}_{a_o}]$.

For sufficiently long signals the $\boldsymbol{\vartheta}_s$ MS estimator is Gaussian distributed with mean equal to its true value $\mathring{\boldsymbol{\vartheta}}_s$ and covariance matrix $\boldsymbol{P}_s$ (see [Poulimenos and Fassois, 2007] for details). Thus, in case that the system in its current state does not present a fault, $\boldsymbol{\vartheta}_{s_o}$ and $\boldsymbol{\vartheta}_{s_u}$ will follow the same normal distribution. Therefore, following a similar procedure with that described in Section 6.4 the following test may be constructed at the α (type I) risk level:

$$\begin{array}{lcl} \chi^2_{\boldsymbol{\vartheta}_s} \leq \chi^2_{1-\alpha}(p_s) & \Longrightarrow & H_0 \text{ is accepted (healthy mechanism)} \\ \text{Else} & \Longrightarrow & H_1 \text{ is accepted (faulty mechanism)} \end{array} \tag{6.F.4}$$

with $\chi^2_{1-\alpha}(p_s)$ designating the χ^2 distribution's $1-\alpha$ critical point.

The fault detection results for this method are shown in Fig. 6.F.2 and although they are slightly better than those obtained by the likelihood-based test the number of missed faults is still large and concerns again the fault cases B and E.

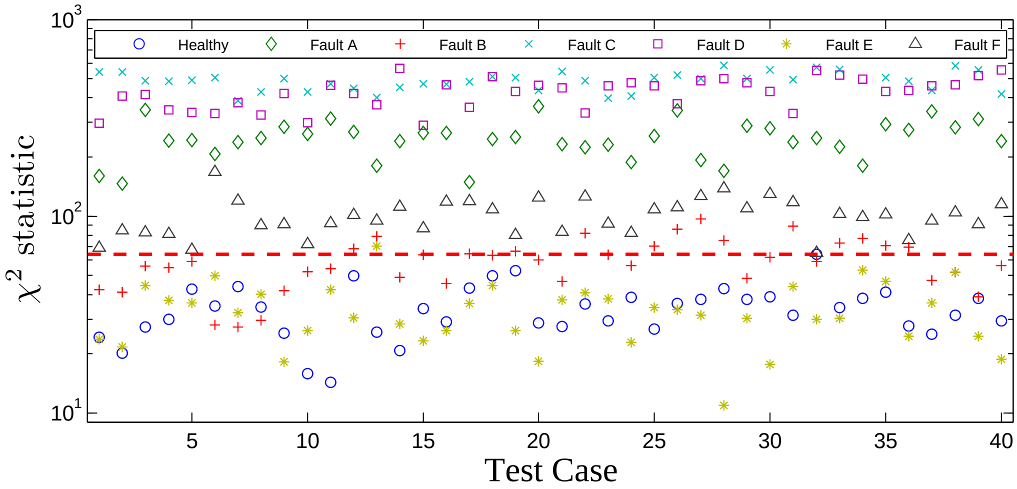

Figure 6.F.2: Fault detection results based on the innovations standard deviation coefficients of projection vector for all 280 test cases at the $\alpha = 10^{-8}$ risk level. A fault is detected if the test statistic exceeds the critical limit (— — —).

Chapter 7

Conclusions and Future Work

The problem of non-stationary random vibration modelling and analysis via Functional Series TARMA was addressed in the present thesis. Within this context, a number of practical and theoretical issues of particular significance for accurate FS-TARMA modelling were considered. An overall discussion and outlook of the issues treated in this thesis, the thesis chapters and their specific objectives is given in Section 7.1, while a brief summary of the main outcomes of this study are discussed in Section 7.2. Future perspectives of the main subjects of the thesis are finally discussed in Section 7.3.

7.1 General Conclusions

Deterministic parameter evolution methods for stochastic identification of TV structures through random output-only vibration data records are mainly based on Functional Series Time-dependent AutoRegressive Moving Average (FS-TARMA) models [Poulimenos and Fassois, 2006, Niedźwiecki, 2000]. Their AR, MA parameters and residual sequence innovations variance that explicitly depend upon time, are described by deterministic functions belonging to specific functional subspaces; and as a consequence the FS-TARMA model is fully parametrized by the corresponding TI coefficients of projection. They were introduced in 1970 by Rao who proposed the truncated Taylor series expansion of a TAR model parameters [Rao, 1970] – this is equivalent to assuming time-dependent parameters that can be described as polynomials of time – and they have played key role in the development and evolution of non-stationary stochastic signal identification and analysis over the last forty years.

They naturally emerged from the necessity for development of effective tools for non-stationary signal analysis in a time where the limitations of stationary analysis into a continuously evolving world had already been recognised. For this reason, and due to their simplicity and the fact that they are based on well known estimation methods FS-TARMA models rapidly evolved and were successfully applied in a number of signal analysis studies in various scientific areas: from financial data modelling [Hinich and Roll, 1981, Gersch and Kitagawa, 1982] to speech analysis [Liporace, 1975, Grenier, 1983b] and the modelling of biomedical processes [Gersch et al., 1983, Amir and Gath, 1989] and from the modelling of communication channels [Tsatsanis, 1995, Jachan and Matz, 2005] to the vibrational analysis of engineering structures [Bardou and Sidahmed, 1994, Conforto and D'Alessio, 1999b, Poulimenos and Fassois, 2009b].

The accumulated experience of forty years of research and development constitute FS-TARMA models today a ripe tool for non-stationary identification. However, despite the progress achieved thus far and the increasing number of successful applications, the FS-TARMA model based non-stationary vibration analysis remains a challenging problem. This is due to the elaborate model structure selection procedures, the complexity of the identification cost functions, as well as problems related to estimated model stability and invertibility and the difficulties these may pose to both estimation and analysis. Furthermore, a number of technologically important issues such as the multivariate FS-TARMA identification have hardly been considered up to date. In order to alleviate some of these problems and significantly facilitate the application of FS-TARMA models the present thesis focused on the development of advanced and complete FS-TARMA identification methods that try to overcome drawbacks of previous approaches.

At first, and in order to assess the effectiveness of FS-TARMA models, a critical overview and comparative assessment of parametric TARMA methods for the identification and model-based analysis of a benchmark laboratory TV structure under unobservable excitation was performed in Chapter 2 of this thesis. The methods were classified according to the mathematical structure imposed on the TV parameter evolution as unstructured, stochastic, and deterministic parameter evolution. The features and relative merits of each class were outlined while a representative method from each was then assessed through its application to the identification and dynamic analysis of a laboratory TV structure consisting of a beam with a mass moving on it. The methods were compared to each other in terms of achievable prediction accuracy and model-based analysis and the results demonstrated the FS-TARMA based methods' applicability, effectiveness, and high potential for parsimonious and accurate identification and dynamic analysis of TV structures under unobservable excitation.

The problem of parametric output-only identification of a time-varying structure based on vector random vibration signal measurements was considered in the third chapter of this thesis. For this reason, a Functional Series Vector Time-dependent AutoRegressive Moving Average (FS-VTARMA) method was introduced and employed for the identification of a "bridge-like" laboratory structure consisting of a beam and a moving mass. The identification was based on three simultaneously measured vibration response signals obtained during a single experiment. The method was judged against baseline modelling based on multiple "frozen-configuration" stationary experiments, and was shown to be effective and capable of accurately tracking the dynamics. Additional comparisons with a recursive Pseudo-Linear Regression VTARMA (PLR-VTARMA) method and a Short Time Stochastic Subspace Identification (ST-SSI) method were made. The identification and model based analysis results demonstrated the ability of the FS-VTARMA method for accurate and parsimonious (economical) output-only multivariate identification of TV structures.

The development of a new class of Adaptable FS-TARMA (AFS-TARMA) models was presented in Chapter 4 of this thesis. AFS-TARMA models utilize adaptable basis functions characterized by a finite number of a-priori unknown parameters which have to be estimated along with the coefficients of projection. Thus, the corresponding functional subspaces used for the expansion of the TV parameters are automatically adapted on the specific identification problem, in contrast to the classical FS-TARMA approach which uses basis functions with fixed and predetermined characteristics. The estimation of the introduced models was based on a Separable Nonlinear Least Squares (SNLS) type procedure which leads to a constrained non-quadratic optimization problem tackled via Particle Swarm Optimization (PSO) and gradient-type refinement. The model orders and subspace dimensionalities were estimated based on suitable criteria and PSO. The method's effectiveness was shown in both simulation and experimental case studies through comparisons with currently available schemes. The results showed excellent performance and superior accuracy achieved by the AFS-TARMA models with adaptable basis functions.

A review of the FS-TARMA models for the identification of non-stationary signals was on the focus of Chapter 5. Toward this end, a critical overview of the available methods for the FS-TARMA model parameter estimation and structure selection problems was presented while special emphasis was placed on promising new methods that aim at overcoming problems of previous approaches. More specifically, the main FS-TARMA and AFS-TARMA estimation methods for both parametric and semi-parametric type of models were summarized. The methods were distinguished in Maximum Likelihood and regression type methods with emphasis given to both theoretical and practical issues. FS-TARMA model structure selection methods were also reviewed and classified in two major categories: the integer optimization methods and those based on the concept of regression (backward or forward). The advantages and disadvantages of each method and the various parameters that are required for the realization of each method were discussed. The performance characteristics of various FS-TARMA and AFS-TARMA estimation methods were also examined via their application to the problem of modelling and analysis of a simulated TARMA model via Monte Carlo experiments. Alternative non-stationary identification methods belonging to the classes of SPE and UPE methods were also employed for this problem and the various models estimated were also compared in terms of various criteria. The simulated non-stationary model was characterized by inhomogeneous evolution of its parameters, that is they were characterized by transitions between smooth and abrupt changes in their values, and its identification was found to be particularly difficult for most of the methods considered. However, the best (in fact excellent) performance characteristics were achieved by the novel AFS-TARMA models.

Finally, this thesis dealt with the development of an efficient statistical time series vibration-based method for fault detection and identification in inherently non-stationary structures. The method is based on non-stationary FS-TAR models and a proper statistical decision making scheme. It employs a single vibration response signal acquired from the structure during its normal operation and it is particularly suitable for non-stationary structures that work repeatedly on an operational cycle characterized by prescribed evolution of their time-varying properties. The method's effectiveness was assessed via its application on the fault detection and identification of a pick-and-place mechanism consisting of two electromagnetic linear motors that follow prescribed motion profiles. Faults of various types and occurrence locations were simulated and a number of experiments was conducted. The considered faults were successfully detected with no false alarms or missed faults while also the faults were correctly identified for most of the test cases.

The main conclusions of the aforementioned studies are summarized in the following section.

7.2 Summary

Chapter 1

Chapter 1 contains an introduction to this thesis. More specifically, the general problem of non-stationary vibration modelling and its significance were described. Furthermore, the current state-of-the-art was reviewed and discussed, and the specific scope of the work was presented. Finally, the thesis chapters were analytically presented and their individual contributions were outlined.

Chapter 2

The main conclusions obtained from the comparative experimental assessment of non-stationary vibration modelling methods via their application to the identification of a "bridge-like" laboratory structure may be summarized as follows:

- Parametric methods are more elaborate and demand increased user expertise compared to their generally simpler non-parametric counterparts. Yet, they were shown to offer increased tracking accuracy and resolution.

- Parametric non-stationary identification methods are particularly adequate for the identification and dynamic analysis of TV structures under unobservable excitation.

- The model-based dynamics, including the resonance and antiresonance natural frequencies and the TV PSD of the vibration response, were most accurately captured by the FS-TARMA method.

- Overall, the results of the study demonstrated the applicability, effectiveness, and high potential for parsimonious and accurate time-varying structural dynamics representation of FS-TARMA models.

Chapter 3

The main issues addressed with respect to the identification of time-varying structures under unobservable excitation through multivariate vibration response measurements and FS-VTARMA models are the following:

- The introduced FS-VTARMA methods applied on the identification of a TV "bridge-like" structure was shown to provide PSD and modal parameter estimates that are in good agreement with those obtained by a baseline "frozen-configuration" model.

- The identified FS-VTARMA model attained better predictive performance than its ST-SSI and PLR-VTARMA counterparts. The FS-VTARMA model provided drastically (by more than an order of magnitude) improved predictions over the corresponding predictions attained previously [Poulimenos and Fassois, 2009a] by a univariate (scalar) FS-TARMA model.

- The estimated FS-VTARMA model was shown to surpass the PLR-VTARMA and ST-SSI models in terms of tracking accuracy for the "frozen-time" structural dynamics.

- The estimated FS-VTARMA model is characterized by a high degree of parametrization parsimony (economy) as compared to its ST-SSI and PLR-VTARMA counterparts. This difference is due to the need of the ST-SSI and PLR-VTARMA models to store their estimated parameter values for each time instant.

- Overall, the identification and model based analysis results demonstrated the ability of the FS-VTARMA method for accurate and parsimonious (economical) output-only multivariate identification of TV structures.

Chapter 4

Chapter 4 which dealt with the introduction of a novel Adaptable FS-TARMA model class and the development of effective identification method lead to the following main conclusions:

- The proposed adaptable basis functions (B-splines and decaying trigonometric) are collectively capable of effectively modelling a wide variety of parameter evolutions, from slow and smooth to fast and abrupt, but also periodic or quasi-periodic. However, a number of other adaptable basis functions may be used within the context of FS-TARMA modelling.

- The introduced AFS-TARMA method was shown to be capable of automatically, and yet effectively, estimating the functional subspaces and coefficients of projection for specified AFS-TARMA models. This is also true for cases of parameter characterized by abrupt or even mixed types of evolution.

- The hybrid optimization scheme utilized for the AFS-TARMA identification method provides accurate solutions even for problems characterized by a large number of local extrema in the fitness function.

- Comparisons with the classical FS-TARMA method, and methods of the UPE and SPE classes confirmed the excellent performance and superior accuracy achieved by the AFS-TARMA method with adaptable basis functions.

- The results of the experimental case study, that is the identification of a TV pick-and-place mechanism, demonstrated the high achievable accuracy of the proposed approach.

Chapter 5

The main conclusions drawn from the review study on the FS-TARMA models and the corresponding parameter estimation and model structure selection methods may be summarized as follows:

- Model structure and basis functional family selection play an important role in achieving high modelling accuracy.
- The classical FS-TARMA model structure selection was shown to be an elaborate procedure which normally requires high user-expertise and inference.
- The classical FS-TARMA methods based on fixed basis and the Smoothness Priors TARMA (SP-TARMA) methods was shown to be incapable of estimating with accuracy parameters which are characterized by inhomogeneous evolution.
- The adaptable approach based on parametrized functional subspaces offers significant improvement regarding parameter tracking accuracy, particularly for cases of inhomogeneous evolution of the time-dependent parameters. This improvement is achieved at the price of increased computational complexity.
- The Multi-Stage (MS) method was found to be superior for classical FS-TAR model estimation, while also of reduced computational complexity when compared to the ML estimates. This result also confirmed practically the fact that the MS method leads to statistically efficient estimators.
- Regarding classical FS-TARMA model estimation again the MS method provided the best results, however the best trade-off between computational complexity and achievable accuracy was provided by the Two Stage Least Squares (2SLS) method.
- The Maximum Likelihood (ML) method was shown to be of increased complexity even for the simple FS-TAR case. The likelihood function was also shown to be characterized by a large number of local extrema making its optimization a difficult task.

Chapter 6

The concluding remarks of the study on the statistical time series vibration-based method for fault detection and identification in inherently non-stationary structures may be outlined as follows:

- The proposed method is particularly suitable for time-varying structures that work repeatedly on an operational cycle characterized by prescribed evolution of their time-varying properties (physical or geometrical). Furthermore, it is noted that the method may work on the basis of a single cycle of operation of the structure.
- The introduced method was shown to effectively tackle fault detection and identification, achieving excellent performance with zero false alarms, missed faults, and low damage misclassification rates.
- The proposed method was also shown to be capable of effectively accounting for stochastic effects and the inherent variability of test data (experimental uncertainty).
- The study has demonstrated the very significant amount of information on the state of the structure embedded even in a single response signal. Thus an important message is that it may not be necessary to employ a “high” number of sensors for precise fault detection; instead, a “few” sensors and powerful signal analysis for extracting the embedded information may be a much more practical and effective approach.

- The availability of data records corresponding to various potential fault scenarios is necessary in order to treat damage identification. This may not be possible with the actual structure itself, but analytical (Finite Element) models may be used for this purpose.

7.3 Suggestions for Future Work

Despite the significant progress that has been achieved on non-stationary vibration modelling through FS-TAR/TARMA models, there are still open issues for further research. Some ideas for further work are:

- The combination of deterministic and stochastic parameter evolution methods for the development of models with parameters characterized by both deterministic and stochastic parts. This extension will give the opportunity to track parameter evolutions that also have stochastic characteristics due to environmental or excitation conditions (temperature, wind, tides, etc).

- The extension of FS-TARMA models to the case of non-stationary linear parameter varying models with parameters dependent not only on time but also to an exogenous measurable variable k (for instance, the weight of a train or a heavy vehicle, the velocity of travelling). This type of models will be able to describe a specific structure under a wide range of operating conditions taking advantage of non-stationary analysis.

- The treatment of algorithmic instability that may occur through FS-TARMA models estimation via Prediction Error (PE) methods where the estimated model is characterized by an unstable MA polynomial.

- The development of criteria to be used within the context of FS-TARMA model structure selection suitable for the non-stationary vibration modelling and analysis problems – it has been observed that the BIC, AIC criteria tend to overestimate the structure of FS-TARMA models, resulting in the identification of a significant number of spurious modes.

- The asymptotic properties of the AFS-TARMA models estimators would facilitate the development of more efficient estimation methods.

- The AFS-TARMA models developed in this thesis may be the basic instrument for the development of statistical frameworks for the problems of change and non-stationarity detection.

- The successful application of FS-TARMA models for the non-stationary vibration modelling and analysis of laboratory time-varying structures, encourages the use of methods on real-world and more complex structures outside the laboratory environment.

Appendix A

Functional Basis Families

A.1 Discrete Fourier Transform (DFT) Functions

The DFT basis functions are given by the following relations:

$$G_0[t] = 1, \quad G_{2k-1}[t] = \cos\left[2\pi k \cdot \frac{t-1}{N}\right], \quad G_{2k}[t] = \sin\left[2\pi k \cdot \frac{t-1}{N}\right], \quad k = 1, 2, 3, \ldots, \quad t = 1, \ldots, N \tag{A.1.1}$$

with N designating the non-stationary signal length (in samples). The first four DFT basis functions are depicted in Fig. A.1.1.

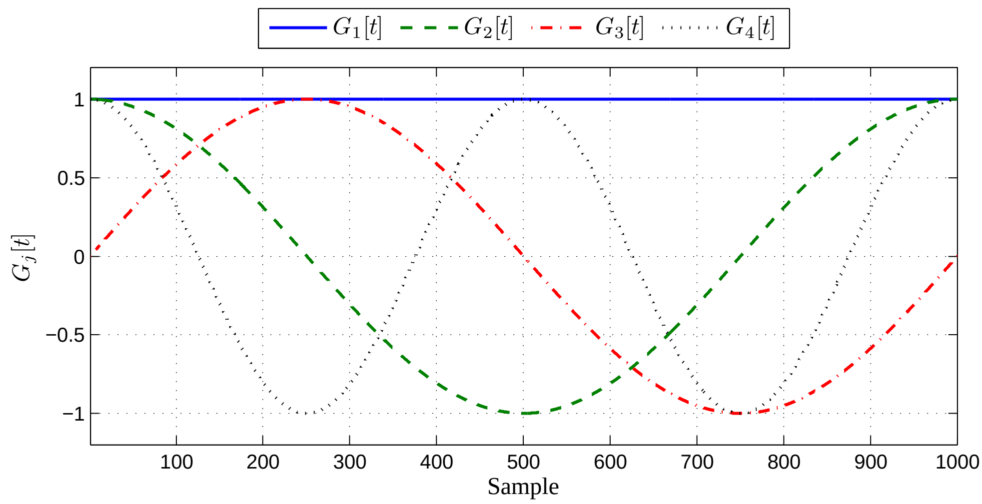

Figure A.1.1: The first four discrete Fourier transform basis functions.

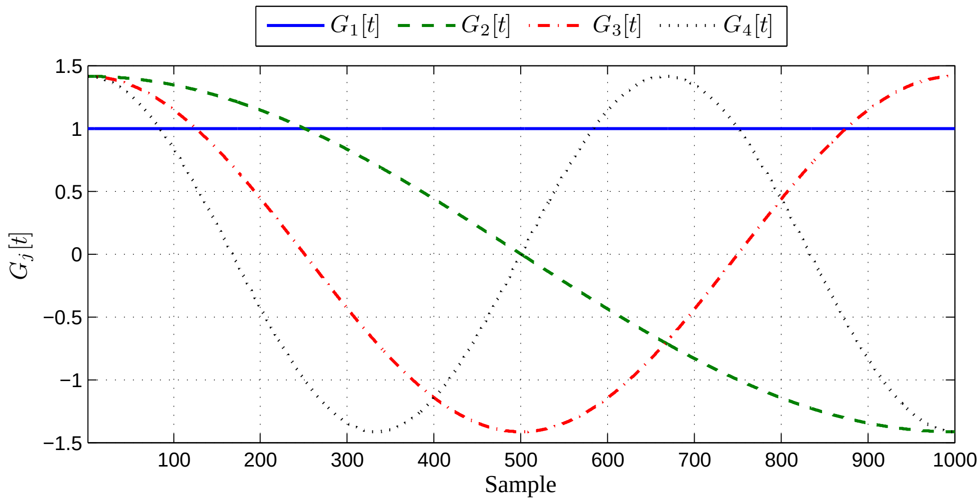

Figure A.2.1: The first four discrete cosine transform basis functions.

A.2 Discrete Cosine Transform (DCT) Functions

The DCT basis functions are given by the following equation:

$$G_k[t] = a_k \cdot \cos\left[\pi k \cdot \frac{2(t-1)+1}{2N}\right], \qquad k = 0,1,2,\dots, \qquad t = 1,\dots,N \tag{A.2.1}$$

with

$$a_k = \begin{cases} \sqrt{\frac{1}{N}} \text{ for } k = 0 \\ \sqrt{\frac{2}{N}} \text{ for } k \neq 0 \end{cases}$$

and N the non-stationary signal length (in samples). The first four DCT basis functions are depicted in Fig. A.2.1.

A.3 Chebyshev Polynomials

The Chebyshev polynomials belong to the broader family of orthogonal polynomials obeying the recurrence relation [Abramowitz and Stegun, 1972, p. 782] :

$$a_1 \cdot G_{k+1}[\tfrac{t-1}{N-1}] = (a_2 + a_3\tfrac{t-1}{N-1}) \cdot G_k[\tfrac{t-1}{N-1}] - a_4 \cdot G_{k-1}[\tfrac{t-1}{N-1}], \quad k = 0,1,2,\dots, \quad t = 1,\dots,N \tag{A.3.1}$$

For $a_1 = a_4 = 1, a_2 = 0, a_3 = 2$, and $G_{-1}[\frac{t-1}{N-1}] = 0$, $G_0[\frac{t-1}{N-1}] = 1$, this expression yields the shifted Chebyshev polynomials of the first kind (see Fig. A.3.1).

A.4 Legendre Polynomials

The Legendre polynomials also obey the recurrence relation of Eq. A.3.1 with $a_1 = k+1, a_2 = 0, a_3 = 2k+1, a_4 = k$, and $G_0[t] = 1, G_1[t] = t$. The first four Legendre polynomials are depicted in Fig. A.4.1.

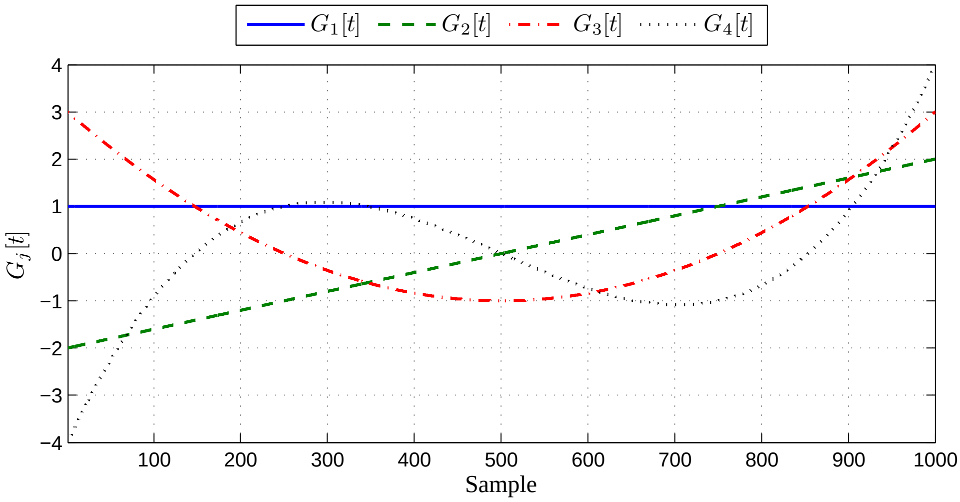

Figure A.3.1: The first four Chebyshev polynomials of the first kind.

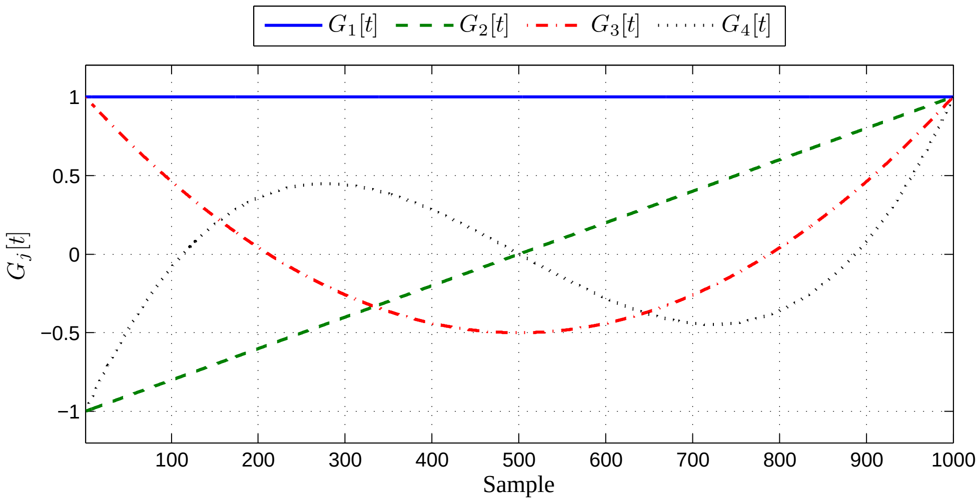

Figure A.4.1: The first four Legendre polynomials.

A.5 Haar Functions

The Haar functions form a group of square waves with magnitude ± 1 in certain intervals and zero elsewhere. The first two are defined as:

$$G_0[t] = 1 \qquad G_1[t] = \begin{cases} 1 & t \in \left[1, \frac{N}{2}\right] \\ -1 & t \in \left[\frac{N}{2} + 1, N\right] \end{cases} \tag{A.5.1}$$

$G_1[t]$ is referred to as the *fundamental square wave* of length N. The rest are defined in families of 2^j, $j = 1, 2, \ldots$, functions ($G_2[t]$ up to $G_3[t]$, $G_4[t]$ up to $G_7[t]$, $G_{2^j}[t]$ up to $G_{2^{j+1}-1}[t]$ in general). In each family (comprising 2^j functions) the interval $[1,\ N]$ is divided into 2^j equal segments of length $\frac{N}{2^j}$ within which $G_1[t]$ is compressed (forming the fundamental square wave of length $\frac{N}{2^j}$) and successively located (from left to right) in each segment, while the remaining portions of the $[1, N]$ interval are filled up with

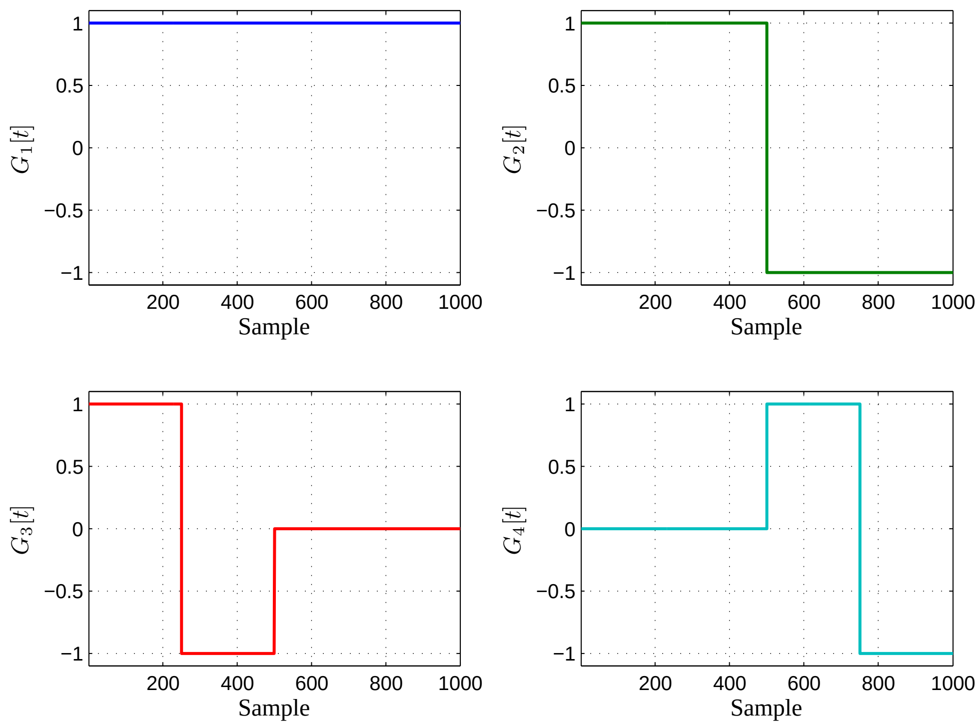

Figure A.5.1: The first four Haar basis functions.

zeros. For instance:

$$G_2[t] = \begin{cases} 1 & t \in \left[1, \frac{N}{4}\right] \\ -1 & t \in \left[\frac{N}{4}+1, \frac{N}{2}\right] \\ 0 & t \in \left[\frac{N}{2}+1, N\right] \end{cases} \qquad G_3[t] = \begin{cases} 0 & t \in \left[1, \frac{N}{2}\right] \\ 1 & t \in \left[\frac{N}{2}+1, \frac{3N}{4}\right] \\ -1 & t \in \left[\frac{3N}{4}+1, N\right] \end{cases} \tag{A.5.2}$$

The first four Haar basis functions are depicted in Fig. A.5.1.

A.6 Normalized B-Splines

Although, there are several ways to define the B-spline functions $G_j^\kappa[t, \boldsymbol{\tau}]$ of order κ, a convenient one is by the means of the Cox-de Boor recursion formula for the normalized B-splines [de Boor, 2001, p. 90].

$$G_j^1[t, \boldsymbol{\tau}] = \begin{cases} 1 & \text{if } \tau_j \leq t < \tau_{j+1} \\ 0 & \text{otherwise} \end{cases} \tag{A.6.1a}$$

$$G_j^i[t, \boldsymbol{\tau}] = w_{j,i}[t] \cdot G_j^{i-1}[t, \boldsymbol{\tau}] + (1 - w_{j,i}[t]) \cdot G_{j+1}^{i-1}[t, \boldsymbol{\tau}], \quad \text{for } 1 < i \leq \kappa \tag{A.6.1b}$$

where

$$w_{j,i}[t] = \begin{cases} \dfrac{t - \tau_j}{\tau_{j+i-1} - \tau_j} & \text{if } \tau_j < \tau_{j+i-1}, \\ 0 & \text{otherwise.} \end{cases} \tag{A.6.1c}$$

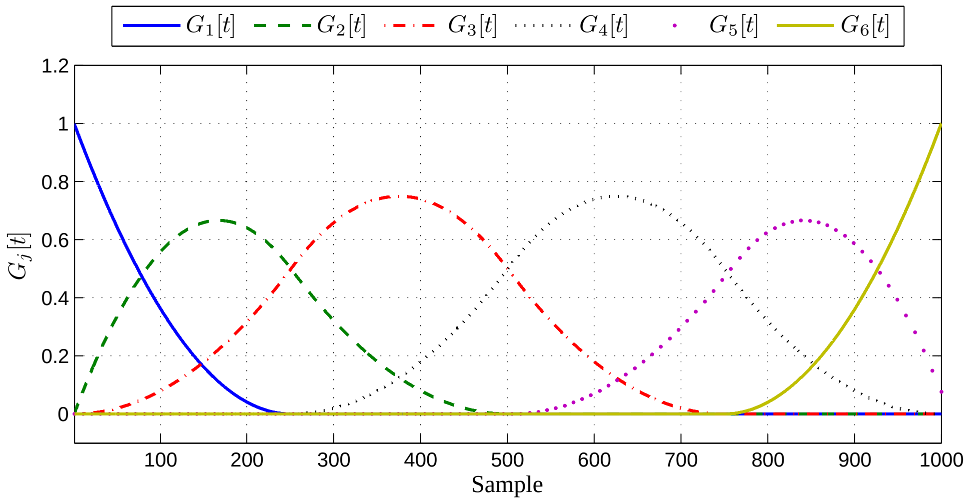

Figure A.6.1: The six functions of a uniform B-spline basis of order $p = 3$ with $N = 1000$ and internal knots $\tau_4 = 250, \tau_5 = 500, \tau_6 = 750$.

In the above relationships, $\boldsymbol{\tau} = [\tau_1, \ldots, \tau_{p+\kappa}] \in [1, N]$ designates the non-decreasing sequence of knots, and p the basis dimensionality. According to the Curry and Schoenberg Theorem [de Boor, 2001, pp. 97-98] and by imposing no continuity conditions at the endpoints, the first κ and last κ knots may be selected as $\tau_1 = \ldots = \tau_\kappa = 1$ and $\tau_{p+1} = \ldots = \tau_{p+\kappa} = N$ with the B-splines basis being fully determined by the $p - \kappa$ free internal knots $[\tau_{\kappa+1}, \ldots, \tau_p]^T$.

The uniform B-spline basis may be obtained by using a grid of equidistant internal knots. For instance, the uniform quadratic B-splines basis ($\kappa = 3$) consisting of six basis functions ($p = 3$) are depicted in Fig. A.6.1.

References

[Abdrabbo, 1979] Abdrabbo, N. (1979). A New Approach to the Problem of Estimating Spectral Parameters of Non-stationary Time Series Models. *Journal of Computational and Applied Mathematics*, 5(2):125–129.

[Abramowitz and Stegun, 1972] Abramowitz, M. and Stegun, I. (1972). *Handbook of Mathematical Functions with Formulas, Graphs, and Mathematical Tables*. Dover Publications, New York.

[Akan and Chaparro, 1994] Akan, A. and Chaparro, L. (1994). Adaptive Time-Varying Parametric Modeling. In *IEEE International Conference on Acoustics, Speech, and Signal Processing (ICASSP-94), Adelaide, Australia*, volume 4, pages 13–16.

[Amir and Gath, 1989] Amir, N. and Gath, I. (1989). Segmentation of EEG During Sleep Using Time-Varying Autoregressive Modeling. *Biological Cybernetics*, 61(6):447–455.

[Auger et al., 1996] Auger, F., Flandrin, P., Gonçalvès, P., and Lemoine, O. (1996). *Time-frequency toolbox - Tutorial*. CNRS France - Rice University. http://tftb.nongnu.org/.

[Augusti et al., 1984] Augusti, G., Baratta, A., and Casciati, F. (1984). *Probabilistic Methods in Structural Engineering*. Taylor & Francis.

[Bakkoury et al., 2000] Bakkoury, J., Roviras, D., Ghogho, M., and Castanie, F. (2000). Adaptive MLSE Receiver Over Rapidly Fading Channels. *Signal Processing*, 80(7):1347–1360.

[Bakrim et al., 1994] Bakrim, M., Aboutajdine, D., and Najim, M. (1994). New Cumulant-Based Approaches for Non-Gaussian Time-Varying AR Models. *Signal Processing*, 39(1-2):107–115.

[Bardou and Sidahmed, 1994] Bardou, O. and Sidahmed, M. (1994). Early Detection of Leakages in the Exhaust and Discharge Systems of Reciprocating Machines by Vibration Analysis. *Mechanical Systems and Signal Processing*, 8(5):551–570.

[Basseville et al., 2007] Basseville, M., Benveniste, A., Goursat, M., and Mevel, L. (2007). Subspace-Based Algorithms for Structural Identification, Damage Detection and Sensor Data Fusion. *EURASIP Journal on Advances in Signal Processing*, 2007:1–13.

[Ben Mrad, 2002] Ben Mrad, R. (2002). Non-linear Systems Representation Using ARMAX Models with Time-dependent Coefficients. *Mechanical Systems and Signal Processing*, 16(5):803–815.

[Ben Mrad and Farag, 2002] Ben Mrad, R. and Farag, E. (2002). Identification of ARMAX Models With Time Dependent Coefficients. *Journal of Dynamic Systems, Measurement, and Control*, 124:464–467.

[Ben Mrad and Fassois, 1991a] Ben Mrad, R. and Fassois, S. (1991a). Recursive Identification of Vibrating Structures from Noise-Corrupted Observations, 1, Identification approaches. *ASME Journal of Vibration and Acoustics*, 113:354–361.

[Ben Mrad and Fassois, 1991b] Ben Mrad, R. and Fassois, S. (1991b). Recursive Identification of Vibrating Structures from Noise-Corrupted Observations, 2, Performance evaluation via numerical and laboratory experiments. *ASME Journal of Vibration and Acoustics*, 113:362–368.

[Ben Mrad et al., 1994] Ben Mrad, R., Fassois, S., and Levitt, J. (1994). Nonstationary Signal Estimation Using Time-Varying ARMA Models. In *IEEE-SP International Symposium on Time-Frequency and Time-Scale Analysis, Philadelphia, USA*, pages 433–436.

[Ben Mrad et al., 1998a] Ben Mrad, R., Fassois, S., and Levitt, J. (1998a). A Polynomial-Algebraic Method for Non-Stationary TARMA Signal Analysis – Part I: The method. *Signal Processing*, 65(1):1–19.

[Ben Mrad et al., 1998b] Ben Mrad, R., Fassois, S., and Levitt, J. (1998b). A Polynomial-Algebraic Method for Non-Stationary TARMA Signal Analysis – Part II: Application to modeling and prediction of power consumption in automobile active suspension systems. *Signal Processing*, 65(1):21–38.

[Bendat and Piersol, 2000] Bendat, J. and Piersol, A. (2000). *Random Data: Analysis and Measurements Procedures*. Prentice-Hall, 3rd edition.

[Bosse et al., 1998] Bosse, A., Tasker, F., and Fisher, S. (1998). Real-Time Modal Parameter Estimation Using Subspace Methods: Applications. *Mechanical Systems and Signal Processing*, 12(6):809–823.

[Boudaoud and Chaparro, 1987] Boudaoud, M. and Chaparro, L. (1987). Composite Modeling of Nonstationary Signals. *Journal of the Franklin Institute*, 324(1):113–124.

[Box et al., 1994] Box, G., Jenkins, G., and Reinsel, G. (1994). *Time Series Analysis, Forecasting and Control*. Prentice-Hall, 3rd edition.

[Carden and Fanning, 2004] Carden, E. and Fanning, P. (2004). Vibration Based Condition Monitoring: A review. *Structural Health Monitoring*, 3(4):355–377.

[Charbonnier et al., 1987] Charbonnier, R., Barlaud, M., Alengrin, G., and Menez, J. (1987). Results on AR-Modelling of Nonstationary Signals. *Signal Processing*, 12(2):143–151.

[Chen, 2005] Chen, L. (2005). *Vector Time-Varying Autoregressive (TVAR) Models and Their Application Downburst Wind Speeds*. PhD thesis, Texas Tech University.

[Chen et al., 1989] Chen, S., Billings, S., and Luo, W. (1989). Orthogonal Least Squares Methods and Their Application to Non-linear System Identification. *International Journal of Control*, 50(5):1873–1896.

[Chengdong et al., 2008] Chengdong, W., Youyun, Z., and Zhenyuan, Z. (2008). Fault Diagnosis for Diesel Valve Trains Based on Time–Frequency Images. *Mechanical Systems and Signal Processing*, 22(8):1981–1993.

[Chevalier et al., 1985] Chevalier, M., Chollet, C., and Grenier, Y. (1985). Speech Analysis and Restitution Using Time-Depedent Autoregressive Models. In *IEEE International Conference on Acoustics, Speech, and Signal Processing, ICASSP '85,*, pages 501–504.

[Chon et al., 2005] Chon, K., Zhao, H., Zou, R., and Ju, K. (2005). Multiple Time-Varying Dynamic Analysis Using Multiple Sets of Basis Functions. *IEEE Transactions on Biomedical Engineering*, 52(5):956–960.

[Chon et al., 2008] Chon, K., Zhong, Y., Moore, L., Holstein-Rathlou, N., and Cupples, W. (2008). Analysis of Nonstationarity in Renal Autoregulation Mechanisms Using Time-Varying Transfer and Coherence Functions. *American Journal of Physiology - Regulatory, Integrative and Comparative Physiology*, 295(3):R821–R828.

[Ciftci and Kahya, 2008] Ciftci, K. and Kahya, Y. (2008). Respiratory Airflow Estimation by Time Varying Autoregressive Modeling. In *30th Annual International Conference of the IEEE Engineering in Medicine and Biology Society (EMBS 2008), Vancouver, BC*, pages 347–350.

[Clergeot, 1984] Clergeot, H. (1984). Filter-Order Selection in Adaptive Maximum Likelihood Estimation. *IEEE Transactions on Information Theory*, 30(2):199–210.

[Cohen, 1995] Cohen, L. (1995). *Time Frequency Analysis*. Prentice Hall PTR.

[Coley, 1999] Coley, D. (1999). *An Introduction to Genetic Algorithms for Scientists and Engineers*. World Scientific.

[Conforto and D'Alessio, 1999a] Conforto, S. and D'Alessio, T. (1999a). Optimal Estimation of Power Spectral Density by Means of a Time-Varying Autoregressive Approach. *Signal Processing*, 72(1):1–14.

[Conforto and D'Alessio, 1999b] Conforto, S. and D'Alessio, T. (1999b). Spectral Analysis for Non-stationary Signals from Mechanical Measurements: A parametric approach. *Mechanical Systems and Signal Processing*, 13(3):395–411.

[Cooper, 1990] Cooper, J. (1990). Identification of Time Varying Modal Parameters. *The Aeronautical Journal of the Royal Aeronautical Society*, 94:271–278.

[Cooper and Worden, 2000] Cooper, J. and Worden, K. (2000). On-Line Physical Parameter Estimation with Adaptive Forgetting Factors. *Mechanical Systems and Signal Processing*, 14(5):705–730.

[Cull et al., 2005] Cull, P., Flahive, M., and Robson, R. (2005). *Difference Equations: From Rabbits to Chaos*. Undergraduate Texts in Mathematics. Springer.

[de Boor, 2001] de Boor, C. (2001). *A Practical Guide to Splines*. Springer-Verlag, Revised edition.

[Dimitriadis et al., 2004] Dimitriadis, G., Fassois, S., Poulimenos, A., and Shi, D. (2004). Identification and Model Updating of a Non-stationary Vibrating System. In *7th Biennial ASME Conference on Engineering Systems Design and Analysis, Manchester, United Kingdom.*

[Doebling et al., 1998] Doebling, S., Farrar, C., and Prime, M. (1998). A Summary Review of Vibration-Based Damage Identification Methods. *The Shock and Vibration Digest*, 30(2):91–105.

[Draper and Smith, 1998] Draper, N. and Smith, H. (1998). *Applied Regression Analysis*. John Wiley & Sons, 3rd edition.

[Engelbrecht, 2006] Engelbrecht, A. (2006). *Fundamentals of Computational Swarm Intelligence*. Wiley.

[Eom, 1999a] Eom, K. (1999a). Analysis of Acoustic Signatures from Moving Vehicles Using Time-Varying Autoregressive Models. *Multidimensional Systems and Signal Processing*, 10(4):357–378.

[Eom, 1999b] Eom, K. (1999b). Time-Varying Autoregressive Modeling of HRR Radar Signatures. *IEEE Transactions on Aerospace and Electronic Systems*, 35(3):974–988.

[Eom, 2000] Eom, K. (2000). Contour Analysis Using Time-Varying Autoregressive Model. In *International Conference on Image Processing, Vancouver, BC, Canada , Canada*, volume 2, pages 891–894.

[Evers and Hopgood, 2007] Evers, C. and Hopgood, J. (2007). Parametric Modelling for Single-Channel Blind Dereverberation of Speech from a Moving Speaker. *IET Signal Processing*, 2(2):59–74.

[Farrar et al., 2001] Farrar, C., Doebling, S., and Nix, D. (2001). Vibration-Based Structural Damage Identification. *Philosophical Transactions of the Royal Society A*, 359(1778):131–149.

[Fassois, 2001a] Fassois, S. (2001a). Identification, Model-Based Methods. In Braun, S., Ewins, D., and Rao, S., editors, *Encyclopedia of Vibration*, pages 673–685. Academic Press.

[Fassois, 2001b] Fassois, S. (2001b). MIMO LMS-ARMAX Identification of Vibrating Structures – Part I: The method. *Mechanical Systems and Signal Processing*, 15:723–735.

[Fassois and Sakellariou, 2007] Fassois, S. and Sakellariou, J. (2007). Time-Series Methods for Fault Detection and Identification in Vibrating Structures. *Philosophical Transactions of the Royal Society A*, 365:411–448.

[Fassois and Sakellariou, 2009] Fassois, S. and Sakellariou, J. (2009). Statistical Time Series Methods for SHM. In Boller, C., Chang, F., and Fujino, Y., editors, *Encyclopedia of Structural Health Monitoring*, pages 443–472. John Wiley and Sons Ltd, Chichester, UK.

[Flaherty, 1988] Flaherty, M. (1988). Application of Polynomial Splines to a Time-Varying Autoregressive Model of Speech. In *International Conference on Acoustics, Speech, and Signal Processing, ICASSP-88*, volume 4, pages 2220–2223.

[Fouskitakis and Fassois, 2001] Fouskitakis, G. and Fassois, S. (2001). On the Estimation of Non-Stationary Functional Series TARMA Models: An isomorphic matrix algebra based method. *ASME Journal of Dynamic Systems, Measurement and Control*, 123(4):601–610.

[Fouskitakis and Fassois, 2002] Fouskitakis, G. and Fassois, S. (2002). Functional Series TARMA Modelling and Simulation of Earthquake Ground Motion. *Earthquake Engineering and Structural Dynamics*, 31(2):399–420.

[Funaki, 2001] Funaki, K. (2001). A Time-Varying Complex AR Speech Analysis Based on GLS and ELS Method. In *EUROSPEECH-2001*, pages 2649–2652.

[Funaki et al., 1998a] Funaki, K., Miyanaga, Y., and Tochinai, K. (1998a). On a Time-Varying Complex Speech Analysis. In *IX European Signal Processing Conference, Island of Rhodes, Greece*.

[Funaki et al., 1998b] Funaki, K., Miyanaga, Y., and Tochinai, K. (1998b). On Robust Speech Analysis Based on Time-Varying Complex AR Model. In Mannell, R. H. and Robert-Ribes, J., editors, *5th International Conference on Spoken Language Processsing (ICSLP'98), Sydney, Australia*, volume 4, pages 1375–1378.

[Garibaldi and Marchesiello, 2006] Garibaldi, L. and Marchesiello, S. (2006). Non Stationary Analysis of a Railway Bridge Scaled Model Under Operational Conditions. In *ISMA2006 International Conference on Noise and Vibration Engineering, Leuven, Belgium*, pages 2851–2862.

[Garthwaite et al., 2002] Garthwaite, P., Jolliffe, I., and Jones, B. (2002). *Statistical Inference.* Oxford University Press, 2nd edition.

[Gersch and Brotherton, 1982] Gersch, W. and Brotherton, T. (1982). Estimation of stationary structural system parameters from non-stationary random vibration data: A locally stationary model method. *Journal of Sound and Vibration*, 81(2):215–227.

[Gersch et al., 1983] Gersch, W., Gevins, A., and Kitagawa, G. (1983). A Multivariate Time Varying Autoregressive Modeling of Nonstationary Covariance Time Series. In *The 22nd IEEE Conference on Decision and Control*, pages 579–584.

[Gersch and Kitagawa, 1982] Gersch, W. and Kitagawa, G. (1982). A Time-Varying Multivariate Autoregressive Modeling of Econometric Time Series. Statistical Research Division RR82/07, Bureau of the Census.

[Gersch and Kitagawa, 1985] Gersch, W. and Kitagawa, G. (1985). A Time Varying AR Coefficient Model for Modeling and Simulating Earthquake Ground Motion. *Earthquake Engineering and Structural Dynamics*, 13(2):243–254.

[Gertler, 1998] Gertler, J. (1998). *Fault Detection and Diagnosis in Engineering Systems*. Marcel Dekker Inc.

[Ghanem and Romeo, 2000] Ghanem, R. and Romeo, F. (2000). A Wavelet-Based Approach for the Identification of Linear Time-Varying Dynamical Systems. *Journal of Sound and Vibration*, 234:555–576.

[Ghosh and Bouthellier, 1993] Ghosh, B. and Bouthellier, P. (1993). Simultaneous Coefficient Assignment of Discrete Time Multi-Input Multi-OutputLinear Time-Varying System: A New Approach for Compensator Design. *SIAM Journal on Control and Optimization*, 31:1438–1461.

[Gill et al., 1981] Gill, P., Murray, W., and Wright, M. (1981). *Practical Optimization*. Academic Press Inc.

[Girault et al., 2000] Girault, J., Kouame, D., Ouahabi, A., and Patat, F. (2000). Estimation of the Blood Doppler Frequency Shift by a Time-Varying Parametric Approach. *Ultrasonics*, 38(1-8):682–687.

[Goethals et al., 2004] Goethals, I., Mevel, L., Benveniste, A., and Moor, B. D. (2004). Recursive Output Only Subspace Identification for In-Flight Flutter Monitoring. In *Proceedings of the 22nd International Modal Analysis Conference (IMACXXII) , Dearborn, Michigan*.

[Golub and Pereyra, 1973] Golub, G. and Pereyra, V. (1973). The Differentation of Pseudo-Inverses and Nonlinear Least Squares Problems Whose Variables Separate. *SIAM Journal on Numerical Analysis*, 10(2):413–432.

[Golub and Pereyra, 2003] Golub, G. and Pereyra, V. (2003). Separable Nonlinear Least Squares: The Variable Projection Method and its Applications. *Inverse Problems*, 19:R1–R26.

[Grenier, 1983a] Grenier, Y. (1983a). Estimation of Non-stationary Moving Average Models. In *IEEE International Conference on Acoustics, Speech, and Signal Processing (ICASSP '83), Boston, USA*, pages 268–271.

[Grenier, 1983b] Grenier, Y. (1983b). Time-Dependent ARMA Modeling of Nonstationary Signals. *IEEE Transactions on Acoustics, Speech, and Signal Processing*, 31(4):899–911.

[Grenier, 1984] Grenier, Y. (1984). Time-Frequency Analysis Using Time-dependent ARMA Models. In *IEEE International Conference on Acoustics, Speech, and Signal Processing (ICASSP '84)*, pages 270–273.

[Grenier, 1985] Grenier, Y. (1985). Nonstationary Signal Modeling with Application to Bat Echolocation Calls. In *CNRS Colloquim on Systemes Sonar Aeriens Animaux, Lyon, France*.

[Grenier, 1986] Grenier, Y. (1986). Nonstationary ARMA Models via Simultaneous AR and MA Estimation. In *IEEE International Conference on Acoustics, Speech, and Signal Processing (ICASSP '86)*, pages 2339–2342.

[Grenier, 1989a] Grenier, Y. (1989a). Model Expansion Applied to Speech Analysis and Source Location. In *International Conference on Acoustics, Speech, and Signal Processing (ICASSP-89), Glasgow , UK*, volume 4, pages 2302–2305.

[Grenier, 1989b] Grenier, Y. (1989b). Parametric Time-Frequency Representations. In Longo, G. and Picinbono, B., editors, *Time and Frequency Representation of Signals and Systems*, number 309 in CISM Courses and Lectures, pages 125–175. Springer-Verlag.

[Ha and Ann, 1995] Ha, P. and Ann, S. (1995). Robust Time-Varying Parametric Modelling of Voiced Speech. *Signal Processing*, 42(3):311–317.

[Haber and Keviczky, 1999] Haber, R. and Keviczky, L. (1999). *Nonlinear System Identification: Input-Output Modelling Approach*. Kluwer Academic Publishers.

[Hall et al., 1983] Hall, M., Oppenheim, A., and Willsky, A. (1983). Time-Varying Parametric Modeling of Speech. *Signal Processing*, 5(3):267–285.

[Hammond and White, 1996] Hammond, J. and White, P. (1996). The Analysis of Non-Stationary Signals Using Time-Frequency Methods. *Journal of Sound and Vibration*, 190(3):419–447.

[Hiltunen et al., 1999] Hiltunen, J., Karjalainen, P., Partanen, J., and Kaipio, J. (1999). Estimation of the Dynamics of Event-Related Desynchronisation Changes in Electroencephalograms. *Medical and Biological Engineering and Computing*, 37(3):309–315.

[Hinich and Roll, 1981] Hinich, M. and Roll, R. (1981). Measuring Nonstationarity in the Parameters of the Market Model. *Research in Finance*, 3:1–51.

[Howe, 2000] Howe, D. (2000). Magnetic Actuators. *Sensors and Actuators A: Physical*, 81(1-3):268–274.

[Huang et al., 2009] Huang, C., Hung, S., Su, W., and Wu, C. (2009). Identification of Time-Variant Modal Parameters Using Time-Varying Autoregressive with Exogenous Input and Low-Order Polynomial Function. *Computer-Aided Civil and Infrastructure Engineering*, 24(7):470–491.

[Jachan and Matz, 2005] Jachan, M. and Matz, G. (2005). Nonstationary Vector AR Modeling of Wireless Channels. In *IEEE 6th Workshop on Signal Processing Advances in Wireless Communications*, pages 625–629.

[Jachan et al., 2007] Jachan, M., Matz, G., and Hlawatsch, F. (2007). Time-Frequency ARMA Models and Parameter Estimators for Underspread Nonstationary Random Processes. *IEEE Transactions on Signal Processing*, 55(9):4366–4381.

[Jachan et al., 2009] Jachan, M., Matz, G., and Hlawatsch, F. (2009). Vector Time-Frequency AR Models for Nonstationary Multivariate Random Processes. *IEEE Transactions on Signal Processing*, 57(12):4646–4659.

[Jiang and Kitagawa, 1993] Jiang, X. and Kitagawa, G. (1993). A Time Varying Coefficient Vector AR Modelling of Nonstationary Covariance Time Series. *Signal Processing*, 33:315–331.

[Johansson and White, 2008] Johansson, A. and White, P. (2008). Instantaneous Frequency Estimation at Low Signal-to-Noise Ratios Using Time-varying Notch Filters. *Signal Processing*, 88(5):1271–1288.

[Jolliffe, 2002] Jolliffe, I. (2002). *Principal Component Analysis*. Springer, 2nd edition.

[Juntunen et al., 1998] Juntunen, M., Tervo, J., and Kaipio, J. (1998). Stabilization of Stationary and Time-Varying Autoregressive Models. In *IEEE International Conference on Acoustics, Speech and Signal Processing (ICASSP'98), Seattle, WA , USA*, volume 4, pages 2173–2176.

[Kacha et al., 2005] Kacha, A., Grenez, F., and Benmahammed, K. (2005). Time-Frequency Analysis and Instantaneous Frequency Estimation Using Two-Sided Linear Prediction. *Signal Processing*, 85(3):491–503.

[Kacha et al., 2008] Kacha, A., Grenez, F., and Benmahammed, K. (2008). Time-Frequency Analysis of Multichannel Signals Using Two-Sided Autoregressive Modeling. *Circuits, Systems, and Signal Processing*, 27(3):309–330.

[Kaderli and Kayhan, 2001] Kaderli, A. and Kayhan, A. (2001). A Spectral Matching Approach for Parameter and Spectral Estimation of Nonstationary Rational Processes. *IEEE Transactions on Signal Processing*, 49(10):2223–2231.

[Kaipio and Karjalainen, 1997] Kaipio, J. and Karjalainen, P. (1997). Estimation of Event-Related Synchronization Changes by a New TVAR Method. *IEEE Transactions on Biomedical Engineering*, 44(8):649–656.

[Kamen, 1988] Kamen, E. (1988). The Poles and Zeros of a Linear Time-Varying System. *Linear Algebra and its Applications*, 98:263–289.

[Kameyama and Ohsumi, 2007] Kameyama, K. and Ohsumi, A. (2007). Subspace-Based Prediction of Linear Time-Varying Stochastic Systems. *Automatica*, 43(12):2009–2021.

[Kirkegaard et al., 1996] Kirkegaard, P., Andersen, P., and Brincker, R. (1996). Identification of Civil Engineering Structures Using Multivariate ARMAV and RARMAV Models. In *International Conference on Identification in Engineering Systems, Swansea, UK*.

[Kitagawa and Gersch, 1985] Kitagawa, G. and Gersch, W. (1985). A Smoothness Priors Time-Varying AR Coefficient Modeling of Nonstationary Covariance Time Series. *IEEE Transactions on Automatic Control*, 30(1):48–56.

[Kitagawa and Gersch, 1996] Kitagawa, G. and Gersch, W. (1996). *Smoothness Priors Analysis of Time Series*. New York: Springer-Verlag.

[Korosec, 2000] Korosec, D. (2000). Parametric Estimation of the Continuous Non-Stationary Spectrum and its Dynamics in Surface EMG Studies. *International Journal of Medical Informatics*, 58-59:59–69.

[Kozin, 1977] Kozin, F. (1977). Estimation and Modelling of Nonstationary Time-Series. In *Symposium of Applications of Computer Method in Engineering, Los Angeles, USA*.

[Kozin and Nakajima, 1980] Kozin, F. and Nakajima, F. (1980). The Order Determination Problem for Linear Time-Varying AR Models. *IEEE Transactions on Automatic Control*, 25(2):250–257.

[Kullaa, 2004] Kullaa, J. (2004). Structural Health Monitoring of a Crane in Variable Configurations. In *ISMA2004 International Conference on Noise and Vibration Engineering, Leuven, Belgium*, pages 457–470.

[Li et al., 2003] Li, J., Su, M., and Fan, L. (2003). Natural Frequency of Railway Girder Bridges under Vehicle Loads. *Journal of Bridge Engineering*, 8(4):199–203.

[Li et al., 2011] Li, Y., Wei, H.-L., Billings, S., and Sarrigiannis, P. (2011). Time-Varying Model Identification for Time-Frequency Feature Extraction from EEG Data. *Journal of Neuroscience Methods*, 196(1):151–158.

[Lima-Veiga and Grenier, 1991] Lima-Veiga, A. D. and Grenier, Y. (1991). Spectral Estimation with Stochastic Coefficients Models. In *13 Colloque sur le Traitement du Signal et des Images*, pages 366–369.

[Lin et al., 2005] Lin, C., Wang, C., Wu, H., and Wang, J. (2005). On-Line Building Damage Assessment Based on Earthquake Records. *Smart Materials and Structures*, 14:S137–S153.

[Liporace, 1975] Liporace, L. (1975). Linear Estimation of Nonstationary Signals. *Journal of the Acoustical Society of America*, 58(6):1288–1295.

[Liu and Deng, 2006] Liu, K. and Deng, L. (2006). Identification of Pseudo-natural Frequencies of an Axially Moving Cantilever Beam Using a Subspace-based Algorithm. *Mechanical Systems and Signal Processing*, 20(1):94–113.

[Ljung, 1999] Ljung, L. (1999). *System Identification: Theory for the User*. Prentice Hall PTR, 2nd edition.

[Ljung and Soderstrom, 1983] Ljung, L. and Soderstrom, T. (1983). *Theory and Practice of Recursive Identification*. The MIT Press.

[Lütkepohl, 1996] Lütkepohl, H. (1996). *Handbook of Matrices*. John Wiley & Sons.

[Mathworks, 2008] Mathworks, T. (2008). *Genetic Algorithm and Direct Search Toolbox User's Guide, Ver. 2.3*. URL: http://www.mathworks.com/access/helpdesk/help/toolbox/gads.

[Mendel, 1973] Mendel, J. (1973). *Discrete Techniques of Parameter Estimation: The Equation Error Formulation*. Marcel Dekker Inc.

[Mevel et al., 2005] Mevel, L., Basseville, M., and Benveniste, A. (2005). Fast In-Flight Detection of Flutter Onset: A Statistical Approach. *Journal of Guidance, Control, and Dynamics*, 28:431–438.

[Mukhopadhyay and Sircar, 1997] Mukhopadhyay, S. and Sircar, P. (1997). Parametric Modelling of Non-Stationary Signals: A unified approach. *Signal Processing*, 60(2):135–152.

[Nathan et al., 1991] Nathan, K., Lee, Y.-T., and Silverman, H. (1991). A Time-Varying Analysis Method for Rapid Transitions in Speech. *IEEE Transactions on Signal Processing*, 39(4):815–824.

[Newland, 1993] Newland, D. (1993). *An Introduction to Random Vibrations, Spectral and Wavelet Analysis*. Addison Wesley Longman, 3rd edition.

[Newland, 1994] Newland, D. (1994). Wavelet analysis of vibration, parts I and II. *Journal of Vibration and Acoustics*, 116:409–425.

[Niedźwiecki, 1987] Niedźwiecki, M. (1987). Recursive Functional Series Modelling Estimators for Adaptive Control of Time-Varying Plants. In *26th IEEE Conference on Decision and Control*, pages 1239–1244.

[Niedźwiecki, 1988] Niedźwiecki, M. (1988). Functional Series Modelling Approach to Identification of Nonstationary Stochastic Systems. *IEEE Transactions on Automatic Control*, 33(10):955–961.

[Niedźwiecki, 1990] Niedźwiecki, M. (1990). Recursive Functional Series Modeling Estimators for Identification of Time-Varying Plants – More Bad News Than Good? *IEEE Transactions on Automatic Control*, 35(5):610–616.

[Niedźwiecki, 2000] Niedźwiecki, M. (2000). *Identification of Time-Varying Processes*. John Wiley.

[Niedźwiecki and Klaput, 2002] Niedźwiecki, M. and Klaput, T. (2002). Fast Recursive Basis Function Estimators for Identification of Time-Varying Processes. *IEEE Transactions on Signal Processing*, 50(8):1925–1934.

[Nocedal and Wright, 2006] Nocedal, J. and Wright, S. J. (2006). *Numerical Optimization*. Springer Series in Operation Research and Financial Engineering. Springer.

[Omenzetter and Brownjohn, 2006] Omenzetter, P. and Brownjohn, J. (2006). Application of Time Series Analysis for Bridge Monitoring. *Smart Materials and Structures*, 15:129–138.

[Ouyang, 2007] Ouyang, H. (2007). Stationary and Non-Stationary Vibration of Atomising Discs. *Journal of Sound and Vibration*, 308:699–708.

[Overschee and Moor, 1989] Overschee, P. V. and Moor, B. D. (1989). *Subspace Identification for Linear Systems: Theory - Implementation - Applications*. Kluwer Academic Publishers.

[Owen et al., 2001] Owen, J., Eccles, B., Choo, B., and Woodings, M. (2001). The Application of Auto-Regressive Time Series Modelling for the Time-Frequency Analysis of Civil Engineering Structures. *Engineering Structures*, 23(5):521–536.

[Pachori and Sircar, 2008] Pachori, R. and Sircar, P. (2008). EEG Signal Analysis Using FB Expansion and Second-Order Linear TVAR Process. *Signal Processing*, 88:415–420.

[Paleologu et al., 2008] Paleologu, C., Benesty, J., and Ciochină, S. (2008). A Robust Variable Forgetting Factor Recursive Least-Squares Algorithm for System Identification. *IEEE Signal Processing Letters*, 15:597–600.

[Papakos and Fassois, 2003] Papakos, V. and Fassois, S. (2003). "multichannel identification of aircraft skeleton structures under unobservable excitation: A vector ar/arma framework". *Mechanical Systems and Signal Processing*, 17(6):1271–1290.

[Paulik et al., 1992] Paulik, M., Das, M., and Loh, N. (1992). Nonstationary Autoregressive Modeling of Object Contours. *IEEE Transactions on Signal Processing*, 40(3):660–675.

[Peng and Chu, 2004] Peng, Z. and Chu, F. (2004). Application of the Wavelet Transform in Machine Condition Monitoring and Fault Diagnostics: A review with bibliography. *Mechanical Systems and Signal Processing*, 18(2):199–221.

[Perez and Behdinan, 2007] Perez, R. and Behdinan, K. (2007). Particle Swarm Approach for Structural Design Optimization. *Computers and Structures*, 85(19-20):1579–1588.

[Petsounis and Fassois, 2000] Petsounis, K. and Fassois, S. (2000). Non-Stationary Functional Series TARMA Vibration Modelling and Analysis in a Planar Manipulator. *Journal of Sound and Vibration*, 231(5):1355–1376.

[Piegl and Tiller, 1998] Piegl, L. and Tiller, W. (1998). Computing the Derivative of NURBS With Respect to a Knot. *Computer Aided Geometric Design*, 15(9):925–934.

[Poulimenos and Fassois, 2003a] Poulimenos, A. and Fassois, S. (2003a). Estimation and Identification of Nonstationary Functional Series TARMA Models. In *13th IFAC Symposium on System Identification (SYSID), Rotterdam, The Netherlands*, pages 162–167.

[Poulimenos and Fassois, 2003b] Poulimenos, A. and Fassois, S. (2003b). Non-Stationary Mechanical Vibration Modeling and Analysis via Functional Series TARMA Models. In *13th IFAC Symposium on System Identification (SYSID), Rotterdam, The Netherlands*, pages 965–970.

[Poulimenos and Fassois, 2004a] Poulimenos, A. and Fassois, S. (2004a). Non-Stationary Random Vibration Modelling and Analysis via Functional Series TARMAX Models. In *ISMA2004 International Conference on Noise and Vibration Engineering, Leuven, Belgium*, pages 2475–2490.

[Poulimenos and Fassois, 2004b] Poulimenos, A. and Fassois, S. (2004b). Vibration-Based On-Line Fault Detection in Non-Stationary Structural Systems via a Statistical Model Based Method. In *2nd European Workshop on Structural Health Monitoring (EWSHM 2004), Munich, Germany*.

[Poulimenos and Fassois, 2006] Poulimenos, A. and Fassois, S. (2006). Parametric Time-Domain Methods for Non-Stationary Random Vibration Modelling and Analysis – A critical survey and comparison. *Mechanical Systems and Signal Processing*, 20(4):763–816.

[Poulimenos and Fassois, 2007] Poulimenos, A. and Fassois, S. (2007). Asymptotic Analysis of Non-Stationary Functional Series TAR Estimators. In *15th Mediterranean Conference on Control & Automation (MED '07), Athens, Greece*.

[Poulimenos and Fassois, 2009a] Poulimenos, A. and Fassois, S. (2009a). Asymptotic Analysis of Non-stationary Functional Series TARMA Estimators. In *15th Symposium on System Identification, Saint-Malo, France*.

[Poulimenos and Fassois, 2009b] Poulimenos, A. and Fassois, S. (2009b). Output-Only Stochastic Identification of a Time-Varying Structure via Functional Series TARMA Models. *Mechanical Systems and Signal Processing*, 23(4):1180–1204.

[Preumont, 1994] Preumont, A. (1994). *Random Vibration and Spectral Analysis*. Kluwer.

[Priestley, 1988] Priestley, M. (1988). *Non-Linear and Non-Stationary Time Series Analysis*. Academic Press.

[Rao, 1970] Rao, T. (1970). The Fitting of Non-Stationary Time-Series Models with Time-Dependent Parameters. *Journal of the Royal Statistical Society. Series B (Methodological)*, 32(2):312–322.

[Reinsel, 1993] Reinsel, G. (1993). *Elements of Multivariate Time Series Analysis*. Springer-Verlag.

[Ruhe and Å. Wedin, 1980] Ruhe, A. and Å. Wedin, P. (1980). Algorithms for Separable Nonlinear Least Squares Problems. *SIAM Review*, 22:318–337.

[Salawu, 1997] Salawu, O. (1997). Detection of structural damage through changes in frequency: A review. *Engineering Structures*, 19(9):718–723.

[Salcedo et al., 2008] Salcedo, G., Sato, J., Morettin, P., and Toloi, C. (2008). Comparing Time-Varying Autoregressive Structures of Locally Stationary Processes. *International Journal of Wavelets, Multiresolution and Information Processing*, 6(1):1–23.

[Sanubari and Tokuda, 1997] Sanubari, J. and Tokuda, K. (1997). Non Stationary Spectral Estimation Based on Robust Time Varying AR Model Excited by a t-Distribution Process. In *IEEE Region 10 Annual Conference on Speech and Image Technologies for Computing and Telecommunications (TENCON '97), Brisbane, Qld., Australia*, volume 1, pages 51–54.

[Sanyal et al., 2005] Sanyal, S., Kukreja, S., Perreault, E., and Westwick, D. (2005). Identification of Linear Time Varying Systems using Basis Pursuit. In *IEEE 27th Annual International Conference of the Engineering in Medicine and Biology Society (IEEE-EMBS 2005)*, pages 22–25.

[Sato et al., 2007] Sato, J., Morettin, P., Arantes, P., and Jr., E. A. (2007). Wavelet Based Time-Varying Vector Autoregressive Modelling. *Computational Statistics & Data Analysis*, 51(12):5847–5866.

[Schnell and Lacroix, 2007] Schnell, K. and Lacroix, A. (2007). Time-Varying Linear Prediction for Speech Analysis. In *15th European Signal Processing Conference (EUSIPCO 2007), Poznan Poland*, pages 2045–2049.

[Senba and Furuya, 2008] Senba, A. and Furuya, H. (2008). Implementation Algorithms for Self-Identification of Adaptive Structures with Variable Geometric Properties. *Mechanical Systems and Signal Processing*, 22:1–14.

[Shi et al., 2007] Shi, Z., Law, S., and Li, H. (2007). Subspace-Based Identification of Linear Time-Varying System. *AIAA Journal*, 45(8):2042–2050.

[Soderstrom and Stoica, 1989] Soderstrom, T. and Stoica, P. (1989). *System Identification*. Prentice Hall.

[Spanos and Failla, 2005] Spanos, P. and Failla, G. (2005). Wavelets: Theoretical Concepts and Vibrations Related Applications. *The Shock and Vibration Digest*, 37(5):359–375.

[Spiridonakos and Fassois, 2009a] Spiridonakos, M. and Fassois, S. (2009a). FS-TARMA Models for Non-Stationary Vibration Analysis: An overview and comparison. In *15th IFAC Symposium on System Identification (SYSID 2009), Saint-Malo, France*.

[Spiridonakos and Fassois, 2009b] Spiridonakos, M. and Fassois, S. (2009b). Multi-Channel Output-Only Identification of an Extendable Arm Structure Under Random Excitation: A comparison of parametric methods. In *4th International Conference on Recent Advances in Space Technologies (RAST '09), Istanbul, Turkey*, pages 161–166.

[Spiridonakos and Fassois, 2009c] Spiridonakos, M. and Fassois, S. (2009c). Parametric Identification of a Time-Varying Structure Based on Vector Vibration Response Measurements. *Mechanical Systems and Signal Processing*, 23(6):2029–2048.

[Spiridonakos and Fassois, 2009d] Spiridonakos, M. and Fassois, S. (2009d). Vibration Based Fault Detection in a Time-Varying Link Structure via Non-Stationary FS-VTAR Models. In *Proceedings of the International Operational Modal Analysis Conference (IOMAC), Ancona, Italy*.

[Spiridonakos and Fassois, 2012] Spiridonakos, M. and Fassois, S. (2012). An FS-TAR Model-Based Statistical Framework for the Fault Detection and Identification in a Time-Varying Pick-and-Place Mechanism. *submitted for publication*.

[Staszewski and Robertson, 2007] Staszewski, W. and Robertson, A. (2007). Time-Frequency and Time-Scale Analyses for Structural Health Monitoring. *Philosophical Transactions of the Royal Society A*, 365:449–477.

[Staszewski et al., 1997] Staszewski, W., Worden, K., and Tomlinson, G. (1997). Time-Frequency Analysis in Gearbox Fault Detection Using the Wigner-Ville Distribution and Pattern Recognition. *Mechanical Systems and Signal Processing*, 11(5):673–692.

[Stavropoulos and Fassois, 2000] Stavropoulos, C. and Fassois, S. (2000). Non-Stationary Functional Series Modeling and Analysis of Hardware Reliability Series: A comparative study using rail vehicle interfailure times. *Reliability Engineering and System Safety*, 68(2):169–183.

[Thonet and Vesin, 1997] Thonet, G. and Vesin, J.-M. (1997). Stationarity Assessment with Time-Varying Autoregressive Modeling. In *IEEE International Conference on Acoustics, Speech, and Signal Processing (ICASSP-97), Munich, Germany*, volume 5, pages 3721–3724.

[Tsatsanis, 1995] Tsatsanis, M. (1995). Time-Varying System Identification and Channel Equalization Using Wavelets and Higher-Order Statistics. In Leondes, C., editor, *Digital Signal Processing Systems: Implementation Techniques*, volume 65 of *Control and Dynamic Systems*, pages 333–394. Elsevier.

[Tsatsanis and Giannakis, 1993] Tsatsanis, M. and Giannakis, G. (1993). Time-Varying System Identification and Model Validation Using Wavelets. *IEEE Transactions on Signal Processing*, 41(12):3512–3523.

[Tsatsanis and Giannakis, 1996a] Tsatsanis, M. and Giannakis, G. (1996a). Equalization of Rapidly Fading Channels: Self-Recovering Methods. *IEEE Transactions on Communications*, 44(5):619–630.

[Tsatsanis and Giannakis, 1996b] Tsatsanis, M. and Giannakis, G. (1996b). Modelling and Equalization of Rapidly Fading Channels. *International Journal of Adaptive Control and Signal Processing*, 10(2-3):159–176.

[Tsatsanis and Giannakis, 1997] Tsatsanis, M. and Giannakis, G. (1997). Subspace Methods for Blind Estimation of Time-Varying FIR Channels. *IEEE Transactions on Signal Processing*, 45(12):3084–3093.

[Verboven et al., 2004] Verboven, P., Cauberghe, B., Guillaume, P., Vanlanduit, S., and Parloo, E. (2004). Modal Parameter Estimation and Monitoring for On-Line Flight Flutter Analysis. *Mechanical Systems and Signal Processing*, 18:587–610.

[Walter, 1994] Walter, G. (1994). *Wavelets and Other Orthogonal Systems with Applications*. CRC Press.

[Wang et al., 2008] Wang, G., Luo, Z., Qin, X., Leng, Y., and Wang, T. (2008). Fault Identification and Classification of Rolling Element Bearing Based on Time-Varying Autoregressive Spectrum. *Mechanical Systems and Signal Processing*, 22:934–947.

[Wang and McFadden, 1993] Wang, W. and McFadden, P. (1993). Early Detection of Gear Failure by Vibration Analysis II – Interpretation of the Time-Frequency Distribution Using Image Processing Techniques. *Mechanical Systems and Signal Processing*, 7(3):205–215.

[Wei and Billings, 2002] Wei, H.-L. and Billings, S. (2002). Identification of Time-Varying Systems Using Multiresolution Wavelet Models. *International Journal of Systems Science*, 33(15):1217–1228.

[Weisstein, 1998] Weisstein, E. (1998). *The CRC Concise Encyclopedia of Mathematics*. CRC Press, New York.

[Xianya and Evans, 1984] Xianya, X. and Evans, R. (1984). Discrete-Time Stochastic Adaptive Control for Time-Varying Systems. *IEEE Transactions on Automatic Control*, 29(7):638–640.

[Xun and Yan, 2008] Xun, J. and Yan, S. (2008). A Revised Hilbert-Huang Transformation Based on the Neural Networks and its Application in Vibration Signal Analysis of a Deployable Structure. *Mechanical Systems and Signal Processing*, 22:1705–1723.

[Yang and Chon, 2010] Yang, B. and Chon, K. (2010). Estimating Time-Varying Nonlinear Autoregressive Model Parameters by Minimizing Hypersurface Distance. *IEEE Transactions on Biomedical Engineering*, 57(8):1937–1944.

[Yang and Lin, 2005] Yang, J. and Lin, S. (2005). Identification of Parametric Variations of Structures Based on Least Squares Estimation and Adaptive Tracking Technique. *Journal of Engineering Mechanics*, 131(3):290–298.

[Yang et al., 2007] Yang, J., Pan, S., and Lin, S. (2007). Least-Squares Estimation with Unknown Excitations for Damage Identification of Structures. *Journal of Engineering Mechanics*, 133(1):12–21.

[Yao and Xu, 2002] Yao, B. and Xu, L. (2002). Adaptive Robust Motion Control of Linear Motors for Precision Manufacturing. *Mechatronics*, 12(4):595–616.

[Zhan and Jardine, 2005a] Zhan, Y. and Jardine, A. (2005a). Adaptive Autoregressive Modeling of Non-stationary Vibration Signals Under Distinct Gear States. Part 1: Modeling. *Journal of Sound and Vibration*, 286:429–450.

[Zhan and Jardine, 2005b] Zhan, Y. and Jardine, A. (2005b). Adaptive Autoregressive Modeling of Non-stationary Vibration Signals Under Distinct Gear States. Part 2: Experimental analysis. *Journal of Sound and Vibration*, 286:451–476.

[Zhan et al., 2006] Zhan, Y., Makis, V., and Jardine, A. (2006). Adaptive State Detection of Gearboxes Under Varying Load Conditions Based on Parametric Modelling. *Mechanical Systems and Signal Processing*, 20(1):188–221.

[Zhang et al., 2010a] Zhang, L., Xiong, G., Liu, H., Zou, H., and Guo, W. (2010a). Time-frequency Representation Based on Time-varying Autoregressive Model With Applications to Non-stationary Rotor Vibration Analysis. *Sadhana*, 35:215–232.

[Zhang et al., 2010b] Zhang, Z., Chan, S., and Hung, Y. (2010b). Local Polynomial Modelling of Time-Varying Autoregressive Processes and its Application to the Analysis of Event-Related Electroencephalogram. In *IEEE International Symposium on Circuits and Systems (ISCAS 2010)*, pages 3124–3127.

[Zhang et al., 2010c] Zhang, Z., Liu, H., Chan, S., Luk, K., and Hu, Y. (2010c). Time-Dependent Power Spectral Density Estimation of Surface Electromyography During Isometric Muscle Contraction: Methods and comparisons. *Journal of Electromyography and Kinesiology*, 20(1):89–101.

[Zheng et al., 2001a] Zheng, Y., Lin, Z., and Tay, D. (2001a). Time-Varying Parametric System Multiresolution Identification by Wavelets. *International Journal of Systems Science*, 32(6):775–793.

[Zheng et al., 2001b] Zheng, Y., Tay, D., and Lin, Z. (2001b). Modeling General Distributed Nonstationary Process and Identifying Time-Varying Autoregressive System by Wavelets: Theory and application. *Signal Processing*, 81(9):1823–1848.

[Zhou et al., 2007] Zhou, Z., Mechefske, C., and Xi, F. (2007). Nonstationary Vibration of a Fully Flexible Parallel Kinematic Machine. *Journal of Vibration and Acoustics*, 129:623–630.

[Zou et al., 2003] Zou, R., Wang, H., and Chon, K. (2003). A Robust Time-Varying Identification Algorithm Using Basis Functions. *Annals of Biomedical Engineering*, 31(7):840–853.

Curriculum Vitae

Minas Spiridonakos

Mechanical & Aeronautical Engineer
Email: mspirid@mech.upatras.gr

Personal

Born on February 26, 1980.

Greek Citizen.

Education

November 2004 - April 2012: PhD Candidate, Department of Mechanical Engineering and Aeronautics, University of Patras, Greece.

PhD Thesis Title: "Advanced and Complete Functional Series Time-Dependent ARMA (FS-TARMA) Methods for the Identification and Fault Diagnosis of Non-Stationary Stochastic Structural Systems".

Supervisor: Prof. S.D. Fassois.

Mechanical Engineering and Aeronautics Diploma obtained from the University of Patras, Greece, (November 2004; with distinction 8.06/10).

Research Interests

Stochastic system identification, time–varying systems, non–stationary vibration analysis, modal testing, statistical methods for Structural Health Monitoring (SHM), damage detection and diagnosis.

Research Experience

Researcher 2006-2008
Greek General Secretariat for Research & Development
Italy-Greece joint research and technology program, project 085-e: Greece-Italy: "Smart space structures stochastic dynamic identification".

Researcher 2005-2008
University of Patras
Karatheodory Grant: "FS-TAR/TARMA Multivariate Methodology Development for Vibration Dynamic Modeling and Damage Detection of Non-stationary Mechanical Systems".

Researcher 2005
Volkswagen Stiftung
Research Project I/76 940: "Nonlinear Dynamics Modeling, Detection, Identification and Fault Diagnosis in Industrial Robotics and Machine Elements".

Academic Experience

Laboratory teaching 2006-2009
University of Patras, Dept. of Mech. Eng. & Aeronautics
Teaching assistant for the "Mechatronic Systems" laboratory exercises (junior year).

Laboratory teaching 2004-2009
University of Patras, Dept. of Mech. Eng. & Aeronautics
Teaching assistant for the "Systems and Automatic Controls I" laboratory exercises (senior year).

Language Skills

Greek (mother tongue)
English (fluently)
Spanish (basic knowledge)

Software Abilities

Programming Languages: C, C++
Technical computing: MATLAB & Simulink, Scilab, Labview
CAD: Autocad
Operating systems: Microsoft Windows and Linux

Instrumentation Experience

Data acquisition, time and frequency domain analysis hardware and software (Siglab, National Instruments)
Vibration analysis actuators and sensors (MB Dynamics, LDS, Data Physics, PCB)

Publications

Journal Articles

M.D. Spiridonakos and S.D. Fassois, "Adaptable Functional Series TARMA Models for Non-Stationary Signal Modelling", *under preparation for publication*.

M.D. Spiridonakos and S.D. Fassois, "Non-Stationary Vibration Modelling and Analysis via Functional Series Time-Dependent ARMA (FS-TARMA) Models – A critical survey", *submitted for publication*.

M.D. Spiridonakos and S.D. Fassois, "An FS-TAR Based Statistical Method for the Modelling and Fault Diagnosis in Time-Varying Structures: A pick-and-place mechanism application study", *submitted for publication*.

M.D. Spiridonakos, A.G. Poulimenos, and S.D. Fassois, "Identification and Dynamic Analysis of Time-Varying Mechanical Structures Under Random Excitation: A comparative assessment of parametric output-only methods", *Journal of Sound and Vibration*, Vol. 329, No. 7, pp. 768-785, 2010.

M.D. Spiridonakos and S.D. Fassois, "Parametric Identification of a Time-Varying Structure Based on Vector Vibration Response Measurements", *Mechanical Systems and Signal Processing*, Vol. 23, No. 6, pp. 2029-2048, 2009.

Proceedings

M.D. Spiridonakos and S.D. Fassois, "Fault Detection and Identification in Time-Varying Structures via an FS-TAR Model Based Method: Application to a Pick-and-Place Mechanism", *6th European Workshop on Structural Health Monitoring (EWSHM)*, Dresden, Germany, July 2012.

M.D. Spiridonakos and S.D. Fassois, "Adaptable Functional Series TARMA Models for Non-Stationary Signal Modelling", *SYSID 2012, 16th IFAC Symposium on System Identification*, Brussels, Belgium, July 2012.

L.D. Avendano-Valencia, M.D. Spiridonakos, and S.D. Fassois, "In-Operation Identification of a Wind Turbine Structure via Non-Stationary Parametric Models", *8th International Workshop on Structural Health Monitoring (IWSHM)*, Stanford University, Stanford,CA, U.S.A, 2011.

M.D. Spiridonakos and S.D. Fassois, "Output-Only Identification of Time-Varying Structures via a Complete FS-TARMA Model Approach", *4th International Operational Modal Analysis Conference (IOMAC)*, Instanbul, Turkey, May 2011.

S.D. Fassois and M.D. Spiridonakos, "Non-Stationary Random Vibration Modelling and Identification - an overview of parametric methods and applications" *(keynote paper)*, *4th International Operational Modal Analysis Conference (IOMAC)*, Instanbul, Turkey, May 2011.

M.D. Spiridonakos and S.D. Fassois, "FS-TARMA Models for Non-stationary Vibration Analysis: An Overview and Recent Advances", *17th International Congress on Sound and Vibration (ICSV17)*, Cairo, Egypt, July 2010.

M.D. Spiridonakos and S.D. Fassois, "FS-TARMA Models for Non-Stationary Vibration Analysis: An overview and comparison", *SYSID 2009, 15th IFAC Symposium on System Identification*, Saint-Malo, France, July 2009.

M.D. Spiridonakos and S.D. Fassois, "Vibration Based Fault Detection in an Extendable Prismatic Link Structure via Non-Stationary FS-VTAR Models", *3rd International Operational Modal Analysis Conference*, Ancona, Italy, May 2009.

M.D. Spiridonakos and S.D. Fassois, "Multi-Channel Output-Only Identification of an Extendable Arm Structure Under Random Excitation: A comparison of parametric methods", *RAST 2009, 4th International Conference on Recent Advances in Space Technologies*, Istanbul, Turkey, June 2009.

M.D. Spiridonakos and S.D. Fassois, "Non-Stationary Random Vibration Modelling in a Retractable Arm Structure", *ISMA 2008*, Leuven, Belgium, September 2008.

M.D. Spiridonakos and S.D. Fassois, "Parametric Output-Only Identification of Time-Varying Structures: The Multiple Measurement Case", *2nd International Operational Modal Analysis Conference*, Copenhagen, Denmark, May 2007.

M.D. Spiridonakos and S.D. Fassois, "Modelling and Simulation of Earthquake Ground Motion via Functional Series TARMA Models with Wavelet Basis Functions", *III European Conference on Computational Mechanics, Solids, Structures and Coupled Problems in Engineering*, Lisbon, Portugal, June 2006.

A.G. Poulimenos, M.D. Spiridonakos, and S.D. Fassois, "Identification of Time-Varying Structures under Unobservable Excitation: An Overview and Experimental Comparison of Parametric Methods", *III European Conference on Computational Mechanics, Solids, Structures and Coupled Problems in Engineering*, Lisbon, Portugal, June 2006.

A.G. Poulimenos, M.D. Spiridonakos, and S.D. Fassois, "Parametric Time-Domain Methods for Non-Stationary Random Vibration Identification and Analysis: An Overview and Comparison", *ISMA 2006*, Leuven, Belgium, September 2006.